

Vol. 13

2020

No. 02

GEOGRAPHY ENVIRONMENT SUSTAINABILITY

Special Issue «Water sustainability at global, regional
and national levels»

«The journal GEOGRAPHY, ENVIRONMENT, SUSTAINABILITY was founded in 2008 by Russian Geographical Society, the Lomonosov Moscow State University Geography Department, and the Russian Academy of Sciences Institute of Geography. Since that time the journal publishes **4 issues per year**, containing original research papers and reviews. The journal issues are open source and distributed through subscriptions, library exchanges of leading universities, and via the website through the world»

FOUNDERS OF THE JOURNAL: Russian Geographical Society, Faculty of Geography, Lomonosov Moscow State University and Institute of Geography of the Russian Academy of Sciences

The journal is published with financial support of the Russian Geographical Society.

The journal is registered in Federal service on supervision of observance of the legislation in sphere of mass communications and protection of a cultural heritage. The certificate of registration: ПИ № ФС77-67752, 2016, December 21.

PUBLISHER

Russian Geographical Society
Moscow, 109012 Russia
Novaya ploshchad, 10, korp. 2
Phone 8-800-700-18-45
E-mail: press@rgo.ru
www.rgo.ru/en

EDITORIAL OFFICE

Lomonosov Moscow State University
Moscow 119991 Russia
Leninskie Gory, 1,
Faculty of Geography, 1806a
Phone 7-495-9391552
Fax 7-495-9391552
E-mail: ges-journal@geogr.msu.ru
www.ges.rgo.ru

DESIGN

Layout designer: Tereshkin Anton I.
Moscow, 115088,
26 Simonovsky Val str., bldg. One
Phone: +7 (903) 108-04-44
E-mail: smile.tai@gmail.com

DOI prefix: 10.24057

Format A4 (210x297mm)

"GEOGRAPHY, ENVIRONMENT, SUSTAINABILITY" is the only original English-language journal in the field of geography and environmental sciences published in Russia. It is supposed to be an outlet from the Russian-speaking countries to Europe and an inlet from Europe to the Russian-speaking countries regarding environmental and Earth sciences, geography and sustainability. The main sections of the journal are the theory of geography and ecology, the theory of sustainable development, use of natural resources, natural resources assessment, global and regional changes of environment and climate, social-economical geography, ecological regional planning, sustainable regional development, applied aspects of geography and ecology, geoinformatics and ecological cartography, ecological problems of oil and gas sector, nature conservations, health and environment, and education for sustainable development.

OPEN ACCESS POLICY. "GEOGRAPHY, ENVIRONMENT, SUSTAINABILITY" is an open access journal. All articles are made freely available to readers immediately upon publication. Our open access policy is in accordance with the Budapest Open Access Initiative (BOAI) definition - it means that articles have free availability on the public internet, permitting any users to read, download, copy, distribute, print, search, or link to the full texts of these articles, crawl them for indexing, pass them as data to software, or use them for any other lawful purpose, without financial, legal, or technical barriers other than those inseparable from gaining access to the internet itself.

Date of publication: July 1st, 2020.

EDITORIAL BOARD

EDITORS-IN-CHIEF:

Kasimov Nikolay S.

Lomonosov Moscow State University,
Faculty of Geography, Russia

Kotlyakov Vladimir M.

Russian Academy of Sciences
Institute of Geography, Russia

DEPUTY EDITORS-IN-CHIEF:

Solomina Olga N. - Russian Academy of Sciences,
Institute of Geography, Russia

Tikunov Vladimir S. - Lomonosov Moscow State
University, Faculty of Geography, Russia

Vandermotten Christian - Université Libre de Bruxelles
Belgium

Chalov Sergei R. - (Secretary-General) Lomonosov
Moscow State University, Faculty of Geography, Russia

Alexeeva Nina N. - Lomonosov Moscow State University,
Faculty of Geography, Russia

Baklanov Alexander - World Meteorological Organization,
Switzerland

Baklanov Petr Ya. - Russian Academy of Sciences, Pacific
Institute of Geography, Russia

Chubarova Natalya E. - Lomonosov Moscow State
University, Faculty of Geography, Russia

De Maeyer Philippe - Ghent University, Department of
Geography, Belgium

Dobrolubov Sergey A. - Lomonosov Moscow State
University, Faculty of Geography, Russia

Ferjan J. Ormeling - University of Amsterdam, Amsterdam,
Netherlands

Sven Fuchs - University of Natural Resources and Life
Sciences

Haigh Martin - Oxford Brookes University, Department of
Social Sciences, UK

Golosov Valentin N. - Lomonosov Moscow State
University, Faculty of Geography, Russia

Gulev Sergey K. - Russian Academy of Sciences, Institute of
Oceanology, Russia

Guo Huadong - Chinese Academy of Sciences, Institute of
Remote Sensing and Digital Earth, China

Jarsjö Jerker - Stockholm University, Department of
Physical Geography and Quaternary Geography, Sweden

Jeffrey A. Nittrouer - Rice University, Houston, USA

Ivanov Vladimir V. - Arctic and Antarctic Research
Institute, Russia

Karthe Daniel - German-Mongolian Institute for Resources
and Technology, Germany

Kolosov Vladimir A. - Russian Academy of Sciences,
Institute of Geography, Russia

Kosheleva Natalia E. - Lomonosov Moscow State
University, Faculty of Geography, Russia

Konečný Milan - Masaryk University, Faculty of Science,
Czech Republic

Kroonenberg Salomon - Delft University of Technology,
Department of Applied Earth Sciences, The Netherlands

Kulmala Markku - University of Helsinki, Division of
Atmospheric Sciences, Finland

Olchev Alexander V. - Lomonosov Moscow State
University, Faculty of Geography, Russia

Malkhazova Svetlana M. - Lomonosov Moscow State
University, Faculty of Geography, Russia

Meadows Michael E. - University of Cape Town,
Department of Environmental and Geographical Sciences
South Africa

Nefedova Tatyana G. - Russian Academy of Sciences,
Institute of Geography, Russia

O'Loughlin John - University of Colorado at Boulder,
Institute of Behavioral Sciences, USA

Paula Santana - University of Coimbra, Portugal

Pedroli Bas - Wageningen University, The Netherlands

Pilyasov Alexander N. - Institute of Regional Consulting,
Moscow, Russia

Radovanovic Milan - Serbian Academy of Sciences and
Arts, Geographical Institute "Jovan Cvijić", Serbia

Sokratov Sergei A. - Lomonosov Moscow State University,
Faculty of Geography, Russia

Tishkov Arkady A. - Russian Academy of Sciences,
Institute of Geography, Russia

Wuyi Wang - Chinese Academy of Sciences, Institute of
Geographical Sciences and Natural Resources Research,
China

Zilitinkevich Sergey S. - Finnish Meteorological Institute,
Finland

EDITORIAL OFFICE

ASSOCIATE EDITOR

Maslakov Alexey A.

Lomonosov Moscow State University,
Faculty of Geography, Russia

PROOF-READER

Troshko Maria M.

Lomonosov Moscow State University,
Faculty of Geography, Russia

ASSISTANT EDITOR

Grishchenko Michail Yu.

Lomonosov Moscow State University,
Faculty of Geography, Russia

CONTENTS

SPECIAL ISSUE

«WATER SUSTAINABILITY AT GLOBAL, REGIONAL AND NATIONAL LEVELS»

Frank Winde

- TURNING WATER POLLUTION SOURCES INTO ASSETS: EXPLORING INNOVATIVE OPTIONS
OF USING ABANDONED MINES FOR GENERATING AND STORING RENEWABLE ENERGY 6

Gabriela Ioana-Toroimac, Liliana Zaharia, Gianina Neculau, Gabriel Minea

- IMPACT OF CHANNEL INCISION ON FLOODS: A CASE STUDY
IN THE SOUTH-EASTERN SUBCARPATHIANS (ROMANIA) 17

Dmitriy V. Magritsky, Natalia L. Frolova, Olga M. Pakhomova

- POTENTIAL HYDROLOGICAL RESTRICTIONS ON WATER USE IN THE BASINS
OF RIVERS FLOWING INTO RUSSIAN ARCTIC SEAS..... 25

Mirza Imran, P. Sheikh Abdul Khader

- FORECASTING WATER LEVEL OF JHELM RIVER OF KASHMIR VALLEY INDIA,
USING PREDICTION AND EARLYWARNING SYSTEM 35

Svetlana A. Agafonova, Alexander N. Vasilenko

- HAZARDOUS ICE PHENOMENA IN RIVERS OF THE RUSSIAN ARCTIC ZONE
UNDER CURRENT CLIMATE CONDITIONS AND THE SAFETY OF WATER USE 43

Alexander V. Martynov

- INFLUENCE OF THE LARGE FLOOD ON THE ELEMENT COMPOSITION
OF FLUVISOLS IN THE AMUR RIVER VALLEY..... 52

Vladimir S. Pashtetsky, Vadim V. Khomenko, Nikolay P. Demchenko,

Natalia Yu. Poliakova, Rinas V. Kashbrasiev

- SUSTAINABLE AND COMPETITIVE AGRICULTURAL DEVELOPMENT OF
A WATER-DEFICIENT REGION (CASE OF THE CRIMEAN PENINSULA)..... 65

Aweewan Mangmeechai

- EFFECTS OF RUBBER PLANTATION POLICY ON WATER RESOURCES
AND LANDUSE CHANGE IN THE NORTHEASTERN REGION OF THAILAND..... 73

Maria B. Kireeva, Ekaterina P. Rets, Natalya L. Frolova, Timothy E. Samsonov,

Elena S. Povalishnikova, Andrey L. Entin, Ivan N. Durmanov, Alexander M. Ivanov

- OCCASIONAL FLOODS ON THE RIVERS OF RUSSIAN PLAIN IN THE 20TH–21ST CENTURIES..... 84

Leonid M. Korytny, Olga V. Gagarinova, Elena A. Ilyicheva, Natalya V. Kichigina

- A GEOGRAPHICAL APPROACH TO WATER RESOURCE MAPPING FOR ATLASES..... 96

Gurveek S. Maan, Jagadish P. Patra, Ripudaman Singh

- A HYDRO-INFORMATIC APPROACH FOR ESTIMATION OF DESIGN FLASH-FLOOD
IN BARGI DAM CROSS-SECTION OF NARMADA RIVER, INDIA.....104

Nguyen Ba Dung, Dang Tuyet Minh, Adeel Ahmad, Nguyen Quoc Long

- THE ROLE OF RELATIVE SLOPE LENGTH IN FLOOD HAZARD MAPPING USING AHP
AND GIS (CASE STUDY: LAM RIVER BASIN, VIETNAM)..... 115

REGULAR ISSUE

Marina A. Chichaeva, Mikhail Yu. Lychagin, Anton V. Syroeshkin, Olga V. Chernitsova HEAVY METALS IN MARINE AEROSOLS OF THE AZOV SEA.....	127
Besfat D. Engdaw ASSESSMENT OF THE TRENDS OF GREENHOUSE GAS EMISSION IN ETHIOPIA	135
Yusra Al-Husban, Ahmad Ayen THE IMPACT OF THE SYRIAN CIVIL WAR ON LAND USE / LAND COVER IN AL-YARMOUK BASIN DURING 2010–2018.....	147
Andrey N. Shikhov, Rinat K. Abdullin, Andrey V. Tarasov MAPPING TEMPERATURE AND PRECIPITATION EXTREMES UNDER CHANGING CLIMATE (ON THE EXAMPLE OF THE URAL REGION, RUSSIA).....	154
Nguyen T. Hung, Irina I. Kosinova, Đang T. L. Anh MODELING AIR POLLUTION IN DONG NAI PROVINCE, VIETNAM.....	166
Si-Son Tong, Thi-Lan Pham, Quoc Long Nguyen, Thi Thu Ha Le, Le Hung Trinh, Xuan Cuong Cao, Adeel Ahmad, Thi-Huyen-Ai Tong THE STUDY OF LAND COVER CHANGE USING CHANGE VECTOR APPROACH INTEGRATED WITH UNSUPERVISED CLASSIFICATION METHOD: A CASE IN DUY TIEN (VIETNAM).....	175

Disclaimer:

The information and opinions presented in the Journal reflect the views of the authors and not of the Journal or its Editorial Board or the Publisher. The GES Journal has used its best endeavors to ensure that the information is correct and current at the time of publication.

TURNING WATER POLLUTION SOURCES INTO ASSETS: EXPLORING INNOVATIVE OPTIONS OF USING ABANDONED MINES FOR GENERATING AND STORING RENEWABLE ENERGY

Frank Winde^{1,2,*}

¹Department Monitoring and Radiation Protection, Wismut GmbH, Jagdschänkenstrasse 29 D-09117 Chemnitz, Germany

² North-West University, Research Unit for Environmental Science and Management, Vanderbijlpark Campus, 1174, Vanderbijlpark 1900, South Africa

*Corresponding author: frank.winde@gmail.com

Received: January 08th, 2020 / Accepted: May 10th, 2020 / Published: July 1st, 2020

<https://DOI-10.24057/2071-9388-2020-03>

ABSTRACT. Through moving large volumes of rock for decades or even centuries from geological underground to surface, industrial scale mining invariably alters the natural local and regional hydrological conditions. Consequences include irreversible changes of flow gradients and water quality in aquifers and streams effected through dewatering, ground subsidence, acid mine drainage, etc. During their lifetime mines spent significant resources and energy on maintaining an ever-increasing diversion from natural hydraulic equilibria through pumping rising volumes of ingress water from ever greater depths, especially if operating below water-rich formations (karst) or in humid climates. Associated pumping costs may even lead to premature mine closure. In cases where complete flooding of closed mines is not an option (e.g. to protect water resources or infrastructure) such costs remain well after mines closed for as long as flooding restrictions apply. In large and densely populated regions in South Africa or Germany, for example, where mining succeeded in triggering urbanisation and self-sustaining economic development it is (currently) assumed that pumping will be needed forever. Accordingly, post-closure water management is no longer only a long-term liability but indeed a perpetual burden placed on future generations that had little direct benefits from earlier mining. This paper focuses specifically on possible ways of reducing perpetual post-closure water management costs specifically of using abandoned mines for generating and storing renewable energy. It discusses successful examples already implemented, concepts investigated but not yet realised as well as technologies that received little, if any, attention to date. The latter range from using mines (included flooded ones) for the storage of electrical energy via different technologies, harvesting geothermal energy from mine water and voids to different ways of transforming chemical energy contained in mine water into electricity.

KEY WORDS: closed mines, mine water, renewable energy, energy storage

CITATION: Frank Winde (2020). Turning Water Pollution Sources Into Assets: Exploring Innovative Options Of Using Abandoned Mines For Generating And Storing Renewable Energy. *Geography, Environment, Sustainability*, Vol.13, No 2, p. 6-16
<https://DOI-10.24057/2071-9388-2020-03>

ACKNOWLEDGEMENTS: The author gratefully acknowledges the supporting advise of Mr. Hans-Jürgen Friedrich (Fraunhofer Institute, IKTS, Germany)

Conflict of interests: The authors reported no potential conflict of interest.

INTRODUCTION

Extracting large amounts of rock from the geological underground at ever increasing depths invariably leads to rising volumes of water ingressing into the created void system. In order to prevent underground workings from gradual flooding this water needs to be continuously removed through pumping. Where pumping rates exceed the natural groundwater recharge for prolonged periods of time this eventually leads to the lowering of groundwater tables and the associated dewatering of overlying aquifers. Through the collapse of near-surface mine tunnels, desiccation of previously saturated soil strata and accelerated subterranean erosion this, in turn, often results in geotechnical ground instability causing subsidences, sinkholes etc.

Worldwide, mine water management is generally among the longest-lasting and costliest parts of post-closure remediation (e.g. Paul et al. 2015; Eberfalvi et al. 2015). In order to reduce associated financial burdens global efforts are underway to find innovative ways of making post-closure water management more affordable and economically as well as ecologically sustainable. This need is especially pressing for developing countries where the bulk of global mining currently takes place, and which have the least resources to mitigate associated impacts that often are more severe than in developed nations. The problem is likely to intensify in future as consumption of mineral resources continuous to grow driven by population growth and improved lifestyles. While mining of conventional fuel such as coal, oil, gas and uranium may decrease in future this is counterbalanced by extracting

growing amounts of partly very rare minerals used, for example, in wind turbines (e.g. neodymium and dysprosium for magnets), solar panels (e.g. indium, cadmium, tellurium), electrical cars (lithium) and electronics. For 2050, predicted requirements for praseodymium, dysprosium, terbium, neodymium and indium range between 4 and 12 times the total annual production in 2017, respectively (Ahmed 2018). Owing to their relatively low natural abundance this will result in ever larger ore volumes to be mined increasingly impacting on the environment. Generally, renewable energy requires more mineral resources per energy unit generated than conventional energy forms (Ghenai and Janajreh 2013; Acatech 2017). As most future mining is set to continue taking place mainly in developing countries where social acceptance is higher than in affluent societies, proactive efforts are needed at an international scale to prevent exacerbating global disparities further fuelling political instability, regional conflict and mass migration.

Against this background the present paper illustrates impacts and costs associated with the post-closure flooding of underground mines using international case studies before exploring a range of existing technologies on generating and storing renewable energy to tackle mine water legacy issues in a sustainable manner. The main objective is not to assess the viability of the various technological options but rather to propose their innovative applications in the context of closed mines.

POST-CLOSURE LEGACY COSTS: CASE STUDIES FROM SOUTH AFRICA AND GERMANY

(i) *South African gold mines:* In dolomitic goldfields of South Africa, where deep-level gold mines dewatered large karst aquifers this led to the drying up of natural karst springs and boreholes previously used for agricultural irrigation as well as to the destruction of infrastructure including roads, railways, residential houses and industrial plants, often with catastrophic consequences and loss of life (Winde and Stoch 2010). Apart from associated economic damage this also changed the hydrological characteristics of the affected landscape, inter alia, through increasing groundwater recharge rates via hundreds to thousands of newly formed sinkholes directly channelling surface runoff underground. Consequently, pumping rates at deep-level mines increased well-above natural levels as indicated, for example, by pre-mining spring flow volumes. Combined with the ever-increasing depth of mining reaching levels of up to 4000 m below surface the rise in pumping volumes placed a significant financial burden onto affected mines some of which have to pump 70 to over 100 Ml per day. If these mines close and are subsequently flooded water flowing into adjacent voids adds to the pumping load and potentially shortens the lifespan of receiving mines. Following the unplanned and haphazard closure of mines in the Western and Central Basins (near Johannesburg, South Africa) subsequent flooding resulted in the uncontrolled decant of highly polluted acidic mine drainage (AMD) contaminating ground- and surface water resources. In order to protect water resources as well as shallow underground infrastructure such as the basements of high-rise buildings, government installed underground pumps to keep mine water from exceeding critical levels. The extracted water is neutralised through liming before being discharged into nearby streams still containing all salts and most contaminants such as uranium. After the storage capacity of adjacent mine tailings was exhausted the toxic sludge generated by liming at the high-density sludge plant is now pumped back to the underground void from which the mine water is extracted essentially creating a closed loop that increases pumping rates as well as pollution levels. For treating a total volume of some 130 Ml/d of AMD in the mid-term (approximately 5 years) government allocated R 15 bn (just under € 1bn) (Winde and Stoch 2010). With all three

flooded mining basins underlying densely populated urban areas the pump-and treat approach needs to be maintained in perpetuity. According to long-term plans the pumped mine water will in future be treated to potable standards via reverse osmosis recovering associated costs through a levy on drinking water. This would effectively burden associated costs onto the general public rather than former mine owners violating the polluter-pays principle.

With more than 300 Ml of mine water per day currently still being pumped by active gold mines future treatment costs are set to almost triple once those mines close. This would render the current pump-and-treat approach unaffordable in the long run especially considering the sluggish economic development and persisting spending priorities such as housing, health, education, social welfare etc.

(ii) *German hard coal mines:* While affordability may be different in Germany, mining-related water problems are similar as, for example, the 'Ruhrgebiet' shows. After more than 200 years, hard coal mining in the Ruhr area, once the economic powerhouse of Germany, finally ceased in December 2018. Mining-induced ground subsidence has left large tracks of land sunken below the natural water level of local rivers such as Rhine, Ruhr, Lippe and Emscher with surface water ponding in drainage-less areas. In some instances, even the direction of stream flow was reversed. This necessitated hydrological engineering employing polders (artificially impounded water bodies) and pumping at surface in order to restore drainage. To avoid that sunken densely populated areas are submerged by rising mine water once mines close, perpetual pumping is required. Pumping volumes in 2016 were around 180 Ml/d (66 Mm³/a) and are predicted to eventually level out at an average of about 300 Ml/d (110 Mm³/a). Together with polder maintenance and limited groundwater treatment (mostly at former cookeries) post-closure water management is estimated to require € 220 million per year from 2019 onward (Dombrowski 2018, RAG 2019).

In contrast to South Africa these costs are not covered by government or levies but by proceeds (interest) from a € 14.3bn-investment controlled by the RAG foundation, a diversified successor of the former Ruhrkohle AG. The latter was founded in 1968 by government to consolidate the many marginal collieries and gradually phase out coal mining. As RAG has received direct and indirect governmental subsidies for decades (including a compulsory levy on coal-based energy termed 'Kohlepfenning', coal penny later found to be unconstitutional) some of the now used capital originally also came from taxes (RAG 2019). Unlike South African gold mines, the Ruhr area is not plagued by excessive AMD-formation allowing to omit costly neutralisation for the bulk of the pumped water. To what extent this may change in future when all mines are flooded to the higher levels at around 600 m below surface (for saving pumping costs) remains to be seen.

(iii) *German lignite mines:* In contrast to hard coal mines in the Ruhr area acidification does occur in former lignite mines in south-east Germany, where large lakes formed in flooded open pits with pH-values below 3 necessitating regular liming among other measures. High sulphate and iron levels reaching the river Spree also pose a challenge for downstream water purification as far away as Berlin. Similar to South Africa, where good quality water from the Vaal Dam is used to keep TDS levels in the AMD-impacted downstream part of the Vaal River below 600 mg/l efforts are made here, too, to keep sulphate levels below 450 mg/l by releasing water from upstream dams in Bautzen and Quitzdorf. This, however, proved to be difficult to maintain during an extended dry-weather-period in 2018 when the dilution capacity of the two dams was exhausted triggering, inter alia, an increase of the maximal permissible sulphate concentration to 500 mg/l sulphate (LfU 2018).

With hundreds of thousands of closed and often abandoned mines worldwide associated challenges truly are of global dimension. As resource-restricted economies in developing countries of the global south are among the most affected, simply copying cost-intensive pump-and-treat approaches employed in affluent countries is not sustainable. This paper thus aims to identify innovative alternatives for avoiding perpetual costs being burdened onto future generations through turning mine legacy sites from liabilities into assets.

To this end, a review of existing technologies was conducted focussing on integrated solutions within the water-energy nexus as an area of growing importance, especially in the field of generating and storing renewable energy. Main criterion for selecting promising technologies was their potential to sustainably reduce long-term costs for post-closure mine water management. The aim is not to exhaustively discuss technical detail but rather to stimulate discussion of alternatives to conventional approaches of remediation. Technologies covered in this paper relate to the following aspects of post-closure mine water management:

- Extracting chemical energy from mine water: PRO, RED.
- Harvesting geothermal energy: wind, water.
- Storing (renewable) energy: PHES, UPHEs, CAS, Redox flow batteries.
- Generating renewable energy: PV, SUT and biofuel.

GENERATING RENEWABLE ENERGY: EXTRACTING CHEMICAL ENERGY FROM MINE WATER

Core concept

Mine water frequently contains significantly higher salt concentrations than freshwater. Through utilising the natural tendency of concentration differences between water bodies being equalised the chemical potential of mine water can be utilised.

One option is to use the osmose-driven pressure differences between interacting freshwater and mine water columns for generating mechanical energy that can be converted into electricity using Pressure Retarded Osmosis (PRO) technology.

Alternatively, the osmotic movement of dissolved cat- and anions from mine water can also be used to directly generate electricity through separating differently charged ions for creating electrical potential differences that drive a direct current (DC), a technology known as Reverse Electrodialysis (RED). Both technologies are briefly outlined below.

Pressure retarded osmosis (PRO)

The salinity gradient between polluted mine water and freshwater (ground- or surface water) drives a natural process of dilution known as osmosis whereby water molecules from the dilute water phase diffusely migrate via a semipermeable membrane into the higher mineralised mine water until differences in salt concentration are equalised. The movement of freshwater molecules does not require any additional fuel but is purely driven by the salinity gradient and therefore also known as «salinity gradient power» or «blue energy» (Siebers 2012).

As freshwater molecules move across the membrane into the mine water column volume and water level are increased in the latter. For seawater, for example, the resulting height difference to the freshwater column is 270 m translating into a hydraulic pressure difference of 26.5 bar that can be converted into electricity via pistons or turbines. Invented in 1973 in Israel, the world's first osmotic power plant based on PRO technology was opened by the

power utility Statkraft in 2009 in the small coastal town of Tofte (Norway) employing the salinity gradient between a local river and seawater yielding a capacity of 10 kW. For Norway alone it is estimated that 12 TWh of 'blue energy' could be produced covering some 10 % of the country's total electricity need (FPTM 2019). Depending on salinity and water throughput (0.5-1 m³/s; ca. 4-9 Ml/d) PRO-plants, under realistic conditions, could produce energy outputs at MW-scale (Siebers 2012).

Application in mine remediation would be best suited for sites with highly saline mine water and sufficiently large resources of clean freshwater nearby (at least about ten times the treated mine water volume depending on salinity) to achieve the required dilution and energy output. While this may limit applications in arid areas suffering from water shortages the technology is well suited for mines with abundant ground and surface water. In addition to humid areas this may also include mines in dry environments operating below water-rich formations as is the case with many South African gold mines.

Apart from supplementing pumping costs through continuously produced, clean free-of-charge energy, no waste product (such as sludge or brine) is to be disposed of like in conventional pump-and-treat approaches such as neutralisation or reverse osmosis (RO). In fact, through diluting mine water with freshwater a good quality water-mix is produced that may either be sold or discharged into nearby water courses without having to consider flow conditions in receiving streams. In view of recent discharge restrictions in Germany due to low dilution capacity of rivers following prolonged dry weather spells in 2018, this may be of increasing future importance for maintaining operational continuity. If RO-based water treatment plants are located near a mine the generated waste brine may be used to increase salinity of the mine water thereby raising the energy output.

Potential applications in Germany may include hard coal mines where overlying Permian evaporites result in highly saline mine water potentially exceeding the dilution capacity of relatively small streams used for disposal. Also, salt mines struggling to dispose of their highly saturated brines are well suited. For all saline mine waters, however, low concentrations of scale-generating constituents such as Ca and Mg (forming calcite) and Fe and Mn (forming iron/manganese hydroxide precipitates) are best as otherwise coatings and scales may damage the membranes.

Applications in semi-arid South Africa are limited by the general scarcity of fresh water at many mines. However, this is different for mines in and around the greater Johannesburg metropolitan areas where large amounts of treated sewage effluents exceeding local mine water volumes by over 10 times could be used.

Current technological challenges mainly relate to the size of the required membrane area approaching millions of square metres. In order to minimise associated space requirements rolled-up membranes are currently investigated. Capital expenditure relates mainly to turbines and pressurised containers as well as membranes. Running cost relate to maintenance, personnel and the regular replacement of membranes.

Reverse electrodialysis (RED)

This type of energy generation is based on the separation of charged ions naturally contained in mine water using successive layers of semipermeable anisotropic membranes through which the mine water migrates. Accumulating the charge differences between salty mine water on the one side of the membrane and clean fresh water on the other

drives a direct current. In 1977, the technology was patented in the USA by S. Loeb from Israel.

Since the end of 2014, a 50-kW-pilot test plant operates on the Afsluitdijk in The Netherlands utilising the difference in electrical potential between freshwater in the IJsselmeer and seawater of the Wadden Sea (part of the North Sea) following a successful 8-year test period. The objective is to demonstrate technical feasibility in real-life conditions. At an increased through-flow of 1 m³/s the plant could produce approximately 1 MW of electricity despite a rather modest salinity gradient. For the future, an extension to 200 MW capacity is envisaged. At an average of 3300 m³ of river water running into the sea per second in the whole of the Netherlands a total of 4.5 GW could be harvested using RED technology (Siebers 2012).

As energy is produced continuously RED could be used to supplement pumping costs. In order to minimise DC-AC conversion losses DC-pumps should be used. RED plants are commonly built modular consisting of stacked cells with a capacity of 250 kW each with each cell the size of a shipping container. The successful testing from 2006 to 2014 and the operation phase thereafter together with the envisaged extension of the pilot plant indicate that the technology is feasible under the testing conditions.

Like with the PRO technology, mines with highly saline water and sufficient freshwater resources are best suited for applying RED.

HARVESTING GEOTHERMAL ENERGY

Core concept

The extraction of geothermal energy is based on the earth's temperature increase from an average of 15°C on surface to over 6000°C at the core creating a so-called geothermal gradient. This gradient varies geographically from around 1°C/100 m in old and stable geological structures (such as cratons within which the South African gold mines are located) to over 20 °C/ 100 m in volcanically active zones. The average gradient in Germany is around 3°C/100 m (<https://www.geothermie.de/bibliothek/lexikon-der-geothermie/g/geothermischer-gradient.html>; accessed 12 May 2019). Depending on the depth of mine and geological settings pumped mine water may be considerably warmer than water on surface. While heat recovery from water is meanwhile well established the same is not true for heated air exhaled by mines. Driven by air temperature differences many mines exhibit natural air movements through shafts

and tunnels in form of lateral and vertical drafts that often are strong enough to drive wind turbines. Technologies extracting energy from wind and water of mines are briefly discussed below.

Geothermal wind energy from mine voids

Increasing rock face temperatures in deeper parts of the mines lead to increased temperature of the ambient air and associated convection driving drafts through tunnels and shafts of the underground void. Rising air leaving the void, in turn, sucks in cooler air from surface which will again be heated in deeper parts of the mine creating a continuous circulation. The escaping air can drive (vertical) wind turbines installed in shaft openings creating renewable energy with the output depending on wind speed. The higher the difference in air temperature between surface and mine void, the higher the wind speed and associated energy yield (Fig. 1).

Of course, this concept provides that shafts are not sealed and exhalation of radon is below permissible limits.

The technology was patented in 2009 in the USA (DuBois 2014, 2018) but has not yet been implemented, not even on pilot scale. However, modelling based on conditions of the Blyvooruitzicht gold mine (South Africa) indicated, in principle, the technical feasibility of the concept.

Advantages of the technology include the relatively low initial capital requirement and the continuous generation of cost-free, clean and renewable electricity. Given the simple structure of the system little maintenance and on-site presence is required rendering the technology suitable for autonomous operation in remote locations especially at sites where no grid connection exists. Compared to intermittent energy supply from solar panels and conventional wind turbines this system operates continuously day and night all year round albeit with fluctuating outputs. Owing to diurnal and seasonal air temperature fluctuations on surface energy outputs vary between maxima in cold winter nights and minima at hot summer days. In addition, in partially flooded mines the technology may also be used to extract water through condensing moisture contained in the warm escaping air. This (essentially distilled) water could either be used directly on site (e.g. in remote arid environments) or be provided to local users. The disadvantage of comparatively small energy yields per turbine (kW-scale) could, to some extent, be overcome by installing several turbines at different shafts.

As the technology is based on temperature differences mines with steep geothermal gradients and constantly low

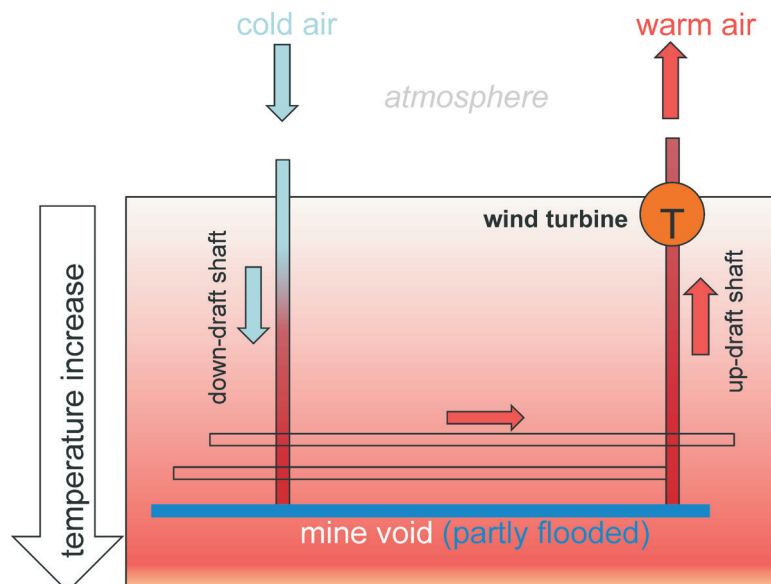


Fig. 1. Schematic sketch of using geothermal drafts from closed mines for wind energy generation

surface air temperature (as found e.g. in mountains or higher latitudes) are suited best. The technology may complement mine-water heat recovery systems provided that flooding the mine void did not unduly reduce temperature differences. Owing to the continuous production of energy and water the system is particularly attractive for remote mines (e.g. in mountainous areas) where little technical infrastructure exists.

Geothermal heat from mine water

Due to the low efficiency of converting heat into electricity, warm mine water is preferably used for directly heating buildings or for cooling if used as energy source for heat pumps. To this end heat exchangers are commonly employed to avoid scaling of warm water distribution pipes and allow for subsequent treatment of the mine water where required. Ramos et al. (2015) list 18 abandoned mines worldwide where geothermal heat is recovered from mine water.

This includes a former colliery in Springhill, Nova Scotia (Canada) as one of the first mines worldwide where the concept has been successfully applied since 1987. It utilises 18 °C-warm water from a 1350-m-deep mine as source for heat pumps at a relatively flat geothermal gradient of just 1.5 °C/ 100 m. Being overwhelmingly used for cooling during summer more heat is returned to the mine void than extracted for heating in winter. The system has significantly lower operating costs than a comparable oil-based equivalent and paid back investment in under one year. In designing the system care was taken that water cooled down on surface to 3 °C is not returned directly to the point of underground extraction in order to avoid an incremental drop of water intake temperature (Jessop 1995). Despite the comparably low geothermal potential of the mine the system remained financially viable over the last 30 years suggesting applications even at sites with sub-optimal conditions. A recently developed screening tool for assessing viability of geothermal system in abandoned mines may assist in this regard (Ramos et al. 2015). For Germany several sites have been investigated (Röder 2015, Penczek 2018).

In order to capitalise on the great depths of South African gold mines approaching 4 km at places and associated rock temperatures of ca. 60°C it has been proposed to drill boreholes of another 4 km depth from the bottom of the mine to tap into underlying rock temperatures of ca. 120 °C by circulating injected mine water through rock fractures (Ntholi 2018).

Advantages of geothermal heat recovery from mine water include the permanent availability of heat energy for heating as well as cooling utilising the large specific thermal capacity of water. Disadvantages include the formation of calcite and iron-hydroxide scales in pipe systems triggered by temperature changes which frequently are also radioactive due to the presence of natural radioisotopes such as uranium, radium and thorium in mine waters. Technologies to effectively prevent radioactive scaling in geothermal systems are developed by Friedrich et al. (2016).

STORING (RENEWABLE) ENERGY

Core concept

Apart from using exhausted mines for generating energy this section explores they could also be used to store energy, especially renewable energy from intermittent sources such as sun and wind. In this regard mines provide two major assets: large cavities in which energy-storage media such as water, compressed air or chemicals can be stored, and depth that allows to transform potential energy into kinetic energy

and visa versa and creates high water pressure. The below discussed technologies exemplify how these properties of mines may be used, either individually or in combination, to store surplus electrical energy and release it back into the grid when needed.

Pumped hydro energy storage

Pumping water against gravity from a lower to a higher reservoir using surplus electricity and releasing it again via turbines in times of need is the base of the over 100 years-old pumped hydro energy storage (PHES) technology. Employed in thousands of hydro power plants worldwide PHES is currently the only technology able to store electrical energy at MW-scale. Based on deriving revenue by using off-peak electricity for pumping (e.g. at night) and selling more expensive electricity generated during peak demand (e.g. during daytime) PHES can operate economically as long as associated energy conversion losses of about 20 % can be recovered by the day-night price spread.

Using off-peak electricity to compress air and let it expand again later the same principle can be used in so-called compressed air storage (CAS) systems. PHES and CAS may be used in surface and underground mines providing much needed storage capacity for intermittently produced renewable solar and wind energy.

In addition, a similar concept based on water pressure may be used to store energy even in underground mines already flooded.

PHES in open pit mines

The worldwide first example of an abandoned mine being successfully converted into a renewable energy hub is the Kidston Goldmine in Queensland (Australia), where two adjacent open pits with different base levels were connected by an underground tunnel housing a pump and two turbines in order to serve as a PHES in which solar energy from an adjacent PV park is stored during night time. The mine now continuously produces 50 MW of solar energy fed into the grid at rates carefully designed to not exceed demand as temporary oversupply could cause prices drop. Following a major weather-related black out of the power grid the project enjoyed political support that helped funding the project in the region a few years earlier. The remoteness of the site is offset by exceptional high yields of solar energy in this part of Australia and the fact that by using existing open pits constructions costs for the PHES were reduced by 60% compared to conventional plants. While similar conditions may be found elsewhere it was the politically motivated financial support by Australia's Clean Energy Finance Corporation that secured the project (Bloomberg 2019, Kidston 2018).

The application of the concept to large lignite open pits was also proposed where low topographic elevation differences are offset by extremely large water volumes. Using only a tenth of the 4.5 bn m³ of water stored in the 68 open-pit lakes in the Lausatia region and around Halle/ Leipzig some 78 GW could be stored assuming a hydraulic head of just 80 m (Schulz 2009). A recent study confirmed the technical feasibility of converting lignite pits into PHES for the Hambach-Garzweiler-Inden region in western Germany, too (Thema and Thema 2019).

Underground mines

As conventional PHES require topographic elevation differences mostly found in (scenic) mountainous areas suitable sites for new plants are rare and often trigger public resistance despite the generally accepted need for storing renewable energy. By converting mines into underground

pumped hydro energy storage (UPHES) plants this problem is averted. The deeper the mine and the larger the circulated water volume, the higher the energy storage capacity easily approaching hundreds to thousands of MW. Various designs have been proposed ranging from closed loop systems circulating a fixed volume of water to open ones integrating continuously generated ingress water. While all UPHES locate the lower reservoir underground either utilising existing tunnels or proposing new excavations, some place the upper reservoir on surface while others use existing underground tunnels at lower depth for that purpose. As underground excavation costs account for the majority of capital expenditure such design differences have significant cost implications. While feasibility studies in German hard coal mines propose to freshly excavate a ring-type of lower reservoir underground resulting in significant costs, studies on South African gold mines propose to utilise the vast underground mine void stretching from surface to several thousands of meters underground (Niemann et al. 2015; Niemann 2018; Zeller 2018; Winde et al. 2017). For specific conditions of deep level gold mines operating below water-rich karst aquifers in South Africa Winde et al. (2016) proposed an open system which integrates the overlying karst aquifer as feed water reservoir providing between 70 to 100 Ml/d of clean ingress water. In addition to exceptional high energy yields of several hundred MW resulting from the large hydraulic head in ultra-deep mines, the interception of ingressing water before flowing through the mine void also prevents water pollution and the need to treat it. Using the concrete example of Driefontein Winde (2018) calculated a total revenue from selling peak electricity and clean water of over R 1.1 bn per annum, with the sale of clean water accounting for some 20% (Fig. 2).

The major advantage of deep-level South African gold mines over German mines in the Ruhr area or the Harz mountains is, however, not so much the greater depth but rather the pronounced peak vs. off-peak price differences varying from 150 % (summer) to 600 % (winter). Owing to the increased input of solar energy during daytime following a change of energy policy in Germany, the formerly utilised day-night differences are now much reduced or have disappeared altogether. At the same time erratic peaks of solar and wind energy that exceed demand increasingly

cause significant costs by grid owners having to sell surplus energy at 'negative prices', i.e. paying neighbouring countries for accepting the expensively generated energy. In 2018, the resulting loss was estimated at approximately € 1bn, i.e. over 4 times the total pumping costs in the Ruhr area further pushing the local price for electricity in Germany which already is the highest in Europe (Bellinger 2018). Since UPHES would be able to easily accept such electricity peaks this may constitute a viable business model. In view of globally rising shares of poorly predictable solar and wind energy market mechanism may soon be developed to pay PHES and UPHES not only for energy generated but also for providing services ensuring grid stability such as energy storage, buffering erratic peaks, providing regulating power, frequency stabilisation as well as black start capacity to name but a few.

Suspended weight gravity energy storage (SWGES)

This technology is based on the same principle as pumped hydro storage except for the fact that it uses a solid weight (e.g. a block of concrete) which is lifted against gravity instead of water. The solid weight is suspended on a rope inside a vertical shaft. During off peak time or excess generation of energy an electrical motor winds up the weight to the surface where it remains suspended until energy is required again. Releasing the weight down into the shaft again turns the motor into the opposite direction. Now acting as a dynamo, the motor feeds electrical energy back into the grid at peak tariffs that are significantly higher than the ones paid for pulling the weight up. According to Menendez et al. (2020) a weight of 3 kt lifted by 600 m could generate 3.81 MWh per cycle with typical cycle times varying between 0.25 to 2 hours. This compares to nearly twenty times the energy output (718 MWh) of a UPHES for 4-16 hours per cycle (i.e. up to 8 x times longer) which utilises the same depth and 0.5 Mm³ of water (i.e. 500 kt). Like UPHES, SWGES would require non-flooded underground mines and open shafts still being intact. While in terms of storage capacity and duration for which peak energy could be provided SWGES is limited compared to competing technologies like UPHES it may be an option in settings where water is not available and peak load periods are short.

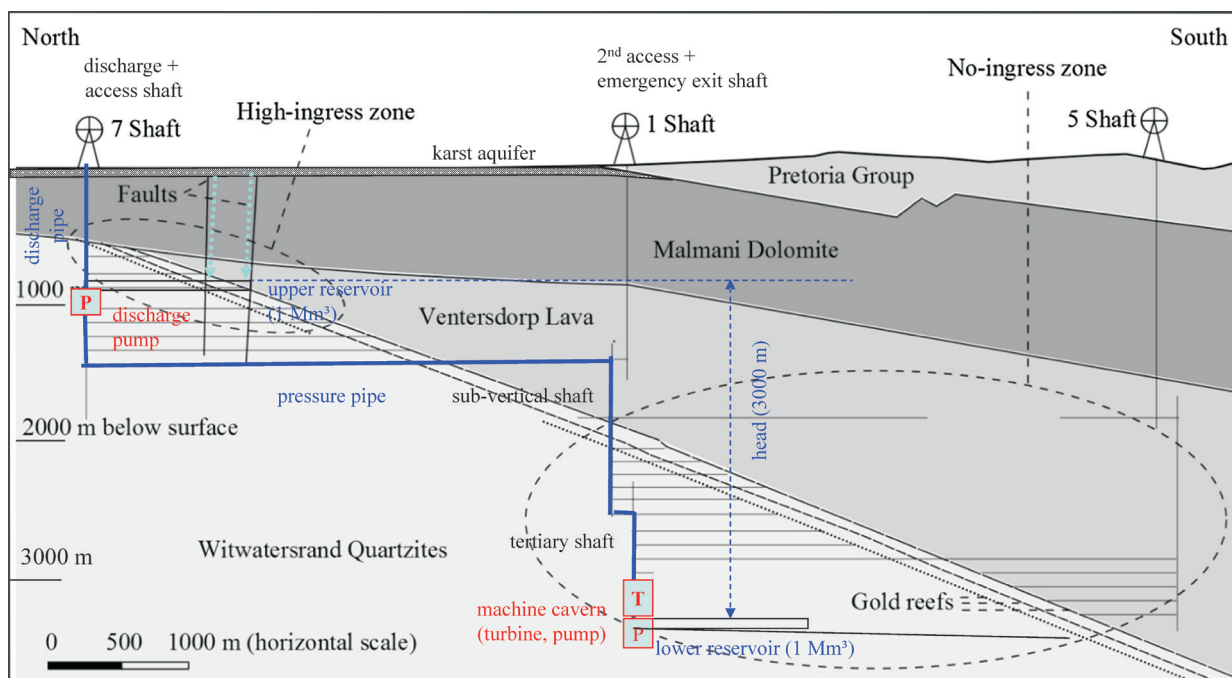


Fig. 2. Proposed UPHES at a deep level gold mine in the dolomitic karst area of the Far West Rand

Water pressure-based energy storage

In order to also utilise underground mine voids already flooded which for other uses would have to be emptied again at significant costs, a new technology is proposed jointly developed by the construction company Hochtief and the Fraunhofer Institute for Energy Economy and Technology (IEE) in Kassel (Germany). In this technology interconnected hollow concrete spheres are lowered into the water and allowed to fill with water via a remotely controlled valve. Pumping out this water with surplus wind energy creates a vacuum inside the concrete balls. During peak time the valve is opened again, and the water allowed to flow back into the balls driving a turbine (which also acts as pump) that generates electricity transmitted via cable to surface (<https://www.ingenieur.de/technik/fachbereiche/energie/betonkugeln-im-bodensee-windstrom-speichern/>, accessed 15 May 2019). In November 2016, a pilot-facility was successfully tested at the Bodensee (Germany). A similar technology substituting the rigid concrete balls by flexible balloons is currently investigated at the MIT in Cambridge, USA. Using the pressure of water surrounding submerged objects water depth impacts on the efficiency of the system. While not specifically designed for mining remediation we believe the technology may hold some promise to be applied in this context especially at flooded mines for which little alternative use exists.

Compressed air-based energy storage (non-flooded underground mines)

CAES is similar to the water-pressure based technology except that it stores electrical energy not in a vacuum but in compressed air. Using underground mine voids for storing pressured air requires airtight structures most commonly found in salt mines (Kaiser et al. 2017). Where flooding of salt mines is not a feasible option (e.g. for protecting groundwater resources from salination) this concept could be considered. For Germany, which produces much of its wind energy at the northern shores salt mines in the nearby lowland of north Germany would constitute an alternative to pumped hydro storage which is mostly confined to far-away mountains in the south that are poorly grid-connected to producers in the north.

Existing pilot projects in Germany (Huntorf) and the USA (McIntosh) are successfully operated for years but are still well below the 100 MW-scale. As compressing air produces heat different systems exist to manage and reduce the increase in temperature (adiabatic vs. isothermal CAES respectively) and the associated energy loss. For offshore applications the use of flexible balloons to store compressed air was also considered which could also be applied to flooded mines. Despite tests on various mines in Japan (hard rock and coal mines) no application in former mines exists to date (Kaiser et al. 2018).

Electrolytic energy storage (EES)

In contrast to the above discussed technologies EES does not primarily use the depth of mine but its underground void space. Energy is stored based on the rechargeable (redox-flow) battery principle. During off-peak times cheap electricity drives electrons from a catholyte solution (positively charged) to an anolyte solution (negatively charged) via an ion-selective membrane separating both solutions. Once charged, the electrolytes are pumped into two separate underground storage caverns of say 100,000 m³ each, where they can be kept for several months. The stored energy is released again by pumping both solutions back to the membrane where electrons spontaneously migrate in reverse direction generating

electricity in the process. A disadvantage of the system is the high toxicity of electrolytes which includes toxic heavy metals (e.g. vanadium) and sulphuric acid, for example. However, recently seawater and recyclable polymers have been identified as suitable non-toxic substitutes (Janoschka et al. 2015). A pilot plant in Jemgum (Germany) using underground salt deposits, since 2017, generates 120 MW. However, to date the concept was not yet applied to closed mines. Watertight, non-flooded underground voids would be potential candidates for future applications.

GENERATING RENEWABLE ENERGY

Core concept

In addition to storing renewable energy generated elsewhere remediated mines may also generate their own renewable energy utilising the abundantly available brownfield areas with long-term use restrictions. Opportunities range from installation of solar panels, wind turbines and solar updraft towers as well as using tailings deposits for growing biofuel.

Photovoltaic (solar panels)

While installation of photovoltaic solar panels on remediated mine dumps and other former brownfield sites is already frequently practiced in Germany (e.g. at former uranium mines in Saxony and East Thuringia Wismut and copper mines in the Mansfeld region of Saxony-Anhalt) it is increasingly also applied to un-remediated sites in order to save costs for decontamination. Arguing that former dumps and land fill sites will not be turned into revenue-generating assets even after costly remediation specialised US-companies now actively seek out cheap contaminated areas where renewable energy is popular but free land scarce. Sites include coal-ash ponds in SW Virginia (USA), mines in eastern Kentucky, landfills in New England and even parts of the nuclear zone at Chernobyl (Ukraine). BHP Group, as the world's largest mining company, plans to install solar panels and energy storage facilities at mine legacy sites in Arizona and New Mexico (USA). The Drayton coal mine in Australia is also planned to be converted into a 25-MW-solar farm (Bloomberg 2019). In China 87 ha of open water surfaces of a flooded coal mine were covered with floating solar panels generating 40 MW (Zhu 2018).

Plans to install solar panels on large flat-topped gold tailings deposits in South Africa comprising hundreds of square kilometres were abandoned despite relatively high solar yields (double as high as in Germany) because of windblown tailings dust potentially scratching and dimming panel surfaces.

Wind turbines, SUT and biofuel

Wind turbines.

Since wind speed exponentially increases with height above ground the placement of turbines on up to 80-m-high tailings deposits in SA goldfields would increase energy output at no additional cost. Given the generally flat topography of the South African interior plateau (Highveld) protruding structures such as tailings dams would elevate wind turbines well above surrounding land and increase energy yields. Generated energy could directly be stored on site using pumped hydro storage provided, of course, that the geotechnical stability of the high-rise turbine structure could be assured in the grainy substrate.

Solar updraft towers (SUT):

Alternatively, large flat tailings areas could also be covered by transparent material (e.g. polyester foil, glass etc.) channelling the heated air below towards a tall chimney

in the centre were convection drives a wind turbine that generates electricity. A pilot model of such SUT operated successfully for 7 years in Manzanares (south of Madrid, Spain) with 46 ha of land feeding a 195-m-high chimney of 10 m in diameter generating 50 kW. In 2010, a SUT was built in Jinshawan (Inner Mongolia, China) for USD 208 million producing 200 kW using a 50-m-high tower and a glass-covered feeding area of 277 ha (https://en.wikipedia.org/wiki/Solar_updraft_tower). A major reason for locating the plant there was to improve local air quality through covering large areas of loose sand with glass in order to reduce wind-blown dust pollution. As large and unvegetated tailings deposits in South Africa are also a major dust source affecting densely populated mining areas SUT would be a possible technology for reducing air pollution and save precious and scarce water resources currently used for dust suppression by simply wetting the tailings surface. With footprint areas of several hundreds to thousands of hectares tailings dams would be sufficiently large to deliver meaningful energy yields given the high insolation typically found in the South African goldfields. By shielding tailings from infiltrating rainwater SUT would also dry up outflow of contaminated tailings seepage as one of the most problematic sources of water pollution in the Witwatersrand basin. Given the tight financial situation of the few remaining gold mines, however, the relatively large capital expenditure required for SUT is likely to present an obstacle for rapid implementation.

Biofuel

Turning vast areas of toxic mine waste into productive use by growing biofuel on top of tailings dams could transform tailings from environmental liabilities requiring

costly maintenance into economic assets that provide local communities with opportunities for sustainable post-closure development. By utilising several hundreds of square kilometres of barren tailings surface, biofuel would no longer compete for land with food production that recently caused global increases in food prices.

Successful test trials of improving soil properties of tailings material to create lasting vegetation covers suggest that certain biofuel plants can indeed be grown in augmented tailings substrate. Through developing non-toxic top soil layers also dust pollution could be reduced at no additional costs. Preferably, plants not requiring extensive irrigation should be employed in order to not inadvertently accelerate seepage-related water pollution.

CONCLUSIONS

Currently driving about 45 % of the global economy mining is, and probably will remain, a crucially important activity that not only creates jobs and revenue but also provides mineral resources needed for sustaining a growing and increasingly resource-hungry human population (Cloete 2019). Given such degree of economic importance, now and in future, it is imperative to make mining ecologically sustainable. While associated impacts on men and environment are generally deemed acceptable as long as benefits are derived, this changes once mines close. No longer providing employment or revenue many closed mines turn into costly legacy sites with associated costs burdened onto taxpayers and future generations. This paper explores a range of innovative technologies aimed at reducing associated costs by turning closed mines from

Table 1. Potential technologies for extracting, generating and storing renewable energy at closed mines

Energy type	Technology	Used media	Suitable mines	Existing applications
Hydro-chemical	PRO	saline mine water	flooded underground voids, salt mines	1 x non-mining pilot project (Norway)
E-generation	RED	saline mine water	flooded underground voids, salt mines	1 x non-mining pilot project (Netherland)
Geothermal heat extraction	heat pump	warm mine water	flooded underground voids	18 x mines (worldwide)
	(vertical) wind turbines	convective mine air/ upward drafts	non-flooded/ partially flooded voids	none
RE-generation	PV SUT conventional wind turbines PHES UPHES SWGES CAES Vacuum EES	solar radiation	on surface, brownfields	several (USA, Germany, Australia, China)
		solar radiation	tailings dams	2 x non-mining pilot projects (Spain, China)
		atmospheric wind	tailings dams	none
		solar radiation, biomass surface water	tailings dams	various test sites
		ingress water	on surface, open pits	1 x gold mine (Queensland, Australia)
		solid weights	non-flooded underground voids	studies in Germany, Finland, South Africa and other countries
		compressed air	underground salt mine caverns	unknown
		mine water	flooded underground voids	2 x non-mining pilot plants (Germany, USA)
		electrolytic solutions	non-flooded underground voids	1 x non-mining pilot test (Bodensee, Germany)
				1 x pilot plant (Jemgum, Germany)

environmental liabilities into economic assets focussing on the extraction, generation and storage of renewable energy. Table 1 provides an overview on technologies discussed.

In some instances, the above technologies can be synergistically combined e.g. by storing renewable energy generated on site in underground mine voids. Combining pumped hydro storage with heat pumps that cool in summer and heat in winter is currently investigated in Switzerland (Gigler 2018). The recovery of geothermal heat from mine water may be complemented by using upward air drafts of mine from the underground void to continuously generate wind energy while covering tailings with solar updraft towers would simultaneously create energy and minimise water and air pollution. In some instances, it may be better to combine several technologies at smaller scale instead of aiming for a single large capital-intensive project that struggles to attract investors. Such incremental steps towards alleviating the financial burden are not confined to energy-related technologies discussed here, but could also include complementary activities like:

- commercially viable extraction of resources from mine water including commodities of economic criticality like rare earth elements, precious metals or salts used in fertilizer (Friedrich 2018; Hoth et al. 2015, Elwert 2018; Zhu 2018)
- using energy from mines for energy-intensive technologies such as data mining, crypto currency generation and tamper-proof certification of critical commodities such as gold, phosphorous, cobalt and diamonds creating a competitive advantage in the promising field of digital technologies (Friedrich et al. 2018)
- food production through horticulture (heating greenhouses with mine water) or aquaculture (suitable water quality provided)
- utilising deep-level mines for scientific research like underground detectors for neutrino beams from CERN as proposed for a Finnish mine or for atmospheric cloud formation processes as suggested for ultra-deep gold mines in South Africa in the 1980s.
- use of ultra-deep mines as safe repository for hazardous material
- establishing revenue-generating land uses such as tourism as successfully implemented in 61 so-called 'mine parks' in China that feature entertainment facilities (Zhu 2018) or water-linked recreation in artificial lakes of flooded open pits in former lignite mining areas of SE-Germany
- reopening closed mines for extracting unmined

commodities following increases in market prices (Goedecke 2015) etc.

In order to make post-closure solutions sustainable close and trust-based consultation with local communities is essential. Where public acceptance of designed after-uses is low or of little benefit to surrounding communities, solutions are unlikely to last. That means socio-economic conditions of host communities must be considered when designing post-closure concepts. E.g., while high-tech solutions, entertainment and recreation may work well in affluent societies, job-intensive agriculture and food production may be more appropriate in resource-restricted settings of developing countries.

Also, solutions for mines in areas with well-developed infrastructure, many potential energy users and a qualified workforce nearby will differ from mines in remote areas with no water or electricity, quite independent from the general economic status of the host country.

In almost all cases, however, political support is required as closing mines generally suffer from shortage of funds and an unwillingness to invest despite the introduction of compulsory remediation funds some years ago.

Furthermore, in deciding on larger capital-intensive projects such as UPHES a macro-economic view often is more appropriate than applying a micro-economic business case approach. E.g., while a UPHES may not be able to generate operational profit on its own it may still be economically viable on national level through saving public funds otherwise spent on perpetually treating polluted water flowing from that mine. Other aspects of national relevance not captured in microeconomic views include strategic water security, stability of the national energy grid, long-term transition of the energy system etc.

Another major obstacle in implementing innovative solutions, especially in government-controlled remediation projects, is the lack of incentives for officials to take risks. While potential failures may be career-threatening there are no mechanisms to reward bold decisions that help saving public funds. In many instances such savings are not even captured by expenditure-focussed accounting systems, leave alone being credited to the responsible official. This often also applies to larger mining companies which tend to be risk and innovation averse. Creating climates that encourage innovative solutions may thus well be the single most important step towards achieving truly sustainable long-term solutions. ■

REFERENCES

- Acatech [ed.] (2017). Rohstoffe für die Energiewende. Wege zu einer sicheren and nachhaltigen Versorgung. Stellungnahme, Berlin (in German).
- Ahmed N. (2018). We don't mine enough rare earth metals to replace fossil fuels with renewable energy. [online] Available at: www.vice.com/en_us/article/a3mavb/we-dont-mine-enough-rare-earth-metals-to-replace-fossil-fuels-with-renewable-energy [Accessed 12 December 2018].
- Bellinger I. (2018). National Geographic Germany: Neue Energien, December 2018, 127-132.
- Bloomberg (2019). 'Land no one else wants' gets solar as coal-and-nukes era fades [online]. Available at: www.miningweekly.com/article/land-no-one-else-wants-gets-solar-as-coal-and-nukes-era-fades-2019-04-25 [Accessed 25 April 2019].
- Cloete K. (2019). Plea for collaboration. Mining Weekly, 22-28 February, 16, quoting M Cutifani, CEO of Anglo American at the Mining Indaba in Cape Town, South Africa.
- Dombrowski B. (2018). Remediating mining legacy site: Case study hard coal mining in the Ruhr area. In: Academy of Science of South Africa [ed.] (2018). Proceedings of the Science Business Society Dialogue conference, Linking science, society, business and policy for the sustainable use of abandoned mines in the SDAC region, 28-30 November 2017, Johannesburg, South Africa, 22-23.
- DuBois JR. (2014). United States Patent No. US 8.677.752 B2, power generation system.
- DuBois JR. (2018). Generating Renewable Energy and Recovering Water from Underground Mines. Hand-out brochure, unpublished, 5.
- Eberfalvi J., Nemeth G., Varhegyi A. (2015). Challenges of the after-care activities on the uranium mining and ore processing legacy sites in Hungary. In: Wismut GmbH [eds.]: Reclaimed mining sites between post-remedial care and reuse. Proceedings of the International Mining Symposium WISSYM 2015, Bad Schlema, 31 August – 3 September 2015, 361-370.

- Elwert T. (2018). Recovery and reprocessing of mine tailings: experiences from Germany. In: Academy of Science of South Africa [ed.] (2018). Proceedings of the Science Business Society Dialogue conference, Linking science, society, business and policy for the sustainable use of abandoned mines in the SDAC region, 28-30 November 2017, Johannesburg, South Africa, 38-39.
- FPTM (Future Power Technology Magazine). (2019). Statkraft Osmotic Power Plant, the First Osmotic Power Or Salinity Gradient Power Generation Plant. [online] Available at: www.power-technology.com/projects/statkraft-osmotic/ [Accessed 26 August 2019].
- Friedrich et al. (2016). Elektrochemische Abtrennung tailingsrelevanter Schwermetallkationen und geogener Radionuklide aus geothermalen Tiefenwässern. In: Proceedings Geothermie Kongress, Essen 2016. [online] Available at: www.geothermie.de/bibliothek/konferenzdatenbank [Accessed 20 May 2020].
- Friedrich H-J. (2018). Resource extraction from mine water. In: Academy of Science of South Africa [ed.] (2018). Proceedings of the Science Business Society Dialogue conference, Linking science, society, business and policy for the sustainable use of abandoned mines in the SDAC region, 28-30 November 2017, Johannesburg, South Africa, 40-41.
- Friedrich H-J., Viehweger K., Winde F. (2018). Innovative Optionen zur Energiegewinnung aus Grubenwasser und gefluteten Grubengebäuden. Projektantrag zum Themenbereich: Inwertsetzung energetischer Nutzungspotenziale von Grubenwasser. Forum Bergbau und Wasser, Deutsches Stiftungszentrum GmbH. Dez. 2018, unveröffentlicht, 31 Seiten. (in German).
- Ghenai C., Janajreh I. (2013). Comparison of resource intensities and operational parameters of renewable, fossil fuel, and nuclear power systems. *Int J of Thermal & Environmental Engineering*, 5(2). [online] Available at: www.researchgate.net/publication/275965432_Comparison_of_Resource_Intensities_and_Operational_Parameters_of_Renewable_Fossil_Fuel_and_Nuclear_Power_Systems, 95-104, DOI: 10.5383/ijtee.05.02.001 [Accessed 20 May 2020].
- Gigler B. (2018). Die Zukunft der Energieversorgung: Kombinierte Energiespeicher als Schlüsseltechnologie. [online] Available at: www.idw-online.de/de/news704503 [Accessed 23 October 2018].
- Goedecke M. (2015). Wismut-Erbe und sächsische Rohstoffstrategie – eine noch nicht abgeschlossene Erfolgsgeschichte. In: Wismut GmbH [eds.]: Reclaimed mining sites between post-remedial care and reuse. Proceedings of the International Mining Symposium WISSYM 2015, Bad Schlema, 31 August – 3 September 2015, 237-250. (in German).
- Helioscsp (2010). China's first solar tower plant starts operating in desert. Solar Thermal Energy News. [online] Available at: www.helioscsp.com/chinas-first-solar-tower-plant-starts-operating-in-desert/, updated 28 Dec. 2010 [Accessed 26 Aug. 2019].
- Hoth N., Wendler C., Kassahun A., Ussath M., Drebenstedt C. (2015). Rückgewinnung wirtschaftstragischer Elemente aus Bergbauwässern – Randbedingungen und Herausforderungen. In: Wismut GmbH [eds.]: Reclaimed mining sites between post-remedial care and reuse. Proceedings of the International Mining Symposium WISSYM 2015, Bad Schlema, 31 August – 3 September 2015, 227-236. (in German).
- Janoschka T., Martin N., Martin U., Friebe C., Morgenstern S., Hiller H., Hager M.D., Schubert U.S. (2015). An aqueous, polymer-based redox-flow battery using non-corrosive, safe, and low-cost materials. *Nature*, 527, 78-94, DOI: 10.1038/nature15746.
- Jessop A. (1995). Geothermal energy from old mines at Springhill, Nova Scotia, Canada. IGA [online]. Available at: www.geothermal-energy.org/pdf/IGAstandard/WGC/1995/1-jessop2.pdf 463-468. [Accessed 20 May 2020].
- Kaiser F., Winde F., Erasmus E. (2018). Storing energy in disused mines: comparing pumped water and compressed air-based technologies. *International Journal of Mining and Mineral Engineering*, 9(3), 177-195, DOI: 10.1504/IJMMME.2018.096096.
- Kidston S. (2018). Implementing pumped hydro energy storage at an open pit mines: a pilot project from Australia. In: Academy of Science of South Africa: Linking science, society, business and policy for the sustainable use of abandoned mines in the SADC region. Proceedings of the science business society dialogue conference, 28-30 November 2017, Indaba Hotel, Johannesburg, Gauteng, South Africa, 28-30, DOI: 10.17159/assaf.2018/0025.
- LfU (Landesamt für Umwelt). (2018). Niedrigwassersituation 2018. Arbeitsgruppe: Bergbaubedingte Stoffeinträge in die Spree und Spree Zuflüsse; Ministerium Ländliche Entwicklung, Umwelt und Landwirtschaft, Land Brandenburg; PowerPoint presentation, 10 slides. [online] Available at: www.braunespreewatch.de/images/studien/20181120_Anlage%2010.pdf [Accessed 20 November 2018] (in German).
- Niemann A. (2018). UPHEs feasibility: Case study from German hard coal mines. In: Academy of Science of South Africa [ed.] (2018). Proceedings of the Science Business Society Dialogue conference, Linking science, society, business and policy for the sustainable use of abandoned mines in the SDAC region, 28-30 November 2017, Johannesburg, South Africa, 31-32.
- Niemann A., Hager S., Lux J-P. (2015). Perspektiven der Bergbaufolgenutzung zur Energiespeicherung – Pumpspeicherwerke unter Tage im Ruhrrevier. In: Wismut GmbH [eds.]: Reclaimed mining sites between post-remedial care and reuse. Proceedings of the International Mining Symposium WISSYM 2015, Bad Schlema, 31 August – 3 September 2015, 199-206.
- Ntholi T. (2018). Geothermal energy as a power source for PUMPS, a geo-engineering system designed for in-situ remediation of acid mine water in abandoned Witwatersrand gold mines. In: Academy of Science of South Africa [ed.]: Proceedings of the Science Business Dialogue Conference «Linking Science, Society, Business and Policy for the Sustainable Use of Abandoned Mines in the SADC Region», 28-30 November 2017, Indaba Hotel, Johannesburg, Gauteng, South Africa, 38, DOI: 10.17159/assaf.2018/0025.
- Paul M., Meyer J., Jenk U., Kassahun A., Baacke D., Forbrig N., Metschies T. (2015). Kernaspekte des langfristigen Wassermanagements an den sächsisch-thüringischen Wismut-Standorten. In: Wismut GmbH [eds.]: Reclaimed mining sites between post-remedial care and reuse. Proceedings of the International Mining Symposium WISSYM 2015, Bad Schlema, 31 August – 3 September 2015, 71-86. (in German).
- Penczek N. (2018). Harvesting geothermal heat from mine water: a pilot project from Germany. In: Academy of Science of South Africa [ed.] (2018). Proceedings of the Science Business Society Dialogue conference, Linking science, society, business and policy for the sustainable use of abandoned mines in the SDAC region, 28-30 November 2017, Johannesburg, South Africa, 33-34.
- RAG (2019). [online] Available at: www.rag.de/ewigkeitsaufgaben/wasserhaltung/ [Accessed 10 May 2019].
- Ramos E.P., Breede K., Falcone G. (2015). Geothermal heat recovery from abandoned mines: as systematic review of projects implemented worldwide and a methodology for screening new projects. *Environ Earth Sci*, DOI: 10.1007/s12665-015-4285-y.
- Röder U. (2015). Geothermische Nutzung von Flutungswässern des Zwickauer Steinkohlereviere. In: Wismut GmbH [eds.]: Reclaimed mining sites between post-remedial care and reuse. Proceedings of the International Mining Symposium WISSYM 2015, Bad Schlema, 31 August – 3 September 2015, 207-214. (in German).
- Schulz D. (2009). Speicherpotenziale von Pumpspeicherwerken in Tagebaurestlöchern ehemaliger Braunkohlereviere. Forum Netzintegration, Deutsche Umwelthilfe Berlin, 30 September, 29. (in German).
- Siebers R. (2012). RED Pilot on the Afsluitdijk, The Netherlands. INES, Singapore. [online] Available at: www.deafsluitdijk.nl/wp-content/uploads/2014/06/2012-10-30-Presentatie-door-Rik-Siebers-over-Blue-Energy.pdf [Accessed 19 October 2012].
- Thema J., Thema M. (2019). Pumpspeicherkraftwerke in stillgelegten Tagebauen am Beispiel Hambach-Garzweiler-Inden. Wuppertal Paper 194, Januar 2019, Wuppertal Institut. [online] Available at: www.epub.wupperinst.org/frontdoor/deliver/index/docId/7211/file/WP194.pdf, 21 [Accessed 20 May 2020].

Winde F. (2018). UPHES pre-feasibility: case study South Africa. In: Academy of Science of South Africa: Linking science, society, business and policy for the sustainable use of abandoned mines in the SADC region. Proceedings of the Science business society dialogue conference, 28-30 November 2017, Indaba Hotel, Johannesburg, Gauteng, South Africa, 27-28, DOI: 10.17159/assaf.2018/0025.

Winde F., Kaiser F., Erasmus E. (2017). Exploring the use of deep level gold mines in South Africa for underground pumped hydroelectric energy storage schemes. *Renewable and Sustainable Energy Reviews*, 78, 668-682, DOI: 10.1016/j.rser.2017.04.116.

Winde F., Stoch E.J. (2010). Threats and opportunities for post-closure development in dolomitic gold mining areas of the West Rand and Far West Rand (South Africa) – a hydraulic view. Part I: Mining legacy and future threats. *Water SA*, 36(1), 69-74.

Zeller E. (2018). UPHES feasibility: case study Finland. In: Academy of Science of South Africa: Linking science, society, business and policy for the sustainable use of abandoned mines in the SADC region. Proceedings of the science business society dialogue conference, 28-30 November 2017, Indaba Hotel, Johannesburg, Gauteng, South Africa, 30, DOI: 10.17159/assaf.2018/0025.

Zhu Q. (2018). Remediating mining legacy sites: case study China. In: Academy of Science of South Africa [ed.] (2018). Proceedings of the Science Business Society Dialogue conference, Linking science, society, business and policy for the sustainable use of abandoned mines in the SDAC region, 28-30 November 2017, Johannesburg, South Africa, 21.

IMPACT OF CHANNEL INCISION ON FLOODS: A CASE STUDY IN THE SOUTH-EASTERN SUBCARPATHIANS (ROMANIA)

Gabriela Ioana-Toroimac^{1*}, Liliana Zaharia¹, Gianina Neculau², Gabriel Minea²

¹University of Bucharest, Faculty of Geography, 1 Nicolae Bălcescu, 010041, Bucharest, Romania

²National Institute of Hydrology and Water Management, 97E Șos. București-Ploiești, 013686, Bucharest, Romania

*Corresponding author: gabriela.toroimac@geo.unibuc.ro

Received: 31st December 2019 / Accepted: May 10th, 2020 / Published: July 1st, 2020

<https://DOI-10.24057/2071-9388-2019-177>

ABSTRACT. Despite numerous researches on river channel incision, there are fewer studies on the impact of channel adjustments on floods. This paper aims to investigate channel adjustments and to analyse their impact on the frequency of floods by estimating the return period of the bankfull discharge of the Prahova River in the South-Eastern Subcarpathians (Romania). The study is based on the analysis of the maximum annual discharges and cross-section profiles of the Prahova River at Câmpina gauging station (1976–2015). To estimate the return period of the bankfull discharge, the log Pearson III distribution was used. Overall, the maximum depth and the cross-section area at the bankfull stage increased during the analysed period, indicating channel incision and lateral stability. The bankfull discharge of 1976 could be reached every year and the one of 2015 could occur almost every 5 years. Therefore, due to channel incision and increased channel capacity, overflowing the bankfull stage is a less frequent hazard on the Prahova River at Câmpina gauging station. River management appears to maintain this situation as no measure is taken to decrease channel incision.

KEY WORDS: channel incision, cross-section profiles, bankfull discharge, return period, floods, river management

CITATION: Gabriela Ioana-Toroimac, Liliana Zaharia, Gianina Neculau, Gabriel Minea (2020). Impact Of Channel Incision On Floods: A Case Study In The South-Eastern Subcarpathians (Romania). *Geography, Environment, Sustainability*, Vol.13, No 2, p. 17-24
<https://DOI-10.24057/2071-9388-2019-177>

ACKNOWLEDGEMENTS: We thank the Romanian National Institute of Hydrology and Water Management for providing data used in this study. We thank the two anonymous reviewers for taking the time to make recommendations, which improved the overall quality of the manuscript.

Conflict of interests: The authors reported no potential conflict of interest.

INTRODUCTION

In the context of the European Union Water Framework Directive (EU-WFD), all water bodies affected by anthropogenic impact should be rehabilitated to a good status (European Commission 2000). One of the key reasons for failing a good ecological status are hydromorphological alterations (e.g., Haase et al. 2013; Richter et al. 2013; Karthe et al. 2018). Nowadays, channel incision is a common process in river channels as sediments are trapped by various human pressures (e.g., Landon et al. 1998; Hajdukiewicz et al. 2019) and all studies aimed at understanding the various effects of this process as scientific and practical interest. Previous studies showed that efforts are made to rehabilitate incised channels (e.g., Beechie et al. 2008; Stähly et al. 2019).

In the context of river basin management, the countries in Eastern Europe have recently made the transition from a legislation based on Soviet water governance to the EU-WFD (Krengel et al. 2018); and Romania, which joined the EU in 2007, is a good example for a country where the goal of a 'good ecological status' was recently introduced. Small scale studies conducted in the Carpathian Mountains reported river channel adjustments due to various natural and anthropic causes such as periods lacking high magnitude

floods, afforestation, river damming, flow control works, and channel dredging/mining (e.g., Korpach 2007; Ioana-Toroimac et al. 2010; Armaș et al. 2012; Chiriloaei et al. 2012; Wyżga et al. 2012; Wyżga et al. 2016a, 2016b; Ioana-Toroimac 2016; Wyżga et al. 2018; Hajdukiewicz et al. 2019). Previous studies in the South-Eastern Subcarpathians showed a decrease of the braiding activity intensity in the last century, shrinking of braided sectors until fluvial metamorphosis, a narrowing process, and an increase of woody riparian vegetation on the riverbanks of the now-abandoned active channel; conversely, in-stream vegetation was severely reduced as a result of changes in the dominant geomorphological processes, namely erosion is more intense than deposition (Ioana-Toroimac 2016). Only few studies investigated the river channel incision in the South-Eastern Subcarpathians (e.g., Armaș et al. 2012; Rădoane et al. 2013).

The impact of channel adjustments on floods was less studied. As example, the increase in flow capacity of the channel was reflected in considerable lowering of stages for low flood discharges and markedly smaller one for high-magnitude floods, with particularities depending on the river type, followed by increasing return period of the bankfull discharge (Armaș et al. 2012; Ioana-Toroimac et al. 2013; Wyżga et al. 2016b). Most of the rivers crossing the South-

Eastern Subcarpathians and the neighbouring areas have high return periods of the bankfull discharge (i.e., up to 8 years at gauging stations without engineering works according to Ioana-Toroimac et al. 2013).

The aim of this paper is to contribute at better understanding the impact of channel alteration on floods based on (i) the analysis of channel adjustments and (ii) the estimation of the return period of the bankfull discharge. The analysis was conducted on the Prahova River in the South-Eastern Subcarpathians (Romania), where the river channel is closely followed by the main national road and railway, of European importance, which cross the Carpathians and connects the capital (Bucharest) to the country's central and western regions, then continuing to Western Europe. In the studied sector, this transport infrastructure of major importance is highly vulnerable to the risk induced by the river channel dynamics and floods (Zaharia et al. 2017), therefore studies on the relationship between channel adjustments and flood features have practical interest, for the proper management of the river in order to mitigate the related risks.

STUDY AREA

The Prahova River is a second-order tributary of the Danube River, in Romania. It has its source in the Carpathians, then crosses the South-Eastern Subcarpathians, and reaches the Romanian Plain (Fig. 1a), having a total length of 193 km and a catchment area of 3754 km². In this paper we investigated the adjustment of the Prahova River channel in the subcarpathian sector, namely at Câmpina gauging station, located 55 km away from the source, controlling a

watershed with an area of 486 km², at 1124 m a.s.l. mean altitude (Aquaproiect 1992). Along the section of the gauging station, the Prahova can be classified as a high energy river on greywacke and marls, with a specific stream power of 665 W m⁻² at bankfull discharge in 2015 and the competence of moving a particle with approximately 160 mm in diameter (Ioana-Toroimac et al. 2017). At this gauging station, during the period 1976–2015, the river had a mean multiannual discharge of 7.55 m³ s⁻¹, with variations of the mean annual flow ranging between 2.64 m³ s⁻¹ (in 2012) and 14 m³ s⁻¹ (in 2005) (Fig. 1b). The maximum annual discharges ranged between 20.7 m³ s⁻¹ (in 2011) and 399 m³ s⁻¹ (in 2005) (Fig. 1c). The premise of all interpretations in this paper consists in the lack of trend in the variability of the mean and maximum annual discharge of the Prahova River at Câmpina gauging station according to the Mann-Kendall test at $\alpha < 0.05$ (Mann 1945; Kendall 1975; Gilbert 1987).

During the analyzed time interval, the subcarpathian sector of the Prahova River was affected by fluvial metamorphosis – most of the braided features have been lost, together with significant expansion of vegetation on the banks and erosion of in-stream vegetated islands to the point of disappearance (Ioana-Toroimac et al. 2010; Ioana-Toroimac 2016). The same sector went through a severe incision, up to 5 m in certain sites (Armaş et al. 2012). The river has a natural long-term tendency for incision due to geological causes (Armaş et al. 2012). It is hazardous to consider the precipitation as responsible for the river incision in this sector, because no statistical trend was detected in the annual amount of precipitation recorded at weather stations in the Upper Prahova catchment (Marin et al. 2014) except

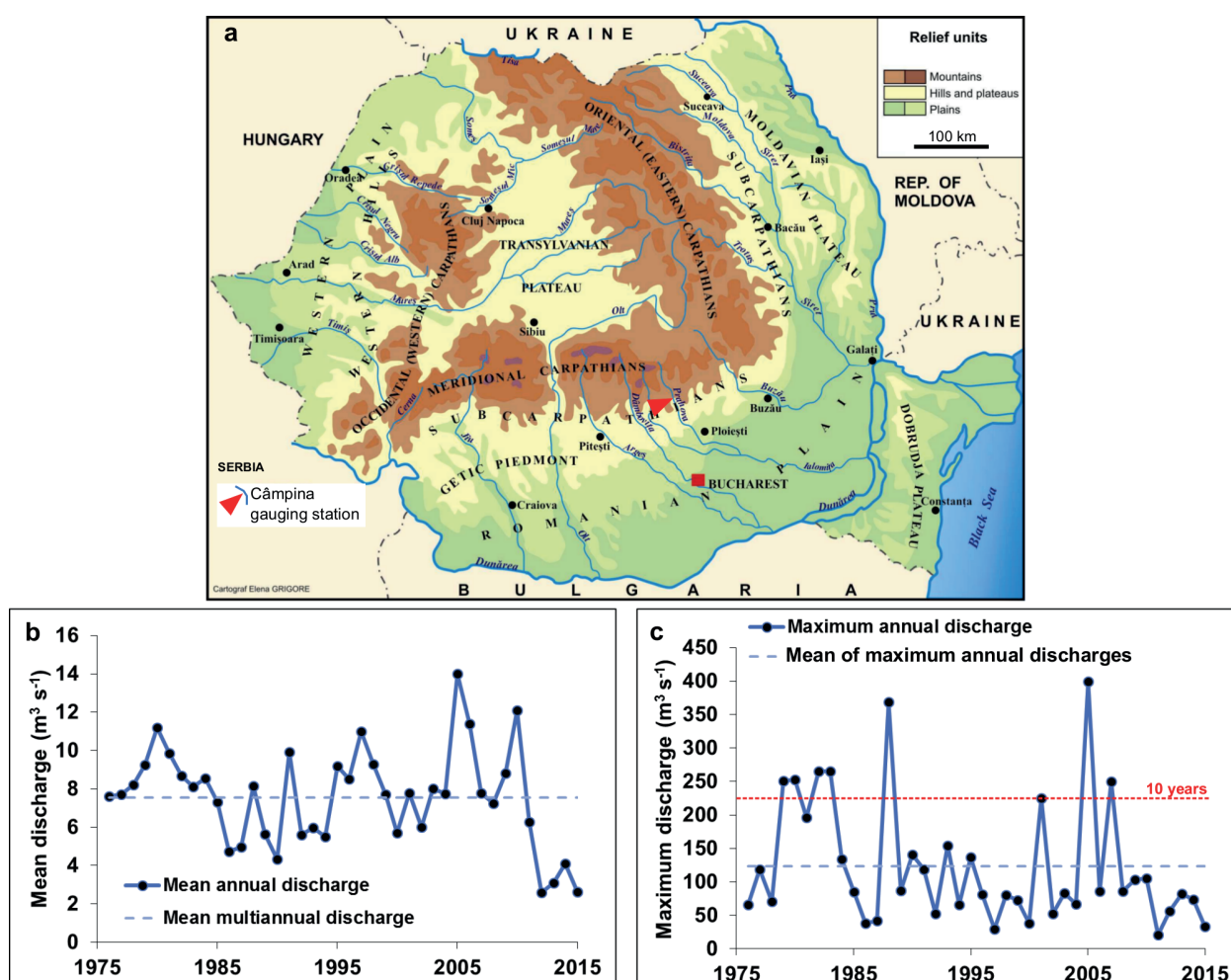


Fig. 1. Study area: a) location in Romania of Câmpina gauging station on the Prahova River; b) variations (1976–2015) of mean and c) maximum annual discharges of the Prahova River at Câmpina gauging station (dashed red line indicates the 10 years return period discharge)

for a decreasing trend in summer in the mountains in the last decennies (Dumitrescu et al. 2014). Daily precipitation characterizes by a negative trend of the number of days with heavy rains and of daily intensity, but a positive trend of the number of consecutive dry days (Croitoru et al. 2016). Despite the deduction of a decrease of the pluvial erosivity, some torrents and landslides were reported as active with socio-economical impact in the Carpathians and Subcarpathians, therefore contributing to the river sediment supply (Ioana-Toroimac et al. 2010). Moreover, several morphogenic floods (e.g., return period > 10 years) have temporally reactivated the floodplain (Ioana-Toroimac et al. 2010) despite its overall trend of narrowing. Therefore, we conclude that the anthropic factor is the main driver of fluvial metamorphosis and river incision (Ioana-Toroimac et al. 2010; Armaş et al. 2012). An example of channel incision is shown in Fig. 2a and b. Human interventions, such as check dams, bank protection, channel rectification, water intakes, micro power plants, torrential works in the catchment, increasing soil sealing, probably diminished the sediment supply of the river and accelerated the channel incision. The Prahova River channel is one of the most altered by various human pressures in the South-Eastern Subcarpathians (Ioana-Toroimac et al. 2017). The high alteration is due mainly to socio-economic stakes in the Prahova upper watershed. In the vicinity of Câmpina gauging station, the management of fluvial processes and hydrological hazards must also consider the international road E60 on the left bank and the railway and small enterprises (i.e., built area) on the right bank.

MATERIALS AND METHODS

To analyse the channel adjustments of the Prahova River, we used cross-section profiles at Câmpina gauging

station. The analysis overlaps the time interval 1976–2015, during which the staff gauge was fixed and represented the landmark used for comparison of all cross-section profiles. The cross-section profiles (randomly chosen 1/year during the studied period) were analysed at the bankfull stage according to the topographic criterion of the lowest bank. The chronological series of cross-section parameters (i.e., depth, width, area, wetted perimeter, hydraulic radius) were analysed by using the non-parametric test of Mann-Kendall to detect a trend of evolution ($\alpha < 0.05$) and the non-parametric test of Pettitt (Pettitt 1979) and the procedure of Hubert (Scheffé 1%, Hubert 2000) to detect a changing point. In order to better understand the vertical dynamics of the riverbed, we analysed the variation of the absolute altitude (in m a.s.l.) of the point of maximum depth (PDmax) for all the available cross-sections during the studied period (approximately 70 values per year during the 40 years of the analysis.) The PDmax was computed for each cross-profile, as difference between the absolute altitude (in m a.s.l.) of the point zero («0») set on the gauging station's staff (this altitude does not change over the years) and «hp oscillation», which expresses the difference between the water stage and the corresponding water maximum depth relative to the point «0» of the gauging station's staff (according to the methodology described by Zaharia et al. 2011).

To characterize the flow of the Prahova River at Câmpina gauging station, the bankfull discharge was calculated based on the Manning equation (Manning 1889), integrating the cross-section parameters at the bankfull stage, the water slope measured simultaneously with the cross-section and Manning roughness coefficient corresponding to bed material grain size (80% medium, coarse gravel and cobble; 20% fine gravel and sand on the latest cross-section



Fig. 2. Dynamics of the Prahova river channel at ca. 200 m upstream of Câmpina gauging station in April 2007 (a) and in November 2017 (b)

profile). Further, the return period of the bankfull discharge was estimated based on the series of maximum annual discharges (1976–2015) by using the log Pearson type III distribution.

RESULTS

During the analysed period, we found that the Prahova riverbed has been deepening. Thus, the maximum depth of the cross-section recorded a positive trend according to the Mann-Kendall test. The maximum depth increased from 1.3 m in 1976 – min to 3.0 m in 2015 – max (mean = 1.9 m; median = 1.7 m; standard deviation = 0.5 m). The maximum depth registered a changing point in 1998 according to Pettitt test and three segments were identified (1976–1991, 1992–2000, and 2001–2015) according to Hubert procedure (Fig. 3a). The PDmax appears to confirm the negative trend in the variability of the maximum depth of the river channel (Fig. 3b). Overall, the PDmax varied on an amplitude of approximately 3.5 m. The deepest incision between two consecutive cross-section profiles of about – 1.3 m occurred in July 1988 followed a few days later by the highest aggradation of +1.3 m in relation to the second peak of the maximum annual discharges of the period 1976–2015 (Fig. 1c), indicating the new equilibrium of the hydrosystem disturbed by a flood. The overall incision was gradually and the PDmax generally maintained under its mean value after 2001 (Fig. 3b).

The cross-section width didn't register a trend in its variability (mean = 44.4 m; median = 44.7 m; standard deviation = 2.6 m). Similarly, the width chronological series had no changing points or segments (Fig. 4a).

The cross-section area had a positive trend during the

analysed time interval according to the Mann-Kendall test. The area increased from 39.7 m² in 1976 to 90.2 m² in 2015 – max (min = 34.0 m² in 1989; mean = 58.1 m²; median = 51 m²; standard deviation = 18.8 m²). The cross-section area recorded a changing point in 1997 according to Pettitt test and several segments were identified (i.e. 1976–1992, 1993–1997, 1998–2000, and 2001–2015), according to Hubert procedure (Fig. 4b).

The wetted perimeter didn't register a trend in its variability (mean = 45.5 m; median = 45.8 m; standard deviation = 2.4 m), with no changing points according to Pettitt test. However, Hubert procedure revealed several segments: 1976–1994, 1995–1996, 1997–2011, and 2012–2015 (Fig. 5a).

The hydraulic radius statistically increased from 0.8 m in 1976 to 1.8 m in 2015 (mean = 1.2 m; median = 1.0 m; standard deviation = 0.4 m). The hydraulic radius time series didn't record a changing point according to Pettitt test, but it is segmented in 1976–1998, 1999–2001, and 2002–2015 according to Hubert procedure (Fig. 5b).

In the morphology of the cross-section of the Prahova River at Câmpina gauging station, different changes were identified (Fig. 6): increase of the maximum depth between 1991–1992; increase of both cross-section area and maximum depth between 1997–1999; and overall drastic channel incision between 1976–2015.

As a consequence of increased channel capacity, during the analysed period, the bankfull discharge increased from 44.9 m³s⁻¹ in 1976 to 163.8 m³s⁻¹ in 2015 (mean = 97.9 m³s⁻¹; median = 61.1 m³s⁻¹; standard deviation = 65.4 m³s⁻¹). The maximum bankfull discharge occurred in 2007, while the minimum bankfull discharge in 1988 (Fig. 7a).

The return period of the bankfull discharge increased

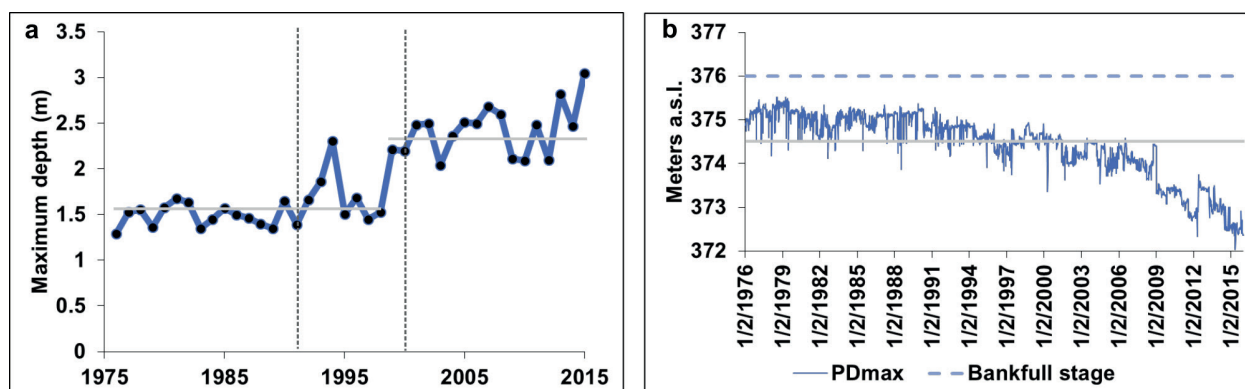


Fig. 3. Variations of channel depth of the Prahova River at Câmpina gauging station (1976–2015): a) maximum value at the bankfull stage (light grey line indicates the mean value of the two intervals according to Pettitt test and dark grey dashed line indicates the Hubert segments); b) point of maximum depth – PDmax (light grey line indicates mean PDmax)

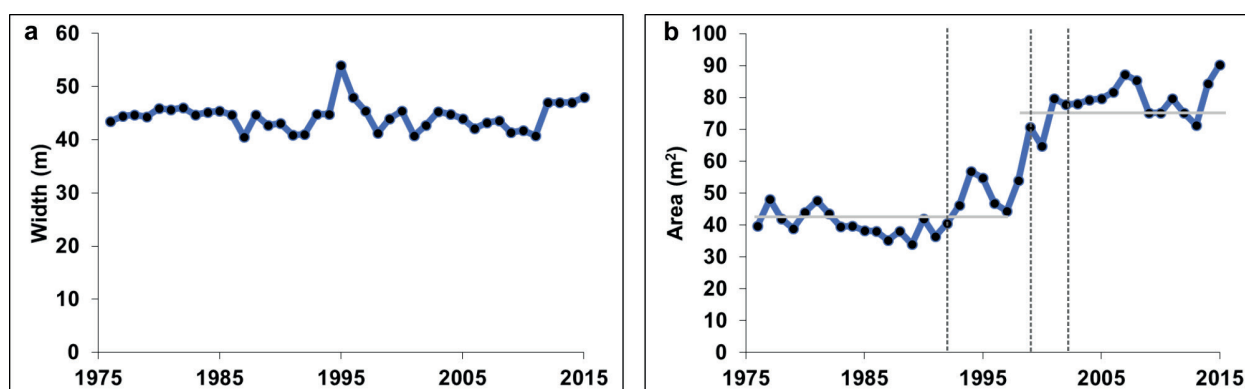


Fig. 4. Variations of a) channel width and b) cross-section area at the bankfull stage of the Prahova River at Câmpina gauging station (1976–2015, light grey line for the mean value of the two intervals according to Pettitt test and dark grey dashed line for Hubert segments)

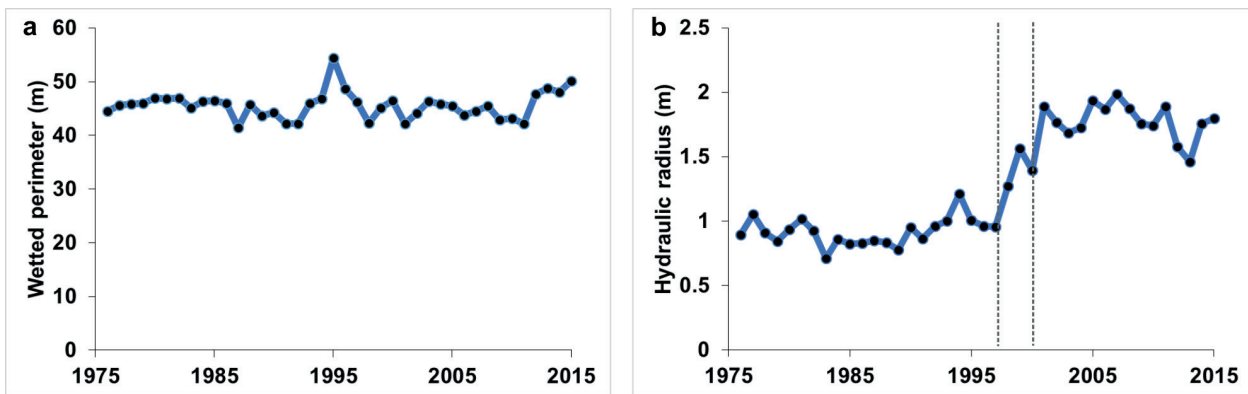


Fig. 5. Variations of a) wetted perimeter and b) hydraulic radius at the bankfull stage of the Prahova River at Câmpina gauging station (1976–2015, dark grey dashed line for Hubert segments)

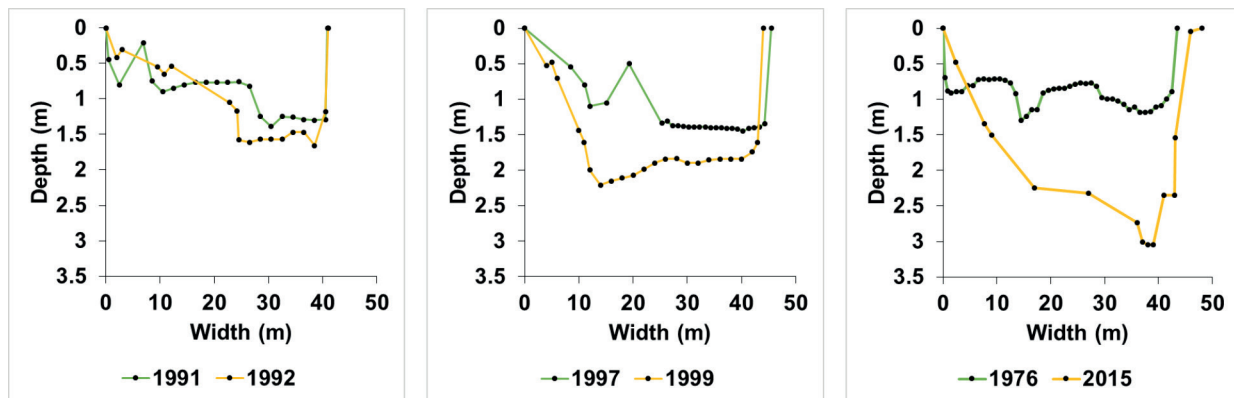


Fig. 6. Variations of the cross-section at the bankfull stage of the Prahova River at Câmpina gauging station, in different periods

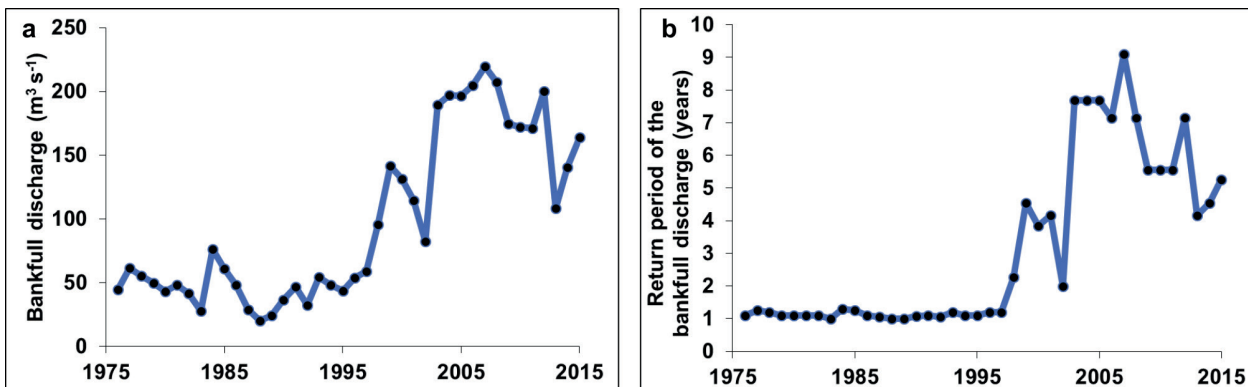


Fig. 7. Variations of a) bankfull discharge and b) associated return period of the Prahova River at Câmpina gauging station (1976–2015)

from 1.1 years in 1976 to 5.3 years in 2015. The maximum value of the return period, i.e. 9 years, corresponded to the high bankfull discharge of 2007 (Fig. 7b).

DISCUSSION

The analysis of the Prahova river channel dynamics at Câmpina gauging station indicated a severe incision of the riverbed and increased channel capacity associated to lateral stability. These processes were followed by a decrease of the probability of flooding over the bankfull discharge.

Understanding channel incision

Our results confirm previous works concerning the incision of the Prahova River in the South-Eastern Subcarpathians (Armaş et al. 2012). The magnitude of the incision is probably maximum in the studied area, while the lower course of the Prahova River was not affected by this process according to Ioana-Toroimac et al. (2015). As response

to disturbances, major channel adjustments occurred in the beginning of 1990s and especially at the end of 1990s. At the beginning of 2000s, the hydrosystem probably relaxed. Since, the hydrosystem preserved the new features, namely channel incision.

The Prahova river channel incision at Câmpina gauging station should be interpreted as part of the entire hydrosystem functioning: the channel incision appears to be the process following the channel narrowing upstream and downstream (Ioana-Toroimac et al. 2010). The incision isn't followed by banks' collapse due to the relatively hard rocks constituting the river channel. Therefore the incision can't naturally be attenuated. The river channel pattern dynamics in our case study is relatively similar to the ones of the Italian rivers described by Surian and Rinaldi (2003).

We can only hypothesise about these disturbances in the Prahova hydrosystem. Finding the precise disturbance responsible for the channel incision, which took place 20 years back, is impossible in lack of detailed registers. We

advance the hypothesis of human pressures as no major flood occurred in the end of 1990s (Fig. 1c); moreover, the highest flood as discharge in 2005 didn't manifest itself by notable channel adjustments. As example of human pressures, dredging was a common practice in the region to avoid river channel aggradation in the vicinity of bridges (Ioana-Toroimac 2014). Therefore, gravel and sand exploitation from the river channel maintained as frequent practice in Romania (Salit and Ioana-Toroimac 2013). Similarly, anthropic increase of the channel capacity is still seen as a way to protect against floods in Romania (ABAS 2015).

There are numerous gaps in the analysis of channel incision of the Prahova River. In lack of other long-term and precise topographic measurements, data from gauging stations are the most suitable and accurate to quantify the channel incision. However, the low number of cross-section profiles diminishes the precision of the results. The decreasing number of points along a cross-section profile (e.g., 46 points on 43.5 m in 1976 versus 15 points on 48 m in 2015 – Fig. 6) also diminishes their fidelity when compared to the studied section. Other measurements compared to stable landmarks, such as the bankfull stage, should complete the ones associated to hydrological variability. Measuring only the PDmax is incomplete as the cross-section area at the bankfull stage also describes the features of the incision. We recommend to enhance cross-section topographic measurements at gauging stations. We recommend as well to continuously and rigorously monitor and inventory human pressures in order to track back disturbances corresponding to channel adjustments.

Remarks on the return period of the bankfull discharge

The return period of the bankfull discharge of the Prahova River increased especially after 1997 in relation to channel capacity growth: from 1.1 years in 1976 to about 5 years in 2015. The latter value is higher than those in the literature, where the return period of the bankfull discharge is thought to be 1–2 years (Leopold 1954) or 1.58 years (Dury et al. 1963) and similar for the majority of stable channels (Doyle et al. 2007), which confirms Prahova river channel adjustments when compared to a normal situation. To better understand the relation between channel incision and floods, the analysis must be completed by estimating the effective discharge that transports the greatest quantity of sediments (Doyle et al. 2007).

However, the values of the bankfull discharge and return period must be carefully interpreted. As shown in Fig. 7a and b, these values appear to have high variability. They strongly depend on the hydrological variability and more precisely on the water slope. In our estimations, the water slope corresponds to the measurement of a random water stage, which probably is lower than the bankfull stage for safety during field work. Therefore, to gain precision in estimating the bankfull discharge, we recommend to enhance knowledge on water slope by field measurements related to the hydraulics of floods or by hydraulic modelling.

Managing complex effects of channel incision

The Prahova River long-term incision and high erosion during floods determined an increase of the channel capacity and return period of the bankfull discharge up to maximum 9 years in the studied section. Additionally, the minimum

annual water stages probably decreased with ecological negative effects. As a consequence, the morphogenic floods are less frequent in the floodplain area and the floodplain accretion is expected to take a longer time. The river became largely disconnected from the floodplain, which reduced delivery of organic matter and wood debris from the riparian zone and limited the availability of remnant channels and ponds in the floodplains for river biota (Wyżga et al. 2011). As incision probably increased the velocity of flood flows in the channel and the river competence, floods may be more destructive now for the structures located within the channel (Wyżga et al. 2016b), which is even more intense in the case of a high energy river such as the Prahova River. In our case study, the loss of floodwater storage in the floodplain area doesn't imply the increase in flood hazard to downstream river sector as the braided river channel becomes very large (up to 300 m according to Ioana-Toroimac 2016) and takes over the capacity to stock floodwater.

As river management practice, Fig. 2a and b shows concrete bank protection structures on the right side built up before 2007 against lateral erosion. Between 2007–2017, a low-invasive rectification was set up (i.e., raise of an in-stream alluvial bar) to deviate the main flow from the right bank. Further field investigations revealed that, after 2015, the left bank of the Prahova River at Câmpina gauging station was protected against lateral erosion by gabions. Hypothetically, the bank stabilisation works further increase the incision (Galia et al. 2015). Therefore, we conclude that river management maintains channel incision in the studied area.

The channel incision of the Prahova River at Câmpina gauging station reduce the frequency of river overflowing, therefore mitigate the flood risk in the studied area. This solution appears to be preferred by river managers probably for socio-economic purposes. Future transdisciplinary studies must analyse the sustainability of this solution.

CONCLUSIONS

This paper showed that the impact of channel incision on floods is translated by an increase of the bankfull discharge and of its return period. In the case of the Prahova River at Câmpina gauging station, during 1976–2015, the total incision was of 1.7 m of maximum depth and the channel capacity doubled. Between the two extreme years of the analysed time interval (1976 and 2015), the bankfull discharge raised from $44.9 \text{ m}^3\text{s}^{-1}$ to $163.8 \text{ m}^3\text{s}^{-1}$, and the associate return periods increased from 1.1 years to 5.3 years. However, these values are oscillating, depending on the dominant fluvial process associated to the hydrological variability. The values also depend on the accuracy of field measurements, which should be a major concern for river managers.

As implications for river management, overflowing became less frequent while floods probably became more competent and destructive in the channel. As no measure was taken so far to diminish the Prahova river channel incision, the situation may be considered worthwhile for flood risk management in the studied area, and should be taken into consideration for river basin planning in the context of the EU-WFD. Future transdisciplinary studies are needed to reveal the sustainability of this solution. ■

REFERENCES

- ABAS (Administrația Bazinală de Ape Siret) (2015). Planul de management al riscului la inundații. București: Administrația Națională Apele Române.
- Armaș I., Gogoșe Nistoran D.E., Osaci-Costache G. and Brașoveanu L. (2012). Morphodynamic evolution patterns of Subcarpathian Prahova River (Romania). *Catena*, 100, 83-99, DOI: 10.1016/j.catena.2012.07.007.
- AQUAPROIECT (1992). Atlasul Cadastrului apelor din România. București: Ministerul Mediului.
- Beechie T.J., Pollock M.M. and Baker S. (2008). Channel incision, evolution and potential recovery in the Walla Walla and Tucannon River basins, northwestern USA. *Earth Surface Processes and Landforms*, 33, 784-800, DOI: 10.1002/esp.1578.
- Chiriloaei F., Rădoane M., Perșoiu I. and Popa I. (2012). Late Holocene history of the Moldova River Valley, Romania. *Catena*, 93, 64-77, DOI: 10.1016/j.catena.2012.01.008.
- Croitoru A.E., Piticar A. and Burada D.C. (2016). Changes in precipitation extremes in Romania. *Quaternary International*, 415, 325-335, DOI: 10.1016/j.quaint.2015.07.028.
- Doyle M.W., Shields D., Boyd K.F., Skidmore P.B. and DeWitt D. (2007). Channel-forming discharge selection in river restoration design. *Journal of Hydraulic Engineering*, 831-837, DOI: 10.1061/(ASCE)0733-9429(2007)133:7(831).
- Dumitrescu A., Bojariu R., Birsan M.V., Marin L. and Manea A. (2014). Recent climatic changes in Romania from observational data (1961–2013). *Theoretical and Applied Climatology*, DOI: 10.1007/s00704-014-1290-0.
- Dury G.H., Hails J.R. and Robbie H.B. (1963). Bankfull discharge and magnitude-frequency series. *Australian Journal of Science*, 26, 123-124.
- European Commission (2000). Directive 2000/60/EC—establishing a framework for community action in the field of water policy. *Official Journal of European Communities*, 327.
- Galia T., Hradechý J. and Škarpich V. (2015) Sediment transport in headwater streams of the Carpathian flysch belt: its nature and recent effects of human interventions. In: P. Heininger, J., Cullmann, eds., *Sediments matters*. Cham: Springer, 13-26, DOI: 10.1007/978-3-319-14696-6_2.
- Gilbert R.O. (1987). *Statistical methods for environmental pollution monitoring*. New York: Wiley.
- Haase P., Hering D., Jähnig S.C., Lorenz A.W. and Sundermann A. (2013). The impact of hydromorphological restoration on river ecological status: a comparison of fish, benthic invertebrates, and macrophytes. *Hydrobiologia*, 704, 475-488, DOI: 10.1007/s10750-012-1255-1.
- Hajdukiewicz H., Wyżga H. and Zawiejska J. (2019). Twentieth-century hydromorphological degradation of Polish Carpathian rivers. *Quaternary International*, 504, 181-194, DOI: 10.1016/j.quaint.2017.12.011.
- Hubert P. (2000). The segmentation procedure as a tool for discrete modeling of hydrometeorological regimes. *Stochastic Environmental Research and Risk Assessment*, 14, 297-304, DOI: 10.1007/PL00013450
- Ioana-Toroimac G. (2014). La dynamique hydro-géomorphologique de la rivière Prahova: fonctionnement actuel, évolution récente et conséquences géographiques. București: Editura Universitară.
- Ioana-Toroimac G. (2016). Inventory of long-term braiding activity at a regional scale as a tool for detecting alterations to a rivers' hydromorphological state: a case study for Romania's South-Eastern Subcarpathians. *Environmental Management*, 58, 1, 93-106, DOI: 10.1007/s00267-016-0701-7.
- Ioana-Toroimac G., Dobre R., Grecu F. and Zaharia L. (2010). Evolution 2D de la bande active de la Haute Prahova (Roumanie) durant les 150 dernières années. *Géomorphologie: relief, processus, environnement*, 3, 275-286, DOI: 10.4000/geomorphologie.7988.
- Ioana-Toroimac G., Minea G., Zaharia L., Zarea R. and Borcan M. (2013). Hydrogeomorphological river typology in the Ialomița and Buzău catchments (Romania). In: G. Arnaud-Fassetta, E. Masson, E. Reynard, eds., *European Continental Hydrosystems under Changing Water Policy*. München: Verlag Dr. Friedrich Pfeil, 261-272.
- Ioana-Toroimac G., Zaharia L. and Minea G. (2015). Using pressure and alteration indicators to assess river morphological quality: case study of the Prahova River (Romania). *Water*, 7, 2971-2989, DOI: 10.3390/w7062971.
- Ioana-Toroimac G., Zaharia L., Minea G. and Moroșanu G.A. (2017). Using a multi-criteria analysis to identify rivers with hydromorphological restoration priority: braided rivers in the south-eastern Subcarpathians (Romania). *Science of the Total Environment*, 599-600, 700-709, DOI: 10.1016/j.scitotenv.2017.04.209.
- Karthe D., Chiffard P. and Büche T. (2018). Hydrogeography – linking water resources and their management to physical and anthropogenic catchment processes. *Die Erde* 149, 2-3, 57-63, DOI: 10.12854/erde-2018-412.
- Kendall M.G. (1975). *Rank correlation methods*. London: Charles Griffin.
- Korpak J. (2007). The influence of river training on mountain channel changes (Polish Carpathian Mountains). *Geomorphology*, 92(3-4), 166-181, DOI: 10.1016/j.geomorph.2006.07.037.
- Krengel F., Bernhofer C., Chalov S., Efimov V., Efimova L., Gorbachova L., Habel M., Helm B., Kruhlov I., Nabyvanets Y., Osadcha N., Osadchyi V., Pluntke T., Reeh T., Terskii P. and Karthe D. (2018). Challenges for transboundary river management in Eastern Europe – three case studies. *Die Erde*, 149, 2-3, 157-172, 101-116, DOI: 10.12854/erde-2018-389.
- Landon N., Piégay H. and Bravard J.P. (1998). The Drôme River incision (France): from assessment to management. *Landscape and Urban Planning*, 43, 119-131.
- Leopold L.B. (1954). *Determination of hydraulic elements of rivers by indirect methods*. United States Government Printing Office: Geological Survey Professional.
- Mann H.B. (1945) Non-parametric tests against trend. *Econometrica* 13, 163-171.
- Manning R. (1889). On the flow of water in open channels and pipes. *Trans. Institution of Civil Engineers of Ireland*, 20 161-166.
- Marin L., Birsan M.V., Bojariu R., Dumitrescu A., Micu D.M., and Manea A. (2014). An overview of annual climatic changes in Romania: trends in air temperature, precipitation, sunshine hours, cloud cover, relative humidity and wind speed during the 1961–2013 period. *Carpathian Journal of Earth and Environmental Sciences*, 9, 4, 253-258.
- Pettitt A.N. (1979). A Non-Parametric Approach to the Change-Point Problem. *Journal of the Royal Statistical Society. Series C (Applied Statistics)*, 28, 2, 26-135, DOI: 10.2307/2346729.
- Rădoane M., Obreja F., Cristea I. and Mihăilă I. (2013). Changes in the channel-bed level of the eastern Carpathians rivers: climatic vs. human control over the last 50 years. *Geomorphology*, 193, 91-111, DOI: 10.1016/j.geomorph.2013.04.008.
- Richter S., Völker J., Borchardt D. and Mohaupt V. (2013). The Water Framework Directive as an approach for Integrated Water Resources Management: results from the experiences in Germany on implementation, and future perspectives. *Environmental Earth Sciences*, 69, 719-728, DOI: 10.1007/s12665-013-2399-7.

- Salit F. and Ioana-Toroimac G. (2013). Actual in-stream mining in alluvial rivers: geomorphological impact and European legislation, 3rd International Geography symposium GEOMED, Symposium Proceedings – Kemel (Antalya)/Turkey (June, 10th-13th 2013), 201-210.
- Stähly S., Franca M. J., Robinson C.T. and Schleiss A.J. (2019). Sediment replenishment combined with an artificial flood improves river habitats downstream of a dam. *Scientific Reports*, 9, 5176, DOI: 10.1038/s41598-019-41575-6.
- Surian N. and Rinaldi M. (2003) Morphological response to river engineering and management in alluvial channels in Italy. *Geomorphology*, 50, 307-326, DOI: 10.1016/S0169-555X(02)00219-2.
- Wyżga B., Oglęcki P., Radecki-Pawlik A. and Zawiejsa J. (2011). Diversity of macroinvertebrate communities as a reflection of habitat heterogeneity in a mountain river subjected to variable human impacts. In: A. Simon, S.J. Bennett, J.M. Castro, eds., *Stream restoration in dynamic fluvial systems. Scientific approaches, analyses, and tools*. American Geophysical Union.
- Wyzga B., Zawiejska J., Radecki-Pawlik A. and Hajdukiewicz H. (2012). Environmental change, hydromorphological reference conditions and the restoration of Polish Carpathian Rivers. *Earth Surface Processes Landforms*, 37, 1213-1226, DOI: 10.1002/esp.3273.
- Wyżga B., Zawiejska J. and Hajdukiewicz H. (2016a). Multi-threat rivers in the Polish Carpathians: occurrence, decline and possibilities of restoration. *Quaternary International* 415, 344-356, DOI: 10.1016/j.quaint.2015.05.015.
- Wyżga B., Zawiejska J. and Radecki-Pawlik A. (2016b). Impact of channel incision on the hydraulics of flood flows: Examples from Polish Carpathian rivers. *Geomorphology*, 272, 10-20, DOI: 10.1016/j.geomorph.2015.05.017.
- Wyżga B., Kundzewicz Z.W., Konieczny R., Piniewski M., Zawiejska J. and Radecki-Pawlik A. (2018). Comprehensive approach to the reduction of riverflood risk: Case study of the Upper Vistula Basin. *Science of the Total Environment*, 631-632, 1251-1267, DOI: 10.1016/j.scitotenv.2018.03.015.
- Zaharia L., Grecu F., Ioana-Toroimac G. and Neculau G. (2011). Sediment transport and river channel dynamics in Romania – variability and control factors. In A.J. Manning, ed., *Sediment transport in aquatic environments*. Rijeka: INTECH, 293-316.
- Zaharia L., Costache R., Prăvălie R. and Ioana-Toroimac G. (2017). Mapping flood and flooding potential indices: a methodological approach to identifying areas susceptible to flood and flooding risk. Case study: the Prahova catchment (Romania). *Frontiers of Earth Sciences*, 11, 2, 229-247, DOI: 10.1007/s11707-017-0636-1.

POTENTIAL HYDROLOGICAL RESTRICTIONS ON WATER USE IN THE BASINS OF RIVERS FLOWING INTO RUSSIAN ARCTIC SEAS

Dmitriy V. Magritsky¹, Natalia L. Frolova^{1*}, Olga M. Pakhomova¹

¹Faculty of Geography, Lomonosov Moscow State University, Leninskie Gory 1, 119991, Moscow, Russia

***Corresponding author:** frolova_nl@mail.ru

Received: June 3rd, 2019 / Accepted: May 10th, 2020 / Published: July 1st, 2020

<http://DOI-10.24057/2071-9388-2019-59>

ABSTRACT. Water consumption has been evaluated for the basins of the rivers flowing into the Arctic seas of the Russian Federation and, separately, for the Arctic zone of Russia (AZR). Long-term dynamics of the major characteristics of water consumption are given for the period from the 1980s to 2017 along with data on its structure. The possible effect of the total water withdrawal and consumptive water use on river water inflow into the Arctic seas has been evaluated for the 1980s (a period of maximal anthropogenic load), for 2006–2017 and up to 2030. The volumes of water consumption in limits of AZR are relatively low. Moreover, the water withdrawal has dropped considerably compared with the situation in the 1980s, in particular, by about 30% in the Pechora, Lena river basins, and from the rivers of Murmansk oblast, and by 50% in the Northern Dvina, Yenisei, and Kolyma river basins. It has increased in the Nenets and Yamalo-Nenets AO because of the intense development of the local oil-and-gas complex. Nowadays, according to the authors' estimates, 21.28 km³/year is being withdrawn in the drainage basins of RF Arctic seas and 2.58 km³/year, within the AZR, or 28.8 and 3.5% of the total volume in Russia. The largest contribution to this value is due to the water-management complexes in the basins of the Ob (14.7 km³/year), Yenisei (2.77), Northern Dvina (0.64), and Murmansk oblast (1.72 km³/year). The volumes of water discharges back into water bodies at the drainage basins of Russian Arctic seas are comparable with the volumes of freshwater withdrawal -71% of water intake. Even lesser is the difference within AZR. The major water users are the industry (with a high proportion of mining plants), thermal power engineering, and municipal economy. But considerable and diverse hydrological restrictions exist at the municipal level and for some water users in AZR. These local hydrological restrictions have been formulated and analyzed in detail, for the first time. They form three large groups. Original maps are given to illustrate the specific features and regularities in the present-day distribution of water-management characteristics over AZR.

KEY WORDS: Russian Arctic Region, water consumption, wastewaters, water-management system, rivers, hydrological restrictions on water use

CITATION: Dmitriy V. Magritsky, Natalia L. Frolova, Olga M. Pakhomova (2020). Potential Hydrological Restrictions on Water Use in the Basins of Rivers Flowing into Russian Arctic Seas. *Geography, Environment, Sustainability*, Vol.13, No 2, p. 25-34
<http://DOI-10.24057/2071-9388-2019-59>

ACKNOWLEDGEMENTS: This study was supported by the Russian Foundation for Basic Research, project no. 18-05-60021-Arctic Study on water quality was done within RFBR project 18-05-60219.

Conflict of interests: The authors reported no potential conflict of interest.

INTRODUCTION

In the present-day world, northern regions and the Arctic are growing in significance because of, first, their role in the formation of global climate and the maintenance of biospheric stability, second, the presence of huge hydrocarbon resources; and, third, the strategic and transport significance of the region, which has a colossal space resource. The exploitation rate of Arctic resources has been growing in the recent decades, accompanied by heavier anthropogenic load onto the Arctic ecosystems. At the same time, the Arctic regions are especially vulnerable to anthropogenic impact because of their extreme natural and climate conditions, the fragility of their ecosystems, the separation from large economic and political centers of the

country, the poor development of transport thoroughfares and infrastructure as a whole, the higher sensitivity of the population to changes in the environment, and the lesser adaptation capacity of the organisms.

The availability of water resources in polar regions has been high enough not to cause troubles regarding their quality. However, the intense development of rich mineral deposits in the Extreme North and the transboundary pollution transport cause rapid disturbance of the fragile environmental equilibrium in many urbanized regions of the Arctic, thus leading to a qualitative depletion of water resources. The further development of the Arctic is also associated with its protection from hazardous natural phenomena, including hydrological. The recent decades have been showing an increasingly extreme character

of changes in the characteristic of water discharges and levels, channel processes, ice phenomena, and water quality. This is largely due to a series of climate changes: a rise of the annual and seasonal air temperature and changes in precipitation depth and the volume and the annual distribution of river runoff.

The requirements to ensure the hydroecological safety of water use in various areas, including the Arctic (Aleksievskii et al. 2011; Khristoforov 2010) are reflected in a system of restrictions on the admissible changes in parameters of the state of water bodies and the economic activity within a period under consideration. The hydrological restrictions take into account the natural specifics of changes in river runoff components and specify the values of hydrological characteristics at which the safe water use is ensured with an admissible level of the risk of hazardous hydrological phenomena. The type and the magnitude of restrictions depend on the type of economic activity in river basins and channels (Frolova 2006).

The hydrological restrictions are of quantitative nature and probabilistic character. The meeting of the hydrological restrictions ensures the safety of the population and water bodies and enables the economically efficient water use (Aleksievskii et al. 2011). Some hydrological restrictions depend only on the natural conditions, changes in which can be forecasted with a degree of reliability for preventing possible adverse effects. Other restrictions are associated with economic activity, and they are introduced in accordance with water user demands.

The determination of hydrological restrictions on water use is hampered by the complexity of the operation of water management systems, the diversity of the approaches to planning and implementing nature-protection measures in the basins of water bodies, and the contradictions in the interests of different sectors of water economy.

The introduction of hydrological restrictions ensures the hydroecological safety of the population, economy, as well as aquatic and nearshore ecosystems. This process is based on the social need, natural admissibility, environmental safety, as well as the technical and juridical provision of water use in the developed segments of river valleys. The regulations determine the activity of water users with respect to water bodies, implying the establishing of a method of their use at which the parameters and the major properties of a hazardous hydrological phenomena are determined and limited as is admissible for the implementation of the water management activity within the boundaries of a water body or its drainage basin

(Aleksievskii et al. 2011). The main types of restrictions that determine the hydroecological safety of water use (HSWU) are given in Fig. 1.

The objective of the study is to evaluate the water use and its long-term changes in the basins of all rivers that flow into RF Arctic seas, including only within the Arctic zone of Russia (AZR) (Fig. 3), and the effect of water use on the water runoff of Arctic rivers and river water inflow, and general effect of hydrological restrictions on water use.

The aim of this work is to quantify water consumption and its long-term dynamics in the basins of all rivers that flow into the Arctic seas of the Russian Federation, including only within the territory of the Arctic zone of Russia (AZR).

MATERIALS AND METHODS

The main source of data on the volumes of the use of surface water and groundwater in RF was the data of the Federal Agency of Water Resources and the Federal Service of State Statistics (State Water Cadastre 1981–2018; Water in Russia 1991–2002; Russian Water Resources and Water Economy 2006–2018). These reference books give the volumes of withdrawn, consumed, and discharged water for constituent entities of the RF and for drainage basins of large rivers and seas, as well as evaporation losses from reservoirs and losses for their filling, and anthropogenic changes in runoff.

The Arctic rivers for which such data are available are the Pechenga, Onega, Northern Dvina, Mezen, Pechora, Ob, Yenisei, Pyasina, Lena, Indigirka, and Kolyma. Long-term series of appropriate water-management characteristics have been obtained for major Arctic rivers over period 1981–2017, for individual RF constituent entities, including Murmansk (since 1996) and Arkhangel'sk (since 2003) oblasts, Yamalo-Nenets (since 2004) and Chukotskii (since 2004) autonomous districts, and for RF as a whole.

In addition, this study uses the materials of «The Schemes of Integrated Use and Protection of Water Bodies» (SIUPWB). They are available on open access, in particular, on the sites of the Amur, Yenisei, Lower-Ob, and Dvina–Pechora Basin Water Management Departments (Amurbvu.ru, Enbvru.ru, Nobwu.ru, Dpbvu.ru). They give much wider list of rivers with data on water intakes and discharges (commonly, for 1–2 years), data on specific water users, and forecasts of changes in the volumes of water consumption by the middle and late 2020s.

Finally, an important sources of data were the open documents of municipal formations, primarily, «Schemes

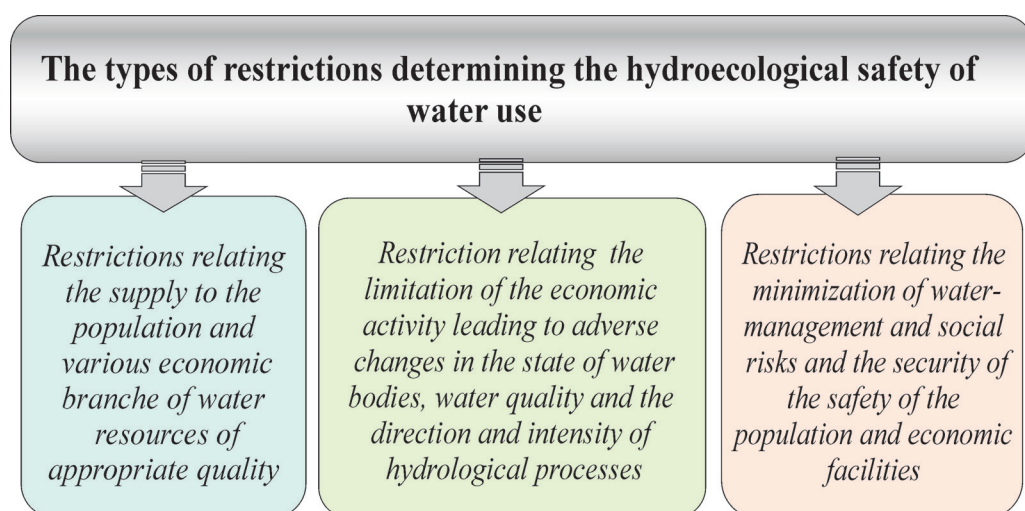


Fig. 1. Diagram of types of restrictions determining the hydroecological safety of water use

of Water Supply and Disposal and Heat Supply,» «The Program of Integrated Development of Community Facilities Infrastructure» in populated localities, as well as annual reports of plants. These documents allowed the authors for the first time to compile an «Electronic Catalogue of Water Users in the Arctic Zone of Russia» (ECWU AZR), though, by now, only for the members of the water-management complex in the territories of the Chukotka Autonomous Okrug, Arctic districts (uluses) in the Republic of Sakha (Yakutiya), and Krasnoyarsk Krai, with various water management data over the past 5–10 years. The number of such members was 229: 70.7% were the enterprises of housing and public utilities (HPU), i.e., in essence, populated localities; 18.8% were mining enterprises; 6.6% were thermal-engineering facilities; and 3.9% were all others. In addition, ECWU AZR contains data on the permanent or occasional problems in water use. The comparison of data from official reference books and those underlying the ECWU AZR showed them to be consistent.

Additionally, materials of other experts and research groups were used in the study and the analysis of its results.

First of all, these are the studies (Zaitseva and Koronkevich 2003; Chernyaev 2000; Shiklomanov 2008; Demin 2011; Ratkovich 2003). The comparison of the characteristics of total water consumption in the drainage basins of Arctic rivers in RF and the values of flow at their mouths was made with the use of data on its magnitude (at the outlet and mouth sections), collected by the authors in earlier studies, processed, and partially published in (Alekseevskii 2007, 2013; Magritsky et al. 2013, 2018; Agafonova et al. 2017).

As a result, it was possible for the first time to reliably assess the values of the present-day withdrawal of surface water and groundwater, as well as wastewater discharge for the basins of the major rivers and the inter-basin areas of the Arctic Zone of Russia; make the thematic maps and diagrams; study the economic sector and hydrographic structure, the spatio-temporal variations of water consumption characteristics; compare data from various sources; improve the results published in (Alekseevskii 2013; Magritsky 2008); and identify major hydrological restrictions of Arctic water use and their correlation with

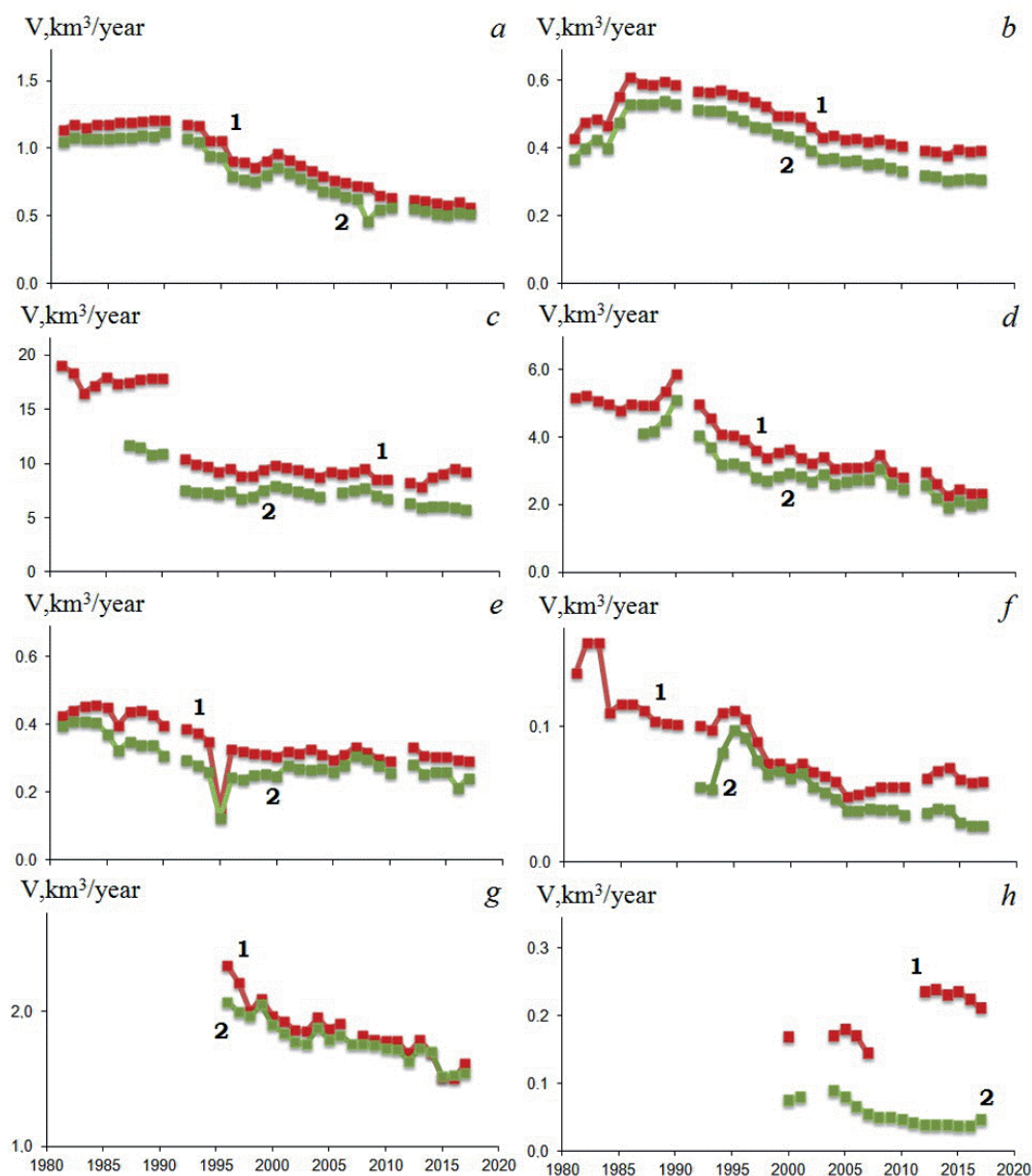


Fig. 2. Charts of long-term variations in the volumes of (1) surface water and groundwater withdrawal and (2) wastewater discharge in the basins of (a) the Northern Dvina, (b) Pechora, (c) Ob, (d) Yenisei, (e) Lena, and (f) Kolyma in the territory of Murmansk oblast (g) and Yamal-Nenets Autonomous Okrug (h). The data for the Ob basin after 1991 are given only for RF territory. The source of primary data is (State Water Cadastre 1981–2018; Russian Water Resources and Water Economy 2006–2018; mpr.gov-murman.ru)

the natural conditions of the territory and the character of nature development.

The collected data were processed with the use of standard software packages Statistica and Excel; the space analysis of hydrological and water management characteristics was made with the use of ArcGIS 10.2.

RESULTS AND DISCUSSION

The availability of a required volume of water resources of appropriate quality in a certain area is a major limiting factor of natural resource and water use. However, the river runoff volumes alone cannot provide adequate knowledge about the sufficiency or deficiency of water resources. To determine whether there is a deficiency in water resources, one has to incorporate data on the use of water resources in different economic sectors.

Water consumption in the basins of Arctic rivers in the 1980s

Water consumption and the disposal (discharge) of wastewater in the basins of RF Arctic rivers has reached its peaks in the second half 1970s and in the 1980s (Fig. 2) – about 28.9 km³/year and 20.7 km³/year, respectively. 15.8% of freshwater was taken on the watersheds of the White and Barents seas, 82% – within the drainage basin of the Kara Sea. For comparison, the total water consumption in Russia from 1981 to 1990 was equal ~111 km³/year (117 km³/year with seawater included) and wastewater volumes were ~75.6 km³/year.

The increase was due to the growing demand of the production complex in the period of extensive development of the country's economy, an increase in the population, and the connection of many populated localities to centralized water and heat supply. Nevertheless, water intake in the basins of many Arctic rivers was relatively small or practically absent. Even in the basins of the best economically developed rivers the volume of water withdrawal in 1981–1990 was 1.26 km³/year (the Northern Dvina), 17.85 km³/year (the Ob: 67% of this volume in Russia and 33% in Kazakhstan) and 5.36 km³/year (the Yenisei), or 1.2. 4.3. and 0.8% of their long-term annual water runoff into seas considering data from (Magritsky et al. 2018). In Murmansk oblast, which is the most industrially developed entity in AZR, ~2.5 km³/year (or 3.6% of annual water runoff) were withdrawn. These volumes are comparable with errors in the calculation of the average annual flow; therefore, we can say that there is no statistically significant anthropogenic effect on river water resources. This area also has not suffered the so-called water stress in the 1980s, which, according to the World Water Assessment Program (UNESCO WWAP), starts to manifest itself at the ratio of water withdrawal to water resources equal to 10% (<http://www.unesco.org/new/en/natural-sciences/environment/water/wwap>).

The largest amounts of freshwater were withdrawn from rivers: from 73–79% in the basins of the Pechora, Lena, and Kolyma to 85–90% in the basins of other rivers under consideration. The remaining part included groundwater (up to 10–20%), lake water, and even seawater (at the mouths of some rivers). The main water consumers in the 1980s were the industry and heat power engineering, as well as municipal services. In the basins of the Ob and Yenisei, these accounted for 80–90% of the withdrawn water, and, in the northern European Russia and Siberia, they reached almost 100% (Alekseevskii 2013). The irrigation and water supply to agricultural enterprises is among the water consumers in the steppe and forest-steppe areas in the Ob, Yenisei, and Lena basins.

Unlike the rivers of the southern seas of Russia, the major portion of water withdrawn in the basins of Arctic rivers is returned into the water bodies (Fig. 2). The difference between these volumes is the irrevocable water use, which leads to a systematic decrease in river water runoff (Shiklomanov 1979). In the case of the Pechora, Northern Dvina, Yenisei, and Lena, the irrevocable water use was 0.15. 0.12. 1.0, and 0.07 km³/year, respectively, or 12, 20, 19, and 16% of the initial water intake from these rivers. At the same time, the direct anthropogenic decrease in the annual runoff (as a difference, on the one hand, the withdrawal of river and ground waters and, on the other hand, the discharge of wastewater into rivers) was lesser: ~0 km³/year for the Onega, 0.09 km³/year for the Northern Dvina, ~0 km³/year for the Mezen, 0.025 km³/year for the Pechora, 0.67 km³/year for the Yenisei, 0.043 km³/year for the Lena, and 0.03 km³/year for the Kolyma, i.e. <0.1% of the annual water resources of those rivers. For other rivers, no data are available for the 1980s and 1990s.

The consumptive water use has reached its maximum values in the 1980s in the Ob–Irtys' basin (6.4 km³/year) because of the arid conditions of water supply, the higher development of the production complex, in particular, agriculture, a larger population, and the inter-basin runoff diversion. With the losses due to evaporation from reservoirs in the Ob basin and the filling of the Shul'binskoe Reservoir in the 1980s taken into account, the consumptive losses increase to 12 km³/year (or 3.1% of the Ob annual runoff in those years). If only wastewater discharges into rivers are taken into account, the value of irrevocable water use increases to 13 km³/year (or 3.4%). At the same time, the error in the average annual runoff is 2.5%. Similar estimates (12 km³/year) are given in D.Ya. Ratkovish's study (2003). For earlier years, he has obtained: 1.6 km³/year in 1936–1940, 2.4 km³/year in 1946–1950, 7.5 km³/year in 1956–1960, 8.1 km³/year in 1966–1970, and 10.2 km³/year in 1976–1980. This is maximally possible anthropogenic impact! Because, if we take into account only additional evaporation losses from reservoirs (Vuglinskii 1991) and the decrease in runoff losses in regulated rivers due to shorter duration and lesser scale of floodplain inundation (Pryakhina 2003), the anthropogenic decrease in the Ob annual runoff would be at least 6 km³/year less. In some rivers in the southern Ob–Irtys' basin and in the Ural Economic Region, the economic management of runoff has reached maximal values at which freshwater deficiency can develop (Stoyashcheva and Rybkina 2014; Magritsky 2008; Frolova and Vorob'evskii 2011). As it has been showed by the authors, in a year with median water abundance (50% exceedance probability) and under current conditions, there is no deficiency of water resources (Frolova and Vorob'evskii 2011). In low-water years (95% reliability), the natural deficiency of water resources can be seen in the basins of the Upper and Middle Irtys', Iset, and Tura. Because of the steady increase in water intake in Kazakhstan territory (from 3.5 to 4.0 km³ per year) and the high rate of increase in the consumptive water use in China (from 1 to 4 km³/year), the deficiency of natural water resources in the Russian part of the Irtys' basin during low-water period can be more than 5 km³.

The anthropogenic decrease in the Yenisei runoff, taking into account the filling of the numerous and huge reservoirs and the total evaporation from their surface, was 5.55 km³/year. According to Ratkovich D. (Ratkovich 2003), in 1936–1940, 1946–1950, 1956–1960, 1966–1970, and 1976–1980, it amounted to 0.2, 0.3, 0.8, 7.6, and 19.4 km³/year.

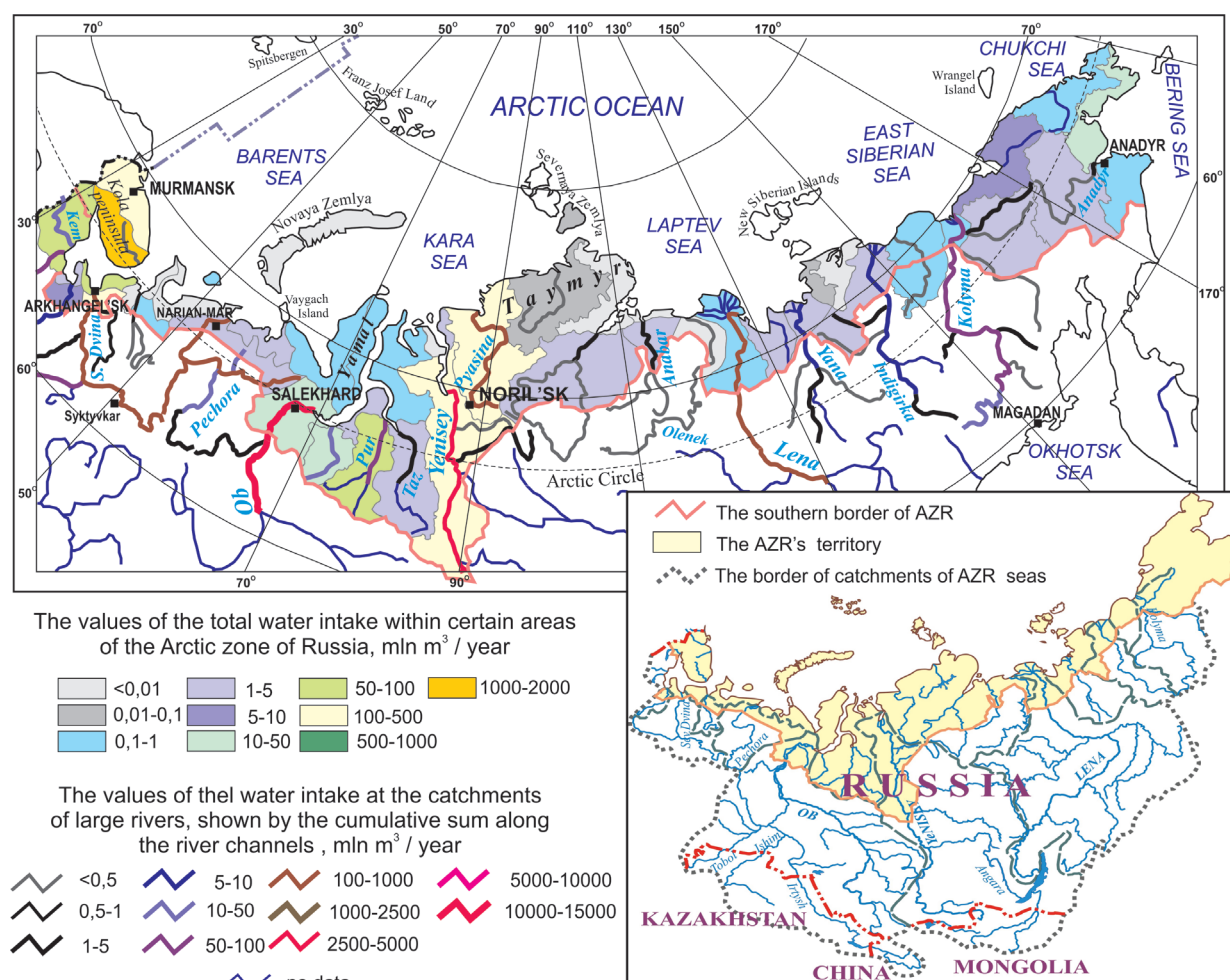


Fig. 3. Map of the present-day (2006–2017) anthropogenic withdrawal of natural waters in the basins of large Arctic rivers and in separate parts of the continental and insular Russian Arctic Zone. The left map shows the boundaries of the Arctic zone and basins of the Arctic seas of Russia

The present-day water consumption in Arctic river basins and its economic sector and territorial features

The period of maximal anthropogenic impact on river water resources was followed by years of economic crisis and a considerable decrease in water use volumes. By 2006–2017 (i.e., by the present-day stage with relatively stable water use characteristics), the total decrease in water intake volume was about 30% in the Pechora, Lena basins and for rivers of Murmansk oblast, and 50% in the Northern Dvina, Yenisei, and Kolyma basins. A part of decrease in water consumption volume is due to the passage to water-saving technologies. A vivid example is the Norilsk Integrated Plant.

Currently, water intake is maximal in Murmansk oblast (1.72 km³/year), in the Northern Dvina River basin (0.64 km³/year); and, obviously, in the Ob River basin (about 14.7 km³/year: ~8.9 km³/year in RF territory, ~2.8 km³/year in Kazakhstan (National Atlas of the Republic of Kazakhstan 2010), and ~3.0 km³/year in China (Kozlov 2018); and the Yenisei River basin (2.77 km³/year) (Table 1). Water intake has increased in the Nenets and Yamalo-Nenets Autonomous Okrugs because of the intense development of the oil and gas complex (Fig. 2). However, many territories and rivers in AZR still remain beyond the water management activity (Fig. 3). Water withdrawal volume in the basins of RF Arctic seas is 21.28 km³/year (Table 2), while only within the AZR is 2.58 km³/year. In Russia in these years, the average water intake volume was 68.3 km³/year (with seawater taken into account, it is about 74). The authors' estimates of water consumption in RF Arctic sea basins given in the first part of Table 2 are in a good agreement with data from (Russian

Water Resources and Water Economy 2006–2018) for the Barents, Laptev, and East-Siberian seas; and they are 2.2 and 1.5 times greater than the characteristics for the White Sea and Kara Sea, respectively. The latter can be explained by the fact that water consumption in the territories of Kazakhstan and China is not taken into account in (Russian Water Resources and Water Economy 2006–2018).

According to SIUPWB estimates, the characteristics given above can increase in RF by a factor of 1.5 within 10–15 years, that is, approximately by 2030. This will not cause adverse changes in water runoff of Arctic rivers, because even now it is compensated for by its climatic increase. For example, in 1976–2015, the annual river water inflow into the seas of the Russian Arctic is about 150 km³/year greater than it was in 1936–1975 (Magritsky et al. 2018).

As can be clearly seen (Table 1), the structure of water intake from some rivers has somewhat changed in compared with the 1980s. In the economic sector structure of water intake and water use, the leading sectors are industry, heat power engineering (TPS) and municipal economy. The water intake for production needs dominates exclusively (from 78 to 93%) in Murmansk oblast and Chukotskii AO (Fig. 4), in the basins of the Northern Dvina, Pechora, Yenisei, Lower Taimyra, Pyasina, Indigirka, and Kolyma rivers. The relative value of water intake for municipal needs is high in the areas where there are no or little development of industrial production. It is 63% in the Mezen basin and 53% in the basin of the Khatanga. It is relatively high in the basins of the Northern Dvina (18–25%), Ob (16–22%), Lena (25–27%), Yana (34%), Anadyr (41%), and generally, in the Arctic part of the Republic of

Table 1. Data on the volumes and structure of water use at key areas of the basins of Russian Arctic Seas in 2006–2017 according to data from (State Water Cadastre 1981–2018; Water in Russia 1991–2002; Russian Water Resources and Water Economy 2006–2018) and Reports on the State and Protection of the Environment for constituent entity of the Russian Federation

Territory	Taken from water bodies, km ³ /year		Discharged wastewater, km ³ /year		The structure of wastewater by the degree of their meeting background quality characteristics ¹ . %		
	total	including river water	total	Including those into river network	clean to meet the standards	cleaned to meet the standards	polluted
Murmansk oblast	1.715	1.526	1.681	1.681	78	1	21
Northern Dvina basin	0.641	0.596	0.549	0.545	17	3	80
Pechora basin	0.405	0.311	0.331	0.320	71	15	14
Ob basin (within RF territory)	8.900	-	6.615	6.396	53	10	37
Yenisei basin	2.765	2.212	2.398	2.350	57	5	38
Pyasina basin ¹	0.280	-	0.160	-	53	2	45
Lena basin	0.309	0.158	0.268	0.222	52	13	35
Indigirka basin ¹	0.008	-	0.004	-	23	3	74
Kolyma basin	0.059	0.053	0.036	0.034	60	20	20
the Chukotka AO	0.026	-	0.020	-	77	1	22

Note. 1 — over period 2009, 2012–2017

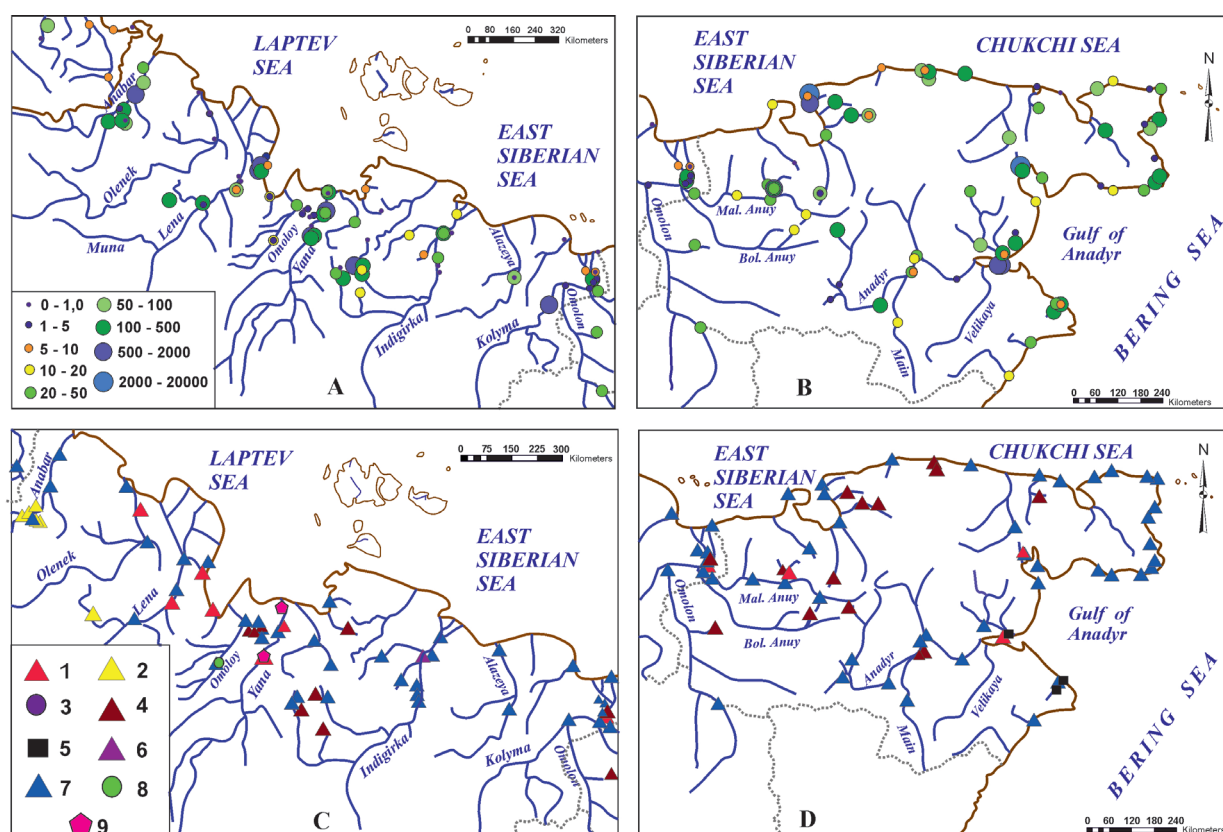


Fig. 4. The volumes of water consumption (thous. m³/year) in Arctic districts of the Republic of Sakha (Yakutia) (A) and in Chukotka Autonomous Okrug (B), and the types and distributions of the major water users (C, D): (1) heat power engineering, (2) diamond mining, (3) metallurgical plants, (4) mining, (5) coal mining, (6) petroleum tank farm, (7) municipal economy, agricultural plant, (8) transport enterprise

Sakha (Fig. 4). In the basins of the Ob, Yenisei, and Lena, a few percent are due to water intake for irrigation: 1, 2, and 7%. The data on the structure of sectoral water intake in the Pur and Taz rivers cause some questions.

The volumes of the present-day wastewater disposal into water bodies, in particular, into rivers (commonly >90%) are comparable with the volumes of their withdrawal 15.19 km³/year, or 71% of the total water intake volume. The difference between water intake and disposal

Table 2. Present-day water intake and discharge volumes in the basins of RF Arctic seas and in RF Arctic zone (AZR)

Sea	Water consumptions in sea basins			Water consumptions in the AZR		
	water withdrawal		discharges, km ³ /year	water withdrawal		discharges, km ³ /year
	total, km ³ /year	including in the basins of large rivers, %		total, km ³ /year	including in the basins of large rivers, %	
Barents	0.54	75.0	0.43	0.161	2.0	0.100
White	2.43	26.8	2.31	1.921	10.9	1.844
Kara	17.9	99.9	12.1	0.457	98.3	0.236
Laptev	0.32	99.1	0.28	0.010	78.2	0.009
East-Siberian	0.07	91.8	0.05	0.012	44.4	0.011
Chukchee	0.001	0	~0	0.001	0	~0
Bering	0.02	2.2	0.02	0.017	2.2	0.016
Total	21.28		15.19	2.58		2.22

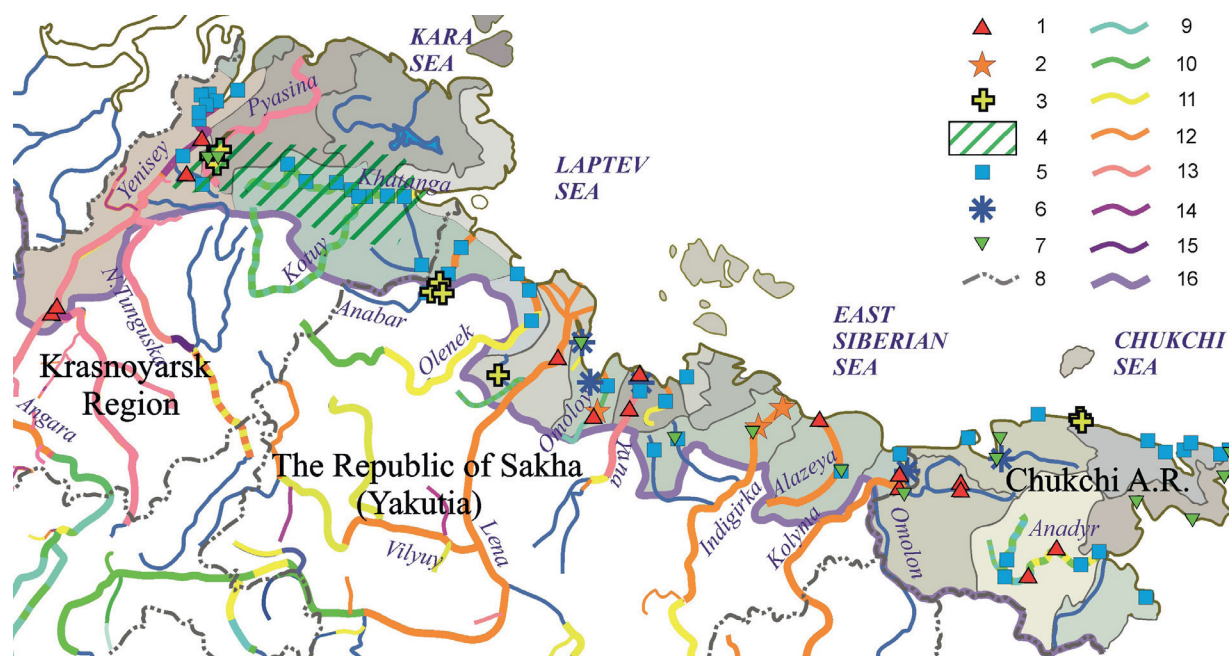


Fig. 5. The features and local features of possible hydrological restrictions in the Arctic regions of the Krasnoyarsk krai and the Republic of Sakha (Yakutia) and in the Chukotskii AO. Denotations: (1) hazard of interruption in water supply because of river flooding, (2) hazard of water supply interruption because of bank erosion and collapse, (3) restrictions because of freezing of a surface water source, (4) restrictions because of low water levels and discharges during summer-autumn dry season, (5) change of water supply sources to ice and imported water, (6) interruption of water supply because of seawater penetration into the water source, (7) other restrictions; water quality classes according to combinatorial water pollution index (KIZV): (9) relatively clean, (10) slightly polluted, (11) polluted, (12) very polluted, (13) dirty, (14) very dirty, (15) extremely dirty, (16) border of AZR

in AZR is even less (Table 2). Therefore, the non-recoverable anthropogenic losses of water runoff here are the far lowest in both the country and the world. Conversely, with the discharge in the rivers taken into account, including the previously withdrawn and used groundwater and lake water, the water use, in some cases, as it follows from Table 1, should lead to an increase in runoff.

Hydrological restrictions on water use in the Arctic

The materials of the previous section, as well as Fig. 4, Tables 1 and 2, indicate strongly that there is no general deficiency of water resources in AZR. This is the consequence, on the one hand, of the abundance of water bodies and the significant river runoff in this area and, on the other hand, the negligibly small volumes of water

intake, especially, consumptive, because of the very sparse population and the extremely low economic development of the area.

However, at the municipal level and for some water users, hydrological restrictions on water use exist (Fig. 5). The character and severity of the hydrological restrictions depend on many factors, including the type and size of the water user, its location, the type of the used natural waters, and the yield and the hydrological regime of the water source. Many factors show spatial, annual, and long-term variations.

The local hydrological restrictions in AZR can be divided into three major groups. The first group includes restrictions on the supply of freshwater to the user of a required amount. This group includes 30.5% of the water

users in the Arctic part of the Chukotskii AO, Yakutia, and Krasnoyarsk krai. The second group is related to the water quality in its source failing to meet the standards (12% does not meet, and 37% does not meet in terms of a small number of characteristics). The third group is related to inundation, damage, destruction, or silting of water intake and discharge structures, the systems of heat and water supply during ice drift, high water discharges and levels (during spring flood and rainfall freshets), as well as because of water freezing in pipes.

The limitations of the 1st type form because of the permanent, periodic, or occasional disagreement between the water abundance (reserves, yield) of a water source and the freshwater demands of a plant or a settlement because of a hydrological–morphological «dying» or seasonal shallowing, freezing, or through-freezing of a water body. Water deficiency can also form because of an increase in the user's demand. These problems can be solved in different ways, including: (1) water transfer; (2) in winter – the change of water supply to river and lake ice and other water sources, including remote, and even to seawater (as is the case with the Chaunskaya TPP in Pevek Town); (3) the construction of water accumulators – ponds and reservoirs (especially, near large populated localities, thermal and power supply facilities, and ore mining plants); (4) the rationalization of water use, e.g., the increase in the share of recycling water supply.

The situation most widespread in the Siberian part of the AZR is the freezing or even freezing through of a surface water source; the absence of acceptable groundwater (in territories with a thick and continuous permafrost stratum, in particular, in the plains of the Arctic Yakutia), and the forced conversion to pre-stored and melted river and lake ice for the heat and water supply in winter, even in populated localities with centralized water supply. The situation with water shortage and low levels in summer and autumn is also possible here, and it even has taken place in the Noril'sk urban district (in 2013 and 2016), in the eastern Taimyr Dolgano-Nenets district. However, the water demand being still not large, along with measures, efficient enough – the prompt construction of a backwater dam on the Norilka river – make this restriction still not serious nor widespread.

The restrictions of the 2nd type are typical of territories and water bodies with: (1) high background concentrations of chemicals limiting the water use, (2) anthropogenic pollution, (3) seasonal or short-time natural deterioration of water quality, for example, during spring flood, under low-water conditions, or because of seawater penetration to the water intakes within river mouths and on sea coasts. It has been found that in six rural settlements (with a total population of 3200), water supply can be occasionally interrupted because of seawater intrusion (during storm surges or low-water periods in rivers). As is known, (Magritsky et al. 2017), the damage caused by seawater intrusion is largest in Arkhangel'sk City. Here, seawater in the Northern Dvina delta can disturb the water supply to the Arkhangel'sk Hydrolysis Plant, pulp and paper plant, TPP, and municipal water supply plant.

It is assumed that the share of polluted water in wastewater structure is not large (Table 1). In fact, however (Zaitseva and Koronkevich 2003), the system of wastewater treatment is far less effective than it is formally stated.

The restrictions associated with water failing to meet quality requirements can be eliminated by water pretreating and temporary or permanent change of water source, e.g., to groundwater. However, the population of the majority of the populated localities of Krasnoyarsk krai

and the Republic of Sakha, which consume water from rivers and have no water treatment stations, have no such opportunity. Moreover, each hydrological season has its own features in the context of water quality deterioration in rivers.

Restrictions of the 3rd type – i.e., caused by a direct effect of flood water on the infrastructure taking freshwater, its treating and distribution, as well as disposal – were identified in 26 populated localities, which lie, fully or partly, in an inundation zone, and in 4 populated localities in river reaches with erodible banks. The population of such areas is 42 thousand. The latest such important event took place in Ust'-Yansk Settlement (Yakutia) in the early June 2018. Overall in AZR, about 80 populated localities suffer inundations by river water and require protection measures. Inundations in sea coasts and at river mouths can be also caused by storm surges. The surge in November 2011, which lasted for less than 2 days, inundated up to 50 km of land at the Northern Dvina mouth with a maximum depth of 1–1.5 m and inflicted damage to the cities of Severodvinsk and Arkhangel'sk with damage of \$1.5–2.0 million (Magritsky et al. 2017).

Clearly, several types of hydrological restrictions can be applicable to some water users and municipalities.

CONCLUSIONS

The Arctic zone of Russia (with islands taken into account) occupies ~18% of its territory. Even greater area (~71%) belong to the drainage basins of Arctic seas. Nevertheless, the volumes of water consumption in these areas, sparsely populated and weakly developed as they are, have been shown in this study to be relatively low. It has no effect on the water resources of Arctic rivers and river water inflow into the seas of the Russian Arctic. Moreover, the water withdrawal has dropped considerably compared with the situation in the 1980s, in particular, by about 30% in the Pechora, Lena river basins, and from the rivers of Murmansk oblast, and by 50% in the Northern Dvina, Yenisei, and Kolyma river basins. It has increased in the Nenets and Yamalo-Nenets AO because of the intense development of the local oil-and-gas complex.

Nowadays, according to the authors' estimates, 21.28 km³/year (Table 2) is being withdrawn in the drainage basins of RF Arctic seas and 2.58 km³/year, within the AZR, or 28.8 and 3.5% of the total volume in Russia. The largest contribution to this value is due to the water-management complexes in the basins of the Ob (14.7 km³/year with 60.5% being the share of RF; 19.0% that of Kazakhstan; and 20.5% that of China), Yenisei (2.77 km³/year), Northern Dvina (0.64 km³/year), and Murmansk oblast (1.72 km³/year). The major water users are the industry (with a high proportion of mining plants), thermal power engineering, and municipal economy. Their contributions vary from one basin to another and within the AZR territory. Many districts and rivers in AZR are not involved in the water management activity. This conclusion is illustrated by the original Map of Anthropogenic Withdrawal of Natural Water in the Basins of Arctic Rivers and in AZR Areas (Fig. 3).

The volumes of water discharges back into water bodies at the drainage basins of Russian Arctic seas are comparable with the volumes of freshwater withdrawal – 71% of water intake. Even lesser is the difference within AZR. That is why the irrecoverable anthropogenic losses of runoff are lower than those either in the country or in the world.

Therefore, the regional deficit of water resources is out of question. However, the economic use of runoff in

the southern part of the Ob–Irtysch basin and in the Ural Economic Region has been classified as critical since the 1970–1980s. Conversely, considerable and diverse hydrological restrictions exist at the municipal level and for some water users in AZR. These conclusions were derived from the data in the Electronic Catalogue of Water Users in AZR. It had been created by the authors, mostly, using the open publications of municipal units, such as «Schemes of Water Supply and Disposal and Heat Supply», «The Program of Integrated Development of Municipal Infrastructure Systems,» as well as SIUPWB. The analysis of these materials has shown that they can be an alternative source of reliable and diverse water-management data.

The features and seriousness of hydrological restrictions depend on many factors, including the economic sector type and the scale of water user, its location, the type of natural water used, and the yield and the hydrological

regime of a water source. Many factors vary over the area, within a year, and from year to year. The restrictions can be combined into three groups. The first is associated with problems relating the supply to a water user of the required amount of fresh water; the second relates to the restrictions because of the withdrawn water failing to meet the standards, and the restrictions of the third group are due to inundation, damage, destruction, or silting of water intake or discharge structures, the systems of heat and water supply during ice drift, high water discharges or levels, as well as water freezing in pipes. Several types of hydrological restrictions can be applicable to some water users and territorial units. These are considered in detail and generalized, in particular, in the form of various maps and diagrams, for water users of Chukotskii AO, Arctic regions of the Republic of Sakha, and Krasnoyarskii Krai. ■

REFER REFERENCES

- Agafonova S., Frolova N., Surkova G. (2017). Modern characteristics of the ice regime of Russian Arctic rivers and their possible changes in the 21st century. *Geography, Environment, Sustainability*, 10(4), 4-15, DOI:10.24057/2071-9388-2017-10-4-4-15.
- Alekseevskii N. (ed) (2007). *Geoecological State of the Russian Arctic Coast and the Safety of Nature Development*. Moscow: GEOS. (in Russian).
- Alekseevskii N., Frolova N. and Khristophorov A. (2011). *Monitoring Hydrological Processes and Improving Water Use Safety*. Moscow: Moscow State University. (in Russian).
- Alekseevskiy, N.I. (ed) (2013). *Atlas The Russian Arctic in the 21st century: environmental conditions and development risks*. Moscow: Feoriya. (in Russian).
- Amurbvu.ru (2017). Amur BWD with SIUPWB for rivers of the Chukchee and Bering seas. Official Website. [online] Available at: www.amurbvu.ru/deyatelnost/skiovo/ [Accessed 12 May 2019].
- Chernyaev A. (ed) (2000). *Water of Russia. River Basins*. Ekaterinburg: AKVA-PRESS. (in Russian).
- Demin A. (2011). *Water resources development in Russia: present-day state and forecasts*. Moscow: Water Problems Institute, Russian Academy of Sciences, 51. (in Russian).
- Dpbvu.ru (2017). Dvinsko-Peshorskoe BWD with SIUPWB of the rivers of the Kola Peninsula, Karelia, Northern Dvina, Onega, Mezen, and Pechora. Official Website. [online] Available at: www.dpbvu.ru/deyatelnost/skiovo-vklyuchaya-ndv. [Accessed 12 May 2019].
- Enbv.ru (2017). Yenisei BWD with SIUPWB for the rivers of Yenisei, Pyasina, Nizhnaya Taymyra, Khatanga, Olenek, and Lena. Official Website. [online] Available at: www.skiovo.enbv.ru [Accessed 12 May 2019].
- Frolova N. (2006). *River Hydrology: Anthropogenic Changes in River Flow*, Moscow: Moscow State University. (in Russian).
- Frolova N. and Vorob'evskii I. (2011). Hydroecological restrictions on water use in the Irtysch Basin. – *Vestn. Mosk. Univ., Ser. 5, Geography*, (6), 34-41 (in Russian).
- Khristoforov A. (2010). *Ecological–Economic Principles of Water Use*. Moscow: Moscow State University, 161. (in Russian).
- Kozlov D. (2018). Problems of transboundary use of water resources in the Irtysch basin and prospects of hydraulic engineering construction in the region. – *SB. scientific. works «Water for reclamation, water industry economy and the natural environment in a changing climate»*, (11), 32-37.
- Magritskiy D. (2008). Anthropogenic Impact on the runoff of Russian rivers emptying into the Arctic Ocean. *Water Resources*, vol. 35, (1), p.1-14, DOI: 10.1134/S0097807808010016.
- Magritsky D. (2018). Climate-induced and anthropogenic changes in water runoff in the major rivers of the Russian Federation in their lower reaches and at marine mouths. – *Present-Day Trends and Development Perspectives of Hydrometeorology in Russia: Proc. All-Russia Sci.-Pract. Conf. Irkutsk: Irkutsk State University*, 285-294. (in Russian).
- Magritsky D., Frolova N., Evstigneev V., Povalishnikova E., Kireeva, M. and Pakhomova O. (2018). Long-term changes of river water inflow into the seas of the Russian Arctic sector. – *Polarforschung*, vol. 87, (2), 177-194.
- Magritsky D., Lebedeva S. & Skripnik E. (2017). Hydrological hazards at mouths of the Northern Dvina and the Pechora rivers, Russian Federation. – *Nat. Hazards*, vol. 88(1), 149-170, DOI: 10.1007/s11069-016-2673-6.
- Magritsky D., Mikhailov V., Korotaev V. and Babich D. (2013). Changes in hydrological regime and morphology of river deltas in the Russian Arctic. – *Proc. of HP1. IAHS-IAPSO-IASPEI Assembly*, IAHS Publ. 358, 67-79.
- Mpr.gov-murman.ru (2017). Ministry of Natural Resources and Ecology of Murmansk oblast. Official Website. [online] Available at: <https://mpr.gov-murman.ru/> [Accessed 12 May 2019].
- National Atlas of the Arctic (2017). Moscow: AO Kartografiya. (in Russian).
- Nobwu.ru (2017). Nizhneobskoe BWD with SIUPWB of the rivers of Ob, Taz, Pur, and Nadym. Official Website. [online] Available at: www.nobwu.ru/index.php/ndvskiovo [Accessed 12 May 2019].
- Pryakhina G. (2003). *Assessing the effect of large reservoirs on river runoff in the lower pool*, Extended Abstract Cand. Sci. (Geogr.) Dissertation, St. Petersburg. (in Russian).
- Ratkovich D. (2003). *Actual problems of water supply*. Moscow: Nauka.
- Russian Water Resources and Water Economy: Statistical Book (2006–2018)*, Moscow: NIA-Priroda (in Russian).
- Shiklomanov I. (1979). *Anthropogenic Changes in River Water Abundance*, Leningrad: Gidrometeoizdat, 302.
- Shiklomanov I. (ed) (2008). *Water Resources of Russia and Their Use*. St. Petersburg, Gos. Gidrol. Inst.. (in Russian).
- State Water Cadastre (1982–2018). Surface and underground water resources, their use and quality*. Annual Publication, Leningrad, St. Petersburg. (in Russian).

- Stoyashcheva N. and Rybkina I. (2014). Water resources of the Ob–Irtys river basin and their use. – *Water Resour.*, 41, (1), 1-7.
- Vuglinskii V. (1991). *Water Resources and Water Balance of Large Reservoirs in the USSR*, Leningrad: Gidrometeoizdat, 223. (in Russian).
- Water in Russia (1991–2002): The State, Use, and Protection.* – Annual Publication 1986–2000: Sverdlovsk, Yekaterinburg. (in Russian).
- Zaitseva I. and Koronkevich N. (eds) (2003). *Anthropogenic Impact on Water Resources of Russia and Nearby States in the Late XX Century*. Moscow: Nauka. (in Russian).

FORECASTING WATER LEVEL OF JHELUM RIVER OF KASHMIR VALLEY INDIA, USING PREDICTION AND EARLYWARNING SYSTEM

Mirza Imran^{1*}, P. Sheikh Abdul Khader¹

¹Department of Computer Applications, B.S. Abdur Rahman Crescent Institute of Science and Technology, Vandalur Ch-600048, India

***Corresponding author:** imranmirza100@gmail.com

Received: 13th December, 2019 / Accepted: May 10th, 2020 / Published: July 1st, 2020

<https://DOI-10.24057/2071-9388-2019-169>

ABSTRACT. The hydrological disasters have the largest share in global disaster list and in 2016 the Asia's share was 41% of the global occurrence of flood disasters. The Jammu and Kashmir is one of the most flood-prone regions of the Indian Himalayas. In the 2014 floods, approximately 268 people died and 168004 houses were damaged. Pulwama, Srinagar, and Bandipora districts were severely affected with 102, 100 and 148 km² respectively submerged in floods. To predict and warn people before the actual event occur, the Early Warning Systems were developed. The Early Warning Systems (EWS) improve the preparedness of community towards the disaster. The EWS does not help to prevent floods but it helps to reduce the loss of life and property largely. A flood monitoring and EWS is proposed in this research work. This system is composed of base stations and a control center. The base station comprises of sensing module and processing module, which makes a localised prediction of water level and transmits predicted results and measured data to the control center. The control center uses a hybrid system of Adaptive Neuro-Fuzzy Inference System (ANFIS) model and the supervised machine learning technique, Linear Multiple Regression (LMR) model for water level prediction. This hybrid system presented the high accuracy of 93.53% for daily predictions and 99.91% for hourly predictions.

KEY WORDS: WSN, Early Flood Warning System, Kashmir Valley, Flood Monitoring, ANFIS, Machine Learning

CITATION: Mirza Imran, P. Sheikh Abdul Khader (2020). Forecasting Water Level Of Jhelum River Of Kashmir Valley India, Using Prediction And Earlywarning System. Geography, Environment, Sustainability, Vol.13, No 2, p. 35-42

<https://DOI-10.24057/2071-9388-2019-169>

ACKNOWLEDGEMENTS: I would like to thank two anonymous reviewers and the editor of this journal for pointing out the necessary changes to be made, which has significantly improved the quality of this manuscript. I wish to pay my gratitude to B.S. Abdur Rahman Crescent Institute of Science and Technology for providing financial support during this research work. I am thankful to Irrigation and Flood Control Department (Srinagar) and India Meteorological Department (Srinagar) NASA SRTM for providing the data.

Conflict of interests: The authors reported no potential conflict of interest.

INTRODUCTION

The Floods are the most damaging disaster in terms of property and life. Flood is the most occurring disaster in the world as compared to other types of natural disasters. (Ahern et al. 2005 & Kiran et al. 2019). Floods are influenced by many factors like precipitation, Snow-melt, Land Use-Land Cover, and built-up (Kim et al. 2009). Out of all other continents, Asia is the most affected continent (Cavallo & Noy 2011; Table 1). As it was predicted by The Intergovernmental Panel on Climate Change (IPCC 2001) that flooding will worsen in decades to come because of the climate change. The climate change induces extreme precipitation (Mishra et al. 2019), Glacier melting at faster rate, (Rafiq & Mishra 2016) extreme temperatures, cyclones, rise in ocean water levels (IPCC 2014). From 2006–2015 annual average of deaths by natural disasters was 69,827. In 2016, \$59 billion worth damages were reported for hydrological disasters and out of the top 10 countries in terms of disaster mortality, five are Asian countries and accounted for 43.2% (Guha-sapir et al. 2017). India is a rich

country when talked about river systems. India has four river systems on a large scale viz. Aravalli, Ganges, Brahmaputra, and Indus that are large both in catchment size and drainage density. All these river systems have several tributaries, which spread along the length and breadth of India which makes it more prone to floods (Mathur 2019). During August 18, 2008, Kosi floods, which impacted India and Nepal, affected more than 3 million people (Bhatt et al. 2010). Apart from this example, there are numerous large-scale hydrological disasters which left parts of India devastated like Leh flashfloods 2010 (Thayyen et al. 2013), Brahmaputra floods 2012 (Pal et al. 2013), Kedarnath flashfloods 2013 (Rafiq et al. 2019), J&K floods 2014 (Mishra 2015), and Tamilnadu floods 2015 (Mishra et al. 2016). Loss of wetlands, deforestation, Population explosion, climate change and inhabitation in high slope zones are the main reasons for the increase in these disasters (Berz 2001., Mcbean 2002. & Rafiq 2017). To mitigate the effects of floods a system is needed which can aware people before the occurrence of this hydrological disaster (Mishra & Rafiq 2019).

Table 1. Large scale flood events since last two decades in India

Event Year	Region	Casualties	Source
2004	Bihar	885	Chandran et al. (2006)
2005	Maharashtra	1,187	Singh, O. & Kumar, M. (2013)
2007	Bihar	1,287	Kumar et al. (2013)
2008	Bihar	434	Bhatt et al. (2010)
2010	Leh	255	Ashrit R. (2010)
2012	Assam	36	Pal et al. (2013)
2013	Bihar	201	Kansal et al. (2016)
2013	Uttarakhand	5,700	Rafiq et al. (2019)
2014	Jammu & Kashmir	268	Mishra et al. (2015)
2015	Chennai	400	Seenirajan et al. (2017)
2017	Bihar	294	Singh S. (2018)
2017	West Bengal	39	Singh S. (2018)
2018	Kerala	445	Vishnu et al. (2019)
2019	Bihar	139	Mishra et al. (2019b)

**Fig. 1. Manual water level monitoring on river Jhelum**

In this work, the hybrid system of Linear Multiple Regression (LMR), and Adaptive Neuro Fuzzy Inference System (ANFIS) are integrated with the wireless sensor technology to develop an early flood warning system which is backed up by solar panels to keep it running in a power failure. The Wireless Sensor Networks (WSN) were chosen because they have low power consumption with high mobility characteristic (Do et al. 2015). The system also uses GPRS and other communication modules for communication. WSN and web monitoring allow remote administration of sensor network which leads to easy maintenance of sensor networks and accuracy in monitoring (Islam et al. 2014). The Webpage, SMS and loudspeakers were used to disseminate the warning to the population, which are the easiest ways to reach out to the people (Natividad & Mendez 2018). The proposed system uses spatially distributed precipitation as input to the model. ANFIS and Multiple Linear Regression models show more accurate forecasts than Artificial Neural Network (ANN) when spatially distributed precipitation is given as input (Rezaeianzadeh et al. 2013). The aim of this work is to propose a system, which is cost effective, accurate and simple to implement. The LMR approach used in the system is fast to fit, easy to interpret and perfect to predict continuous response like water level. The proposed system uses wireless sensors to measure parameters like temperature, rainfall, and water level because of its low cost, quick response, stability, and

flexibility (Niranjan 2012), which is feasible for a developing country (Basha & Rus 2007). To monitor the water level by WSN and communication through GPRS and SMS makes it a real-time monitoring system (Sunkpho & Ootamakorn 2011). By combining sensor networks, artificial intelligence, and modern communication technology, better early warning systems can be built, as this methodology was employed by (Pengel et al. 2013) in a system which uses wireless sensors and Artificial intelligence to predict dike and embankment failure. Furthermore, WSN and machine learning when integrated together can predict floods efficiently (Roy et al. 2012).

STUDY AREA

The Jhelum River is the main river of Kashmir division, which runs along its entire length of 140 km. Most of the towns and villages are located on its banks. The width of the Jhelum river varies between 69 to 113 meters from Sangam to Ram munshibagh (Romshoo et al. 2018). The most flood-affected districts of Kashmir are Anantnag, Pulwama, Srinagar, and Bandipora. The valley does not have any Early flood warning system right now and the flood monitoring is a manual one (Fig. 1). The study area has the total area of 8603 sq/km, with 14 catchments having tributaries draining from Pir Panjal range and joining the river on the left bank and on the right

side tributaries join the river from the Himalayan range (Bhatt et al., 2017) as shown in the (Fig. 2). Sandran river, Bringi, Arapath, Lidder, Vaishow, Rambhara, Watalara, Arpal, Sasara, and Romushi are those tributaries which join the Jhelum river in Anantnag and Pulwama districts and contribute a lot to the water flow of Jhelum river (Fig. 2). For this reason, the Sangam gauge station was taken into consideration, because after Kakapora village, no other tributary joins Jhelum up to Srinagar.

DATA USED

The daily precipitation and temperature data of 30 years ranging from 1980–2010 from three meteorological stations, Pahalgam, Kokernag and Qazigund were obtained from the India Meteorological Department. The daily water-level data from 1980–2019 of Jhelum river at three gauging stations, Sangam, Rammunshibagh, and Asham was acquired from the Department of Irrigation and Flood Control Jammu and Kashmir. The watershed of the study area was generated using the SRTM Digital Elevation Model (DEM) using ArcGIS software.

METHODOLOGY

In this system, we have four base stations out of which three base stations were equipped with wireless sensors to measure different parameters and one base station namely

Sangam, where sensors are not used and data was acquired from the meteorological station. All the three WSN equipped base stations have the same architecture (Fig. 3). The system mainly depends on the wireless communication for data transmission and not on the internet because of the volatile situation of the Kashmir valley which experiences frequent internet blockade by the government for security reasons (Iqbal 2017).

The ANFIS is a multilayer feed-forward network, being so specific operations were performed on incoming signals by each node (neuron). The ANFIS is a Takagi-Sugeno model with five layers in which membership functions, inputs, and derived rules determine its structure. An optimal number of epochs (iterations in learning phase) and type of membership function determines the efficiency of the model. The ANFIS employs «if-then» rules to perform an operation (Jang 1993) which is described below for a first-order model of common two fuzzy rules (Younes et al. 2015).

Rule 1: If x_1 is A_1 and x_2 is B_1 then $f_1 = p_1x_1 + q_1x_2 + r_1$

Rule 2: if x_1 is A_2 and x_2 is B_2 then $f_2 = p_2x_1 + q_2x_2 + r_2$

Where A and B denote grade like «Low» or «Less» whereas p_1, q_1, p_2, q_2 are parameters. The Root Mean Square Error (RMSE), Mean Absolute Error (MAE) and Coefficient of Determination (R^2) statistical methods were used to evaluate the performance of the model (Antanasijevic et al. 2013).

$$RMSE = \sqrt{\sum_{i=1}^n \frac{(X_i - X_o)^2}{X}} \quad (1)$$

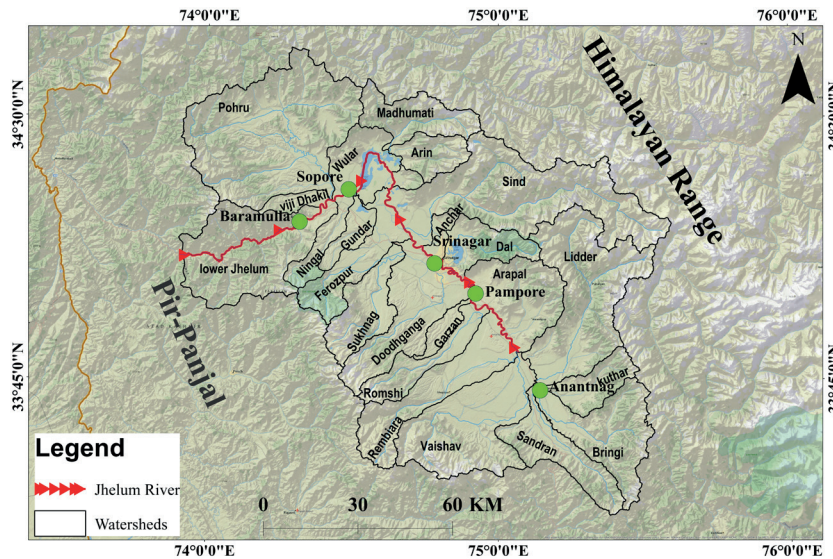


Fig. 2. Watersheds of kashmir valley with tributaries draining in river Jhelum

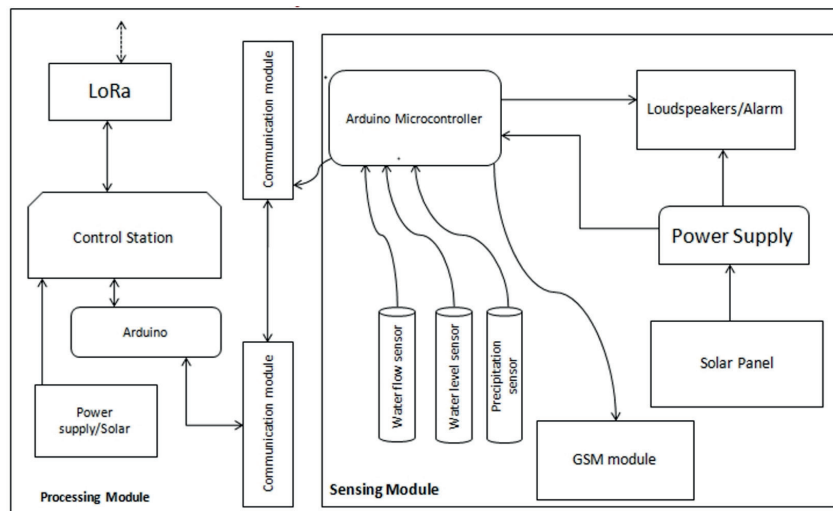


Fig. 3. Architecture of base station

$$MAE = \sum_{i=1}^n \frac{|x_i - x_0|}{n} \quad (2)$$

Coefficient of determination

$$(R^2) = 1 - \frac{\sum (x_i - x_0)^2}{\sum (x_i - \bar{x})^2} \quad (3)$$

The first and foremost thing is to select the optimal variables, which are admissible to the desired output. 120 tests were done to get the optimal number of inputs and based on these tests, the best number of inputs turned out to be four. Furthermore, the best type of membership function was determined by testing all eight types of membership functions and the hybrid type of training algorithm was used. The epoch number and membership function number was kept constant at 40 and 3 respectively. The Triangular membership function showed the best results when compared to the other membership functions as shown in table 2. This model was selected for further modification in order to enhance its performance. To finalize the best performing structure of the model, it was necessary to determine the optimum number of functions. The number of membership functions were varied from 3-6 and the epochs were kept constant at 40. The tests revealed that the optimum number of membership functions is four. The best performing membership function was selected on the basis of the smallest RMSE for training and testing.

PROPOSED SYSTEM WORKFLOW

The process of flood monitoring and early warning starts from the sensing module. The CS475A radar sensor is ideal for outdoor rough condition, calculates the distance between the sensor and the water by measuring the elapsed time between the emission and return of pulses. This data along with the data from rain measuring, tipping, self-emptying bucket, temperature sensor, and the magnetic hall-effect water-flow sensor is transmitted to the microcontroller. The Arduino 2560, which has 54 digital I/O pins with Atmega 2560 microcontroller sends the sensor data to the processing module of the base station via the HC-12 communication module, which is processed and a localised prediction about the future water level at this base station is made by finding a correlation between the rainfall and the water level.

$$L(t+Q) = L(t) + \sum_{a=-n}^{a=0} a_a R_a \quad (4)$$

Where L is the river water level, Q is the lag time, R is the rainfall, and α is the coefficient, which illustrates the correlation between water level and rainfall. The increase in the water level is directly proportional to the intensity of the rain. The data acquired through sensors is transmitted to the control center via the SX1272LoRa module. At the control center, the data is received by another SX1272 LoRa module and stored in the database. This data is later used to update the database and retrain the model. For the accurate water level prediction, the system makes use of weather forecasts from IMD (Indian Meteorological Department). The trained ANFIS model at the control center takes the forecasted values as inputs and produces an output which is the predicted value of the water level at Sangam. As we have from hourly to day to day forecasts available so this model can predict the water levels accordingly. Now, as the water level prediction for Sangam, Kakapora, Pampore and Ram munshibagh are available, The Multiple Linear Regression model takes these four predicted values as input and generates the future water level of Ram munshibagh as output which can be denoted by the equation:

$$B_4 = \beta_0 + \beta_1 B_1 + \beta_2 B_2 + \beta_3 B_3 + e \quad (5)$$

$$B_4 = 1.771 + 0.0448 B_1 + 0.4440 B_2 + 0.9260 B_3 \quad (6)$$

Where B_4 is the response variable, β_i are the coefficients, where $i = 0, 1, 2$ and 3 are regression coefficients. B_1 , B_2 , and B_3 are independent variables. The summary of the model is shown in table 3.

Then this predicted water level is compared against the five warning levels which are shown in Table 3 to determine the intensity and possibility of a flood. The intervals between the data acquisition from sensors depend upon the intensity of rain and the water level. The interval of per data acquisition from sensors starts from 15 minutes, which decreases with an increase in every warning level which is shown in (eqn. 7).

$$T_j = T_j - k_i \quad (7)$$

Where T_j is the time interval between the two consecutive measurements, Δt is the increment unit, $k_i \in \{0, 1, 2, 3, 4, \text{ and } 5\}$ is the warning level. This equation means the interval between the two measurements decreases as the warning level increases. Therefore, we will have predictions that are more accurate.

Our system has five warning levels viz. Normal, High, Very High, Critical, and Flood. The time intervals of these warning levels are shown in Table 4.

Table 2. Membership functions with respective test values

Function Type	RMSE ^{train}	RMSE ^{test}	MAE ^{train}	MAE ^{test}	R-sq ^{train}	R-sq ^{test}
triangular Membership function (trimf)	2.1357	3.3613	0.286	0.561	0.997	0.993
trapezoidal membership function (trapmf)	2.2750	3.6257	0.317	0.601	0.991	0.987
generalized bell membership function (gbellmf)	2.1485	7.4029	0.292	1.013	0.963	0.959
gaussian membership function (gaussmf)	2.1556	4.2192	0.307	0.843	0.981	0.976
gaussian combination membership function (gauss2mf)	2.2727	4.5048	0.319	0.775	0.978	0.969
pi-shaped membership function (pimf)	2.3343	3.8190	0.395	0.741	0.981	0.975
Difference between two sigmoidal membership functions (dsigmf)	2.2188	7.9834	0.296	1.107	0.985	0.905
Product of two sigmoidal membership functions (psigmf)	2.2201	7.8919	0.399	1.091	0.957	0.893

Table 3. Summary of LMR model

S	R-sq	R-sq(adj)	R-sq(pred)
0.180179	98.82%	98.78%	98.68%

Table 4. Warning levels and corresponding time intervals

Level 1	Level 2	Level 3	Level 4	Level 5
Normal	High	Very High	Critical	Flood
15 Minutes	10 minutes	5 minutes	1 minute	1minute

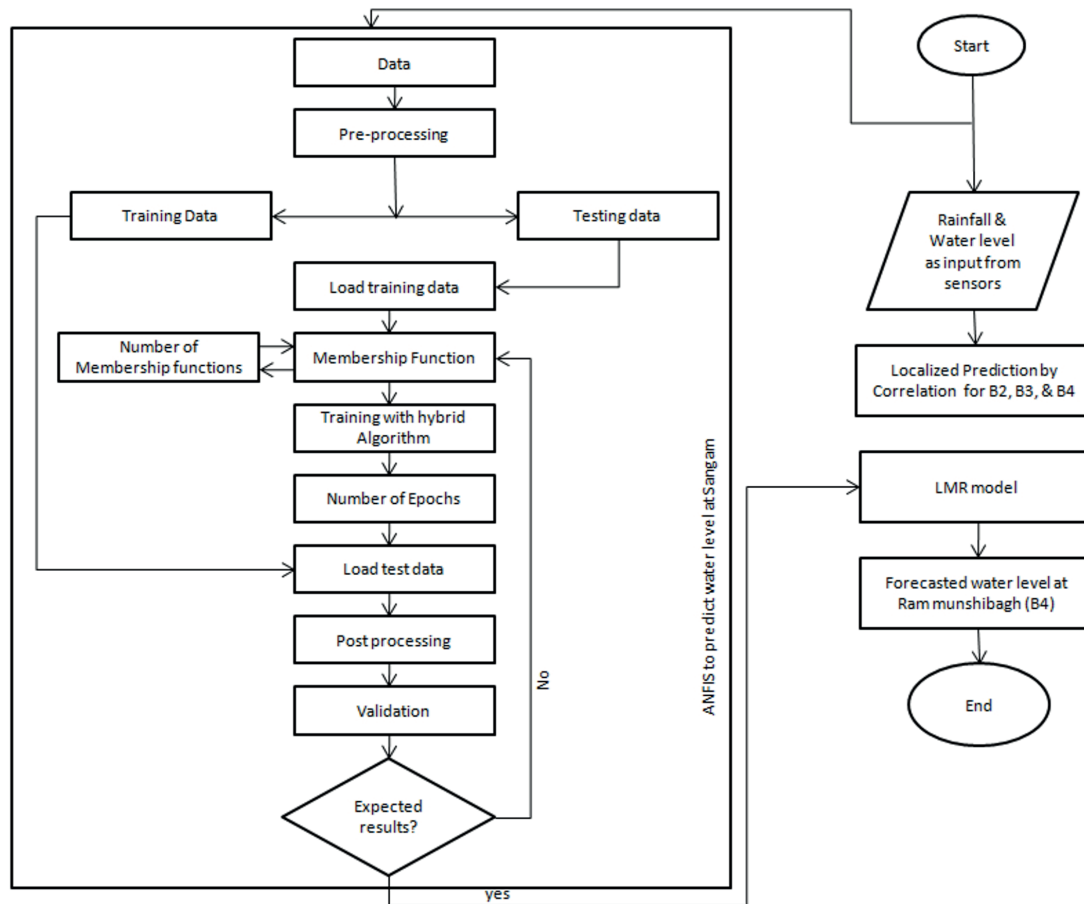


Fig. 4. Flowchart of The Proposed system

RESULTS AND DISCUSSION

The proposed system was used to predict the water levels of river Jhelum at Srinagar. The ANFIS model was used to predict water level at Sangam or base station B1 because all the data was available to develop the model. The developed model has 256 rules, four-member functions for each input parameter and one output function. The efficiency of the ANFIS was evaluated using RMSE, MAE and R2 tests. The model achieved RMSEtrain (0.4306), RMSEtest (0.6109), MAEtrain (0.0623), MAEtest (0.0783), R2train (0.972) and R2test (0.966). These results were achieved at epoch number 230 and increasing epochs after that did not show any improvement in the model. The model showed that the predicted values and the measured values were almost equal with residuals falling between ± 1 which signifies the efficiency of the model. The results were accurate with an accuracy of 93.53% for daily predictions and 99.91% for hourly predictions (Fig. 5, 6)

The accuracy of the system in short-term predictions is better than the long-term predictions. The accuracy of the system depends on the accuracy of forecasted values of the precipitation and temperature.

In our regression model The R-sq is the regression coefficient, which determines how well the model fits our data (Dar 2018) and 98.82% is quite acceptable in our scenario (Table 5). The Adjusted R-sq value fuses the

number of indicators in the model to enable you to pick the right model. The difference in the R-sq and Adjusted R-sq value for a predictor shows the contribution of that predictor in improving the model. A model with higher predicted R2 values has better prediction ability and in our case 98.68% is excellent. Usually, 0.05 significance level works well but, in our model, we got the P-value of 0.038, 0.015, 0.014, 0.008 this signify that the association between response and each term is statistically significant. The Variance Inflation Factor of 3.36, 3.39, and 4.27 for respective variables is moderate inflation of variance of a coefficient due to correlation among the predictors in our model. The acceptable range is 10 and the regression coefficient is poorly estimated if the VIF value is greater than 10 (Babin & Anderson 2014).

In Fig. 6, The probability plot of residuals approximately follows a straight line with the least number of outliers. The residuals versus fits plot verify that there is no recognizable pattern in the points and the residuals are randomly distributed and fall randomly on both sides of 0 (Fig. 7). For all observations, the distribution of residuals is shown by the histogram of the residuals and which shows only two outliers. The order in which data were collected is displayed by the residuals versus order plot. No trends or patterns are shown in residuals and thus indicating that there is no correlation between independent variables.

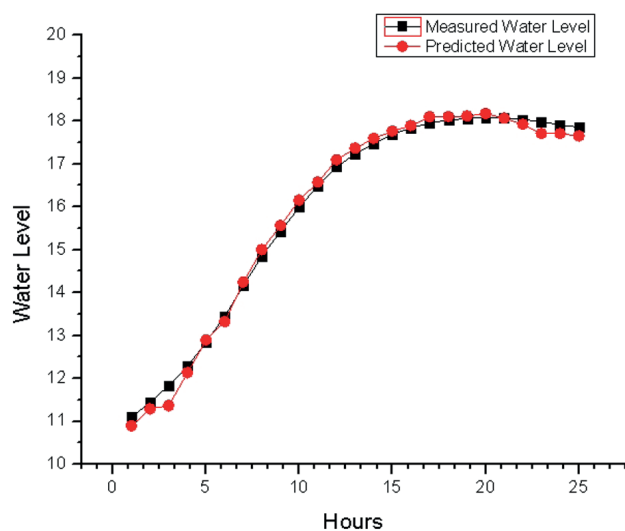


Fig. 5. Hourly Prediction Results

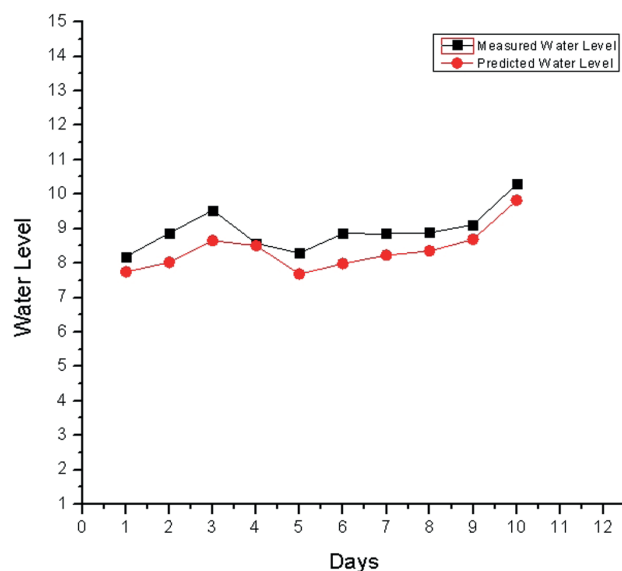


Fig. 6. Daily Prediction Results for 12 Days

Table 5. Coefficients of Regression model

Term	Coef	SE Coef	T-Value	P-Value	VIF
Constant	1.771	0.215	8.24	0.038	
B1	0.0448	0.0228	20.35	0.015	3.36
B2	0.1440	0.0791	22.57	0.014	3.39
B3	0.9260	0.0241	38.35	0.008	4.27

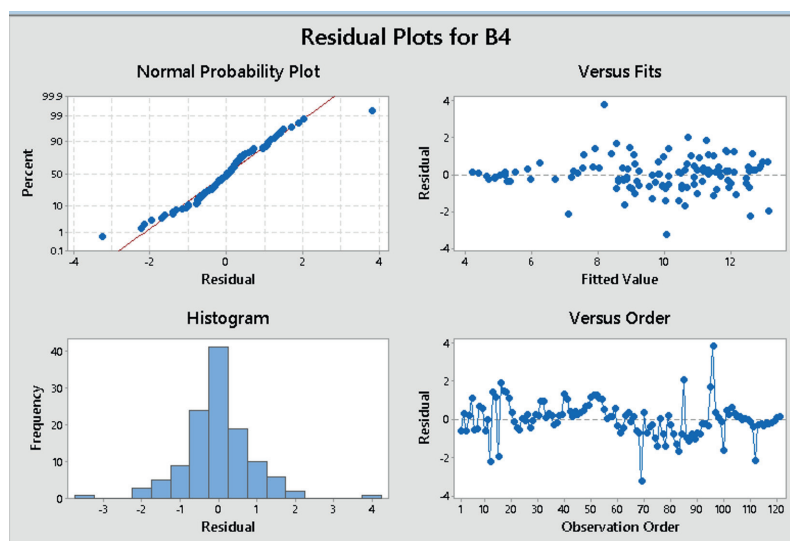


Fig. 7. Residual Plots

CONCLUSION AND FUTURE WORK

The system will have a direct effect on the resilience index of the valley and will contribute to the economy of the valley. As the system will provide lead time in flood warning which can be used in evacuation. This will lead to saving of many human lives; livestock and valuables. The system uses wireless sensors to measure the different factors contributing to the floods. Machine learning methods used the data to predict the possible water level. The system uses two machine learning models and wireless sensor network to perform the task of river monitoring and early flood warning. This hybrid approach paves the way to look into more possible and efficient hybrid methods to predict the various aspects and behaviors of this river under certain

circumstances. The proposed system is the first Early Flood Warning system devised for Jhelum basin and covers 52.3 km of Jhelum basin from Sangam village of Anantnag district to Ram munshibagh (Srinagar). In the future, we will integrate remote sensing and GIS with machine learning methods to cover the whole Jhelum basin in Kashmir from Anantnag to Baramulla district. We can use satellite-derived rainfall (Mishra & Rafiq 2017a) temperature (Rafiq et al. 2012) and other datasets (Mishra & Rafiq 2017b) to estimate run-off and develop a sophisticated, multi-dimension early warning system. To cover the whole Jhelum basin in Kashmir we have to find some cost-effective alternatives in hardware and communication between nodes for such a long basin would be a challenging task. ■

REFERENCES

- Ahern M., Kovats R.S., Wilkinson P., Few R. & Matthies, F. (2005). Global Health Impacts of Floods : Epidemiologic Evidence. *Epidemiologic Reviews* (27), 36-46, DOI: 10.1093/epirev/mxi004.
- Antanasijevi D.Z., Pocaj V.V., Povrenovi D.S., Risti M. Đ. & Peri A.A. (2013). PM 10 emission forecasting using artificial neural networks and genetic algorithm input variable optimization. *Science of the Total Environment*, (443), 511-519, DOI: 10.1016/j.scitotenv.2012.10.110.
- Ashrit R. (2010). Investigating the Leh 'cloudburst'. National Centre for Medium Range Weather Forecasting. Ministry of Earth Sciences, India.
- Basha E. & Rus D. (2007). Design of Early Warning Flood Detection Systems for Developing Countries. *Information and Communication Technologies and Development. ICTD 2007*, 1-10, DOI: 10.1109/ICTD.2007.4937387.
- Berz G., Kron W., Loster T., Rauch E. & Schimetschek J., Schmieder J., Siebert A., Smolka A., Wirtz A. (2001). World Map of Natural Hazards – A Global View of the Distribution and Intensity of Significant Exposures. *Natural Hazards*, (23), 443-465.
- Bhatt C.M., Rao G.S., Farooq M., Manjusree P., Shukla A., Sharma S.V.S.P., Dadhwal V.K. (2017). Satellite-based assessment of the catastrophic Jhelum floods of September 2014, Jammu & Kashmir, India. *Geomatics, Natural Hazards and Risk*, 8(2), 309-327, DOI: 10.1080/19475705.2016.1218943.
- Bhatt C.M., Srinivasa Rao G., Manjushree P. & Bhanumurthy V. (2010). Space based disaster management of 2008 Kosi floods, North Bihar, India. *Journal of the Indian Society of Remote Sensing*, 38(1), 99-108, DOI: 10.1007/s12524-010-0015-9.
- Cavallo E. and Noy I. (2011) Natural Disasters and the Economy – A Survey. *International Review of Environmental and Resource Economics*, (5), 63-102, DOI: 10.1561/101.00000039.
- Chandran R., Ramakrishnan D., Chowdary V., Jeyaram A. & Jha A. (2006). Flood mapping and analysis using air-borne synthetic aperture radar: A case study of July 2004 flood in Bagmati river basin, Bihar. *Current Science*, 90(2), 249-256.
- Dar A.A. and Anuradha N. (2018). An Application of Taguchi L9 Method in Black Scholes Model for European Call Option, *International Journal of Entrepreneurship*, 22(1), 1-13.
- Do H.N., Vo M., Tran V., Tan P.V. and Trinh C.V. (2015). An early flood detection system using mobile networks. In 2015 international conference on advanced technologies for communications (ATC), 599-603. IEEE.
- Guha-sapir D., Hoyois P. and Below R. (2017). Annual Disaster Statistical Review 2016: The numbers and trends. *Review Literature And Arts Of The Americas*, 1-50, DOI: 10.1093/rof/rfs003.
- IPCC. (2001). Third Assessment Report (TAR) of the Intergovernmental Panel on Climate Change, Parts 1, 2 and 3, Cambridge University Press, Cambridge, UK. (1, 2, 3).
- IPCC. (2014). Climate Change 2014 Impacts, Adaptation, and Vulnerability Part B: Regional Aspects, Cambridge University Press, Cambridge, UK.
- Iqbal M. (2017). Ethnographers Lens Reviews Life in a Conflict Zone Kashmir. *International Journal of Research Culture Society*, 1(8) 80-86.
- Islam A., Islam T., Syrus M.A. and Ahmed N. (2014). Implementation of Flash Flood Monitoring System Based on Wireless Sensor Network in Bangladesh, 3rd International Conference on Informatics, Electronics & Vision 2014.
- Jang J.R. (1993). ANFIS : Adaptive-Network-Based Fuzzy Inference System. *IEEE transactions on systems, man, and cybernetics*, 23(3), 665-685.
- Joseph F., Hair Jr., William C. Black, Babin B.J. and Anderson R.E. (2014). *Multivariate Data Analysis*, 7th ed. Pearson education limited, Eidenburgh gate, Harlow.
- Mathur D.K. (2019). Application of Geospatial technologies in flood vulnerability analysis. *Disaster Advances*, 12(12), 40-45.
- Kansal M.L., Kumar P. and Kishore K.A. (2016). Need of Integrated Flood Risk Management (IFRM) in Bihar. In National conference on Water Resources and Flood Management with special reference to Flood Modelling (WRFM-2016), Surat.
- Kaur A., Ghawana T. and Kumar N. (2019). Preliminary Analysis of Flood Disaster 2017 in Bihar and Mitigation Measures. In *Proceedings of International Conference on Remote Sensing for Disaster Management*, 455-464.
- Kim S., Kim J. & Park K. (2009). Neural Networks Models for the Flood Forecasting and Disaster Prevention System in the Small Catchment. *Disaster Advances*, 2(3), 51-63.
- Kiran K.S., Manjusree P. & Viswanadham M. (2019). Sentinel-1 SAR Data Preparation for Extraction of Flood Footprints-A Case Study. *Disaster Advances*, 12(12), 10-20.
- Kumar S., Sahdeo A. and Guleria S. (2013). Bihar Floods 2007: A Field Report. National Institute of Disaster Management, Ministry of Home Affairs, Government of India, New Delhi.
- Mcbean G. (2002). Climate Change and Extreme Weather : A Basis for Action, *Natural Hazards*, 31, 177-190.
- Mishra A.K., Chandra S., Rafiq M., Sivarajan N. and Santhanam K. (2016). An observational study of the Kanchipuram flood during the northeast monsoon season in 2015, *Weather*, 9-10, DOI: 10.1002/wea.3271.
- Mishra A.K. (2015). A study on the occurrence of flood events over Jammu and Kashmir during September 2014 using satellite remote sensing. *Natural Hazards*, 78(2), 1463-1467, DOI: 10.1007/s11069-015-1768-9.
- Mishra A. K. and Rafiq M. (2017b). Analyzing snowfall variability over two locations in Kashmir , India in the context of warming climate. *Dynamics of Atmospheres and Oceans*, 79 (May), 1-9, DOI: 10.1016/j.dynatmoce.2017.05.002.
- Mishra A.K., Nagaraju V., Rafiq M. and Chandra S. (2019). Evidence of links between regional climate change and precipitation extremes over India. *Weather*, 74(6), 218-221.
- Mishra A.K., Meer M.S. and Nagaraju V. (2019b). Satellite-based monitoring of recent heavy flooding over north-eastern states of India in July 2019. *Natural Hazards*, 97(3), 1407-1412.
- Mishra A.K. and Rafiq M. (2019). Rainfall estimation techniques over India and adjoining oceanic regions. *Current Science*, (January), DOI: 10.18520/cs/v116/i1/56-68.
- Mishra A.K. and Rafiq M. (2017a). Towards combining GPM and MFG observations to monitor near real time heavy precipitation at fine scale over India and nearby oceanic regions. *Dynamics of Atmospheres and Oceans*, 80 (October), 62-74, DOI: 10.1016/j.dynatmoce.2017.10.001.
- Natividad J.G. and Mendez J.M. (2018). Flood Monitoring and Early Warning System Using Ultrasonic Sensor. *IOP Conference Series: Materials Science and Engineering*, 325(1). DOI: 10.1088/1757-899X/325/1/012020.
- Pal I., Singh S., and Walia A. (2013). Flood Management in Assam , INDIA : A review of Brahmaputra floods 2012. *International Journal of Scientific and Research Publications*, 3(10), 1-5, www.ijsrp.org/research-paper-1013/ijsrp-p2214.pdf.

- Pengel B., Shirshov G.S., Krzhizhanovskaya V.V., Melnikova N.B., Koelewijn A.R., Pyayt A.L. and Mokhov I.I. (2013). Flood early warning system: sensors and internet. *Floods: From Risk to Opportunity* (January), 445-453, DOI: 10.1177/1745691612459060.
- Rafiq M. and Mishra A.K. (2016) Investigating changes in Himalayan glacier in warming environment: a case study of Kolahoi glacier. *Environmental Earth Sciences*. 1; 75(23):1469.
- Rafiq M. and Mishra A.K. (2017). A study of heavy snowfall in Kashmir, India in January 2017. *Weather*, 99 (January), 23-25.
- Rafiq M., Mishra A.K., Romshoo S.A. and Jalal F. (2019). Modelling Chorabari Lake outburst flood , Kedarnath , India. *Journal of Mountain Science*, 16 (October 2018), 64-76.
- Rafiq M., Rashid I. and Romshoo S.A. (2012). Estimation and validation of Remotely Sensed Land Surface Temperature in Kashmir Valley. *Journal of Himalayan Ecology & Sustainable Development*, 9, 1-13.
- Rezaeianzadeh M., Tabari H., Yazdi A.A., Isik S. & Kalin L. (2013). Flood flow forecasting using ANN, ANFIS and regression models. *Neural Computing and Applications*, 25(1), 25-37, DOI: 10.1007/s00521-013-1443-6.
- Romshoo S.A., Altaf S., Rashid I., Dar R.A. (2018). Climatic, geomorphic and anthropogenic drivers of the 2014 extreme flooding in the Jhelum basin of, of Kashmir, India. *Geomatics, Natural Hazards and Risk*, 9(1), 224-248.
- Roy J.K., Gupta D. & Goswami S. (2012). An improved flood warning system using WSN and artificial neural network. 2012 Annual IEEE India Conference, (INDICON 2012), (December), 770-774, DOI: 10.1109/INDCON.2012.6420720.
- Singh Y., Deep K. and Niranjana S. (2012). Multiple Criteria Clustering of Mobile Agents in WSN, *International Journal of Wireless & Mobile Networks*, 4(3), 183-193.
- Singh O. and Kumar M. (2013). Flood events, fatalities and damages in India from 1978 to 2006. *Natural Hazards*, 69, 1815-1834, DOI: 10.1007/s11069-013-0781-0.
- Seenirajan M., Natarajan M., Thangaraj R. and Bagyaraj M. (2017) Study and Analysis of Chennai Flood 2015 Using GIS and Multicriteria Technique. *Journal of Geographic Information System*, 9, 126-140, DOI: 10.4236/jgis.2017.92009.
- Sunkpho J. and Ootamakorn C. (2011). Real-time flood monitoring and warning system. *Songklanakarin Journal of Science and Technology*, 33(2), 227-235, DOI: 10.1016/s0959-8049(11)72694-6.
- Thayyen R.J., Dimri A.P., Kumar P. and Agnihotri G. (2013). Study of cloudburst and flash floods around Leh, India, during August 4-6, 2010. *Natural Hazards*, 65(3), 2175-2204, DOI: 10.1007/s11069-012-0464-2.
- Younes M.K., Nopiah Z.M., Basri N.E.A., Basri H., Abushammala F.M., Maulud K.N.A. and Maulud K.N.A. (2015). Solid waste forecasting using modified ANFIS modeling. *Journal of the Air & Waste Management Association*, 65(10), 1229-1238, DOI: 10.1080/10962247.2015.1075919.

HAZARDOUS ICE PHENOMENA IN RIVERS OF THE RUSSIAN ARCTIC ZONE UNDER CURRENT CLIMATE CONDITIONS AND THE SAFETY OF WATER USE

Svetlana A. Agafonova^{1*}, Alexander N. Vasilenko¹

¹Faculty of Geography, Lomonosov Moscow State University, Leninskie Gory 1, 119991, Moscow, Russia

*Corresponding author: sv_andreevna@mail.ru

Received: January 21st, 2019 / Accepted: May 10th, 2020 / Published: July 1st, 2020

<https://DOI-10.24057/2071-9388-2020-12>

ABSTRACT. The ice regime of the Russian Arctic rivers and its hazardous manifestations under current climate conditions are characterized. The ice phenomena in rivers in the region determine the conditions of navigation, water supply, hydropower station (HPS) operation, and the construction of temporary ice bridges and roads. Data of more than 100 hydrological gages over period from 1936 to 2016 were used to compile various cartographic materials and to analyze the spatial variations of the dates of ice phenomena, the duration of ice-free and ice cover periods, and the maximal ice thickness. Special attention is paid to the characteristics of level regime in periods with ice phenomena. Data on the frequency of floodplain inundation during spring ice run, the hazard of ice jams, and the seasonal features of the passage of maximal annual water level are generalized.

The observed changes in ice regime characteristics and ice hazard are analyzed. The years of the start of statistically significant shift of the periods of ice phenomena, caused by both climate changes and anthropogenic impact, are identified. The increase in the duration of the ice-free period was found to be not greater than 3–4 days for East Siberian rivers, 5–6 days for the Middle and West Siberian rivers, and up to 10–12 days for the rivers in the European part. A decrease in the maximal ice thickness is most pronounced in the rivers of the Northern European Russia, where it is 10–15 cm. The frequency of floodplain inundation during spring ice run remains constant.

KEY WORDS: river ice regime, hazardous ice phenomena, climate changes, ice jams

CITATION: Svetlana A. Agafonova, Alexander N. Vasilenko (2020). Hazardous Ice Phenomena In Rivers Of The Russian Arctic Zone Under Current Climate Conditions And The Safety Of Water Use. Geography, Environment, Sustainability, Vol.13, No 2, p. 43-51

<https://DOI-10.24057/2071-9388-2020-12>

ACKNOWLEDGEMENTS: The study was supported by the Russian Foundation for Basic Research (№ 18-05-60021-Arctic).

Conflict of interests: The authors reported no potential conflict of interest.

INTRODUCTION

Studying the present-day trends in changes in the ice regime of arctic rivers and its hazardous manifestations is an important scientific and practical problem. Ice phenomena in Arctic rivers are taking place over the major part of the year. The ice regime of the rivers determines the character of water economy functioning in the territory under consideration. The time and duration of ice phenomena determine the

periods of summer navigation, and the conditions of water supply, the operation of HPSs, and temporary ice bridges and roads. The hazardous ice phenomena and processes include ice jams and hanging ice dams, which cause floods, dense ice run at high water level, through freezing of rivers, the formation of frazil ice and sludge, weak and thin ice, unstable ice cover, aufeis, earlier ice formation, and delayed ice disappearance at low water levels (Table 1) (Agafonova et al. 2017).

Table 1. Hazardous ice phenomena in Russian rivers

Engineering problem		Ice phenomena and processes
Increased water levels and flooding		Ice jams, hanging ice dams
Violation of operating conditions of various facilities	Water intakes	Through freezing, underwater ice
	Ice crossings	Low strength and thickness of ice, unstable freeze-up
	Roads and bridges	naleds (aufeis)
	Water transport	Early dates of ice appearance, late breakup and ice clearing at low water level
Damage to hydraulic structures and fleet		Ice run at high water level, ice pile-up

The study region is the Arctic zone of Russia, the boundary of which is determined by the Presidential Decree of May 2, 2014 (the most recent amendments of May 13, 2019, Kremlin.ru 2019). The Arctic zone includes several administrative formations: Murmansk oblast, some regions of the republics of Karelia and Komi, Arkhangelsk oblast, Nenets and Yamalo-Nenets Autonomous districts, some regions in Krasnoyarsk krai and the Republic of Sakha (Yakutia), the Chukotka Autonomous District, as well as the continental lands and islands in the Arctic Ocean (Fig. 1).

The climate of the Arctic zone shows a long and severe winter and a short and cool summer. The length of the period with negative air temperature averages 200–230 days for the European sector and 240 days and more for the Asian part of the territory and the lower reaches of the Pechora. The mean temperature of January decreases from west to east from -10°C in Kola Peninsula to -30°C in Taimyr peninsula and to -40°C in the basins of the Lena, Yana, and Indigirka. The number of days with temperature below -30°C in the northeastern European part of the Arctic zone is 30 and that for the central regions of Siberia is 120. The annual precipitation varies from 200 mm on the coast of the East Siberian Sea to 500 mm in the European sector. Stable snow cover lies on the average 200–250 days per year. Permafrost is common for the Arctic zone of Russia; it is insular in Kola Peninsula, mostly discontinuous from Kanin Peninsula to the Urals and continuous in the Asian part (Alekseevsky 2007; Kasimov 2017).

The major rivers in the territory are the Northern Dvina, Pechora, Ob, Yenisei, Khatanga, Olenek, Lena, Yana, Indigirka, and Kolyma, which belong to the basin of the Arctic Ocean. The water regime shows a spring (or spring–summer) flood and a stable winter low-water period. In the northeastern part, the high summer–autumn floods can be caused by the melting of snow cover, glaciers, and high-mountain snowfields, aufeis, and underground ice (Frolova et al. 2018). Because of the severe natural conditions, the runoff of the winter low-water season in the drainage basins of the Laptev, East Siberian, and Chukchi seas is very low. Some large and medium northern rivers (the Anabar, Olenek, Yana, Alazeya, Palyavaam, Amguema, etc.) will freeze through in winter.

Many rivers in Kola Peninsula and Karelia are used to generate electric power. HPS chains have been constructed on the Niva, Kovda, Tuloma, Paz, Suna, Kem, Vyg, and other rivers (Magritsky 2008). In the lower pools of HPS, ice-related problem can be due to the formation of hanging ice dams and ice jams. Considerable level rises, caused by ice jams, lead to a decrease in electric power production, which makes it necessary to regulate the regime of releases and water temperature in the lower pools. During the operation of water intakes, the intensive formation of frazil ice leads to its deposition in water intake systems, freezing and clogging of grates (Shatalina et al. 2013; Beltaos 2013).

The arctic territory of Russia is a key region of the country producing raw materials. The transport infrastructure of the Arctic zone of Russia is poorly developed, especially in its Asian part. Water transport is used for both passenger and freight traffic. Navigable rivers are used every year for Northern Delivery of Freight, primarily, fuel, into hard-to-reach areas. In the Republic of Sakha (Yakutia), for example, the route of the Northern Delivery of Freight runs downstream the Lena River toward the mouths of the Khatanga, Anabar, Olenek, Yana, Indigirka, and Kolyma and further upstream these tributaries on shallow-draft vessels. In the lower reaches of large rivers (Northern Dvina, Mezen, Pechora, Khatanga, Yenisei, etc.), large seaports are in operation. Winter navigation is taking place in the lower reaches of the Northern Dvina (Arkhangelsk port) and the Yenisei (Dudinka port) (Nokelaynen 2019). The ice conditions for river navigation are determined not only by the period of possible summer navigation (i.e., the period of ice-free channel), but also variations of the dates of ice phenomena, the periods of freezing and clearing of ice. The early freeze-up can result in a forced wintering of ships in places not adequately equipped for this.

In winter, temporary ice bridges are constructed on the Northern Dvina, Pechora, Ob, Nadya, Yenisei, and Khatanga. In large cities occupying islands or both river banks, communication between the banks are preserved, where possible, in the transitional autumn and spring periods. For example, towboats with ice reinforcement are used for this in Arkhangelsk. Another feature of river crossings in Arkhangelsk is that they cross the channel of the Northern

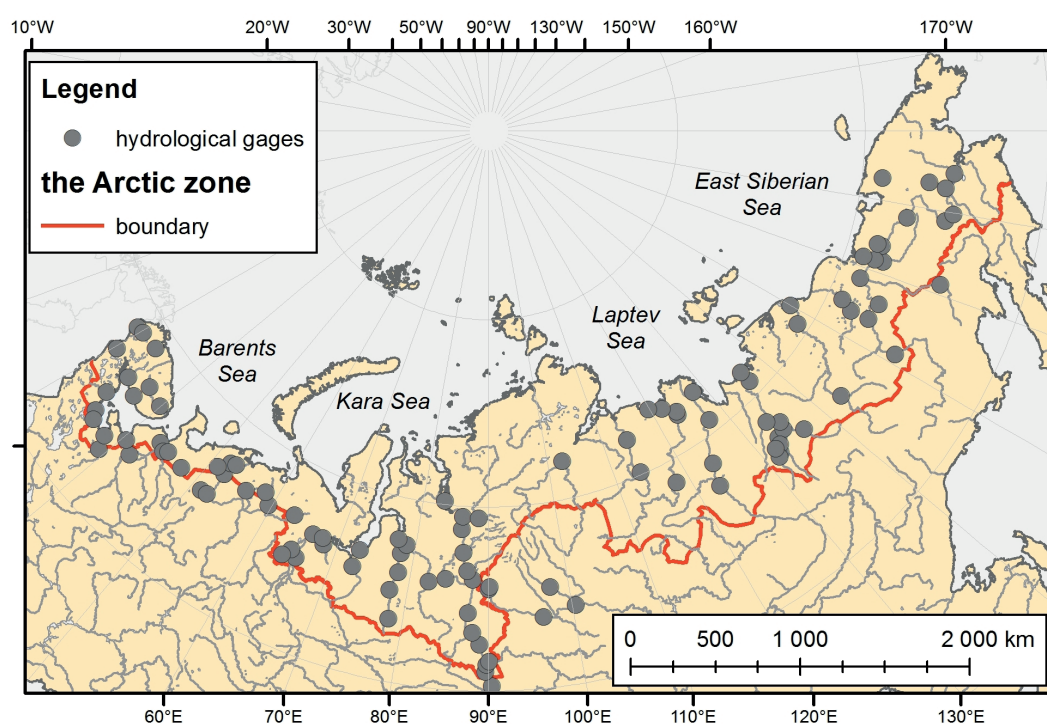


Fig. 1. The study area

Dvina with year-round navigation. In Western Siberia, because of the high density of river network, 80% of the winter road Aksarka–Salemal–Panaevsk–Yar-Sale are ice bridges. In the Republic of Sakha (Yakutia), some segments of winter roads run along the channels of rivers or branches (as, for example, part of the winter road «Arktika» from Burustakh town on the federal road R504 Kolyma to Cherskii) (Plyusnin 2014). The bearing capacity of the ice cover depends on its thickness and structure. The operation of ice bridges becomes difficult during thaws and in the cases of disturbances of ice cover with the formation of fractures and holes.

By the early XX century, only general data, mostly of descriptive character, were available on the ice regime of the major arctic rivers of Russia. Active studies of this region started in the 1930s, mostly to meet the needs of the developing navigation through the Northern Sea Route. Among the present-day studies of the hazardous ice phenomena and processes in Arctic rivers, of interest are the works analyzing the formation of hazardous water levels in periods with ice phenomena, including those that form during ice jam formation (Magritsky 2013, 2017). Earlier, the authors have assessed the hazards of the ice regime in the European sector of the Russian Arctic zone (Agafonova et al. 2016). This article, generalizes the data on the ice regime and its hazardous manifestations for the entire Arctic zone and nearby territories.

MATERIALS AND METHODS

The network of hydrological gages on rivers in the arctic region is sparse. Even at the peak of this network development in the 1980s, the researchers mentioned that its density is not satisfactory. After the 1980s, the network started rapidly declining: the number of gages on rivers had decreased by 43 and that of mouth gages, by 48%; as of January 1, 2018, the number of gages in operation in the rivers of the Arctic zone was 174, of which 58 were located at river mouths (Aari.ru 2018).

This study uses data of 100 gages, which have been operating for more than 50 years and have a drainage area of more than 5 000 km² (Fig. 1). To improve the maps for rivers in Karelia and Kola Peninsula, data from eight gages

with drainage areas from 2000 to 5000 km² were also used. The collected data included the dates of ice phenomena (appearance of ice, freeze-up, break up, and clearance of ice), their duration (period with ice phenomena, ice cover period, autumn and spring ice run), the recurrence of jams, maximal water levels during spring ice run and jam formation, the maximal ice thickness since 1936 or from the start of observations until 2016. Gaps and short series were restored by the method of hydrological analogy with the use of data on gages on rivers with similar physiographic conditions and catchment characteristics. Earlier, the authors have proposed to characterize the hazardous phenomena in ice regime by the following parameters, derived from data of observations on hydrological gages: the duration of physical navigation (i.e., a period without ice phenomena), variations of dates of ice phenomena and the duration of the periods of freezing up and breakup, the recurrence of water flooding the floodplain in the period with ice phenomena, and the frequency of the years when a maximal annual water level is accompanied by ice phenomena (Agafonova et al. 2016). The characteristic of ice regime under current conditions is based on data averaged over the past 30 years (a period from 1987 to 2016). The time variability of ice characteristics was estimated for the period from 1936 to 2016. The study used statistical methods for the analysis of data with testing series for agreement with statistical hypotheses (at a significance level of $\alpha = 5\%$) with the use of Fisher's (F-test), Student's (t-test), Andersen's (t(A)), and Spearman's coefficient of rank correlation (Spearman RCC or r_s). The statistical treatment of data and the application of the above criteria followed the recommendations given in (Kalinin et al. 2014; Ginzburg 1992, 2005). When Fisher's and Student's test were used, the break year was chosen by successively trying all years, provided that each period was longer than 30 years.

Ice Regime of the Russian Arctic Zone

The duration of the period with ice phenomena in the Arctic rivers varies, on the average, from 180 days for White Sea rivers to 260 days for northeastern rivers and rivers in the Taimyr Peninsula. The ice cover in the rivers is stable, the only exceptions being rapids, outlets from large lakes, and river segments in regions with specific hydrogeological

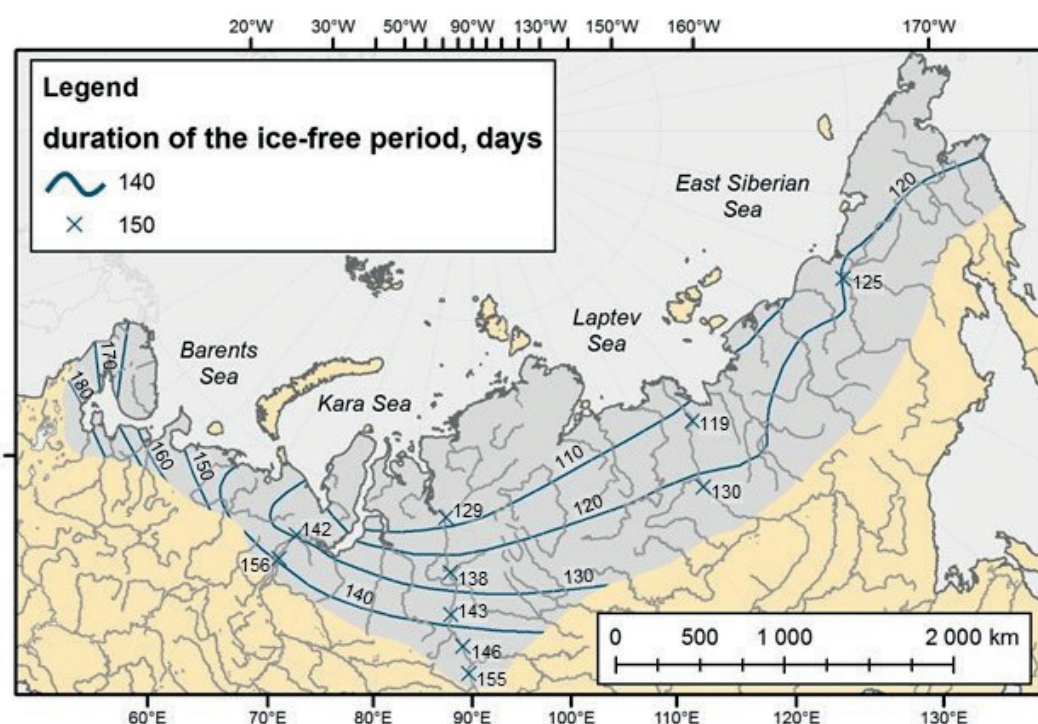


Fig. 2. Duration of the ice-free period (the average mean over 1987–2016)

conditions. Rivers do not freeze up in the zones near industrial wastewater discharge sites and downstream of HPS dams. The duration of the ice cover period varies over the area from 5 to 8.5 months. The periods with ice phenomena and ice cover in the Ob, Yenisei, Lena, and Kolyma rivers are somewhat shorter than the respective periods for the medium-size rivers. According to (Donchenko 1987), the effect of the drainage area on the shortening of these period can be seen at values in excess of 500 000 km². For example, for the Ob River at Salekhard, the average duration of the physical navigation (i.e., the period when the river is free of ice) over 1987–2016 is 15 day longer than the zonal values, the same difference for the Lena River downstream of Zhigansk is 7 days (Fig. 2).

The first ice phenomena appear, on the average, in late September in the rivers of Omolon, Malyi Anyui, in the upper part of the Yana River basin and in the Olenek River; in the rest part of the Asian Arctic sector, they appear by the middle October, and by late October–early November, they appear in the rivers of the southern White Sea coast. The freezing up of medium and large rivers is accompanied by autumn frazil and ice run. The variability of freeze-up dates determines the conditions of organization of operations on rivers – the long freezing periods reduce the period of possible operation of ice bridges. The average length of the freezing period in European rivers is about a fortnight, and that for Siberian rivers is 10 days. The average duration of the freezing period in rapid reaches of rivers in Karelia and Kola Peninsula is somewhat longer (for example, this period in the Varzuga River at Varzuga Village is 24 days long); in such river reaches hanging ice dams may occur all over the freeze-up period with water level rise reaching 3 m. The length of the freezing period in the Yenisei River varies from 6–7 (Karaul Vil., Dudinka City) to 35 days (Yartsevo Vil.). In the northwestern part of the territory, open water holes tens and hundreds kilometers in length can be seen, notwithstanding the low air temperature in winter. These holes are confined to the discharges of subpermafrost water through tectonic faults or under-bed taliks (Bol'shoi and Malyi Anyui, Omolon, etc.) (Arzhakova 2001). Aufeises can be seen in all rivers in the permafrost zone. They are of hazard to transport safety, as they clog the holes in artificial structures and cause inundation of railroads and motor roads on the nearby areas. River aufeises form at freezing up of rivers, at subsidence of ice cover under the pressure of snow or transport, at channel clogging by sediments or ice. The melting of aufeises can extend all over the warm season (Alekseev 1987).

In the majority of rivers in the Arctic zone, ice thickness is increasing throughout the ice cover period, reaching its maximal values in the last month of this period. The thickness of ice determines the loads onto the structures accompanying the thermal expansion of ice cover and changes in water level, as well as the dynamic loads during ice run and ice jam formation. Abrupt increases in ice thickness are due to water flowing over ice and freezing on it, as well as the formation of snow ice. A considerable increase in ice thickness in small rivers is often due to freezing of downstream river segments down to the bed and the absence of flow at the gage. A decrease in water flow in winter can cause the formation of ice consisting of several layers separated by spaces without water (sushnyak, sushchenets). The maximal ice thickness by the end of ice cover period vary in Kola Peninsula rivers from 0.5 in warm to 1.0 m in cold winters; the respective values in the Pechora are from 0.7 to 1.4 m. In the rivers of the Western Siberia, ice thickness for sections north of the polar circle can exceed 2.0 m; the rivers of the Yamal and Gydanskii peninsulas freeze through every year (e.g., the Shchuch'ya River at the villages of Labrovaya and Shchuch'ya remains frozen over up to 5 months). In the rivers of Eastern Siberia, ice thickness can reach over 3 m (the Lena

River, the Bykovskaya Branch, p.st. Stolb: 3.35 on May 20, 1971 and 3.04 m on May 20, 1976). For rivers of the northeastern part of the territory, because of the diverse hydrogeological conditions, at the accumulated freezing degree days (AFDD) greater than 5000°C, the average ice thickness by the end of ice cover period varies from 0.8 m (the Enmyvaam (En'muveem) River–HMS En'muveem (Mukhomornoe V.) and the Bol'shoi Anyui River–HMS Konstantinovskaya) to 2.0 m and more (the Olenek River and the Yana River with tributaries).

The main rivers of the Russian Arctic zone flow in the general direction from the south toward the north at the direction of their debacle front movement from the upper to the lower reaches. The spring ice run in the majority of rivers is accompanied by high water levels, in particular, because of the formation of ice jams. The floods induced by ice-jams are especially hazardous because they take place in cold seasons and they are accompanied by ice moving onto the banks and destroying the structures located in the flooded zone. The losses caused by ice jams are commonly far in excess of those caused by floods in ice-free periods. In addition to the inundation of the territory and damage to hydroengineering structures, long-term jams hamper the removal of ice from the river, thus reducing the navigation period. Water level rises caused by ice jams and hanging ice dams downstream of HPS dams reduce electric power production (Kozlov 2015). The rivers of Karelia, and the Onega and Northern Dvina rivers break up on the average in the late April–early May; those of Kola Peninsula, in mid-May; and the lower reaches of the Pechora River, on May 20. In the rivers of Karelia and the southern coast of the White Sea, maximal annual water levels are accompanied by ice phenomena in half of cases or more; in the lower reaches of the Ponoi, Varzuga, Northern Dvina, Mezen, and Pechora rivers, this takes place in 70–80% of cases. Large ice jams with water level rise above 3 m form in the lower reaches of the rivers of Northern Dvina, Mezen, and Pechora. Note that now the regime of spring ice run and jam formation at the delta of the Northern Dvina is changed by the annual ice-breaking operations. In the lower reaches of the Mezen and Pechora, the recurrence of floodplain inundation during spring ice run is 90% and more. In the rivers of Kola Peninsula and Karelia, water level rise at the formation of jams most often does not increase 0.5–1.0 m. The only exception is the Varzuga gage on the Varzuga River, where jam-induced water level rises can reach 3 m and more (as, for example, in 1999 and 2013). In rivers of the Belomorsko–Kulaiskoe Plateau (the Kotuga, Kepina, and Kuloi rivers), no spring ice run takes place, and maximal water levels pass after their clearing of ice (Figs. 3 and 4).

The spring ice run in the Ob River upstream of Salekhard City begins on the average in the mid-May, while the lower reaches of the Pur and Taz rivers break up in early June. Because of the high swampiness of the area, the break up period in the river is extended and the ice is far less strong at the beginning of ice run. The jam-induced water levels never exceed 1–2 m, the duration of the spring ice run in the Nadym, Pur, and Taz rivers and in the Lower Ob is 3–5 days. The duration of the spring ice run in the Polar Ural rivers is somewhat longer (in the rivers of Shchuch'ya and Sob it lasts for 7–10 days). The maximal annual water levels for most rivers in the territory were recorded during spring flood (in late May–early June). The recurrence of floodplain inundation during spring ice run for medium and large rivers is 90–100%. For such rivers (the Ob, Nadym, Pur, and Taz), maximal annual water levels coincide with ice phenomena in 80–90% of cases, while in the rest 10–20%, maximal levels are recorded in the first week after it becomes free of ice.

The average date of the start of spring ice run along the Yenisei River varies from May 5 at Yartsevo Village to June 9 (Karaul Village), and the average date of the passage of maximal

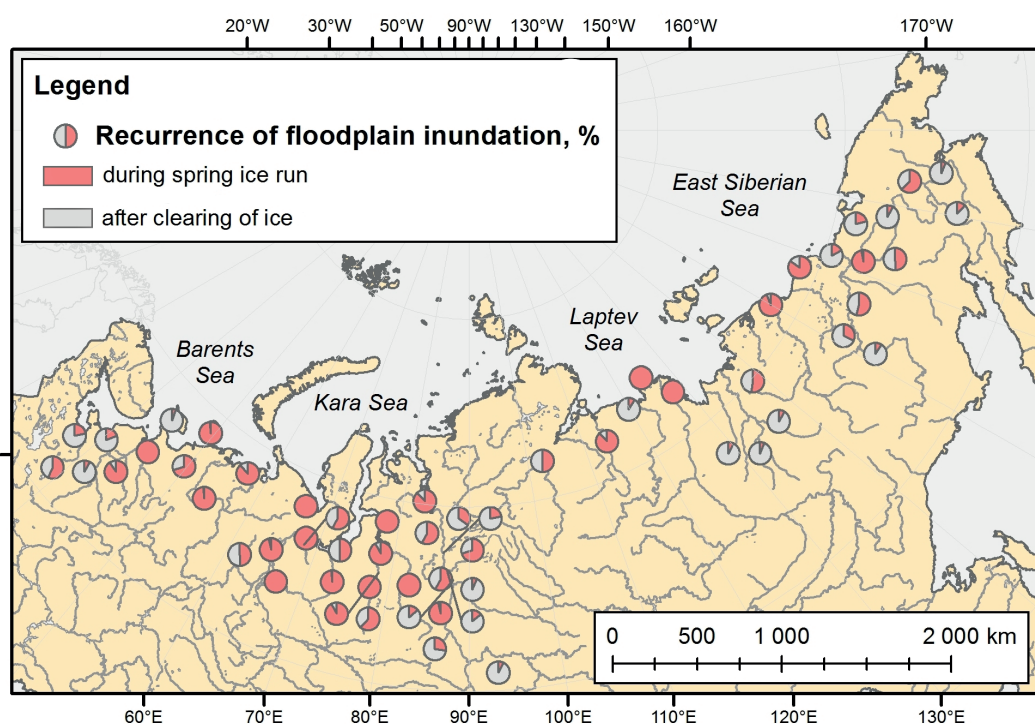


Fig. 3. Recurrence of floodplain inundation during spring ice run

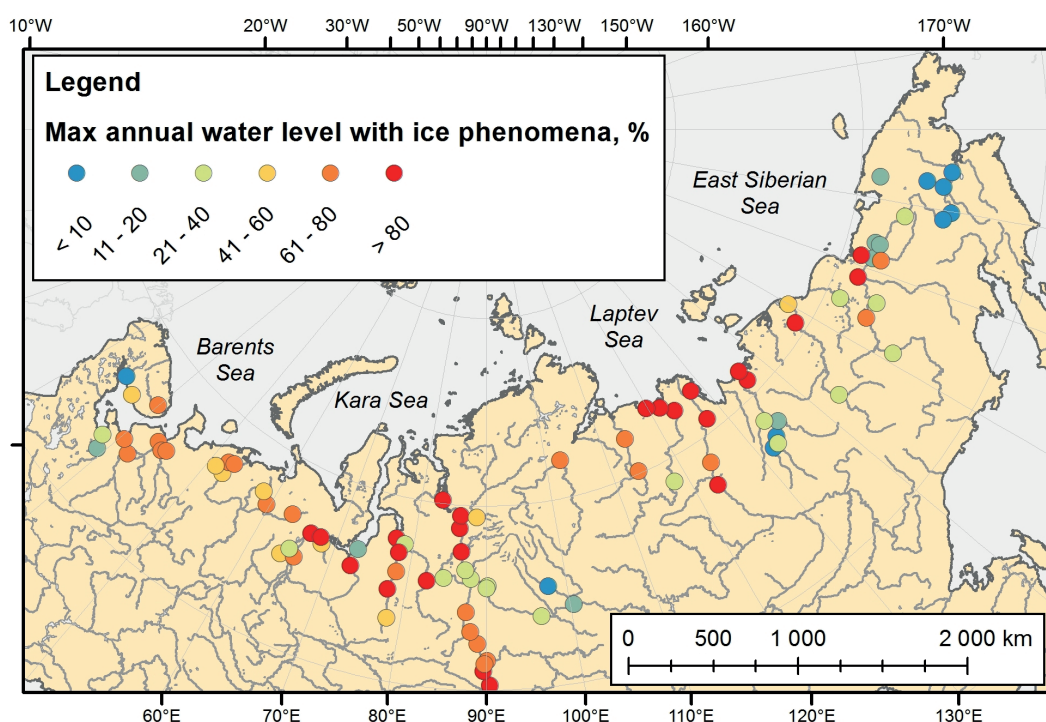


Fig. 4. Recurrence of the passage of peak water levels in periods with ice phenomena

annual water level varies from April 21 to June 9, respectively. The duration of the spring ice run in the Yenisei River in the Arctic zone of Russia decreases downstream from 13 to 5 days. Ice jams form every year during spring ice run. The depth of floodplain inundation at the formation of large jams reaches 6.5 m near Dudinka City (1999) and 3.7 m near Igarka City (1999 and 2001). In this case, the recurrence of water levels above critical marks is not high – the most recent flood in Dudinka City was recorded in 1999.

In the late May–early June, spring ice run passes in the Lena River downstream of Zhigansk Village. A characteristic feature of ice run in the lower Lena is the simultaneous break up of long river reaches and the formation of large ice jams, which stop the propagation of break up for up to 5 days. According to (Buzin 2015), the length of ice jams in the lower

part of the river is up to 150 km. The rivers that break up in the late May are the Yana (in the segment Verkhoyansk City– polar base Yubileinaya), Kolyma (Srednekolymsk C.–Kolymskoe V.), Bol'shoi and Maliy Anyui, and Anadyr; those that break up in early June are the Olenek, Indigirka (Chokurdakh V.), and Alazeya. No ice run takes place in the reaches that freeze through or where ice is thick (the ice here melts on the site). In the medium and large rivers in Eastern Siberia, the spring ice run is taking place at high water level. In the lower reaches of the Olenek, Lena, and Yana rivers, annual maximums of water level occur during spring ice run in 90% of years or more. The jam-induced level rises in the Yana, Indigirka, and Kolyma reach 5 m. In Srednekolymsk T., water levels during ice run in the recent 30 years are in excess of the critical level in 40% of cases; the latest floods during break up were recorded in

this river reach in 2012 and 2013. In the upper reaches of the Yana, Indigirka, and Kolyma and in the northeastern part of the territory, maximal annual water levels occur after clearing of ice in the period of summer–autumn rain floods.

The time variations of the dates and duration of ice phenomena in Arctic zone rivers show regularities of the spatial distribution that are common for all ice characteristics. The least values of the root-mean-square deviation are recorded in East Siberian rivers and the largest, in the rivers of the southern coast of the White Sea, and the rivers of Karelia and Kola Peninsula. In the European Sector of the Arctic, the root-mean-square deviation of the dates of ice appearance is less than that of the freeze-up. In the Asian sector of the Russian Arctic zone, the variations of the autumn dates differ only slightly. The root-mean-square deviation of ice appearance in the European sector of the Russian Arctic zone is 10–12 days, and that of freeze-up dates varies from 12 days for the Pechora to 14–16 days for the rivers of Karelia and Kola Peninsula. For the major portion of the Asian sector, variation in the autumn dates of ice phenomena is 5–7 days. The dates of debacle and clearance of ice are interrelated and have the same values of root-mean-square deviation: 7–10 days for the European sector, 7–8 days for the Western Siberia and the Yenisei, and 5–6 days for the Eastern Siberia and Northeast within the Russian Arctic zone.

Changes in ice regime characteristics in rivers

Studying the observed changes in the hydrological regime of rivers, including ice regime, is the focus of considerable recent attention. Under the project SWIPA (Snow, Water, Ice, Permafrost in the Arctic) of the Arctic Council, an international group of scientists in 2008–2011 generalized the main results of studying changes in the ice regime of Arctic rivers and the effects of these changes. This project was a continuation of ACIA Program (Arctic Climate Impact Assessment), the results of which were published in 2005. In the article (Prowse et al. 2011) the authors reveal a displacement of ice phenomena dates and correlate these changes with the global atmospheric processes. The main present-day features of Arctic climate changes are given in (Barros et al. 2014). The ice characteristics of rivers change with changes in climate conditions and water regime. The article characterizes variations in ice characteristics over period from 1936 to 2016. The data on the northeastern part of the territory are too scarce to determine variations in ice characteristics over a long period. The data contain gaps, which cannot be filled because of the lack of analogues. In fact, only data from the gage at Srednekolymsk Town on the Kolyma River are available for filling the gaps.

Analysis of the series of ice phenomena dates with the use of Anderson test showed the violation of independence only for individual gages: the autumn dates of ice appearance in the Yenisei River (in the zone of influence of runoff regulation) and the Kolyma River at Srednekolymsk City; and the spring dates in the rivers of Kola Peninsula and the lower Onega River.

In the northern European Russia, including the rivers of Kola Peninsula and Karelia, changes in the dates of ice appearance are 5–6 days for the major portion of the territory and 9–11 days for the Onega and southern Karelia. The shift of the freeze-up dates at most gages is somewhat greater (by 1–2 days) than that for ice appearance. Changes in ice appearance dates are statistically significant for the Onega River since the mid-1970s; the freeze-up dates show no statistically significant trend (by Spearman's test). The shift of the break up toward earlier dates is 6–8 days. Changes in the mean values have been statistically significant since

1972–1973 for all rivers, except for the Pechora tributaries (the Sula and Tsil'ma rivers). According to (Agafonova et al. 2007, 2009), the earlier break up of rivers in the Northern European Russia was accompanied in the recent years by low water discharges and the formation of long-term jams. This results in a smaller shift of the dates of clearance of ice (by 4–6 days toward earlier times). The longer clearance of ice reduces the navigation period not only in medium and small rivers, but also in the segments of branching in large rivers.

In West Siberian rivers within the Arctic zone of Russia, the shifts of ice appearance and freeze-up dates coincide and amount to 4–6 days toward later time; the shift of the spring dates is 6–7 days toward earlier time. The observed changes in the dates are more pronounced at the gage the Ob River–Salekhard (where the ice cover period is of particular importance because of the operation of the Labytnangi–Salekhard ice bridge) and are not observed further upstream; the shift of the average dates of ice appearance and break up are statistically significant since 1975 and 1972, respectively. At other gages, the analysis of the series with the use of Spearman coefficient of rank correlation showed that there is no statistically significant trend in any date of ice phenomena.

In the recent years, the shift of the autumn dates of ice phenomena (the appearance of ice and freeze up) toward later dates decreases along the Yenisei from Yartsevo V. to Igarka C. These changes are caused by both climatic and anthropogenic factors. Yenisei runoff regulation had its effect, primarily, on the freeze-up dates: the shift of freeze-up dates after 1963 in the segment from Yartsevo V. to Podkamennaya Tunguska V. varied from 11 to 5 days, in the downstream reach, the dates in these years did not change. In addition, runoff regulation has caused a considerable disturbance in the homogeneity of freeze-up dates in terms of variance. The breakup dates shift toward earlier times by 2–4 days for gages from Yartsevo V. to Selivanikha V. and by 5–7 days further downstream. For the gages on the Nizhnyaya Tunguska R., the autumn dates of ice phenomena changed by 2–3 days, and the spring dates, by 4–5 days. Changes in the breakup dates are statistically significant for Potapovo V., Dudinka C., and gages on the Nizhnyaya Tunguska R. since 1980.

In the rivers of Eastern Siberia, the changes in the dates of ice phenomena do not exceed 2–3 days with appreciable changes having been observed since the early 2000s. The only exception is the Olenek R.: the dates of ice appearance and break up at the gages of Sukhana HMS and Tyumeti polar base shifted by 5 days. A statistically significant trend is typical of the series of spring dates of ice phenomena at gages on the Lena R. (Zhigansk V., Dzhardzhan HMS, and Kyusyur V.). The dates of ice phenomena in the Kolyma R. at Srednekolymsk T. change, in particular, because of runoff regulation by a chain of HPSs (the Kolymskaya HPS since 1982 and the Ust-Srednekanskaya HPS since 2013); the shift of the dates is 3–4 days toward later times for autumn phenomena and 3 days toward earlier times for spring phenomena. The observed trends are statistically significant. Because of the lack of analogs, the changes in ice characteristics of rivers east of the Kolyma R. were evaluated with the use of data since 1957. In the Omoloi and Malyi and Bol'shoi Anyui rivers, the shift of ice phenomena does not exceed 2 days, and that for the Anadyr R. does not exceed 4–6 days toward later times for autumn phenomena and ~4 days toward earlier times for spring phenomena.

The decrease in the ice cover duration and the period with ice phenomena shows some spatial regularities, which

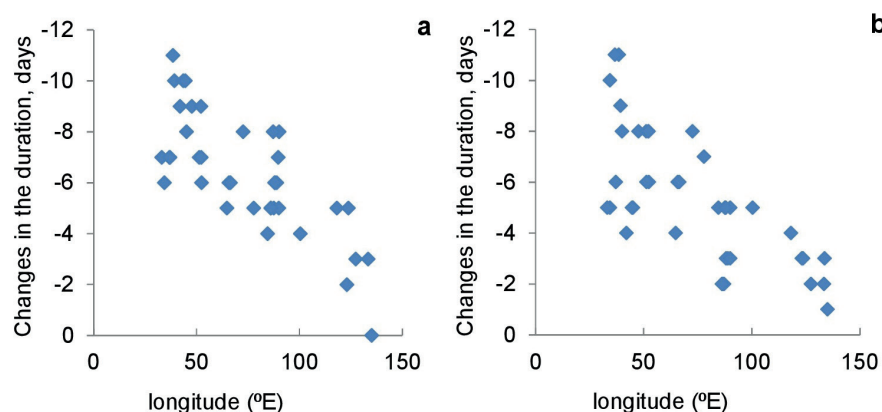


Fig. 5. Changes in the duration of ice cover (a) and ice phenomena (b) after 1987

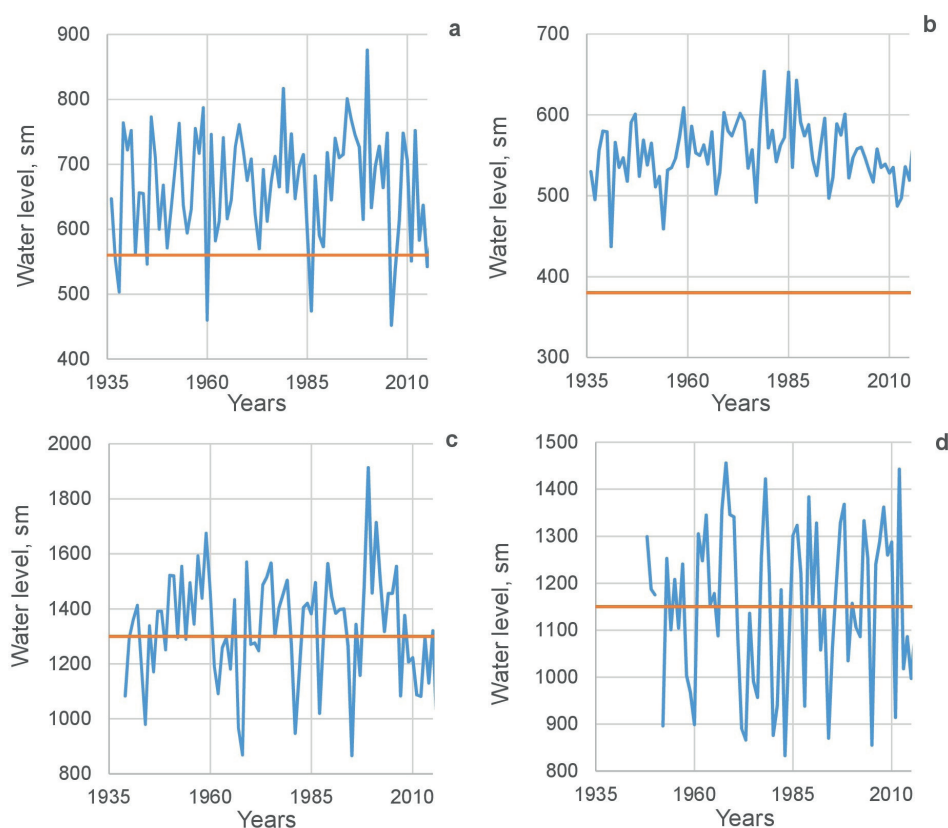


Fig. 6. Maximal ice-run water levels. (a) Mezen–Dorogorskaya, (b) Ob–Salekhard, (c) Yenisei–Dudinka, (d) Yana–Jubilejnaja (red line – level of floodplain)

are difficult to map because of the sparse gage network, but which can be expressed in terms of a dependence on the longitude. The changes are more pronounced on the European sector (up to 10–12 days for ice cover duration) and decrease eastward (they do not exceed 2–3 days for East Siberian rivers) (Fig. 5).

The observed decrease in the accumulated freezing degree days (AFDD) in winter does not lead to a considerable decrease in ice thickness in the major portion of the territory. The ice thickness in Siberian rivers sometimes reaches maximal values by the middle of the ice cover period, and the further accumulation of the accumulated freezing degree days (AFDD) has no effect on the maximal ice thickness. The result is that the change in ice thickness in East Siberian rivers does not exceed 5 cm, it can reach up to 10 cm in other Siberian rivers and the large rivers of European north, and it is only in Karelian rivers that it can increase to 10–15 cm. Changes in the temperature regime in winter, i.e., frequent thaws, may have an effect on ice cover structure in the rivers of European Arctic sector. The long freeze-up periods along with ice-holes

contribute to the formation of a large amount of frazil ice and sludge. After winter breakups the ice cover is often hummocky. Slush ice with water interlayers becomes more and more frequent in the ice structure. The changes in the characteristics of ice strength by the end of winter in the rivers of northern European Russia change the passage conditions of spring ice run in the lower reaches of the Onega, Northern Dvina, Mezen, and Pechora. It is worth mentioning that winter breakups are still few even in the European Arctic zone. For example, in winter of 2015–2016, long reaches of hummocky ice cover formed in the Northern Dvina basin with slush under ice in the upper and middle parts of the basin. In the spring of 2016, a jam formed in the Northern Dvina delta, which required the use of icebreakers to destroy.

In the recent years, the maximal ice-run water levels in the rivers of the European sector, West Siberia, and Northeastern territory showed a tendency toward a decrease. At the same time, the recurrence of floodplain inundation during spring flood remains constant for most rivers (Fig. 6). The frequency of ice jam has not changed. In

addition, there still is a hazard of formation of large jams with jam-induced floods. In the rivers of the European part, this is facilitated by the special conditions of freezing and winter breakups of rivers, as shown by various studies (Buzin et al. 2014; Agafonova et al. 2017).

CONCLUSIONS

Observation data from 100 hydrological gages in the Arctic zone of Russia over the past 30 years (since 1987 to 2016) were used to characterize the present-day ice regime and its hazardous manifestations. Periods with ice phenomena and ice cover last for the major portion of the year and average from 180 (150) days in Karelian rivers to 260 (250) days in the rivers of the northern East Siberia. The Ob, Yenisei, Lena, and Kolyma show the duration of ice phenomena somewhat shorter than the characteristic zonal values (by 15 days for the Lower Ob and by 7 days for the Lower Lena). The first ice phenomena appear, on the average, in late September in the rivers of Kolyma and Yana. The average duration of the freeze-up period in European rivers is about 2 weeks, and that for Siberian rivers is 10 days. Along the Yenisei, the duration of freezing varies from 6–7 (Karaul V., Dudinka C.) to 35 days (Yartsevo V.). The late dates of freeze-up reduce the operation periods of ice bridges, and the long freeze-up periods imply the formation of frazil ice and slush. In the river reaches with rapids in Karelia and Kola Peninsula, hanging ice dams can occur all over the ice cover period and cause water level rises up to 3 m.

In the majority of rivers in the Arctic zone, ice thickness increases all over the ice cover period, reaching its maximal values in the last month of the ice cover period. The maximal ice thickness averages ~1.0 m for the Pechora and up to 2.0 m and more for rivers in Western and Middle Siberia; it can exceed 3.0 m in some years in the Lena R. and in the upper parts of the Yana Basin. In the rivers of the northwest of the territory, because of the diversity of hydrogeological conditions, at the values of the accumulated freezing degree days (AFDD) greater than 5000°C, the average ice thickness by the end of ice cover period can vary from ~0.8 m to more than 2 m. The thickness and structure of ice cover on the rivers determines the carrying capacity of ice bridges and characterizes the ice load onto the hydroengineering structures during spring ice run.

The major rivers in the Arctic zone of Russia flow in a general direction from the south to the north with the direction of breakup front propagation from the upper to the lower reaches. The breakup of rivers is accompanied by the formation of ice jams, high water levels, and inundation of the floodplain. The damage caused by ice jams is commonly much larger than that of floods during ice-free period. In addition to inundation of the territory and damage to hydroengineering structures, long-term jams hamper the removal of ice and reduce the navigation period. In the rivers of the Northern European Russia, maximal annual water levels are accompanied by ice phenomena in 70% of cases, while in large Siberian rivers,

this share can reach 100%. The large populated localities suffering inundation during spring ice run include Arkhangelsk (Northern Dvina R.), Nar'yan-Mar (Pechora R.), Salekhard (Ob R.), Nadym (Nadym R.), Igarka and Dudinka (Yenisei R.), and Srednekolymsk (Kolyma R.).

The time variations of the dates and duration of ice phenomena in the rivers of the Arctic zone characterize the conditions of navigation planning and organization in a river. The least root-mean-square deviations are typical of rivers in Eastern Siberia (from 4 days for autumn dates and from 5 days for spring dates); and their largest values, of the rivers of the southern coast of the White Sea, and the rivers of Karelia and Kola Peninsula (14–16 days for freeze-up dates). The high variability of the dates of ice appearance and breakup requires the development of methods for ice forecasts for navigable segments of rivers.

The hazardous ice phenomena that take place in Arctic rivers largely restrict the development of water economy in territories and determine the conditions of economic development of the territory and the living conditions for the population. The result is that the economic activity mostly develops in the regions where it is economically sound. Changes in ice regime characteristics can cause new ice-related problems: a considerable reduction of the operation period of ice bridges, destructive ice jam-induced floods in winter, disturbance of water intake operations because of the excessive formation of slush, frazil ice, etc.

The observed changes in the dates and duration of ice phenomena in Arctic rivers in the period from 1936 to 2016 have taken place under the effect of natural and anthropogenic factors. In the rivers of the European north and West Siberia, statistically significant shifts of the dates of ice phenomena have been observed since the early 1970s. The decrease in the ice cover period and the period with ice phenomena over the past 30 years varies from 6 days for the Ob to 10–12 days for the Onega, Mezen, and Varzuga rivers. The shift of the autumn dates of ice phenomena toward later times decreases along the Yenisei from Yartsevo V. to Igarka C. The effect of runoff regulation in the Yenisei R. can be seen primarily in the freeze-up dates: after 1963, the change varied from 11 to 5 days in the river segment from Yartsevo V. to Podkamennaya Tunguska V. and from 5 to 7 days further downstream. In the rivers of Eastern Siberia, the shift of the dates of ice phenomena can be seen only since the early 2000s.

Notwithstanding the recent trends toward a decrease in the maximal ice-run water levels in rivers of the European sector, Western Siberia, and the northeastern part of the territory, the recurrence of flood inundation during spring ice run keeps constant in most river segments. The changed autumn–winter conditions of ice cover formation in rivers contribute to the preservation of the high recurrence of hazardous ice jams in the European sector of the Arctic. The recurrence of ice jams in Siberian rivers shows almost no changes. ■

REFERENCES

- Aari.ru. (2018). Review of the state and operation of the hydrological network in the Arctic zone of the Russian Federation, including river mouths for 2017. [online] Available at: www.aari.ru/dept/science/hydrology/review2017.pdf [Accessed 20 Dec.2018] (in Russian).
- Agafonova S., Frolova N. (2007). Specific features of ice regime in rivers of the Northern Dvina basin. *Water Resources*, 34(2), 123-131, DOI: 10.1134/S0097807807020029.
- Agafonova S., Frolova N. (2009). Influence of ice regime of the northern rivers of European Russia on the hydroecological safety under the climate changes. *Bulletin of the Moscow University. Geography*, 4, 55-61. (in Russian with English summary).
- Agafonova S., Frolova N., Krylenko I., Sazonov A., Golovlev P. (2017). Dangerous ice phenomena on the lowland rivers of European Russia. *Natural Hazards*, 88, 171-188, DOI: 10.1007/s11069-016-2580-x.
- Agafonova S., Frolova N., Vasilenko A., Shirocova V. (2016). Ice regime and dangerous hydrological phenomena on rivers of the Arctic zone of European Russia. *Bulletin of the Moscow University. Geography*, 6, 41-48. (in Russian with English summary).
- Alekseev V. (1987). *Aufeis*. Novosibirsk: Nauka (in Russian).
- Alekseevsky N. (ed) (2007). *Geoecological state of the Arctic coast of Russia and safety of environmental management*. Moscow: GEOS (in Russian).
- Arzhakova S. (2001). The winter flow of the rivers of the permafrost zone of Russia. St. Petersburg: Gidrometeoizdat (in Russian).
- Barros V., Field C., Dokken D. et al (eds.) (2014). IPCC: climate change 2014: impacts, adaptation, and vulnerability. Part B: Regional aspects. Contribution of working group II to the fifth assessment report of the intergovernmental panel on climate change. Cambridge University Press, Cambridge, United Kingdom and NewYork.
- Beltaos S. (2013). *River ice formation*. Edmonton: Committee on River Ice Processes and the Environment, Canadian Geophysical Union Hydrology Section.
- Buzin V. (2015). Hanging ice dams and ice jams on the rivers of Russia. St. Petersburg: GGI. (in Russian).
- Buzin V., Goroshkova N., Strizhenok A. (2014). Maximum ice-jam water levels on the northern rivers of Russia under conditions of climate change and anthropogenic impact on the ice jamming process. *Russian Meteorology and Hydrology*, 39(12), 823-827, DOI: 10.3103/S1068373914120061.
- Donchenko R. (1987). The ice regime of the rivers of the USSR. Leningrad Gidrometeoizdat (in Russian).
- Frolova N., Magritsky D., Kireeva M., Agafonova S., Povalishnikova E. (2018). Anthropogenic and climate-related changes in water flow and ice phenomena in Russian Arctic rivers. *Geography issues*, 145, 233-251. (in Russian).
- Ginzburg B. (2005). River freeze-up and breakup dates in the late 20th century and their possible changes in the 21st century. *Russian meteorology and hydrology*, 12, 65-72.
- Ginzburg B., Polyakova K., Soldatova I. (1992). Secular changes in dates of ice formation on rivers and their relationship with climate change. *Soviet meteorology and hydrology*, 12, 57-64.
- Kalinin V., Chichagov V. (2014). Long-term variability of ice formation dates on the rivers of the Votkinsk reservoir catchment. *Russian meteorology and hydrology*, 39(7), 491-497, DOI: 10.3103/S1068373914070085.
- Kasimov N. (ed) (2017). *National Atlas of the Arctic*. Moscow: Roscartography (in Russian).
- Kozlov D. (ed) (2015). *Dangerous ice phenomena on rivers and water reservoirs of Russia*. Moscow: RGAU–MSHA (in Russian).
- Kremlin.ru (2019). Decree of the President of the Russian Federation No. 296 of 02.05.2014. On the land territories of the Arctic zone of the Russian Federation [online] Available at: www.kremlin.ru/acts/bank/38377 [Accessed 20 Dec.2019] (in Russian).
- Magritskii D. (2008). Anthropogenic impact on the runoff of Russian rivers emptying into the arctic ocean. *Water Resources*, 35(1), 1-14, DOI: 10.1134/S0097807808010016.
- Magritsky D., Lebedeva S., Polonsky V., Skripnik E. (2013). *Journal of geographical institute «Jovan Cvijic»*, 63(3), 133-145, DOI: 10.2298/IJGI1303133M.
- Magritsky D., Lebedeva S., Skripnik E. (2017). Hydrological hazards at mouths of the Northern Dvina and the Pechora rivers, Russian Federation. *Natural Hazards*, 88(1), 149-170, DOI: 10.1007/s11069-016-2673-6.
- Nokelaynen T. (2019). Mapping the navigation conditions of arctic rivers of Russia. *Intermap. Intergis*, 25(2), 175-185. (in Russian with English summary), DOI: 10.35595/2414-9179-2019-2-25-175-185.
- Plyusnin V. (ed) (2014). *Geography of Siberia in the Early 21st Century. Vol. 3. Economy and Population of Siberia*. Novosibirsk: GEO (in Russian).
- Prowse T.D., Alfredsen K., Beltaos S., Bonsal B.R., Duguay C., Korhola A., McNamara J., Pienitz R., et al. (2011). Past and future changes in Arctic lake and river ice. *AMBIO A Journal of the Human Environment*, 40, 53-62, DOI: 10.1007/s13280-011-0216-7.
- Shatalina I., Tregub G. (2013). Ice problems of construction and operation of hydraulic structures. St. Petersburg: VNIIG. (in Russian).

INFLUENCE OF THE LARGE FLOOD ON THE ELEMENT COMPOSITION OF FLUVISOLS IN THE AMUR RIVER VALLEY

Alexander V. Martynov^{1,*}

¹ Institute of Geology and Nature Management of the Far East Branch of the Russian Academy of Sciences, Blagoveshchensk, Russia

*Corresponding author: lexx_1981@list.ru

Received: January 9th, 2019 / Accepted: May 10th, 2020 / Published: July 1st, 2020

<https://DOI-10.24057/2071-9388-2019-03>

ABSTRACT. Floodplain soils function as long-lasting stock or source of different substances, including pollutants. The main factor determining biochemical processes in fluvisols is flooding. Global climate change, which is causing more frequent and massive floods, is urging us to assess the potential environmental risks and create appropriate environmental management strategies. This study was performed to estimate the impact of a heavy flood on the total content of major elements and both total and mobile trace elements in fluvisols of one of the longest rivers in the world, the Amur. The study was conducted in field conditions by sampling from the same soil profiles before and after the flood. As a result, 10 major and 42 trace elements were distinguished. Major-element composition was determined with X-ray fluorescent method, trace-element composition - with the inductive coupled plasma mass spectroscopy. Maximum decrease of concentration was determined for CaO, MnO, P₂O₅ (up to 60%) and Sr, Cd, Ba, Tl and Pb (up to 40%). Significant increase was in concentration of Ni, Cu, and Mo (up to 160%). Among mobile trace elements, increase was observed in concentration of Sc, Ni and Th (up to 400%). With the correlation analysis, it was also established that the main causes of changes in elemental composition of the soils were decrease of pH, development of redox environment and washing out of organic matter. The main factor determining the influence of the flood on fluvisols was floodplain relief, which affected the length of the inundation, flood water velocity and the way allochthonic matter retained.

KEY WORDS: catastrophic flood, fluvisols, major elements, trace elements, Amur River

CITATION: Alexander V. Martynov (2020). Influence Of The Large Flood On The Element Composition Of Fluvisols In The Amur River Valley. *Geography, Environment, Sustainability*, Vol.13, No 2, p. 52-64

<https://DOI-10.24057/2071-9388-2019-03>

Conflict of interests: The authors reported no potential conflict of interest.

INTRODUCTION

Floodplains and fluvisols perform the function of natural drainage system in global circulation of matter since they transport major and trace elements from land to rivers, and further to seas and oceans (Zocatelli et al. 2013). Part of the migrating matter is retained in different geochemical barriers within of fluvial soils in the floodplain area, which provides their high biological efficiency and fertility (Wei & Jin-liang 2002). However, fluvisols may be subjected to heavy contamination in presence of high element contents within catchment area, of geogenic or anthropogenic origin (Förstner et al. 2004; Lair et al. 2009). Subsequently, the soils might cause pollution of the downstream areas due to remobilization, transportation and redistribution of elements (Förstner et al. 2004; Hilscherova et al. 2007). One of the main factors regulating distribution and retention of major and trace elements in fluvial soils are floods (Day et al. 1988; Zerling et al. 2006). Flood waters bring silt deposits, which vary in chemical composition and in texture (Gerrard 1987). They also feed ground waters, which determine transport of major and trace elements in soils of floodplains (Pirastu & Niedda 2013). Flood waters influence the processes of soil formation by changing redox potential (Eh), soil reaction and microbial activity, which significantly affects mobility of

elements (Abgottspon et al. 2015; Shrestha et al. 2014). The frequency and capacity of floods have recently increased, which probably caused by global climate change (Oriola & Chibuike 2016; Wölz et al. 2009). Growing events of extreme flood occurrence increases necessity to assess their impact on the element composition of soils and estimate possible environmental risks.

The main problem impeding the study of flood impact on floodplain soils is in little possibility to predict floods as well as their capacity and length (Silvestro et al. 2017). Consequently, most of the existing results showing the influence of long-lasting inundations on soil properties and their elemental composition have been obtained in laboratory or on model experiments (Abgottspon et al. 2015; Frohne et al. 2014; Unger et al. 2009). However, these results do not reflect in situ processes due to heterogeneity in time and area of content of major and trace elements in floodplains (Schulz-Zunkel et al. 2013). The latter is attributed to strong variability of biochemical and soil-forming processes occurring in floodplains (Lair et al. 2009; Tockner et al. 2016). Furthermore, most scientific works dealing with the content and behavior of major and trace elements in fluvisols take into consideration narrow range of elements (Antić-Mladenović et al. 2016; Martin 2015), whereas, analysis of wide range of elements would allow us

to distinguish associations of elements prone to accumulation or losses and, as a result, to forecast the flood consequences in the future.

In 2013, the severest in the last 120 years inundation struck the Amur River basin situated on the border of Russia and China (Makhonov & Liu Shuguang 2013; Verbitskaya 2015; Sokolova 2015). However, it was difficult to estimate the consequences of the flood for the floodplain soils due to lack of research of the fluvial soils in the area. Studies of elemental composition of fluvisols have mostly been conducted in the tributaries of the Amur, and even those were not numerous (Makhonov & Makhonova 2017; Martynov 2015; Sorokina & Zarubina 2013; Sorokina & Gusev 2014; Sorokina & Gusev 2018; Wang 2015). The only study of elemental composition of fluvisols was performed in the middle reach of the Amur River, Russian side, in 2011. Short time period between the 2011 research and the flood gave us a unique opportunity to analyze the flood consequences. Therefore, the objective of our study was to assess the impact of the severe 2013 flood on elemental composition of the fluvisols of the Amur floodplain based on comparative analysis of the soil composition before and after the flood. We also investigated the changes in relationships of different element fractions and properties of the fluvisols after the flood. We also investigated the changes in relationships of different element fractions and properties of the fluvisols after the flood. The research expands understanding of the natural procedures of element migration in fluvisols and contributes to study of soil formation processes which occur in the Amur floodplain. One of the largest rivers in the world, which has important environmental significance for Russia and China and is experiencing anthropogenic impact (Ermoshin et al. 2013).

MATERIALS AND METHODS

Study site and the properties of the soils under research

The site of study locates along the middle reach of the Amur River in Amur region, Russian Far East (Fig. 1). The River starts at the Mongolian Plateau and flows into the Sea of Okhotsk reaching the length of 4,440 km and the catchment area of 1,855 km². The River mostly has rain nourishment which comprises significant 70%. The region has monsoon climate which means that precipitation is unequal during the year. During warm period precipitation may reach 80% of annual volume which causes significant fluctuation of the river flow. Within the middle reach of the Amur River, sum of annual precipitation is 900 mm. Mean temperature during the year is

0°C, absolute temperature minimum is -45°C ranging 45–70°C during the year. The period of mean temperature over 0°C is 165–195 days, over 10°C – 120–130 days (Muranova 1966).

The study area is a floodplain area up to 10 km wide, up to 5 km long and up to 14 meters high. Soil studies were conducted in 2011 and 2014, during which 31 soil profile were set, of which samples were taken from genetic horizons. According to the results of the work, a soil map was compiled (Fig. 2). The flood in 2013 made it possible to assess its impact on various aspects of the process of soil formation, including the elemental composition of alluvial soils. For this, three soil profiles were reestablished with sampling from the same horizons. Despite the fact that most of the studied floodplain was flooded (Fig. 3), repeated sections were laid only within the riverbed floodplain. The choice of these sections is due to the fact that they are located in the zone of the longest flooding and the strongest hydromechanical impact, which is confirmed by published data (Makhonov 2017).

The hydrological characterization of the study area was performed according to the nearest hydrological post provided by the Amur Center for Hydrology and Environmental Monitoring (table 1). The post is located in the Poyarkovo village, 60 km upstream. Based on these data, in 2011 and 2012 the studied floodplain was not flooded. In 2013, the maximum level of water rise was 7.3 meters, as a result, a column of water up to 3 meters stood above the soil located within the coastal rampart. The period of direct flooding of the floodplain lasted from July 27 to September 2, which amounted to 38 days. Flooding of hydromorphic alluvial soils by groundwater was recorded even in 2014. The soil samples were classified according to the World Reference Base for soil resources (WRB 2014). We identified Haplic Fluvisols, Umbric Fluvisols and Umbric Fluvisols (HypoGleyic).

Analytical investigations

The properties of the fluvisols and their major-elemental composition were analysed in the analytical centre of mineralogy-geochemical research Institute of Geology and Nature Management FEB RAS. Granulometric composition was determined with pipette-sampling technique, organic matter was measured with wet combustion method, pH was determined with potentiometric method, cation-exchange capacity was represented by scope of calcium and magnesium, aluminum and hydrogen cations (CEC). All the analyses were conducted in accordance with generally accepted methods (Pansu 2006). Major-elemental composition was determined with X-ray fluorescent method on the spectrometer XRF-1800 Simadzu (Japan).

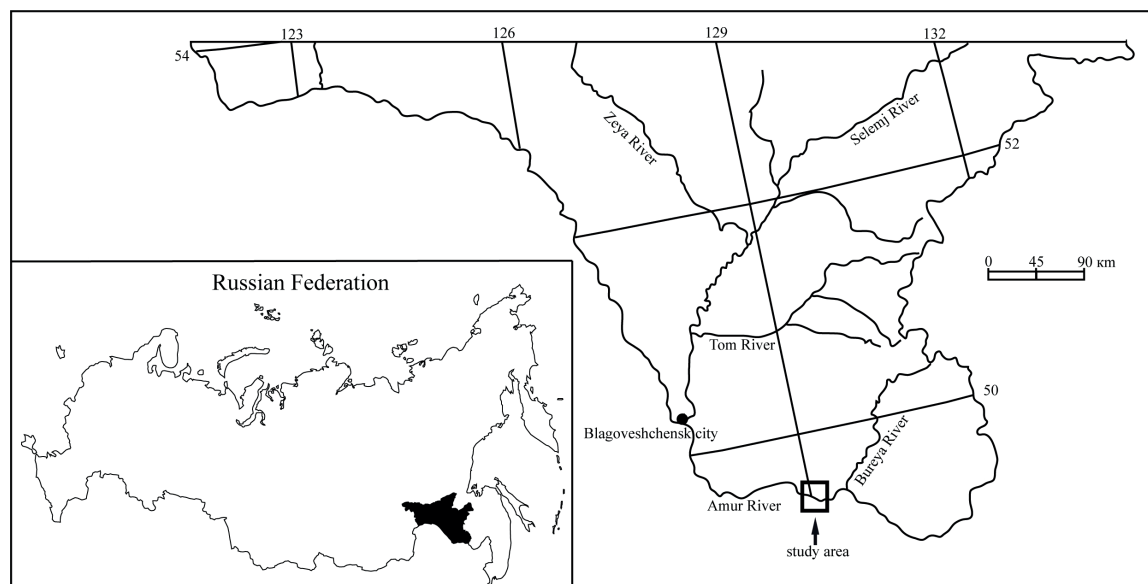


Fig. 1. Location of the study area on the territory of the Amur Region

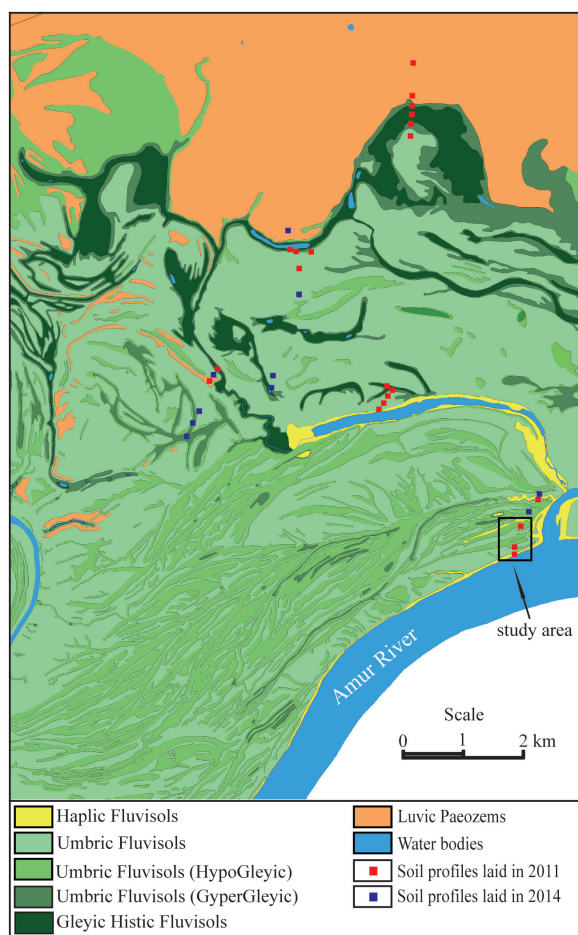


Fig. 2. A soil map of a part of the floodplain of the middle course of the Amur River based on materials from expeditions 2011 and 2014

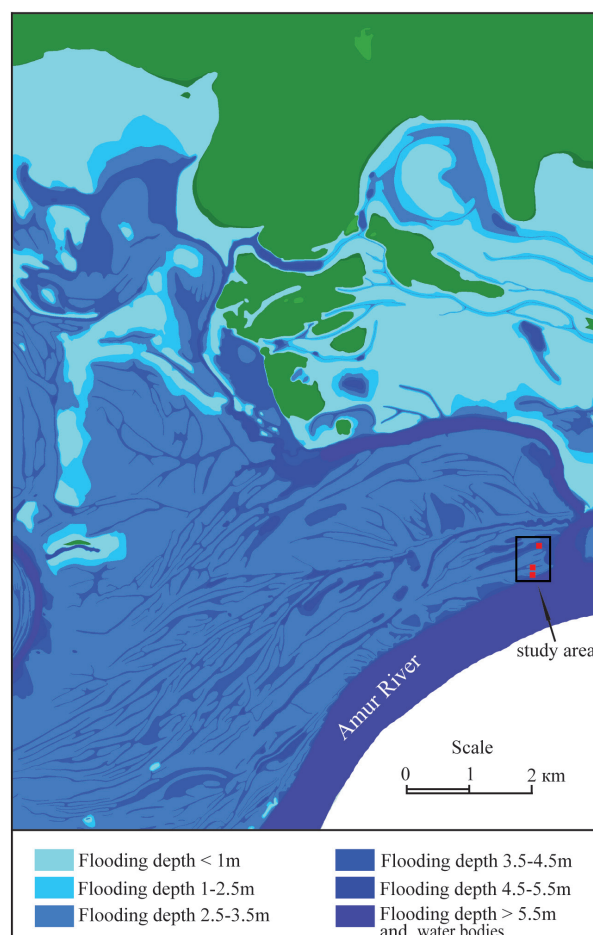


Fig. 3. Flooding model when the water level in the Amur River rises by 7 meters

Table 1. Potential technologies for extracting, generating and storing renewable energy at closed mines

	Water edge in the Amur River (cm)	The maximum level of water rise in the Amur River, relative to the edge (cm)			The height of the river bank of the shore, relative to the edge (cm)
		years			
		2011	2012	2013	
Poyarkovo village	104.0	279	285	729	476
Study area	98.4	285	291	735	460

Determination of total and mobile forms of trace elements (Zn, Cu, Cd, Pb, Be, Sc, V, Cr, Ga, As, Zr, Nb, Hf, Ta, Sr, Ba, Li, Co, Ni, Rb, Y, Mo, Sn, Sc, W, Ti, Th, U, La, Ce, Pr, Eu, Nd, Sm, Gd, Tb, Dy, Ho, Er, Tm, Yb, Lu) was carried out in the accredited analytical centre of Far Eastern Geological Institute FEB RAS (the accreditation certificate number is RA.RU.518986). Total content of trace elements was determined applying acid digestion method in mixture of acids HF, HNO₃, and HClO₄ at ratio 2,5:1:0,5. Extraction of mobile trace elements was conducted with ammonium acetate buffer at pH 4.8. The soil solutions were mineralized in microwave oven MARS-5 (CEM Corporation, USA). Analysis of wide range of elements was performed with the inductive coupled plasma mass spectroscopy Agilent 7700x (Agilent Technologies, Japan). Source data on major and trace elements contents are given in Appendix A.

Statistical analysis

The influence of the flood on the content of major and trace elements is introduced in percentage ratio of the content of the elements after the flood to the content of the elements before the flood. To visualize the ratio we applied k-means clustering. The

number of clusters was chosen in advance by using hierarchical approach (Ward's method, Manhattan distance) at a distance of 4 steps. The length of each step was 20 for major elements, 50 for total trace elements and 100 for mobile trace elements.

To determine relationships between soil properties, major and trace elements Pearson's correlation analysis was applied. Before the analysis, the variables with abnormal distribution were standardized. The found correlation coefficients were averaged according to k-means clustering. The number of clusters was chosen in advance by using hierarchical approach at a distance of 1 step with the length 10. For all calculations software STATISTICA v.7.0 was used. To create a soil map and hydrological model software «Panorama 2011» was used.

RESULTS

The properties of fluvisols before and after the flood

Profile №1 (P1). Haplic Fluvisols (Epiarenic). Soil profile (N49°24'08.38" E129°12'16.15") was set up on the foot of levee close to towpath. After the flood, the soil got slightly firmer, and humus horizon got darker.



Fig. 4. Change in the morphological appearance of profile №2 after the flood

Profile №2 (P2). Haplic Fluvisols (Epiarenic). Soil profile (N49°24'08.85" E129°12'15.72") was set up on the top of levee. After the flood, the soil was covered by sandy alluvia deposition 30 cm. The latter indicates significant water flow force in the area during the flood (Fig. 4).

Profile №3 (P3). Haplic Fluvisols (HypoGleyic). Soil profile (N49°24'23.70" E129°12'19.62") was set up in the depression of the floodplain on the bottom of a dry creek distancing 500 m from the river. After the flood, organic horizon was partially washed out, and mixed with bottom silt particles. Such morphological changes indicate high water flow velocity at the beginning of the flood. Later, the area was long inundated by waters.

After the flood, we observed decrease of soil pH and decrease of organic matter content in all studied soils. In profile 1 and 2 silt and clay contents decreased (Table 2).

Changes of major and trace element content after the flood

In terms of major-element composition, the content of elements belonging to C1 did not change much in P1 and P2, whereas in P3 the elements accumulated in upper horizon and were washed out in lower horizon (Fig. 5). Content of the elements belonging to C3 lessened in all soils, especially in P3. Content of the elements belonging to C2 differed widely in all soils though it increased in organic horizons.

Total content of trace element in P1 and P3 mostly rose after the flood (Fig. 6) though it lessened or did not change in P2. Trace elements in P1 and P3 mainly accumulated in lower horizons. Among the trace elements maximum increase in content is characterized by Ni, Cu and Mo, whereas maximum dispersion for Sr, Cd, Ba, Pb and Tl.

Content of mobile trace elements belonging to C2, C3 and C4 increased significantly in organic horizons, especially in P1 and P3. Content of elements belonging to C1 decreased almost in all studied soils (Fig. 7). Most accumulation was typical for Sc, Ni and Th.

Analysis of correlation coefficients of soil properties, major and trace elements before and after the flood

Total concentrations of trace element were divided into four clusters according to correlation coefficient (R) before the flood (Fig. 8). Clusters 2 and 4, which encompassed greater part of elements, had similar values of R. The elements had strong positive R to aluminum and magnesium oxides and to exchange cations of calcium and magnesium, characterizing cation exchange capacity (CEC). Elements belonging to C1 showed

strong R to clay particles, CEC, manganese oxide, phosphorous oxide and calcium oxide. However, Sr and Ba belonging to C3 significantly differed from other trace elements (Fig. 8), i.e. they had significant negative R to clay particles, CEC, organic matter, aluminum and magnesium oxides, but they had positive R only to potassium oxide. Significant correlations to pH and iron oxides were not revealed in trace elements.

After the flood, almost all elements united into a single cluster according to their R (Fig. 9) with the exception of Sr and Ba, whose R mirrored values of other elements. Besides, all trace elements belonging to C2 had strong correlation to clay particles, CEC, carbon, hydrogen cations, aluminum cations and aluminum and magnesium oxides.

Clusters based on relations between the content of mobile trace elements, major elements and soil properties before the flood can be divided into two groups (Fig. 10). Elements belonging to clusters 1 and 4 appeared to have strong correlation to organic matter, clay particles and also positive R to manganese and calcium oxides and pH. Clusters 2 and 3 had strong correlation to aluminum and sodium oxides, but negative R to calcium, manganese, phosphorous oxides and pH.

After the flood, mobile trace elements grouped into 3 clusters, and variation of R values between variables decreased (Fig. 11). All mobile trace elements had positive, Rs to clay particles, organic matter, CEC and oxides of aluminum, iron, magnesium and phosphorous. Elements belonging to C1 had near zero R to pH and calcium oxide though C2 and C3 elements had perfect negative R to pH and calcium oxide.

DISCUSSION

It is considered to be that floods enrich fluvisols with different elements and substances (Saint-Laurent et al. 2014; Wei & Jinliang 2002). On the other hand, there are results suggesting that floods can generate negative conditions for soil formation due to destruction of organic horizon and remobilization of organic, silt and clay particles (Saint-Laurent et al. 2010), major and trace elements (Izquierdo et al. 2012; Schulz-Zunkel et al. 2015). Our research is consistent to both assumptions to be correct as inundations wash out some elements but retain others.

Analysis of the flood impact on the content of major elements

Long-lasting inundation did not have any considerable impact on the content of Si, Al, Mg, Na or K since difference in their content was less than 10% from those values before the flood (Fig. 2). The mentioned elements being part of river

Table 2. Properties of alluvial soils before and after the flood

Profiles	Layers	Depth (cm)	Clay (%)	pH KCl	total C (%)	Ca+Mg, (mg-eq)	H+Al (mg-eq)	Clay (%)	pH KCl	total C (%)	Ca+Mg (mg-eq)	H+Al (mg-eq)
			Before flood					After flood				
P1	A	0-5	6	6.2	1	5.33	0.03	4	5.2	0.6	2.58	0.02
	C	10-15	4	5.9	0.03	0.58	0.02	3	4.8	0.06	1.84	0.01
P2	A1	0-5	8	5.4	1.3	5.94	0.06	7	5.0	0.9	5.39	0.03
	A2	20-25	12	4.1	0.9	4.31	0.49	8	4.0	0.8	4.53	0.60
	C	40-45	15	3.9	0.6	2.43	1.00	10	4.3	0.07	1.47	0.16
P3	A	0-5	20	7.3	11.3	16.49	0.04	22	4.5	5.3	17.15	0.87
	Cgi1	15-20	12	4.7	2.3	13.51	0.18	13	3.8	1.9	9.44	4.22
	Cgi2	40-45	13	4.3	1.7	9.37	0.53	14	3.9	1.8	6.98	3.11

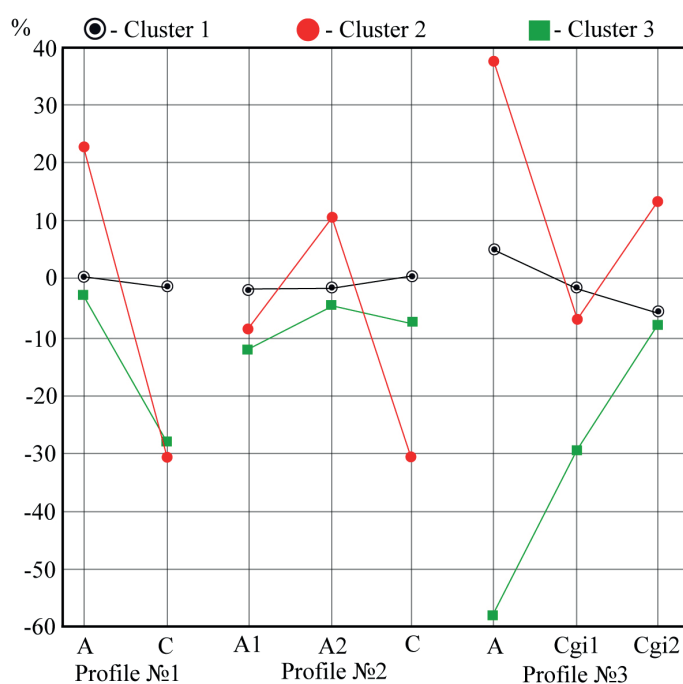


Fig. 5. Graph of average changes in the content of major elements after flooding, %:

C1: SiO₂, Al₂O₃, MgO, Na₂O, K₂O;C2: TiO, Fe₂O₃;C3: MnO, CaO, P₂O₅

deposits retaining in channel-near floodplain were mostly presented in the form of primary minerals. As primary minerals are big in size, infiltration of their oxides down the soil profile is insignificant.

Content of Mn, Ca and P oxides decreased after the flood (Fig. 2). The latter may be attributed to destruction of the upper horizons and washing out of fine particles, like in partially eroded organic horizon P3, where reduction of the elements was the severest after the flood. Besides, the decrease of the element content may be a result of redox regime change.

Long stay of flood waters favors development of redox processes (Ponnamperuma 1984). In P1 and P2, which are situated in floodplain depression, and consequently, stayed longest under the water after the flood, significant reduction of calcium oxide was observed. The latter is consistent with the reports concerning strong leaching of calcium oxides in humid conditions due to water saturation (Orlov & Bezuglova 2000). Most phosphorous in young fluvisols is concentrated in the form of primary minerals (Zehetner et al. 2008), which are not subjected to substantial influence of changes of soil properties, and are only exposed to physical loss caused by washing out

of soils. Floods may have negative influence on the content of non-mineral form of phosphorous due to reduction of sorption capacity of phosphorous under hydration conditions (Lair et al. 2009). Manganese exists in the form of primary minerals as well, but Mn+2 is prone to leaching by river waters (Sharma et al. 2016).

Iron and titanium oxides accumulated in upper horizons of P1 and P3 and were washed out in lower horizons though in P2 they retained in the middle part of the soil profile (Fig. 2). Therefore, iron and titanium oxides moving with allochthonic matter were present in smaller particles, which were able to get inside the soil profile and retain in upper horizon. In mineral horizons iron and titanium compounds were leached down the profile. Titanium is not a mobile element, and it mostly exists in the form of primary minerals (uddevallite or rutile) resistant to erosion (Cornu et al. 1999). Although titanium oxides can sometimes be mobile, in our case, physical displacement may have occurred due to washing out of soil profile by flood water. Iron oxides behaved the same way, which indicated that they were also presented in mineral form in the fluvisols. In redox environment, which accompanies inundation of soils,

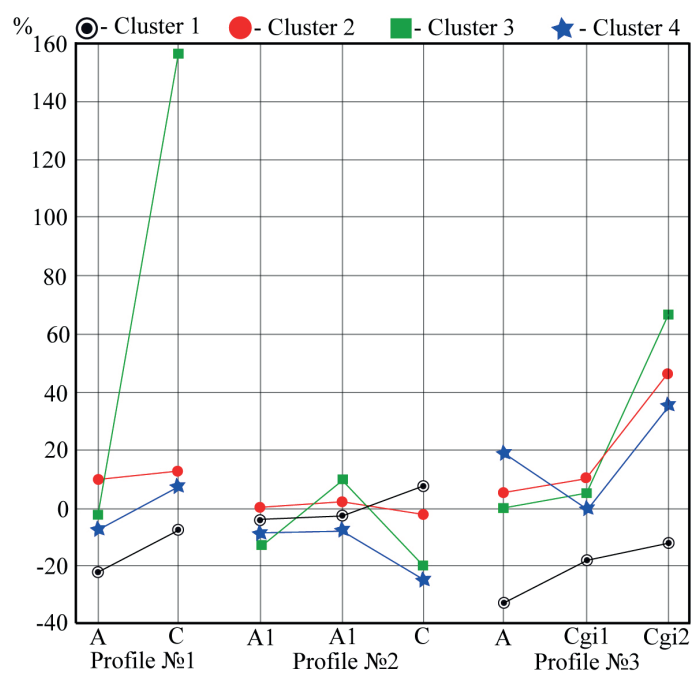


Fig. 6. Graph of average changes in the content of trace elements after flooding, %:

C1: Sr, Cd, Ba, Tl, Pb;
 C2: Be, Sc, Zn, Y, REE;
 C3: Ni, Cu, Mo;
 C4: Li, V, Cr, Co, Ga, As, Rb, Zr, Nb, Sn, Cs, Hf, Ta, W, Th, U

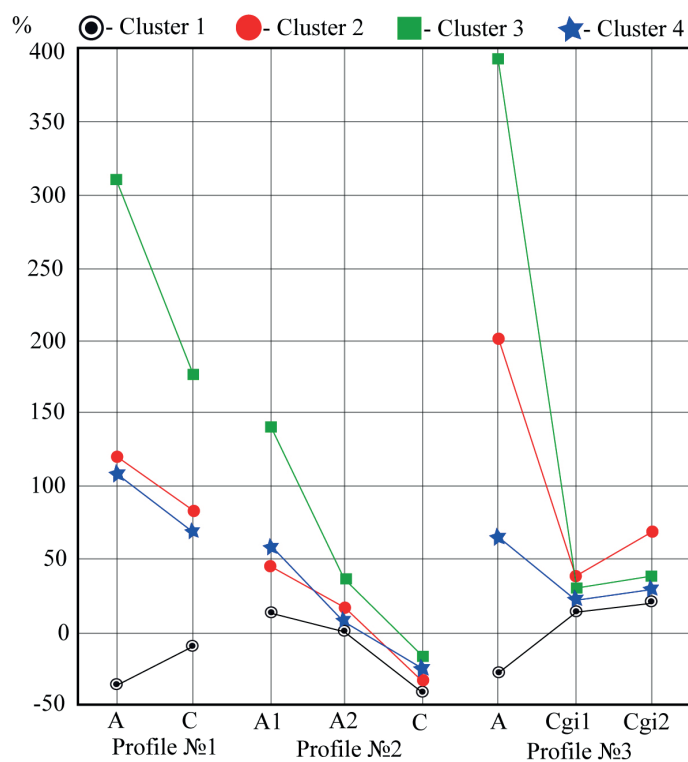


Fig. 7. Graph of average changes in the content of mobile trace elements after flooding, %:

C1: Li, Cr, Co, Zn, Rb, Sr, Mo, Cd, Cs, Ba, W, Tl;
 C2: Be, Cu, Hf, U, Ce, Pr, Nd, Sm, Eu, Gd, Tb, Dy, Ho, Er, Tm, Yb, Lu;
 C3: Sc, Ni, Th;
 C4: V, Ga, As, Y, Zr, Pb, La

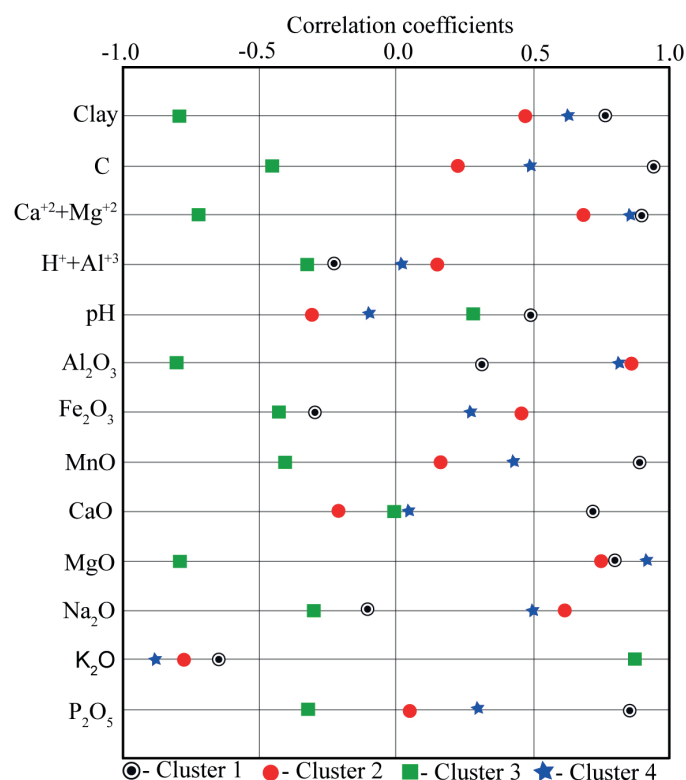


Fig. 8. Graph of average coefficients of correlation between the content of the total trace elements, major elements and properties of soils before the flood:

C1: Zn, Cu, Cd, Pb;

C2: Be, Sc, V, Cr, Ga, As, Zr, Nb, Hf, Ta, Eu;

C3: Sr, Ba;

C4: Li, Co, Ni, Rb, Y, Mo, Sn, Sc, W, Tl, Th, U, La, Ce, Pr, Nd, Sm, Gd, Tb, Dy, Ho, Er, Tm, Yb, Lu

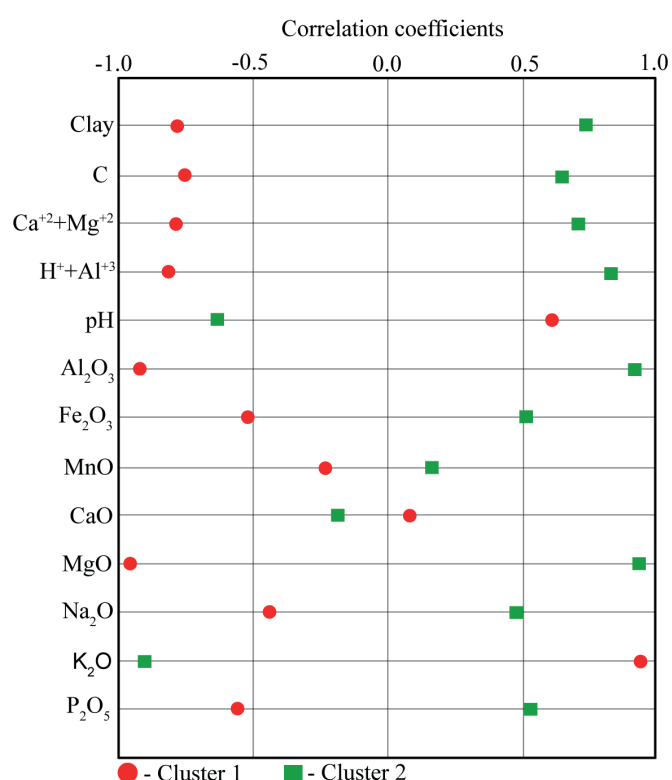


Fig. 9. Graph of average coefficients of correlation between the content of the total trace elements, major elements and properties of soils after the flood:

C1: Sr, Ba;

C2: All other elements

iron oxides disintegrate and mobilize (Vodyanitsky 2010) due to high acidity, being, consequently, intensively washed out by flood waters.

The most substantial changes of major element composition were observed in P3, which was inundated for longer period of time due to its location on the bottom of a dry creek. Minimum changes occurred in major element composition of P2, which located on the top of levee and was the first to come out of flood waters. As the location was on the way of the flood waters entering the floodplain, the soil was covered by a thick layer of alluvia, which preserved the soil from washing out and significant changes in element composition. Hence, length of inundation and water flow velocity were the main factors determining the influence of flood on element composition of fluvisols. In turns, the impact of water flow was affected by floodplain landscape, which goes in line with supposition that floodplain relief is the key pedogenic factor in fluvial soil formation (Du Laing 2009).

Analysis of the flood impact on total content of trace elements

Flood caused rise of trace elements content in P1 and P3. In lower horizons elements belonging to clusters 2, 3 and 4 mainly accumulated, whereas in upper horizons their content did not change or rose insignificantly (Fig. 3). The maximum rise in content of Ni, Cu and Mo was observed, which could be explained by great content of the elements in allochthonic matter. Our conclusion is consistent with the data about greater concentrations of the elements in bottom sediments (Sorokina & Zarubina 2011). Elements belonging to C1 were washed out of all the soil horizons, but most intensively out of upper horizons. Reduction of the content of C1 elements and insignificant accumulation of C2, C3 and C4 elements

in organic horizon can be attributed to influence of redox potential. Changes of redox potential are faster and bigger in organic horizons of redundantly wet soils than in mineral horizons. Decrease of Eh during the flood results in drastic rise of acidity (Shaheen et al. 2016). In such conditions trace elements are washed out of soils or displaced down the soil profile. The latter is supported by the data (Antić-Mladenović et al. 2016; Kuznetsov et al. 2017; Shaheen et al. 2014) on high mobility of Sr, Cd and Pb at low pH as well as numerous studies of the influence of redox potential on accumulation of trace elements (Cao et al. 2001; Frohne et al. 2011; Schulz-Zunkel et al. 2015). In organic horizon of P2 the content of the most trace elements did not change (Fig. 3). In the lower horizon both processes, washing out and accumulation, were observed. There were some differences in accumulation of trace elements between fluvisols, which could be explained by longer inundation of P1 and P3, eventually, leading to greater amount of allochthonic matter. In P2, sedimentary cover of alluvia impeded arrival of new elements. However, the location of the soil in the area of high dynamics of water flow caused intensive washing through the soil, and afterward, decreases in concentration of most elements, especially in sandy horizon.

The flood did not have much influence on the relationships between soil properties, content of major elements and total trace elements (Fig. 5, 6). Before the flood, content of trace elements was mostly dependent on mineral composition of the soils (Fig. 5). That is indicated by positive correlation to Al and Mg oxides, which, in youth fluvisols, exist in the form of the substances having strong sorption potential (Du Laing et al. 2009), namely: primary aluminosilicates and secondary clay minerals (Scriabina 2011). Organic matter also did not have much influence on total content of trace elements, which might have been caused by youth of the studied soils. The only

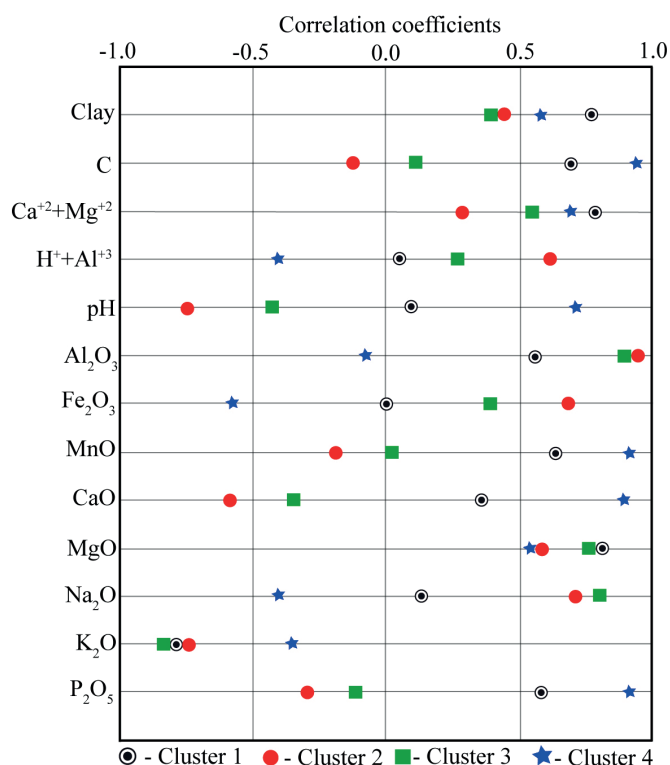


Fig. 10. Graph of average coefficients of correlation between the content of the mobile trace elements, major elements and properties of soils before the flood:

C1: Rb, Ba, W, Tl, Pb;
C2: Be, Sc, Cr, Ga, Y, Hf, Th, REE
C3: Co, Ni, Cu, Zr, Cs, U;
C4: Li, V, Zn, As, Sr, Mo, Cd

elements bound to carbon of organic matter were Zn, Cu, Cd and Pb. The elements standing apart were Sr and Ba as they had positive R only to potassium oxides (Fig. 5). The behavior of Ba was dependent on its association to potassium in rocks and its frequent existence in alkaline feldspars and biotites (Kabata-Pendias 2011). Sr can display similar behavior, as it is geochemically isomorphous with Ba and is contained in great amount in plagioclases and feldspars (Ivanov 1994). On the bases of origin of Sr and Ba and lack of positive or negative Rs to soil properties, we may presume that Sr and Ba mainly exist in the composition of primary minerals or that they are absorbed by the minerals. After the flood the relationships between trace elements, major elements and soil properties changed insignificantly though reduction of diversity of Rs was observed (Fig. 6). All trace elements, apart from Sr and Ba, had near values of R to major-element composition and soil properties. The latter indicated reduction of spatial variability of fluvial soil properties after the flood.

Thus, the flood caused increase of the concentration of most trace elements, except Sr, Cd, Ba, Tl and Pb. Accumulation of elements mainly occurred in lower horizons, whereas composition of upper horizons did not change much due to rise of acidity and development of reduction environment during inundation. Also, the flood developed the conditions in fluvisols which make all trace elements, except Sr and Ba, show similar behavior in relation to soil properties.

Analysis of the flood impact on the content of mobile trace elements

Mobile fractions of trace elements are very dynamic and their content in soils can change in a short period of time (Kovda 1973). As a result, it is hard to estimate the influence a flood has on them. However, mobile trace elements strongly react to changes of soil properties, so their content allows us to identify the processes occurring in soils after inundations. After

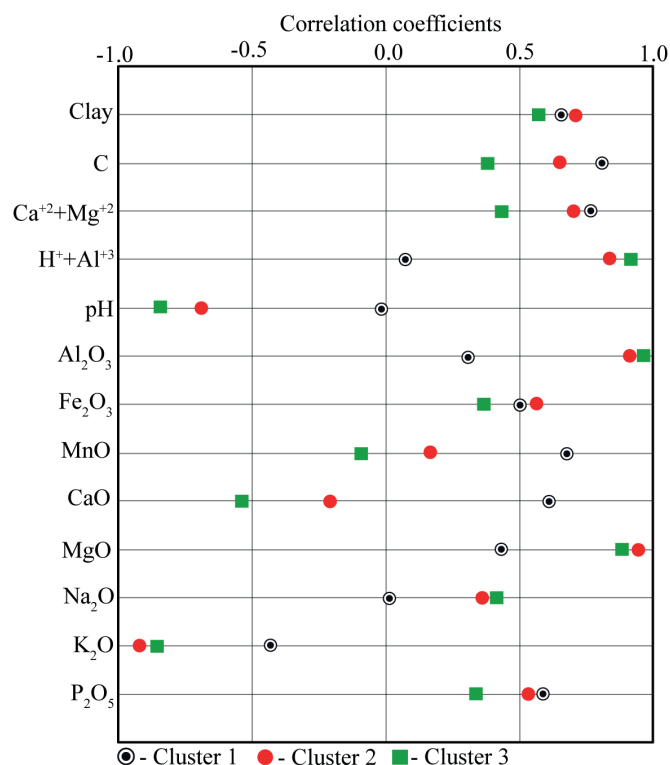


Fig. 11. Graph of average coefficients of correlation between the content of the mobile trace elements, major elements and properties of soils after the flood:

C1: Li, V, Ni, Zn, As, Sr, Mo, Cd, W;
C2: Be, Cr, Co, Rb, Zr, Ba, Hf, Pb;
C3: Sc, Cu, Ga, Y, Cs, Ti, Th, U, REE

the flood, most analyzed mobile trace elements accumulated on organic horizons (Fig. 4), whereas total content of trace elements did not change significantly. The main factor of mobility of trace elements both in soils and soil solutions is pH (Zeng et al. 2011). Thus, increase of content of mobile trace elements belonging to C2, C3 and C4, as well as decreasing of content of C1 elements (Fig. 4) was dependent on increase of acidity. The reason for decrease of the content of C1 elements in Fig. 4 was in positive correlation of the elements to pH and CaO (Fig. 7). This the elements stayed mobile in neutral or slightly acidic pH, whereas strengthening of acidity after the flood caused their immobilization. The latter is proved by Rs of the trace elements to pH close to 0 after the flood (Fig. 8).

Content of mobile trace elements also depended on their selective sorption. Unlike total content of trace elements, part of mobile trace elements (C1 and C4) was accumulated by organic matter, but the other part (C2 and C3) was accumulated by soil minerals (Fig. 7). Trace elements adsorbed by organic matter had linkage to contents of manganese, phosphorous and calcium oxides. While comparing element composition of C1 (Fig. 4) and element composition of C2 and C3 (Fig. 7), we noticed that content of elements adsorbed by organic matter reduced after the flood. That was assumptive consequence of decrease of the content of organic matter, or oxides, which bind with the trace elements. After the flood differences of selective sorption by the components of the soils of mobile trace elements became less pronounced (Fig. 8). Therefore, the flood caused homogenization of relationships between the content of mobile trace elements and soil properties. However, the process was weaker than that of total content of trace elements.

All things considered, the flood caused immobilization of Li, Cr, Co, Zn, Rb, Sr, Mo, Cd, Cs, Ba, W and Tl in fluvisols as a result of increase of acidity, reduction of organic matter content and of content of calcium, manganese and phosphorous oxides.

Other trace elements which were mainly connected with mineral composition of soils mobilized in the conditions of high acidity. The flood had stronger influence on mobility of trace elements in organic horizons, which was caused by development of reduction environment in the horizons during the flood and, as a result, higher acidity of organic horizons compared to mineral ones.

CONCLUSION

Our study of the influence of the severe flood on element composition of fluvisols in the middle reach of the Amur River demonstrated that main influence revealed in enhancement of the fluvisols acidity, washing out of organic and silt fractions and retention of allochthonic matter. As a result of

these processes, the content of calcium, manganese and phosphorous oxides decreased in major-element composition. Concurrently, in trace-element composition, washing out of Sr, Cd, Ba, Tl and Pb occurred. Besides, immobilization of mobile Li, Cr, Co, Zn, Rb, Sr, Mo, Cd, Cs, Ba, W and Tl was observed. After the flood, total content of Ni, Cu, Mo and mobile forms of Sc, Ni, Th accumulated. The consequences of the flood mostly depended on floodplain landscape, which made topography the key soil-forming factor in development of element composition of fluvisols. Content of other major and trace element altered insignificantly. The attained results contribute to fundamental knowledge of flood consequences for fluvisols and floodplain landscapes in general, and are critical to study of geochemical processes in one of the longest rivers of the world, the Amur. ■

REFERENCES

- Abgottspon F., Bigalke M., Wilcke W. (2015). Fast colloidal and dissolved release of trace elements in a carbonatic soil after experimental flooding. *Geoderma*, 259-260, 156-163, DOI:10.1016/j.geoderma.2015.06.005.
- Antić-Mladenović S., Frohne T., Kresović M., et al. (2016). Biogeochemistry of Ni and Pb in a periodically flooded arable soil: Fractionation and redox-induced (im)mobilization. *Journal of environmental management*, 186, 141-150, DOI: 10.1016/j.jenvman.2016.06.005.
- Cao X., Chen Y., Wang X., Deng X. (2001). Effects of redox potential and pH value on the release of rare earth elements from soil. *Chemosphere*, 44, 655-661, DOI: 10.1016/S0045-6535(00)00492-6.
- Cornu S., Lucas Y., Lebon E., et al. (1999). Evidence of titanium mobility in soil profiles, Manaus, central Amazonia. *Geoderma*, 91, 281-295. DOI:10.1016/S0016-7061(99)00007-5.
- Day F.P., West S.K., Tupacz E.G. (1988). The influence of groundwater dynamics in a periodically flooded ecosystem, the Feat Dismal Swamp. *Wetlands*, 8, 1-13.
- Du Laing G., Rinklebe J., Vandecasteele B., et al. (2009). Trace metal behavior in estuarine and riverine floodplain soils and sediments: A review. *Science of the Total Environment*, 407, 3972-3985, DOI: 10.1016/j.scitotenv.2008.07.025.
- Ermoshin V., Ganzey S., Shiraiva T. (2013). Land use changes in the trans-boundary Amur River basin in the 20th century. *Geography, Environment, Sustainability*, 6(2), 4-19, DOI: 10.24057/2071-9388-2013-6-2-4-19.
- Förstner U., Heise S., Schwartz R., et al. (2004). Historical contaminated sediments and soils at the river basin scale. *Transport*, 4, 247-260, DOI: 10.1007/BF02991121.
- Frohne T., Diaz-Bone R.A., Du Laing G., Rinklebe J. (2014). Impact of systematic change of redox potential on the leaching of Ba, Cr, Sr and V from a riverine soil into water. *Journal of Soils and Sediments*, 15, 623-633, DOI: 10.1007/s11368-014-1036-8.
- Frohne T., Rinklebe J., Diaz-bone R.A., Du G. (2011). Controlled variation of redox conditions in a floodplain soil: Impact on metal mobilization and biomethylation of arsenic and antimony. *Geoderma*, 160, 414-424, DOI: 10.1016/j.geoderma.2010.10.012.
- Gerrard J. (1987). *Alluvial Soils*. New York: Hutchinson Ross.
- Hilscherova K., Dusek L., Kubik V., et al. (2007). Redistribution of organic pollutants in river sediments and alluvial soils related to major floods. *Journal of Soils and Sediments*, 7, 167-177, DOI: 10.1065/jss2007.04.222.
- IUSS Working Group. (2014). World reference base for soil resources. International Soil Classification System for Naming Soils and Creating Legends for Soil Maps. *World Soil Resources Report* (106), Rome: FAO.
- Ivanov V.V. (1994). *Ecological geochemistry of element. (1)*. Moscow: Nedra Publish. (in Russian).
- Izquierdo M., Tye A.M., Chenery S.R. (2012). Sources, lability and solubility of Pb in alluvial soils of the River Trent catchment, U.K.. *Science of the total environment*, 433, 110-22, DOI: 10.1016/j.scitotenv.2012.06.039.
- Kabata-Pendias A. (2011). *Trace Elements in Soils and Plants*. Boca Raton: CRC Press.
- Kovda V.A. (1973). *Foundations of the doctrine of soils. General theory of the soil-forming process. Vol. 2*. Moscow: Publishing house «Science» (in Russian).
- Kuznetsov P.V., Chuparina E.V., Proidakova O.A., Aisueva T.S. (2017). Specifics of strontium accumulation in the floodplain soils of the Kuda River, Irkutsk Region. *Geochemistry International*. 55, 299-305, DOI: 10.1134/S001670291703003X.
- Lair G.J., Zehetner F., Fiebig M., et al. (2009). How do long-term development and periodical changes of river-floodplain systems affect the fate of contaminants? Results from European rivers. *Environmental Pollution*, 157, 3336-3346, DOI: 10.1016/j.envpol.2009.06.004.
- Lair G.J., Zehetner F., Khan Z.H., Gerzabek M.H. (2009). Phosphorus sorption-desorption in alluvial soils of a young weathering sequence at the Danube River. *Geoderma*, 149, 39-44, DOI: 10.1016/j.geoderma.2008.11.011.
- Makhinov A.N., Liu Shuguang. (2013). Formation of the riverbed relief and river banks. Khabarovsk: FEB RAS. (in Russian).
- Makhinov A.N. (2017). The water regime of the floodplain of the Amur River and the features of floodplain sedimentation during the extreme flood of 2013. *Meteorology and Hydrology*. 3, 87-92. (in Russian).
- Makhinov A.N., Makhinova A.F. (2017). Flood impacts on the geochemical flows in the soils of river valley. *Advances in current natural sciences*. 1, 58-63 (in Russian).
- Martin C.W. (2015). Trace metal storage in recent floodplain sediments along the Dill River, central Germany. *Geomorphology*, 235, 52-56, DOI:10.1007/s00254-008-1557-9.
- Martynov A.V. (2015). Content and distribution of trace elements in alluvial soil of floodplain of major rivers on Zeya-Selemdja plain. *Geography and Natural Resources*. 3, 138-145. (in Russian).
- Muranova A.P. (1966). *Resources of surface waters of the USSR. vol. 18. Far East. (1). Upper and middle Amur*. Leningrad: Hydrometeorological Publishing House. (in Russian).
- Orlov D.S., Bezuglova O.S. (2000). *Biogeochemistry*. Rostov-on-Don: Phoenix Publish. (in Russian).
- Oriola E., Chibuike C. (2016). Flood risk analysis of a local government area (Kwara State, Nigeria). *Geography, Environment, Sustainability*, 9(3), 106-116, DOI: 10.15356/2071-9388_03v09_2016_07.

- Pansu M., Gautheyrou J. (2006). Handbook of soil analysis mineralogical, organic and inorganic methods. Berlin: Springer-Verlag.
- Pirastu M., Niedda M. (2013). Evaluation of the soil water balance in an alluvial flood plain with a shallow groundwater table. *Hydrological Sciences Journal*, 58, 898-911, DOI: 10.1080/02626667.2013.783216.
- Ponnamperna F.N. (1984). Effects of Flooding on Soils, In T.T. Kozłowski, et al. ed., *Flooding and plant growth*, London: Academic Press, 9-46, DOI: 10.1017/S0014479700013272.
- Saint-Laurent D., Gervais-Beaulac V., Berthelot J.S. (2014). Variability of soil properties in different flood-risk zones and link with hydroclimatic changes (Southern Québec, Canada), *Geoderma*, 214-215, 80-90, DOI: 10.1016/j.geoderma.2013.09.025.
- Saint-Laurent D., Lavoie L., Drouin, et al. (2010). Floodplain sedimentation rates, soil properties and recent flood history in southern Québec. *Global and Planetary Change*, 70, 76-91, DOI: 10.1016/j.gloplacha.2009.11.009.
- Schulz-Zunkel C., Krueger F., Rupp H., et al. (2013). Spatial and seasonal distribution of trace metals in floodplain soils. A case study with the Middle Elbe River, Germany. *Geoderma*, 211-212, 128-137, DOI: 10.1016/j.geoderma.2013.07.010.
- Schulz-Zunkel C., Rinklebe J., Bork H-R. (2015). Trace element release patterns from three floodplain soils under simulated oxidized-reduced cycles. *Ecological Engineering*, 83, 485-495, DOI: 10.1016/j.ecoleng.2015.05.028.
- Shaheen S.M., Frohne T., White J.R., Delaune R.D. (2016). Redox-induced mobilization of copper, selenium and zinc in deltaic soils originating from Mississippi (U.S.A.) and Nile (Egypt) River Deltas: A better understanding of biogeochemical processes for safe environmental management. *Journal of Environmental Management*, 186, 131-140, DOI: 10.1016/j.jenvman.2016.05.032.
- Shaheen S.M., Rinklebe J., Rupp H., Meissner R. (2014). Temporal dynamics of pore water concentrations of Cd, Co, Cu, Ni and Zn and their controlling factors in a contaminated floodplain soil assessed by undisturbed groundwater lysimeters. *Environmental Pollution*, 191, 223-231, DOI: 10.1016/j.envpol.2014.04.035.
- Sharma B.D., Choudhary O.P., Chanay J.K., Singh P.K. (2016). Forms and uptake of manganese in relation to soil taxonomic orders in alluvial soils of Punjab, India. *Communications in Soil Science and Plant Analysis*, 47, 313-327, DOI: 10.1080/00103624.2015.1123722.
- Shrestha J., Niklaus P.A., Pasquale N., et al. (2014). Flood pulses control soil nitrogen cycling in a dynamic river floodplain. *Geoderma*, 228-229, 14-24, DOI: 10.1016/j.geoderma.2013.09.018.
- Silvestro F., Rebora N., Cummings G., Ferraris, L. (2017). Experiences of dealing with flash floods using an ensemble hydrological now casting chain: implications of communication, accessibility and distribution of the results. *Journal of Flood Risk Management*, 10, 446-462, DOI: 10.1111/jfr3.12161.
- Skryabina O.A. (2011). Mineralogical composition of soils and soil-forming rocks. Perm: Perm State Agricultural Academy Publish (in Russian).
- Sokolova G.V. (2015). Analyzing the Amur River water regime for the period preceding the catastrophic flood in 2013. *Russian Meteorology and Hydrology*, 40, 477-479, DOI: 10.3103/S1068373915070067.
- Sorokina O.A., Gusev M.N. (2014). The content of rare-earth elements in the floodplain soils of the Zeya River valley (the Amur River basin). *Bulletin of the North-Eastern Scientific Center DVO RAN*, 3, 36-40. (in Russian).
- Sorokina O.A., Gusev M.N. (2018). Weathering reflected by the chemical composition of alluvial soils from the Zeya and Seledzha river valleys. *Science China Earth Sciences*, 61, 604-613, DOI: 10.1007/s11430-017-9162-5.
- Sorokina O.A., Zarubina N.V. (2011). Chemical composition of the bottom sediments in the middle reaches of the Amur River. *Russian journal of pacific geology*, 30, 105-113. (in Russian).
- Sorokina O.A., Zarubina N.V. (2013). The content of chemical elements in alluvial soils and bottom sediments of the Urkan River (the Amur River basin). *Eurasian Soil Science*, 46, 644-653, DOI: 10.1134/S1064229313060094.
- Tockner K., Mark S.L., Jack A.S. (2010). River flood plains are model ecosystems to test general hydrogeomorphic and ecological concepts. *River research and applications*, 26, 76-86, DOI: 10.1002/rra.1328.
- Unger I.M., Motavalli P.P., Muzika R. (2009). Changes in soil chemical properties with flooding : A field laboratory approach. *Agriculture, Ecosystems and Environment*, 131, 105-110, DOI: 10.1016/j.agee.2008.09.013.
- Verbitskaya E.M., Ageeva S.V., Dugina I.O., et al. (2015). Catastrophic flood on the Amur River in summer 2013: Features and Causes. *Russian Meteorology and Hydrology*, 40, 683-690, DOI: 10.3103/S1068373915100064.
- Vodyanitsky Y.N. (2010). Iron compounds and their significance in soil conservation. Moscow: Soil Institute V.V. Dokuchaeva (in Russian).
- Wang L. (2015). The effect of reclamation on the distribution of heavy metals in saline-sodic soil of Songnen Plain, China. *Environmental Earth Sciences*, 73, 1083-1090, DOI: 10.1007/s12665-014-3464-6.
- Wei D., Jin-liang Z. (2002). Total N, total P and organic matters content in floodplain soils of Xianghai Nature Reserve. *Journal of Geographical Sciences*, 12, 58-64. DOI:10.1007/BF02837428.
- Wölz J., Cofalla C., Hudjetz S., et al. (2009). In search for the ecological and toxicological relevance of sediment re-mobilisation and transport during flood events. *Soils and Sediments*, 9, 1-5, DOI: 10.1007/s11368-008-0050-0.
- Zaydelman F.R. (2009). Genesis and ecological basis of soil and landscape reclamation. Moscow: KDU. (in Russian).
- Zehetner F., Lair G.J., Maringer F-J., et al. (2008). From sediment to soil: floodplain phosphorus transformations at the Danube River. *Biogeochemistry*, 88, 117-126, DOI: 10.1007/s10533-008-9198-3.
- Zeng F., Ali S., Zhang H., et al. (2011). The influence of pH and organic matter content in paddy soil on heavy metal availability and their uptake by rice plants. *Environmental Pollution*, 159, 84-91, DOI: 10.1016/j.envpol.2010.09.019.
- Zerling L., Hanisch C., Junge F.W. (2006). Heavy metal inflow into the floodplains at the mouth of the river Weibe Elster (Central Germany). *Acta Hydrochimica et Hydrobiologica*, 34, 234-244, DOI: 10.1002/aheh.200400624.
- Zocatelli R., Moreira-Turcq P., Bernardes M., et al. (2013). Sedimentary evidence of soil organic matter input to the Curuai Amazonian floodplain. *Organic Geochemistry*, 63, 40-47, DOI: 10.1016/j.orggeochem.2013.08.004.

APPENDIX

Table A.1. Content major elements in alluvial soils before and after flood

Major elements	Content major elements, %							
	Profile 1		Profile 2			Profile 3		
	A	C	A1	A2	C	A	Cgi1	Cgi2
Before flood								
Si ₂ O	72.54	72.44	69.2	69.97	68.85	64.19	66.38	67.99
TiO ₂	0.77	0.83	1.02	1.01	1.07	0.81	0.99	0.77
Al ₂ O ₃	11.59	10.77	12.47	13.14	13.92	13.1	15.82	15.93
Fe ₂ O ₃	4.58	5.43	6.69	6.79	7.17	4.76	7.17	6.26
MnO	0.13	0.14	0.18	0.18	0.12	0.38	0.18	0.14
CaO	3.17	2.96	2.9	2.11	1.91	6.47	1.78	1.57
MgO	0.6	0.58	0.72	0.71	0.74	1.21	1.16	1.14
Na ₂ O	1.7	1.53	1.56	1.54	1.57	1.36	2.02	2.17
K ₂ O	3.98	4.72	4.14	3.52	3.61	2.96	2.96	2.76
P ₂ O ₅	0.32	0.21	0.32	0.26	0.32	0.77	0.24	0.26
After flood								
Si ₂ O	71.48	75.4	70.72	68.83	72.63	66.72	66.8	64.99
TiO ₂	0.95	0.56	0.92	1.11	0.75	1.01	0.94	1.02
Al ₂ O ₃	11.22	10.06	12.16	13.57	11.61	14.77	17.31	16.97
Fe ₂ O ₃	5.61	3.85	6.21	7.57	4.93	7.15	6.56	5.89
MnO	0.14	0.1	0.16	0.16	0.13	0.21	0.1	0.14
CaO	3.18	2.56	2.72	1.99	2.1	1.94	1.07	1.09
MgO	0.57	0.48	0.67	0.72	0.56	0.98	1.12	1.04
Na ₂ O	1.74	1.7	1.6	1.39	1.8	1.74	1.99	1.78
K ₂ O	4.31	4.89	3.95	3.5	4.45	2.96	2.59	2.68
P ₂ O ₅	0.27	0.12	0.26	0.27	0.19	0.31	0.23	0.28

Table A.2. Content of the total and mobile form of trace elements in alluvial soils before flood

Trace element	Content trace element, mg/kg															
	Profile 1				Profile 2						Profile 3					
	A		C		A1		A2		C		A		Cgi1		Cgi2	
	total	mobile	total	mobile	total	mobile	total	mobile	total	mobile	total	mobile	total	mobile	total	mobile
Li	16.2	0.048	11.7	0.028	22.0	0.064	22.2	0.051	22.6	0.041	37.0	0.581	44.0	0.116	33.7	0.108
Be	1.5	0.030	1.3	0.039	1.8	0.055	1.8	0.132	1.8	0.136	1.9	0.047	2.4	0.189	2.1	0.193
Sc	5.4	0.007	3.0	0.015	6.6	0.018	6.1	0.066	5.9	0.084	7.6	0.017	10.9	0.134	8.7	0.173
V	48.3	0.037	27	0.027	60.0	0.024	56.7	0.016	56.5	0.020	69.3	0.155	99.6	0.037	84.0	0.032
Cr	36.0	0.085	13	0.230	31.4	0.336	29.6	0.427	27.6	0.519	38.1	0.334	56.7	0.653	43.1	0.720
Co	6.5	0.172	3.9	0.151	8.4	0.191	8.7	0.224	8.8	0.209	11.6	0.316	15.3	0.459	13.7	0.560
Ni	11.5	0.078	6.7	0.059	15.0	0.093	15.7	0.237	14.5	0.097	27	0.345	28.3	0.642	22.9	0.687
Cu	7.1	0.003	3.1	0.042	10.8	0.024	10.7	0.082	8.9	0.036	37.2	0.065	25.0	0.310	20.0	0.305
Zn	49.5	2.759	21.4	0.178	57.9	0.604	51.1	0.165	49.3	0.079	168.1	9.285	101.1	0.582	78.8	0.676
Ga	15.0	0.006	13.0	0.007	17.3	0.011	16.5	0.044	16.7	0.049	15.6	0.025	22.3	0.064	19.6	0.064
As	5.3	0.105	4.9	0.086	7.6	0.064	7.7	0.056	8.1	0.077	10.1	0.719	14.7	0.125	14.6	0.117

Rb	91.8	0.270	85.2	0.032	98.9	0.197	94.2	0.526	93.2	0.557	101.7	2,822	114	1,469	103.8	1,603
Sr	418.1	14,978	428.8	4,951	396.6	9,957	356.7	10,842	341.4	7,196	295.8	72,258	261.2	19,058	316.8	13,387
Y	11.0	0.138	7.8	0.175	12.8	0.275	12.2	1,178	10.5	1,211	17.0	0.575	19.5	1,775	16.0	1,799
Zr	40.1	0.017	17.4	0.020	38.1	0.023	42.8	0.048	43.1	0.051	50.9	0.053	75.5	0.105	63.9	0.131
Nb	6.8	0.000	4.4	0.000	7.9	0.000	7.5	0.000	7.6	0.000	7.2	0.000	9.9	0.000	7.5	0.000
Mo	0.4	0.003	0.3	0.005	0.5	0.003	0.5	0.004	0.5	0.000	1.0	0.008	1.4	0.003	1.1	0.001
Cd	0.2	0.043	0.1	0.006	0.1	0.017	0.1	0.007	0.1	0.003	1.1	0.164	0.2	0.013	0.1	0.017
Sn	1.3	0.000	0.7	0.000	1.5	0.000	1.4	0.000	1.4	0.000	2.2	0.000	2.5	0.000	2.0	0.000
Cs	2.3	0.008	1.5	0.002	3.0	0.006	3.4	0.053	3.3	0.062	5.6	0.042	6.9	0.088	5.2	0.097
Ba	973.0	26.92	1,103.0	12.68	915.0	28.88	858.0	51,700	850	30,700	835.3	81.22	792.2	66.23	891	61.51
Hf	1.2	0.001	0.6	0.001	1.2	0.001	1.4	0.002	1.3	0.002	1.5	0.001	2.2	0.004	1.7	0.004
Ta	0.5	0.000	0.4	0.000	0.6	0.000	0.5	0.000	0.6	0.000	0.5	0.000	0.7	0.000	0.5	0.000
W	0.6	0.001	0.4	0.000	0.9	0.002	1.2	0.002	1.0	0.001	1.4	0.002	1.7	0.001	1.3	0.001
Tl	0.5	0.003	0.5	0.001	0.5	0.002	0.5	0.005	0.5	0.005	0.6	0.017	0.6	0.011	0.6	0.010
Pb	19.2	0.372	16.3	0.177	20.5	0.286	18.7	0.431	19.1	0.600	39.2	0.786	25.2	0.793	25.3	0.816
Th	4.2	0.012	3.5	0.028	5.5	0.034	6.1	0.131	6.0	0.142	8.3	0.033	11.1	0.239	9.0	0.237
U	1.2	0.099	0.8	0.129	1.6	0.172	1.7	0.321	1.8	0.324	3.2	0.224	4.2	0.889	3.6	0.861
La	21.7	0.178	12.8	0.275	28.6	0.383	25.3	1,570	27.3	1,776	35.5	0.690	37.2	2,027	33.4	1,991
Ce	47.5	0.297	28.8	0.28	61.3	0.630	52.7	2,916	59.2	3,158	68.6	1,206	77.7	4,370	70.2	4,420
Pr	5.2	0.039	3.4	0.060	6.8	0.088	5.7	0.387	5.9	0.423	7.2	0.151	8.2	0.521	7.4	0.514
Nd	19.2	0.169	12.9	0.244	24.9	0.372	20.6	1,648	20.9	1,778	26.5	0.666	29.8	2,268	27.5	2.22
Sm	3.4	0.036	2.4	0.049	4.2	0.079	3.6	0.329	3.5	0.349	4.8	0.132	5.6	0.472	4.9	0.459
Eu	0.8	0.007	0.7	0.010	0.9	0.015	0.8	0.063	0.8	0.068	0.9	0.025	1.1	0.088	1.1	0.086
Gd	2.6	0.034	1.9	0.045	3.2	0.072	2.9	0.298	2.7	0.316	4.3	0.121	4.7	0.421	4.2	0.410
Tb	0.4	0.005	0.3	0.006	0.5	0.010	0.5	0.044	0.4	0.047	0.6	0.017	0.7	0.063	0.6	0.062
Dy	2.1	0.024	1.5	0.033	2.6	0.050	2.4	0.219	2.1	0.236	3.3	0.086	3.8	0.32	3.1	0.319
Ho	0.4	0.004	0.3	0.006	0.5	0.009	0.5	0.040	0.4	0.043	0.6	0.016	0.8	0.059	0.6	0.06
Er	1.1	0.011	0.8	0.016	1.4	0.022	1.3	0.101	1.2	0.107	1.8	0.039	2.2	0.148	1.8	0.153
Tm	0.2	0.001	0.1	0.002	0.2	0.002	0.2	0.012	0.0	0.012	0.3	0.004	0.3	0.017	0.3	0.018
Yb	1.1	0.006	0.8	0.011	1.3	0.014	1.2	0.066	1.1	0.069	1.6	0.022	1.9	0.097	1.6	0.103
Lu	0.2	0.001	0.1	0.002	0.2	0.002	0.2	0.010	0.2	0.010	0.2	0.003	0.3	0.014	0.2	0.016

Table A.3. Content of the total and mobile form of trace elements in alluvial soils after flood

Trace element	Content trace element, mg/kg															
	Profile 1				Profile 2						Profile 3					
	A		C		A1		A2		C		A		Cgi1		Cgi2	
	total	mobile	total	mobile	total	mobile	total	mobile	total	mobile	total	mobile	total	mobile	total	mobile
Li	15.3	0.055	12.1	0.040	19.5	0.042	23.3	0.051	14.8	0.034	37.2	0.086	48.5	0.070	49.9	0.054
Be	1.6	0.06	1.6	0.033	1.7	0.085	2.0	0.161	1.6	0.056	2.1	0.175	2.7	0.251	2.9	0.269
Sc	6.8	0.028	4.1	0.048	8.1	0.037	7.8	0.075	6.8	0.078	12.4	0.095	14.9	0.213	15.8	0.242
V	49.6	0.094	30.6	0.038	56.5	0.036	56.5	0.017	45.1	0.020	93.4	0.188	105.3	0.031	116.3	0.024
Cr	28.1	0.107	16.2	0.033	33.9	0.145	32.9	0.324	24.7	0.070	56.4	0.665	65.3	1,084	68.4	0.956
Co	6.5	0.125	4.6	0.046	8.1	0.076	8.9	0.284	7.2	0.064	13.8	0.264	15.1	0.332	17.5	0.258
Ni	11.0	0.371	13.4	0.151	13.4	0.293	19.4	0.443	12.2	0.054	27.2	1,099	31.3	0.457	32.1	0.59

Cu	6.5	0.037	8.3	0.125	7.7	0.021	13.4	0.069	8.0	0.078	25.6	0.255	26.0	0.255	28.4	0.468
Zn	41.3	1,334	31.8	0.570	47.5	0.387	57.4	0.139	41.8	0.133	102.7	4,105	102	0.515	102.3	0.393
Ga	14.9	0.013	14.1	0.016	16.5	0.016	16.8	0.049	15.8	0.026	20.4	0.047	23.8	0.092	24.2	0.109
As	6.0	0.257	4.4	0.106	6.7	0.078	7.4	0.054	4.9	0.048	13.5	0.462	11.5	0.110	22.1	0.139
Rb	87.0	0.116	96.4	0.007	93.9	0.314	95.3	0.561	94.9	0.287	113.5	1,162	110.2	1,914	110.6	1,884
Sr	375.5	8,279	382.9	3,168	376.8	10,941	323.4	12,825	391.9	3,676	226.1	22.84	206.1	9,592	202.4	10,251
Y	11.5	0.294	8.5	0.317	13.8	0.380	12.5	1,342	11.8	0.725	18.4	1,213	21.7	2,262	25.7	2,818
Zr	37.6	0.024	25.7	0.019	42.9	0.028	42.1	0.022	31.6	0.022	68.6	0.101	77.9	0.123	85.0	0.14
Nb	6.5	0.000	4.6	0.000	6.3	0.000	6.3	0.000	5.9	0.000	9.1	0.000	10.4	0.000	10.1	0.000
Mo	0.4	0.001	0.9	0.001	0.5	0.001	0.4	0.001	0.3	0.001	1.3	0.003	1.4	0.001	2.4	0.002
Cd	0.1	0.025	0.1	0.007	0.1	0.013	0.1	0.004	0.1	0.002	0.2	0.077	0.1	0.016	0.1	0.014
Sn	1.1	0.000	0.8	0.000	1.3	0.000	1.3	0.000	1.2	0.000	2.3	0.000	2.4	0.000	2.5	0.000
Cs	2.2	0.005	1.9	0.001	2.8	0.017	3.5	0.053	2.0	0.014	6.4	0.042	7.3	0.181	7.6	0.211
Ba	844.1	22.36	904.0	12,270	829.6	38.85	865.5	60.41	906.4	11.27	700.9	77.94	705.2	66.49	691.7	62.28
Hf	1.0	0.001	0.7	0.001	1.4	0.001	1.1	0.001	0.9	0.001	1.8	0.004	2.0	0.005	2.2	0.006
Ta	0.4	0.000	0.3	0.000	0.4	0.004	0.4	0.005	0.4	0.001	0.6	0.002	0.7	0.001	0.7	0.001
W	0.7	0.002	0.4	0.001	0.8	0.003	0.9	0.006	0.7	0.002	1.5	0.012	1.6	0.030	1.8	0.032
Tl	0.4	0.753	0.5	0.365	0.5	0.770	0.5	0.73	0.5	0.237	0.6	1,319	0.6	1,400	0.6	1,076
Pb	15.6	0.043	14.7	0.071	17.2	0.069	17.7	0.146	21.7	0.059	22.2	0.199	23.3	0.356	24.7	0.403
Th	4.0	0.198	3.5	0.112	5.2	0.292	6.1	0.407	4.7	0.186	9.4	0.758	11.4	1,286	12.4	1,649
U	1.2	0.395	0.9	0.553	1.5	0.590	1.5	1,881	1.2	1,853	3.0	1,475	4.2	2,898	5.0	3,568
La	25.8	0.769	15.3	1,029	27.0	0.942	28	3,048	21.1	1,029	33.5	3,124	40.2	6,502	47.1	7,758
Ce	54.4	0.093	32.3	0.128	55.7	0.137	53.9	0.451	46.6	0.332	69.4	0.371	83.5	0.753	97.1	0.909
Pr	6.2	0.387	3.9	0.474	6.3	0.530	5.8	1,903	4.9	1,212	7.6	1,609	8.9	3,210	10.5	3,877
Nd	22.1	0.082	14.2	0.091	23.0	0.110	20.0	0.376	17.9	0.196	27.2	0.335	32.4	0.695	38.2	0.827
Sm	3.7	0.016	2.6	0.016	4.1	0.022	3.5	0.073	3.3	0.037	5.1	0.066	6.7	0.127	7.1	0.15
Eu	1.0	0.075	0.8	0.08	1.1	0.102	0.9	0.344	0.9	0.169	1.1	0.323	1.3	0.624	1.5	0.738
Gd	3.3	0.011	2.3	0.012	3.7	0.015	3.35	0.051	3.0	0.027	4.7	0.046	5.6	0.089	6.6	0.112
Tb	0.4	0.055	0.3	0.059	0.5	0.073	0.4	0.255	0.4	0.138	0.6	0.233	0.8	0.474	0.9	0.573
Dy	2.1	0.010	1.6	0.011	2.5	0.013	2.2	0.047	2.2	0.024	3.3	0.044	4.0	0.084	4.7	0.102
Ho	0.4	0.025	0.3	0.029	0.5	0.032	0.4	0.118	0.4	0.060	0.6	0.109	0.8	0.210	0.9	0.256
Er	1.2	0.003	0.9	0.003	1.4	0.004	1.3	0.013	1.2	0.007	1.8	0.012	2.2	0.024	2.6	0.029
Tm	0.2	0.017	0.1	0.021	0.2	0.021	0.2	0.076	0.2	0.037	0.3	0.072	0.3	0.137	0.4	0.167
Yb	1.0	0.002	0.7	0.003	1.3	0.003	1.1	0.011	1.1	0.005	1.7	0.011	1.9	0.020	2.3	0.025
Lu	0.2	0.000	0.1	0.000	0.2	0.004	0.2	0.005	0.2	0.001	0.2	0.002	0.3	0.001	0.3	0.001

SUSTAINABLE AND COMPETITIVE AGRICULTURAL DEVELOPMENT OF A WATER-DEFICIENT REGION (CASE OF THE CRIMEAN PENINSULA)

Vladimir S. Pashtetsky¹, Vadim V. Khomenko², Nikolay P. Demchenko¹, Natalia Yu. Poliakova¹, Rinas V. Kashbrasiev^{2*}

¹FSBSI Research Institute of Agriculture of Crimea, Simferopol, Russia

²Kazan Federal University, Kazan, Russia

*Corresponding author: rkashbra@gmail.com

Received: September 6th, 2019 / Accepted: May 10th, 2020 / Published: July 1st, 2020

<https://DOI-10.24057/2071-9388-2019-122>

ABSTRACT. The transition of water-deficient regions to sustainable agricultural development requires taking into account natural, economic and social factors, and restructuring of the sectoral and territorial structure of agriculture. In the case of the Crimean Peninsula, the most important factor was the interruption of water supply through the North Crimean Canal (April 2014). Hence, there was a need to revise the possibility of growing crops in dryland conditions. It has become practically impossible to grow rice, soybean, some vegetables, potatoes, grain corn, pome and stone fruits, etc. Farmers were forced to review grain and fodder crop rotation. They stopped growing crops that required systematic irrigation. Given these realities, a special place in crop rotation should have such plants as pea, chickpea, lentil, sainfoin, etc. The studies conducted by Crimean scientists and experience in commercial production stimulated farmers to grow essential oil crops since they are among the most promising. Viticulture based on the well-developed agriculture and vine growing in favourable areas of the Republic is also promising. Some pome and stone fruits that demand less irrigation are very promising for the Crimea too. Special attention should be paid to filbert, jujube, sweet almond, hazelnut, etc. Considerable efforts should be made to develop animal husbandry. The search for water at depths of 1-1.2 kilometres should be one of the ways to solve problems in the agro-industrial complex (AIC) of the Crimea, as well as wastewater treatment and their use for irrigation purposes. All the aforementioned changes are already taking place in the AIC. But they require significant acceleration and investments in prospective economic sectors.

KEY WORDS: water-deficient area, structure of agriculture, sustainable development, agricultural competitiveness, food security, drought-resistant agriculture, soil-climatic zones

CITATION: Vladimir S. Pashtetsky, Vadim V. Khomenko, Nikolay P. Demchenko, Natalia Yu. Poliakova, Rinas V. Kashbrasiev (2020). Sustainable And Competitive Agricultural Development Of A Water-Deficient Region (Case Of The Crimean Peninsula). *Geography, Environment, Sustainability*, Vol.13, No 2, p. 65-72
<https://DOI-10.24057/2071-9388-2019-122>

Conflict of interests: The authors reported no potential conflict of interest.

INTRODUCTION

Sustainable development of the territories is possible when the use of natural, industrial and financial resources, as well as technological development and institutional transformations, are mutually agreed and meet the needs of present and future generations (Kotlyakov et al. 1999). In different regions of the world, depending on natural conditions, the goals of sustainable development are achieved differently (Golubchikov et al. 2017). In this article, we explore the conditions for sustainable development of water-deficient regions on the example of the Crimean Peninsula.

The purpose of this research was to identify trends in the agriculture of the Crimean Peninsula and changes in its territorial and sectoral structure depending on changing natural, social and economic conditions.

Dryland farming is labour-intensive and costly industry. Investing in it is associated with natural, technological and

financial risks. An analysis of the production of grain crops in the Crimea shows that even under relatively favourable conditions it is impossible to harvest more than 25 cwt/ha (Gerasimova 2006; Gormashov 2006; Pashtetsky 2015; Morozov 2017). Hence, it is impossible to compete with farmers, for example, from the Krasnodar Territory, who harvested over 60 cwt/ha over the past five years.

Lack of water from the North Crimean Canal since April 2014 is further exacerbating the situation. Currently, a little over 13 thousand hectares are irrigated from various water sources in the Crimea, mainly by drip irrigation. In 2015, only 10.1 thousand hectares were irrigated, though in 2013 this number was nearly 136 thousand hectares.

The shortage of water resources led to the disappearance of entire sectors of agricultural production, such as rice growing, soybean cultivation, as well as the sharp decline in the production of fodder, vegetables, melons, etc. At the same time, resource – and energy-intensive technologies, as well as non-renewable natural resources are still being used

(Polovitskiy and Gusev 2004; Pashtetsky 2015). It does not contribute to the structural restructuring of the agricultural economy in terms of its sustainability and remains an obstacle to the production of high-quality and competitive agricultural products.

Crimean farmers will have to choose new and economically feasible ways to develop the AIC on the peninsula based on dryland farming.

There are many positive prerequisites on the peninsula, such as the large domestic demand for products due to the significantly increased number of tourists (more than 6 million in 2018), significant reserves of unused land, as well as the possibility to develop such attractive and economically viable industries like horticulture, viticulture and essential oil crop cultivation.

MATERIALS AND METHODS

The presented results are based on the data provided by the Ministry of Agriculture of the Republic of Crimea, primary data and analytical materials provided by the Federal State Budget Scientific Institution «Research Institute of Agriculture of Crimea» for 1989–2019.

In our research, we used the abstract and logical methods, comparative analysis, observation and collection of facts. They made it possible to study changes in the structure of agricultural production in the Crimea, as well as trends in the transition of agriculture of the Crimean Peninsula to sustainable and competitive development.

RESEARCH RESULTS

In Soviet times, agriculture in the Crimea developed rapidly due to the centrally planned economy. The economy of the peninsula had specific characteristics:

- Optimal, smart and proper work planning, efficient decision-making process and timely control of results for every region, district and even each agricultural enterprise taking into account soil, climate, economic and even social characteristics;
- Optimal balance of sectors in the agricultural enterprises, which allowed the rational use of land, agricultural machinery, and labour;
- There were irrigated arable lands on the peninsula. 460 thousand hectares were irrigated at the state level and 150 thousand hectares were so-called «satellites». At that time

one irrigated hectare was said to work just like four hectares of dry land;

- There were such dynamically developed branches as horticulture, viticulture, olericulture (vegetable growing), and rice cultivation;
- Strong food-canning industry (there were five large state canning enterprises and 157 canning factories with refrigerators);
- Strong livestock farming based on a good fodder base and sectors of dairy and beef cattle breeding, poultry farming, pig, rabbit and sheep breeding;
- People's work ethic;
- High level of technologies in agriculture and animal husbandry based on the research results of Crimean scientists.

Since the 1990s, with the transition to a market economy, the above mentioned factors of intensive agricultural production have not worked anymore. Fig. 1 illustrates the outcome of the AIC reform process in the Crimea.

As we can see from Fig. 1, from 1985 to 2019 the number of sheep and goats has decreased by 5.8 times, cows – by 5.1 times. The trend is the same for other livestock industries. Over the past six years, the trend towards a decrease in the number of cattle and poultry continues. This leads to a decline in livestock production in the Crimea and to the need to import almost 400 thousand tons of milk and dairy products, as well as 38 thousand tons of meat from other regions.

An important factor for sustainable growth of milk and meat production is the development of cattle breeding in large agricultural enterprises. These enterprises have opportunities for investment to organize production at the global level, as well as for the development of the necessary fodder base, corresponding to high technologies for the production of final products (Van Lynden 2000). To date, this trend, for many reasons of a political and economic nature, is absent; there is a decrease in the number of livestock and volumes of its production. Sanctions against the Crimea continue to discourage both foreign investors and Russian banks and companies. There are no large Russian banks, insurance companies or large agricultural holdings in the region. The agriculture of the peninsula needs investment not only in the livestock, but also in the processing industry (Ingersent and Rayner 1999). The only example of serious investment – the development of the «Krym-farming» (Crimea-Farming) dairy enterprise. It works consistently and systematically; its activity is based on foreign investments.

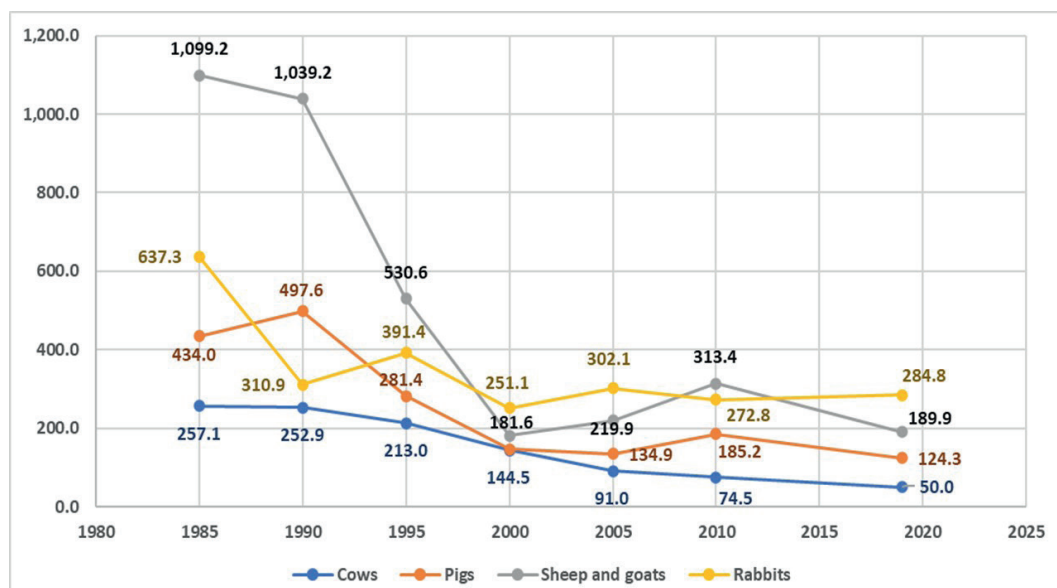


Fig. 1. Dynamics of livestock on the Crimean Peninsula, 1985–2019, thousands of head

This enterprise successfully solved the problems of building its own plant for processing dairy raw materials into high-quality products.

Under these conditions, the state budget is the main source of investment. Indeed, government investment in agriculture is effective, but it is clearly not enough to reverse stagnation in the Crimean economy.

Recovery of cattle, pig and sheep breeding and fattening is also a very promising way of farms and peasant enterprises development. During 1990-s and from 2000 to 2019, the number of cattle on farms increased (including cows), as well as the number of pigs, sheep and goats. Farmers more efficiently address issues on improving livestock arid fodder production, placing the animals in temporary barns without the significant costs on their maintenance and repair.

S. Garmashov (2006), V. Pashtetskiy (2016) and other scientists from the Crimea agree that the Crimea itself renews only half the amount of water resources needed for the peninsula. However, these water reserves clearly not enough for the development of agriculture, which is believed to be a priority in the life of any society and state. The situation in the region forces us to begin the search for a fundamentally new harmonious doctrine of economic policy on a qualitatively new level. New consistent state policy is critical for the Republic of Crimea. It should be aimed at striving to implement the environmentally sound principles of sustainable development into real business practices and social life (Van Lynden 2000; Gormashov 2006; Pashtetsky et al. 2016).

A serious challenge to the economy of the region is the impossibility to use the Dnieper water for irrigation. In this regard, the fodder supply on the peninsula has deteriorated. In the 1980s, there were 1.2 million hectares of agricultural lands (half of which was irrigated), in 2010 – 866 thousand hectares, and in 2017, agricultural lands were reduced to 768 thousand hectares.

With the interruption of water supply through the North Crimean Canal, the prospect of vegetable growing development on the peninsula has become insignificant. The cultivation of vegetables is possible only by individual private farms and households, as they can use water from the rivers and the moisture accumulated during the winter-spring period in ponds and reservoirs.

Furthermore, the growing demand for water caused changes in crop rotations. Farmers unwisely grow only grain and industrial crops, stop the production and use of organic fertilizers. The attitude of the Crimean authorities to

the provision of eastern Crimea with drinking water is also short-sighted. The transfer of water to the North Crimean Canal from the reservoirs of the Belogorsky district, as well as replenishment of water from Novogrigoryevsky, Nezhinsky and Prostornensky intakes with a volume of 200 thousand cubic meters per day, are dangerous. Such water intake in the near future can lead to a limitation of drinking water supplies and can leave the population of Dzhankoy and Nizhnegorsk districts without fresh water.

A much more effective and promising option is to drill wells to a depth of 1.0-1.2 kilometres. It is necessary to use the similar experience of other countries, such as Saudi Arabia, which managed to grow 55 million palm trees in the desert using water from one-kilometre-deep wells.

The forage crop area and the fodder production decreased the most significantly during the 1990s. But even in 2010–2017, during a period of stabilization in agricultural production, this negative trend continues to occur: for example, the sown area of annual plants decreased by 2.7 times, perennial plants – by 2.3 times (Fig. 2).

Fig. 2 illustrates that the fodder crop acreage decreased not very much after 2014. However, the lack of irrigation affects their productivity. For example, today agricultural enterprises receive 15–19 tons of fodder root crops per hectare, while in the 1980s the yield was 60–80 tons/hectare.

At the same time, there is a positive experience of a number of agricultural enterprises that demonstrate the benefits of the introduction of new technologies. They are «Karkinitzky», «Partizan», «Krym Farming», etc. They quickly responded to the interruption of water supply and changed fodder crop rotation. This experience shows that even without irrigation it is possible to have a stable fodder base, increase production volumes and improve economic indicators. Currently, the volumes of fodder production on the peninsula is approximately equal to that of one of the fourteen regions of the Crimea in the 1980s. This reflects potential prospects for growth in fodder and livestock production.

In recent years, unnecessarily significant areas were sown with sunflower (Pashtetsky et al. 2013). Some farmers began to plant sunflower every three and sometimes even every two years that sharply worsened the state of arable lands. Despite the fact that in some dry years the sunflower was not even harvested, the economic efficiency of this crop makes farmers violate the agricultural technology of its cultivation. In addition, soybean, which gives a good

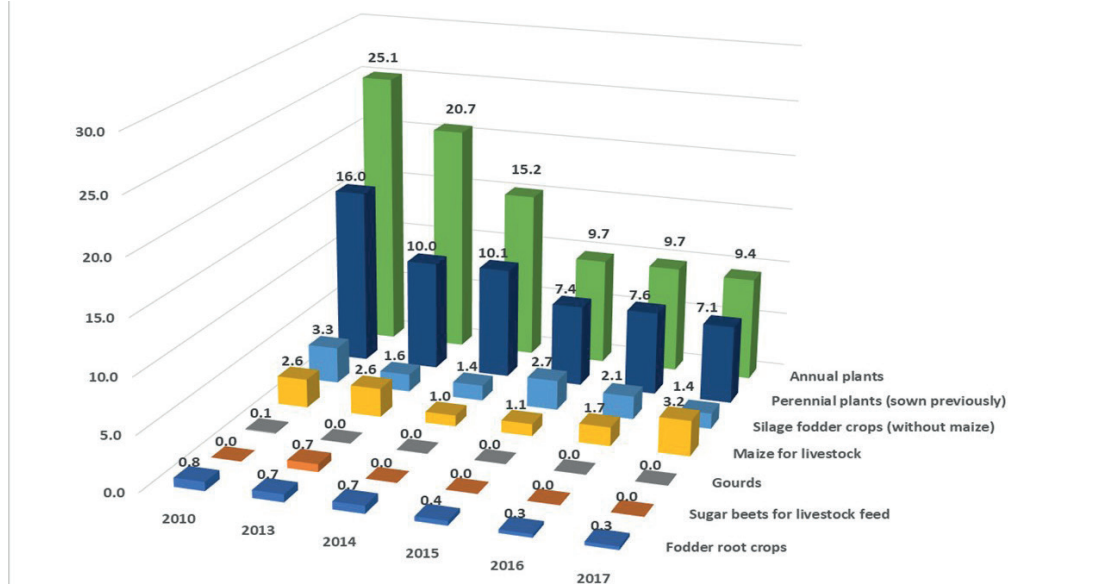


Fig. 2. Sown area of fodder crops on the Crimean Peninsula (thousand hectares)

yield under irrigation and was earlier cultivated on an area of up to 12 thousand hectares, stopped to be grown because of the interruption of water supply to the Crimea. Due to the lack of stable demand for rapeseed in the region, its cultivation areas decreased from 22 thousand hectares in 2010 to 11.8 thousand hectares in 2017 (Table 1).

The next aspect of sustainable and competitive development of the region is the cultivation of new types of crops. The Crimea, with its arid climate, cannot compete with agricultural producers of the Krasnodar Krai. After all, over the past five years, the yield of grain crops was up to 60 kg/ha there, and the costs were almost the same. This creates the prerequisites for the cultivation of essential oil crops. They can be grown on dry land and provide good economic indicators. In the 1980s Crimean essential oil industry was the leading one in the USSR. Crimean farmers produced 60% of the country's needs in lavender oil, 30% of rose oil and 52% of sage essential oil. However, like all other branches in the region, the cultivation of essential oil crops during the transition to a market economy was minimized (Fig. 3).

According to Fig. 3, from 1989 to 2017, the lavender growing area decreased by 4.4 times, the area of clary sage – by 5.5 times, of rose – by forty three times. Only coriander production volumes increased: from 2.556 hectares in 2007 to 30.547 hectares in 2017. The essential oil industry can quickly and greatly improve the economic situation in the Crimean villages due to significant demand for essential oil. The success of the industry is largely determined by the presence on the peninsula such institutions as FSBSI «Research Institute of Agriculture of Crimea» with its specialists, technologies, varieties and the ability to provide Crimean farms with seedlings and seeds of essential oil crops. Sustainable development of essential oil production requires also strengthening the role of the Ministry of Agriculture of the Crimea in involving farms in this promising industry.

For sustainable feed production and growth in livestock production, it is necessary to change radically not only the structure of crop rotations, but also optimize the use of water resources available on the peninsula (Pashtetsky 2015). They are groundwater reserves, river flows in the mountainous

Table 1. Industrial crops production on the Crimean Peninsula

	2010	2013	2014	2015	2016	2017
Sown area, thousand hectares						
Sunflower	26.6	81.3	83.8	82.7	117.0	122.3
Soybean	11.6	13.2	4.1	0.7	0.4	-
Rapeseed	18.4	8.5	17.8	6.4	0.9	6.0
including						
winter	18.4	8.4	17.4	6.4	0.8	6.0
spring	0.0	0.1	0.4	0.0	0.1	-
Production, thousand hectares						
Sunflower	36.2	109.3	101.2	107.4	152.0	119.2
Soybean	34.0	33.6	2.2	0.7	0.7	-
Rapeseed	22.0	16.4	14.1	10.9	1.7	11.8
including						
winter	21.9	16.4	13.7	10.9	1.5	11.8
spring	0.1	0.0	0.4	0.0	0.2	-

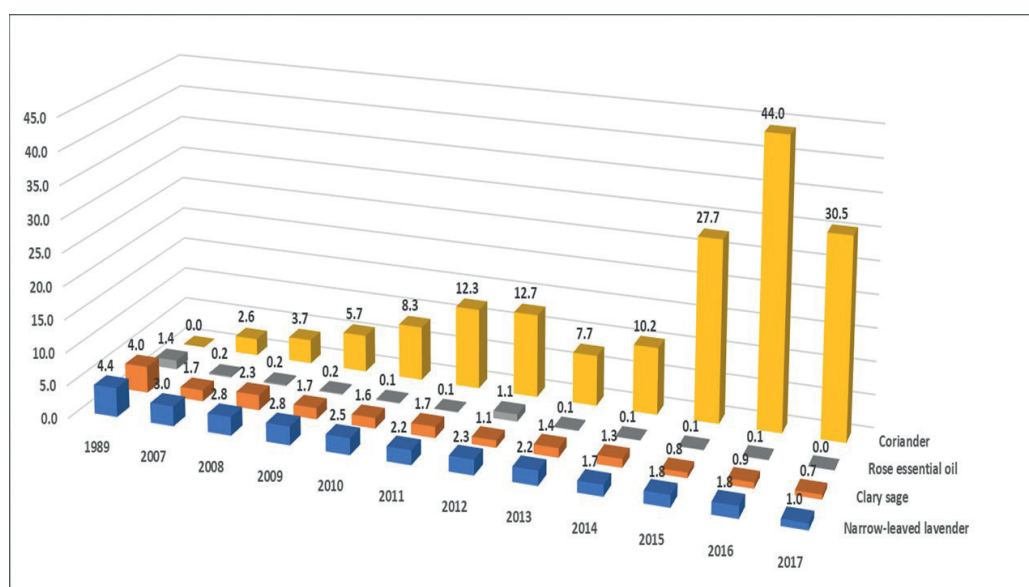


Fig. 3. Dynamics of the areas of the main essential oil crops in the Crimea in 1989–2017, thousand hectares

and foothill regions, reservoirs and ponds, water from other rivers of the peninsula. An example of the optimal use of water is the agricultural company «Chernomores» (situated in the Bakhchisarai district), which accumulates the water of the Belbek River in irrigation ponds during the winter-spring period and irrigates 400 hectares of vineyards. It is necessary to monitor the availability of water everywhere in the peninsula, as well as adopt the measures to increase the number of water sources and rationally use it. As the experience of the Soviet period shows, excessive pumping of groundwater from horizons up to 200 meters led to the depletion of aquifers and the replacement of freshwater by the salt one from the Black Sea and Sivash (Pashtetsky et al. 2016). Currently, in the Crimea, a little over 13 thousand hectares are irrigated from various water sources, mainly by drip irrigation. In 2015, only 10.1 thousand hectares were irrigated, though in 2013 this number was nearly 136 thousand hectares.

The reuse of water resources is promising. In the future, wastewater treatment can provide up to 70 million cubic meters of water. It can be used in the steppe of the peninsula for irrigation agricultural crop (Pashtetsky et al. 2013).

Investment in agriculture is unattractive to investors, both foreign and domestic, due to the high risk of natural anomalies, the lack of short return periods and lower than in other sectors dividends. One of the problems is sanctions. They discourage large Russian banks, insurance companies, etc. and they do not open their branches in the region. Only the government is a reliable investor for the Crimea as a whole, and agriculture in particular. Stimulating investment activity in such conditions is vital and is the most important for the economic development of agriculture. Therefore, it will be extremely important to search for options for real investment in the near future (Bugueva 2017). Moreover, there are many positive prerequisites on the peninsula, such as the large domestic demand for products due to the significantly increased number of tourists (more than 6 million in 2018), significant reserves of unused land, as well as the possibility to develop such attractive and economically viable industries like horticulture, viticulture and essential oil crop cultivation. In addition, the investment attractiveness of the Crimea is based on its favourable geographical position, popularity for tourists, high-quality winemaking, warm climate, and highly educated population.

The potential of the Crimean farmers is large. They are able to provide products not only for its residents and tourists, but also for the northern regions of Eurasia, as it was during the Soviet period. In this case, the role of a strong middle class is growing. Development of the village is impossible without farms and households that use natural resources and biological features and advantages of plants and animals much more efficient (Vorobeveva 2014). In this regard, it should be noted that the Crimean authorities do not pay necessary attention to the emergence and functioning of private farms in the region. Farms have not yet become the locomotive of rural production in such industries as vegetable growing, viticulture, horticulture and livestock. In 2018, over 1,200 farms are registered in the Crimea. Their contribution to the sector of crop production was 16.0% in 2017, to livestock – 2.1%, and it is constantly growing. The state takes some measures to support financially some farms and allocates grants for dairy and beef cattle breeding and all branches of crop production (Vorobeveva 2014; Bugueva 2017).

Viticulture, in spite of the lack of water, is very promising too, because the Crimean winemakers have both traditions and experience in the field of winemaking.

The organization of vegetables production, by contrast, is not so promising. The most powerful factors influencing

vegetable growing are warm climate, availability of water, and modern technologies. Additionally, the market infrastructure and the development of logistics seriously affect the efficiency of the vegetable growing industry. During the Soviet period, specialized collective farms of the vegetable and milk trust, the «Krymkonserv» associations, as well as many collective farms with their own canning plants and refrigerators, were engaged in the cultivation of vegetables. The vegetables were processed at five large canning plants located in Simferopol, Dzhankoy, Nizhnegorsk, and Bakhchisaray. All state farms specializing in the cultivation of vegetables had large areas of irrigated arable land, certain crop rotations, and considerable labor resources. Currently, the cultivation of vegetables is only possible near water sources. Despite the obvious shortage of vegetables on the peninsula, vegetable producers face challenges in their efforts to sell them, as it is unprofitable for trade enterprises to cooperate with a large number of small farms.

All the above listed has determined the specialization of regions of the Crimea, taking into account soil-climatic conditions, economic characteristics of the areas and location of markets. Early vegetables, as well as early potatoes, early cabbage, pumpkin, peppers, and eggplant must be grown in Simferopolsky, Bakhchisaraysky and Saksy districts. In Dzhankoy and Krasnogvardeisk districts, it is necessary to grow vegetables for conservation. The supply of cities of the southern coast, Simferopol, Sevastopol, and Yevpatorya with large stocks of onions for sale in winter should also be given to these districts. In the north-eastern and eastern zones of the peninsula, it is necessary to cultivate a full set of vegetables to meet the needs for fresh vegetables of residents and vacationers in the resorts of the cities of Feodosia, Sudak, and Kerch. In Krasnoperekopsky and Razdolnensky districts, it is necessary to develop melon farming, potato growing, as well as growing vegetables for canning production.

Such zoning will increase the efficiency of the industry and will contribute to meeting the urgent needs in the vegetables of the population and guests of the Crimea. The sanctions also affect the activity of Crimean producers in foreign markets. The sanctions regime does not allow Crimean producers to sell grain, wine, and essential oil products of enterprises outside the Peninsula. It's difficult to buy abroad highly productive breeds of dairy cattle breeding, pigs and sheep, as well as raw materials, seeds, and equipment of foreign production. The most important consequence of the sanctions is the almost complete cessation of investment from abroad. All this affects the competitiveness of products, food security, profit, and quality of rural development.

The external factors mentioned above leading to an increase in the cost of production are not the only problems of the Crimean producers. There are also problems connected with land use, production equipment, and etc. Not all manufacturers have finished the preparation of the documents establishing the right to property and land. This creates significant organizational difficulties for sustainable and competitive agricultural development in the Crimea.

The practical implementation of the principles of sustainable development of a water-deficient region depends on the solution of many problems associated with the shortage of water resources, the development of an appropriate infrastructure for dryland farming, the system of financial support for agricultural production and rural areas. As for the Crimean Peninsula, these problems can be clarified as the tasks that require a priority solution. These include:

- moral and physical depreciation of basic production equipment,
- decrease in soil fertility of the peninsula,
- underdevelopment of drought-tolerant agriculture,
- application of organic fertilizers in volumes recommended by scientists,
- modification of crop rotations according to the changed economic conditions,
- recovery of livestock industries in the volumes necessary to ensure food security for the inhabitants of the peninsula,
- recovery of enterprises processing agricultural products,
- insufficient access to markets of agricultural products for Crimean producers,
- lack of introduction of innovative technologies in all sectors of the Crimean village,
- low level of rural social infrastructure.

The solution of these problems will allow organising agricultural production taking into account economic feasibility and addressing such an important and urgent social problems as the employment of the population in rural areas. So, the question of the proper financing of agriculture is relevant.

In 2019, the Ministry of Agriculture of the Republic of Crimea plans to allocate 212 million rubles for the development of small business in the countryside. 172 million rubles will be allocated to «new» farmers for the development of family livestock farms based on peasant enterprises and farms. The budget also provides 40 million rubles for the development of the material and technical base of the peasant enterprises and farms. Such an important issue as land reclamation will not be left without attention, too. 360 million rubles will be allocated to solve this problem. Money is also pledged to reimburse part of the costs incurred in the fight against especially dangerous pests, uprooting of unproductive perennial plantations, payment of electricity bills for the production of vegetables in greenhouses. The task of the Crimean producers is the targeted and reasonable use of the allocated funds to bring the agricultural economy of the Crimea to a sustainable development path.

Microloans today are the most popular among the Crimean businessmen. The micro-financing fund provides the opportunity to take a loan of up to five million rubles. 165 entrepreneurs used that opportunity in 2017. In 2018, 312 million rubles have already been allocated to 170 entrepreneurs. This gives the necessary benefits to the economy of the Republic of Crimea. Such financial help will be extended for several years (Borsch et al. 2016).

The second popular type of support for entrepreneurship is the lending programmes under which regional Guarantee Funds provide loan security for small and medium-sized enterprises. 164 representatives of small business have borrowed more than 1.2 billion rubles. Moreover, in 2018, the Crimean businesspersons have the opportunity to take agricultural machinery and equipment in leasing at six percent yearly. This will be continued in the future (Borsch et al. 2016).

Among the many problems existing in the agriculture of the Crimea is the reduction of soil fertility (Polovitskiy and Gusev 2004; Pashtetsky et al. 2013). Scientists from FSBSI «Research Institute of Agriculture of Crimea» found that the humus content has decreased on average from 2.7% to 2.2% over the past 50 years. This happened because of land resources long-time exploitation that was focused on meeting the current economic and social needs of society. Other problems, including environmental ones, were solved on the «residual principle». During the Soviet period, accumulation and application of fertilizers were organized

systematically. From 10 to 12 tons of organic fertilizers were introduced in all crop rotations annually. In the vegetable crop rotations or fields where fodder beets or corn were grown, up to 60 tons of manure was introduced. This provided high yields and fertility conservation. However, the organic fertilizer application in recent years has decreased in the Peninsula to 0.4 tons per hectare. A clear violation of crop rotation (e.g., cultivation only winter crops and sunflower) has exacerbated the problem of humus accumulation and preservation. The decrease of soybean, forage and other crops that accumulate nitrogen in the soil in the structure of crop rotation led to the same results. Organizational problems also «work» in the same way when the owner of 3-5-8 hectares of land, even having cattle on the farm, without the necessary equipment for introducing manure into the soil, cannot bring organic fertilizer to his/her land. We can say that society continues to exploit land haphazardly. At the same time, agricultural enterprises «Karkinitzky», «Partizan» and a number of other farms work systematically and introduce organic fertilizers into the soil. It was readily recognized by experts (Pashtetsky 2015) that sustainable agricultural development is possible if the following preconditions are in place: ecological conversion of human activities aimed at implementing state and regional programmes of the environmental protection; rational use of natural resources; environmental and food security.

However, over the last three decades, an unbalanced structure of the resources using has developed because of unsustainable agricultural activity. They are the use of resource- and energy-intensive technologies, the predominant use of non-renewable natural resources that do not contribute to the structural transformation of the agrarian economy from the point of view of its stability, the impede production of high-quality and competitive agricultural products. Insufficient investment in the development of agriculture and resources-protected-activity increase the risk of the accelerating economic decline of the AIC of the Crimea.

Therefore, now it is a necessity to find new ways of balanced development of agriculture of the Peninsula. Each agrarian should direct his/her efforts to ensure agricultural balance. It is necessary to form an agricultural mechanism that ensures appropriate sustainable development of the environment. Consideration of characteristics, resource, landscape, economy, and prospect specific to each farm are the most important tasks. A long period of growing crops on the same field leads to the spread of such weeds as bentgrass, scentless chamomile, brome grasses, *Atriplex cana* and other like ragweed (*Ambrosia*), *Chenopodium album* L., and field thistle. Experience has shown that after three years of growing spring barley, even the double treatment with herbicides could not fully suppress weeds (Ivanov 1976; Polovitskiy and Gusev 2004).

It is well known that different weeds have different biological characteristics and they can grow in any agriculturally-valuable crop. So, in winter crops grow winter and perennial weeds; in spring crops – spring weeds. In vegetable crop rotations weeds that are adapted to their biology are common. And, here, the role of the scientifically substantiated crop rotation, which without the use of chemical fertilizer can get rid of most types of weeds, is very important

Crops i.e. winter rye and winter wheat that are sown densely effectively compete with weeds. Such row crops as corn and sunflower, the plants which come close only in summer, require at first inter-row cultivation. Weed-sensitive crops must be sown after those that contribute to cleaning the fields of weeds, for example, spring crops after row crops.

After that, it is necessary to grow crops that contribute to reducing the number of weeds.

In 2018, weather conditions in the Crimea were unfavourable for the cultivation of agricultural crops. In spring, in the meter layer of soil, there were 70–90 mm of moisture, which is clearly insufficient for the development of the crops. The same situation with moisture was in the spring and summer. This created great problems for the farmers because the harvest of grain and forage crops almost throughout the Peninsula was very low. Precipitations in May were only in the foothill areas (Bakhchisaraysky, Belogorsky and Simferopolsky district). Only some farms could harvest the amount of grain usual for these regions. For example, Research Institute of Agriculture of Crimea harvested 36 cwt/ha (in Simferopolsky and Bakhchisaraysky districts). At the same time, agricultural enterprise «Karkinitsky» (situated in the Razdolnensky district), consistently receiving more than 40 cwt/ha, got only 17.9 cwt/ha. Grain yield in the Crimea as a whole was only 1.6 t/ha, oilseeds – 5.5 cwt/ha.

For timely agricultural operations, the critical issue is the availability of the necessary number of machines. On the first of January 2019, the Republic of Crimea had 20,878 units of agricultural machinery, including 5,270 tractors, 1,317 harvesters, 1,596 plows, 2,393 cultivators, 1,910 seed drills, and 1,129 harrows. To harvest crops in optimal agro-technological terms, there are three main organizations that assist farmers in harvesting grain and leguminous crops, mulching crop residues, tillage, sowing, fertilization, and plant protection.

Agrarians of the Crimea should know and use agro-climatic conditions of the territory. Concluding our investigation, we distinguish 7 zones in the Crimea according to various sources (Ivanov 1976; Polovitskiy and Gusev 2004; Pashtetsky 2015). These 7 soil-climatic zones are important for the sustainable and competitive development of AIC of the Crimea:

The zone of solonetzic steppes. In this zone (Krasnoperekopsky, Dzhankovsky area, Nizhnegorsky, Sovetsky and Kirovsky districts) the climate is very dry, moderately hot with mild winters. The soil cover of this zone is represented by dark-chestnut weakly and medium solonetzic soils. These should orient the farmers on the cultivation of such winter crops like wheat, barley, rye, and perennial grasses. To obtain stable yields, wheat should be planted after bare fallows, cropped fallows, and perennial grasses. Onobrychis and Melilotus are the most promising perennial grasses in this area. And if the irrigation is possible, Medicago can be grown too. High-quality winter wheat should be grown there, as well as perennial grasses to provide feed and livestock industry.

The zone of the steppe with chestnut soils. This zone includes Pervomaysky, Razdolnensky districts, and southern part of the Dzhankovsky and Krasnoperekopsky districts. Here climate is very dry with moderately mild winters. The soil represented by dark-chestnut weakly and medium solonetzic soils. These natural factors «help» in cultivating high-quality winter wheat, large areas of perennial grasses, and essential oil crops such as mint, coriander, wormwood, sage, and lavender.

The zone of black soil steppe. It includes Krasnogvardeisky district, northern part of Simferopol and Belogorsky district, south of Nizhnegorsky, Sovetsky and Kirovsky districts, and eastern part of Saksy district. The climate of the region is arid and hot with temperate mild winters. The largest area in the zone is presented by southern and calcareous chernozems. The area is the most suitable for growing traditional for the Peninsula crops: winter wheat and winter barley, early spring crops (oats and barley), pea and bean, sunflower, mustard and flax. Sainfoin, alfalfa, clover, and winter vetch should

be sown as the basis for forage. To balance fodder in sugar, triticale, sudangrass or sorghum-sudangrass hybrids are the best. The area is prospective for growing traditional oil-bearing plants. And if the irrigation is available, it is possible to grow vegetables and sugar beet seeds.

The zone of high rocky steppes. Farms of Chernomorsky and the eastern part of the Saksy district are located in the rocky steppes. The region's climate is very arid, with mild winters. In dry years, winter and spring crops begin to die here first of all because of lack of moisture in the soil. The soils in the area are calcareous chernozems, weak and sod-calcareous soils. The only crop that provides the best yields is winter barley. Farmers should focus on such perennial herbs as Onobrychis and Melilotus, and such forage crops as winter vetch, triticale, and sudangrass. The area fits for growing lavender, sage, and coriander.

The zone of the lowland complex solonetzic steppe. There are the farms of Leninsky district. The climate of the zone is arid, of the coastal strip – very arid, with moderately hot summers and mild (centre and Priazovye) and very soft (Prichernomorje) winter. The soils in the area are very diverse. They are represented by southern chernozems, weak and medium solonetzics, as well as by the solonetzic chernozems in the Western part of the Peninsula. Soil and climatic conditions of the zone are hard for crop growing. For agricultural activities in the area, there should be 20% of bare fallows and the same amount of cropped ones. This allows cultivating winter wheat. Forage should be based on Onobrychis and Melilotus. It is possible to cultivate aromatic crops. And if the irrigation is possible, sugar beet for seeds may be grown.

The zone of the foothill calcareous-chernozem steppe. It includes the agroenterprises of Bakhchisaraysky, Belogorsky, Bakhchisaraysky districts, southwestern part of the Kirovsky district, the Simferopolsky district (except the northern part), and the city of Sevastopol. The climate of the region is arid, warm with moderately mild winters. The soils of the region are calcareous chernozems, in some places sod-calcareous. The region is suitable for growing fruit crops, grapes, as well as essential oil crops and tobacco. The basis of the feed is alfalfa and sainfoin. In the eastern foothill region of the zone, there are agricultural enterprises of Simferopolsky, Belogorsky and the southwestern part of Kirovsky districts. The climate is semi-arid, moderately warm with mild winters. This makes it possible to grow traditional Crimean crops, namely essential oil crops, tobacco, medicinal herbs, pome and stone fruits, grapes.

The southern coastal mountain zone. They are agricultural lands of the cities of Yalta, Alushta and Sudaksky district. The climate of the zone is subtropical (western part of the zone), arid, with warm winters. In the central part – arid, hot, with mild winters. In the eastern – very arid. The soil is represented mainly by brown soils. Due to insufficient moisture in the soil and air, all agricultural methods of crop cultivation should be aimed at preserving and accumulating it in the soil. The main crop in the area is grapes, which accumulate 26% of sugar in berries and is used for the production of strong and dessert wines.

CONCLUSIONS

1. The most important tasks for the AIC of the Crimea in the current economic situation should be: a) formation of a competitive, investment-active agricultural producer; b) development of the most economically profitable industries, which will ensure the needs of the region in the food and raw materials for the food industry.

2. All farms of the peninsula need to review production plans as soon as possible and change crop rotation in the light of the current economic situation.

3. The only real and effective option for investing in the Crimean village is the financial support of the state that provides a transition to dryland farming, create conditions for the active economic growth and ensure food security for the residents of the Crimea and vacationers.

4. Production experience and the effectiveness of cultivation in arid climate orient the AIC of the Crimea on the cultivation of essential oil crops.

5. The promising industry is viticulture, based on existing experience in cultivating crops in favourable soil-climatic zones of the Crimea.

6. In horticulture, it is necessary to develop plantations of undemanding (drought resistant) pome and stone fruit crops, as well as cultivate hazelnuts, sweet almonds, and walnuts.

7. Special efforts of farmers should be aimed at expanding the food supply and developing all branches of animal husbandry.

8. The development of vegetable growing sectors should be guided by the availability of local irrigation and meet the needs of the residents of the Crimea with fresh vegetables throughout the year.

9. Sustainable cultivation of crops depends on the soil and climatic characteristics of the regions of the Crimean Peninsula, which can be distinguished as 7 soil-climatic zones.

10. The most intensively developing forms of integration in the AIC of the Crimea should be processing enterprises for joint processing and sale of products that ensure its competitiveness. ■

REFERENCES

- Borsch L.M., Gerasimova S.V., Tishchenko E. (2016). Priorities for implementation of the state policy of socioeconomic development of agriculture in the Republic of Crimea. *Tavrisheskiy nauchny obozrevatel*, 8(13), 39-43. (in Russian).
- Bugaeva T.N. (2017). The agriculture of the Crimea: problems and prospects. *Scientific Bulletin: finance, banking, investment*, 2, 126-131. (in Russian).
- Gerasimova S.V. (2006). Management of investment activities of joint stock companies. Kiev: Znanie. (in Russian).
- Golubchikov Y.N., Eremchenko E.N., Markova I., Tikunov V.S., Tikunova I.N., Il'ina I.N. (2017) Sustainable development of polar and high-mountain regions of the world – the change of the polar paradigm. *International Journal of Sustainable Development and World Ecology*, 24(4), 328-337.
- Gormashov V.I. (2006). Variability of winter wheat productivity in the south of Ukraine and ways of its stabilization. *Visnik agrarnoi nauki Pivdenного regionu*, 2, 50-57. (in Russian).
- Ingersent K. and Rayner A. (1999). *Agricultural Policy in Western Europe and the United States*. Cheltenham: Edward Elgar.
- Ivanov V.N. (1976). *Soils of the Crimea and their land reclamation*. Simferopol: Tavriya, 1976. (in Ukrainian).
- Kotlyakov V.M., Trofimov A.M., Kashbraziev R.V., Seliverstov Yu.P. (1999). Complex ecological-economical systems: problems of study (economical aspect). *Izvestiya Akademii Nauk, Seriya Geograficheskaya*, 1, 7-12. (in Russian with English summary).
- Morozov V.A. (2017). Main strategic directions of the regional agribusiness. In: *Scientific support for the development of agribusiness in the context of import substitution: collection of scientific works of the International Scientific and Practical Conference*. St. Petersburg: SPbSAU, 59-62. (in Russian).
- Pashtetsky V.S. (2015). Scientific basis of agrolandscapes optimization and effective agrarian sector development in the Republic of Crimea. Simferopol: Publishing House ARIAL. (in Russian).
- Pashtetsky V., Ergin S., Ergina Ye., Verdysh M., Kapralova Ye., Pirozhok A. (2016). Ecological-economic strategies of the agrarian sector in the Crimea. *AIC: economy, management*, 7, 4-15. (in Russian).
- Pashtetsky V.S., Radchenko L.A., Melnichuk T.N., Tarasenko V.S., Parkhomenko T.Yu., Babina R.D., Lyashevsky V.I., Nemtinov V.I. (2013). Strategy of development of the Crimean agrarian industry and their scientific and investment support. *Taurian Journal of Agricultural Science*, 1, 6-8. (in Russian).
- Polovitskiy I.Ya. and Gusev P.G. (2004). *Soils of the Crimea and ways to increase their fertility*. Moscow: Publishing House of MSU, Publishing House «Kolos» (in Russian).
- Van Lynden G.W.J. (2000). *Guidelines for the Assessment of Soil Degradation in Central and Eastern Europe*. FAO and ISRIC.
- Vorobeva E.I. (2014). State financial regulation in Russia. *Scientific Bulletin: finance, banking, investment*, 3(28), 6-12. (in Russian).

EFFECTS OF RUBBER PLANTATION POLICY ON WATER RESOURCES AND LANDUSE CHANGE IN THE NORTHEASTERN REGION OF THAILAND

Aweewan Mangmeechai^{1*}

¹National Institute of Development Administration, Bangkok, Thailand

*Corresponding author: aweewan.m@nida.ac.th

Received: November 9th, 2019 / Accepted: May 10th, 2020 / Published: July 1st, 2020

<https://DOI-10.24057/2071-9388-2019-145>

ABSTRACT. The Thai government launched Phase 3 of its Rubber Plantation Project in 2011 aiming to expand the total area of new plantations to 128,000 ha. The northeastern region contains the largest areas for new rubber plantation areas, yet it is known to have unfertile areas and regular encounters with water scarcity during summer. This leads to research questions as to how the policy affects land and water use in the country. This study shows that the water requirement of rubber trees is 14,221 m³/ha/year which is higher than that of other local crops (e.g., rice, cassava, sugarcane, and corn). Thus, irrigation systems must be utilized during certain months. The land use changes from the cultivation of edible crops to rubber do not threaten the amount of food available for domestic consumption since Thailand generally exports more of its crops than it consumes. From this policy, total rubber yield would increase to 742 M kg and rice, corn, and cassava would disappear about 1613 M kg (24% of the total amount of rice exported in 2012), 7837 M kg, 8926 M kg, respectively. The government should provide a better plan on crop water requirements suitable for each region and knowledge on increasing crop-per-drop efficiency to all farmers.

KEY WORDS: Rubber water consumption; Agricultural policy; Land use; Irrigation system

CITATION: Aweewan Mangmeechai (2020). Effects Of Rubber Plantation Policy On Water Resources And Landuse Change In The Northeastern Region Of Thailand. *Geography, Environment, Sustainability*, Vol.13, No 2, p. 73-83
<https://DOI-10.24057/2071-9388-2019-145>

ACKNOWLEDGEMENTS: This research was supported by Thai National Research Council. The author thanks associate professor Prasert Pavasant and terms for assistance with for data collection and comments that greatly improved the manuscript. They may not agree with all of the interpretations/conclusions of this paper.

Conflict of interests: The authors reported no potential conflict of interest.

INTRODUCTION

Water is becoming a scarce resource for agricultural plantations. Most of the water (up to 90%) provided for domestic purposes can be reused and recycled, while most of the water (40–90%) provided to agriculture to grow food is consumed (evapotranspired) and cannot be re-used (Rijsberman 2006). Small farmers and the poor are particularly disadvantaged and can face acute water scarcity if they do not have access to water to satisfy their needs for either food security or sustainable livelihoods.

Thai farmers rely tremendously on rainfall to grow their agricultural products. Any change in rainfall, especially overall precipitation levels and distribution patterns, carries huge consequences for the farming sector. Farm holding lands for was 23.9 million ha, or 46.5% of the country, in 2017. A breakdown of where these agricultural areas were located can be summarized as follows: 5.2 million ha in the northern part, 10.2 million ha in the northeastern part, 5.0 million ha in the central part, and 3.5 million ha in the southern part (National Statistic Office 2019). Note that, of this figure, the area within irrigation was only 4.0 million ha in 2017 (Royal Irrigation Department 2018).

Based on the frequency of droughts monitored over the past two decades, some experts have predicted that Thailand may now be facing a prolonged water crisis in spite of the fact that the country receives an average rainfall of 1,200 mm to 1,600 mm, annually. With this amount of rainfall, the country is considered to be a water-surplus country. However, the yearly droughts have become an emerging problem in recent years, mostly because farmers have expanded agricultural activity beyond irrigated zones.

Thailand has developed into the world's largest producer and exporter of natural rubber, in alignment with the government's new policy of promoting rubber plantations. Rubber cultivation has expanded throughout many areas in Thailand. The country has produced more than three million metric tons of natural rubber annually, making it a significant source of income. One of the important changes in land use during the past few years has been the expansion of rubber tree plantations. Initially, most rubber plantations of Thailand were located in the South and the East, where there are short dry seasons and adequate rainfall throughout the year.

Since the government added a subsidy that encouraged expansion, rubber plantations have emerged in new areas such as the Northeast. Para rubber has become a major cash crop of the Northeast since then. The northeastern region

contains the largest agricultural area, yet it is known to have unfertile areas, a long dry season, and regular encounters with water scarcity during summer months. With its large areas of plantation, water shortages can be a major constraint to agricultural production. In some of these areas, long dry periods, high temperatures, and high air vapor deficits are reported as being major constraints (Priyadarshan 2005; Rao et al. 1998).

The management of land and water are inextricably linked (Wheater 2009). With the land utilization changes in the northeastern region, it is important to understand the actual water requirement of rubber compared to those of local crops. An understanding of actual water requirements could affect the views of policy makers on the urgency at which to address water issues as well as their views on the most effective policies addressing land utilization and the economic value of crops.

Land for food production could be limited. Kastner and Nonhebel (2010) reported that in Philippines the combined effect of dietary change and population growth led again to increased land requirements for food. Thus, strong increases in yields were enabling constant land requirements for about two decades. The findings suggested that developments in land requirements for food and underlying factors are often non-linear. Caution is warranted when discussing futures of global food supply, based on assumptions of linear or continuous trends (Kastner 2010). Indonesia and Malaysia may also face similar trend due to an expansion areas of palm oil (Wicke 2011).

According to the government policy on rubber plantation promotion, this study aims to understand the consequences of this policy on water and land use change issues. The objectives of this study are 1) to estimate the water requirements of rubber plantations in Thailand associated with the expansion encouraged by Phase 3 of the Rubber Plantation Project. 2) to understand the linkage between land use changes and edible crops associated to the Rubber Plantation Project 3) to discuss and provide suggestions on water management and land use changes. Water footprint concept was applied in this study.

MATERIALS AND METHODS

Rubber plantation policy

Rubber has been a significant source of income for the country. The most important agricultural export sectors are rice, natural rubber, sugar, and cassava (FAO 2011). Rice and rubber generate the top two highest incomes from agricultural exports. From 2005 to 2008, rubber had the highest export value. As exporter of agricultural products, however, the country exploits domestic natural resources through, for example, its misuse of water resources and fertilizer in agricultural practices (Office of Agricultural Economics 2012a).

Nevertheless, the government has promoted an integration of rubber agro-forestry into the farming systems, especially in the North and Northeast. The first phase was from 2004 to 2006, and the second phase was from 2006 to 2011. The collective aim of these two consecutive projects was to increase the amount of land used for rubber plantations by 320,000 ha.

The Thai government announced plans to launch the next phase of its initiative to expand rubber plantations nationwide. The third phase is from 2011 to 2013. Again, the aim is to expand the area used for rubber plantations; this time the goal is an additional 128,000 ha. Of these, a total area of 16,320 ha has been approved for participation in the Northeastern region (Fig. 1). Farmers who have their own lands (0.8-2.4 ha) and have never planted rubber trees before could now participate in the governmental program. For the third phase of the Rubber Plantation Project, the government is providing subsidized tree seedlings (18 baht/seed or US\$0.6/seed), fertilizer, and also subsidizes of 21,870 baht/ha or US\$729/ha for the first three years and technical expertise to help local farmers take up rubber production and move out of poverty. This includes lower tariffs resulting from the country's free trade agreements with trading partners such as China, Australia, New Zealand, and the ASEAN member states.

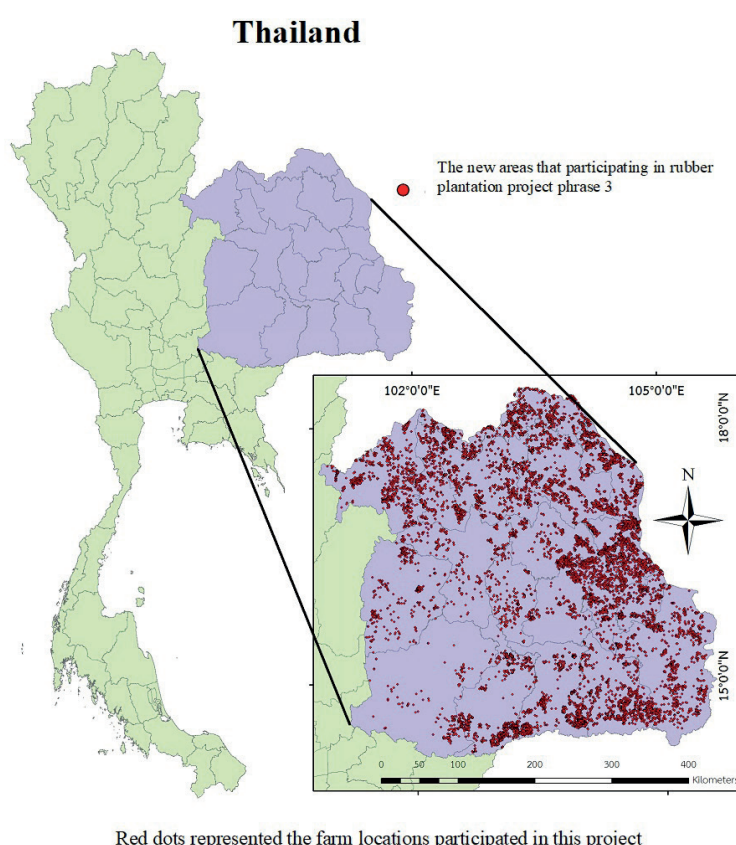


Fig. 1. Total rubber plantation areas in the Northeastern region in alignment with rubber plantation project phase 3

North-eastern region topography

Northeast region topography is mostly plateau at an altitude 120–400 meters above sea level. The climate in the northeast region is like a savannah which is hot and humid, alternating with the dry season with moderate rain. The rainy season starts from May to October and the summer season starts from February to May. During summer, the weather is hot and very dry because it is far from the sea. In addition, there are 3 large basins including the Mekong River, the Chi River and the Moon river. The main river basin of the region is the longest river in Thailand with a length of approximately 765 kilometers. Soil in the Northeast region is sandy soil and lack of nutrients. Underground there are rock salt, making the soil salty and dry which is not suitable for planting crops and farming. Since the northeast region is sandy soil, it cannot hold water, causing water shortages, especially during the summer. Therefore, it requires irrigation system and water storages e.g. dam or reservoir (Regional Development Policy Board 2019).

Factors related to rubber growth and yield

The rubber tree (*Hevea brasiliensis*) is indigenous to the tropical rainforest of the Amazon Basin near the equator, at altitudes that do not surpass 200 m above sea level. The suitable conditions for rubber tree growth include high temperatures of between 24–28 °C and ample annual rainfall averaging 1,500–2,500 mm (Jiang 1988; Office of Research and Development for Land Management 2005). Rao et al. (1998) identified the weekly weather conditions associated with optimum yields at 22.8 to 30.4 °C, with 5.9 h of sunshine. Any deviation from these meteorological conditions for a period of up to 6 months had a significant impact on latex production.

All factors related to rubber growth and yields are summarized in Table 1. For rubber growth, water is an important issue because it is required for photosynthetic growth and prevents the stagnation and wilting of plant cells. During the crop growth period, particularly when negative and reproductive growth takes place simultaneously, plants need large quantities of water for photosynthesis to occur. In contrast, reproductive organs require less water (Samarasinghe 2003).

In studies by Vijayakumar (1988, 1998), tree loss was as high as 18% in the rainfed plots, while tree loss was only 3.7% in the irrigated plots. Variations in girth were also greater among rainfed plants than irrigated plants (Vijayakumar 1988; Vijayakumar 1998).

In addition, the study indicates that reductions in the photosynthetic rate and leaf area index caused by water stress significantly inhibited growth. Higher solute concentrations in latex tended to lower the photosynthetic rate. The immaturity period could thus be reduced to 6 years by irrigation (Vijayakumar 1998).

Clermont-Dauphin (2013) reported, for the first time, that soil water shortage is unexpectedly and arguably not the main cause of low growth rates. Dry air in the dry season and waterlogging in the rainy season can be even greater constraints.

With regard to yield, Rao et al. (1998) reported latex is 65–70% water and hence moisture stress influences the yield. Low latex solute potentials and sufficient available water are the conditions required for a good flow of latex. Lower yields are associated with moisture stress conditions and the withering of the tree. During a recorded drought period, for instance, a 61% lower yield than average was experienced. Of similar fluctuation was the highest yield, at 77% above the average yield. Yields of rubber trees tend to be dependent on the genotype, soil and atmospheric conditions. Most of the nutrient and water uptakes take place in the surface layers during the wet season and the same are absorbed from the deeper layers of the soil during the dry season (Rao et al. 1998). Seasonal variations of yields and yield components show that maintenance of higher soil moisture status and low vapor pressure deficits are essential to maintaining optimum water relations in rubber trees (Devakumar et al. 1988; Rao et al. 1990). Regional variations in annual rubber yields are associated with the intensity and duration of moisture stress. About 40–62% of the total variations in monthly rubber production could be explained by prevailing environmental and technological factors (Daud 1989; Jiang 1988). Rainfall exceeding 9–11 mm per rainy day is not congenial to high yields owing to harvesting difficulties. Above 34 mm of rainfall in a day can make tapping difficult (Rao et al. 1998).

There were some differences in the root distribution patterns, yet the total root density per unit soil volume did not vary between irrigated and rainfed trees in a study by Devakumar et al. (1998). Irrigated trees intercepted nearly 88% of solar radiation during the summer and 90% in the post-monsoon season; meanwhile, rainfed trees intercepted 49% and 88% during the summer and post-monsoon season, respectively. The biomass produced by irrigated trees was significantly higher (60%) than the biomass produced by the rainfed trees.

Table 1. Factors related to rubber tree growth and yields

Factors	Rubber tree	References
Sufficient water (irrigation system)	Reduced tree loss (approximately 15%) Low variations in girth/growth rate Diluted latex Reduce immaturity period (approximately 1 year) Increased shrub and resin yields (approximately 6%)	(Vijayakumar 1988) (Vijayakumar 1998) (Rao et al. 1990) (Clermont-Dauphin 2013) (Njukeng 2011) (Miyamoto 1984) (Ferraris 1993)
Meteorological parameters, irradiance, ambient temperature, and vapor pressure deficit	Increased shrub and resin yields (approximately 6%) Maintenance of plant water status through their effects on stomatal resistance and transpiration, thereby influencing latex vessel turgor and latex outputs	(Rao et al. 1990)
Genotype, soil moisture, low vapor pressure deficit, and atmospheric conditions	Seasonal variations of yields and yield components	(Rao et al. 1998)

Trunk volume was 57% greater in the irrigated than that of the rainfed trees (Devakumar et al. 1998).

Meteorological parameters, irradiance, ambient temperature and vapor pressure deficits, play important roles in the maintenance of plant water status through their effects on stomatal resistance and transpiration, thereby influencing latex vessel turgor and latex outputs (Rao et al. 1990).

The results indicate that when there is a short dry period, rubber plants are not seriously affected if there is sufficient soil moisture to support nutrient uptake and evapotranspirational demand. At low soil moisture levels, the rate and duration of latex flow are reduced. Beyond a threshold, the non-availability of soil moisture in the root zone of rubber plants leads to changes in plant water relations and thus affects overall productivity.

A prolonged dry period may significantly affect yield components, such as the initial flow rate, plugging index and dry rubber content. Likewise, heavy rainfall for a prolonged period can negatively affect yields. A shorter duration of sunshine, associated with high rainfall, results in low photosynthetic efficiency. Heavy rainfall also causes nutrient loss by erosion and leaching. Cloudy weather associated with heavy rainfall may lead to disease outbreaks and also affect the photosynthetic efficiency of the plantation. When rain occurs after latex collection, an increase in the volume of latex is expected on the next day of tapping. A higher moisture status in soil may also lead to a dilution of the latex. At low soil moisture levels, the rate and duration of latex flow are dramatically reduced. These factors may be responsible for day-to-day latex yield variability (5–6%). Also seasonal changes in rubber yield are associated with the weather and climatic conditions experienced by the plantation (Njukeng 2011).

Miyamoto (1984) reports that shrub and resin yields increased linearly with increased irrigation, while rubber contents generally decreased with increased irrigation. Resultant rubber yields were highest under the lowest stress treatment, yielding about 840 kg/ha. Thus, a dry irrigation regime may be preferred in areas with a critical water shortage if rubber production is the sole purpose of growing guayule and the economics justify low rubber yields per land area (Miyamoto 1984). In a study by Ferraris (1993), rubber yield was highest under the wet regime, mainly because of its large biomass but also because rubber contents remained relatively high (about 6% on the average) (Ferraris 1993).

Crop water requirement (CWR)

The crop water requirement is the water needed for evapotranspiration under ideal growth conditions; it is measured from planting to harvesting. Conditions are ideal when adequate soil water is maintained by rainfall and/or irrigation so that it does not limit plant growth and crop yields. The crop water requirement is calculated by multiplying the reference crop's evapotranspiration (ET_0) by the crop coefficient (K_c): $CWR = K_c \times ET_0$. It is assumed that when the CWR is fully met, the actual crop ET_0 will be equal to the CWR (Hoekstra et al. 2009). The ET_0 is the evapotranspiration rate from a reference surface. The reference is a hypothetical surface with extensive green grass cover possessing specific characteristics. The only factors affecting ET_0 are climatic parameters. ET_0 expresses the evaporating power of the atmosphere at a specific location and time of year and does not consider crop characteristics and soil factors.

Rainfall contributes to a greater or lesser extent in satisfying the CWR, depending on the location. During the rainy season in tropical and some semi-tropical regions, a great part of a crop's water needs are covered by rainfall, while during the dry season, the major supply of water should come from irrigation. How much water is coming from rainfall and how much water should be covered by irrigation is, unfortunately, difficult to predict as rainfall varies greatly from season to season. In order to estimate the rainfall deficits for irrigation water requirements, a statistical analysis needs to be made from long-term rainfall records. In addition to the variability of rainfall from year to year, not all rain that falls is used by the crop. The intensity of rain may be such that part of the rainfall is lost due to surface runoff or due to deep percolation below the root zone. In order to determine the part of the rainfall that effectively contributes to the CWR, a number of definitions are first given. It is then subsequently explained how the different rainfall values can be calculated and how they are incorporated in the CWR calculations.

Water footprint (WF)

The WF of a product (commodity, good or service) is defined as the volume of freshwater that is used for its production. The WF of crop cultivation can be estimated following the 2011 WF assessment manual of Hoekstra et al. (2009). Total water use is a summation of the green water, blue water, and gray water. The green WF refers to rainwater that evaporates during the production process. This is particularly relevant for crop growth. The blue WF refers to surface water and groundwater used for irrigation that evaporate during production process. The gray water is the volume of polluted water as well as the volume of dilution water that is discharged during the production process; it is defined as the amount of water needed to dilute pollutants emitted to natural water systems during the production process to the extent that the quality of the ambient water remains within agreed upon water quality standards. Green and blue water can be estimated by CROPWATS. The grey component of crop or tree growth ($WF_{proc, grey}$, m^3/ton) is calculated as the chemical application rate per hectare (AR , kg/ha) times the leaching fraction (α) divided by the maximum acceptable concentration (c_{max} , kg/m^3) minus the natural concentration for the pollutant considered (c_{nat} , kg/m^3) and then divided by the crop yield (Y , ton/ha).

$$WF_{proc, grey} = \frac{(\alpha \times AR) / (C_{max} - C_{nat})}{Y}$$

The pollutants generally consist of fertilizers (e.g., nitrogen, phosphorus), pesticides and insecticides. One has to consider only the "waste flow" to freshwater bodies, which is generally a fraction of the total application of fertilizers or pesticides to the field. One needs to account for only the most critical pollutant; that is, the pollutant yielding the highest water volume using the above calculation.

CWR, green, and blue water estimation method

The CROPWAT 8.0 program can be applied to estimate green and blue water of crop and help with the design and management of irrigation schemes, taking the user, with the help of an actual data set, through the different steps required to calculate evapotranspiration, crop water requirements, scheme water supply and

irrigation scheduling. Since the cultivation of most crops relies on rainfed systems, in this study, blue water represents the additional water needed from irrigation system when rainfall is insufficient. The model requires the types of input summarized in Table 2.

The FAO Penman-Monteith equations were used to produce the ET_0 data in Table A1 reported by the Royal Irrigation Department (2011). ET_0 was calculated with weather data from 120 weather stations within 64 provinces from 1981 to 2010. ET_0 data was reported by the Royal Irrigation Department (2011).

The rainfall data comprises the average rainfall values from 2002 to 2012 (10 years) provided by the Thai Meteorological Department. The crop coefficient (K_c) varies over the length of a growing period. The K_c -Penman Monteith value of crops were obtained from the Royal Irrigation Department (Irrigation Water Management Research Group) and are summarized in Table 3. The K_c was divided into three stages: the initial, mid-season, and final stages. The lengths of the individual growth stages were also used as input data for the program. For example, the growth stages for cassava total 360 days; for corn, 99 days; and for rubber, 25 years. The rooting depth of rubber ranges from 1.5 to 2 m for primary roots and secondary roots, while lateral roots can spread as far as 20 meters (Office of Research and Development for Land Management 2005). Critical depletion occurs at

about 40% of the total available soil moisture (Homyarnyen 2007). The yield response factor represents relative yield that decreases in relative to evapotranspiration deficit. The yield response factors of rubber were calculated and were in the range of 0.33-0.49.

Gray water calculation method

According to gray water calculation equation, in this study, α is the amount of nitrogen leaching using the rate of 10% (Nevison). According to interview with approximately 300 farmers, the nitrogen (chemical fertilizer) application rate per hectare (AR) is 118 kg-N/ha/yr for rubber, 98 kg-N/ha/yr for sugarcane, 98 kg-N/ha/yr for corn, 58 kg-N/ha/yr for rice, and 80 kg-N/ha/yr for cassava. These rates were obtained from interviews with farmers. The C max is the nitrogen standard concentration 0.005 kg/m³, C nat = 0, and Y is the average yield per area (Office of Agricultural Economics 2012b). For the water footprint calculation, the average time for planting a rubber tree is 25 years. The tree can be tapped after year 7. Then total water footprint of a rubber tree is its 25 years of growth divided by its 18 years of yields. The sum of the blue, green, and gray water is called the water footprint of crop cultivation (for use in a hypothetical situation or an actual crop water requirement). The functional unit is the actual crop water requirement (L) per yield (kg).

Table 2. Input parameters for CROPWAT

Input	Parameters	Data sources
Weather	- Evapotranspiration (ET_0) - Rainfall data	- The Royal Irrigation Department - The Thai Meteorological Department
Crop data	- Crop coefficient (K_c) - Growing stage - Rooting depth - Critical depletion - Yield response factor	- FAO and Ministry of Agriculture - Literature - Literature - Literature - Calculations
Soil data	- Total available soil moisture - Max rain infiltration rate - Rooting depth	- Literature - Laboratory and literature - Literature

Table 3. K_c -Penman Monteith values of crops

Month	Sugarcane	Cassava	Rubber	Week	Rice	Corn
1	0.65	0.3	0.65	1	1.03	0.63
2	0.86	0.3	0.86	2	1.07	0.72
3	1.13	0.3	1.13	3	1.12	0.86
4	1.35	0.8	1.35	4	1.29	1.13
5	1.56	1.1	1.56	5	1.38	1.35
6	1.29	1.1	1.29	6	1.45	1.52
7	1.20	1.1	1.20	7	1.50	1.61
8	0.93	0.5	0.93	8	1.48	1.63
9	0.63	0.5	0.63	9	1.42	1.58
10	0.52	0.5	0.52	10	1.34	1.50
11	-	0.5	0.52	11	1.23	1.38
12	-	0.5	0.52	12	0.94	1.15
13	-	-	-	13	0.86	0.90
14	-	-	-	14	-	0.67

RESULTS

Water consumption

The results show that rubber plantations require larger amounts of water than other crops (e.g., sugarcane, rice and corn). On average, the water requirement for rubber is 14,221 m³/ha/year (41% blue water, BW and 59% green water, GW); sugarcane, 12,177 m³/ha/year (36% BW and 64% GW); cassava, 9668 m³/ha/year (52% BW and 48% GW); rice, 5220 m³/ha/year (-27% BW and 73% GW); and corn for animal feed, 4417 m³/ha/year (46% BW and 54% GW) (Fig. 2 (a)). This implies that rainfall alone is not enough, especially during the dry season. One exception is rice, which we assumed was planted in a semi-flooded area. Green water counts for approximately 59% of the actual rubber crop water requirement, which is comparable to sugarcane at 64%, cassava at 48%, and corn at 54%. Thus, irrigation systems must be utilized during certain months.

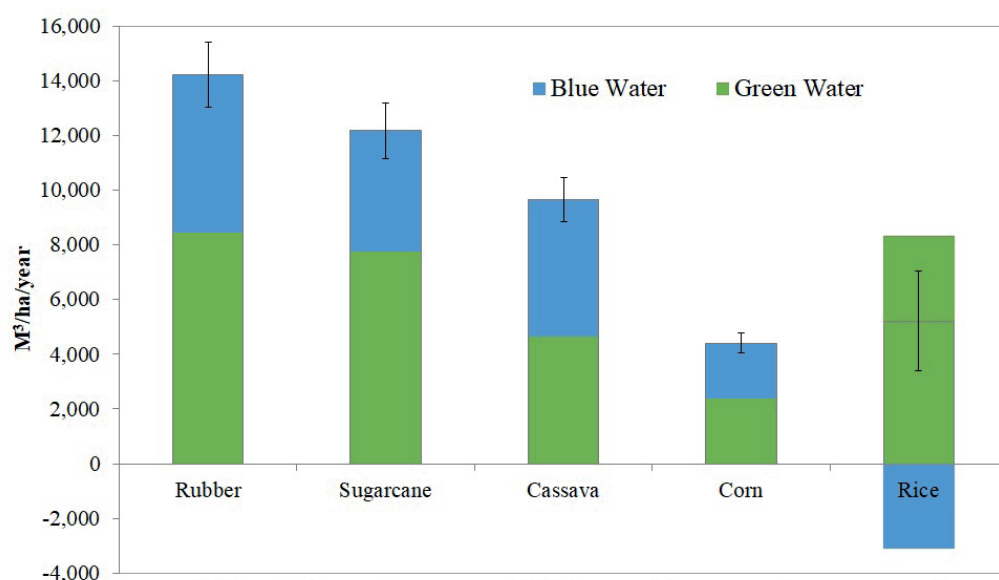
The water footprint of each crop was estimated. The study boundary is only in the field or plantation process only. The water footprint for rubber is 13,067–17,257 L/kg yield; for sugarcane, it is 188–209 L/kg yield; for cassava, it is 512–625 L/kg yield; for corn, it is 1,413–1,877 L/kg yield; and for rice, it is 2,716–3,366 L/kg yield (Fig. 2 (b)). Rubber produced the most gray water (1,600 L/kg yield), followed by rice (550 L/kg yield), corn (500 L/kg yield), cassava (80 L/kg yield), and

sugarcane (30 L/kg yield). If farmers increased their rubber yields, the amount of gray water would lessen.

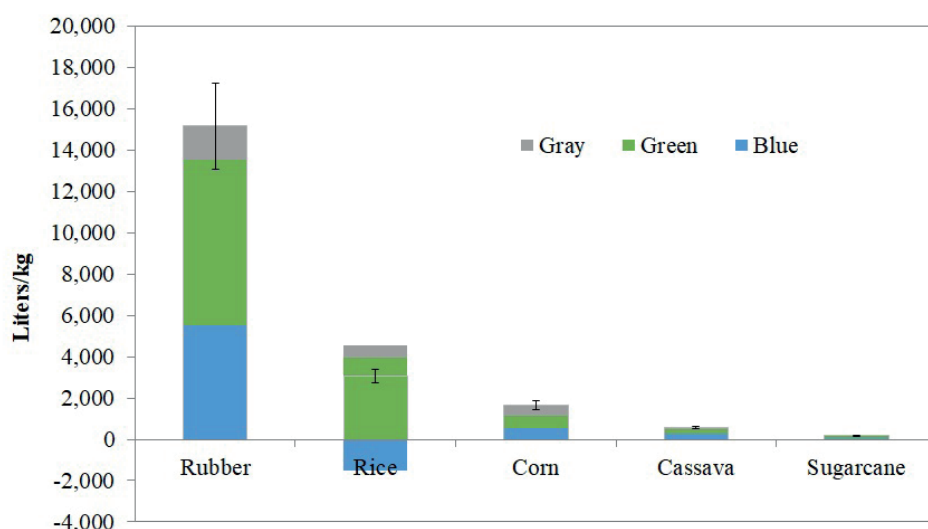
The mean annual rainfall in the northeastern region from 2001–2010 was 1,530 mm, and the rainfall was most concentrated between the months of June and September. Plants, however, experienced stress conditions from mid-October to April. Figure 3, results of the CROPWATS model, showed rubber's water requirement to meet optimal condition during each month of different types of northeastern soil. The green bars represent effective rainfall and the blue bars represent the additional irrigation water requirement. From the Figure 3, there are not much different variation of water requirement between different types of soil due to their soil characteristics in the region that cannot hold water. The region experienced an average water deficit of 580 mm during the summer months. Drought survival is important in the northern part of Thailand, where long dry periods can threaten tree survival the first year after planting, as tree growth is more easily affected in the early stage of development during a drought period (Sangsing 2004).

Land use changes and local water requirements

According to Phase 3 of the Rubber Plantation Project, the quota for the Northeast region is 80,000 ha. Of these, a total area of 16,320 ha was approved for participation. Only 4,456 ha (or 27%) of the total approved area has actually



(a) The actual crop water requirement is the sum of blue water and green water volumes



(b) Green, blue, and gray water of each crop

Fig. 2. Crop water requirements in the northeastern part of Thailand

been used for planting rubber trees, while the rest (11,908 ha) have not yet been used for planting rubber. This is partly due to the fact that the government terminated a subsidy policy on Jan. 4, 2013 – also due to the rapid drop in rubber price – Of the 11,908 ha, 7,979 ha is home to rice paddies, cassava, sugarcane, and corn fields. The rest of 3,929 ha is destroyed forestland and grassland.

To maintain the status quo, in the new rubber plantation areas (4,456 ha), the actual water requirement for planting rubber is 60-65 million m³/yr, more than double the regular water requirement for edible crops of around 27-29 million m³/yr. If all the approved areas in the project (100%) were converted to rubber tree plantations, the total rubber yield

would be 20.6 M kg and the additional water requirement in the region would be 53-57 million m³/yr (Table 4). Expected rubber yield, if adequate irrigation is provided, could increase rubber yield at a rough estimate of 6% or 1.2 M kg. However, this large amount of water cannot be acquired unless the support from the government to promote irrigation systems and individual or village reservoirs. Otherwise, this can lead to policy failure in a long run.

Thailand is also an exporter of food and agricultural products. A change from the planting of edible crops to rubber plantations does not affect the amount of food available for domestic consumption since Thailand exports more crops than it consumes domestically, with the

mm

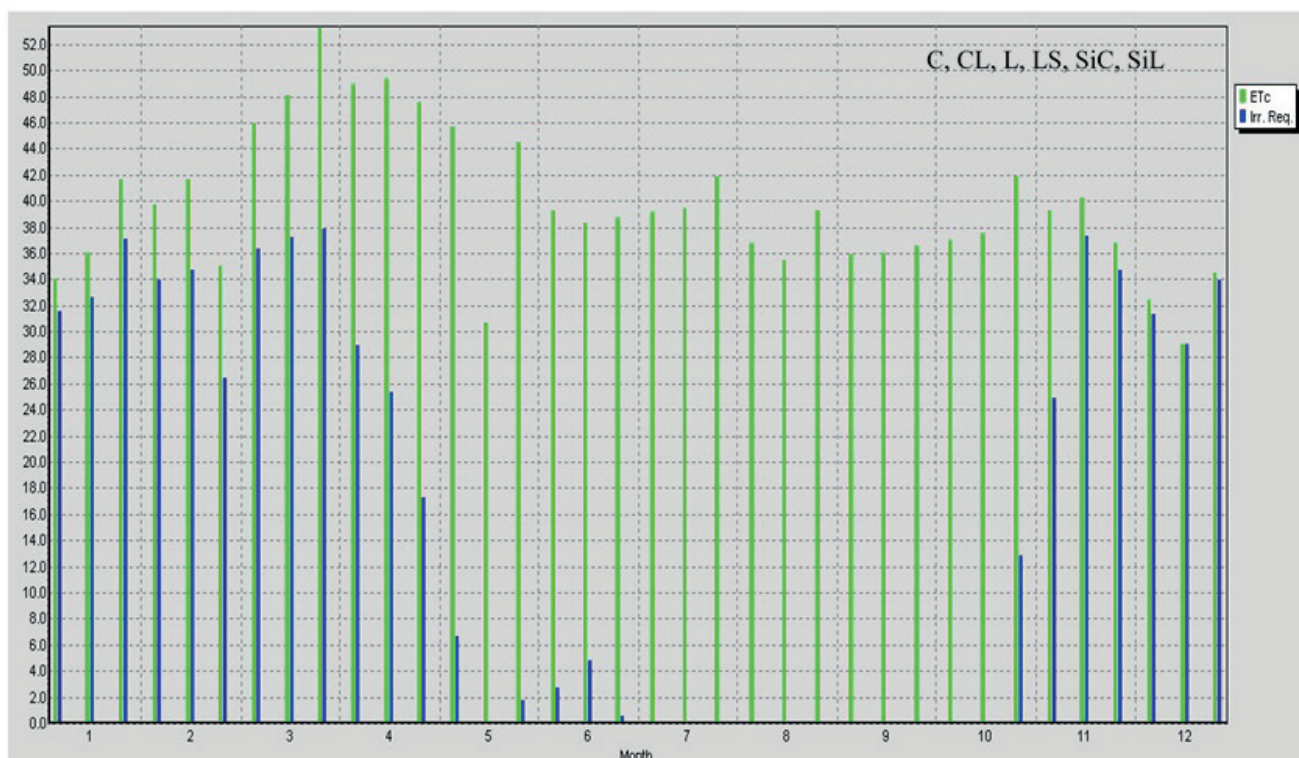


Fig. 3. Rubber's water requirement during each month (the green bars represent effective rainfall and the blue bars represent the additional irrigation water requirement needed to meet the optimal condition) of Clay (C), Clay Loam (CL), Loam (L), Sandy Loam (LS), Silty Clay (SiC), Silty Loam (SiL) (y-axis is month and x-axis is mm)

Table 4. Land use and water requirements of the agricultural products subject to the rubber plantation policy

	Area (ha)			Water requirement (M m ³)			Products (M kg)			
	Rubber plantation	Incremental Rubber plantation	Mix crop	Rubber	Mix crop	Incremental water	Rice	Corn	Cassava	Rubber
Status quo	4,456	-	7,979	61.2 -65.9	56.7-60.7	-	16.9	10.3	24.0	7.4
10%	5,254	798	7,181	72.2-77.7	96.2-104.0	50.4 -55.1	14.5	8.9	20.6	8.7
20%	6,052	1,596	6,383	83.1-89.5	85.5-92.4	50.7 -55.3	9.8	6.0	14.0	10.0
30%	6,850	2,394	5,585	94.1-101.4	74.8-80.9	50.9 -55.6	6.9	4.2	9.8	11.3
40%	7,647	3,192	4,787	105.1-113.2	64.1-69.3	51.2 -55.9	4.8	3.0	6.8	12.7
50%	8,445	3,990	3,990	116.0-125	53.4-57.8	51.5 -56.1	3.9	2.4	5.6	14.0
60%	9,243	4,787	3,192	127.0-136.8	42.7-46.2	51.8 -56.4	3.0	1.8	4.3	15.3
70%	10,041	5,585	2,394	138.0-148.6	32.1-34.7	52.0 -56.6	1.2	0.8	1.7	16.6
80%	10,839	6,383	1,596	148.9-160.4	21.4-23.1	52.3 -56.9	0.8	0.5	1.2	17.9
90%	11,637	7,181	798	159.9-172.2	10.7-11.6	52.6 -57.1	0.8	0.5	1.1	19.3
100%	12,435	7,979	-	170.8-184.0	-	52.9 -57.4	-	-	-	20.6

exception of rice. This should not pose a problem. In 2012, for example, Thailand exported 6,734 M kg of rice (Office of Agricultural Economics 2012b). The production of rice in the areas under Phase 3 development, however, was only 17 M kg, accounting less than 1% of the total amount of rice exported. When combine all the 3 phase projects together with the total areas of rubber plantation of 448,000 ha, total rubber yield would increase to 742 M kg and rice, corn, and cassava would disappear about 1613 M kg (24% of the total amount of rice exported in 2012), 7837 M kg, 8926 M kg, respectively. When standardize crop water requirement with value gain from export, every thousand US dollar gain from rubber requires 547–629 m³ of water (Mangmeechai 2013).

Crop per drop

The total volume of water used globally for crop production is 6390 Gm³/yr at field level. Rice is responsible for the largest share of the total water volume used for global crop production. It consumes about 1359 Gm³/yr, which is about 21% of the total volume of water used for crop production at field level. The second largest water consumer is wheat (12%) (Hoeskstra 2007).

Given the importance of agriculture to Thailand, production efficiency needs to be a priority. When comparing the water requirements for growing crops in the Northeastern region with the world averages reported by (Hoeskstra 2007). The water per yield averages of Thai rice and maize were higher than their corresponding world averages (Table 5).

Based on the Hoeskstra (2007) report, the four most important direct factors explaining high water footprints are (1) gross national income, (2) a water-intensive consumption pattern, (3) climate, and (4) water-inefficient agricultural practices. The third and fourth factors are clear explanations for the high water consumption of agriculture in Thailand. With regard to climate, the regions with high evaporative demands have relatively large water requirements per unit of crop production. A fourth factor that can explain high water footprints is the use of agricultural practices that utilize water inefficiently, which means that water productivity in terms of output per drop of water is relatively low. This factor partly explains the high water footprints of countries such as Thailand, Cambodia, Turkmenistan, Sudan, Mali and Nigeria

(Hoeskstra 2007). Yield is an indicator of the efficiency of an agricultural practice. For example, the yield for the major Thai export, rice, was lower than the world average: the world average rice yield was 4.3 tons/ha, while the Thai rice yield was 2.9 tons/ha (Office of Agricultural Economics 2012b). Thailand's cassava yield (22.7 tons/ha) was higher than the world average (12.5 tons/ha). The sugarcane yield of Thailand (69.3 tons/ha) was slightly lower than the world average (70.2 tons/ha). The Thai rubber yield was 1.7 tons/ha, slightly greater than the world average of 1.2 tons/ha (Office of Agricultural Economics 2012b).

In order to increase its crop-per-drop efficiency in the face of increased water shortage issues, Thailand needs to develop irrigation systems that enhance crop yields and improve the efficiency of water applications, rather than endlessly seeking new supplies. More storage and decentralized micro-irrigation are necessary to save water in times of water surplus for use in times of water shortage (Bouwer 2000; FAO 2002; Rijsberman 2006; Sosothikul 2010). All of these activities must be implemented under the framework of river-basin management to ensure coherent planning, policy-making with wide public participation, and the implementation of effective water-resource, land-use and flood management measures (Editorial 2007). The government should move toward on promoting rubber plantation policy since it provides higher revenue for farmers, in the meantime, irrigation systems should be developed to improve crop per drop and land use efficiency.

DISCUSSION

The Thai government launched Phase 3 of its Rubber Plantation Project in 2011. The project aims to expand the total area of new plantations to 128,000 ha, from 2011 to 2013. The northeastern region contains the largest areas for new rubber plantation areas, yet it is known to have unfertile areas, a long dry season, and regular encounters with water scarcity during summer months. This objective leads to research questions as to how the policy affects land and water use in the country. The results of this study can thus be used to introduce recommendations on water management for more sustainable rubber plantations in the area and maximized land use.

Table 5. Average virtual water content of some selected products for a number of selected countries (m³/ton)

Country	Rice (paddy)	Maize	Sugar cane
USA	1275	489	103
China	1321	801	117
India	2850	1937	159
Russia	2401	1397	-
Indonesia	2150	1285	164
Australia	1022	744	141
Brazil	3082	1180	155
Japan	1221	1493	120
Mexico	2182	1744	171
Italy	1679	530	-
Netherlands	-	408	-
World average	2291	909	175
Thailand	2488	1143	171

This study shows that the water requirement of rubber trees is higher than that of other local crops (e.g., rice, cassava, sugarcane, and corn). On average, the water requirement for rubber is 14,221 m³/ha/year (41% blue water, BW and 59% green water, GW); sugarcane, 12,177 m³/ha/year (36% BW and 64% GW); cassava, 9,668 m³/ha/year (52% BW and 48% GW); rice, 5,220 m³/ha/year (-27% BW and 73% GW); and corn for animal feed, 4,417 m³/ha/year (46% BW and 54% GW). In the study, agricultural green water refers to water from effective rainfall, while blue water refers to the additional water supplied to meet optimal growing conditions. This implies that the rainfall, especially during the dry season, cannot sufficiently meet the actual crop water requirements. Thus irrigation systems must be utilized in certain months. The results show that during the dry months, Nov. to April, water is insufficient; meanwhile, water is provided in excess from May to Oct. Thus, irrigation systems must be utilized during certain months. The land use changes from the cultivation of edible crops to rubber do not threaten the amount of food available for domestic consumption since Thailand generally exports more of its crops than it consumes.

Regarding to the verification and uncertainty of the data, this study used primary data and secondary data from government reports. The methodology and data collection

for primary data followed crop water requirement manual which has been used worldwide. The CROPWAT model was verified by comparing the estimation of crop water requirement from equation and the CROPWAT program. The results showed that the difference between the two methods did not exceed more than 10% (Fig. 4).

CONCLUSIONS

The Thai government launched Phase 3 of its Rubber Plantation Project in 2011 aiming to expand the total area of new plantations to 128,000 ha. This policy attempts to create a more stable income for farmers without concerning other aspects e.g. climate, geographic, and water resources suitable for rubber plantation, fluctuation of rubber market price, land use changes, and food security etc.

By taking these aspects into account, the findings of this study suggests the government and local government to provide a better plan for the rubber plantation project by considering crop water requirements suitable for each region. Irrigation system or individual or community reservoir should be planed. In addition, education provided to all farmers on increasing crop-per-drop efficiency is necessary. ■

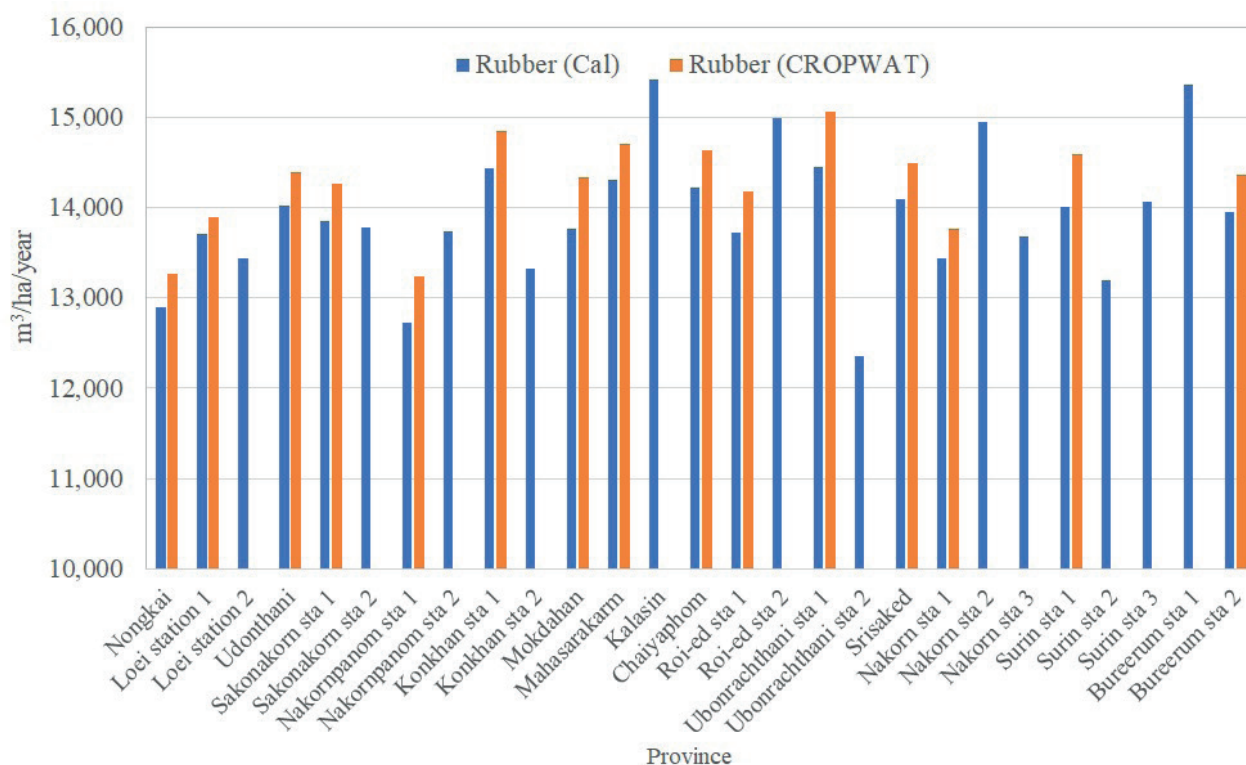


Fig. 4. Rubber water consumption from calculations and from the CROPWAT program

REFERENCES

- Bouwer H. (2000). Integrated water management: emerging issues and challenges. *Agricultural Water Management*, 45, 217-228.
- Clermont-Dauphin C., Suvannang N., Hammecker C., Cheylan V., Pongwichian P. and Do F. (2013). Unexpected absence of control of rubber tree growth by soil water shortage in dry subhumid climate. *Agronomy for Sustainable Development*, 33, 531-538.
- Daud N., Nayagam N., and Veramuthoo P. (1989). Effects of selected environmental and technological factors on rubber production. A case study of RRIM economic laboratory. *Journal of Natural Rubber Resource*, 4(1), 66-74.
- Devakumar A., Rao G., Rajgopal R., Rao P., George M., Vijayakumar K. and Sethuraj M. (1988). Studies on soil-plant-atmosphere system in Hevea: II. Seasonal effects on water relations and yield. *Indian Journal of Natural Rubber Resource*, 1(2), 45-60.
- Devakumar A., Prakash P., Sathik M. and Jacob L. (1998). Drought alters the canopy architecture and micro-climate of *Hevea brasiliensis* trees. *Trees*, 13, 161-167.
- Editorial. (2007). Solving Thailand's water crisis: A comprehensive approach is needed in resource management to effectively deal with flood and drought problems. [online] *The Nation*. Available at: www.nationmultimedia.com/2007/03/11/opinion/opinion_30028990.php [Accessed 30 Mar. 2015].
- FAO. (2002). Crops and Drops: Making the best Use of Water for Agriculture. [online] Available at: www.fao.org/3/Y3918E/Y3918E00.htm [Accessed 1 Mar. 2015].
- FAO. (2011). Thailand and FAO Achievements and success stories. [online] Available at: www.fao.org/3/a-at017e.pdf [Accessed 1 Apr. 2015].
- Ferraris R. (1993). Effect of plant density on yield and rubber accumulation in guayule (*Parthenium argentatum*) in south-eastern Queensland. *Journal of Experimental Agriculture*, 33(1), 71-82.
- Hoeskstra Y. and Chapagain K. (2007). Water footprints of nations: Water use by people as a function of their consumption pattern. *Water Resources Management*, 21, 35-48.
- Homyarnyen K. (2007). Water irrigation for growing asparagus in Nakorn Pratom Province. Bangkok: Ministry of Agriculture and Cooperatives.
- Irrigation Water Management Research Group. Crop Coefficient (Kc) 40 crop types. [online] Available at: water.rid.go.th/hwm/cropwater/CWRdata/Kc/kc_th.pdf [Accessed 25 Dec. 2014].
- Jiang A. (1988). Climate and natural production of rubber (*Hevea brasiliensis*) in Xishuangbanna, southern part of Yunnan province, China. *International Journal of Biometeorology*, 32, 280-282.
- Kastner T. and Nonhebel S. (2010). Changes in land requirements for food in the Philippines: A historical analysis. *Land Use Policy*, 27, 853-863.
- Mangmeechai A. (2013). Environmental externalities in relation to agricultural sector in Thailand with tradelinked analysis. *Environment, Development and Sustainability*, DOI: 10.1007/s10668-013-9509-2.
- Miyamoto S., David J. and Piela K. (1984). Water use, growth and rubber yields of four Guayule selections as related to Irrigation regimes. *Irrigation Science*, 5, 95-103.
- National Statistic Office. (2019). Statistics of Land Utilization by Region and Province Year: 2008–2017. [online] Available at: www.statbbi.nso.go.th/staticreport/page/sector/en/11.aspx [Accessed 5 Feb. 2015].
- Nevison C. Good Practice Guidance and Uncertainty Management in National Greenhouse Gas Inventories: Indirect N₂O Emissions from Agriculture. Water Evaluation and Planning. Yield Response to Water Shortage. [online] Available at: www.weap21.org/webhelp/Mabia_Alg_Yield.htm [Accessed 20 Feb. 2015].
- Njukeng J., Muenyi P., Ngane B. and Ehabe E. (2011). Ethephon Stimulation and Yield Response of Some Hevea Clones in the Humid Forests of SouthWest Cameroon. *International Journal of Agronomy*. [online]. Available at: DOI: 10.1155/2011/257340 [Accessed 2 Feb. 2015].
- Office of Agricultural Economics. (2012a). Agricultural Situation and Trend 2012. [online] Available at: www.oae.go.th/assets/portals/1/files/ebook/trends2555.pdf [Accessed 25 Feb. 2015].
- Office of Agricultural Economics. (2012b). *Agricultural Statistics of Thailand*. Bangkok: Ministry of Agriculture.
- Office of Research and Development for Land Management. (2005). *Rubber*. Bangkok: Land Development Department.
- Priyadarshan P., Hoa T., Huasun H. and Goncalves P. (2005). Yielding Potential of Rubber (*Hevea brasiliensis*) in Sub-Optimal Environments. *Journal of Crop Improvement*, 14(1-2), 221-247.
- Rao G., Rao P., Rajagopal R., Devakumar A., Vijayakumar K. and Sethuraj M. (1990). Influence of soil, plant and meteorological factors on water relations and yield in *Hevea brasiliensis*. *International Journal of Biometeorology*, 34(3), 175-180.
- Rao P., Saraswathiyamma C. and Sethuraj M. (1998). Studies on the relationship between yield and meteorological parameters of para rubber tree (*Hevea brasiliensis*). *Agricultural and forest meteorology*, 90, 235-245.
- Regional Development Policy Board. (2019). Northeast Development Plan in the 12th National Economic and Social Development Plan (2017–2021). [online] Available at: www.nesdb.go.th/ewt_dl_link.php?nid=7526&filename=index [Accessed 1 Mar. 2015].
- Rijsberman F. (2006). Water scarcity: Fact or fiction? *Agricultural Water Management*, 80, 5-22.
- Royal Irrigation Department. (2018). Annual Report 2018. [online] Available at: www1.rid.go.th/main/_data/annual-conclusion/RID-Annual/RID_Annual_2018.pdf [Accessed 25 Jan. 2015].
- Samarasinghe B. (2003). Growth and yields of Sri Lanka's major crops interpreted from public domain satellites. *Agricultural Water Management*, 58, 145-157.
- Sangsing K., Kasemsap P., Thanisawanyangkura S., Sangkhasila K., Gohet E., Thaler P. and Cochard H. (2004). Xylem embolism and stomatal regulation in two rubber clones (*Hevea brasiliensis* Muell. Arg.). *Trees*, 18, 109-114.
- Sosothikul P. (2010). The water shortage: crisis of opportunity? [online] Bangkok post. Available at: www.eng.moac.go.th/ewt_news.php?nid=58&filename=index [Accessed 25 Feb. 2015].
- Vijayakumar R. (1988). Physiology of drought tolerance of Hevea. *Compte-Rendu du Colloque Exploitation Physiologic et Amelioration de l'Hevea*, 269-281.
- Vijayakumar K., Dey S., Chandrasekhar R. and Austin D. (1998). Irrigation requirement of rubber trees (*Hevea brasiliensis*) in the subhumid tropics. *Agricultural Water Management*, 35, 245-259.
- Wheater H. and Evans E. (2009). Land use, water management and future flood risk. *Land Use Policy*, 26, 251-264.
- Wicke B., Sikkema R., Dornburg V. and Faaij A. (2011). Exploring land use changes and the role of palm oil production in Indonesia and Malaysia. *Land Use Policy*, 28, 193-206, DOI: 10.1016/j.landusepol.2009.08.019.

APPENDIX

The FAO Penman-Monteith equations were used to produce the ET_0 data in Table A1 reported by the Royal Irrigation Department (2011). ET_0 was calculated with weather data from 120 weather stations within 64 provinces from 1981 to 2010. ET_0 data was reported by the Royal Irrigation Department (2011).

Table A.1. Reference evapotranspiration by Penman – Monteith (ET_0) of each province from 1951-1995 (45 years) in the northeastern region

ET_0 (mm/day)	Jan	Feb	Mar	Apr	May	June	July	Aug	Sep	Oct	Nov	Dec
Nong Khai	3.11	3.78	4.62	4.62	4.03	3.56	3.51	3.41	3.51	3.63	3.31	3.04
Loei	3.28	4.06	4.81	5.06	4.43	4.07	3.66	3.55	3.55	3.55	3.23	3.04
- Loei agricultural station	3.19	3.95	4.73	4.76	4.2	3.89	3.87	3.39	3.84	3.5	3.42	3
Udon Thani	3.32	4.07	4.85	5.21	4.56	4.08	3.71	3.55	3.61	3.73	3.7	3.22
Sakon Nakhon	3.44	4.09	4.87	5.02	4.4	3.99	3.57	3.44	3.86	3.9	3.64	3.25
- Sakon Nakhon agricultural station	3.14	3.75	4.48	5	4.36	4.26	3.86	3.69	3.98	3.77	3.38	3.09
Nakhon Phanom	3.33	3.86	4.3	4.5	3.95	3.47	3.42	3.33	3.48	3.6	3.6	3.16
- Nakhon Phanom agricultural station	3.52	4.03	4.48	4.96	4.28	4.25	3.81	3.32	3.83	3.57	3.59	3.25
Khon Kaen	3.65	4.18	5.09	4.97	4.67	4.29	3.88	3.68	3.61	3.79	3.83	3.63
- Khon Kaen agricultural station	3.2	3.81	4.48	4.76	4.25	3.91	3.88	3.36	3.48	3.59	3.48	3.18
Mukdahan	3.65	4.18	5	5.15	4.11	3.64	3.56	3.43	3.57	3.8	3.95	3.53
Maharakham	3.57	4.19	4.71	5.22	4.62	4.22	3.84	3.64	3.62	3.76	3.83	3.58
Kalasin	4.15	4.89	5.4	5.45	4.8	4.32	4.22	3.65	3.71	4.06	4.3	4.1
Chaiyaphom	3.6	4.2	5	5.12	4.47	4.13	3.77	3.61	3.6	3.78	3.89	3.51
Roi-et	3.49	4.13	4.66	4.83	4.22	3.9	3.84	3.64	3.61	3.63	3.68	3.51
- Roi-et agricultural station	4.04	4.44	4.92	5.25	4.59	4.62	4.21	3.9	3.6	3.78	4.1	3.9
Ubonrajthanee	4	4.53	4.93	5.03	4.45	3.96	3.87	3.71	3.43	3.71	4.23	4.22
- Ubonrajthanee agricultural station	3.63	3.68	4.23	4.13	3.65	3.64	3.56	2.87	3.22	3.34	3.64	3.42
- Srisakad agricultural station	3.4	3.92	4.56	4.75	4.42	4.43	4.19	3.71	3.85	3.62	3.79	3.45
Nakornrajchasma	3.37	3.95	4.39	4.64	4.2	3.95	3.89	3.79	3.36	3.42	3.51	3.41
- Pakchong	4.71	4.71	5.01	4.81	4.2	4.54	4.26	4.04	3.38	3.5	4.44	4.52
Chockchai	3.47	4.21	4.68	4.74	4.09	4.18	3.82	3.72	3.31	3.6	3.57	3.42
Surin	3.76	4.36	4.83	4.87	4.21	4.12	3.71	3.61	3.62	3.7	3.84	3.8
- Surin agricultural station	3.52	3.97	4.38	4.56	3.96	3.98	3.53	3.45	3.58	3.6	3.67	3.43
- Tha Tum	3.54	4.2	4.78	4.99	4.43	4.03	3.96	3.52	3.55	3.72	3.89	3.62
Bureerum	4.17	4.81	5.27	5.49	4.74	4.66	4.14	3.67	3.64	3.86	4.12	3.98
- Nangrong	3.62	4.16	4.81	4.94	4.38	4	3.94	3.55	3.6	3.75	3.92	3

OCCASIONAL FLOODS ON THE RIVERS OF RUSSIAN PLAIN IN THE 20TH–21ST CENTURIES

Maria B. Kireeva^{1*}, Ekaterina P. Rets², Natalya L. Frolova¹, Timothy E. Samsonov¹, Elena S. Povalishnikova¹, Andrey L. Entin¹, Ivan N. Durmanov¹, Alexander M. Ivanov¹

¹Faculty of Geography, M.V. Lomonosov Moscow State University, Leninskie Gory, 1, Moscow, 1199911, Russia

²Water Problems Institute RAS, Gubkin str., 3, Moscow, 119333, Russia

*Corresponding author: kireeva_mb@mail.ru

Received: January 31st, 2019 / Accepted: May 10th, 2020 / Published: July 1st, 2020

<https://DOI-10.24057/2071-9388-2020-29>

ABSTRACT. The article focuses on the study of flood flow changes on the rivers of the European Territory of Russia (ETR) in the last thirty years. This is an extremely important problem, as with floods, whose contribution to the structure of the annual flow of European rivers in recent decades has been increasing, the most destructive floods are associated. On the example of 55 representative hydrological gauge stations located on the ETR in regions with different conditions of runoff formation, the features of both summer and winter floods formation are considered. It has been established that over the past thirty years on the most rivers there has been an intensive reduction in the ratio of volumes and maximum flood discharges in relation to the similar characteristics of the basic runoff. Increased groundwater supply is observed, and the absence of significant freezing of the soil leads to an increase in infiltration. The volumes of flood runoff and the basic runoff become comparable or the proportion of the latter begins to prevail. The main reason for the increase in minimum water discharge is associated with an increase in flood flow under the influence of more intense and prolonged thaws. A distinctive feature of the water regime of recent decades has been the flood peaks in almost any season of the hydrological year. In the middle and southern part of the ETR – in the basins of the Volga, Oka, Vyatka, Don Rivers – there is an increase in low-water flow and in the quota of flood in annual flow. On some rivers of the ETR, the spring flood runoff currently accounts for less than 50% of the annual runoff.

KEY WORDS: thaws, floods, changes in hydrological regime, ETR rivers

CITATION: Maria B. Kireeva, Ekaterina P. Rets, Natalya L. Frolova, Timothy E. Samsonov, Elena S. Povalishnikova, Andrey L. Entin, Ivan N. Durmanov, Alexander M. Ivanov (2020). Occasional Floods On The Rivers Of Russian Plain In The 20th–21st Centuries. *Geography, Environment, Sustainability*, Vol.13, No 2, p. 84-95

<https://DOI-10.24057/2071-9388-2020-29>

ACKNOWLEDGEMENTS: The study was supported by the Russian Science Foundation (grant no. 19-77-10032) regarding data calculation and analysis methods, the Russian Foundation for Basic Research (grant No. 18-05-60021) regarding the preparation and calculations for the rivers of the Arctic zone, the Russian Foundation for Basic Research (grant No. 20-35-70024) regarding the calculations and data analysis for the rivers of the North Caucasus.

Conflict of interests: The authors reported no potential conflict of interest.

INTRODUCTION

The study of occasional floods is vital because the phenomenon is often associated with the world's most destructive floods (Blöschl et al. 2017). An analysis of foreign studies shows that the water regime of the rivers not only in the European territory of Russia (ETR), but also of other rivers of Eastern and Western Europe, has undergone significant changes in nature and structure over the past decades.

For example, according Parajka et al. (2010), significant changes in the processes of floods caused by rain have been observed on the rivers of the Alpine-Carpathian region; the role of autumn floods is increasing in proportion to the total volume of peak flow. Thus, due to an increase in the volume of autumn floods, a decrease in summer runoff is observed. Parajka et al. mainly attribute this to changes in the climatic regime of the region, primarily the precipitation regime and the trends of air mass movement. The authors note that floods typically have a pronounced seasonality,

especially for foothill or semi-mountain terrain. However, the precipitation maxima that historically occurred in July and August for the territory as a whole have moved to the end of summer and the end of autumn, and for other sections there was a shift in the maximum and intensity of precipitation in the spring. This happened as a result of the confrontation of cold air masses from the north and warm from the Mediterranean Sea.

Studies conducted in Germany (Beurton and Thielen 2009) show that country has three regions with different flood regimes. Winter floods prevail in western and central Germany, while in the north and east spring and summer floods dominate, and in southern Germany the peak flood season is in summer. These differences are most likely associated with a change in the western circulation of air masses. Since 1971, the flood regime of German rivers has undergone substantial changes in structure and character, leading Beurton and Thielen to consider two periods, 1971–2000 and 1940–2000. The occurrence of floods on the Rhine,

Odra, Danube, and Elbe over the past two decades has led to discussions about climate change and its consequences for river floods. Their analysis of flood development trends revealed greater changes for winter floods than for summer floods. The work of other researchers (Petrow and Merz 2009) has revealed that the observed changes in flood formation are influenced by climatic factors. Thus, milder winters and more frequent rains can cause an increase in the share of winter floods during the entire year for all of Western Europe.

Flood typing and classification is of interest to researchers (Marsh and Hannaford 2007). The vast majority of studies are based on cluster analysis – a multidimensional statistical procedure that collects data offering information about the objects. The clustering task relates to statistical processing, as a result of which typologies and classifications are obtained, and schemes or models are developed. Research results show that floods are least active in summer (Finch et al. 2007). Over recent decades, the share of floods in summer has been rapidly decreasing due to the strong influence of vegetation cover and evaporation. At the same time, the significance of winter floods has been increasing, due to western transport and the influence of the Atlantic, which determine the thermophysical features of the region and the presence of precipitation.

According to the authors of a 2001 article (Cunderlik and Burn 2001), an understanding of the hydroclimatic processes that determine the occurrence of floods is fundamental to assessing their recurrence. With this approach, the flood regime of the river is a reflection of the properties of the catchment. Many authors have noted that over the past few decades floods have become more frequent due to changes in peak flow, the contribution of which to the structure of the total runoff of rivers is becoming more significant.

Many studies are based on a description of seasonal peaks that caused flooding that led to significant damage to the urban infrastructure and offer analysis of the factors that caused them. In one example, the articles published with the support of the national hydrological monitoring program analyze the floods that occurred in England and Wales in 2007 (Marsh and Hannaford 2007; Finch et al. 2007) as a result of summer peak flow. The authors found uniformity and almost no change in the timing of flooding during the summer season in this territory. They note that the cause of the flood is abnormal synoptic conditions. Air flows under the influence of the North Atlantic weather system changed their direction to the south, contributing to the establishment of high pressure over Great Britain (Azores anticyclone), which prevented summer weather from coming to the region. Citing studies on climate modeling, note that the result of climate change will increase the intensity of rainfall, especially in the middle and high latitudes, as well as an increased risk of summer floods in some regions.

The seasonality of the maximum water discharge on the rivers of Europe is analyzed in an article published in Science (Blöschl et al. 2017) and is directly related to their genesis. The authors compare the coincidence of the maximum discharges with soil moisture, 7-day maximum precipitation

and maximum winter snowpack. For most rivers of the ETR, there is a shift of the maximum water discharge to an earlier date. At the same time, for individual rivers of the northwest, dates of maximum discharge are in the winter months and are associated with thaw floods. An analysis of the spatial distribution of the seasonality of maximum discharge has been carried out by Hall and Blöschl (2018). Their findings show that all rivers of European Russia fall into a cluster with spring discharge peaks associated with seasonal spring floods. Their article describes methods that can be used in the future to pinpoint regions that give rise to floods on the rivers of the ETR.

The study of winter floods on the rivers of Belarus is extremely important, since it is a border region with Russia. The results of one study (Volchek and Shelest 2012) echo the trends in the growth of winter floods on the rivers of Central Russia and the north-west. The authors revealed statistically significant increases in the maximum winter peak discharge for 10 of the 30 rivers studied. The authors attribute these trends mainly to the increasing role of the western type of atmospheric circulation. The article (Volchek and Shelest 2012) identifies groups of years with extreme floods observed on many rivers. The authors also analyzed the number of floods during the years of prevalence of various types of circulation. It is shown that the number of floods on most rivers is greater in years with western atmospheric circulation (W). As a result of the work, it was revealed that the increase in maximum water discharge on most rivers in Belarus is about 10%, only on the rivers of the Polesye region the maximum winter discharge increases by 20–40%.

MATERIALS AND METHODS

The time-series of daily water discharges for the observation period 1936–2015 is used as initial information. At the data preparation stage, large and medium rivers with a basin area from 2000 to 50,000 km² were selected in the ETR. Calculations were also carried out for individual closing sections of large rivers with a catchment area of 150,000 to 250,000 km². Medium rivers were used to assess the background changes in the water regime, and the closing sections of large rivers were used to study the transformation of runoff and water regime characteristics of large river basins. As a result, 55 gauging stations located in the regions with different flow formation conditions were selected for the ETR; priority was given to gauges with the most comprehensive hydrological data. Initial data for calculations (Table 1) were prepared for the selected sections, including a continuous series of water discharges. As the main method for processing the initial data, we used GrWat automated hydrograph partition algorithm (Kireeva et al. 2019). Partly this algorithm based on the same principals, described in several research papers (Nathan and McMahon 1990; Eckhardt 2005; Shevnina 2013). As a result of this partition, four genetic components of the runoff were obtained for each day of the water year: base flow, thawed snow (main flood wave), thawed snow (thawing peaks during the winter) and rain.

Table 1. Representative basins that were used to assess the characteristics of the flood flow of rivers in the European territory of Russia (ID numbers correspond to Fig. 1)

No.	River	Station	Watershed area, km ²	Observation period	Natural zone
Russian North					
1	North Dvina	Ust-Pinega	348,000	1930–2014	taiga
2	Sykhona	Kalikino	49,000	1930–2014	taiga
3	Vym'	Veslyana	19,100	1928–2014	taiga, forest-tundra

4	Onega	Nadporozhskiy Pogost	12,800	1926–2014	taiga
5	Mezen	Malonisogorskaya	56,000	1930–2014	taiga, forest-tundra
6	Pechora	Ust-Tsilma	248,000	1932–2014	taiga, forest-tundra
7	Izhma	Ust-Ukhta	15,000	1913–2014	taiga, forest-tundra
8	Usa	Petrin	27,500	1915–2014	taiga, forest-tundra
Kolskiy peninsula					
9	Umba	Payalka	6,470	1932–2015	forest-tundra
10	Ponoi	Kanevka	10,200	1932–2015	forest-tundra
Volga basin					
11	Volga	Staritsa	21,100	1920–2010	mixed forest
12	Tvertsa	Madnoe	5,400	1877–2015	mixed forest
13	Mologa	Ustuzhna	19,100	1934–2015	mixed forest
14	Kostroma	Buy	8,870	1896–2015	forest-steppe
15	Unzha	Makarjev	18,500	1900–2015	mixed forest
16	Vetluga	Vetluga	22,200	1938–2015	mixed forest
17	Tsivil	Tuvs	4,040	1945–2015	forest-steppe
18	Sura	Poretskoe	15,400	1935–2015	forest-steppe
19	Alatur	Turgenjevo	11,000	1933–2015	forest-steppe
20	Samara	Elshanka	22,800	1878–2015	forest-steppe
Oka (main right tributary of Volga) Basin					
21	Oka	Kaluga	54,900	1876–2015	forest-steppe
22	Oka	Murom	190,000	1936–2015	forest-steppe
23	Ugra	Tovarkovo	15,300	1935–2015	forest-steppe
24	Moksha	Temnikov	15,800	1935–2015	forest-steppe
25	Tsna	Knyazhevo	13,600	1932–2015	forest-steppe
26	Klyasma	Kovrov	24,900	1878–2015	mixed forest
Don basin					
27	Don	Kazanskaya	102,000	1928–2015	forest-steppe
28	Sosna	Elets	16,300	1927–2015	forest-steppe
29	Krasivaya Mecha	Efremov	3,240	1944–2015	forest-steppe
30	Khoper	Besplemyanovskiy	44,900	1929–2015	forest-steppe
31	Medveditsa	Archedinskaya	33,700	1928–2015	forest-steppe, steppe
32	Medveditsa	Lisie Gory	7,610	1936–2015	forest-steppe
33	Ilovlya	Aleksandrova	6,520	1915–2015	steppe
34	Chir	Oblivskaya	8,470	1923–2015	steppe
35	Tikhoya Sosna	Alekseevka	2,060	1941–2015	forest-steppe
36	Bitug	Bobrov	7,340	1936–2015	forest-steppe
Kama (main left tributary of Volga) basin					
37	Kama	Gayni	27,400	1911–2015	taiga
38	Vishera	Ryabinino	30,900	1930–2015	taiga
39	Chusovaya	Lyamino	21,500	1956–2015	mixed forest
40	Sylva	Podkamennoe	19,700	1931–2015	mixed forest
41	Ufa	Krasnoufimsk	14,200	1971–2015	mixed forest
42	Dema	Bochkarevo	12,500	1946–2015	mixed forest

43	Belaya	Sterlitamak	21,000	1931–2015	mixed forest
44	Cheptsya	Glazov	9,750	1927–2015	mixed forest
45	Vyatka	Vyatskie Polyani	124,000	1918–2015	mixed forest
North Caucasus basins					
46	Terek	Vladikavkaz	1,490	1960–2017	altitudinal zone
47	Terek	Kotlyarevskaya	8,920	1960–2017	altitudinal zone
48	Baksan	Zaykovo	2,100	1960–2017	altitudinal zone
49	Kambileevka	Olginskoe	359	1960–2017	altitudinal zone
50	Nalchik	Belaya Rechka	140	1960–2017	altitudinal zone
51	Kuban	Armavir	16,900	1960–2017	altitudinal zone
52	Marukha	Marukha	301	1960–2017	altitudinal zone
53	Urup	Steblyitskiy	3,190	1960–2017	altitudinal zone
54	Bolshaya Laba	Nizhe Aziatskogo Mosta	1,180	1960–2017	altitudinal zone
55	Belaya	Kamennomostskiy	1,850	1960–2017	altitudinal zone

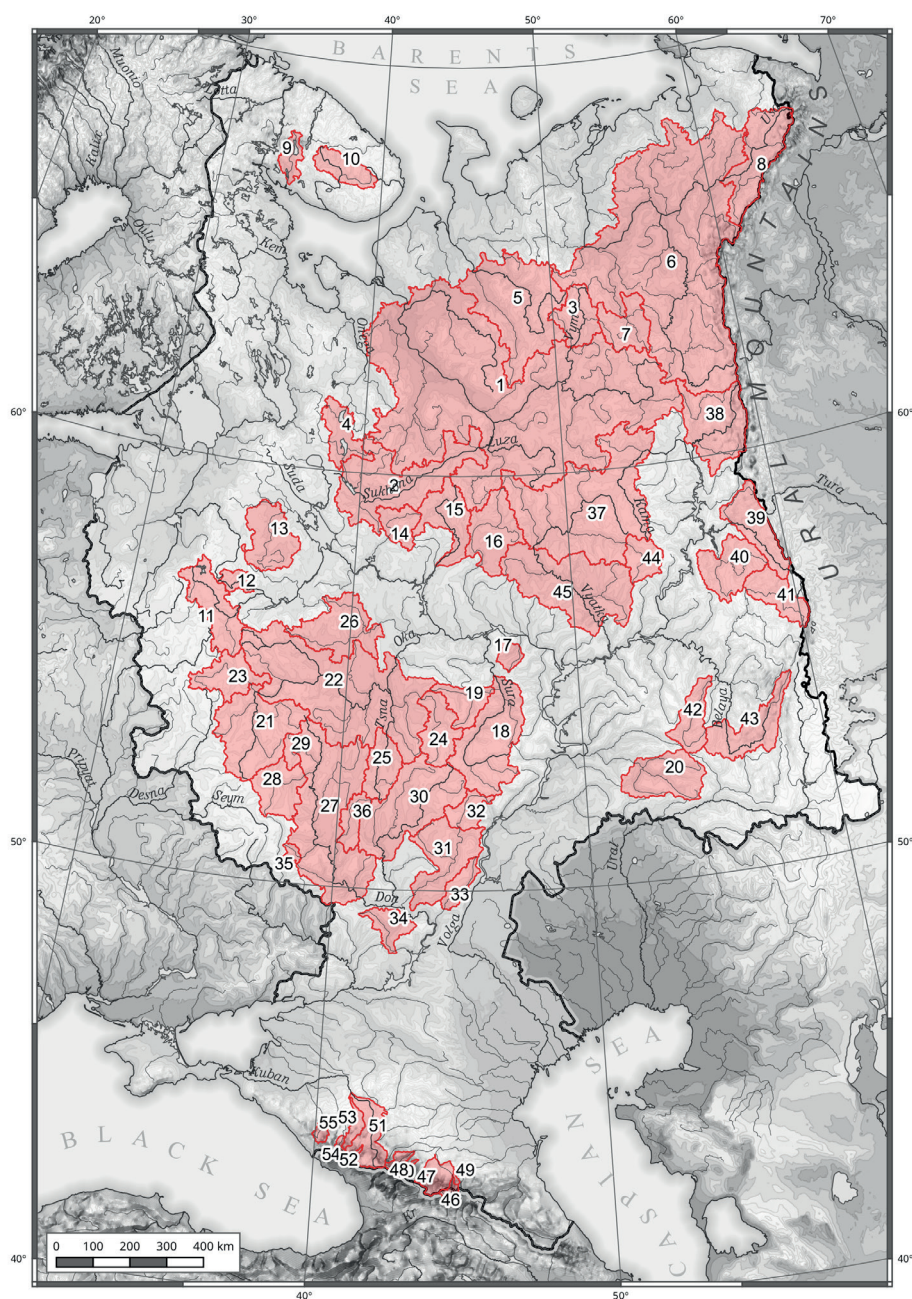


Fig. 1. Basins used in the analysis of occasional floods on the rivers of the European territory of Russia

For each output parameter from GrWat package statistical criteria's were calculated. Analysis include Fisher, Student and no parametric all Spearman criteria as well as Mann-Kendall test, t-test and petit test for threshold year.

RESULTS

As the result, all indicators characterizing the seasonal runoff, seasonal flood runoff, summer–autumn and winter low flow periods. Fourteen indicators were calculated for occasional floods (Table 2). A total of 1,680 hydrographs were analyzed. Despite the universality of the proposed algorithm, separation errors were observed for 45 hydrographs (2.7% of the total). Regardless, this can be considered a good result, as the same parameter set was used for the entire observational period each gauging station. The characteristics of the occasional floods were calculated for two seasons: the summer–autumn period (from this point, «rain floods») and the winter period («thaw floods»). The end of the summer–autumn period is set to a stable transition of the air temperature to negative values for five days during each year in each watershed.

Recently, occasional river floods have been observed almost annually for most rivers of the European Russia. Moreover floods have been observed in most hydrological seasons in recent decades. This process is clearly visible in the long-term oscillations of the dates of the peak annual discharges of rain and thaw floods.

Trends in the characteristics of rain floods vary with the geographic location of the catchment. For the rivers of the Russian north, northwest and most rivers of central Russia rain floods, which were previously observed mainly in July, have shifted noticeably earlier, now characteristic of May and June (Fig. 2). Additionally, the number of autumn floods in the north of the ETR has generally decreased significantly. In the North Caucasus, the dates of the peak runoff have shifted from July–August to June–July for rivers with a significant share of alpine snow and glacial snowmelt runoff. The trend toward an increased «spread» of the dates of annual maximum water discharge of flash-floods is characteristic of the steppe and forest-steppe regions – the Don basin, tributaries of the lower reaches of the Oka River, and rivers of the Middle and Lower Volga basin. So,

for example, on the Samara river the maximum discharge of rain floods was mainly observed in May–August until the mid-1970s (Fig. 2a) and was associated with intense summer rains. In the following decades another «cluster» of dates is distinguished – rain floods observed in October–December.

Trends in annual maximum discharges of rain floods are multidirectional. The annual maximum discharges of rain floods of the Mezen river increase in a statistically significant manner, while the same feature of the neighboring Northern Dvina and Pechora, and their tributaries – the Sukhona, Vym, and Usa – has not changed appreciably. There is a slight increase in rain flood maximums in the upper reaches of the Oka and the Don, while the left-bank tributaries of the Volga exhibit the opposite trend. An increase in annual maximum discharges of rain floods is observed in the foothills of the Kuban basin, and there are no statistically significant trends in the mountainous part and in the Terek basin. The only pronounced trend is a statistically significant increase in annual maximum discharges of rain floods for all rivers of the Kama basin (Fig. 3).

Changes in the volume of rain floods runoff has a noticeable pattern. In general, an increase in the volume of rain floods runoff is observed for most of the rivers of the ETR. This tendency is especially pronounced in the northern territories. Statistically significant trends were identified for the rivers Pechora, Severnaya Dvina, Mezen and Ponoï (Fig. 4). For the rivers of Central Russia and the left-bank tributaries of the Upper Volga – Unzha, Kostroma, Vetluga and the upper Kama River – this trend is less pronounced and not statistically significant (Fig. 4d). At the same time, no increase in the volume of rain floods was observed for the eastern Kama tributaries. Multidirectional trends are characteristic of the south of Russia; in most cases this is a slight decrease, with the exception of the Kuban basin, where a statistically significant increase was detected.

The amount of rain floods has changed insignificantly for all the rivers of the ETR, on average 3–4 floods per year are observed for the rivers of the north. Among the rivers of the Kola Peninsula, an average of 8–10 rain floods occur annually under the influence of the Gulf Stream and Atlantic cyclones, and in some years the number of occasional floods can reach 15. In central Russia, the number of flood

Table 2. List of characteristics in the output file of the GrWat algorithm

Group	No.	Title	Units	Characteristics
Runoff volume	1	Wpavs1	km ³	Total volume of occasional rain flood runoff with groundwater component
	2	Wpavs2	km ³	Total volume of occasional rain flood runoff without groundwater component
	3	Wpavthaw1	km ³	Total volume of occasional thaw flood runoff with groundwater component
	4	Wpavthaw2	km ³	Total volume of occasional thaw flood runoff without groundwater component
Parameters of maximum flow	5	Qmaxpavs	m ³ /s	Daily maximum discharge of rain occasional floods
	6	datemaxpavs	date	Date of daily maximum discharge of rain occasional floods
	7	Qmaxpavthaw	m ³ /s	Daily maximum discharge of thaw occasional floods
	8	datemaxpavthaw	date	Date of daily maximum discharge of thaw occasional floods
	9	DaysPavsSum	days	Number of days, classified as occasional flood, during summer-autumn low flow period
	10	DaysThawWin	days	Number of days, classified as occasional flood, during winter low flow period
Other	11	CvWin	–	The relative variability of winter low flow period
	12	CvSum	–	The relative variability of winter low flow period
	13	CountPavs	number	Number of rain peaks
	14	CountThaws	number	Number of thaw peaks

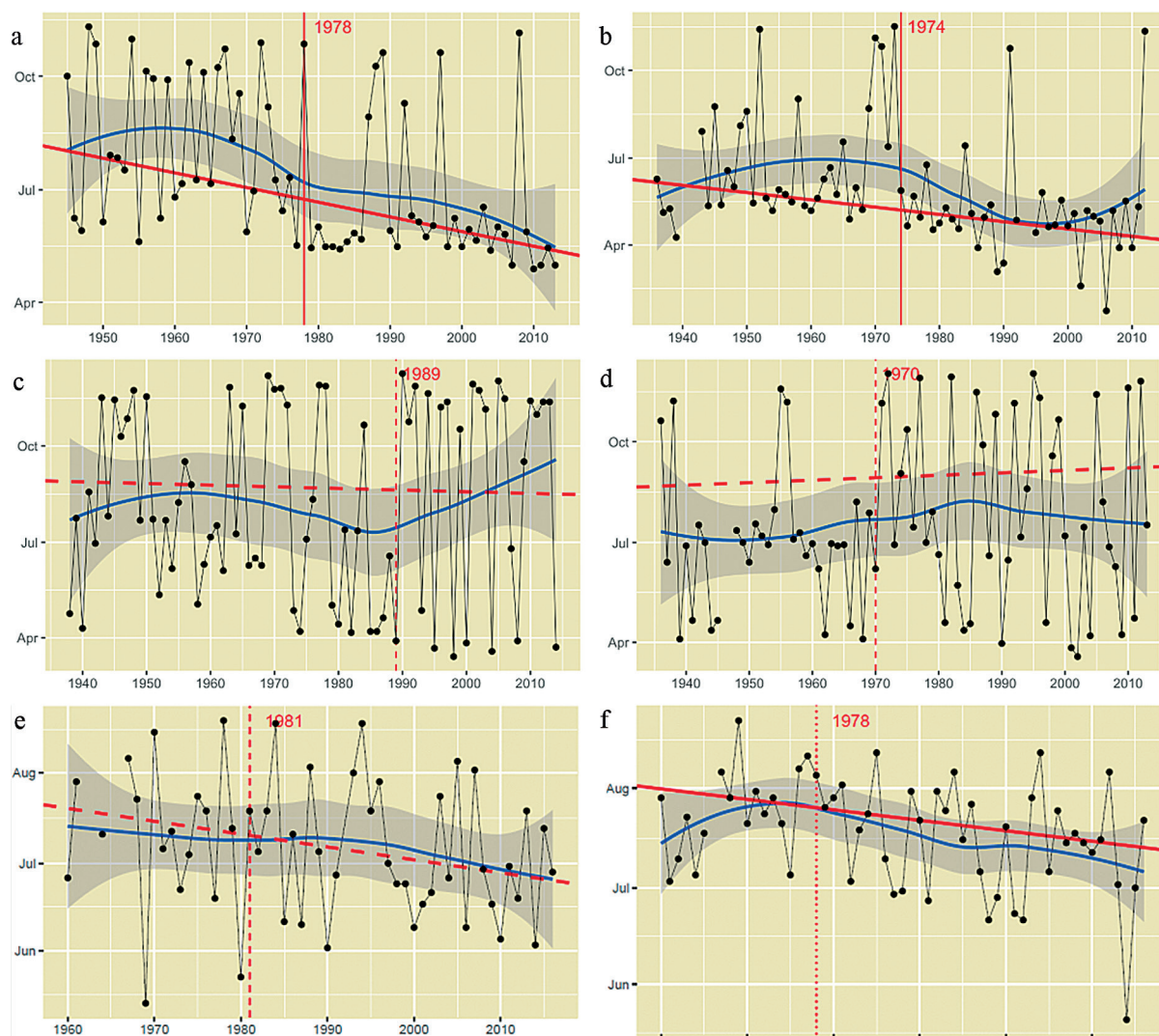


Fig. 2. Dates of maximum discharge of rain floods for: (a) the Mezen River – village Malonisogorsk, (b) the Oka River – Kaluga city, (c) the Hoper River – Besplemyanovsky farm, (d) the Samara River – village Yelshanka, (e) the Terek River – Vladikavkaz city, (f) the Baksan River – village Zayukovo

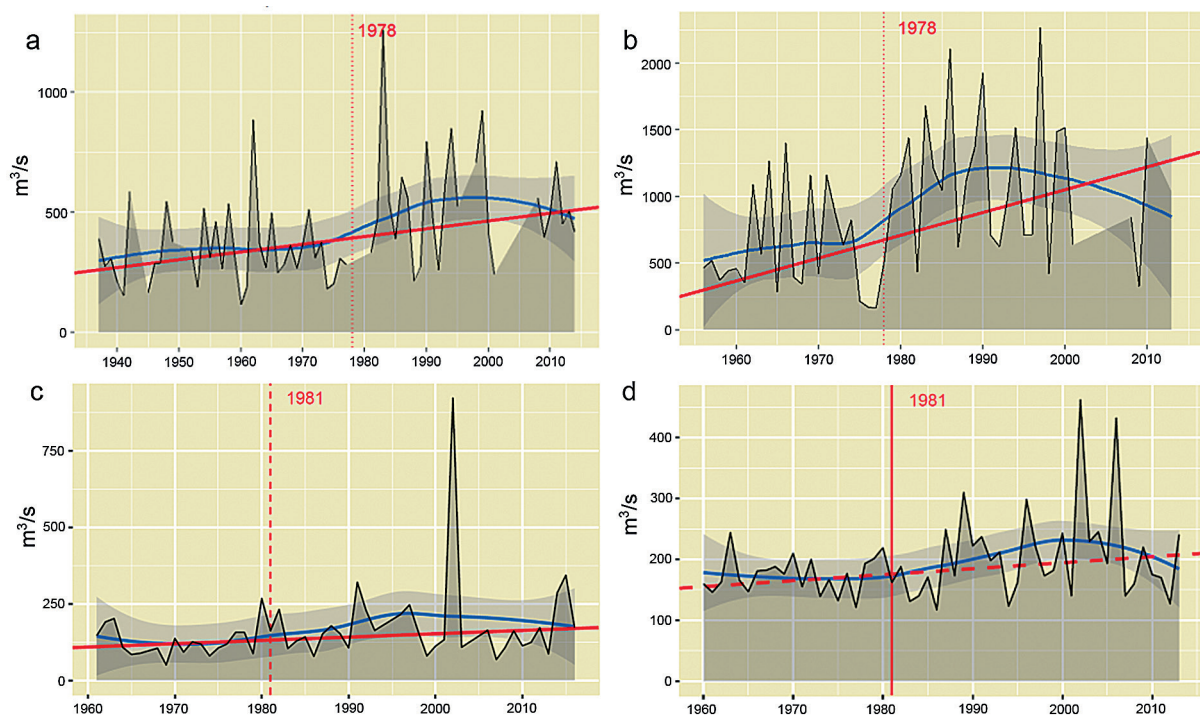


Fig. 3. Annual maximum discharge of rain peaks for: (a) the Kama River – village Guines, (b) the Chusovaya River – village Lyamino, (c) the Urup River – Steblitsky farm, (d) the B.Laba River – below the Asian Bridge

waves associated with liquid precipitation averages 6–7 events and has a statistically insignificant upward trend. In the North Caucasus, there are 7–13 rain floods per year in the highlands and up to 15–19 in the foothills. Along rivers with an insufficient zone of humidification, including tributaries of the Don and Lower Volga, the number of rain floods has halved in the last 10 years. While 1–2 rain floods a year were previously observed there, it is common in recent years for none to occur. However, data for a 10-year period is not sufficient to draw reliable conclusions about the trend in number of rain floods in the region.

When assessing the contribution of flash floods to the increase in annual runoff, two characteristics should be considered: the thaw floods' volume including the basic ground flow and without it. The latter indicator reflects the volume of water that enters the channel network relatively quickly as a result of melting snow during thaws and liquid precipitation events. The thaw flood runoff with the basic component include partial melt or liquid precipitation runoff entering the riverbed as an underground component; and depends on the water content of the previous period. Almost everywhere, the volume of thaw runoff without a base component has no statistically significant tendency to increase. Explicit growth is recorded only for the rivers of Central Russia, the Oka basin and its tributaries. For the Kama basin, there is a decrease in the volume of thaw runoff without base component, as well as for the left-bank tributaries of the Volga. In the south, a series of thaw runoff volumes constitute small values with separate pronounced

emissions; thus, it is not possible to identify trends for this region. Apparently, the main manifestation of the role of thaw flash floods is expressed in the growth of the base component, reflecting the relationship between surface runoff and groundwater.

The maximum discharges of thaw floods are growing in almost every part of the ETR. In the north, this growth is insignificant; with a move southward, to the Volga basin, this signal is more pronounced (Fig. 5). The strongest growth is recorded for the Oka basin, the left-bank tributaries of the Upper Volga—Unzha, Kostroma and Vetluga (Fig. 5 b, c, e). Among the rivers of the arid zone, the maximum discharge of thaw floods are also increasing in a statistically significant manner. Simultaneously, a shift in the dates of thaw floods to the spring is recorded for the most of gauges (from December–January to February–March). During autumn, the occasional floods, previously classified mostly as thaw floods, occur during rain events in more recent observations.

An increase of the thaw floods number is observed for a few rivers in the ETR; this is most pronounced for the rivers of central Russia, as well as for rivers originating from the slopes of the Southern Urals, Belaya and Dema (Fig. 6). In the South and North Caucasus thaws' number has not changed significantly.

A series of maps of the flood flow characteristics were drawn for the ETR. The maximum specific discharge of rainfall floods is distributed according to geographical zonality. The highest values for lowland rivers – up to 50 L/(s·km²) – are observed in the north of European Russia in the Pechora and Mezen river basins, in the rivers of the Kola Peninsula (Fig. 7).

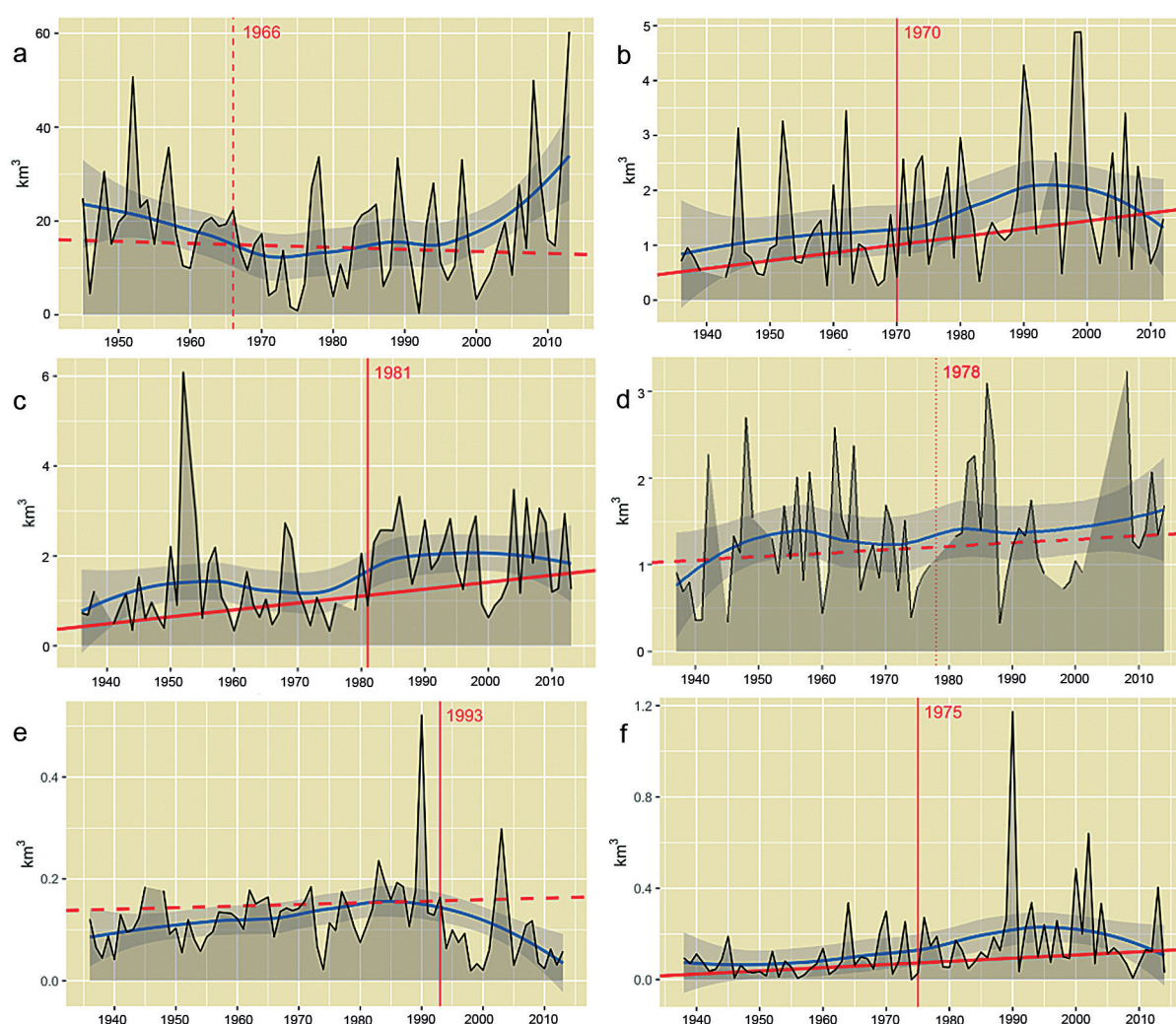


Fig. 4. Volumes of maximum discharge of rain floods for: (a) the Northern Dvina River – village Ust-Pinega, (b) the Oka River – Kaluga city, (c) the Unzha River – Makaryev city, (d) the Kama River – village Gayny, (e) the Samara River – village Yelshanka, (f) the Hoper River – Besplemyanovsky farm

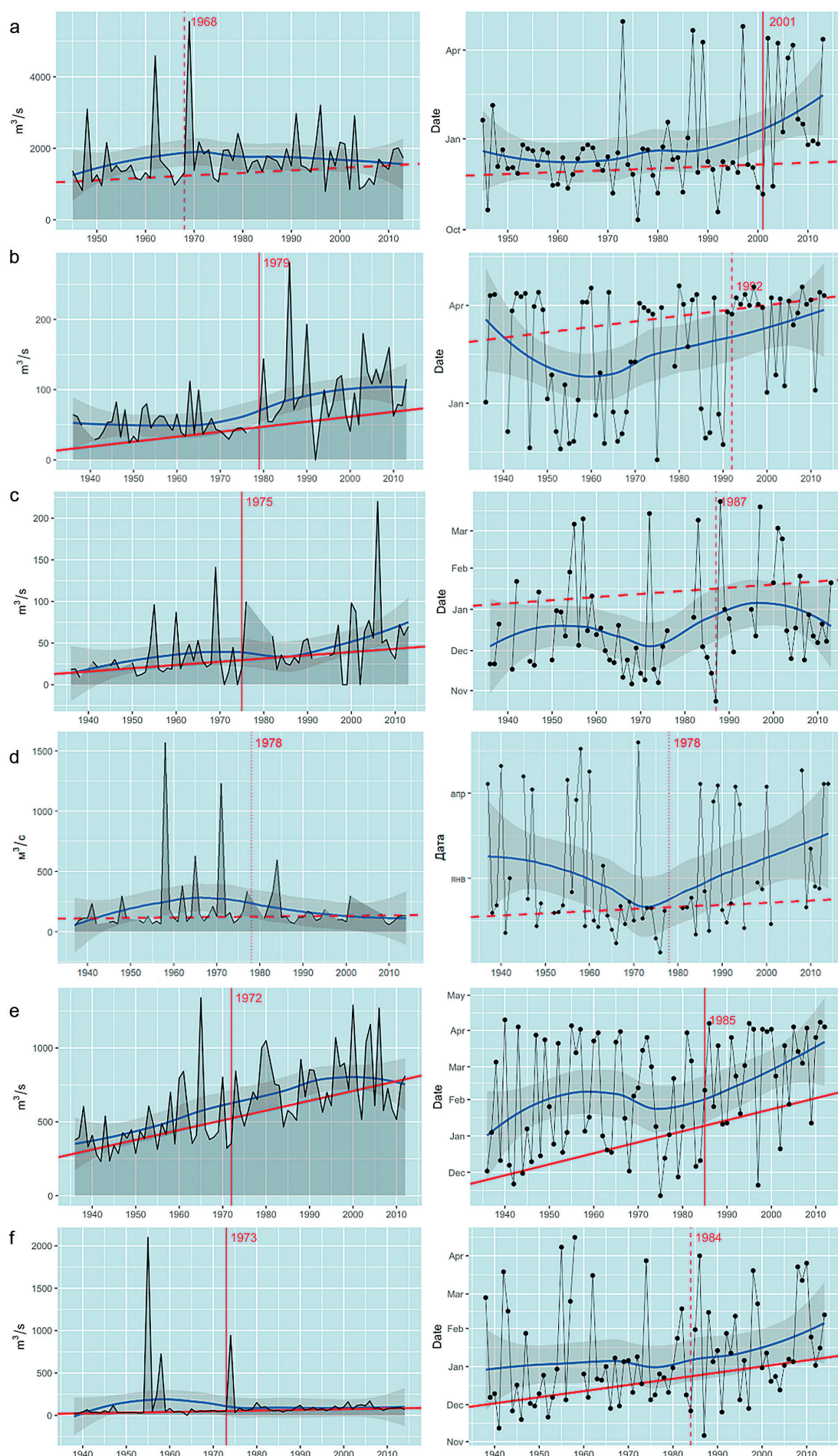


Fig. 5. Change in the maximum discharge rate of thaw floods (left) and its date (right) for : (a) the Severnaya Dvina River – Ust-Pinega village, (b) the Unzha River – Makaryev city, (c) the Moksha River – Temnikov, (d) the Kama River – Gayny village, (e) the Oka River – Murom city, (f) the Hoper River – Besplemyanovsky farm

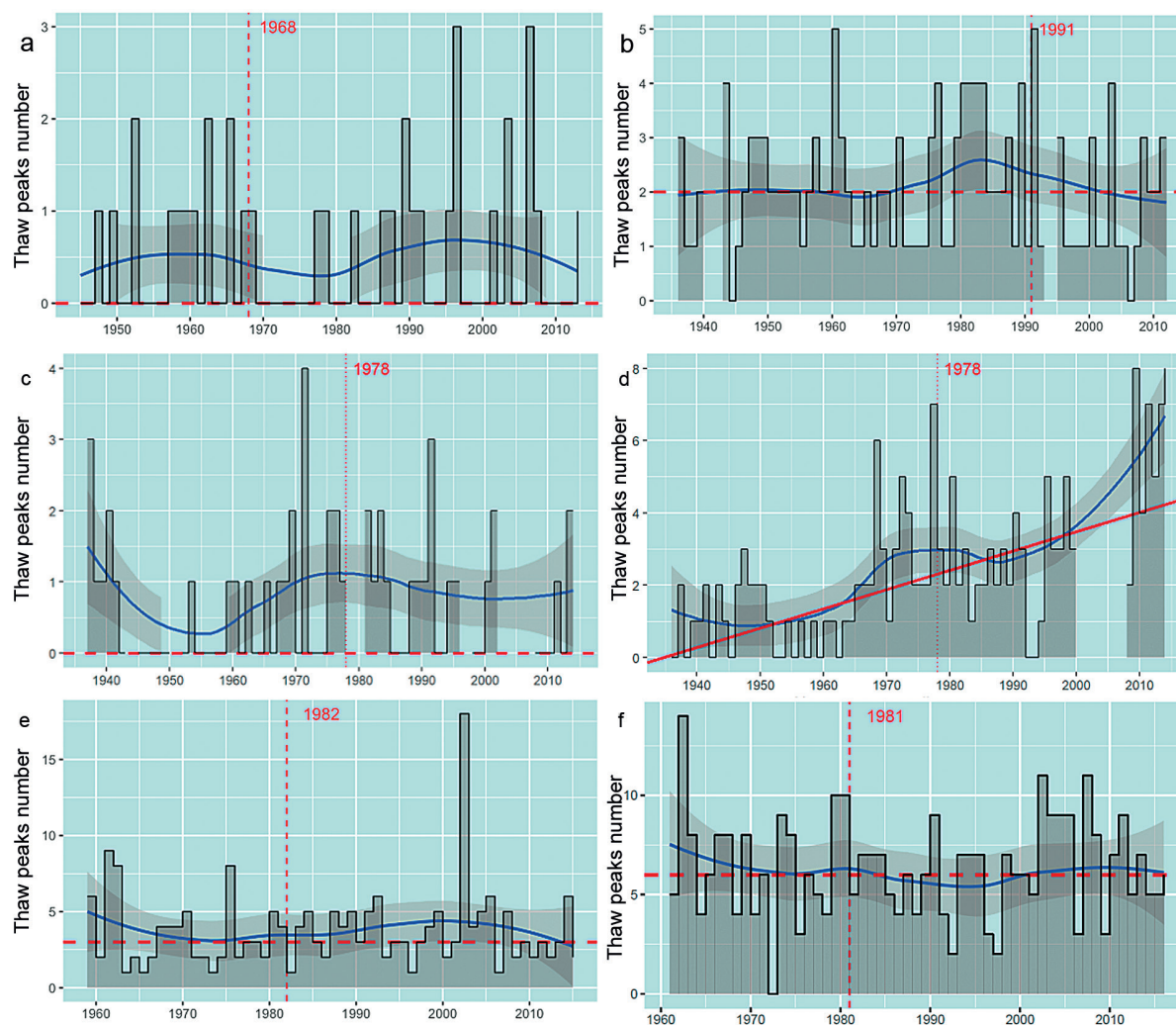


Fig. 6. Change in the number of thaw peaks for: (a) the Mezen River – village Malonisogorskaya, (b) the Oka River – Murom city, (c) the Kama – Gainy village, (d) the Belaya River – Sterlitamak city, (e) the Sosna River – Yelets town, (f) the Urup River – Steblitsky farm

This maximum corresponds to the climatic ridge of the runoff. The highest values are typical for the Pechora and Kama river basins that originate from the western slopes of the Urals. An interesting feature is the high values (from 20 to 50 L/(s·km²) in the Upper Volga and the Upper Oka. The specific discharge for thaw runoff is an order of magnitude lower than the values for the rain floods runoff; in addition, thaw runoff exhibits a slightly different spatial pattern. The highest values are also typical for the northeast of the region and the Kola Peninsula. The rivers of the Upper Volga basin have a high specific discharge of thaw floods (Fig. 7) of more than 10 L/(s·km²). In the west of the North Caucasus more than 100 L/(s·km²).

The runoff depth of rain and thaw floods varies throughout the territory quite smoothly and almost completely corresponds to changes in the continental climate. Orographic relief forms are distinguished—the Valdai Upland and the slopes of the Urals, where the rain runoff reaches 80 mm and thaw runoff depth is 30 mm (Fig. 8). In the North Caucasus, the runoff depth of rainfall floods is closed to that observed for the rivers of the Russian north, 50–90 mm, while in the catchments of small rivers it can exceeds 130 mm. In recent decades, the thaw runoff depth of rivers of central Russia has markedly increased to 20–30 mm per year.

An extremely interesting indicator is the average number of occasional floods, observed on the rivers. The number of rain peaks varies from 1 to more than 10, depending on the geographic location of the catchment. The rivers of the western half of the ETR, the left-bank tributaries of the Upper Volga – the Kostroma, Unzha and Vetlug rivers, as well as the

rivers of the North Caucasus have the largest number of local rain maximums. The number of thaw occasional floods clearly divides the ETR into the western and eastern half. In the western parts of the Oka basin, the Upper Volga, Don and the North Caucasus it reaches 5–8 or more (Fig. 9), in the eastern part it rarely exceeds 1. Only the left-bank tributaries of the Kama, originating from the slopes of the Southern Urals, are characterized by 2–3 thaw peaks.

DISCUSSION

An increase in the amount of liquid precipitation in the winter is typical for the modern climate of the ETR (Kireeva 2019). It is closely associated with an increase in the average winter temperature and the number of thaws. The mechanisms of the water regime transformation of the rivers are difficult to interpret due to the lack of direct measurements of all components of the water balance that were previously carried out at water-balance stations (Barabanov et al. 2018). Based on indirect indications (an increase in the level of groundwater, reduction of soil freezing depth, and a decrease of the main seasonal flood volume), it can be concluded that the processes of runoff formation on catchments in the middle latitudes (mixed forest zone) and in the south (forest-steppe zone) of the Russian Plain have begun to occur somewhat differently (Barabanov et al. 2018).

Presumably, this change is due to the influence of warmer air masses, which are increasingly invading from the Atlantic and from the southern latitudes, including the

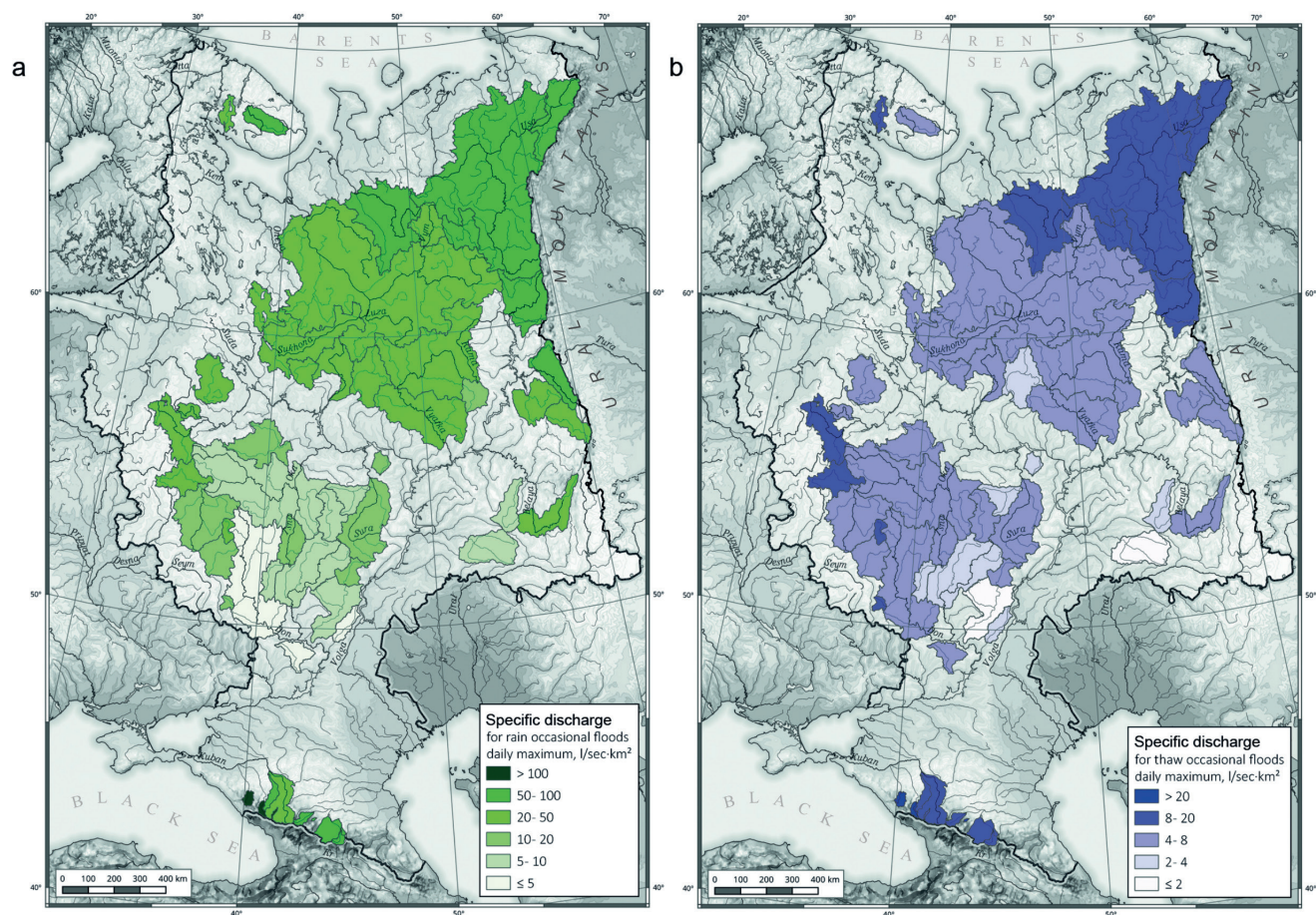


Fig. 7. Maximum daily specific discharge of occasional (a) rain and (b) thaw floods (averaged for 1978–2015)

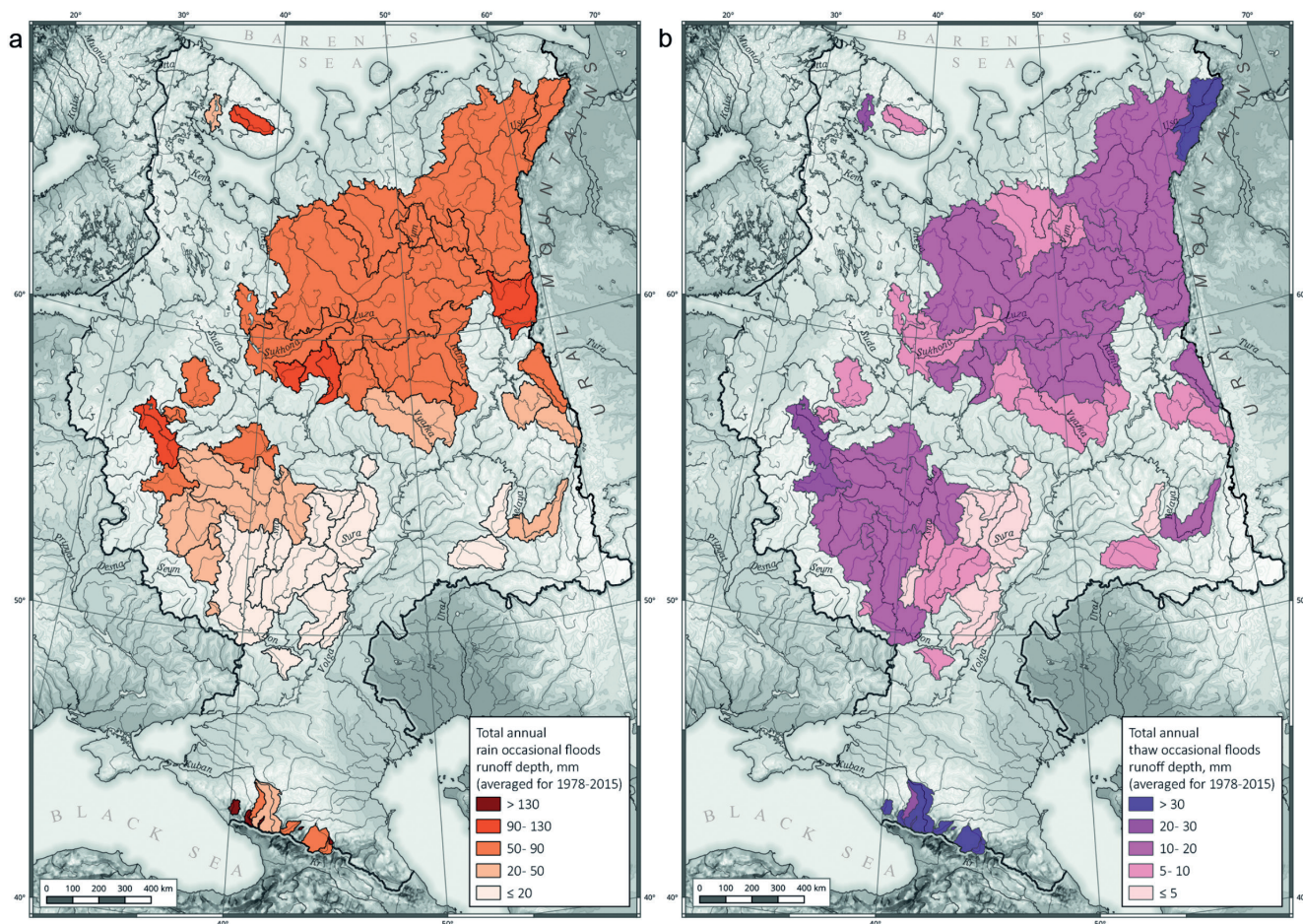


Fig. 8. The runoff depth of occasional (a) rain and (b) thaw floods (averaged for 1978–2015)

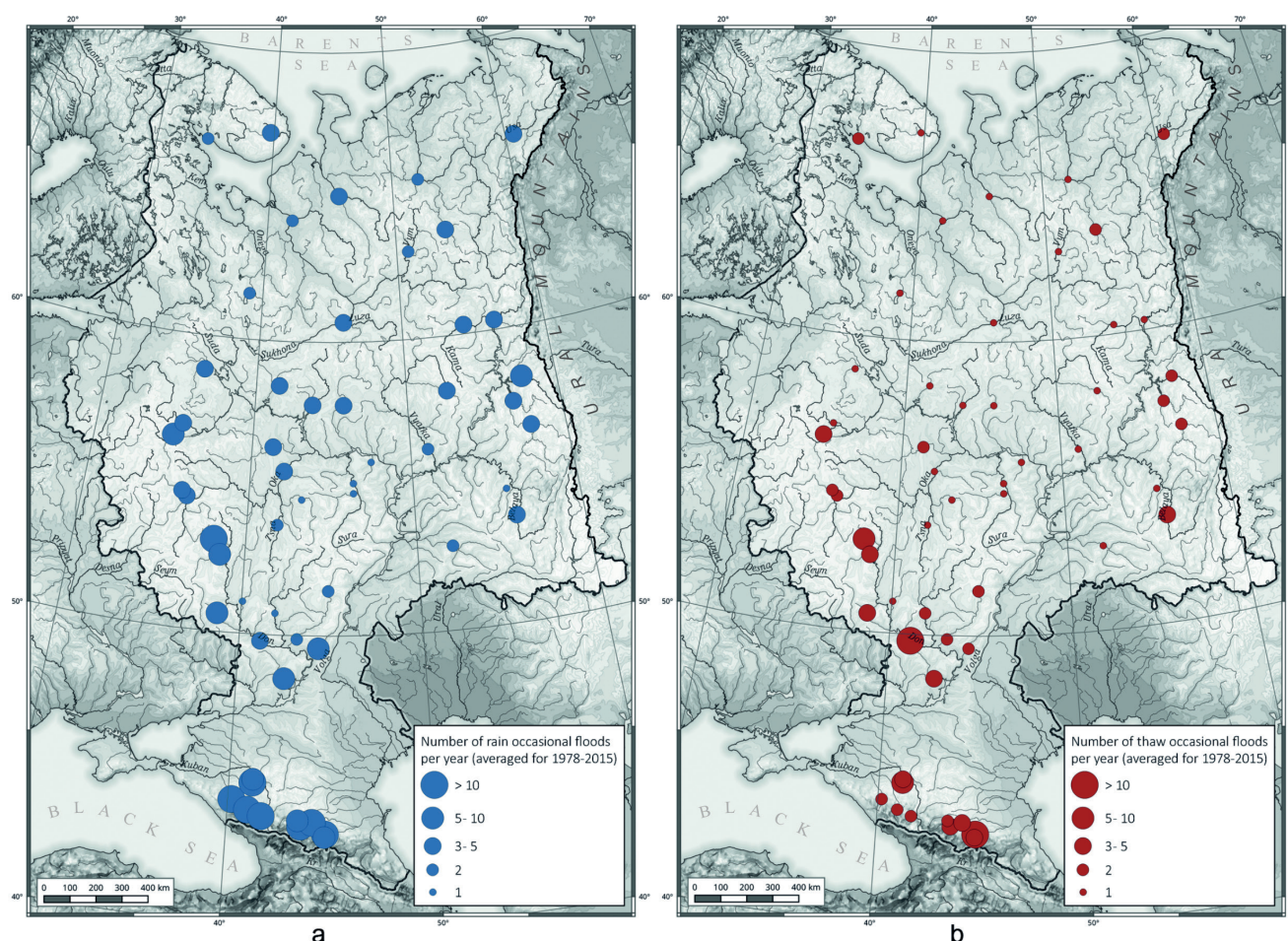


Fig. 9. The number of occasional (a) rain and (b) thaw floods for 1978–2015

Black Sea. This leads to multiple increases in temperature in the winter, its transition through zero and changes in the phase of precipitation from solid to liquid. In addition, according to recent studies (Kislov et al. 2017), anomalous amounts of precipitation play a significant role in blocking anticyclones. The Euro-Atlantic sector fully covers the ETR and experienced an increase in the frequency of blocking in the northern hemisphere during the 20th – early 21st centuries. Under current conditions, it was hypothesized that a change in the process of runoff formation in the winter period has qualitatively changed the characteristics of seasonal runoff over the past 30 years. By the end of the 1970s, most of the ETR was characterized by relatively cold winters with stable snow cover and a high annual snowmelt maximum in spring. Snow cover moisture-yielding ability was followed by the beginning of surface flow and replenishment of surface and underground water resources and runoff of surplus into the river network (Koronkevich 2018).

Currently, the replenishment of soil and groundwater horizons and the filling of surface depression are associated with thaws and occur several times during the winter. Water flows to the surface of the catchment area throughout the winter. By filtering into soil horizons, it causes increased loss of melt water during the winter low-flow season. At the same time, no pronounced seasonal flood occurs in the spring; the increase in discharge due to surface melt water inflow has changed, presumably, to subsurface inflow with many lower gradients. Such hydrographs are now typical for the rivers of the Don basin and the southern part of the Oka basin as well as Samara, Sura and the Moksha basin. Levelling of the hydrograph led to no «washing» of the riverbed during the flood period; thus, small rivers gradually silt and disappear. The «snowmelt droughts» that stand out on rivers

with water peaks during snowmelt season have the same mechanism (Van Loon 2015). All these processes observed while the annual runoff is more or less stable (Frolova 2017).

The formation of thaw floods in winter is especially dependent on the state of the soil surface – its moisture content, freezing depth and the presence of an ice crust on the surface. These three factors determine the possibility of water seepage, that is moisture loss due to infiltration. If the soil freezing depth and its humidity are small, a significant part of the melt water yield will go into the subsurface and ground horizons and the peak flow on the river, most likely, will not form. If there is an ice crust on the surface, it actually turns into a water-repellent and the peak flow most likely will be very high. In the central part of Russia, in the Upper Don and the Oka Basins, significant trends in the minimum soil temperature at a depth of 40 cm have been observed over the past 30–40 years. In the late 1970s and mid-1980s it averaged -4...-6 degrees, reaching -8...-10 degrees in some years; then, in the 2000s, its average value moved toward 0...-1 degrees (average for 2000–2013) (Kireeva et al. 2019). In about half of the measurements the minimum winter soil temperature was positive. Thus, freezing was not already observed at a depth of 40 cm. The minimum temperature of the soil is also influenced by the presence of snow cover – the greater its height, the more noticeable the heat-insulating effect that prevents deep freezing. Therefore, in the more southern regions, for example, in the Lower Don, the tendency to increase the minimum soil temperature is less pronounced. In the northwestern portion of the ETR similar trends are observed; an increase in the minimum soil temperature is less pronounced in the eastern regions of the Kama basin, the Middle and Lower Volga the Urals.

Summing up, we can state that an increase in the minimum soil temperature and, as a consequence, a

decrease of the soil freezing depth leads to an increase in subsurface and ground water replenishment. At the same time, melt water losses due to surface retention and evaporation increase during the winter and especially during the spring. The combination of these trends leads to an increase in losses to infiltration and waterlogging of the soil in winter due to the occurrence of frequent thaws and a decrease in surface runoff in spring. As a result, the supply of groundwater increases, in turn leading to an increase in the share of underground river nourishment. The increased discharges of the low-flow period contributes to the formation of occasional floods. Liquid precipitation or a strong and prolonged thaw leads to a sharp increase in water yield. If the soil is already saturated with moisture at this moment the surface runoff begins, superimposed on the previous growth of the river groundwater supply.

CONCLUSIONS

In recent years, a significant transformation of the water regime has been taking place on the most rivers of Russian Plain. Occasional floods play an important role in this process. Intensive reduction in the ratio of volumes and maximum discharge of main seasonal flood wave correspond to an increase of the base flow component. This growth is presumably associated with the effect of overlapping occasional floods. Changes in the processes of flow formation in the closing section of the river are associated with increased groundwater supply. A vicious cycle arises: the occurrence of thaws leads to higher water yield to the catchment surface during winter; if the soil is not frozen, this water seeps out, filling the soil horizons; if it is frozen, surface runoff and flash flooding occur. In further thaws, high soil moisture contributes to the formation of flow peaks, since the water has nowhere to be filtered. The calculated results presented in this work confirm a number of previous findings about the change and transformation of the water regime of the ETR Rivers. ■

REFERENCES

- Barabanov A.T., Dolgov S.V., Koronkevich N.I., Panov V.I., Petelko A.I. (2018). Surface runoff and melt infiltration into the soil on arable land in the forest-steppe and steppe zones of the East European Plain, *Soil Science*, 1, 62-69.
- Beurton S. and Thieken A. (2009). Seasonality of floods in Germany, *Hydrological Sciences Journal*, 54, 1, 129-141.
- Blöschl G., Hall J., Parajka J., Rui P. A.P., Merz B., Arheimer B., Giuseppe A.T., Bilibashi A., Bonacci O., Borga M., Čanjevac I., Castellarin A., Giovanni C.B., Claps P., Fiala K., Frolova N., Gorbachova L., Gül.A., Hannaford J., Harrigan S., Kireeva M. et al. (2017). Changing climate shifts timing of european floods, *Science*, 357, 6351, 588-590.
- Cunderlik J.M. and Burn D.H. (2001). The use of flood regime information in regional flood frequency analysis, *Hydrological Sciences-Journal-des Sciences Hydrologiques*, 47, 1.
- Eckhardt K. (2005). How to Construct Recursive Digital Filters for Baseflow Separation, *Hydrological Processes*, 19(2), 507-515.
- Finch J., Marsh T., McKenzie A. (2007). A preliminary risk assessment of the potential for groundwater flooding during the winter of 2007/8 – an update, Wallingford, NERC/Centre for Ecology and Hydrology-British Geological Survey, 23.
- Frolova N.L., Agafonova S.A., Kireeva M.B., Povalishnikova E.S., Pakhomova O.M. (2017). Recent changes of annual flow distribution of the Volga basin rivers in *Geography, Environment, sustainability*. 10(2), 28-39, DOI: 10.24057/2071-9388-2017-10-2-28-39.
- Hall J. and Blöschl G. (2018). Spatial patterns and characteristics of flood seasonality in Europe, *Hydrol. Earth Syst. Sci.*, 22, 3883-3901, DOI: 10.5194/hess-22-3883-2018.
- Kireeva M., Frolova N., Rets E., Samsonov T., Entin A., Kharlamov M., Telegina E., Povalishnikova E. (2019). Evaluating climate and water regime transformation in the European part of Russia using observation and reanalysis data for the 1945–2015 period, *International Journal of River Basin Management*, DOI: 10.1080/15715124.2019.1695258.
- Kislov A., Sokolikhina N., Semenov E., Tudriy K. (2017). Blocking Anticyclone in the Atlantic Sector of the Arctic as an Example of an Individual Atmospheric Vortex, *Atmospheric and Climate Sciences*, 7, 323-336, DOI: 10.4236/acs.2017.73024.
- Koronkevich N.I., Georgiadi A.G., Dolgov S.V., Barabanova E.A., Kashutina E.A., Milyukova I.P. (2018). Change in snow flood flow in the southern macro-slope of the Russian Plain in the period 1930–2014, 58 (4), 498-506 (in Russian), DOI: 10.15356/2076-6734-2018-4-498-506.
- Marsh T.J. and Hannaford J. (2007). The summer 2007 floods in England and Wales – a hydrological appraisal, Wallingford, Centre for Ecology and Hydrology, 30.
- Nathan R.J. and McMahon T.A. (1990). Evaluation of Automated Techniques for Baseflow and Recession Analysis, *Water Resources Research*, 26(7), 1465-1473.
- Parajka J., Kohnová S., Bálint G., Barbuc M., Borga M., Claps P., Cheval S., Dumitrescu A., Gaume E., Hlavčová K., Merz R., Pfandl M., Stancalie G., Szolgay J., Blöschl G. (2010). Seasonal characteristics of flood regimes across the Alpine–Carpathian range, *Journal of Hydrology* 394, 78-89.
- Petrov T. and Merz B. (2009). Trends in flood magnitude, frequency and seasonality in Germany in the period 1951–2002, *Journal of Hydrology*, 371, 1-4.
- Shevnina E.V. (2013). Methodology for calculating the characteristics of spring flood according to daily water discharge, *Problems of the Arctic and Antarctic*, 1(95), 44-50 (in Russian).
- Van Loon A.F. and Laaha G. (2015). Hydrological drought severity explained by climate and catchment characteristics, *Journal of Hydrology*, 526, 3-14, DOI:10.1016/j.jhydrol.2014.10.059.
- Volchek A.A. and Shelest T.A. (2012). Formation of winter floods on the rivers of Belarus, *Scientific notes of the Russian State Hydrometeorological University*, Rubric: Hydrology, 25, 5-19 (in Russian).

A GEOGRAPHICAL APPROACH TO WATER RESOURCE MAPPING FOR ATLASES

Leonid M. Korytny^{1*}, Olga V. Gagarinova¹, Elena A. Ilyicheva^{1,2}, Natalya V. Kichigina¹

¹V.B. Sochava Institute of Geography, Siberian Branch, Russian Academy of Sciences, Russian Federation, Irkutsk; 1, Ulan-Batorskaya St., 664033

²Department of Hydrology and Environmental Sciences, Irkutsk State University, Russian Federation, Irkutsk; 126, Lermontov St., 664033

*Corresponding author: kor@irigs.irk.ru

Received: December 18th, 2019 / Accepted: May 10th, 2020 / Published: July 1st, 2020

<https://DOI-10.24057/2071-9388-2019-171>

ABSTRACT. We examine water resource mapping as an important component of the geographical approach in land hydrology and in the water sector which serves to assist considerably in dealing with water problems and water resource management. We suggest that seven groups of water resource maps be distinguished: introductory maps, maps of formation of surface and subsurface water regimes, maps of assessments of water resource potential, maps of water management, maps of anthropogenic impacts on water, maps of hazardous hydrological phenomena and maps of water protection measures. Characteristic properties water resource mapping for atlas products are identified using a case study of territory surrounding Lake Baikal as a site of global significance. We compiled an inventory of water resource themes covered by various atlases of the Baikal region and determined gaps relating to economic aspects of water and to maps on water protection. Limitations of the traditional isoline method in geographical water resource mapping are shown. At hillslope level where atmospheric precipitation transforms to surface runoff further to stream flow, it is recommended that the indication localization method be used, which is based on interdependencies of components of the geosystem. Water runoff mapping at the regional level in the hydrographic network uses the technique of long-channel (epure) mapping based on tools of structural hydrographic and Horton-Strahler classification. A technique of regionalization is described for flood hazards, water protection and recreation zoning of Baikal's shores as well as cartographic modeling of processes in the Selenga river delta.

KEY WORDS: water resource maps, Baikal region, atlases, indication localization, long-channel mapping, delta

CITATION: Leonid M. Korytny, Olga V. Gagarinova, Elena A. Ilyicheva, Natalya V. Kichigina (2020). A Geographical Approach to Water Resource Mapping for Atlases. *Geography, Environment, Sustainability*, Vol.13, No 2, p. 96-103

<https://DOI-10.24057/2071-9388-2019-171>

ACKNOWLEDGEMENTS: This work was supported by the Russian Foundation for Basic Research [project no. 17-29-05043/18 and 17-29-05052], Research Project No. 0347-2019-0003

Conflict of interests: The authors reported no potential conflict of interest.

INTRODUCTION

Water resources have a number of special features which distinguish them from other natural resources. They are characterized by a dual natural-social essence: the water as the component of the natural environment and, at the same time, one of the major elements of productive forces, plays a large social-historical, infrastructural and region-forming role. Not only do water resources have mass and energy properties but they also provide a basis for human livelihoods and economic development.

Problems caused by scarcity or surplus of water and by pollution of water bodies are growing at an ever increasing pace worldwide. Today about 1.3 billion people are in dire need of freshwater, and about one-fourth of a billion are experiencing enormous water stress. Pollution has currently affects up to 17,000 km³ of water, or half the maximum estimated volume available for use. So far it is impossible to determine whether a global water crisis is approaching.

Over the last several decades, climate and human-caused have changed of water regime and water quality, showed insufficient hydrological and hydrochemical observations. Assessment of the current hydrological conditions requires the use geographical methods of analogy and zoning, the use of indirect and indicative characteristics, and the widespread introduction of remote methods and GIS technologies. The need to take into account the parameters and functions of specific landscapes of the catchment, the manifestation of local and regional natural relationships is especially relevant in the Eastern regions of Russia, which is determined by the variety of natural conditions, the complexity of economic tasks and the lack of hydrometeorological network.

Water resource mapping is an important geographical tool for assisting with water management. Mapping has been widely used for long periods of time in scientific research and practical applications. «The map as any other model reproducing an object for scientific inquiry is able to substitute it in such a way so that its study provides a possibility of scooping new, intrinsically important information» (Sochava 1978).

The underlying cartographic atlas products are the result from accumulated knowledge of different sectors and disciplines of Earth sciences as well as from various territorial subdivisions of countries and regions. Atlas maps reflect achievements of these sciences stimulating new ideas. In this paper, we examine the characteristic properties of water resource atlas mapping by using the Baikal region as an example.

In this case, four main tasks are solved:

- to propose a new classification of water resource maps according to the mapped characteristics and purpose;
- to consider the experience of water resource mapping of the Baikal region;
- to identify the methodological features of water resource atlas mapping;
- to outline the prospects for water resource mapping in the Baikal region.

RESULTS AND DISCUSSION

Classification of water resource maps

According to its content, we propose to distinguish several groups of maps:

(1) *Hydrographic (introductory)* maps of the hydrographic network, river basins, the river network density and other hydrographic indicators, river sailing directions, valleys, presence of lakes, dams and bogs etc.. This group also includes schematic maps of the network of water resource monitoring: hydrometric sections, gauging stations, sampling locations, etc.

(2) Maps on *formation of surface and subsurface water regimes*. As the largest group it incorporates maps on water balance elements, rates of streamflow, ice phenomena as well as thermal, hydrochemical, hydrobiological and microbiological regime and status, channel processes, usable resource and regimes of subsurface waters, and hydrological and hydrogeological regionalization.

(3) The group on *assessment of water resource potential* includes maps on the availability water and its energy production, water supply, transport and fishing.

(4) The group on the *water sector and its management* includes maps of water infrastructure such as intakes, canals, water transport routes, irrigation and drainage systems etc.

(5) *Consequences of anthropogenic impacts* on water bodies and their catchments are represented in this group. Central to it are maps depicting changes in water status such as pollution, clogging, depletion, salinization and disturbances of natural flow regimes.

(6) The group *hydrological risks* comprises maps on hazards and risks related to floods, debris flows, avalanches, water erosion, bank abrasion, etc.

(7) Finally, the group *«Water protection measures»* includes maps on water protection facilities and zones and recommended water protection measures.

Presentation of water resource themes in atlas products for the Baikal region

The Baikal region includes three territorial units of the Russian Federation: the Irkutsk oblast, the Republic of Buryatia, and the Zabaikalskii krai. The total area of the region is 1.56 million square kilometers, its population is 4.45 millions (3% of the population of the Russian Federation, as of 01.01.2019). The region has all attributes of landscape-ecological and economic-cultural integrity where a significant role is played by water resource relationships. The region is an integral entity primarily because a significant part of its territory lies within the drainage basin of Lake Baikal, a water body of global significance. Baikal is one

of the greatest lakes of on Earth and a UNESCO World Heritage site. The reserves of freshwater in the lake are 23.6 thousand cubic kilometers, or 26% of the world reserves of lake freshwater and 90% of Russia's lake water, and 5.5% of all freshwater of the world. The lake is unique in its flora and fauna, in the diversity and degree of endemism of the species inhabiting it, and in unprecedented self-purification mechanisms. It is the world's oldest lake with an estimated age of 20–25 million years, or several orders of magnitude older, than any other reservoir across the globe.

Baikal's waters are central to the immense hydroelectric and water-supply potential of the region, which largely determines the economic profile of the territory. The region is among the main sources satisfying domestic and export needs of Russia for diverse natural resources. The largest industrial-economic complex has been created in the east of the country. Therefore, it has rightfully served (and continues to do so) as a powerful base for development of Far Eastern and northern regions of Russia and as the testing grounds for prospective implementation of a number of programs of national significance relating to energy, transport, gold and furs; various sectors of the defense complex, and recreation and tourism.

It is appropriate to carry out the planning of socio-economic development of the Baikal region using a powerful cartographic information base represented by atlas products. Many years of efforts of the Irkutsk-based V.B. Sochava Institute of Geography SB RAS managed to achieve Russia's highest level of cartographic presentation and information support (Batuev & Korytny 2018).

Let us consider the way in which water resource maps are presented in the atlases of three classes, basing ourselves on the atlases produced in the ex-Soviet Union and in today's Russia. The first class includes atlases of a global level, i. e. of the world, parts of the world and Russia in general. Small-scale maps provide a means of positioning the indicators of the federal subjects of the Baikal region in Russia and in the world. This applies for comprehensive atlases, such as the (Atlas of natural resources of the world 1998) or the (National atlas of Russia 2004–2008) as well as for specialist water resource atlases: the (Atlas of the world water balance 1974) and the (Atlas of snow-ice resources of the world 1998). We now consider in greater detail three atlases for the territory of Russia that were published in the last decade.

The (Atlas of socio-economic development of Russia 2009) offers a comprehensive multi-purpose model, with its 240 maps making it possible to analyze the qualitative and quantitative changes that occurred in Russia in the late 20th – early 21st centuries in the economy and in social relations. A characteristic of the atlas is the only regional section that includes 50 maps of the Baikal region. And the territory of the region is displayed on most of the other small-scale maps: on a total of 94.7% of all maps in the atlas. But the water resources and their use are neglected in the atlas; not a single water resource map can be found even in the regional section, with the exception of the water transport block on Russia's map of water transport systems.

A next atlas offers a different situation. An encyclopedic compilation of information on the full spectrum of natural, technogenic and socio-biological hazards and risks is provided in the (Atlas of natural and technogenic hazards and risks from emergency situations 2011). The atlas contains 323 maps and is intended for a wide range of users. The Baikal region is presented on 268 maps, or 83% of all maps. Out of them, 28 maps are water resource maps; of course, most of these maps belong in the group «Hazardous hydrological phenomena».

The latest example is provided by the (Ecological atlas of Russia 2017) that reflects spatio-temporal information on the formation conditions for the ecological situation, economic impacts on the natural environment, the ecological status of the environment, and on the measures undertaken for environmental sanitation and optimization of the ecological situation at the beginning of the 21st century. The atlas was developed on the basis of the latest scientific-methodological and technological achievements in the array of modern subject sciences (geography, biology, ecology, informatics, etc.) and in mapping by ensuring continuity with the best examples of national and foreign cartographic products; it contains 262 maps accompanied by texts, satellite images and other illustrative material. The Baikal region is presented on 178 maps (68%), and 36 maps are devoted to the water resource themes in the seven groups but the maps of anthropogenic transformations and hazardous hydrological phenomena are dominant.

The second class is represented by two atlases of lakes. The first of them, the (Atlas of Lake Hovsgol), situated in the Mongolian part of the Baikal drainage basin, was published in 1989. The atlas contains a total of 91 maps. The maps in the first part of the atlas characterize the surface and subsurface, the climate and waters, soils and vegetation, wildlife, the population and the economy of the Hovsgol region; the second part contains information on the characteristics of the lake bed, the morphology and dynamics of its shores, wind-driven wave, water temperature, chemistry of waters and bottom sediments, and the organic world of the lake. It is logical that one-third of the maps are water resource maps, and an absolute predominance corresponds to the group of formation of regimes and in this group, to hydrochemical and hydrobiological maps.

The situation with the (Atlas of Lake Baikal 1993) is somewhat different. It is structured in the same way, i. e. the water area and its surroundings are considered but about 60% of all maps now refer to water resource maps. And most of the maps refer to the second group (formation of regimes of the lake) but the geophysical properties: currents, wave disturbances, the ice and thermal regime, etc. are presented on about half of the maps.

The third class is comprised of the ecological atlases of the Baikal region. The first of them is entitled (Irkutsk region: ecological conditions of development 2004). The purpose of 90 maps in the atlas is to furnish a means of linking the ecological connections and phenomena displayed on the maps to a broad geographical background of a diverse thematic spectrum as well as showing the concrete indicators of particular deviations in the nature management system in order to eliminate them through the measures for its rationalization. Furthermore, about 30% of the maps are water resource maps, and the maps of formation of regimes and anthropogenic impacts carry basic and equal «weight». It is for the first time that the (Ecological atlas of the Lake Baikal basin 2015) reflects the spatial formation patterns of the ecological situation throughout the entire catchment of Baikal and its water area, which provides a means of determining and substantiating the future directions of ecologically balanced and sustainable development of Russia and Mongolia. The atlas was published in the Russian, English and Mongolian language. Out of the 142 maps of the atlas, about 16% refer to water resource themes. Although more than half of them belong in the group of formation of regimes, almost all other groups are presented.

The (Ecological atlas of the Baikal region) that was posted on the online geoportal maintained by the Institute of System Dynamics and Control Theory SB RAS in 2017 is yet another completed cartographic compilation product. It

serves as a base component of the cartographic information system for sustainable development of the Baikal region and is intended primarily for managerial bodies of the subjects of the Russian Federation on the territory of the region. The atlas contains 348 maps, and about a hundred of them refer to the water area of Lake Baikal. Thus the number of water resource maps reached 20%, although the group of formation of regimes is dominant, but all groups of maps are presented.

The final analysis shows that sufficient attention is paid to water resource maps and, especially, to lake maps in particular. However, the groups of maps presented are nonuniform, the least – the maps of the water economy, and the water protection maps. This should be taken into account in future mapping of the Baikal region.

Methodological foundations of geographical water resource mapping

Geographical mapping of water resources uses most of the procedures and methods employed in thematic mapping. However, there are limitations as regards the conventional isoline method. It is based on the assumption that changes are continuous in the space of hydrometeorological elements, which is, to a large extent, typical for the radiation balance, air temperature and evaporation and, to a lesser extent, to atmospheric precipitation, mostly on flat territories, with the type of latitudinal zonality predominating, and with a significant spatio-temporal averaging. However, when streamflow characteristics are represented by isolines, a very important factor is neglected: if atmospheric precipitation occurs at any point of the terrestrial surface, then the channeled runoff is, essentially, a point characteristic which can be regarded as an area characteristic (in the form of moduli or a layer of flow) as a result of generalizations and statistical transformations. Therefore, the drawing of isolines where river channels are absent altogether is quite arbitrary in character and the values of the flow obtained from such a map have rather crude and, often, simply empty values.

Certainly, the main spatial mapping cell in hydrology is the basin (catchment), and we substantiated this in the theoretical development of the basin concept in nature management (Korytny 2001; Korytny 2017). The difference of the main mapping procedures for elements of the hydrographic network and landscapes of the catchment is due to this.

At the hillslope level, i. e. where atmospheric precipitation transforms to the runoff, to the overland runoff first, and then to the channeled runoff, it is recommended that the method of *indicative localization* be used, which is based on interdependences of geosystem components (Gagarinova 2012). For instance, the map «Long-term average flow» in (Ecological atlas of the Baikal region 2017) reflects the formation patterns of the water regime of the territory which are based on the properties of landscapes to transform meteoric moisture (rainfall, fog, snow etc.) into runoff (Fig. 1). The value of the runoff from landscape complexes is determined by solving the inverse problem, i. e. identifying the relationship of the water discharge in the outlet section of the catchment with the runoff from landscape units occupying its area, and calculating on the basis of the equation $Q_j = \sum q_i f_{ij}$, where j is the river basin index; Q_j is the runoff from it, L/s; q_i is the modulus of flow from the i th landscape complex, L/s km², and f_{ij} stands for the areas of the j th basin occupied by the i th landscape, km². The map is constructed on the basis of the long-term average values of river flow and landscape characteristics of the Lake Baikal drainage basin. The lake's catchment encompasses different landscape zones and altitudinal belts, which is responsible

for a high degree of generalization and a large contrast of the values of the flow. The amplitude of fluctuations in the modulus of annual flow varies from more than 10 L/s km² in goletz and mountain-taiga landscapes to virtually 0 L/s km² in deserts areas of Mongolia (the Selenga basin). A similar procedure was used in constructing maps of minimum summer flow and maximum flood flow within the Lake Baikal drainage basin which were included in (Ecological atlas of the Lake Baikal basin 2015).

Other requirements should be taken into account in the event of mapping the streamflow at the regional level in the hydrographic network. First, it is desirable to show the true magnitude of streamflow in river systems in channel water discharges rather than the characteristics averaged over the territory. Second, it is important to cover on a single map the maximum possible spectrum of rivers of a different size (except for the smallest rivers). And, third, in order for the map to have a practical importance, it is necessary for users

to be able to rapidly obtain specific and sufficiently accurate information on the magnitude of streamflow in any given river section.

These requirements are satisfied by the technique of *longchannel mapping*, based on the tools of structural hydrography (Korytny 2001; Ilyicheva 2009). Large-scale topographic maps are used to construct the river network graph for the region, based on the principles of the Horton-Strahler river order classification. A calculation of the structural measures taking into account hierarchy, order, braiding and subordination of all elements of the river system saturates all topological space of the graph of the river system with structural information, and a close linkage of the structural measure to the mean magnitude of streamflow permits the flow to be determined at almost every point of the system. The relationships of the mean magnitude of streamflow, represented as an average long-term water discharge, with the structural measure in the same river section are constant

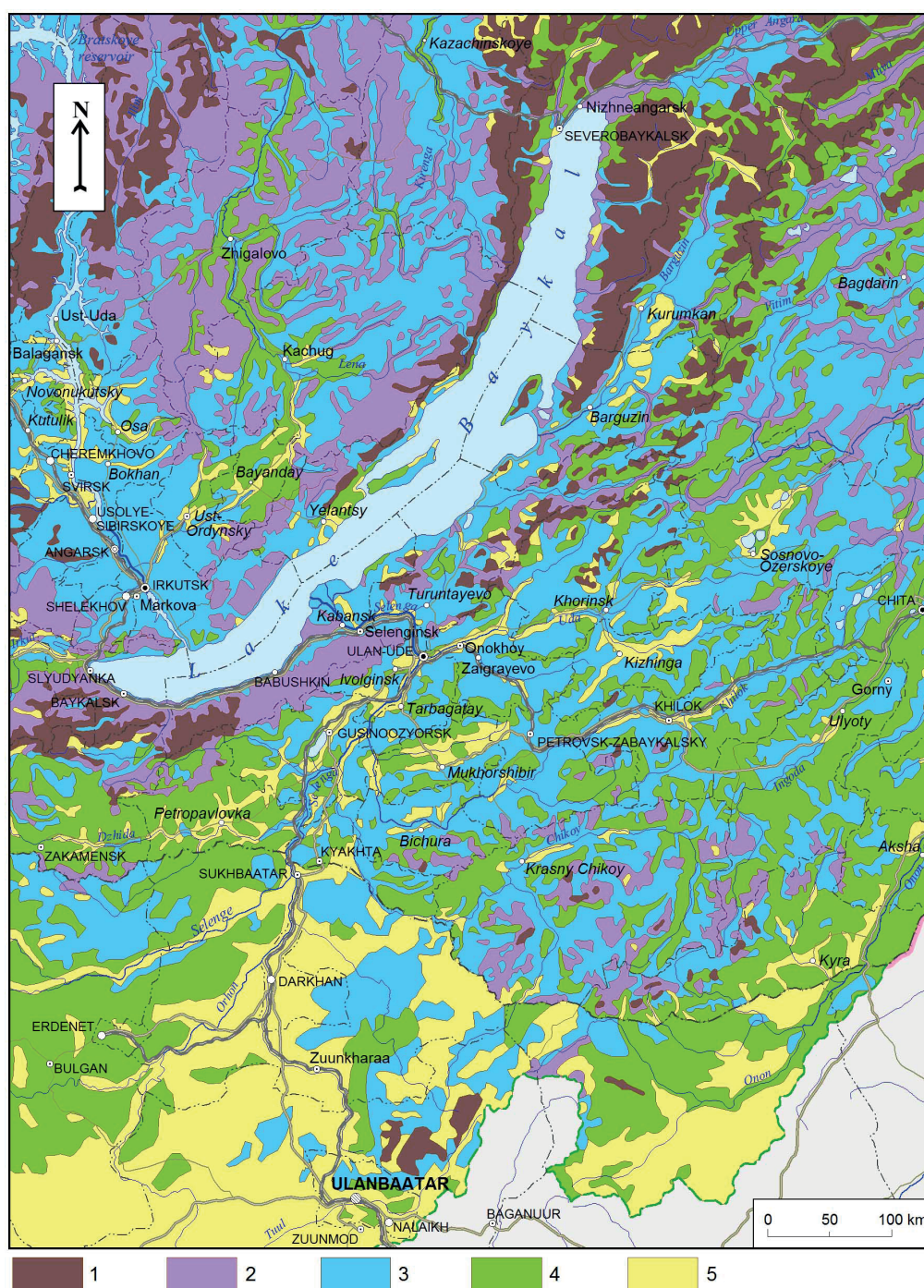


Fig. 1. Average annual runoff in the Baikal region. Modulus of flow, l/s/ km²: 1 – more than 10, 2 – 5–10, 3 – 3–5, 4 – 1–3, 5 – less than 1

for geologically homogeneous territories and constitute a statistical model of the river system as the set of permanent streams displayed on topographic maps, which corresponds to a stable average long-term flow.

The maximum or extremely high water runoff can be assessed using the dynamical model for the river system constructed from SRTM images. The dynamical model is represented by the set of thalwegs more than 75 m in length, whose activity is responsible for an increase of the number of elementary water-erosion components which operate solely in the period of maximum humidification at the passage of extreme water runoff. The calculated maximum water runoff (extremely high flow) shows a complete capacity of the water-erosion network. The calculated values exceed many times the observed values, in some cases by a factor of several tens or hundreds, and the reliability of such values is less than 0.1% (Amosova, Ilyicheva 2018).

This technique was used to prepare maps of water resources in the ecological atlases of the Baikal region. Structural parameters were calculated for each point of confluence of the streams on the basis of the river network graph. Structural modules were determined, which represent the ratio of water discharge to the structural measure at this point. The basic characteristic, water runoff of the river systems, is shown as a longchannel scale band (epure) (Fig. 2). This procedure refers to the group of localized diagrams, a method of mapping phenomena that are of continuous or linear (bank-like) occurrence. In this case, the epures are assigned to the linear element of space, i. e. to the river channel. The epures are drawn on both sides of the river channel proportional to the flow. The width of the epures varies smoothly along the length of the river, at the points of confluence with tributaries, depending of their water runoff.

A similar technique was also used for the other maps. Thus, on L.A. Bezrukov's map that was included in (Ecological atlas of the Baikal region 2017), where the spatial characteristics of the distribution of a stable streamflow were determined through a special zoning of the territory of the Baikal region from the conditions of the organization of large-scale centralized water supply from surface sources, the zone of different water availability are highlighted as bands running parallel to surface sources, i. e. water bodies: rivers, lakes, and reservoirs.

Regionalization also refers to traditional geographical methods. Thus, for generating the flood hazard maps the aforementioned atlas used the approach in which a flood hazard is characterized by the flood genesis and frequency, strength of flood impact, the size of damage and by the possibility of forecasting a hazardous situation. An integral flood hazard is determined by a different combination of these characteristics, and hazard classes are identified (low, moderate, significant, high and very high) (Kichigina 2018). Three classes of hazard (significant, high, and very high) are singled out for periodically flooded settlements. A combination of all characteristics analyzed is used to identify districts with a different integral flood hazard; in this case, the genesis of floods in river sections is designated by symbols (Fig. 3).

Based on the dual (socio-economic and natural) character of the spatial aspect, the flood hazard was determined for municipalities in the rank of administrative districts, with due regard for basin approach. Such an approach provides a means of making targeted practical use of results obtained. A **very high hazard** of flooding is characteristic for the most developed agglomerations of Irkutsk oblast, the Republic of Buryatia and Zabaikalskii krai (district). A **high hazard**

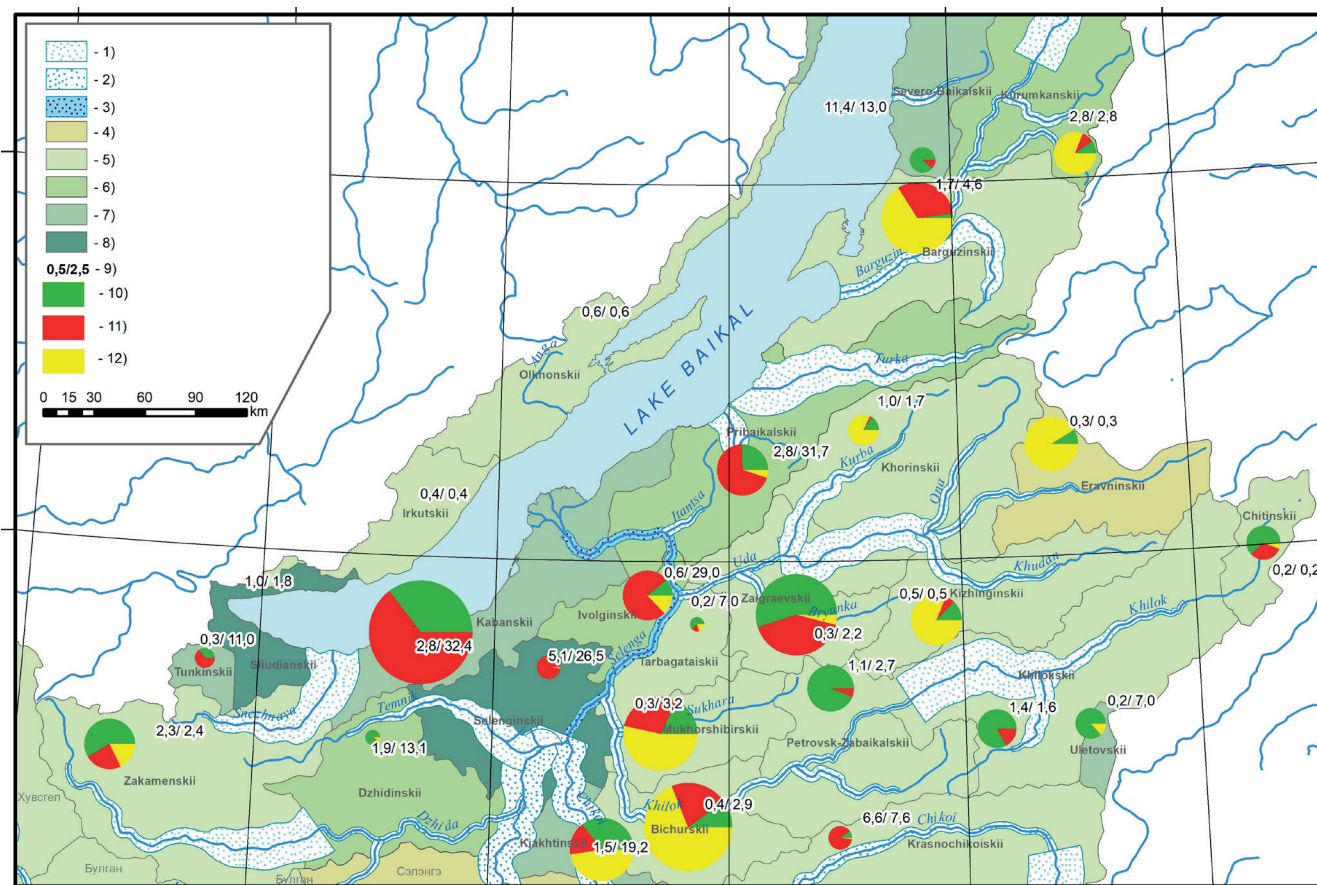


Fig. 2. A fragment of the map of water-carrying capacity and water use in the Baikal region
 Water bearing capacity, m^3s^{-1} : 1 - 1 mm; 2 - 1 mm: 50; 3 - 1 mm: 500. Water availability, $\text{km}^3/1000 \text{ km}^2$: 4 - less than 0.005; 5 - 0.005-0.15; 6 - 0.15-0.25; 7 - 0.25-0.35; 8 - more than 0.35; 9 - local flow/total flow, km^3/year .
 Water use, %: 10 - Household and drinking; 11 - Industrial; 12 - Agricultural

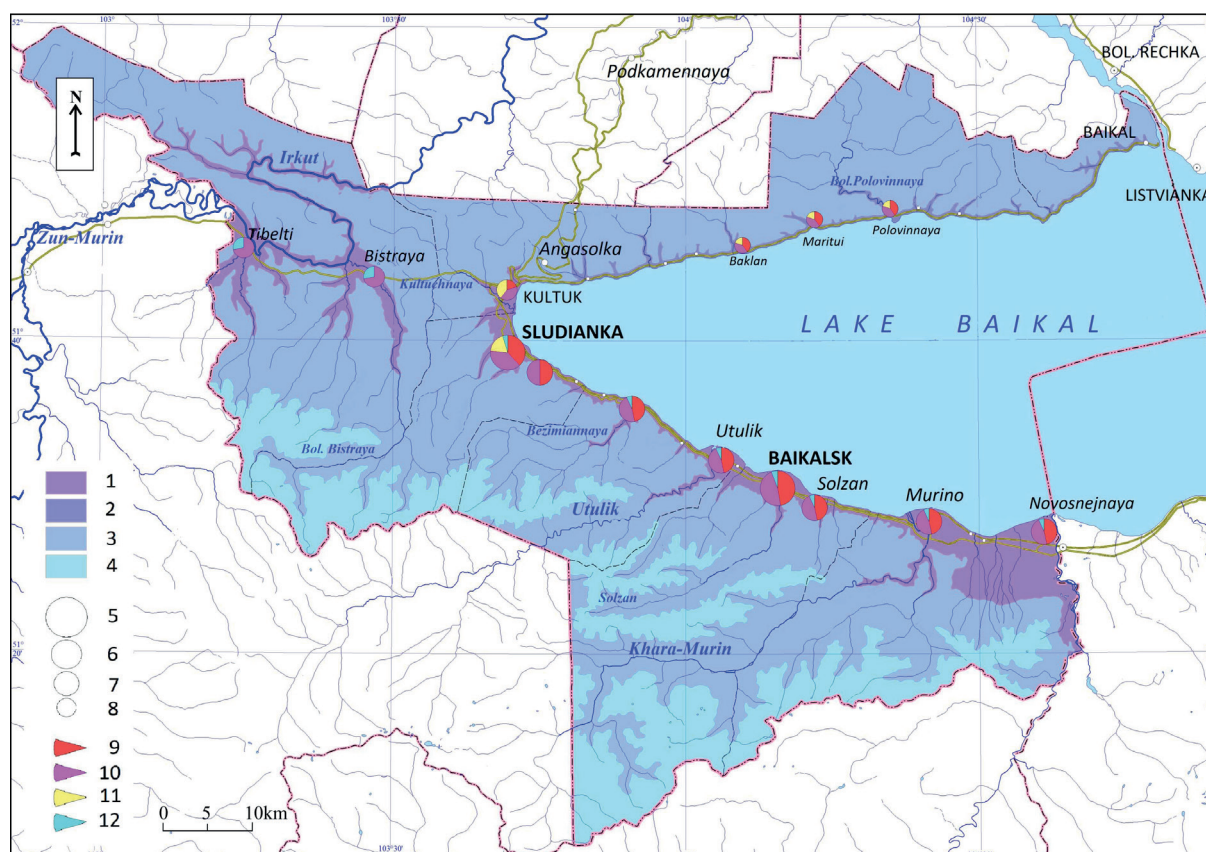


Fig. 3. Flood hazard for the Slyudyanskii district of Irkutsk oblast

Hazard: 1 – high, 2 – moderate, 3 – low, 4 – no floods. Degree of flood hazard for settlements: 5– very high, 6 – high, 7 – moderate, 8 – low. Flood genesis: 9 – debris flows, 10 – rainfall, 11 – aufeis, 12 – snow melt

also occurs in the southern districts of these subjects with the largest number of flooded settlements, including the cities of Tulun, Nizhneudinsk, Irkutsk, Cheremkhovo, Zima, Angarsk, Ulan-Ude, Chita, Shilka, Nerchinsk and Sretensk. Floods present the highest hazard, although flooding of a mixed genesis is also possible (floods coupled with ice jams or rainfall). Damage to settlements and to agricultural and industrial enterprises in these densely populated and well developed areas can be very large. A *high hazard* is also typical for the northern districts of Irkutsk oblast within the Lena river basin: in the Kachugskii, Kazachinsko-Lenskii, Ust-Kutskii and Kirenskii districts. In spite of a relatively small population size of these districts, most settlements are situated along the river banks and have long been affected by flooding of a different genesis, such as Zhigalovo, Ust-Kut, Kirensk, Alekseevka, and others. Flooding of a different genesis is possible to occur there: ice-jam floods, snow-melt floods, rainfall floods and mixed floods (snow-melt floods coupled with ice jams or rainfall). A high hazard potential of rainfall-induced floods occurs in Mongolia in densely populated areas of the city of Ulaanbaatar and its vicinities in the Töv aimag.

Prospects for water resource mapping in the Baikal region

The cartographic program in the Baikal region is continued with the creation of a new fundamental atlas entitled «The Baikal region: society and nature». The contents of all relevant maps will be distributed in the following three large thematic directions: socio-economic factors for formation of the ecological situation, ecological status and transformation of the environment, and the medical-geographical situation; environmental protection, and rational nature management. It is intended to use a multilevel system of mapping to include maps of Baikal-Mongolian Asia, federal subjects of the Baikal region and

their municipalities, and large-scale maps of local areas influencing the natural environment.

Water resource maps should occupy an important place. But the lags in previous cartographic products must be filled in. In particular, special attention should be paid to the block of water economy maps to focus on the present status and future hydroelectric energy, water supply, water transport and water recreation uses of natural resources. The decision on the boundaries of the water protection zone of Baikal was taken. The theoretical framework for projecting the water protection zone is provided by the landscape-hydrological principles permitting the size and configuration of the water protection zone to be determined in accordance with the spatial differentiation of landscapes having individual hydrological properties. The processes of flow formation and control and natural water accumulation and filtration in vegetation and soil elements of landscapes are responsible for the different flow and purification regimes as the water mass approaches the lake.

The same principles of landscape-hydrological organization of the territory were used as a basis for the recreational zoning of an area on the southwestern coast of Lake Baikal within the boundaries of the Central Ecological Zone of the Baikal Natural Area. The landscape-hydrological map of recreational zoning illustrates a need for territorial restrictions in tourism development of the territory, defining the zones of absolute preservation and regulated use (Fig. 4).

Mapping and modeling of processes in deltaic systems opens up brand new vistas. It is suggested that river mouths be treated as open geosystems, volumetric geological bodies which are end components of global river systems. Special attention is given to the Selenga river delta, the main tributary of Lake Baikal. Cartographic material from different time periods was used to generate morphodynamical models of subaerial surfaces and neighboring aquatic areas which

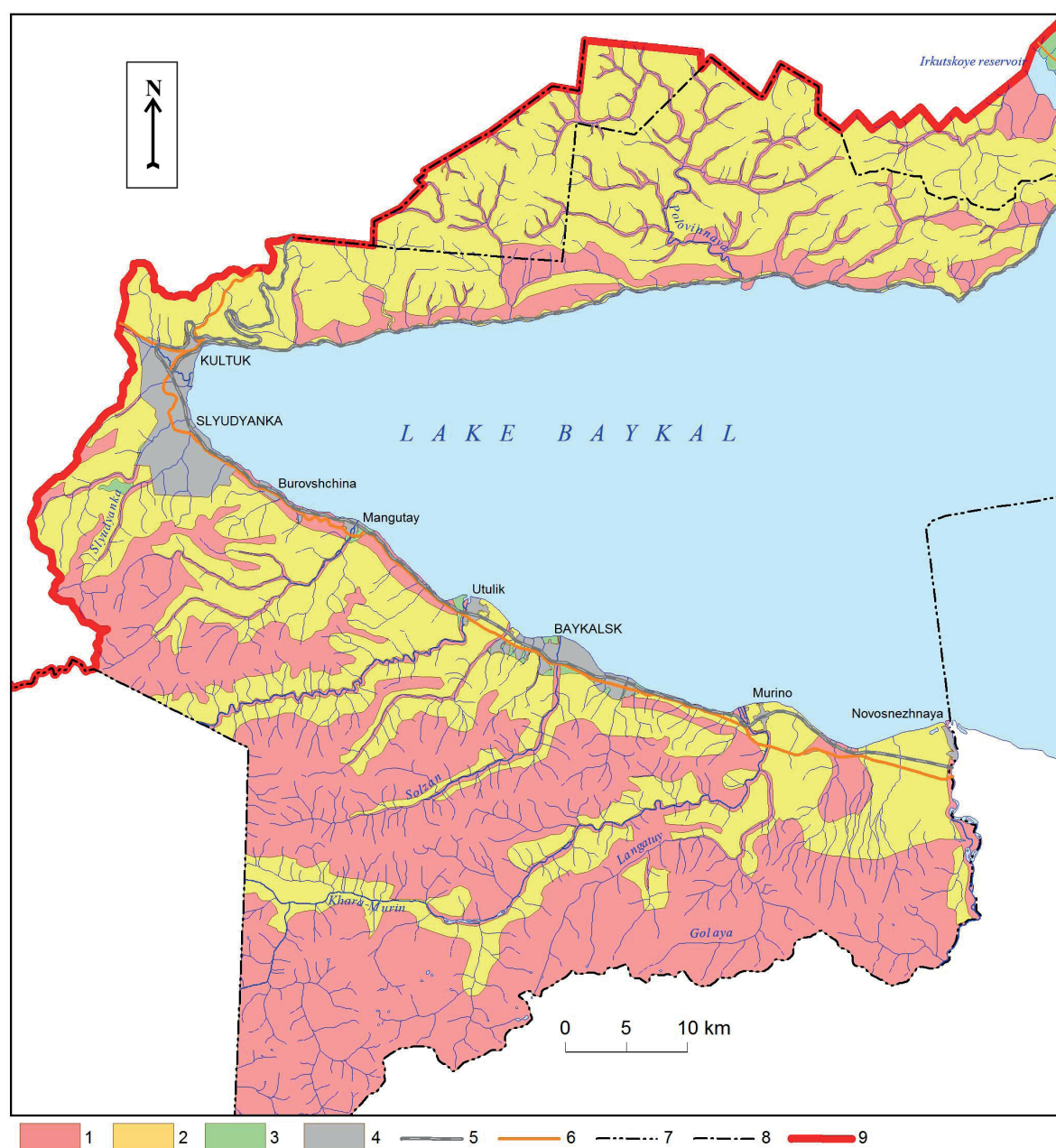


Fig. 4. Landscape-hydrological zoning of a section along Baikal's coast. Zones: 1 – preservation of the present status, 2 – limited development, 3 – development, 4 – settlements; roads; 5 – motor road, 6 – railroad; boundaries: 7 – boundary of the Slyudyanskii district, 8 – boundary of the Irkutskii district, 9 – boundary of the Central Ecological Zone of the Baikal Natural Area

characterize the dynamics of the bank line, the position of channels in plan, and hypsometry of the surface and bottom elevations of the channel network. An important applied aspect of these efforts is represented by schematic maps of natural risks, showing a relative stability of different portions of the river mouth geosystem for land use planning in particular hydroclimatic conditions. Many years of field investigations within the Selenga river delta and the implementation of the historical-cartographic method enabled us to determine zones of the most intense manifestation of erosion and accumulation processes within the main morphological elements of the deltaic plain (Dong et al. 2016, 2019). An objective rationale is given for the zones of relative stability and for the zones undergoing continual changes in the rate and direction of bank erosion. Long-term manifestations of modern tectonic processes are taken into consideration. The maps prepared by this technique were included in the latest (Ecological-geographical atlas-monograph Selenga-Baikal 2018).

CONCLUSIONS

In view of an ever-increasing role of water resources across the globe, it is emphasized that the role of water resource mapping conducted from the geographical perspective must become more prominent in atlas products. A wealth of experience gained from such mapping in the Baikal region might also prove useful in this regard. As our research has shown, the experience of which is summarized in this article, it is important:

- to consider a set of water resource maps as a system of interconnected works, covering all aspects of formation, spatial-temporal distribution and use of water objects and water resources;
- take into account the methodological specifics of creating of different groups of water resource maps in different geographical conditions;
- to recommend for study and application the examples of water resources maps of the Baikal region, including the continuation of atlas mapping. ■

REFERENCES

- Amosova I.Yu. & Ilyicheva E.A. (2018). Structural and hydrographic approach to the determination of extremely high flow. *Izvestiya Bulletin of Irkutsk State University. Series «Earth Sciences»*, 23, 17-27.
- Batuev A.R. & Korytny L.M. (2018). Multilevel atlas environmental cartography (As exemplified by the Baikal region). *Geogr. Nat. Resour.*, 39(4), 296-306.
- Batuev A.R. & Korytny L.M. (Eds.). (2015). *Ecological atlas of the Lake Baikal basin*. Irkutsk: V.S. Institute of Geography SB RAS.
- Bogoyavlenskii B.A. (Ed.). (1989). *Atlas of Lake Hovsgol (Mongolian People's Republic)*. Omsk: GUGK SSSR (in Russian).
- Dong T.Y., Nittrouer J.A., Czapiga M.J., Ma H., Elroy B., Il'icheva E., Pavlov M., Chalov S. and Parker G. (2019). Roles of bank material in setting bankfull hydraulic geometry as Informed by the Selenga River Delta, Russia, *Water Resour. Res.*, 55(1), 827-846.
- Dong T.Y., Nittrouer J.A., Ilicheva E.A., Pavlov M., McElroy B., Czapiga M.J., Ma H. and Parker G. (2016). Controls on gravel termination in seven distributary channels of the Selenga River Delta, Baikal Rift basin, Russia. *Geol. Soc. Am. Bull.*, 128(7), 1297-1312.
- Gagarinova O.V. (2012). Landscape-hydrological regularities of runoff formation within the Lake Baikal watershed basin. *Geogr. Nat. Resour.*, 33(3), 218-222.
- Galazii G.I. (Ed.). (1993). *Baikal. Atlas*. Moscow: Roskartografiya (in Russian).
- Ilyicheva E.A. (2009). Structural patterns of river systems within the Lake Baikal drainage basin. In V.I. Shmykov (Ed.), *Proceedings of the 3rd international conference «Ecological-geographical investigations within river basins»*, 43-48. Voronezh: VGU (in Russian).
- Kasimov N.S. (Ed.). (2019). *Ecological-geographical atlas—monograph «Selenga–Baikal»*. Moscow: Faculty of Geography MSU.
- Kichigina, N.V. (2018). Flood hazard on the rivers of the Baikal region. *Geogr. Nat. Resour.*, 39(2), 120–129.
- Korytny L.M. (2001). *The basin concept in nature management*. Irkutsk: Institute of Geography SB RAS (in Russian).
- Korytny L.M. (2017). The Basin concept: From hydrology to nature management. *Geogr. Nat. Resour.*, 38(2), 111-121.
- Korzun V.I. (Ed.). (1974). *Atlas of the world water balance [Supplemental material]. The world water balance and Earth's water resources*. Leningrad: Gidrometeoizdat (in Russian).
- Kotlyakov V.M. (Ed.). (1997). *Atlas of snow-ice resources of the world (1–2)*. Moscow: Institute of Geography RAS (in Russian).
- Kotlyakov V.M. (Ed.). (1998). *Resources and environment. World atlas (1–2)*. Moscow: Institute of Geography RAS (in Russian).
- Plyusnin V.M. (Ed.). (1917). *Ecological atlas of the Baikal region*. Irkutsk: V.B. Sochava Institute of Geography SB RAS; Matrosov Institute of System Dynamics and Control Theory. [online] Available at: www.atlas.isc.irk.ru [Accessed 20 May 2020].
- Pozdnyak G.V. (Ed.). (2004–2008). *National atlas of Russia (1–4)*. Moscow: Roskartografiya (in Russian).
- Shoigu S.K. (Ed.). (2011). *Atlas of natural and technogenic hazards and risks from emergency situations*. Moscow: Feoriya (in Russian).
- Sochava V.B. (1978). *An introduction to the theory of geosystems*. Novosibirsk: Nauka (in Russian).
- Tikunov V.S. (Ed.). (2009). *Atlas of socio-economic development of Russia*. Moscow: PKO Kartografiya (in Russian).
- Vorobyev V.V., Antipov A.N. & Khabarov V.F. (Eds.). (2004). *Irkutsk region: Ecological conditions of development*. Moscow: Roskartografiya; Irkutsk: Institute of Geography SB RAS, DOI: 10.4236/oalib.1103893.

A HYDRO-INFORMATIC APPROACH FOR ESTIMATION OF DESIGN FLASH-FLOOD IN BARGI DAM CROSS-SECTION OF NARMADA RIVER, INDIA

Gurveek S. Maan¹, Jagadish P. Patra², Ripudaman Singh^{1*}

¹Department of Geography, School of Humanities, Lovely Professional University, Phagwara 144411, Punjab, India

²National Institute of Hydrology, Roorkee 247667, India

*Corresponding author: ripudaman.17178@lpu.co.in

Received: December 31st, 2019 / Accepted: May 10th, 2020 / Published: July 1st, 2020

<https://DOI-10.24057/2071-9388-2019-178>

ABSTRACT. Estimation of design flood is imperative for hydraulic designs of spillways and various other water resources development projects as well as very essential for flood risk assessment. The objective of the present study is to apply Geographical Information System (GIS) supported hydro informatics approach for estimation of design flash-flood in Bargi dam cross-section. A criterion used for estimation of design flash flood is validated by central water commission (CWC). A hydrologic modelling software (HEC-GeoHMS) is used for the delineation of basin characterises for simulation of the precipitation-runoff process of the dendritic basin system. The SUH (Synthetic Unit Hydrograph) and flood hydrographs for 25, 50 and 100 year return periods are computed along with time distribution curve which can be used to derive the time distribution co-efficient of storm rainfall in the sub-basins for the rainstorm of any duration. It is observed in this research that the peak characteristics of the design flash-flood are more perceptive to the various design storm pattern. It is demonstrated that flood hydrographs are important in flood-risk management. The results attained exhibit the capability of the flood hydrograph to describe the effects of different hydraulic systems.

KEYWORDS: Basin delineation, Synthetic Unit Hydrograph, Flood Hydrograph, Design Flood, Time distribution curve, HEC-GeoHMS

CITATION: Gurveek S. Maan, Jagadish P. Patra, Ripudaman Singh (2020). A Hydro-Informatic Approach For Estimation Of Design Flash-Flood In Bargi Dam Cross-Section Of Narmada River, India. Geography, Environment, Sustainability, Vol.13, No 2, p. 104-114

<https://DOI-10.24057/2071-9388-2019-178>

ACKNOWLEDGEMENTS: Major limitation of the present research is that it is based on the data and study conducted in July 2011. Extending its comparison and changes taking place from that point of time to the later periods would be taken in the upcoming researches. Present paper is part of various studies carried out at National Institute of Hydrology (NIH), Roorkee, India. Researchers acknowledge the data provisions for this publication from NIH and are thankful for this collaboration and taking such collaborative researches in future as well.

Conflict of interests: The authors reported no potential conflict of interest.

INTRODUCTION

The study related to the safety of a structure in flash flood event is very crucial and need to be carried out at regular intervals. The hydrograph of extreme floods is valuable information for any hydrologic design. A most important parameter is the peak flood for better assessment of flood-related studies. Design flood studies are used to assess maximum flood that a hydraulic structure can bear. In design flood estimation a prominent concept of return period is used with non-exceedance probability. Giuliano et al., 2009 explained various methods such as empirical method, hydrograph technique, rational method, and flood frequency analysis to compute peak flood. The frequency analysis method is generally incorporated to calculate flood for a specific return period. In the case of inadequacy of primary data, frequency analysis recorded storm data is made and the storm of a particular frequency is applied to unit hydrograph for deriving design flood (Rowe et al. 2018). India is divided into 7 zones and 26 hydro-meteorological homogeneous sub-zones by Indian Meteorological

Department in association with Central Water commission and for each zone-specific flood estimation guidelines are formed for 25, 50 and 100 years return period (CWC 2002). The Bargi Dam on river Narmada is one of a series of 30 dams designed by the Central Water and Power Commission and was developed for creating irrigation and generating hydroelectric power for the country (CWC 2010). The transformation of rainfall into runoff has been a wide research topic and problem for hydrologists. To estimate and compute this difference many method, techniques, formulae has been tried and used with physiographic and climatic characteristics. Bernard's (1935) model was the first step to estimate unit hydrograph from watershed characteristics. Snyder (1938) derived a set of formulas relating to the physical geometry of watershed to three basic parameters of the unit hydrograph. Clark (1945) created a technique to compute the unit hydrograph of any desired unit period. The shape and channel slope create the peak of the instantaneous unit hydrograph (IUH) which is a function of watershed length Taylor and Schwarz (1952). According to Minshall (1960), the unit hydrograph's peak flow and

time are dependent upon storm and rainfall intensity. Then Nash (1957) develops a model that has two parameters (n and k). Nash explained these two parameters as relating to the first and second moment off unit hydrograph about the origin. But these two parameters were calculated from the watershed characteristics. Then Boyd (1978, 1982) developed a linear watershed boundary network (LWBN) to estimate the unit hydrograph from and hydrological properties of the watershed. National Institute of Hydrology (1985) has been done a regional unit hydrograph study for the Narmada basin from the Clark model. For this HEC-1 package was used (HEC-GeoHMS Reference Manual 2010; Parhi et al. 2012). Janusz Zelazinski (1986) gave a method for estimating flow velocity. This relation was between velocity and peak discharge. But this was the trial and error method to estimate the maximum value of velocity for each flood event. Rodriguez-Iturbe (1979, 1982 and 1997) gave the potential application to develop a unit hydrograph. According to him the effect of climatic variation is incorporated by having a dynamic parameter velocity in the formulation of the geomorphological instantaneous unit hydrograph (GIUH). By using manning's equation Panigrahi (1991) developed a system of computing velocity. GIUH approach is developed by Yen et al. (1997) on two hilly catchments in the eastern United States in Illinois. Bhaskar et al. (1997) derived GIUH from watershed geomorphological characteristics with the Nash model using ARC/INFO GIS for twelve watersheds in a big sandy river basin in eastern Kentucky. Which model he used was watershed hydrology simulation (WAHS). Maidment et al. 1996, Jenson and Domingue 1988, Maidment 2002 and Olivera and Maidment 1999 used DEM data to drive GIUH for three mountain basins in Italian Alps. Then Lee K. T. (1998) developed a design hydrograph by DEM with the help of geographic runoff simulation.

Many regional and national agencies apply the concept of Probable Maximum Precipitation or Flood (PMP or PMF) instead of statistical approaches for large dams (WMO 2009). There are four approaches to acquire synthetic design hydrograph (SDH): Synthetic Unit Hydrograph (SUH), Traditional Unit Hydrograph (TUH), Statistical Method (SM) and Typical Hydrograph (TH). In last two methods frequency analysis approach are followed to attain SDH Yue et al. (2002). Sauquet et al. (2008) established a 'representative hydrograph', attained by standardizing the dimensionless hydrographs $Q(t)/Q_p$ middling around the peak position. Mediero et al. 2010; Xiao et al. 2009, examined that it is very imperative to evaluate the shape of flood hydrograph and flood volume to prevent flood damage and designing hydraulic structures. Rosbjerg et al. 2013 also determined the magnitude of flood peak resultant to a specific return period during flood estimation. Design flood hydrograph plays a very vital contribution to calibrate physical properties of a flood occurrence for any particular return period and to obtain the event rarity through statistical information (Serinaldi and Grimaldi 2011). Parkes and Demeritt 2016; Nakamura and Oki, 2018 have shown estimation of design flood below definite return period is of major concern for flood studies, such as developing flood management and mitigation scheme, designing hydraulic structure. Probabilistic and deterministic methods are two approaches which is primarily used for design flood estimation (Smithers 2012; Rogger et al. 2012). Probabilistic approach considers the occurrence of flood events and on other side deterministic approach is based on rainfall data and some basin processes. The calibration of design is a very time taking process in geomorphic parameter measurement on topographic maps. This study is performed for peak flow analysis in an un-gauged watershed. The design storm is

applied to the geomorphic runoff simulation model to obtain the design hydrograph (NIH 1997, 1998). In the science of hydrology, the time of 1900–1930 was empirical. The intensity of rainfall can be obtained from Rainfall-Intensity – Duration-Frequency curves, if the information is available. Current criteria for design flood estimation are given by the Central Water Commission (CWC) and Bureau of Indian Standard (BIS). The method of design flood was headed by Dr. A. K. Khosla with a team of engineers. And they had recommended that design discharge should be a maximum flood on record for a period not less than 50 years. They also suggested that in the case where data is not available in that situation design floods should be decided on the bases of hydro meteorological data.

Using this formula CWC and IMD have published flood estimation report for 26 subzones of India like Lower Ganga Subzone 1(g), upper Narmada and Tapi subzone 3(c) which is indicated in figure 1. This study is conducted to estimate design flood at the Bargi dam cross-section with these objectives: (a) Delineation of basins up to Bargi dam and estimation of catchment characteristics (b) Estimation of synthetic unit hydrographs for different delineated sub-basins and (c) Estimation of flood hydrographs for various return periods (25, 50, 100 years) at the Bargi dam cross-section.

DATA AND METHODOLOGY

Study Area and Data Availability

The Narmada, also known as Rewa is one of the largest rivers in India. It bifurcates North India and South India as flowing westward by covering 1,312 km and drains into Gulf of Cambay (Khambhat) into the Arabian Sea. The Narmada basin lies between Vindya and Satpura ranges by covering an area of 98,796 km² lying on the northern extremity of the Deccan Plateau. The Bargi dam on river Narmada is of 69 m height and 5.4 km length. The water spreading is of the reservoir is over 267.97 km² with about 75 km in length and 4.5 km width. The basin area is around 14,556 km². In Basin Atlas, CWC 2014, the Narmada Basin is divided into 3 Sub-basins viz. Narmada Upper, Narmada Middle and Narmada Lower Sub-basin which are shown in figure 2. Basin area up to Bargi Dam in Narmada Upper Sub-basin is considered as a study area for computation of various basin characteristics.

SRTM 90 m resolution DEM which is developed by NASA is considered in this study to capture the morphological characteristics of drainage basin. Accuracy at 90 m resolution is detailed enough to capture drainage basin characteristics. The more specific aim of this paper is to estimate design flash-flood, for which only SRTM DEM data are currently available. The spatial resolution of SRTM DEM is analysed and validated by Smith and Sandwell, 2003. The SRTM 90 m (3-arc seconds) was downloaded from <http://www.cgiar-csi.org/> on July, 2010. Average rainfall is collected from the Indian Meteorological Department (IMD) for rainfall level analysis for three rain gauge stations covering proposed plant area. The topographical survey was carried out in the proposed plant field, and cross-section of drains was also calculated. The bathymetry is built from surveyed contours, SRTM DEM and spot height of Survey of India (SOI) toposheet.

METHODOLOGY

This research computes design flash flood to estimate flood hydrograph of at project site in Narmada River using HEC HMS model. The synthetic unit hydrographs are derived from basin characteristics of the study area and flood hydrographs for 25, 50 and 100 year return periods

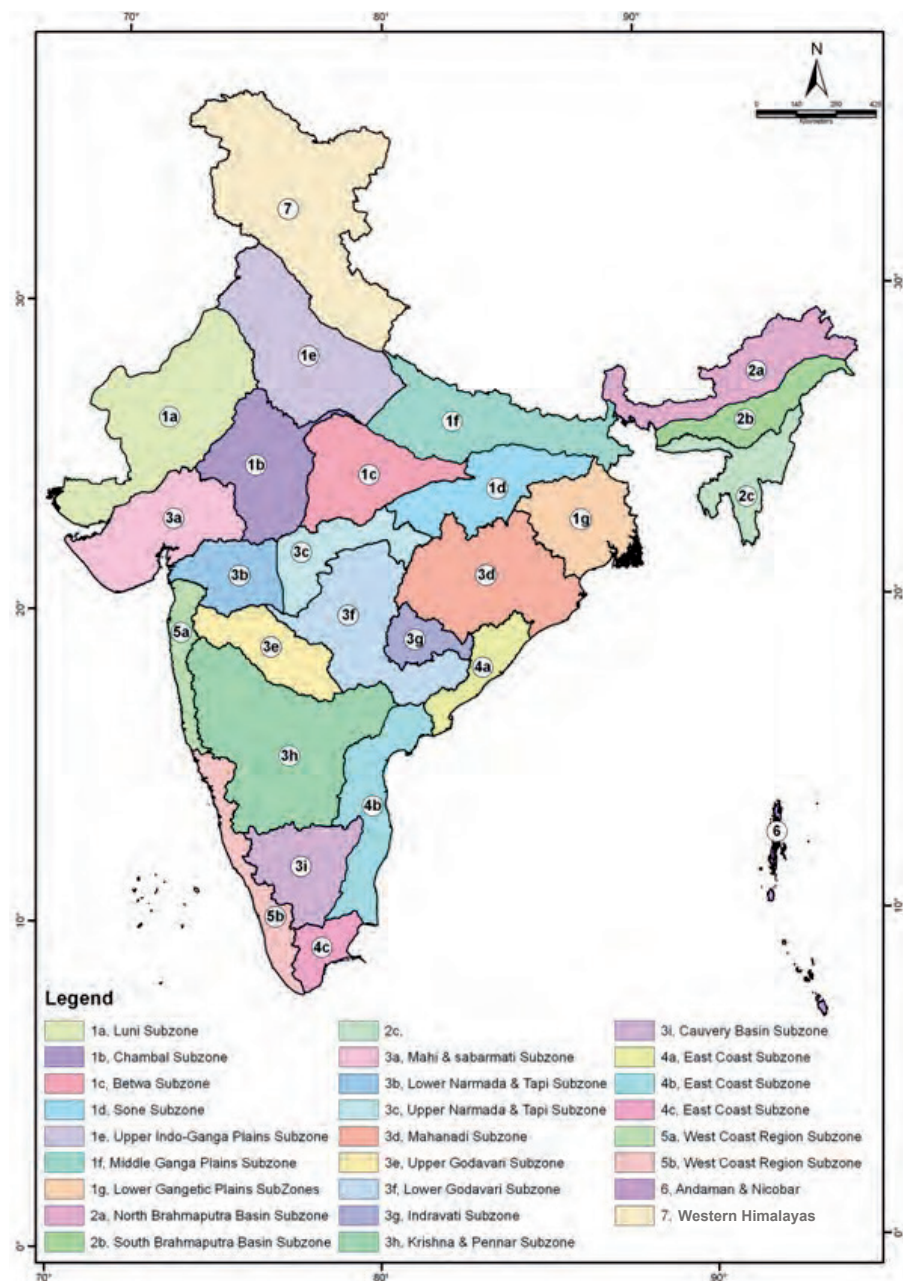


Fig. 1. Hydrological Zone Map of India
Source: CWC (Central Water Commission)

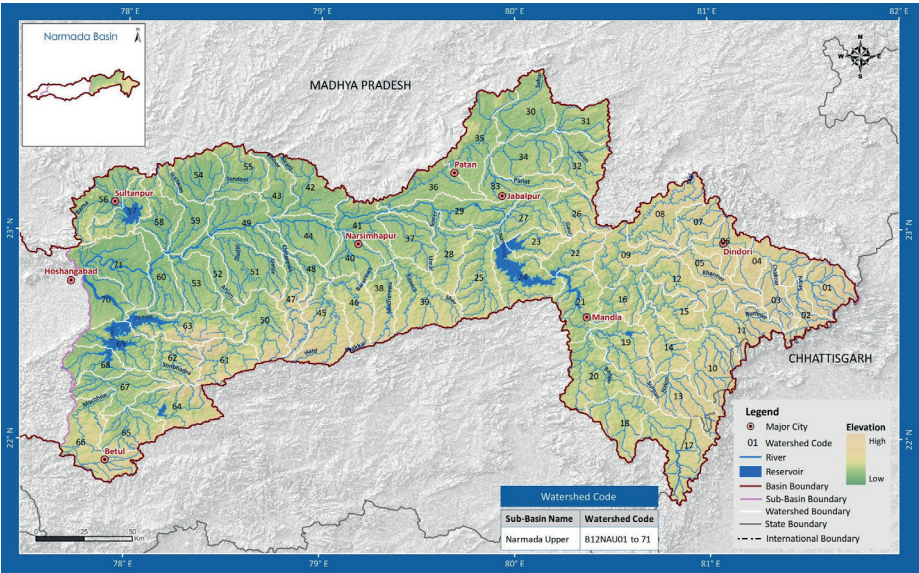


Fig. 2. Upper Narmada Sub-Basin (Sub-Zone 3c)
Source: CWC (Central Water Commission)

are computed for Bargi dam situated on Narmada River. The basin area up to the Bargi dam is divided into five sub-basin and synthetic unit hydrographs for each sub-basins are derived from the basin characteristics estimated using Arc GIS and Arc Hydro tools. A hydrologic model is setup in HEC-HMS for estimating flood hydrographs at outlet of each sub-basin and finally at the project site by hydrologic flood routing through the two reaches.

Basin Delineation

HEC-Geo HMS software is used for the delineating basin area of the Bargi dam from the SRTM DEM. There MSS image is used to identify land use and land cover pattern. The DEM is projected to the UTM projection system in ArcGIS before processing with HEC-Geo HMS (HEC-GeoHMS Reference Manual 2010; Parhi et al. 2012). A basin is all the land area that topographically drains surface water to a particular point of interest (outlet), often a water body such as a stream, lake or reservoir.

Project Setup

After terrain processing, layers of drainage network and polygon layers of all small basins are obtained. In this step outlet of the basin is defined and HEC-Geo HMS automatically copies all the terrain preprocessing data for the area upstream of the outlet location (HEC-GeoHMS Reference Manual 2010; Parhi et al. 2012). Thereafter using basin processing tools, sub-basin and stream networks can be subdivided and merge to meet the study objectives. In this study the Bargi dam site is selected as the outlet and the corresponding project area is delineated for further basin processing. The DEMs (digital elevation models) of the study areas were processed using HEC-GeoHMS, an ArcView GIS extension for catchment delineation, terrain pre-processing, and basin processing. The research methodology is explained in fig. 3.

Basin Processing

After completion of terrain processing and project set up the projected area with projected points are established. In this step polygon layer for multi basins and drainage network layer are generated. The different tools allow visualizing delineation results, assessing outcomes, and accepting or denying the resulting delineation. In basin processing, different sub-basins are merged and divided into a total of 5 sub-basins each having an area less than 5000 km².

Stream and Sub-basin Characteristics

After finalizing stream and sub-basin delineation, various physical characteristics can be extracted. Fig. 3 shows the flow chart of various steps involved in this process. First, the river length for selected or all routing reaches in the river layer are computed and then the river slope is calculated. From the river slope, elevation and slope of the river are calculated for downstream and upstream. After getting river length and slope, the longest flow path is calculated for each basin. It is one of the physiographic parameters to draw a unit hydrograph. It computes the longest flow length in every sub-basin, upstream elevation, downstream elevation, and slope between the endpoints. Then, the average basin slope is computed for all the five basins. It took average basin slope value from a slope grid. It is also a necessary parameter to draw a unit hydrograph. Basin centroid is computed because based on its interactive longest flow path are further considered. For calculation of centroid normally four methods are recommended. Three methods may be estimated basin centroid based on different algorithms and the fourth method is user-defined. In this research, the first method (center of gravity method) is used to extract basin centroid. Based on basin centroid, centroid elevation is calculated. And After this process, the last physiographic parameter, the centroidal flow path is

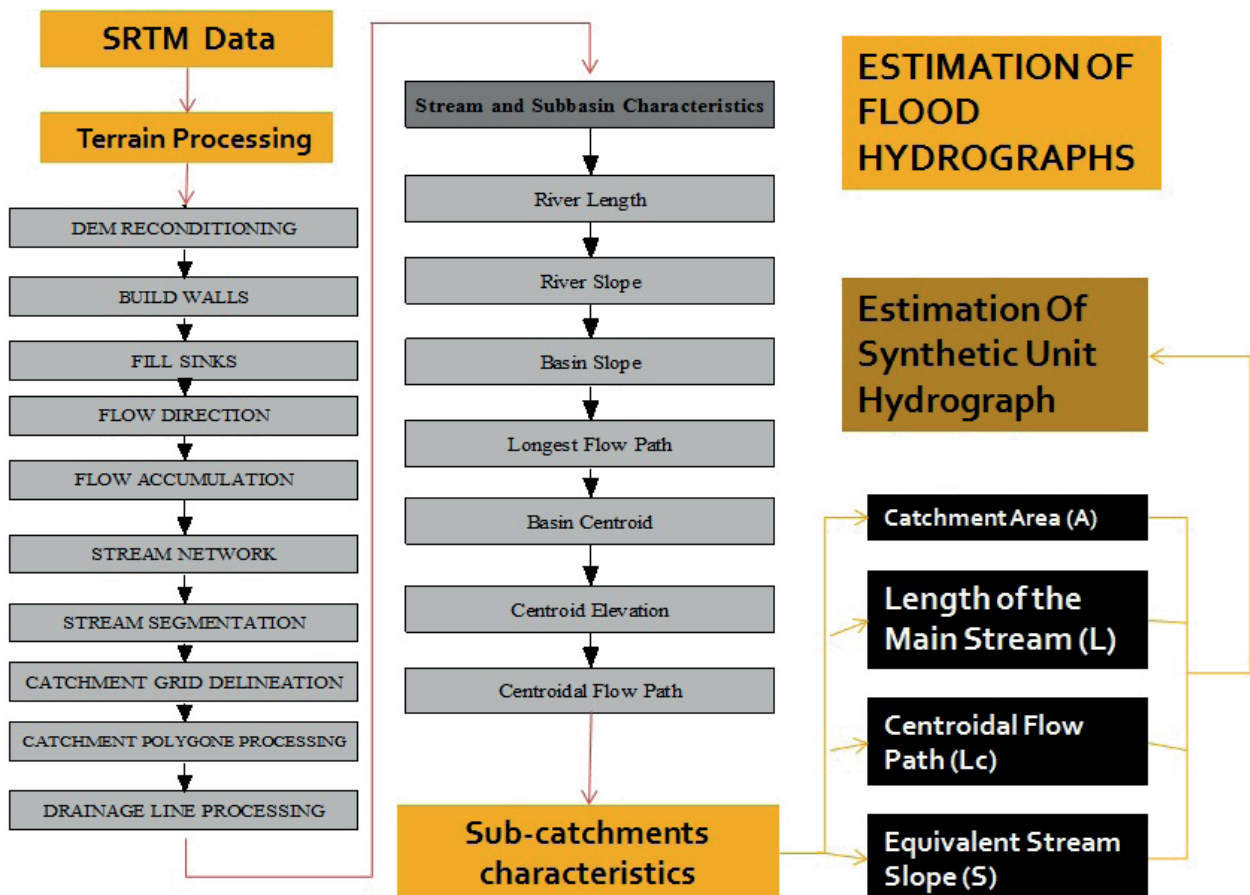


Fig. 3. Flow chart of the methodology

computed. The centroidal flow path tells us the aspect of the flow path from basin Centroid to outlet for a basin. For this process, the values of the longest flow path, basin Centroid, and sub-basin layer are used because this parameter gives a hydrological significance to estimate design flood and storm flood.

Estimation of Synthetic Unit Hydrograph

SUH is the unit hydrograph of unit duration for a basin developed from relation established between physiographic and unit hydrograph parameters of the representative gauged basins in a hydrometeorological homogeneous region (subzones). In this approach, the design storm after converting it into effective rainfall (input) is applied to the unit hydrograph (transfer function) to obtain a design flood (basin response). It is possible to develop unit hydrograph if site-specific concurrent rainfall-runoff data is available for 5-8 years or few selected severe storm events. The collection of adequate concurrent rainfall-runoff data for every site is, however, neither practicable nor economically feasible. In such a situation, the regional method for developing SUH is advisable. Hence, in this case, the SUH is developed using procedures described in the CWC report (2002) for subzone-3(c).

Physiographic Parameters

The physiographic parameter considered in the present study is basin area (A), length of the mainstream (L), length of the mainstream from a point nearest to the center of gravity of the basin area to the observation site (L_c) and the equivalent stream slope (S). The parameters for each sub-basin are extracted from the HEC-Geo HMS (HEC-GeoHMS Reference Manual 2010; Parhi et al. 2012). The upstream and downstream elevation and slope are added to the river layer's attribute table with the column headings: «ElevUP», «ElevDS», and «Slp».

Derivation of One Hour Unit Hydrograph

The following parameters of SUH are estimated from the derived physiographic parameters (NIH 1997):

1. Time from the center of unit excess rainfall to the peak of unit hydrograph in hours (T_p)

$$T_p = 0.995 \left(\frac{LLc}{\sqrt{S}} \right)^{0.2654}$$

2. Peak discharge of unit hydrograph in cubic meters per second (Q_p). This is the product of peak discharge per sq.km (qp) and basin area (A)

$$Q_p = qp * A$$

3. The base width of unit hydrograph in hours (T_b)

$$T_b = 5.04537(tp)^{0.71637}$$

4. Width of unit hydrograph measured at discharge ordinates equal to 50% of Q_p in hours (W_{50}).

$$W_{50} = 1.9145(qp)^{-1.2582}$$

5. Width of unit hydrograph measured at discharged ordinates equal to 75% of Q_p (W_{75}).

$$W_{75} = 1.1102(qp)^{-1.2088}$$

6. Width of the rising site of unit hydrograph measured in hours at discharge ordinates equal to 50% of Q_p (WR_{50})

$$WR_{50} = 0.7060(qp)^{-1.3859}$$

7. Width of the rising site of unit hydrograph measured in hours at discharge ordinates equal to 75% of Q_p (WR_{75}).

$$WR_{75} = 0.45314(qp)^{-1.3916}$$

8. Time from the start of the rise to the peak of the unit hydrograph (T_m). This is the summation of T_p and $0.5 * T_r$ where T_r is the unit duration of unit hydrograph

$$T_m = tp + \frac{tr}{2}$$

9. Peak discharge of unit hydrograph per unit area in cumec per sq.km

$$qp = 1.665(tp)^{-0.71678}$$

1-hour UH is plotted using the estimated parameters (T_m , T_b , Q_p , W_{50} , w_{75} , WR_{50} and WR_{75}). While plotting the unit hydrograph the sum of discharge ordinates of 1-hr is obtained and compared with the theoretical value found by using the following general equations:

$$\sum Q_i = \frac{[2.78 * A]}{tr}$$

Where, Q_i = Discharge ordinates at 1-Hour interval (cumec), A = basin area in sq.km and tr = unit duration in hours. Suitable adjustment is made in the falling limb region from W_{50} point to the tail of the UH and a smooth curve is drawn to make the volume equal to the volume of the UH.

Estimation of Flood Hydrographs

The flood hydrographs for various return periods (25, 50, 100 years) were estimated for rainfall for corresponding return periods as provided in the CWC (2002) report. Other input parameters required for deriving flood hydrograph are discussed below. Design Loss Rate- Conversion of gross storm rainfall units into effective rainfall units for application to unit hydrograph is normally done by subtraction of constant rate for the basin, even though the loss rate in the basins is complex phenomena, varying due to soil conditions, soil cover and topology along with temporal and spatial variations of storm rainfall. There can be a wide variation in the loss rate. Because the estimation of basin rainfall depends upon the location of the rain gauge stations, which also affects the estimation of the areal rainfall depth for runoff observed at the outlet of the basins. So design loss rate of 0.10 cm/hr for subzone-3(c) is used in this study. CWC (2002) has analyzed a total of 172 flood events for estimating base flow. The recommended value of the base flow of 0.05 cumec per sq. km for subzone-3(c) is used in this study. Design Storm Duration-The duration of storm rainfall which causes maximum discharge in a drainage basin is called design storm duration. The design storm (T_d) is estimated as $T_d = 1.1 \times t_p$. Where t_p is basin lag time.

Time Distribution Curves

These curves can be used to derive the time distribution co-efficient of storm rainfall in the subzone for the rainstorm of any duration. The applied method was validated by CWC in its 2002 report.

Conversion of Point to Areal Rainfall

The areal reduction factors (ARF) are factors which when applied to point rainfall values for a specified duration and return period give areal rainfall for the same duration and return period. The areal to point rainfall ratios versus basin area for design storm duration of different periods was validated by CWC in its 2002 report. The areal to point rainfall ratio is also called Areal Reduction Factor (ARF).

RESULT AND DISCUSSION

HEC-HMS Model Application

Hydrologic modeling software has been developed for simulation of the precipitation-runoff process of the

dendritic basin system. By using its components like basin model manager and meteorological model manager a hydrologic response is computed. By using its model manager component the element of the basin is settled including sub-basin, reach and junction. A model component gives the environment to set up the main feature of a basin. Background map for basin is taken as a shapefile, output of the HEC-Geo HMS project (HEC-GeoHMS Reference Manual 2010; Parhi et al. 2012). The sub-basin element is used to show physical basin. The outflow is computed by using precipitation, loss rate, and base flow. Five sub-basins are created. And four junctions are settled at the junction point of the river network for five sub-basins. After setting up the model component, meteorological data is filled. By using synthetic unit hydrograph ordinates and storm rainfall values flood hydrograph for 100, 50 and 25 years are computed in HEC-HMS by setting all the data in HEC-Geo HMS components (HEC-GeoHMS Reference Manual 2010; Parhi et al. 2012).

In meteorological models specified hyetograph method is selected for all five basins. Flood hydrograph is derived for the one-hour interval for dated 25 January 2010 to 26 January 2010. For rainfall data, precipitation gages method is adopted for five basins. All the values of storm rainfall in gages one to five are given in the table.

Basins Delineation and Characteristics

By using HEC-GeoHMS model a total 57 sub-basins from the DEM are delineated. After terrain processing, the sub-basins are merged and subdivide to 5 major basins as shown in fig. 5. The total area of the basin is found to be 15032.73 sq km. The basins characteristics required for deriving SUH are given in table 1.

Synthetic Unit Hydrographs

Using the relationships derived in CWC (2002) report the SUH parameters are estimated from basin characteristics. These parameters are given in Tables 2 and 3. The 1 hour-UH

(unit hydrograph) for all five basins are also plotted using these parameters (Fig. 6).

Estimation of design rainfall

After the estimation of the synthetic unit hydrograph, flood hydrographs are computed for the various return periods. At the beginning of depth duration frequency analysis, design storm duration is computed using $T_d = 1.1 \times t_p$ for all five basins for 25, 50, and 100 years given in table 2. The values of the design storm are taken rounded off to the nearest full hour. After this Point rainfall is estimated from isopluvials maps for 25, 50, 100 years by using the arithmetic mean method is given in the CWC (2002) report. A conversion factor is read from CWC (2002) report for all the basins to get 25, 50, 100-year point rainfall for various storm duration (T_d). Now 25, 50, 100-year point rainfall, thus worked out to be (conversion factor \times point rainfall) for all five basins given in table 2. The next step is carried towards the areal reduction factor. The areal reduction factor is read from the CWC (2002) report corresponding to the area of all five basins given in table 2. After getting the areal reduction factor point rainfall is converted into areal rainfall. Now storm duration of 25, 50, 100 years, areal rainfall works out to be (areal reduction factor from each basin point rainfall of basin) values are given in table 3. Further storm duration of 25, 50, 100-year areal rainfall has been split into a 1-hour rainfall increment given in table 3 using the time distribution coefficient read from in CWC (2002) report. The design loss rate of 0.10 cm/hr is used to get effective hourly rainfall.

Time Distribution Curve

Using the relationship is given in CWC (2002) report time distribution curve is derived for 25, 50 and 100 years for all five basins. The blue line depicts the relationship between storm rainfall and storm duration for 50 years. As it is red line gives the same relation for 25 years. And a yellow line shows the 100-year relationship in storm hydrograph between storm rainfall and storm duration. The relationship of storm duration (T_d) and storm rainfall is given in the table.

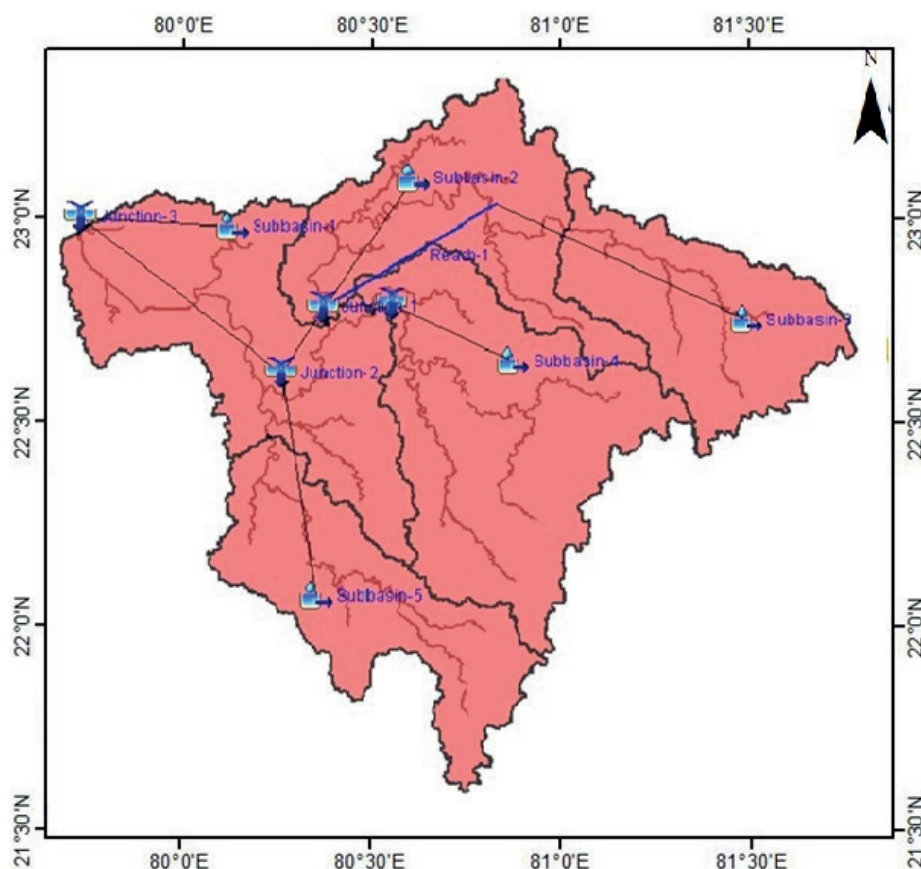


Fig. 4. HEC-GeoHMS Basin Model setup

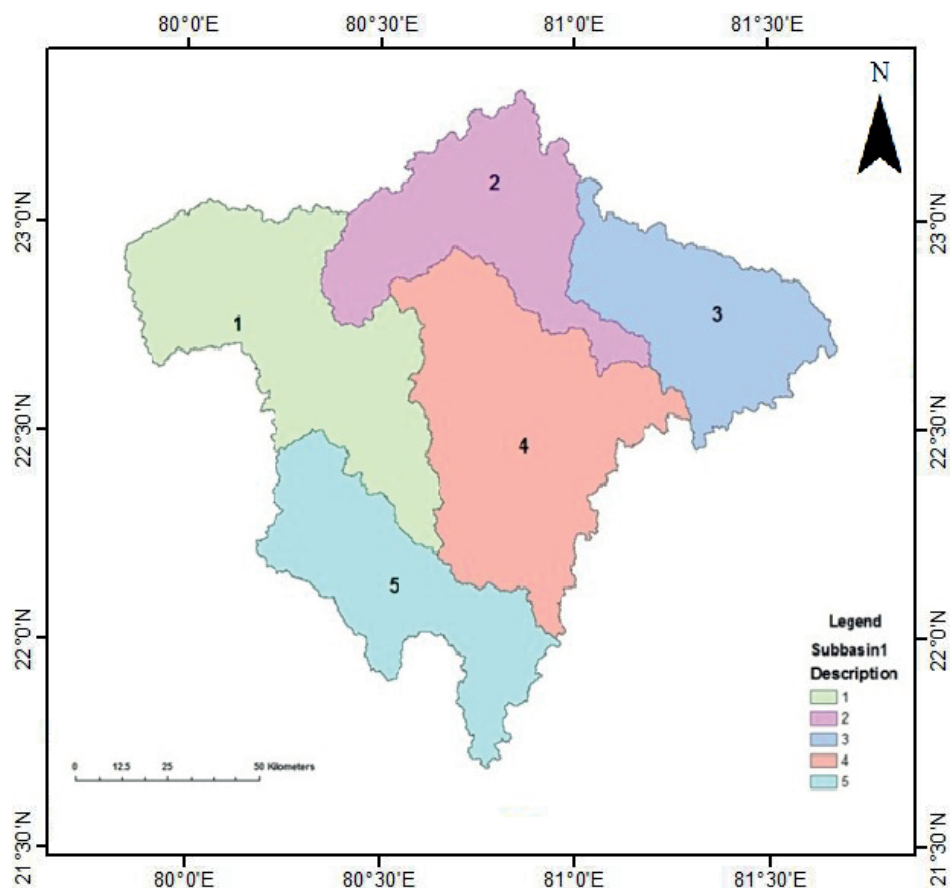


Fig. 5. Five major sub-basins

Table 1. Sub-Basins characteristics

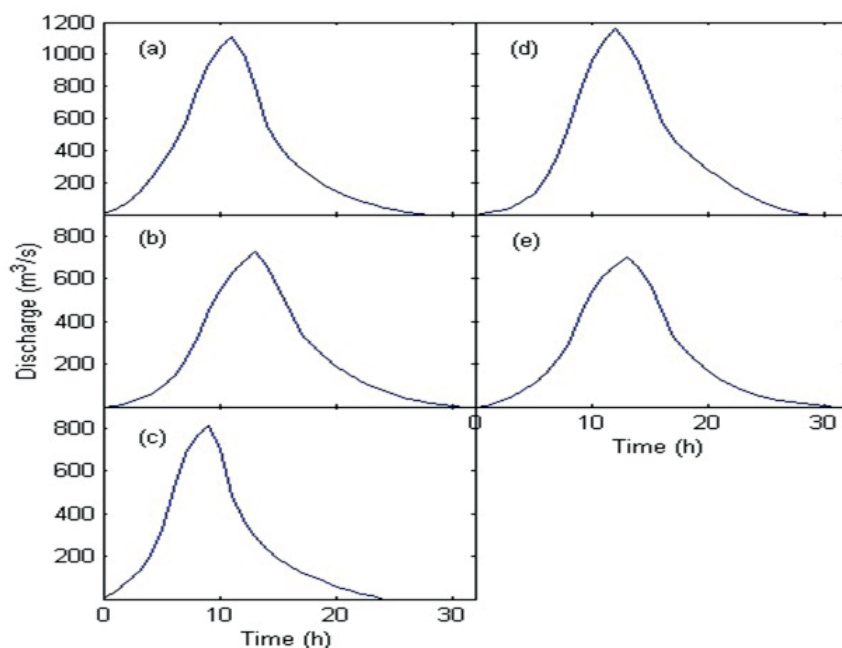
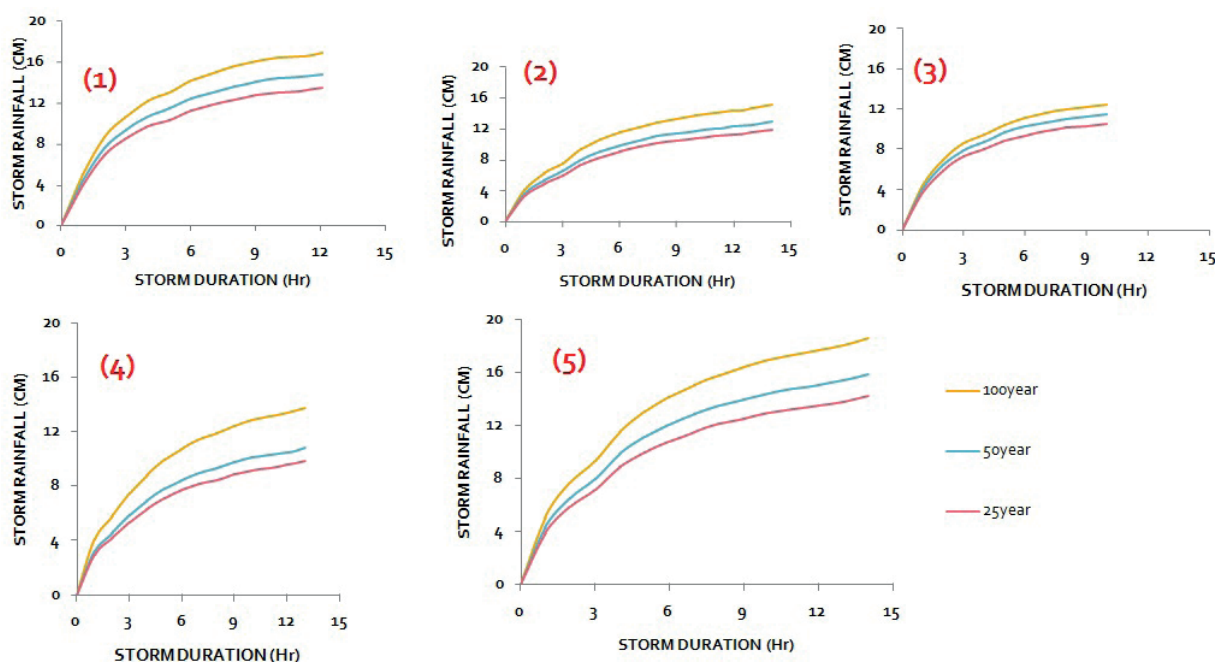
Sub basin No.	Basin Area (A) (km ²)	Length (L) (km)	Centroidal Longest Flow Path (Lc) (km)	Equivalent Slope (S) (m/km)
1	3,596.30	170.72	66.86	2.53
2	2,612.27	206.88	97.65	2.59
3	2,311.98	111.00	55.47	2.77
4	3,978.36	173.33	88.83	2.59
5	2,533.82	172.60	91.52	1.47

Table 2. Parameters of unit hydrograph

Parameters	Basin No.				
	1	2	3	4	5
Time from the center of unit excess rainfall to the peak of unit hydrograph in hours (Tp)	10.5	12.5	8.5	11.5	12.5
Base width of unit hydrograph in hours (Tb)	27.19	30.24	23.97	28.71	30.45
Peak discharge of unit hydrographs (Qp) (m ³ /s)	1,110	724.89	809.42	1,162.5	698.16
Width of unit hydrograph measured at discharge ordinates equal to 50% of Qp in hours (W50)	8.4	9.6	7.17	9.001	9.69
Width of unit hydrograph measured at discharge ordinates equal to 75% of Qp in hours (W75)	4.59	5.22	3.94	4.91	5.27
Width of the rising site of unit hydrograph measured in hours at discharge ordinates equal to 75% of Qp (WR75)	2.32	2.69	1.95	2.51	2.72
Width of the rising site of unit hydrograph measured in hours at discharge ordinates equal to 50% of Qp (WR50)	3.6	4.17	3.02	3.88	4.21
Peak discharge of unit hydrograph per unit area of basin (qp) (m ³ /s/km ²)	0.3	0.27	0.35	0.29	0.27
Time from the start of the rise to the peak of the unit hydrograph (Tm)	11	13	9	12	13
Discharge ordinates at 1-Hour interval (Qi) (cumec)	9,990.5	7,256.9	6,422.7	11,052	7,039

Table 3. Storm Hydrograph parameters for five basins for 100, 50, 25-year storm rainfall

Return period for	100 year					50 year					25 year				
C. No.	1	2	3	4	5	1	2	3	4	5	1	2	3	4	5
Storm duration (Td)	12	14	10	13	14	12	14	10	13	14	12	14	10	13	14
Conversion factor	0.79	0.84	0.76	0.82	0.84	0.79	0.84	0.76	0.82	0.84	0.79	0.84	0.76	0.82	0.84
Mean rainfall	25.33	22	22	20	26	28	24	24	22	29	32	28	26	28	34
Point rainfall	20.01	18.48	16.72	16.4	21.84	22.12	20.16	18.24	18.04	24.36	25.28	23.52	19.76	22.96	28.56
Areal reduction factor	0.67	0.64	0.63	0.60	0.65	0.67	0.64	0.63	0.60	0.65	0.67	0.64	0.63	0.60	0.65
1Hour rainfall	13.41	11.82	10.53	9.84	14.19	14.82	12.90	11.49	10.82	15.83	16.94	15.05	12.44	13.77	18.56

**Fig. 6. Estimated SUH for five sub-basins****Fig. 7. Time distribution curve for five basins for 25, 50 and 100 years**

Flood Hydrographs

After computing the simulation process the result is gathered at junction three. The results of the simulation also present the individual result of sub-basins, junctions and reach also. Subbasin-1 gives peak discharge at 14160.6

cumec at 12:00. Subbasin-2 contributes peak discharge at 7526.6 cumec at 14:00. Subbasin-3 is giving 7,564.5 cumec peak discharge at 10:00. At Subbasin-4 peak, discharge is 11024.2 cumec at 14:00 and at subbasin-5 it is 9288.1 cumec at 15:00.

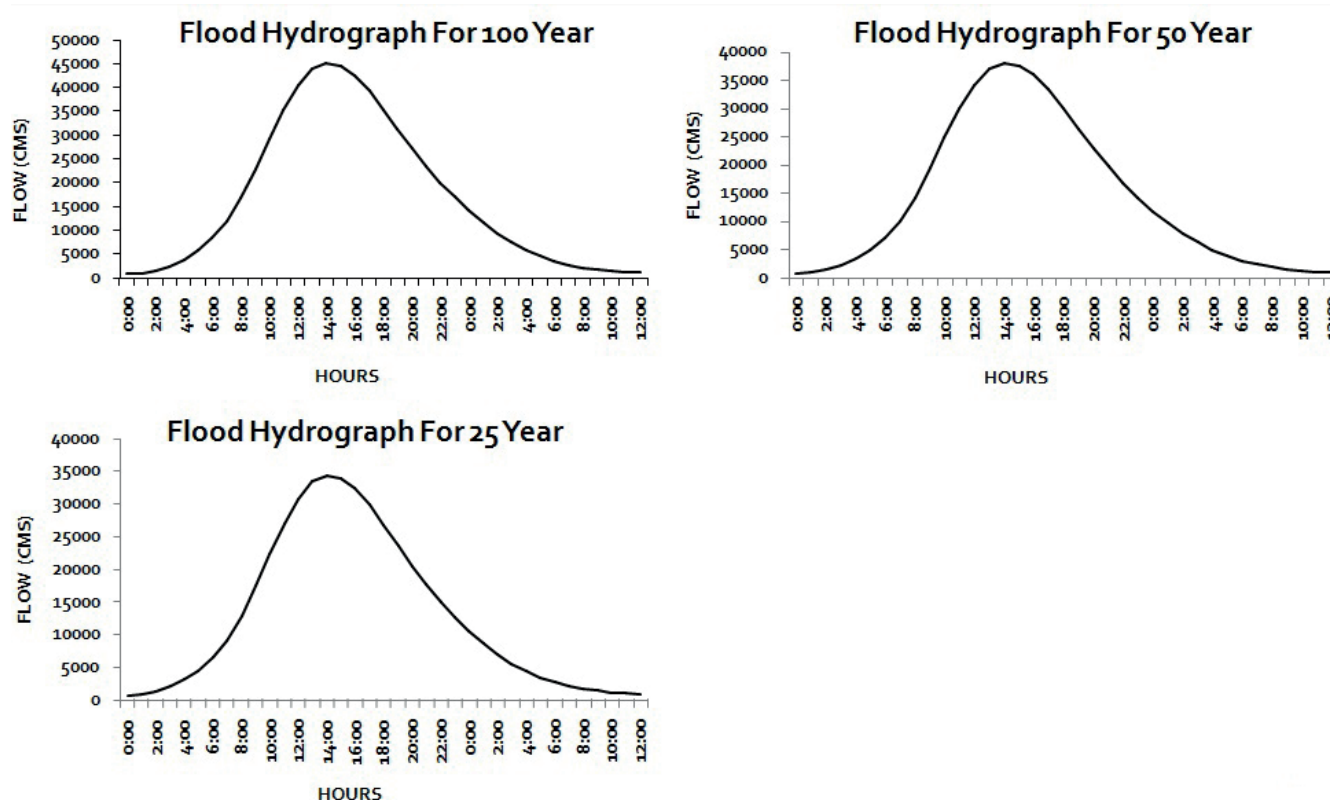


Fig. 8. Flood Hydrographs for 25, 50 and 100 years

Flood hydrograph for 100 years

The result at junction three depicts the peak outflow is 45004.7 cumec and the total outflow is 147.24 (mm). The peak outflow is computed on dated 25 January 2010 at time 14:00. In fig. 7 flood hydrograph depicts outflow at junction-3 which has the contribution of junction-2 and subbasin-1. At Junction-1, 2, 3, 4 peak flow is 24,515.3; 33,803.4; 45,004.7; 11,024.2 cumec respectively. The rising limb of the 100-year flood hydrograph at starting hour 00:00 to 07:00 hour shows the normal flow of the river (Fig. 8). After 07:00 hours outflow is increasing and outflow is above 10,000 cumec. At 14:00 hours outflow reaches peak discharge 45,004.7 cumec. Recession limb starts after 14:00 hours and it is continuously decreasing up to 04:00 hours shown in the table. After 04:00 hour to 12:00 hour, it is rapidly decreased.

Flood hydrograph for 50 years

The result of the flood hydrograph of 50 years gives the peak outflow 38012.2 cumec at 14:00 hours and the total outflow is 124.59 mm at junction-3. Starting 3 hours of rising limb shows the general flow of the river and from 04:00 to 14:00 hours it depicts the rising side of discharge. The peak discharge is 38,012.2 cumec at 14:00 hours. After 14:00 hours decreasing limb starts and it goes up to 04:00 hours with a great recession rate and then 04:00 to 12:00 hours it decreases with average rate. These time-series data are shown in table 3.

Flood hydrograph for 25 years

Junction-3 is the main outlet of all discharges. So at junction-3 peak discharge is 34,326 cumec. Discharge from

subbasin-1 is 11,109.5 cumec and at a junction, it is 25,625.9 cumec. Discharge from these two elements reaches junction-3. And discharge from subbasin-2, 3, 4 and 5 is 5,840.6; 6,355.7; 7,722.8; 7,016.2 cumec respectively. Flood hydrograph of 25 years has a peak value of 34326 cumec at 14:00 hours. And the total outflow is 112.54 mm. Starting the first hour has a normal discharge value of 944.4 cumec from 02:00 hour to 14:00 hour rising limb is increasing with rapid speed. And 14:00 hour to 07:00 hour recession limb have also the rapid rate of discharge but from 06:00 to 12:00 discharge rate is normal.

CONCLUSIONS

This study utilized a hydro informative approach to analyze design flash flood for better understanding of flood control to provide safety for a proposed project site and mitigating flood hazard. The flood hydrograph for various periods were analyzed in an ungauged basin, and the simulation results were satisfactory. The Geospatial analysis techniques which are used in combination of HEC-HMS and HEC-GeoHMS are practical for obtaining basin topographic parameters as well as it makes hydrological forecast more reliable and demonstrated high simulation accuracy in the basin. The flood volume and timing along with peak discharge predicted fairly accurate. It is observed that the application of HEC-HMS should be expectant to corroborate its suitability for the Indian basins. ■

REFERENCES

- Bernard M. (1935). An approach to determinate stream flow. *Transactions of the American Society of Civil Engineers*, 100, 347-362.
- Bhaskar N.R., Parida B.P. and Nayak A.K. (1997). Flood estimation for ungauged catchments using the GIUH. *Journal of Water Resources Planning and Management*, 123 (4), 228-238, DOI: 10.1061/(ASCE)0733-9496(1997)123:4(228).
- Boyd M.J. (1979). A storage-routing model relating drainage basin hydrology and geomorphology. *Hydrological Sciences Bulletin*, 24, 43-69.
- Boyd M.J., Pilgrim D.H. and Cordery I. (1979). A storage routing model based on catchment geomorphology. *Journal of Hydrology*, 42 (3-4), 209-330.
- Central Water Commission (CWC). (2002). Flood Estimation Report for Upper Narmada and Tapi subzone-3(c) (revised), 5-28.
- Central Water Commission (CWC). (2010). Development of Hydrological Design Aids project (Surface Water) under HP-II. [online]. Available at: www.cwc.nic.in/Training_Workshop_in_CWC/Hydrology_Workshop_Feb%206-7,06.pdf [Accessed 24 October 2011].
- Clark C.O. (1945). Storage and unit hydrograph. *Transactions of the American Society of Civil Engineers*, 110, 1419-1446.
- Giuliano D.B., Francesco L.B. and Alberto M.C. (2009). Design flood estimation using model selection criteria, *Physics and Chemistry of the Earth*, 34, 10-12.
- Janusz Zelazinski (1986). Application of the geomorphological instantaneous unit hydrograph theory to the development of forecasting model in Poland, *Hydrological Science Journal*, 31, 2, 6/1986.
- Jenson S.K. and Domingue J.O. (1988). Extracting topographic structure from digital elevation data for geographic information system analysis. *Photogrammetric Engineering and Remote Sensing*, 54(11), 1593-1600.
- Jenson S.K. (1985). Automated derivation of hydrologic basin characteristics from digital elevation model data. In: *Proceedings of the digital representations of spatial knowledge (Auto-Carto 7)*, 11-14 March, Washington, DC. Falls Church, VA: American Society for Photogrammetry and American Congress on Surveying and Mapping, 301-310.
- Maidment D. (2002). *ArchHydro-GIS for water resources*. Redlands, CA: ESRI Press, 220.
- Maidment D.R., et al. (1996). Unit hydrograph derived from a spatially distributed velocity field. *Hydrological Processes*, 10, 831-844, DOI: 10.1002/(SICI)1099-1085(199606)10:6<AID-HYP374>3.0.CO;2-N.
- Minshall N.E. (1960). Predicting storm runoff on small experimental watersheds. *J. Hydraul. Div. Am. Soc. Civ. Eng.*, 86 (HY 8), 17-38.
- Mediero L., Jiménez-Alvarez A. and Garrote L. (2010). Design flood hydrographs from the relationship between flood peak and volume, *Hydrol. Earth Syst. Sci.*, 14, 2495-2505.
- Nash J.E. (1957). The form of the instantaneous unit hydrograph. *Hydrological Sciences Bulletin*, 3, 114-121.
- National Institute of Hydrology (NIH). (1997). Rainfall-runoff modelling of morel catchment for design flood estimation. [online]. Available at: www.nih.ernet.in/TechnicalPapers/Rainfall_runoff_modelling_of_morel_catchment_for_design_flood_estimation_NIH_1997-98.pdf [Accessed 24 October 2011].
- National Institute of Hydrology (NIH). (1998). Application of GIUH, and GIS-Based Approach for Design Flood Estimation Report. [online]. Available at: www.nih.ernet.in/TechnicalPapers/Application_of_GIUH_and_GIS_Based_Approach_for_Design_Flood_Estimation.pdf [Accessed 24 October 2011].
- Nakamura S., Oki T. (2018). Paradigm shifts on flood risk management in Japan: Detecting triggers of design flood revisions in the modern era. *Water Resour. Res.* 54 (8), 5504-5515.
- Olivera F. and Maidment D.R. (1999). GIS tools for HMS modeling support. *Proceedings of the 19th ESRI users conference*, July 26-30, San Diego, CA.
- Parkes B., Demeritt D. (2016). Defining the hundred year flood: A Bayesian approach for using historic data to reduce uncertainty in flood frequency estimates. *J. Hydrol.* 540, 1189-1208.
- Panigrahi R.K. (1991). «Derivation of nash model parameters from geomorphological instantaneous unit hydrograph» M.E. Dissertation, DOH, UOR, Roorkee, India.
- Parhi P.K., Sankhua R.N. and Roy G.P. (2012). Calibration of Channel Roughness for Mahanadi River, (India) Using HEC-RAS Model. *Journal of Water Resource and Protection* 04(10), 847-850, DOI: 10.4236/jwarp.2012.410098.
- Rodríguez-Iturbe I. and Rinaldo A. (1997). *Fractal river basins; chance and self-organization*. Cambridge University Press.
- Rodríguez-Iturbe I. and Valdés J. (1979). The geomorphologic structure of the hydrologic response. *Water Resources Research*, 15(6), 1409-1420, DOI: 10.1029/WR015i006p01409.
- Rodríguez-Iturbe I., González-Sanabira M. and Caamaño G. (1982b). On the climatic dependence of the IUH: a rainfall runoff analysis of the Nash model and the geomorpho-climatic theory. *Water Resources Research*, 18(4), 887-903, DOI: 10.1029/WR018i004p00887.
- Rowe T.J. and Smithers J.C. (2018). Continuous simulation modelling for design flood estimation – a South African perspective and recommendations. *Water SA*, Pretoria, 44(4), 691-705.
- Rosbjerg D. et al. (2013). Prediction of floods in ungauged basins, in *Runoff Prediction in Ungauged Basins. A Synthesis Across Processes, Places and Scales*, edited by G. Bloschl, et al., 189-226, Cambridge Univ. Press: Cambridge, U.K.
- Rogger M., Kohl B., Pirkel H., Viglione A., Komma J., Kirnbauer R., Merz R. and Bloschl G. (2012). Runoff models and flood frequency statistics for design flood estimation in Austria—Do they tell a consistent story?, *J. Hydrol.*, 456, 30-43, DOI: 10.1016/j.jhydrol.2012.05.068.
- Smith B. and Sandwell D. (2003). Accuracy and resolution of shuttle radar topography mission data. *Geophysical Research Letters*, 30(9), 1467.
- Snyder F.F. (1938). Synthetic unit-graphs. *Transactions American Geophysical Union*, 19, 447-454, DOI: 10.1029/TR019i001 p00447.
- Sauquet E., Ramos M.H., Chapel L., Bernardara P. (2008). Stream flow scaling properties: investigating characteristic scales from different statistical approaches. *Hydrol. Process* 22(17), 3462-3475, DOI: 10.1002/hyp.6952.
- Serinaldi F. and Grimaldi S. (2011). Synthetic design hydrographs based on distribution functions with finite support, *J. Hydrol. Eng.*, 16, 434-446.
- Smithers J.C. (2012). Methods for design flood estimation in South Africa, *Water SA*, 38, 633-646.
- Taylor A.B. and Schwarz H.E. (1952). Unit hydrograph lag and peak flow related to basin characteristics. *Transactions, American Geophysical Union*, 33, 235-246, DOI: 10.1029/TR033i002p00235.
- US Army Corps of Engineers, HEC-GeoHMS, Hydraulic Reference Manual Version 4.1, 2010: Hydrologic Engineering Center.
- WRIS. (2012). *River Basin atlas of India*, Publication of Ministry of Water Resources, Government of India, jointly created by Central Water Commission (CWC) and Indian Space Research Organization (ISRO) under India WRIS project, 144.

(WMO) World Meteorological Organization. (2009). Extreme Values Analysis in: The Guide to Hydrological Practices. Volume II: Management of Water Resources and Application of Hydrological Practices [online]. Available at: www.whycos.org/hwrp/guide/index.php [Accessed 25 May 2020].

Xiao Y., Guo S., Liu P., Yan B. and Chen L. (2009). Design flood hydrograph based on multi characteristic synthesis index method, J. Hydrol. Eng., 14(12), 1359-1364.

Yen B.C. and Lee K.T. (1997). Unit hydrograph derivation for ungauged watersheds by stream order laws. Journal of Hydrologic Engineering, 2(1), 1-9, DOI: 10.1061/(ASCE)1084-0699(1997)2:1(1).

Yue S., Ouada T., Bobee B., Legendre P. and Bruneau P. (2002). Approach for describing statistical properties of flood hydrograph, J. Hydrol. Eng., 7(2), 147-153.

THE ROLE OF RELATIVE SLOPE LENGTH IN FLOOD HAZARD MAPPING USING AHP AND GIS (CASE STUDY: LAM RIVER BASIN, VIETNAM)

Nguyen Ba Dung^{1*}, Dang Tuyet Minh², Adeel Ahmad³, Nguyen Quoc Long⁴

¹Hanoi University of Natural Resources and Environment, Hanoi, Vietnam

²Thuyloi University, Vietnam, Hanoi, Vietnam

³Department of Geography, University of the Punjab, Lahore, Pakistan

⁴Hanoi University of Mining and Geology, Hanoi, Vietnam

*Corresponding author: nbdung@hunre.edu.vn

Received: March 4th, 2020 / Accepted: May 10th, 2020 / Published: July 1st, 2020

<https://DOI-10.24057/2071-9388-2020-48>

ABSTRACT. In addition to the five main factors affecting the formation of floods including slope, rainfall, drainage density, soil, and land cover, the relative slope length factor has also been considered to be one of the fundamental causes that contribute to flood hazard. The paper analyzes the theoretical basis for choosing the relative slope length criterion when zoning flood hazard in Lam river basin. The important role of this factor was evaluated by the results of the flood risk zoning map established by the method of integrating AHP and GIS technology in two cases: using 5 flood influence criteria and using 6 flood influence criteria. Flood hazard zoning maps for 2 cases were tested with 3 historic floods occurring on Oct 2010, Oct 2013 and Oct 2016. The results showed that the map established with six influence factors is more detailed and accurate than the one created with five factors affecting flood hazard because of the similarity with the reality of that map. The results of the study are applicable to other river basins which their geographical features are similar to characteristics the Lam river basin.

KEY WORDS: Relative slope length, slope length, flood hazard zoning, AHP algorithm, Lam river basin

CITATION: Nguyen Ba Dung, Dang Tuyet Minh, Adeel Ahmad, Nguyen Quoc Long (2020). The Role Of Relative Slope Length In Flood Hazard Mapping Using Ahp And Gis (Case Study: Lam River Basin, Vietnam). *Geography, Environment, Sustainability*, Vol.13, No 2, p. 115-123

<https://DOI-10.24057/2071-9388-2020-48>

Conflict of interests: The authors reported no potential conflict of interest.

INTRODUCTION

Floods are among the most common and most destructive natural disasters in Vietnam causing serious consequences (El Alfy 2016; Chau et al. 2013), threatening people's lives and slowing down the progress of socio-economic development. In period 1989 to 2014, floods caused considerable losses including at least 14,867 dead and missing people, asset damages equivalent to 1% of GDP for Vietnam (Chinh et al. 2018) and especially in agriculture, the extreme flood can affect more than 40% of wet rice production (Chau 2013). Floods also bring sediments with it (Bastawesy et al. 2009) and more sedimentation can result in clogging of drainage systems (El Alfy 2016). Widespread flooding with dramatic damages has shown the importance of flood mitigation and disaster response. In order to solve this problem, the first important mission is that building the flood hazard-zoning map, one of the powerful tools to identify flood-prone zones. The production of flood hazard maps is an important component of flood risk assessment and management activities (Chau et al. 2013; Luu et al. 2018).

There are many methods to establish the flood hazard zoning map such as the Hydrological method, Analytic Hierarchy Process (AHP) method, Statistic method, etc., but the AHP method is one of the most effective procedures because of its easy usage and high flexibility (Minh 2017a). In Vietnam, this approach has

appeared in the early years of the previous decade with some typical studies in Vu Gia – Thu Bon river (Tu et al. 2013), Hương river (Phường et al. 2015), Lam basin river (Minh and Dung 2017), river system in Quang Nam province (Chinh et al. 2018; Luu et al. 2018). AHP is a mathematical model for assigning the weight and rank to each factor used in the multi-criteria decision-making process (Souissi et al. 2019). When developing a flood risk zoning map using the Analytical Hierarchy Process (AHP) method, the selection of the factors leading to the formation of floods will determine the accuracy of the research results. Using AHP technique, the criteria that have a significant influence on flood formation in the river basins and other geographical areas have been published by many scientists in research of the different geographical areas including rainfall, slope, soil, land use, drainage density, land cover, irrigation system, etc. (Radwan et al. 2019; Seejata et al. 2018; Vojtek and Vojteková 2019). In fact, there are many various factors affecting flood generation such as physical geography, socio-economic, infrastructure factors (Elkhrachy 2015; Kazakis et al. 2015; Rahmati et al. 2016). According to (Tran et al. 2008), the flood is not a pure risk disaster but this phenomenon has deep roots in social vulnerabilities and inappropriate environment management. For each geographical area, the criteria as well as the level of impact on the flood are also different and there are no specific factors for flood susceptibility (Rahmati et al. 2016).

In the Lam river basin, apart from the aforementioned factors, the slope length factor is also one of the main causes affecting the flood risk. Slope length is defined as the distance from the point of origin of overland flow to the point where the slope decreases to the extent that deposition begins or to the point where runoff enters a defined channel (Zhang et al. 2017). This factor is known as one of the key factors that impact the flow volume (Yongmei et al. 2011) and runoff velocities (Gilley et al. 1987). The slope length has been studied a lot when assessing its effect on erosion. The effect of slope length on erosion occurs through an increase in the volume and the speed of runoff, resulting in increased capacity of the runoff to disaggregate and transport sediments (Bagarello and Ferro 2010). The research of (Bagio et al. 2017) revealed that the increase in erosion with the length of the slope is explained by the greater erosive power of surface runoff, determined mainly by the increase in the volume and speed of runoff (Bagio et al. 2017). Therefore, the longer the slope length, the higher the flow velocity and the greater the runoff volume. This leads to the slope length also significantly affecting the flood formation. There are two kinds of slope length: absolute and relative slope length. However, it is not easy to implement the absolute length hierarchy of all slopes in the study area by AHP, so the latter one will be mentioned in this study. The objective of the current study is to analyze the importance of relative slope length factor in making a flood hazard zonation maps using AHP associated with GIS techniques.

RESEARCH AREA

The Lam river system is located within 103°14' to 106°10' E and 17°50' to 20°50' N, lasts approximately 350 km in the NW-SE direction (Fig. 1). In Vietnam, more than 80% of the area is mountainous (Kieu 2011). The topography of the Lam river basin is complex distribution, the upstream and middle areas are steep terrain, while the terrain of downstream areas is quite flat. The terrain of the river basin is like a sloping roof that the peak is the Truong Son mountain range in the west and descending to the east. This makes it easy to concentrate the flow downstream quickly to create large floods. The average annual rainfall in the Lam river basin in the period 1961–2017 measured at Muong Xen station is 1,039,883 mm (lowest) and at the Ky Anh station is 2,899,900 mm (highest) (Kieu 2011).

As one of the nine major river systems of Vietnam, the Lam River system has two major tributaries, the Ca river and

the La River. The drainage density of the Lam river basin is approximately equal to that of the central rivers (0.67 km/km²). The soil in the mountainous area of the Lam river basin is quite good, the thickness of the soil layer is more than 50 cm, the good soil structure consists of 38 different soils which are unevenly distributed throughout the basin and can be divided into the main land groups including alluvial soil, red yellow feralit soils, coastal sand groups, and mangrove groups. The Lam river basin is rich in land cover including broadleaf evergreen forest, renew forest, mixed bamboo forest, residential land, shrubs, agricultural land, bare lands, cultivated aquatic land, other lands. Currently, the area of vacant land, bare hills on the Lam River basin is quite high, about 20% of natural land area (Kieu 2011).

Thus, with such natural conditions, the factors which can cause flooding in the Lam river basin including heavy rainfall on large areas, rich soils, thick drainage density, steep slope, land use for many purposes. These are the most important factors for the formation of the floods when heavy rainfall occurs for long periods. However, the watershed line of the southern and southwestern regions of the Lam river basin passes through mountains with an average elevation of 1,300–1,800 m. Also, the average slope of the sub-basins of the research area varies from 1% to 40%, so the slope length will be relatively great leading to higher risks of flooding. In the mountainous areas, the slope is different, the value of slope length is different, that means flood hazard also different. Therefore, it is necessary to consider the slope length element or the distance from the watershed line to the location where assessing the flood hazard (Minh 2019b).

DATA AND METHODS

Analyzing the effects of slope length on flood hazard

The concept of slope length

Slope length is the distance from the origin of overland flow along its flow path to the location of concentrated flow or deposition. According to (Widchmeier and Smith 1978), slope length has been defined as «the distance from the starting point of overland runoff (the top of the hillslope) to one of two following locations: (a) the point where the slope decreases sufficiently for deposition to occur, (b) the position where flow concentrates a clearly-defined channel (wet or dry) that may be a part of a drainage network or a constructed channel such as a terrace or diversion» (Wischmeier and Smith 1978). Thus, this length is equal to the distance calculated from the watershed line

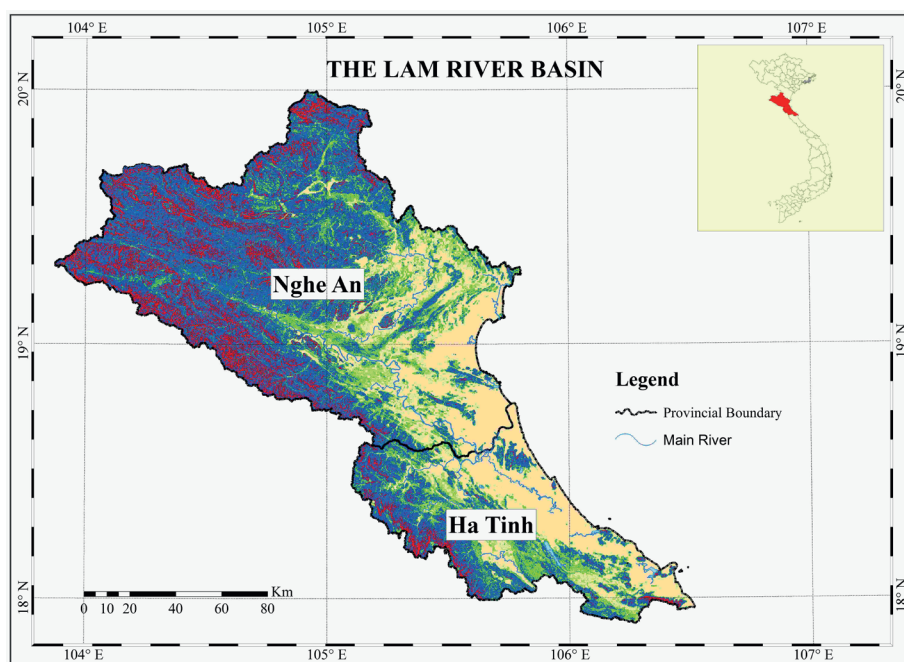


Fig. 1. The Lam river basin

to the valley line. A watershed is an area of land that drains to a stream, river, lake or ocean. It is a land surface feature that can be identified by connecting the highest elevations between two areas. During rainstorms, some water runs off both parts of the watershed but meets in the valley, stream, river, etc.

When measuring in units of distance, it is the absolute slope length. In some cases, for example, according to National Standards TCVN 5299: 2009, the erosion calculation caused by rain, slope length can be segmented by distance from the top of the slope to the base of the slope (Ministry of Science and Technology 2009), then the slope length is a relative slope length. In fact, there will be two concepts existed: the relative slope length and the absolute slope length. The relative slope length is the length of a segment relative to the entire slope length. The absolute slope length is normally measured in length measurement units, meaning "absolute" in terms of quantitative while the relative slope length is hierarchized based on the percentage of absolute slope length, so it means "relative" in terms of quantitative. The absolute slope length will be more meaningful in calculating the hydrological, hydraulic models but it is difficult in the hierarchy to determine the weight for the AHP model (Minh 2019b). Therefore, this paper uses a relative slope length.

The theoretical basis for choosing the relative slope length factor in zoning flood hazard

In reality, because water accumulates gradually in the process of moving along the slope from high to low and flood usually only occurs in the lower area, so the slope length is a factor that affects both floods as well as the possibility of flooding. According to Begarello and Ferro, an increase in slope length will increase flow volume and flow speed as well (Bagarello and Ferro 2010; Kinnell 2004). The longer the slope length, the greater the volume of water, flow speed, and inertia force. That is, the further the distance from the watershed line, the greater the kinetic energy of the flow, the higher the velocity of the flow leading to an increase in flood risk. Moreover, when the slope length increases, the tilted area will increase as well, hence the further the distance from the watershed line is, the more the volume of water accumulated

on the surface will be. This conclusion is also consistent with the research of (Yongmei et al. 2011). In the research, the authors conducted an experiment to observe rain-flow in areas with different slope lengths, and the results have shown that the flow volume increases with an increasing slope length (Yongmei et al. 2011). With the same results, (Liu & Singh 2004) studied runoff generation for four types of slope lengths. The modeling showed that the unit discharge increased remarkably as the slope length increased. The longer the slope was, the larger the unit discharge was (Liu & Singh 2004).

Thus, on the same slope, the volume of water, flow velocity as well as the ability to accumulate water will increase gradually as the water flows from the watershed line to the valley line. Moreover, the capacity of water accumulation on the slope is dependent on the time of water concentration. The time of rainwater concentration on the slope depends on the hydrogeological coefficient of the slope (Φ_{sd}) and the rain zone (Fig. 2) calculated by the formula (Directorate for Roads of Vietnam 2013): in which

$$\phi_{sd} = \frac{L_{sd}^{0.6}}{m_{sd} J_{sd}^{0.3} (\phi H_p)^{0.4}} \quad (1)$$

L_{sd} : Average slope length of the basin (m)

J : Slope in %

ϕ : Flood flow coefficient depending on the soil type, design daily rainfall and basin area.

H_p : design daily rainfall

m_{sd} : Parameter of roughness characteristics on the slope, depending on the surface condition of the basin slope

According to (Directorate for Roads of Vietnam 2013), the time of water concentration on the slope increases when the geomorphology and hydrological coefficient of the slope increases. The relevance between these two values is expressed in a line chart, where X-axis uses for Φ_{sd} , Y-axis for the time of water concentration, and separate lines represent rain zones as Fig. 2. Also, formula (1) shows that coefficient Φ_{sd} is proportional to the slope length. This proves that the greater the slope length, the more the time of water concentration and the greater the flood risk. Thus, the slope length is also one of the main causes of flooding.

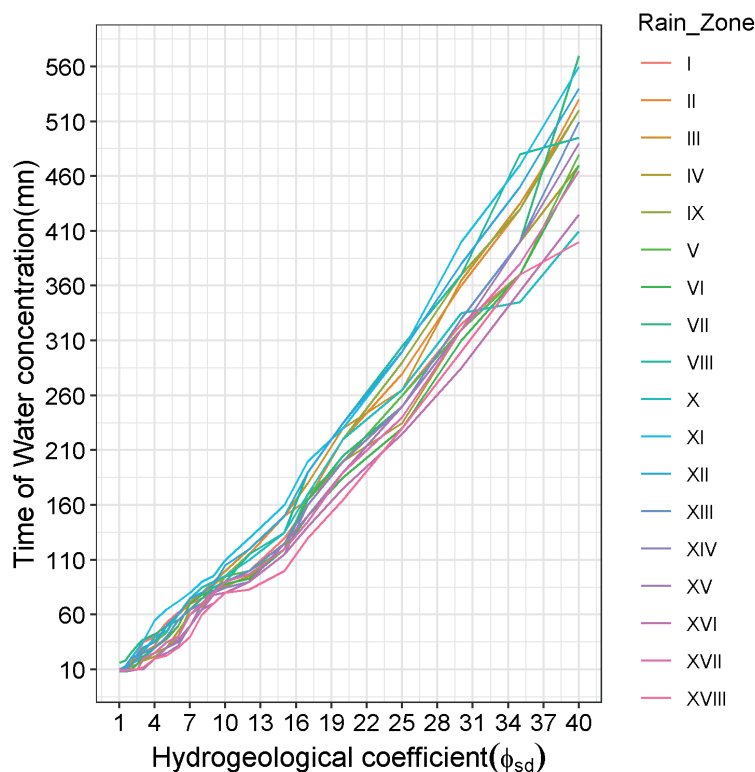


Fig. 2. The time of water concentration on the slope based on the hydrogeological coefficient of the slope and the rainy areas

DATA SETS AND METHODOLOGY

Data Sets

There are many indicators affecting flood hazard, and they vary from one study area to another. This paper used a composite flood hazard map index based on six variables—criteria, the flood causative factors, namely, the rainfall, the slope, the soil, the land cover, the drainage density, and the relative slope length. The selection of these elements was actually based on their relevance to flood occurrences as well as physical conditions of the study area. The study used various sources of documents including the topographic map, current land use map, administrative boundary map, map of river and stream system of Lam river basin, location map of hydrological stations in Lam river basin in scale 1:50,000 and the average rainfall data at some locations on Lam river basin in the period 1961 to 2017. These data obtained from concerned government agencies such as Vietnam National Space Center, Department of Natural Resources and Environment of Ha Tinh, Nghe An, and Thanh Hoa provinces and National Centre for Hydrometeorological Forecasting.

METHODOLOGY

Based on digitized topographic maps (20 m interval) in scale 1:50,000 and the geo-referenced in the National coordinating system, the digital elevation model (DEM of 30m grid cell resolution) was derived. The slope map and relative slope length map will be created from this DEM. Also based on the DEM and map of river and stream system of Lam river basin, the subbasins boundaries were also determined and several calculations were finally made as far as the flow direction and accumulation, the main flow length of each river tributary, the subbasin area and the drainage density index. From that, the drainage density map is built. Furthermore, average annual rainfall dataset for a large time period (1961–2017) from 20 meteorological stations covering the regional area was obtained from the National Centre for Hydro-Meteorological Forecasting (NCHMF). This kind of data helped to make the rainfall distribution map for the study area. In addition, through the current land use map (2015), the study area's land cover was identified and categorized according to flood susceptibility. Simultaneously, this map is used to establish a soil map. Taking into account the soil map within the Lam river basin, each soil type was assorted and ranked

according to its texture, penetration, and vulnerability to flood event. Each criterion was spatially visualized in a thematic map after processing in a GIS environment and was classified into five classes: Very Low; Low; Moderate; High and Very High by the Arcmap version 10.2 (Link: <http://desktop.arcgis.com/en/arcmap/>).

The evaluation of the accuracy of the map factors affecting the flood is done by comparing the result with the actual ones. The drainage density map is verified by alarm level and corresponding risk level at 5 hydrological stations in the Lam river basin with three historical flood events: October 16–18, 2010; October 15–16, 2013; and October 15–16, 2016. The verification results show that there is a similarity between the map of land cover (Minh 2017b), soil (Minh 2017c), drainage density (Minh 2019a), relative slope length (Minh 2019b) and risk level at hydrological stations: Hoa Duet, Linh Cam, Nam Dan, Chu Le, and Do Luong. For the slope map and the rainfall map, besides comparing these maps to the actual situations, these products are examined by making a comparison with the same type of maps establishing by other methods in research of Kieu (2015). Therefore, it is reasonable to infer that the results are almost consistent with reality and previous research.

In this paper, the authors have adopted an AHP method associated with GIS environment to manipulate the physical factors in the production of flood hazard zoning map. Fig. 3 presents a flowchart of the methodology applied in this research. Being a systematic approach developed in the 1970s, the AHP method gives decision-making based on experience, perception, and heuristics acquired from logical mathematical principles (Bhushan and Rai 2004) and help in organizing the complex problem in a simple way to follow and analyze. This algorithm aims in detecting the flood risk areas in the study region by recognizing the most flood-affected parameters based on the decision-makers' preferences being capable of altering subjective assessments of importance into a set of weights, (Kandilioti et al. 2012; Myronidis et al. 2009; Stefanidis et al. 2013). In other words, personal evaluations are transformed into numerical values and handled to rank each alternative in this study on a numerical scale. In the AHP implementation, a pairwise comparison technique is used to derive the priorities for the criteria in terms of their importance in achieving the goal. In this study, there are 6 factors that contribute to flood formation, so the number of comparisons will be $6 \times (6-1)/2$. The score of pairwise comparison of these criteria will

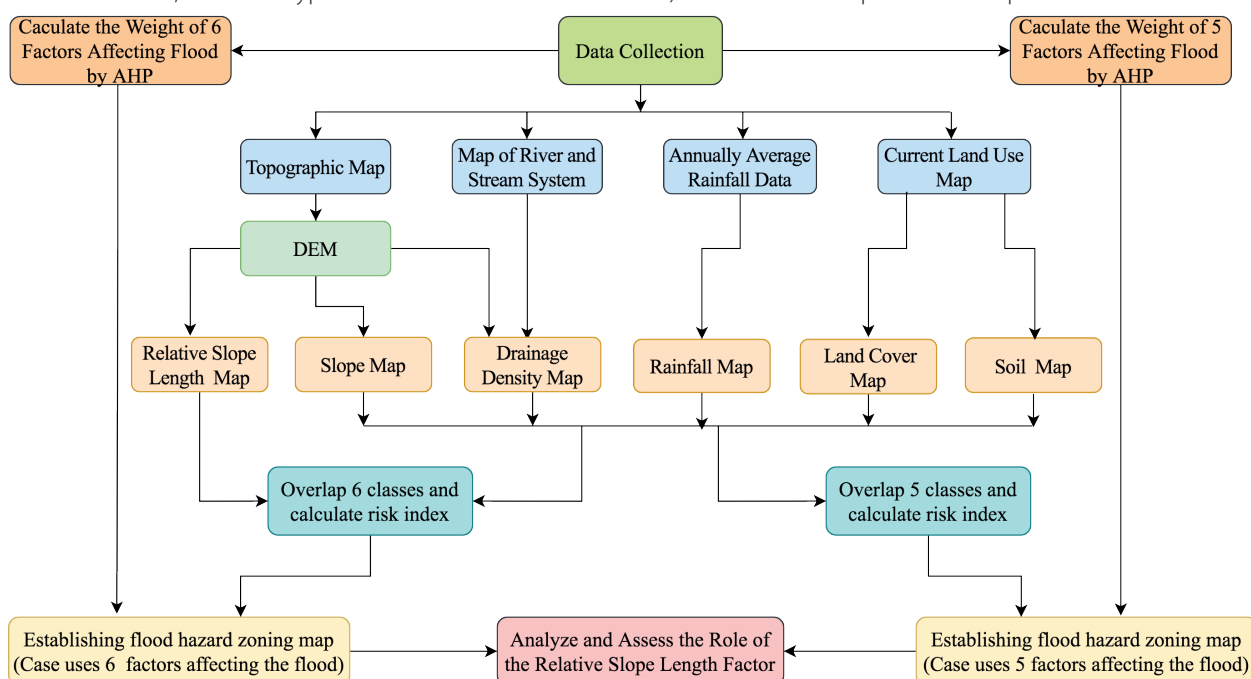


Fig. 3. Methodology flowchart

be the coefficient of the pairwise comparison matrix. The relative significance between the factors is assessed along the row from 1 to 9 pinpointing less important to much more important criteria, respectively whereas the corresponding column assigns the reciprocal of the weight (from 1/2 to 1/9) (Lappas and Kallioras 2019). The weight of the parameters can be computed using two methods: eigenvector method and normalization matrix method. The priority vector shows relative weights among the things that we compare. In this paper, the second method is employed to obtain the weight of the factors. A higher weight value of the factors represents more priority or more impact than others within the study. That means, the greater the weight of a factor becomes, the more that factor influences the flood hazard. However, there are existed errors in pairwise comparison and this leads errors in evaluation. To check and eliminate errors as well as examine the importance of the factors, according to (Saaty 2012), using consistency ratio (CR) of data. A Consistency Ratio (CR) indicates the probability that the matrix ratings were randomly generated and when CR is less than or equal to the threshold 0.1 signifies an acceptable reciprocal matrix, while ratio over 0.1 implies that the matrix should be revised indicating inconsistent judgments.

Once the weights for the factors are determined, a multi-criteria evaluation is performed by utilizing the specific weights and the maps for six factors to create the flood hazard zoning map. The basis of flood risk zoning will be generalized into the equation for calculating the risk score according to the hierarchy score of six factors:

$$HI = \sum_{i=1}^6 w_i * X_i \quad (2)$$

in which

HI: Hazard Index (risk score)

X_i : Hierarchy score of factor i ($i = 1 - n$)

w_i : The weight of factor i

RESULTS AND DISCUSSION

The research carries out in 2 cases. The first case uses 5 factors affecting the flood hazard to calculate the weights and makes a flood hazard zoning map including rainfall, slope, soil, land cover, drainage density. The remaining alternative, using five elements of the above plan and adding a relative slope length criterion to calculate a model and generate a flood hazard zoning map. Table 1 shows the weight of the criteria calculated according to the AHP method in 2 cases (Minh 2019b; Dung et al. 2020).

Based on the weight of factors calculated as Table 1, combined with the map of the influence criteria, the flood hazard zoning map of the river Lam basin is created by the spatial analysis method in the GIS environment. With the different numbers of influence parameters, flood risk zoning results are also different. It can be seen the difference between the results of flood risk zoning in two cases: five influence factors (Fig. 4) and six influence factors (Fig. 5).

Obviously, the results of the flood hazard zoning map using six influence factors are more detailed and specific than the remaining case. While this map indicates high-risk areas that are concentrated mainly in the districts of Huong Khe, Huong Son, Duc Tho, Can Loc, Thach Ha, Vu Quang, and Hung Nguyen, the results of the flood hazard zoning using five influence factors do not highlight this high-risk area.

Table 1. The weight of influencing factors

Criteria	Weight (case of 5 factors affecting flood)	Weight (case of 6 factors affecting flood)
Rainfall	0.495	0.45
Slope	0.276	0.255
Drainage desity	0.082	0.077
Soil	0.071	0.068
Land cover	0.077	0.073
Relative slope length		0.077

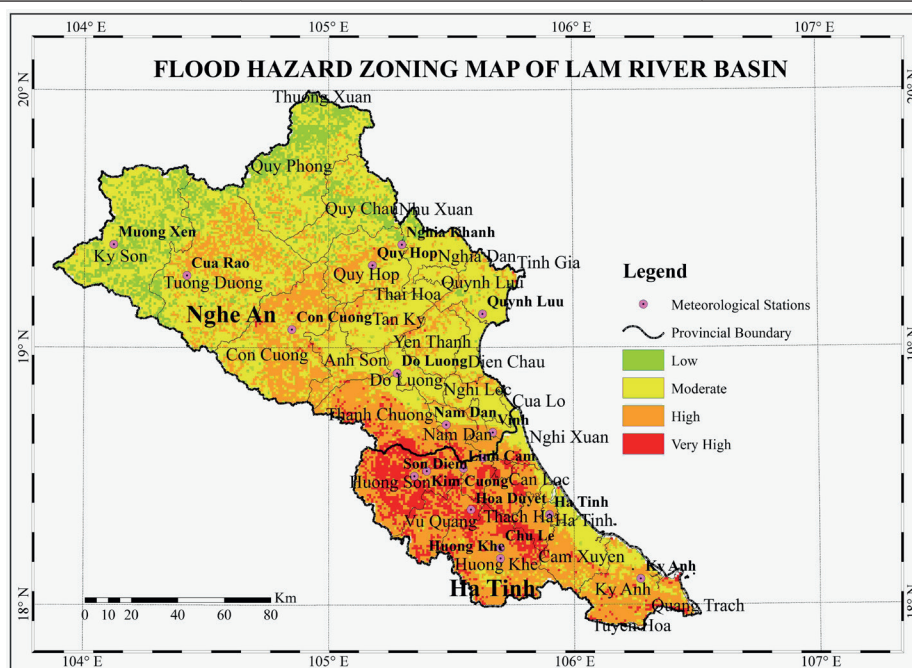


Fig. 4. Flood hazard zoning map of Lam river basin (using 5 influence factors)

The research results can be verified based on the flood alarm level at the hydrological stations on the river of the study area (Do Luong, Son Diem, Hoa Duyet, Linh Cam and Nam Dan) with three typical flood events including October 16-18, 2010; October 15-16, 2013; and October 15-16, 2016. Three levels of flood alarms can assess corresponding to the hazard level in the study as follows: Above alarm 3 – the risk of flooding is very high; Above alarm 2 – high flood risk; Above alarm 1- average flood risk; Under alarm 1- low flood risk.

According to decision No. 05/2020/QĐ-TTg signed on January 31, 2020 of the prime minister, the water levels corresponding to the flood alarm levels on the Do Luong, Nam Dan, Son Diem, Hoa Duyet, Linh Cam, Chu Le hydrological stations on the rivers of the river Lam basin are shown on Table 2. Compare the water levels of the hydrological stations in the historical floods to flood alarm levels in corresponding stations (Table 2), this indicates the relevance of the research results with the historical floods in reality.

Tables (from 3 to 5) show flood alarm levels and respective hazard levels at hydrological stations during the

three floods. The similarities of the research results and the reality can be compared based on risk levels on the hazard zoning map for 2 cases (using 5 factors and using 6 factors affecting flood formation). The comparison result shows the level of conformity between alarm levels on some hydrographic stations and the results of the flood hazard zoning of the study in the three flood events as follows:

The above test results show that there is very little mismatch on the map using 5 criteria affecting flood hazard, while most of the areas with very high flood risk in the flood risk zoning map using 6 influence factors are similar to reality. This is clearly shown in columns 7 and 9 in Table 3, 4, and 5. In particular, the Chu Le area is always at very high flood risk and suitable for over alarm level 3 of many floods. According to the survey data of Ha Tinh Committee for Flood and Storm Control, in addition to 3 flood events mentioned above, alarm level at the Chu Le station of most historical floods is over alarm level 3. For example, a flood of September 29 – October 2, 2009 (over alarm 3, 3.06 m); a flood of October 4, 2010 (over alarm 3, 1.52 m); a flood of September 26, 2013 (over alarm 3, 0.3 m); a flood of October 29 – November 4, 2016 (over alarm 3, 0.21 m);

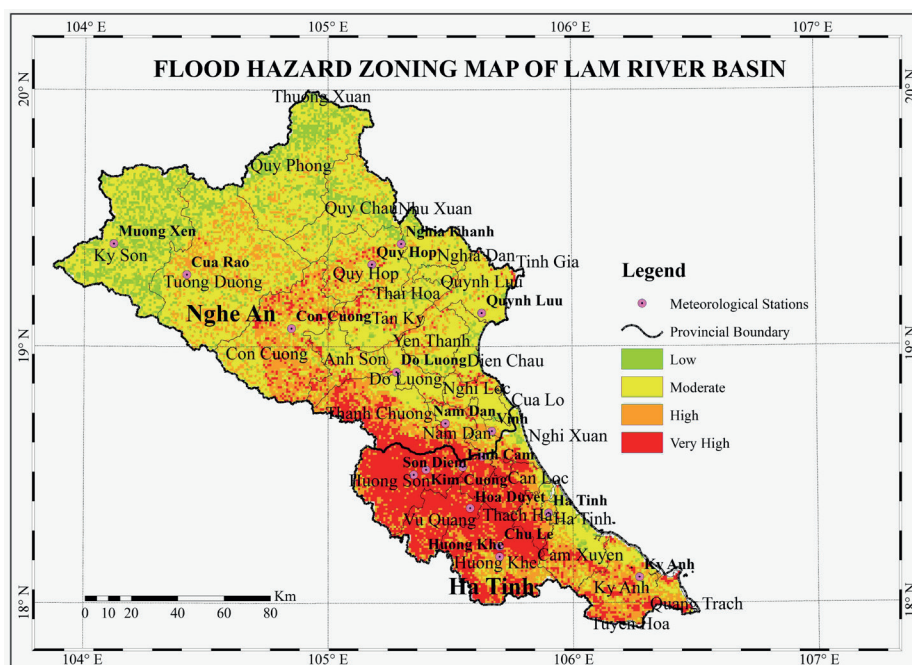


Fig. 5. Flood hazard zoning map of Lam river basin (using 6 influence factors)

Table 2. The water levels corresponding to the flood alarm levels on the rivers of the river Lam basin

No.	Province	River	Hydrological stations	Water level corresponds to the alarm level (m)		
				I	II	III
1	Nghe An	Ca	Nam Dan	5.4	6.9	7.9
2			Do Luong	14.5	16.5	18.0
3	Ha Tinh	La	Linh Cam	4.5	5.5	6.5
4		Ngan Pho	Son Diem	10.0	11.5	13.0
5			Hoa Duyet	7.5	9.0	10.5
6		Ngan Sau	Chu Le	11.5	12.5	14.0

(Sources: Decision No. 05/2020/QĐ-TTg of Prime Minister's: Regulation of water levels corresponding to the flood alarm levels on nation-wide rivers)

* With the flood on October 16-18, 2010

- The flood hazard zoning map using six influence factors: Flood risk level in this map is suitable to the actual risk level at 5/5 hydrological stations.

- The flood hazard zoning map using five influence factors: Flood risk level in this map is only suitable to the actual risk level at Son Diem hydrological station.

Table 3. Water level, Alarm level and hazard level at Hydrological stations in flood event October 16-18, 2010

No.	Hydro-logical stations	Water level (m)	Alarm level	Hazard level in reality	Risk level on a map using 6 factors	Comparison Results	Risk level on a map using 5 factors	Comparison Results
1	Son Diem	13.00	Over alarm level 3 (0,78 m)	Very high	Very high	Similarity	Very high	Similarity
2	Hoa Duyet	12.37	Over alarm level 3 (1,87 m)	Very high	Very high	Similarity	High	No Similarity
3	Linh Cam	7.28	Over alarm level 3 (0,78 m)	Very high	Very high	Similarity	High	No Similarity
4	Nam Đan	6.2	Over alarm level 1 (0,8 m)	Medium	Medium	Similarity	High	No Similarity
5	Chu Le	16.56	Over alarm level 3 (3.06 m)	Very high	Very high	Similarity	High	No Similarity

(Data Source: Ha Tinh Committee for Flood and Storm Control)

* With the flood on October 15 -16, 2013

- The flood hazard zoning map using six influence factors: Flood risk level in this map is suitable to the actual risk level at 5/6 hydrological stations, except Linh Cam station.

- The flood hazard zoning map using five influence factors: Flood risk level in this map is suitable to the actual risk level at two hydrological stations, Son Diem and Linh Cam.

Table 4. Water level, Alarm level and hazard level at Hydrological stations in flood event October 15-16, 2013

No.	Hydro logical station	Water level (m)	Alarm level	Hazard level in reality	Risk level on a map using 6 factors	Comparison Results	Risk level on a map using 5 factors	Comparison Results
1	Do Luong	13.19	Under alarm level 1 (1.31 m)	Low	Low	Similarity	Medium	No Similarity
2	Son Diem	14.62	Over alarm level 3 (1.62 m)	Very high	Very high	Similarity	Very high	Similarity
3	Hoa Duyet	11.26	Over alarm level 3 (0.76 m)	Very high	Very high	Similarity	High	No Similarity
4	Linh Cam	5.74	Over alarm level 2 (0.24 m)	High	Very high	No Similarity	High	Similarity
5	Nam Đan	6.5	Under alarm level 2 (0.4 m)	Medium	Medium	Similarity	High	No Similarity
6	Chu Le	14.42	Over alarm level 3 (0.92 m)	Very high	Very high	Similarity	High	No Similarity

(Data Source: Ha Tinh Committee for Flood and Storm Control)

* With the flood on October 15 -16, 2016

- The flood hazard zoning map using six influence factors: Flood risk level in this map is suitable to the actual risk level at 4/6 hydrological stations, except Linh Cam and Son Diem station.

- The flood hazard zoning map using five influence factors: Flood risk level in this map is only suitable to the actual risk level at Linh Cam hydrological stations.

Table 5. Water level, Alarm level and hazard level at Hydrological stations in flood event October 15-16, 2016

No.	Hydrological station	Water level (m)	Alarm level	Hazard level in reality	Risk level on a map using 6 factors	Comparis-on Results	Risk level on a map using 5 factors	Comparis-on Results
1	Do Luong	13.00	Under alarm level 1 (1.12 m)	Low	Low	Similarity	Medium	No Similarity
2	Son Diem	12.8	Below alarm level 3 (0.2 m)	High	Very high	No Similarity	Very high	No Similarity
3	Hoa Duyet	10.91	Over alarm level 3 (0.41 m)	Very high	Very high	Similarity	High	No Similarity
4	Linh Cam	5.5	Alarm level 2	High	Very high	No Similarity	High	Similarity
5	Nam Đan	5.66	Over alarm level 1 (0.26 m)	Medium	Medium	Similarity	High	No Similarity
6	Chu Le	15.64	Over alarm level 3 (2.14 m)	Very high	Very high	Similarity	High	No Similarity

(Data Source: Ha Tinh Committee for Flood and Storm Control)

From the study results, it is observed that AHP provides a flexible, simple, step-by-step and transparent approach of analyzing complex problems in a multi criteria decision analysis (MCDA) environment based on experts and end-user preferences, knowledge, experience, and judgments. Further, the AHP- GIS based method to flood hazard assessment as utilized in this study is seen as a relatively inexpensive, easy to use, and more importantly, permits interactive implementation by flood managers for continuing improvement. Therefore, it was found that the changes in the set of criteria contributing to flood creation significantly affect the result of the hazard zoning map, and the changes were reasonable and acceptable. The results prove that adding the relative slope length parameter to calculate the model will increase the reliability of the research method. Also, the different results obtained from these two cases indicate the importance of the relative slope length factor in mapping flood hazard zoning.

These results also introduce a way to improve the accuracy of developing flood risk zoning map with AHP by adding a factor leading to the formation of floods when calculating the model. However, it is carefully considered to decide which factors can be supplemented and the matching capacity of these elements on the hierarchy and computation by the AHP algorithm. In addition, it is not

recommended to add too many criteria, only a maximum of 9 criteria is sufficient because psychologists conclude that, nine objects are the most that an individual can simultaneously compare and consistently rank (Pawel 2010).

CONCLUSION

When studying flood hazard zoning by the AHP method, the criteria affecting the flood may change depending on data collection. However, besides using the common factors contribute to flooding in most terrain and geographic areas such as rainfall, slope, drainage density, land cover, and soil, it is advisable to add the relative slope length parameter as input data. This is the important criterion when studying the flood risk zoning for many basins in general and the Lam river basin in particular. This factor affects the volume of water, water accumulate ability, and flow velocity, thereby this contributes to flood risk. Results of flood hazard zoning using the relative slope length are more specific and accurate, thus accuracy and reliability of the warning work will be improved significantly. Especially for river basin with high flood frequency, areas with high elevations, high slope, and area with a long distance from the watershed line to the valley line, using the slope length in the flood risk study is necessary. ■

REFERENCES

- Bagarello V. and Ferro V. (2010). Analysis of soil loss data from plots of differing length for the Sparacia experimental area, Sicily, Italy. *Biosystems Engineering*, [online]. 105(3), 411-422. Available at: www.sciencedirect.com/science/article/pii/S153751101000005X?via%3Dihub [Accessed March 2010].
- Bagio B., Bertol I., Wolschick H.N., Schneiders D., Santos M.A.D.N.D. (2017). Water Erosion in Different Slope Lengths on Bare Soil. *Revista Brasileira de Ciência do Solo*, [online]. 41. Available at: www.scielo.br/scielo.php?script=sci_arttext&pid=S0100-06832017000100505 [Accessed 09 March 2017].
- Bastawesy M. El., White K. & Nasr A. (2009). Integration of remote sensing and GIS for modelling flash floods in Wadi Hudain catchment, Egypt. *Hydrological Processes*, [online]. 23(9), 1359-1368, DOI: 10.1002/hyp.
- Bhushan N. and Rai K. (2004). *Strategic Decision Making: Applying the Analytic Hierarchy Process*; Springer: London, UK.
- Chau V.N., Holland J., Cassells S., Tuohy M. (2013). Using GIS to map impacts upon agriculture from extreme floods in Vietnam. *Applied Geography*, [online] 41, 65-74. Available at: www.sciencedirect.com/science/article/abs/pii/S0143622813000805 [Accessed July 2013].
- Chinh L., Meding J. (2018). A Flood Risk Assessment of Quang Nam, Vietnam Using Spatial Multicriteria Decision Analysis. *Water*, [online] 10(4), 461. Available at: www.mdpi.com/2073-4441/10/4/461 [Accessed 8 April 2018].
- Directorate for Roads of Vietnam, TCVN 9845:2013. (2013). Calculating of flood flow characteristics (in Vietnamese with English summary). Available at: www.vanbanphapluat.co/tcvn-9845-2013-tinh-toan-cac-dac-trung-dong-chay-lu [Accessed 20 May 2020].
- Dung N.B., Minh D.T., Long N.Q., Ha L.T.T. (2020). Weights of factors contributing to flood formation in the Lam river basin, Vietnam. *Journal of Southwest Jiaotong University*, 55(2). Available at: www.researchgate.net/publication/341121252_WEIGHTS_OF_FACTORS_CONTRIBUTING_TO_FLOOD_FORMATION_IN_THE_LAM_RIVER_BASIN_VIETNAM [Accessed April 2020].
- El Alfy M. (2016). Assessing the impact of arid area urbanization on flash floods using GIS, remote sensing, and HEC-HMS rainfall-runoff modeling. *Hydrology Research*, [online] 47(6), 1142-1160, DOI: 10.2166/nh.2016.133.
- Elkhrachy I. (2015). Flash Flood Hazard Mapping Using Satellite Images and GIS Tools : A case study of Najran City , Kingdom of Saudi Arabia (KSA). *The Egyptian Journal of Remote Sensing and Space Sciences*, [online] 18(2), 261-278, DOI: 10.1016/j.jejrs.2015.06.007.
- Gilley J.E, Finkner S.C., Varvel G.E. (1987). Slope Length and Surface Residue Influences on Runoff and Erosion. *Biological Systems Engineering: Papers and Publications*, 148-152. Available at: www.digitalcommons.unl.edu/cgi/viewcontent.cgi?article=1120&context=biосyengfacpub [Accessed 20 May 2020].
- Kandilioti G. and Makropoulos C. (2012). Preliminary flood risk assessment. The case of Athens. *Natural Hazards*, [online] 61(2), 441-468. Available at: www.link.springer.com/article/10.1007/s11069-011-9930-5 [Accessed 20 May 2020].
- Kazakis N., Kougiass I. & Patsialis T. (2015). Science of the Total Environment Assessment of flood hazard areas at a regional scale using an index-based approach and Analytical Hierarchy Process : Application in Rhodope – Evros region, Greece. *Science of the Total Environment*, [online] 538, 555-563, DOI: 10.1016/j.scitotenv.2015.08.055.
- Kinnell P.I.A. (2000). The Effect of Slope Length on Sediment Concentrations Associated with Side-Slope Erosion. *Soil Science Society of America Journal*, [online] 64, 1004-1008. Available at: www.researchgate.net/publication/235936764_The_Effect_of_Slope_Length_on_Sediment_Concentrations_Associated_with_Side-Slope_Erosion [Accessed December 1999].
- Kieu T.D. (2011). Research on large flood management in the Lam River basin, Ph.D. Thesis, Thuyloi University (in Vietnamese with English summary).
- Lappas I. and Kallioras A. (2019). Flood Susceptibility Assessment through GIS-Based Multi-Criteria Approach and Analytical Hierarchy Process (AHP) in a River Basin in Central Greece. *International Research Journal of Engineering and Technology (IRJET)*, [online] 6(3), 738-751. Available at: www.irjet.net/archives/V6/i3/IRJET-V6I3137.pdf [Accessed 3 March 2019].
- Liu Q.Q. and Singh.V.P. (2004). Effect of Microtopography, Slope Length and Gradient, and Vegetative Cover on Overland Flow through Simulation. *Journal of Hydrologic Engineering*, [online] 9(5), 375-382, DOI: 10.1061/(ASCE)1084-0699(2004)9.

- Luu C., Von Meding J., Kanjanabootra S. (2018). Assessing flood hazard using flood marks and analytic hierarchy process approach: A case study for the 2013 flood event in Quang Nam, Vietnam. *Natural Hazards*. [online] 90, 1031-1050. Available at: www.researchgate.net/publication/320757449_Assessing_flood_hazard_using_flood_marks_and_analytic_hierarchy_process_approach_a_case_study_for_the_2013_flood_event_in_Quang_Nam_Vietnam [Accessed November 2017].
- Minh D.T. (2017a). Modeling methods and application for building a flood hazard zoning model. *Journal of Mining and Earth Science*, 58(4), 128-135 (in Vietnamese with English summary).
- Minh D.T. (2017b). The application of GIS technology in establishing a land cover hierarchy map for zoning flood hazard in Lam river basin. *Mining Industry Journal*, 5, 37-40 (In Vietnamese with English summary).
- Minh D.T. (2017c). The application of GIS technology to build a soil classification map following level of flood risk in Lam river basin. *Journal of Science on Natural Resources and Environment*, 16, 68-74 (in Vietnamese with English summary).
- Minh D.T. (2019a). Application of GIS technology to establish a drainage density hierarchical map for flood hazard zoning in Lam river basin. *Journal of Mining and Earth Sciences*, 59(6), 32-42 (in Vietnamese with English summary).
- Minh D.T. (2019b). Research on the application of special modeling in zoning flood hazard in flood warning in lam river basin, Ph.D. thesis, university of mining and geology (in Vietnamese with English summary).
- Minh D.T and Dung N.B. (2017). Flood Hazard zoning in Lam river basin, Vietnam, using GIS and analytic hierarchy process (AHP). *Proceedings of International Conference on Geo-Spatial Technologies and Earth Resources*, 837-843.
- Ministry of Science and Technology. (2009). Soil quality – Method for determination of soil erosion by rain. National Standards TCVN 5299: 2009, (in Vietnamese). Available at: www.vanbanphapluat.co/tcvn-5299-2009-chat-luong-dat-xac-dinh-muc-do-xoi-mon-dat-do-mua [Accessed 20 May 2020].
- Myronidis D., Emmanouloudis D., Stathis D., Stefanidis P. (2009). Integrated flood hazard mapping in the framework of E.U directive on the assessment and management of flood risks. *Fresenius Environ Bull.* [online] 18(1), 102-111. Available at: www.researchgate.net/publication/259451282_Integrated_flood_hazard_mapping_in_the_framework_of_the_EU_directive_on_the_assessment_and_management_of_flood_risks [Accessed 20 May 2020].
- Pawel C. (2010). Using the analytic hierarchy process in evaluating decision alternative. *Operations research and decisions*. [online] 1. Available at: www.researchgate.net/publication/227653945_Using_the_Analytic_Hierarchy_Process_in_Evaluating_Decision_Alternatives [Accessed 20 May 2020].
- Phuong T.T., Minh P.T., Ngoc N.B. (2015). Application GIS and AHP to build the flood hazard zoning map in the Huong River basin, Thua Thien Hue province. *Hue University Journal of Science*. [online] Volume 13(112) (in Vietnamese). Available at: www.jos.hueuni.edu.vn/index.php/TCKHDDH/article/view/2232 [Accessed 20 May 2020].
- Radwan F., Alazba A.A. & Mossad, A. (2019). Flood risk assessment and mapping using AHP in arid and semiarid regions. *Acta Geophysica*, [online] 67(1), 215-229, DOI: 10.1007/s11600-018-0233-z.
- Rahmati O., Zeinivand H. & Besharat M. (2016). Flood hazard zoning in Yasooj region, Iran, using GIS and multi-criteria decision analysis. *Geomatics, Natural Hazards and Risk*. [online] 7(3), 1000-1017, DOI: 10.1080/19475705.2015.1045043.
- Saaty T.L. (2012). Decision making in complex environments: The Analytic Network Process (ANP) for Dependence and Feedback. Pittsburgh. Available at: www.superdecisions.com/sd_resources/v28_man02.pdf [Accessed 20 May 2020].
- Seejata K., Yodying A., Wongthadam T., Mahavik N. & Tantane S. (2018). Assessment of flood hazard areas using Analytical Hierarchy Process over the Lower Yom Basin, Sukhothai Province. *Procedia Engineering*. [online] 212, 340-347, DOI: 10.1016/j.proeng.2018.01.044.
- Souissi D., Zouhri L., Hammami S., Msaddek M. H., Zghibi A. & Dlala M. (2019). GIS-based MCDM-AHP modeling for flood susceptibility mapping of arid areas, southeastern Tunisia. *Geocarto International*. [online] 1-27, DOI: 10.1080/10106049.2019.1566405.
- Tran P., Marincioni F., Shaw R., Sarti M., Van An L. (2008). Flood risk management in Central Vietnam: Challenges and potentials. *Natural Hazards*, 46(1), 119-138. Available at: www.link.springer.com/article/10.1007/s11069-007-9186-2
- Tu L.H., Hong N.T., Liem N.D., Loi N.K. (2013). Integrating Analytic Hierarchy Process and GIS for Flood risk zoning in Vu Gia Watershed, Quang Nam Province, VNU Journal of Science. [online] 3(29), 64-72 (in Vietnamese with English summary). Available at: [file:///Users/ad/Dowloads/1110-1-2162-1-10-20160519%20\(1\).pdf](http://file:///Users/ad/Dowloads/1110-1-2162-1-10-20160519%20(1).pdf) [Accessed 20 May 2020].
- Vojtek M. & Vojteková J. (2019). Flood susceptibility mapping on a national scale in Slovakia using the analytical hierarchy process. *Water (Switzerland)*. [online] 11(2), DOI: 10.3390/w11020364.
- Yongmei D., Xihuan S., Xianghong G., Shijun N. & Juanjuan M. (2011). Analysis of Slope Length on Water Soil Erosion. *International Conference on Consumer Electronics, Communications and Networks, CECNet*. [online] 2943-2946, DOI: 10.1109/CECNET.2011.5769391.
- Zhang H., Wei J., Yang Q., Baartman J.E.M., Gai L., Yang X., et al. (2017). An improved method for calculating slope length (λ) and the LS parameters of the Revised Universal Soil Loss Equation for large watersheds. *Geoderma*. [online] 308, 36-45. Available at: www.sciencedirect.com/science/article/pii/S0016706116310059 [Accessed 15 December 2017].
- Wischmeier W.H. and Smith D.D. (1978). Predicting rainfall erosion losses: a guide to conservation planning with Universal Soil Loss Equation (USLE) Agriculture Handbook, Department of Agriculture, Washington, DC. (703). Available at: www.naldc.nal.usda.gov/download/CAT79706928/PDF [Accessed 20 May 2022].

HEAVY METALS IN MARINE AEROSOLS OF THE AZOV SEA

Marina A. Chichaeva^{1*}, Mikhail Yu. Lychagin², Anton V. Syroeshkin¹, Olga V. Chernitsova²

¹Peoples Friendship University of Russia (RUDN University), Moscow, Russia

²Lomonosov Moscow State University, Moscow, Russian Federation

*Corresponding author: machichaeva@gmail.com

Received: January 1st, 2020 / Accepted: May 10th, 2020 / Published: July 1st, 2020

<https://DOI-10.24057/2071-9388-2020-11>

ABSTRACT. The content of heavy metals and Al in the aerosol matter over the Sea of Azov has been studied. According to the special test the vast majority of samples were attributed to the type of marine aerosol. The ranges of contents were determined as following: Fe (200 – 2000 ng / m³), Al (20 – 200 ng / m³), Zn (10 – 280 ng / m³), Cu (2 – 23 ng / m³), Ni (1 – 16 ng / m³), Pb (3 – 30 ng / m³), Cd (0.4 – 2.8 ng / m³); Mn (3 – 23 ng / m³), Cr (1 – 15 ng / m³). The spatial distribution of HMs in the marine aerosol of the Sea of Azov depends on the influence of the river-sea geochemical barrier zone in the Taganrog Bay and the anthropogenic impact of the coastal industrial cities. HM concentrations decrease from the northern coast of the bay and the mouth of the Don River towards the open sea. The maximum HM content in marine aerosol observed in the mouth area of the Don River. It may be associated with the HM accumulation at the river-sea geochemical barrier, and also with the anthropogenic impact of the cities of Rostov-on-Don, Azov and Taganrog. Anthropogenic impact of the city of Mariupol cause the maximum values of Fe, Cr, and Cd in marine aerosol matter of the western part of the Taganrog Bay.

KEY WORDS: heavy metals, spatial distribution, aerosol, micro particles, sea surface microlayer, pollution, Don River, Taganrog Bay

CITATION: Marina A. Chichaeva, Mikhail Yu. Lychagin, Anton V. Syroeshkin, Olga V. Chernitsova (2020). Heavy Metals In Marine Aerosols Of The Azov Sea. Geography, Environment, Sustainability, Vol.13, No 2, p. 127-134

<https://DOI-10.24057/2071-9388-2020-11>

Conflict of interests: The authors reported no potential conflict of interest.

INTRODUCTION

The aerosol of the surface layer of the atmosphere, including over water areas, is a mixture of particles of various genesis – from the local sources to the long-range atmospheric transport. Calculations show that over the territory of Europe, marine aerosol accounts for about 25-36% of the total aerosol matter (Georgoulas et al. 2016). Aerosol transport from the continent to water bodies is currently well reported (Marín-Beltrán et al. 2019; Akinori et al. 2019; Mahowald, 2018; Von Glasow 2013; Jordi et al. 2012; Paytan et al. 2009). The phenomena of transcontinental transport of aerosols and abundant atmospheric deposition to the surface of the ocean in the Arctic zone, over the waters of the North Atlantic are known (Vinogradova et al. 2019; Maslennikova et al. 2018; Sullivan et al. 2017; Lukashin et al. 2018; Vinogradova et al. 2017). It is shown that among the sources of marine aerosol generation (marine, dust, urban, black carbon, volcanic), the ocean surface is the most powerful, delivering up to 10¹⁶ kg per year (Kondratiev et al. 1999). The reverse process of transporting aerosol matter of marine origin towards coastal territories is also being investigated.

The concentrations of chemical elements in the Sea Surface Microlayer (SSM), their interaction and removal with marine aerosol have been reported in a number of papers (Li et al. 2019; Li et al. 2018, Rastelli et al. 2017). It has been shown that marine aerosol is formed mainly from SSM during the destruction of air bubbles that occur in the thickness of the sea water during gas evolution in the dispersed phase. In addition, it is formed by a direct wind breakdown of water droplets from the sea surface when waves collapse. Aerosol particles formed under these conditions are referred by dimension to the PM 10 group. The mechanisms of marine aerosol formation suggest a significant similarity between

the chemical composition of aerosol particles and the surface microlayer (Lapshin et al. 2002; O'Dowd et al. 2007; O'Dowd et al. 2002).

The climatic role of marine aerosols is significant (Van Dolah et al. 2000; Li et al. 2019). Cloudiness is strongly modulated by the emission of aerosols from the sea surface, affecting its formation and microphysical properties. The mechanism of the effect of aerosol on cloudiness in general can be described as follows. An increase in the concentration of aerosol in the atmosphere changes the water content of clouds and the size of cloud droplets, prolonging the lifetime of the cloud and thus reducing the amount of precipitation (Brooks et al. 2017; Chandrakar et al. 2016; Buseck et al. 1999; Takata et al. 2009).

Many studies are currently devoted to studying the concentration of heavy metals (HM) in aerosol particles. Scientific research is carried out within the framework of the UN programs: GESAMP, National Institute of Health, USA – Marine biotoxins. The mechanisms of toxicant concentrating in SSM and their further aerosol transportation in coastal areas are studied (Li et al. 2018). The accumulation and transfer of toxic substances at the ocean-atmosphere boundary can lead to significant pollution of the near-water layer of the atmosphere (Song et al. 2019; Qureshi et al., 2009; Kolesnikov et al. 2005). The studies are carried out by groups of scientists in various areas of the world (Furness et al. 2017), the North Sea (Salomons et al. 1988), the Arctic Seas (Shevchenko et al. 2003; Golubeva et al. 2011), the Atlantic and Indian Oceans (Witt et al. 2006; Rädlein et al. 1992), Antarctic seas (Tuohy et al. 2015). HMs were found in aerosol matter above the Ross Sea off the Antarctic coast.

HMs as part of aerosol particles are involved in global atmospheric circulation processes, and therefore HM monitoring in marine aerosol considered urgent. The European

Monitoring and Evaluation Program (EMEP; <http://www.emep.int>) and the Acid Deposition Monitoring Network in East Asia (EANET; <http://www.eanet.cc>) internationally cover the origin, spatial distribution aerosols, monitor their chemical composition, use methods of computer simulation of migration flows (Sajeev et al. 2014). The EMEP and EANET monitoring programs rely on satellite-based atmospheric sounding data, as well as data on the chemical composition of aerosols (including HM concentrations) from a network of reference stations in Eurasia, where aerosol sampling is carried out. Computer simulation is corrected by observations on the ground. Thus, remote monitoring methods rely on routine monitoring of aerosol composition.

Toxic substances entering the atmosphere with marine aerosol microparticles, along with urban aerosol sources, pose a serious potential threat to public health in the coastal zone of the seas and oceans (Mahowald et al. 2018; Aryasree et al. 2015; Van Dolah et al. 2000; Syroeshkin 2002; Lapshin 2002). HM entering the body through the respiratory system, penetrating the skin, inhalation and swallowing pathways (Wang et al. 2018) can increase morbidity and mortality from cardiovascular, respiratory diseases, cirrhosis, anemia, neuropathy (Liu et al. 2018), and also affect the kidneys, liver and gastrointestinal tract, causing cancer (Csavina et al. 2013; Izhar et al. 2016; Sánchez-Rodas 2017). There is an increased risk of pulmonary (asthma) and allergic diseases (Walsh et al. 2017; Kirkpatrick et al. 2011; Fleming et al. 2009). The role of marine aerosol as a carrier of palitoxins and endotoxins to the coastal zone has been shown (Patocka et al. 2018; Lang-Yana et al. 2014).

The ecological state of the Sea of Azov, despite the long decline in production activity that began in the 1990s, remains tense. The sea has a relatively small area and depth, there are large industrial centers along its shores, and thereby it is one of the most polluted seas in Russia (Klenkin et al. 2009). The mouth area of the Don River presents hydrodynamic and geochemical barrier. That's why the Sea of Azov considered an interesting and extraordinary subject for studying aerosol matter in the lowest atmosphere. The purpose of this work was to establish the levels of content and spatial distribution of HMs in the marine aerosol microparticles of the Sea of Azov.

MATERIALS AND METHODS

The paper presents data on the concentration of heavy metals in aerosol microparticles of the Sea of Azov obtained by the Azov-2006 complex ship expedition from the Taganrog Bay to the port of Temryuk. The studies were carried out in 2 stages: July 16 – 25 and September 25 – October 1, 2006. Each aerosol sampling period lasted 3-5 hours. Points of change of aerosol filters are marked at the map (Fig. 1). Simultaneously, the content of HM in the sea surface microlayers of 0.2 and 1 mm thick was studied. It has been previously shown that the main source of pollution of the atmospheric near-water layer is aerosol emission from the sea surface, which enables enrichment of the SSM due to the heterogeneous convection (Lapshin et al. 2005; Kolesnikov et al. 2005). A total of 54 aerosol filters and 168 samples of the bulk water and sea surface micro layer were collected.

Aerosol sampling was carried out on AFA-RMP-3 analytical filters using a Karcher NT 351 ECO vacuum cleaner with a maximum air flow rate of 78 dm³/s. The basis of the AFA filter is Petryanov's filter cloth made of perchlorovinyl fiber, in accordance with state specifications TU 951892-89. This is a fibrous material using mechanical methods of particle capture, as well as the electrostatic attraction of aerosol particles to charged filter fibers. Due to this, the material is characterized by high capture efficiency. The canvas is characterized by an irregular arrangement of polymer fibers of the different thickness, so the filter has a different pore diameter. Using the sampling technique methodology, these filters provide collecting 99.9% of aerosol particles with a linear size more than 0.3 microns. 3 filters were exposed simultaneously, the exposure time was 3-5 hours. The volume of pumped air was 16.0±0.1 m³/h, the height of the filter holder was not more than 10 m above the water edge in the headwind. Aerosols were not collected in the rain, and the sampler was not visibly sprayed. During the selection, the following meteorological parameters were controlled: wind direction and speed, air temperature, humidity, pressure, cloud cover (Syroeshkin et al. 2005).

For the elemental analysis, filters were packaged in a special snap-on polypropylene bags. After being delivered to the laboratory, the filters were incubated in Teflon bombs in 10 ml of aqua regia for 1 day. The samples were mineral-

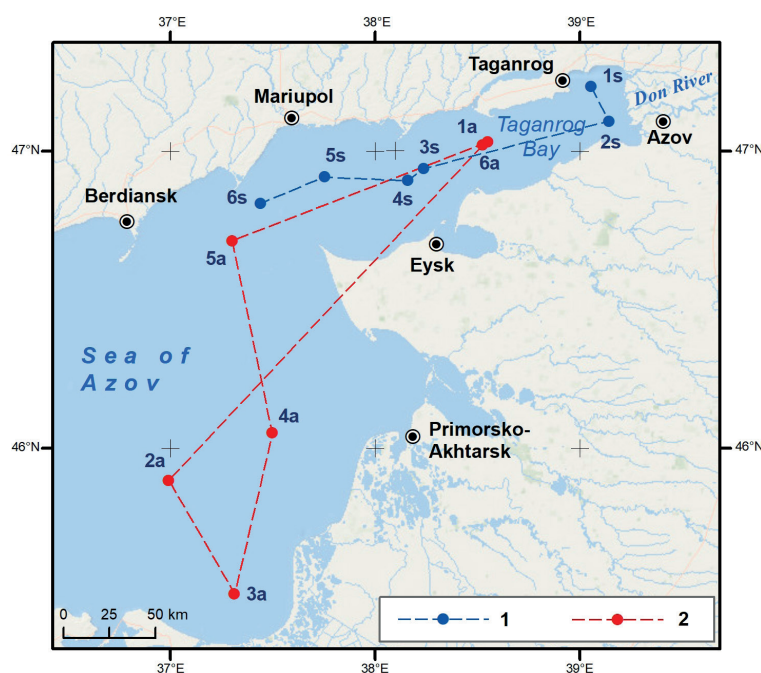


Fig. 1. Aerosol filter change points in the expedition Azov-2006: 1 – July, 2 – September – October

ized under pressure in an MDS2000 microwave oven in the following mode: 2 min. 20 sec – at 80% power, 5 min. – at 100% power. In all experiments, processing and subsequent analysis of the control filter were carried out.

The concentrations of HM in aerosol samples were determined using a SpectrAA-800 atomic absorption spectrometer with electrothermal atomization and the Zeeman effect according to the Varian protocol with modifications according to the results of international intercalibration with the IAEA MEL laboratory (Coquery et al. 2001; Kolesnikov 2005). In parallel, an analysis of 3-5 samples was carried out. The content of elements in the reference sample, see Appendix (Table 2). In all series of measurements, the background content of elements in the AFA control filters was taken into account. The volume of air pumped through the filters allowed the elements to accumulate in an amount significantly exceeding the background content. The average relative error in determining parallel samples did not exceed 20% with a confidence level of 0.95 (Syroeshkin et al. 2005).

The size spectrum of aerosol particles was not studied. However, according to the published data, it is possible to assume the size of aerosol matter generated by the sea surface. The amount of aerosol particles in the drive layer of air sharply increases at winds of about 7-10 m/s. This is due to the emergence of a direct wind failure of water droplets from the ridges of sea waves. This mechanism was noted as one of the first. O'Dowd in the article "Marine aerosol production: A review of the current knowledge" gives a graph of the dependence of the generation of the aerosol substance on the wind speeds for the particles of Aitken and for particles from 10 to 100 nm (O'Dowd et al. 2007). Process of destruction of the air bubbles on the surface of the sea is the most important for the generation of marine aerosol on a global scale producing two types of droplets of film (0.9 microns) and reactive (2 – 2.5 microns) (Syroeshkin et al. 2005; Syroeshkin et al. 2006; Syroeshkin et al. 2014).

RESULTS AND DISCUSSION

To determine the genesis of aerosol particles, a method was used based on their dispersed composition and element content normalized to Al content. The test showed mainly marine origin of the aerosol collected during the studies (Kole-

nikov et al. 2005; Syroeshkin et al. 2006; Syroeshkin 2005).

It is known that heavy metals can be found in natural waters in dissolved and suspended forms and have both natural and anthropogenic origin. A significant part of the suspended forms of HM entering the seas with river runoff is deposited on the river-sea geochemical barrier. The suspended matter remaining in the water column tends to be distributed at the water-bottom (sedimentation process) and water-air (particle flotation) interfaces. Marine aerosol formed from the surface microlayer of the sea inherits its chemical composition. It can include both sea salts and solid microparticles of various origin.

In most cases, the concentration of elements in sea waters is significantly lower than in river waters, where up to 75% of Fe, Mn, Ni, Cu are transported in conjunction with organic substances. Fe, Al, Mn, Ni, and Cu migrate in river waters in forms of colloids, simple and complex ions with a positive and negative charge. The river-sea barrier zone acts as a trap for the most substances (Gordeev 1983).

The main source of pollutants for the Sea of Azov is the runoff of large and small rivers: Don, Kuban, Mius, Eya, Beisug, Kagalnik, etc. (Mikhailenko et al. 2018). The catchment area of the Sea of Azov is about 570 000 km², with the Don and Kuban River catchments account for about 85% of the total (Matishov et al. 2002). The ratio of dissolved and suspended forms of HM at the marine edge of the Don River delta is different. For Fe, Mn, Cr, Pb, the predominance of suspended forms is noted. For Zn, Ni, Cu, and Cd, dissolved forms are prevailing. The flows of metals in the lower reaches of the Don River are largely determined by the influence of the city of Rostov-on-Don. Flows of dissolved and suspended forms of Ni, Cu, Zn, Cd and other HMs significantly increase downstream the city (Tkachenko et al. 2017). As shown below, this also affects the chemical composition of aerosols, especially in the mouth area of the Don River.

Spatial distribution of Heavy Metals and Al in marine aerosols

Iron. The Fe distribution is characterized by the presence of two regions with elevated elemental abundances (Fig. 2). Concentration increases from the open central part of the sea towards the northern and northeastern parts, especially sharply in the Taganrog Bay. On average, the concentration of

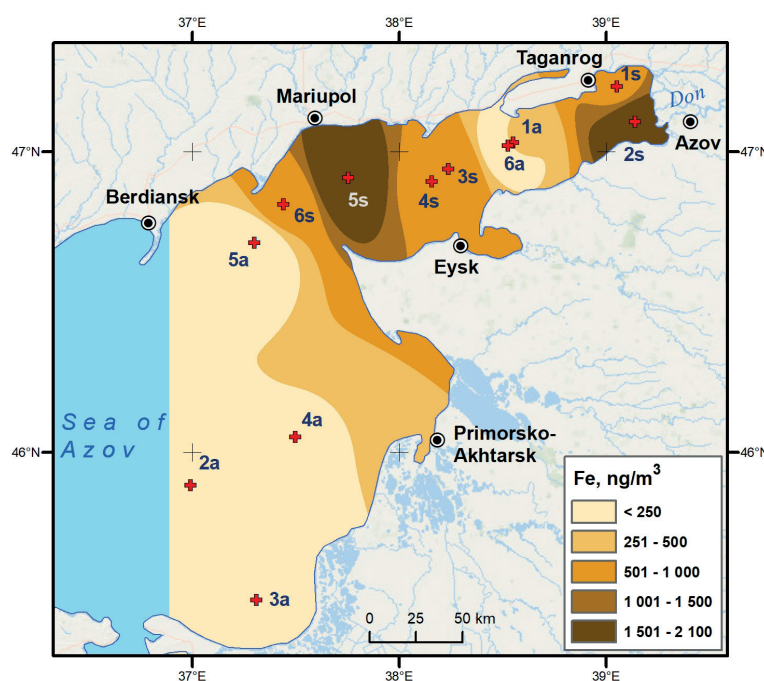


Fig. 2. Distribution of Fe in marine aerosols

Fe in the open sea is 200-1000 ng/m³. The gulf zone is marked by Fe values of about 1800-2000 ng/m³, which is an order of magnitude higher than the average concentration over the entire water area.

Perhaps this fact is explained by the presence of a dynamic geochemical barrier in the mixing zone of fresh and salt waters, the stirring up of bottom sediments and the lifting of suspended particles to the sea surface, where they can be captured in marine aerosol during wind-wave disruption and other processes of formation of marine aerosol. The zone of the northern coast also stands out, in the area of Mariupol, Fe is about 1800 ng / m³, which can be associated with the technogenic influence of the city. Pollutants can also come from the precipitation, as well as from the coastal abrasion, which provides the terrigenous material (Mikhailenko 2018).

Aluminum. The average concentration of Al in marine aerosols in most of the water area is 20–50 ng / m³ (Fig. 3). It rises up to 90-100 ng / m³ at the northern coast in the region of Mariupol, and even higher up to 200 ng / m³ in the Don River mouth area and the Taganrog Bay. This is an order of magnitude higher than the average concentration over the sea. Probably, the maximum in the Taganrog Bay can be explained by the secondary mobilization of aluminosilicate particles and their lift to the surface due to the turbulent mixing and flotation processes. Aerosol particles are enriched with Al, since their main source is the sea surface.

The maximum of Al in the area of Mariupol is less pronounced than for the most part of chemical elements, which indicates a low Al content in wastewaters.

Lead. The distribution of Pb in the marine aerosol is characterized by a maximum content at the mouth of the Don River, where it reaches 30 ng / m³. Moving towards the sea, the Pb content at first sharply (5 times), and then gradually decreases (Fig. 4). The high content of Pb in the aerosol of the Taganrog Bay may be due to the anthropogenic impact of Taganrog, which is an industrial city, port and center of ferrous metallurgy.

Cadmium. The average Cd value in marine aerosols over the Sea of Azov is about 0.4 – 0.6 ng / m³. Its content increases up to 2.2 ng / m³ in the mouth of the Don River and Taganrog Bay. The concentration of Cd reaches maximum values up to 2.8 ng / m³ in the north-western part of the sea nearby Ukrainian town of Mariupol (Fig. 5). Since the greatest values are comparable and located close to the industrial centers of the northern coast of the sea, it can be assumed that the supplier of Cd is mainly atmospheric emissions and wastewater from industrial cities.

Zinc. In the open part of the Sea of Azov, the Zn content in aerosol particles is from 10 to 60 ng / m³ (Fig. 6). For the Zn distribution, as for Cd, 2 peaks were noted – in the area of Mariupol (100-110 ng / m³) and in the mouth of the Don River. The second maximum is more contrasting, the values here are 200-280 ng / m³. It is caused by water pollution in the lower reaches of the

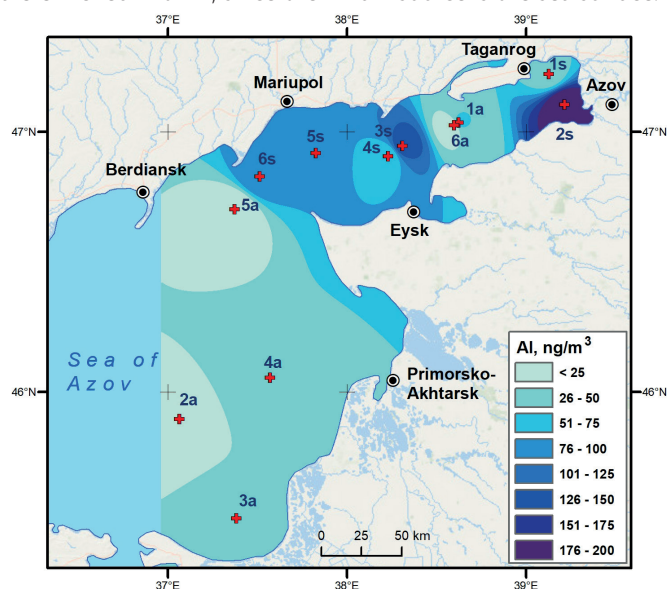


Fig. 3. Distribution of Al in marine aerosols

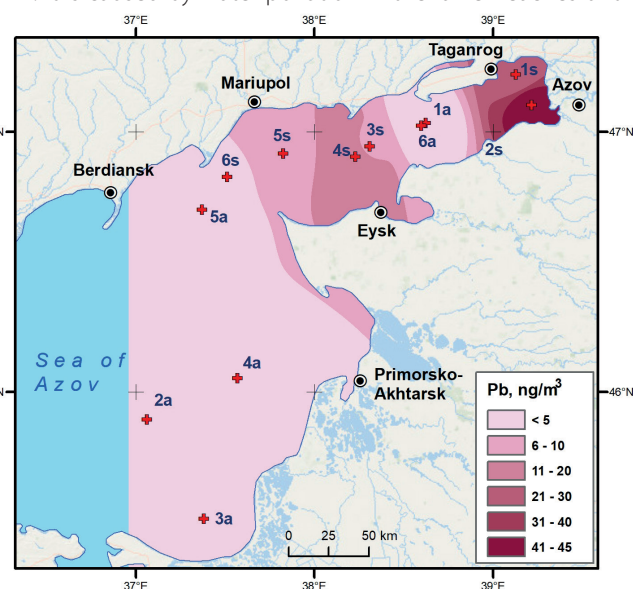


Fig. 4. Distribution of Pb in marine aerosols

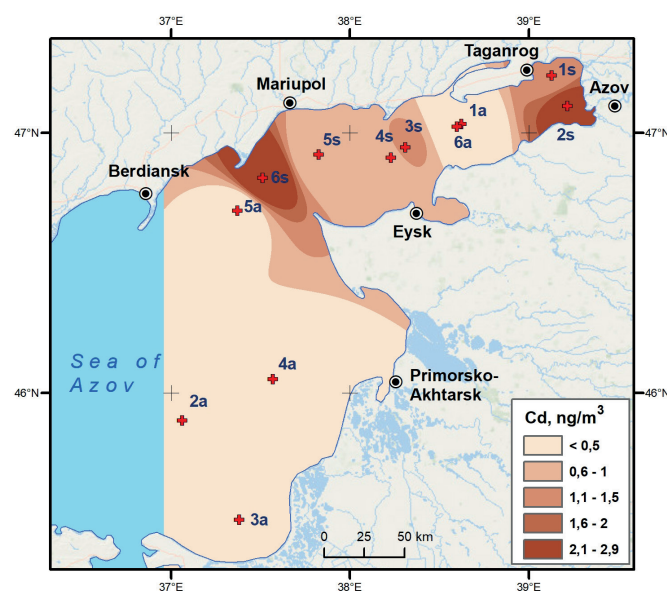


Fig. 5. Distribution of Cd in marine aerosols

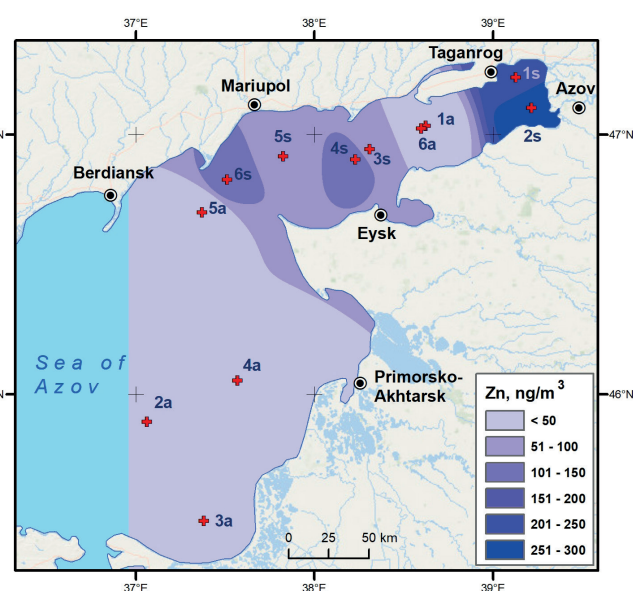


Fig. 6. Distribution of Zn in marine aerosols

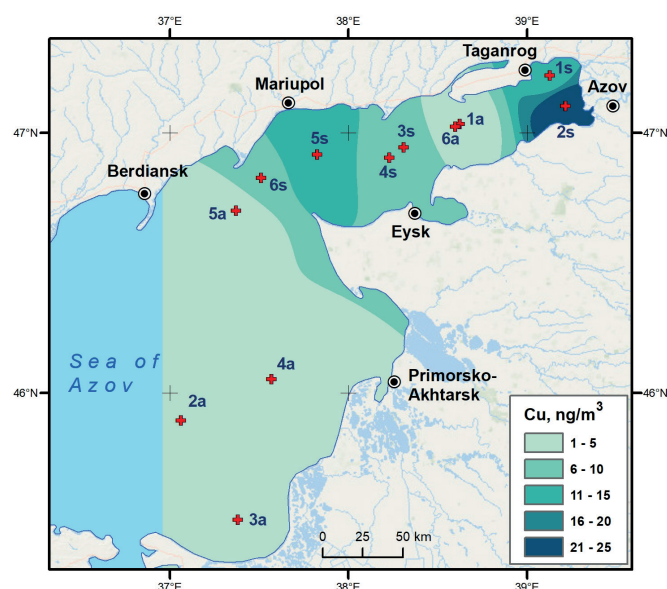


Fig. 7. Distribution of Cd in marine aerosols

river by wastewaters of Rostov-on-Don and Azov town, which is noted by many authors (Tkachenko et al. 2017; Bufetova et al. 2019; and others).

Copper. The average Cu content in the open part of the Sea of Azov is 2–8 ng / m³. The Cu concentration increases as it approaches the coast of Ukraine, reaching 12–16 ng / m³ in the area of Mariupol (Fig. 7). Taganrog Bay is a zone of high Cu content in marine aerosol. Here, the concentration increases to 20–23 ng / m³, which can be attributed to the influence of the city of Taganrog, as well as the barrier zone of mixing of salt waters of the Sea of Azov and fresh water of the Don River, which acts as the main source of Cu for the adjusting water area (Bufetova et al. 2019).

Cromium. The Cr distribution in the marine aerosol (Fig. 8) is characterized by a slow increase from the southern part of the open sea, where it is 1–5 ng / m³ to the northern (15 ng / m³ in the region of Mariupol) and the northeastern part up to the entrance to the Taganrog Bay, where it reaches 18 ng / m³. This is consistent with trends in concentrations of the most HMs. High contents are confined to industrial centers on the north and north-east coast of the Sea of Azov (Mariupol, Taganrog), as well as to the water area of the Taganrog Bay.

Thus, for most of the heavy metals, the concentrations increase as they move from the open part of the sea towards the northern coast and the mouth of the Don River, where under the influence of industrial centers and the geochemical river-sea barrier, local maximums of values are associated with increase in anthropogenic load. Maximum contents of Fe, Cr, and Cd are confined to the mouth part of the Don River, and the city of Mariupol. For Pb, Zn and Cu, the main maximum content in the aerosol is observed in the eastern part of Taganrog Bay and the mouth of the Don River.

A large role in the pollution of the Sea of Azov belongs to the cities located on the coast and in the Don River Delta: Azov, Taganrog, Yeysk, Primorsko-Akhtarsk, Temryuk – due to the discharge of insufficiently purified “conditionally clean” water from enterprises directly into water bodies and streams (Khovansky et al. 1990). It is also worth noting the contribution of ports, shipping, landfills and dumping.

Taganrog is one of the leading industrial centers on the coast of the Sea of Azov, in which industrial enterprises are located: car assembly enterprises (TagAZ), steel manufacturing, pipe production (TagMet), energy and heating boilers, repair and reconstruction of ships, aircraft, etc. There are 51 organizations that have emissions of harmful substances into the atmosphere. The general indicators of pollutant emissions into the atmosphere of Taganrog range from 3.6% to 5.1% of the pollutant emissions of the entire region (Nechipurenko et al. 2019).

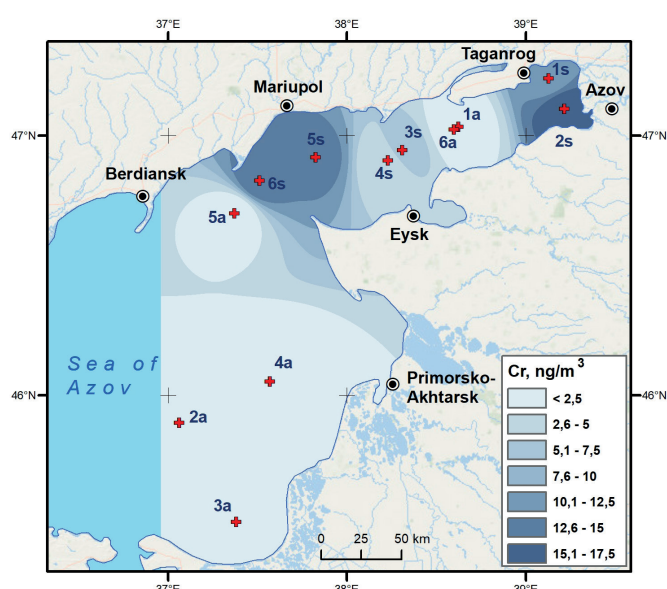


Fig. 8. Distribution of Cr in marine aerosols

Mariupol is one of the most disadvantaged cities in Ukraine in terms of air pollution in Pb, Zn, Cu, Ni, Mn, Cr and Cd compounds. Two large metallurgical enterprises are located on the territory of the city, which are powerful sources of atmospheric emissions (Grishchenko et al. 2018; Voityuk et al. 2018). Industrial dust includes toxic oxides of Fe, Si, Al, Mg, Mn, Cr, etc. (Monin et al. 2012).

The behavior and distribution of trace elements is influenced by the mixing of fresh and salt waters of the rivers and the Sea of Azov, where the great majority (70–95%) of river suspended matter precipitates at the river-sea geochemical barrier, capturing pollutants brought by the river, including heavy metals (Mikhailenko et al. 2018). Shallow-water Taganrog Bay also belongs to the such zones. Here HM content in the marine aerosol rises sharply due to the enrichment SSM with pollutants. Concentrations of HM in the water of the Sea of Azov in places exceed MPC, especially in the Taganrog Bay. The sum of multiples of the MPC TM for the Taganrog Bay in 2005 amounted to 4.7 MPC, while for the open sea it is less (3.7 MPC), which is consistent with the data obtained during the study of the composition of the sea aerosol of the Sea of Azov (Klenkin et al. 2009).

Based on the comparison with the data from other regions, the Sea of Azov can be attributed to the group of seas with the medium or high HM content in marine aerosol. The research of aerosol particles was carried out: 2002–2007 in Black Sea (Yablokov et al. 2002; Lapshin et al. 2003; Syroeshkin et al. 2004; Syroeshkin et al. 2014; Syroeshkin et al. 2006), 2005–2008 in the Kara, Barents and White Seas (Syroeshkin et al. 2010), 2001–2004 in the Baltic Sea (Syroeshkin et al. 2004), 2006–2008 in the Atlantic Ocean (Syroeshkin et al. 2012), 2007–2009 in the Arctic Ocean (Lapshin et al. 2010). The concentration levels of Ni and Cr are shown in Fig. 9 A. It is clearly seen that aerosols of the Sea of Azov contain these metals in low concentrations 10–100 ng / m³ comparable with the Arctic seas. The concentration range of Cd and Mn (Fig. 9 B) is 2 orders of magnitude with the lowest levels in the Arctic Ocean, and the highest values in the Baltic, Azov and Mediterranean Seas. The content of Pb in the marine aerosols (Fig. 9 C) varies from 0.1 – 10 ng / m³ in the group of subjects with a relatively low anthropogenic impact (White, Barents, and Kara seas, Arctic and Atlantic oceans), to 10–100 ng / m³ in the group of southern seas (Black, Azov, Mediterranean, and Baltic seas), subjected to the strong anthropogenic pressure.

In general, the HM content in aerosol microparticles is determined by a number of factors. The first group includes the natural factors, primarily climate related and associated with the geographical position of seas, such as precipitation, evaporation, water salinity, etc. The second group is associated with the hu-

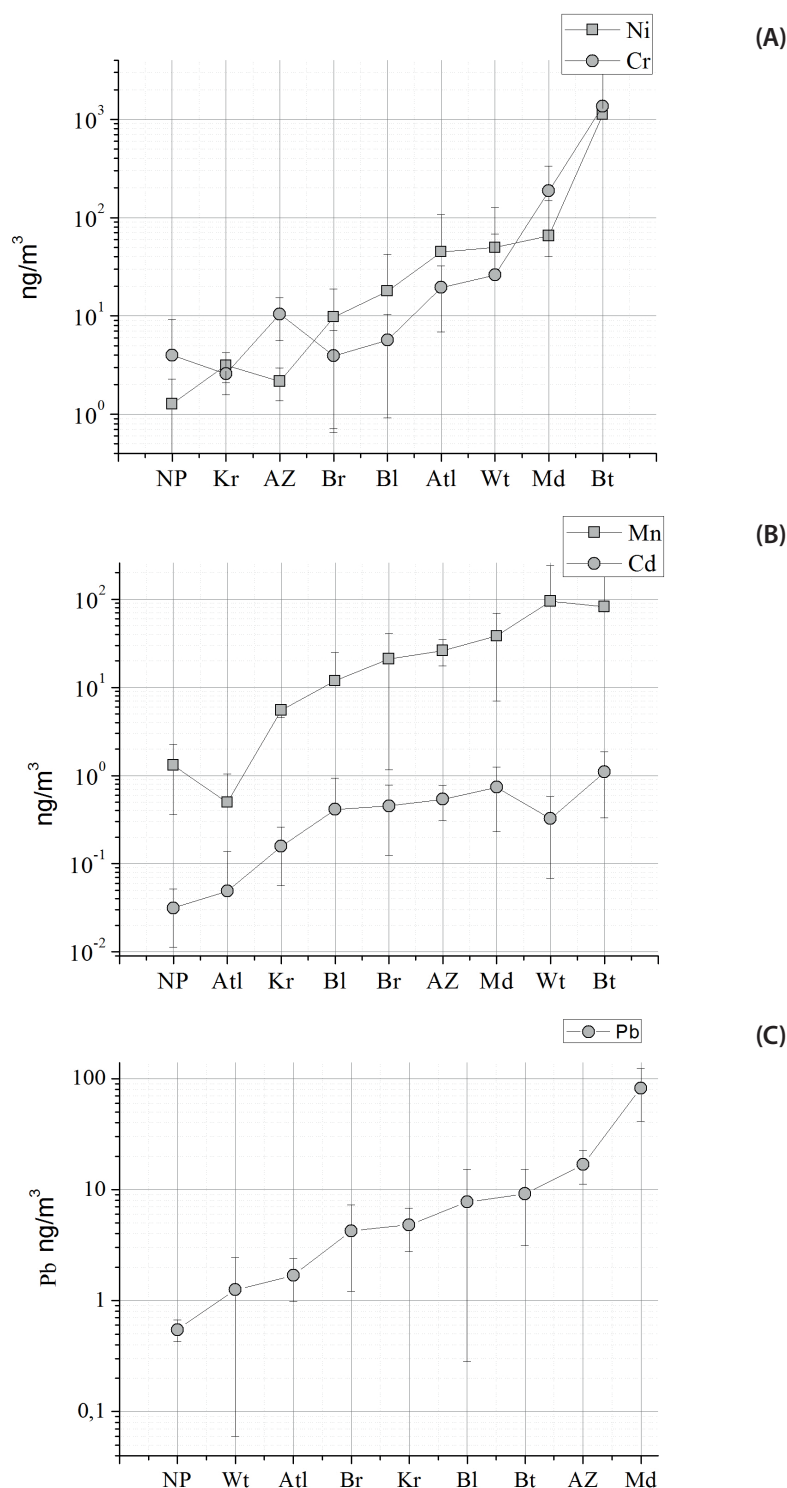


Fig. 9. Concentration of Ni and Cr (A), Mn and Cd (B), Pb (C) in marine aerosols of different areas: NP- North Pole; Wt- White Sea; Atl- South Atlantic; Br – the Barents Sea; Kr – Kara Sea; Bl – Black Sea; Bt – the Baltic Sea; Az.- Sea of Azov; Md – the Mediterranean Sea

man economic activity. The Mediterranean Sea, the Black Sea, and in particular the shallow enclosed Sea of Azov are subjected to the high anthropogenic pressure, which affect the content of various elements in the sea water, and therefore in the sea surface microlayers and marine aerosols. The natural distribution of elements plays a subordinate role here. It is worth considering that it is almost impossible to determine the specific pollution sources while studying aerosol particles in the vast water areas.

CONCLUSIONS

1. The spatial distribution of heavy metals in the marine aerosol of the Sea of Azov is determined by the influence of the river-sea geochemical barrier zone in the Taganrog Bay and

the anthropogenic impact of the coastal industrial cities. HM concentrations increase from the open part of the sea towards the northern coast and the mouth of the Don River.

2. The maximum content of HM in marine aerosol was observed in the mouth area of the Don River in the eastern part of the Taganrog Bay, which can be associated with the anthropogenic impact of the cities of Rostov-on-Don, Azov and Taganrog. High contents of Fe, Cr, and Cd were also found in the western part of the Taganrog Bay, due to the technogenic impact of the city of Mariupol.

3. The Sea of Azov can be attributed to the group of seas with the moderate or high HM content in marine aerosol in comparison with the data from other regions. ■

REFERENCES

- Akinori I., Myriokefalitakis S., Kanakidou M., Mahowald N. M., et al. (2019). Pyrogenic iron: The missing link to high iron solubility in aerosols. *Science Advances*, 5(5), 7671, DOI: 10.1126/sciadv.aau7671.
- Aryasree S, Nair PR, Girach IA, Jacob S. (2015). Winter time chemical characteristics of aerosols over the Bay of Bengal: continental influence. *Environmental Science and Pollution Research*, 22(19), 14901-14918, DOI: 10.1007/s11356-015-4700-7.
- Brooks S.D., Thornton D.C. (2018). Marine Aerosols and Clouds. *Annual Review of Marine Science*, 3(10), 289-313, DOI: 10.1146/annurev-marine-121916-063148.
- Buseck P. R., Posfai M. (1999) Airborne minerals and related aerosol particles: Effects on climate and the environment. *Proceedings of the National Academy of Sciences*, 96(7), 3372–3379, DOI:10.1073/pnas.96.7.3372.
- Chandrakar K.K., Cantrell W., Chang K., Ciochetto D., et al. (2016). Aerosol indirect effect from turbulence-induced broadening of cloud-droplet size distributions. *Proceedings of the National Academy of Sciences USA*, 113(50), 14243-14248, DOI: 10.1175/JAS-D-18-0006.1.
- Coquery M., Villeneuve J.P. (2001). Final report on the split sampling exercises and quality assurance activities. EU Project № ENV RM S9602, Amsterdam, ICWC, 51.
- Csavina J., Field J., Taylor M.P., Gao S., et al. (2012). A Review on the Importance of Metals and Metalloids in Atmospheric Dust and Aerosol from Mining Operations. *Science of the Total Environment*, 433, 58-73, DOI: 10.1016/j.scitotenv.2012.06.013.
- Fleming L.E., Bean J.A., Kirkpatrick B., Cheng Y.S., et al. (2009). Exposure and effect assessment of aerosolized red tide toxins (brevetoxins) and asthma. *Environmental Health Perspectives*, 117(7), 1095-1100. DOI: 10.1289/ehp.0900673.
- Furness R.W. (2017). *Heavy Metals in the Marine Environment*. CRC press.
- Garrett W.D. (1965). Collection of slick-forming materials from the sea surface. // *Limnol. Oceanog*, 10, 602-605.
- Georgoulas A.K., Alexandri G., Kourtidis K.A., Lelieveld J., et al. (2016). Spatiotemporal variability and contribution of different aerosol types to the Aerosol Optical Depth over the Eastern Mediterranean. *Atmospheric Chemistry And Physics*, 16(21), 13853-13884, DOI: 10.5194/acp-16-13853-2016.
- Golubeva N.I., Burtseva L.V., Gromov S.A. (2011). Heavy Metals in Atmospheric Air in the Kara Sea Water Area in September–October. *Oceanology*, 58, 870-878. DOI: doi.org/10.1134/S000143701806005X.
- Goncharuk V.V., Lapshin V.B., Chichaeva M.A., Samsoni-Todorov A.O., et al. (2012). Heavy metals, aluminum and arsenic in aerosols of the oceans. *Chemistry and Water Technology*, 34(1), 1-15, DOI: 10.3103/S1063455X12010018.
- Gordeev V.V. (1983). *River runoff into the ocean and features of its geochemistry*. Moscow: Nauka.
- Grebennikova T.V., Syroeshkin A.V., Chichaeva M.A., Esper S.A., Lvov D.K. (2017). Natural foci of influenza A in the western Arctic. *Voprosy Virusologii*, 62(1), 11-17, DOI: 10.18821/0507-4088-2017-62-1-11-17.
- Grishchenko S.V., Grishchenko I.S., Kostenko V.S., Basenko I.N. et al. (2018). Hygienic assessment of atmospheric air pollution of populated areas of Donbass by heavy metals. *Bulletin of Hygiene and Epidemiology*, 22(1), 11-15.
- Izhar S., Goel A., Chakraborty A., Gupta T. Annual trends in occurrence of submicron particles in ambient air and health risk posed by particle bound metals. (2016). *Chemosphere*, 146, 582-590, DOI: 10.1016/j.chemosphere.2015.12.039.
- Jordi A., Basterretxea G., Tovar-Sánchez A., Alastuey A., Querol X. (2012). Copper aerosols inhibit phytoplankton growth in the Mediterranean Sea. *Proceedings of the National Academy of Sciences USA*, 109(52), 21246-21249, DOI: 10.1073/pnas.1207567110.
- Kirkpatrick B., Fleming L.E., Bean J.A., Nierenberg K., et al. (2011). Aerosolized Red Tide Toxins (Brevetoxins) and Asthma: Continued health effects after 1 hour beach exposure. *Harmful Algae*, 10(2), 138-143, DOI:10.1016/j.hal.2010.08.005.
- Kolesnikov M.V., Matveeva I.S., Lapshin V.B., Pletenev S.S., et al. (2005). Heavy metals in marine aerosols of the Russian part of the Black sea. *Oceanology*, 45(1), 102-111.
- Lang-Yona N., Lehahn Y., Herut B., Burshtein N., Rudich Y.. (2014) Marine aerosol as a possible source for endotoxins in coastal areas. *Science of the Total Environment*, 499, 311-8, DOI: 10.1016/j.scitotenv.2014.08.054.
- Li J., Han Z., Yao X., Xie Z., Tan S. (2019). The distributions and direct radiative effects of marine aerosols over East Asia in springtime. *Sci Total Environ*. 651(2), 1913–1925, DOI: 10.1016/j.scitotenv.2018.09.368.
- Li S., Du L., Tsona N.T., Wang W. (2018). The interaction of trace heavy metal with lipid monolayer in the sea surface microlayer. *Chemosphere*. 196, 323-330, DOI: 10.1016/j.chemosphere.2017.12.157.
- Liu Y., Li S., Sun C., Qi M., et al. (2018) Pollution Level and Health Risk Assessment of PM_{2.5}-Bound Metals in Baoding City Before and After the Heating Period. *International Journal of Environmental Research and Public Health*, 15(10), 2286. DOI: 10.3390/ijerph15102286.
- Mahowald N.M., Hamilton D.S., Mackey K.R., Moore J.K., et al. (2018). Aerosol trace metal leaching and impacts on marine microorganisms. *Nature Communications*, 9(1), 2614, DOI: 10.1038/s41467-018-04970-7.
- Marín-Beltrán I., Logue J.B., Andersson A.F., Peters F. (2019). Atmospheric Deposition Impact on Bacterial Community Composition in the NW Mediterranean. *Frontiers in Microbiology*, 10(858), 1-14, DOI: 10.3389/fmicb.2019.00858.
- O'Dowd C.D., Jimenez J.L., Bahreini R., Flagan R.C., et al. (2002). Marine aerosol formation from biogenic iodine emissions. *Nature*, 417 (6889), 597-598. DOI: 10.1038/nature00775.
- O'Dowd C.D., de Leeuw G. (2007). Marine aerosol production: a review of the current knowledge. *Philosophical transactions. Series A, Mathematical, physical, and engineering sciences*, 365(1856), 1753-1774, DOI: 10.1098/rsta.2007.2043.
- Patocka J., Nepovimova E., Wu Q., Kuca K. (2018). Palytoxin congeners. *Archives of Toxicology*, 92(1), 143-156, DOI: 10.1007/s00204-017-2105-8.
- Paytan A., Mackey K.R.M., Chen Y., Lima I.D., et al.(2009). Toxicity of atmospheric aerosols on marine phytoplankton. *Proceedings of the National Academy of Sciences USA*, 106(12), 4601-4605, DOI: 10.1073/pnas.0811486106.
- Qureshi A, MacLeod M, Hungerbühler K. (2009). Modeling aerosol suspension from soils and oceans as sources of micropollutants to air. *Chemosphere*, 77(4), 495-500, DOI: 10.1016/j.chemosphere.2009.07.051.
- Rädlein N., Heumann K.G. (2006). Trace Analysis of Heavy Metals in Aerosols Over the Atlantic Ocean from Antarctica to Europe. *International Journal of Environmental Analytical Chemistry*, 48, 127-150.
- Rastelli E., Corinaldesi C., Dell'Anno A., Lo Martire M., et al. (2017). Transfer of labile organic matter and microbes from the ocean surface to the marine aerosol: an experimental approach. *Scientific Reports*, 7, 11475, DOI: 10.1038/s41598-017-10563-z.
- Sajeev P., Randall V.M., Van Donkelaar A., et al. (2014). Global Chemical Composition of Ambient Fine Particulate Matter for Exposure Assessment *Environmental Science & Technology*, 48(22), 13060-13068, DOI: 10.1021/es502965b.
- Salomons W., Bayne B. L., Duursma E.K., Förstner U. (1988). *Pollution of the North Sea*. Springer, Berlin, Heidelberg, 300-347.

- Sánchez-Rodas D., Alsioufi, L., Sánchez de la Campa A.M., González-Castanedo Y. (2017). Antimony speciation as geochemical tracer for anthropogenic emissions of atmospheric particulate matter, *Journal of Hazardous Materials*, 324(B), 213-220, DOI: 10.1016/j.jhazmat.2016.10.051.
- Song S.K., Shon Z.H., Choi Y.N., Son Y.B., et al. (2019). Global trend analysis in primary and secondary production of marine aerosol and aerosol optical depth during 2000–2015. *Chemosphere*, 224, 417-427, DOI: 10.1016/j.chemosphere.2019.02.152.
- Sullivan R.C., Levy R.C., da Silva A.M., Developing and diagnosing climate change indicators of regional aerosol optical properties. *Scientific Reports*, 7(1), 1-13, DOI: 10.1038/s41598-017-18402-x.
- Syroeshkin A.V., Chichaeva M.A. (2010). Concentration level of heavy metals within marine aerosols of Western Arctic seas, Southern Atlantic and Arctic ocean. *Trace elements in medicine*, 11(2), 15.
- Takata K., Saito K., Yasunari T. (2009). Changes in the Asian monsoon climate during 1700–1850 induced by preindustrial cultivation. *Proceedings of the National Academy of Sciences USA*, 106(24), 9586-9589, DOI: 10.1073/pnas.0807346106.
- Tuohy A., Bertler N., Neff P., Edwards R., Emanuelsson D., et al. (2015). Transport and deposition of heavy metals in the Ross Sea Region, Antarctica. *Journal of Geophysical Research: Atmospheres*, 120, 996-11,011, DOI: 10.1002/2015JD023293.
- Van Dolah F.M. (2000). Marine algal toxins: origins, health effects, and their increased occurrence. *Environmental Health Perspectives*, 108(1), 133-41, DOI: 10.1289/ehp.00108s1133.
- Von Glasow R., Jickells T.D., Baklanov A., Carmichael G.R., et al. (2013). Megacities and Large Urban Agglomerations in the Coastal Zone: Interactions Between Atmosphere, Land, and Marine Ecosystems. *AMBIO A Journal of the Human Environment*, 42(1), 13-28, DOI: 10.1007/s13280-012-0343-9.
- Vinogradova A.A., Ivanova Yu.A. (2017). The transfer of air masses and pollution to the Arctic islands of Russia (1986–2016): long-term, interannual and seasonal variations. *Geophysical processes and biosphere*. 16(4), 5-20, DOI: 10.21455/GPB2017.4-1.
- Vinogradova A.A., Kotova E.I. (2019). Heavy metal pollution of the northern seas of Russia: flow from the atmosphere and river runoff. *Geophysical processes and biosphere*. 18 (1), 22-32, DOI: 10.21455/GPB2019.1-3.
- Voityuk Yu. Yu., Kuraeva I.V., Loktionova E.P. (2018). Sources of heavy metal pollution in the territories of industrial agglomerations of ferrous metallurgy. *Materials of the VI International Scientific Conference. Modern problems of landscape science and geoecology (on the 100th anniversary of the birth of Professor V.A. Dementiev)*. Ed. A.N. Witchenko.
- Walsh J.J., Lenes J.M., Weisberg R.H., Zheng L., et al. (2017). More surprises in the global greenhouse: Human health impacts from recent toxicmarine aerosol formations, due to centennial alterations of world-wide coastal food webs. *Marine Pollution Bulletin*, 116(1-2), 9-40, DOI: 10.1016/j.marpolbul.2016.12.053.
- Wang X., He S., Chen, Zhang Y, et al. (2018). Spatiotemporal Characteristics and Health Risk Assessment of Heavy Metals in PM_{2.5} in Zhejiang Province. *International Journal of environmental research and public health*, 15(4), 583, DOI: 10.3390/ijerph15040583.
- Witt M., Baker A. R., Jickells T. D. (2006). Atmospheric trace metals over the Atlantic and South Indian Oceans: Investigation of metal concentrations and lead isotope ratios in coastal and remote marine aerosols. *Atmospheric Environment*, 40, 5435-5451, DOI: 10.1016/j.atmosenv.2006.04.041.
- Zatsepa S.N., Lapshin V.B., Oradovsky S.G., Simonov A.I. A device for sampling water from a surface microlayer. Copyright certificate No. 1375974 of December 3, 1985.
- Klyonkin A.A., Korablina I.V., Korpakova I.G. (2007). Description of the current level of pollution of water and bottom sediments of the Sea of Azov by heavy metals. *Ecology and industry of Russia*, 5, 30-33.
- Kondratiev K. Ya., Moskalenko N.I., Pozdnyakov D.V. (1983). *Atmospheric aerosol*. Leningrad: Hydrometeoizdat.
- Lapshin V.B., Chichaeva M.A., Matveeva I.S., Chichaev A.N., et al. (2010). Heavy metals, aluminum and arsenic in aerosols of the Atlantic, Arctic Oceans and European seas of Russia. *Investigated in Russia*, 34, 393-403.
- Lapshin V.B., Yablokov M.Yu., Matveeva I.S., et al. (2002). Are marine aerosols toxic? *Investigated in Russia*, 118, 1302-1316.
- Lukashin V.N., Klyuvitkin A.A., Bobrov V.A., Dara O.M., Shevchenko V.P. (2018). The chemical composition of the aerosols of the North Atlantic. *Oceanology* 58(5), 781-791, DOI: 10.1134/S0030157418050052.
- Maslennikova A.V., Shevchenko V.P., Belogub E.V., Maslov A.V., Blinov I.A. (2018). Sedimentary material from the drifting ices of the Ermak Plateau and the Fram Strait: new data on spore-pollen spectra, mineralogy, and geochemistry. *Mineralogy*, 4(4), 102-118.
- Matishov G.G. (2002). *Ecosystem studies of the Sea of Azov and the coast*. Volume 4, Apatity: Publ. KSC RAS.
- Mikhailenko A.V., Fedorov Yu.A., Dotsenko I.V. (2018). Heavy metals in the components of the landscape of the Sea of Azov. *Rastov-on-Don: Southern Federal University*.
- Monin V.L. (2012). Monitoring of technogenic air pollution in the city of Mariupol. *Bulletin of the Azov State Technical University*, 24, 327-334.
- Nechipurenko V.V., Merinova Yu.Yu. (2019). Industrial complex as a factor in the pollution of urban systems of the Rostov region. *Collection of scientific papers based on the materials of the 9th International Scientific and Practical Conference*. Edited by E.I. Tikhomirova. 81-85.
- Savenko V.S. The geochemistry of ocean aerosol. (1998). *Bulletin of Moscow University. ser. 5. Geography*, 1, 28-32.
- Smirnov A.N., Lapshin V.B., Balyshv A.V., Lebedev I.M., Syroeshkin A.V. (2004). Supranadmolecular complexes of water. *Investigated in Russia*, 38, 413-421.
- Smirnov A.N., Lapshin V.B., Balyshv A.V., Popov P.I., Lebedev I.M., Syroeshkin A.V. (2003). Cooperative anisotropic motion of the dispersed phase in aqueous solutions. *Investigated in Russia*, 39, 422-425.
- Syroeshkin A.V., Popov P.I. (2005). «Marine Aerosols. Toxicity, research methods», Moscow: RUDN.
- Syroeshkin A.V., Smirnov A.N., Goncharuk V.V., Uspenskaya E.V., et al. (2006). Water as a heterogeneous structure. *Investigated in Russia*, 88, 843-854.
- Syroeshkin A.V., Chichaeva M.A., Matveeva I.S. (2014). Repeatability of one-to-one relationships between concentrations of heavy metals and dispersion of marine aerosol (as exemplified by two expeditionary studies on the Black Sea. *Heliogeophysical studies*, 10(10), 113-127.
- Tkachenko A.N., Tkachenko O.V., Lychagin M.Yu., Kasimov N.S. (2017). Heavy metal flows in aquatic systems of the Don and Kuban deltas. *Doklady Academy of Sciences*, 474(2), 234-237.
- Khovansky A.D. (1990). *Geochemical assessment of the state of the river system of the Lower Don, Rostov-on-Don*: Publishing House of the University of Rostov.

ASSESSMENT OF THE TRENDS OF GREENHOUSE GAS EMISSION IN ETHIOPIA

Besfat D. Engdaw^{1*}

¹Bahir Dar University, Tana Sub-City, Bahir Dar, 6000, 79, Ethiopia

*Corresponding author: besflov@gmail.com

Received: November 6th, 2018 / Accepted: May 10th, 2020 / Published: July 1st, 2020

<https://DOI-10.24057/2071-9388-2018-61>

ABSTRACT. This paper assesses the trends of greenhouse gas emissions in Ethiopia. To assess the trends of greenhouse gas emissions, the paper uses quantitative data ranging from 1990–2013. This data is ascertained from United Nations Framework Convention on Climate Change Data interface. The Paper analyzed these data using descriptive methods of data analysis. Accordingly, the paper revealed that Ethiopia has shown increasing trends of emission in most sectors, except land use-land use change, and forestry. Having an average emission of 50739.73 GgCO_{2e}, land use-land use change, and forestry is the largest sector that contributes to greenhouse gas emissions in Ethiopia. The agricultural sector played the second largest role with an average emission level of 47093.63 GgCO_{2e}. Following the above two sectors, the energy sector, ranked third, has contributed an emission of 17670.13 GgCO_{2e}. Other sectors like waste, industrial, and international bunkers have contributed a trivial amount to the country's greenhouse gas emissions, with average greenhouse gas emissions of 3081.21 GgCO_{2e}, 881.21 GgCO_{2e}, and 458.65 GgCO_{2e} respectively. However, the annual emissions growth rate of the bunker sector is very high accounting for 57.53%. The industrial sector has shown a 20.05% average annual growth rate followed by land use-land use change and forestry with an annual emission growth rate of 19.76%. The energy sector and waste sector have 9.45% and 7.4% average annual growth rates. The agricultural sector has a 3.11% of average annual growth rate. The country has introduced different policy instruments. However, most of the policy instruments are not effective enough.

KEY WORDS: Greenhouse Gas emission, Carbon dioxide, Methane, Nitrous oxide, LULUCF

CITATION: Besfat D. Engdaw (2020). Assessment Of The Trends Of Greenhouse Gas Emission In Ethiopia. Geography, Environment, Sustainability, Vol.13, No 2, p. 135-146

<https://DOI-10.24057/2071-9388-2018-61>

ACKNOWLEDGMENTS: I would like to acknowledge Professor David W. Tushaus, US Ambassador's Distinguished Scholar at School of Law, Bahir Dar University and Fulbright Scholar Liaisons, for his unreserved comments, insights, and intense proofreading to further develop the manuscript. I would also like to acknowledge the anonymous reviewers for their valuable and important comments, their comments are scientifically very important to advance value of the manuscript.

Conflict of interests: The author reported that there is no conflict of interest.

INTRODUCTION

Greenhouse gases are gaseous substances that help to regulate the temperature of our planet. Without greenhouse gases, our planet would be too cold. However, rigorous recent human activity has led to an increased greenhouse gas emission in the atmosphere. This affects the natural system in which the atmosphere regulates the temperature of the earth. Due to increased greenhouse gas emissions induced by man, the planet is now getting hotter and hotter. Consequently, global warming becomes one of the major environmental challenges that the world has faced. Among the greenhouse gases, carbon dioxide, nitrous oxide, methane, and fluorinated greenhouse gases are the major ones. They have contributed more than 76% of the globally increased greenhouse effects (See 2001). The total greenhouse gas including land use-land use change and forestry increases gradually. During the 1990s, it was 22219.63mt/co_{2e}. However, toward the turn of 2000, the total greenhouse emission including land use-land use and forestry change was around 27205.08 mtco_{2e}. In the year 2013, the total greenhouse gas emission, including LULUCF, have reduced to 18739.21mt/co_{2e}. From 1990 – 2013 the average growth of world green-

house gas emissions was around 1.544% (CAIT 2017). On the other hand, the total greenhouse emission excluding land use-land use change and forestry was around 22866.8 mtco_{2e}. From 1990–2013 the average growth of world greenhouse gas emissions, excluding LULUCF, was around 2.05%. This statistical data has proved that the global greenhouse gas emissions with and without LULUCF have increased on average at 1.54 and 2.05% per year respectively (UNFCCC 2017). As a result of this, greenhouse gas emission has become a global, national and local policy issue that many countries around the world are trying to address.

Although developing countries have less contribution to global greenhouse gas emissions, they have shown increasing trends and patterns. Despite the fact that developing countries, particularly Africa, produce less anthropogenic greenhouse gas emissions, they are highly exposed and vulnerable to climate variability and climate-related events (Sarkodie and Strezov 2019). Developing countries have shown 270.66% of average growths in 2013 as compared to the 1990s net total greenhouse gas emissions. From 1990–2013, developing countries have an average growth rate of 65.6% annual greenhouse gas emissions per year (UNFCCC 2017). As a part of developing countries, Sub Saharan coun-

tries have also shown increasing trends in greenhouse gas emissions. The total greenhouse gas emission of Sub Saharan African countries was 3,867 MtCo_{2e} in 1990 and reached 4542.4 MtCo_{2e} in 2010 with an average growth of 17.5% (IEA 2012). CAIT (2017) has also revealed that the region has an average growth rate of 13.3 % in 2013 as compared to the 1990s. Therefore, Ethiopia is not an exception as there have been increased trends in greenhouse gas emissions.

There are several causes for greenhouse gas emissions, but the major causes are fossil fuel burning, forestry harvest and land-use change, agricultural activities and industrial processes. Sectors like agriculture, energy, wastes, bunker fuels, land-use change and forestry (LULUCF), and industries have been contributing immensely to greenhouse gas emissions. In developed countries, the energy sector (fossil fuel) and the industrial sector are the main sources of greenhouse gases. However, in developing nations, like Ethiopia, land-use change and the forestry (LULUCF) and the agricultural sector are the main sources of greenhouse gas emission. In Ethiopia, the agricultural sector and land-use change and forestry contributed a huge share for greenhouse gas emissions (FDREMoEF 2015; USAID 2015). Other sectors like manufacturing, industry, energy, and wastes have insignificant contributions to greenhouse gas emissions. However, in terms of average annual growth rates some sectors like industrial sectors and wastes, have shown despicable increments in their contribution to greenhouse gas emissions (USAID 2015).

This paper will contribute to the existing literature by analyzing the trends of greenhouse gas emissions in Ethiopia, examining the contributions of agricultural, land use-land use change and forestry, energy, industry, waste and bunkers fuel sectors in greenhouse gas emission. It depicts out the trends of greenhouse gas emissions in these sectors, and investigate the policy instruments and measures of greenhouse gas emissions in Ethiopia.

MATERIALS AND METHODS

A qualitative research methodology has been employed. The paper applied a qualitative research methodology because the prime goal of the paper, assessing the trends of greenhouse gas emissions, needs a descriptive research approach, which is purely qualitative. Moreover, making inferences, or association of variables, is not the objective of the paper. So the paper finds qualitative research methodology best addresses its objective. The paper is entirely de-

pendent on secondary data, which are ascertained from the UNFCCC (United Nations Framework Convention on Climate Change). The greenhouse gas emission data from UNFCCC is supposed to be the most reliable source of data as they are directly collected from concerned countries. It draws data from annex I and non-annex I countries using consistence reporting mechanisms. This paper draws Ethiopia's 24-year data of greenhouse emissions that are already found at the UNFCCC. The paper covers data ranging from 1990–2013. The paper disregards data after 2013 due to a lack of statistical data. These quantitative data are presented using graphs, diagrams, and charts.

RESULTS AND DISCUSSION

Greenhouse Gas Emissions in Ethiopia

There has been a rising trend in aggregated national greenhouse gas emissions in Ethiopia. Estimated emissions in 2013 were about 927.46% higher than in 1990, but 29.35% and 28.86% lower than the 2000 and 2010 emission respectively. Generally, the net greenhouse gas emissions, removal with LULUCF, have increased on average 28.89% per year from 1990–2013. However, after 2011 the net greenhouse gas emissions have shown decreasing trends as it was 192,336.5 GgCo_{2e}, 124,656.7GgCo_{2e}, and 120,500.6GgCo_{2e} in 2011, 2012 and 2013 respectively. (Fig. 1).

Greenhouse gas emissions estimations are very important to have informed decisions about emission reduction strategies. However, it is affected by a number of uncertainties. So, it is vital to acknowledge that the greenhouse gas emission estimates have a certain level of uncertainty that needs to be taken into account. In Ethiopia, the main activity data used to build the national inventory were gathered from official annual reports produced by the government institutions. However, the data do not include metadata showing the uncertainty levels nor do they provide the statistics needed to estimate the uncertainty of the activity data they generate. Since these institutions do not calculate the uncertainties associated with the data that they submit, it is impossible to determine the uncertainty associated with emission calculations in the national inventory. Nevertheless, the uncertainty levels resulting from the use of default factors have been computed. The uncertainty assessment of the total inventory was estimated with a total inventory uncertainty of 4.2% and trend uncertainty of 27.9% (FDREMoEF 2015).

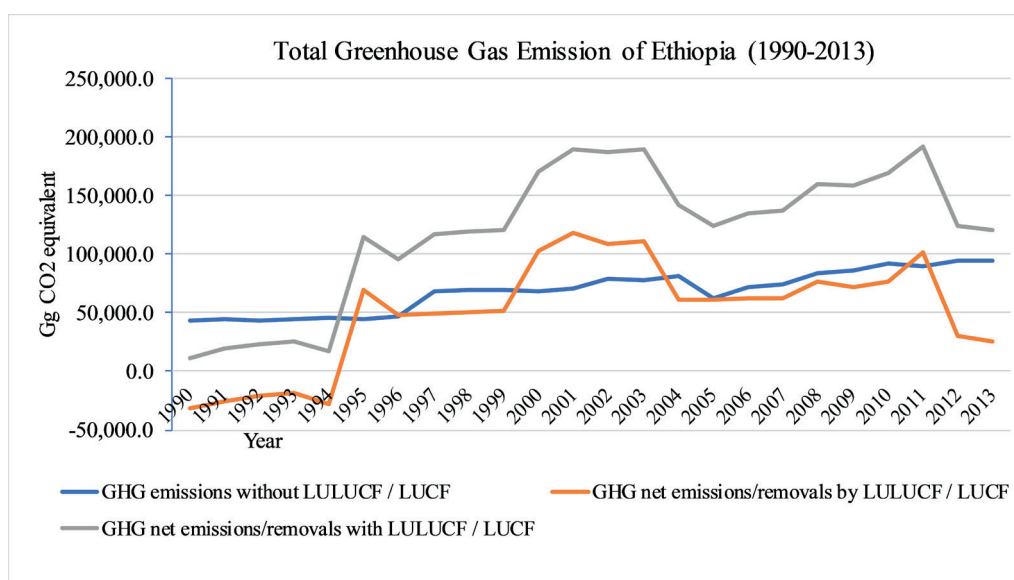


Fig. 1. Computed from UNFCCC Data Interface

Carbon dioxide

The Intergovernmental Panel on Climate Change indicated that global warming and climate change have become the world's most critical issues in recent decades, with a significant increase in carbon dioxide emissions. Natural and human activities are the causes of CO₂ emissions. However, the primary cause of CO₂ emission nowadays is attributed to human activities, particularly economic activities (IPCC 2001). It has an immense contribution to world greenhouse gas emissions. Anthropogenic factors have contributed to a 9.8% emissions growth rate from 1990–1997. This growth rate has been doubled in the subsequent years as a 20.5 % growth rate was evident from 1998–2005. However, the growth rate in carbon emission has shown little decrement from 2006–2013 as it was around 16% (CAIT 2017). This might be because of the policy measurements that were taken by the global environmental regimes.

The emission of carbon in developing countries has shown a gradual increase, though little when it is compared with the emissions of developed nations. The major sources of carbon emission in developing nations, excluding China, India, and Brazil, are related to agricultural activities and land use-land use change and forestry. In Ethiopia, like other developing nations, the major sources of carbon emissions are LULUCF and agricultural activities. The carbon emissions including/excluding LULUCF have a colossal variation. The level of carbon emission including LULUCF is higher than the level of carbon emission excluded LULUCF. Since 1990, the average carbon emission in Ethiopia, including LULUCF, has been around 55966.23 Ggtco_{2e}, however, the carbon emission except LULUCF is around 5293.67 Ggtco_{2e}. The disparity between excluding and including LULUCF emission is because the country does not produce carbon emissions from the combustion of fossil fuels. Even though the country has 320 million tons of potentially exploitable coal, it has exploited zero percent of it (FDREMoEF 2015). Except for the transport sector, Ethiopia does not produce carbon emissions as it does not generate power/energy by burning fossil fuels. Hence, most of the carbon emissions in Ethiopia are attributed to land-use change and forestry and the transport sector. According to FDREMoEF, (2015) the carbon dioxide emission from land use and land use changes in cropland and grassland contributed 92% (cropland 59% and grassland 33%). Transport and the energy sector followed as the other

main sources CO₂ emission, which accounted for 3% and 1% respectively. However, looking at the average growth rate of carbon emissions, LULUCF (Land use- Land use change and forestry) included carbon emissions are greater than LULUCF excluded carbon emission as the former increased by 17.3 %, while the later increased with 7.5 % since 1990 (Fig. 2). With all these increasing and decreasing trends of CO₂ emissions, the economic activities of the country have played great roles. The CO₂ emission, including LULUCF, has shown a drastic increment after 1994. This can be because of the extensive deforestations (i.e. an estimate of annual deforestation ranges from 39,000 hectares in 1990 to more than 143,000 hectares after 1994 and the percentage of forest rent to the country's GDP has also raised from 11.88% in 1990 to 22.75 in 1994), population growth and economic activities. According to World Bank (2013) the GDP per capita of the country has shown colossal variabilities from 1990–2003, with the lowest GDP per capita growth rate of -11.893% in 1991, the time when the country had the highest reduction of Co₂ emissions. However, after 2004 the country had no negative GDP per capita with the highest growth rate of 10.408% in 2004. The CO₂ emission, which has started falling from 2002–2003, has started rising again after 2004. In 1990 the carbon dioxide per capita emission, including LULUCF, was around -2.96 GgCo_{2e} / 1 billion USD. However, in 2013 it reached 0.89 GgCo_{2e} / 1 billion USD (UNFCCC 2017). Besides this, as carbon dioxide and methane are the primary greenhouse gases emitted through human activities in Ethiopia, population growth has a negative impact on Co₂ emissions. Hence the population of the country had been growing at 2.53 % on average from 1990–2013. And in 1990 the carbon dioxide per capita emission, including LULUCF, was around -0.61GgCo_{2e}/ thousands of populations. However, in 2013 it reached 0.42GgCo_{2e}/ thousands of populations (UNFCCC 2017).

Nitrous Oxide

The other major greenhouse gas emission is nitrous oxide. Nitrous oxide emission is largely caused by anthropogenic factors; the combustion of fossil fuels, industrial processes, transport sectors, land-use change and clearing of the forest, agricultural activities like use of fertilizer, manure or animal wastes are the major anthropogenic source of nitrous oxide (IPCC, 2001; Olivier and Janssens 2012). From

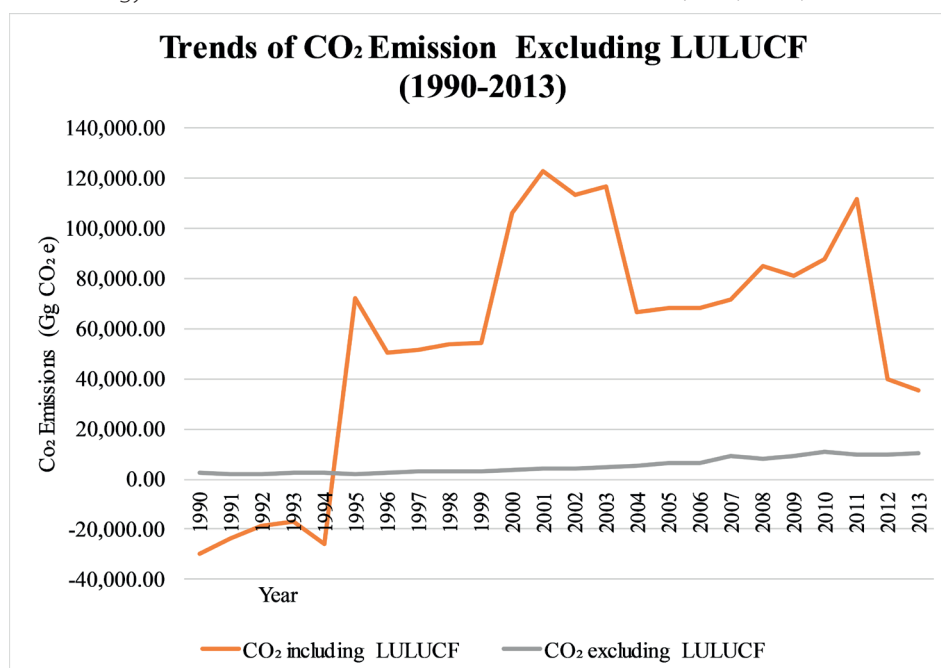


Fig. 2. Computed from UNFCCC Data Interface

1980–1998 the atmospheric emission of N_2O continues to increase at a rate of 0.25% per year. Despite it has shown a reduction at around 50% from 1991–1993, the emission of N_2O after 1993 was at rates closer to those observed during the 1980s (IPCC 2001). The amount of nitrous oxide emission in Sub Saharan Africa is attributable to agricultural activities and land-use change and forestry.

Ethiopia has economies dominated by the agricultural sector. As a result of this, nitrous oxide emissions emanating from nitrogenous fertilizer and other agricultural activities become evident. The application of nitrogenous fertilizer and other agricultural activities have contributed to 356,000tcoe nitrous oxide emissions in 2001/02 in Ethiopia. The average agricultural land on which fertilizers applied was 17.012kg/ha in 2002. The level of nitrous oxide emission in Ethiopia have shown increases from 1990–1994 (3,410Ggco_{2e}–12134.98 Ggco_{2e}). However, in 1995 it decreases from 12134.98 Ggco_{2e} to 11025.4Ggco_{2e} with a growth rate of -9.14%. The rise of the emission has reached 21,952.74Ggco_{2e} in 2008. Five years later, the emissions of nitrous oxide become 24,123.86Ggco_{2e}. The level of nitrous oxide emission with and without LULUCF had a slight difference only in 1990 as nitrous oxide with and without LULUCF was around 3410 Ggco_{2e} and 3100 Ggco_{2e}. Respectively however, for the rest of the years, it had similar emission values. It is for this reason that the paper has only displayed N_2O excluding LULUCF in figure 3. The average growth rate of nitrous oxides emission from 1990–2001 was approximately 21.97%. However, it had shown a drastic downward shift from 2002–2013 with an average growth of 8.07% (Fig. 3). Moreover, according to FDREMoEF, (2015), manure management has contributed the largest share of N_2O emissions with 45% of the contribution. It is followed by soil management with 40% of N_2O emissions. The rest of N_2O emission has been contributed by fuel combustion activities, other energy sectors, and wastewater treatment and discharge with 5%, 5%, and 4% respectively. Despite the consumption of fertilizer fluctuating considerably, the average kilogram of fertilizer applied to agricultural land in the same period was around 16.5Kg/ha (FDREMoEF 2015). From 2002–2007 the average kilograms of fertilizers applied in agricultural land were 11.85Kg/ha. From 2008–2013 an average of 21.13 Kg/ha of fertilizers were applied. Besides this, FAO (as cited in FDREMoEF 2015) has also estimated that 141,000 ha of forest has been lost annually between 1990 and 2010 and that the average annual deforestation rate, based on the change in forest cover from 2005 to 2010, was estimated to be 1.1 percent of total forest cover.

Methane

Methane is the third but important greenhouse gas that has a contributory effect on greenhouse emissions. Since the period of the industrial revolution, the atmospheric methane emission has been doubled and contributed to more than 20% of the greenhouse gas effect. Methane is produced through the natural process by bacteria and anthropogenic factors like mining, burning of fossil fuels, and livestock husbandry. Livestock production is the main source of methane emission in developing nations. It has two primary sources of emission; enteric fermentation and manure management. In enteric fermentation, methane emitted when cattle eat plants and ferment it in their stomach and exhale methane. The second source of methane is manure management. In manure management, methane is emitted when cattle excrete manures containing methane. The total emission of methane from enteric fermentation in Ethiopia is very high, which accounts for 40.55Mt co_{2e}/year, as compared with other east African countries. For example, Kenya, Tanzania, and Uganda have 11.55, 13.46, and 5.64 mtco₂/year of methane respectively which is very low as compared with Ethiopia. The total methane emission from manure management is also around 1.41Mtco₂/year, which is very high as compared with the other East African countries' practices (Brown et al. 2012).

The total methane emissions with and without LULUCF have very little difference from 1990–1993. The average methane emission with LULUCF was 37,826.25 Ggco_{2e} and the average methane emission without LULUCF was 37,500.75 Ggco_{2e} from 1990–1993. However, from 1993–2013 both LULUCF included and excluded methane emission was similar. The total methane emission, including LULUCF, in Ethiopia, was around 37,821Ggco_{2e} in 1990. The emission of methane has slight progression and retroversion from year to year until 1996. However, after 1996, as graph4 vividly showed there is a continuous upsurge. As graph4 depicted well, the emission of methane including LULUCF reached 60,729.02 Ggco2e in 2013. The growth rate of methane emission from 1990–1994 was around -4.50%. From 1995–1999 the average annual emission growth rate of methane was raised by 11.39%. However, from 2000–2004 the average annual emission growth rate of methane was around 2.52%. From 2005–2009, the average annual emission growth rate of methane was 0.14%, and it turns out to be 2.5% from 2010–2013. Generally, the emissions of methane increase on average by 2.71% per annum from 1990–2013 (Fig. 4). As Ethiopia has the largest livestock population

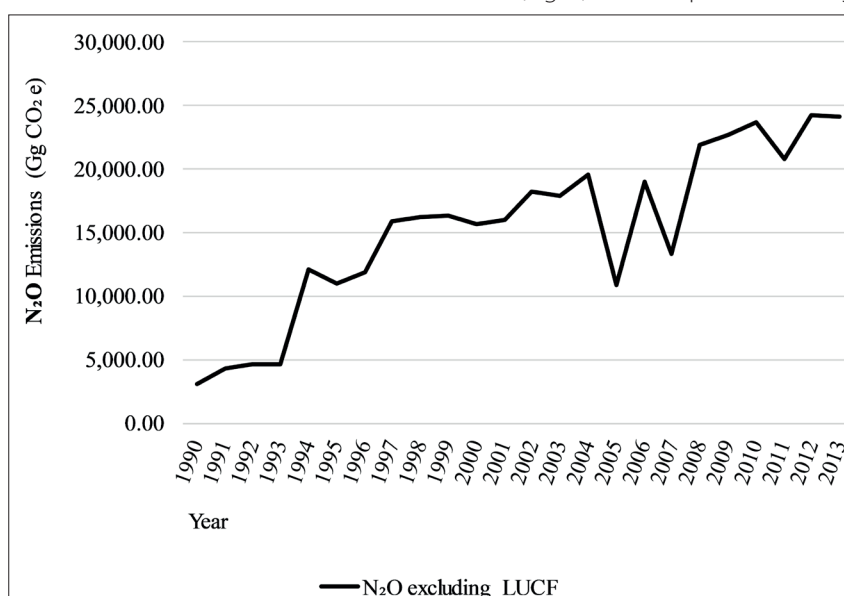


Fig. 3. Trends of N_2O emission excluding LUCF (1990–2013)

in Africa consisting of cattle (53 million), sheep (26 million), goats (23 million) and birds (50 million), emission from enteric fermentation, which was associated with domestic live-stock, has contributed to the largest CH_4 emissions accounting for 26% of the emissions. Other energy sectors, which primarily come from the use of fuelwood and wood waste in the residential and commercial institutions, have also contributed to 26% of the emission, and solid waste disposal and decomposition have contributed to 25%. The reset of methane emission comes from wastewater treatment and discharge (6%), manure management (5%), biomass burning (5%), rice cultivation (3%), transport (2%), solid fuels or coal (1%) and energy industries (1%) (FDREMoEF 2015). Generally, the agriculture sector contributed the most methane emissions, constituting 53% of all national methane emissions in 2013.

Sectorial Contributions of Greenhouse Gas Emissions in Ethiopia

Agriculture

Agriculture covers the lion share of the gross domestic product of many developing nations. It has also provided employment opportunities for the vast majority of the population in Sub Saharan countries. However, this sector of the economy produces a large share of greenhouse gas emissions next to land-use change and forestry. The biggest sources of emission in this sector are the encroachment of pasture and cropland into forested areas; livestock manure and digestive processes; burning of Savannah; and cropland management and cultivation practices (Brown et al. 2012).

The greenhouse gas emissions from agricultural practice are basically in the form of nitrous oxide resulting from the application of fertilizer and/or manure in a form of methane resulted from livestock emission and animal manure or rice cultivation. Therefore, agriculture is the main source of nitrous oxide and methane emission. In Ethiopia, agriculture has contributed to the vast majority of greenhouse gas emissions. It has contributed around 35856.67 Ggco_{2e} per year from 1990–1994. As compared with 1990, greenhouse gas emission has increased by 1.4% in 1994. From 1990–1994, the greenhouse gas emission from the agricultural sector has an average growth rate of 0.13% per annum. From 1995–1999, the average total greenhouse gas emission traced from the agricultural sector reached 38852.47 Ggco_{2e} per year. However, unlike the preceding period, this period has shown upward trends of greenhouse gas emissions. The total greenhouse gas emission from this sector increased by 19.26%

from 1995 to 1999 and it had a 3.11% increase per annum for the respective years. From the year 2000–2004, the total greenhouse gas emission traced from the agricultural sector was averaged around 44216.04 Ggco_{2e} per year. It increased by 25.12% from 2000–2004. On average the greenhouse gas emission from this sector increased by 6.01% per annum. From 2005–2009, the agricultural sector has an average greenhouse gas emission of 54773.65 Ggco_{2e} , as compared with the 2005 emissions, the total greenhouse gas emissions in 2009 has increased by 43.28%. It also had a 9.75% average annual increase each year. From 2010–2013 the total greenhouse gas emission from this sector increased by 1.65% as the emission stood at 65438.18 Ggco_{2e} emissions on average per year. It also had a 1.74% average annual increase each year during these periods. Generally, from 1990–2013 the total greenhouse gas emission traced from the agricultural sector increased by 3.11% on average per annum. As it is depicted in Fig.5, agriculture has paramount contributions to the total greenhouse gas emission in Ethiopia (Fig. 6, 7, and 8). The main sources emission in this sector included enteric fermentation (67.48%), manure management (20.52%), agricultural soils (8.75%), and prescribed burning of savannas (3.22%) and rice cultivation (0.017%) (UNFCCC 2017).

Land Use and Land Use Change and Forestry (LULUCF)

Land use and change and forestry is the first leading sector that has contributed to the largest greenhouse gases emission in Ethiopia. This sector contributed to greenhouse gas emissions in changing and modifying the use of landscape. This, perhaps, happens in the form of forest degradations, deforestation, shifting cultivation, wildfire, etc. (MESTI and EPA 2015). Developing countries have shown continuous upward trends of greenhouse gas emissions from the sector. In confirming this fact, Brown et al. (2012) said that from 2001–2006 the native ecosystems underwent a land-use change and about 5.5 million ha/year were converted into cropland in East Africa countries and 1.2 million ha per year in western African countries. Ethiopia also has had the largest native vegetation land converted to cropland from 2001–2006 which is almost 3.6 million hectares. As a result of this, the land use change and forestry is the first largest sector that has contributed to greenhouse emissions. This sector has contributed 43.31% of greenhouse gas emissions in Ethiopia. From 1990–1994 the total greenhouse gas emanated from land use-land use change and forestry was -1.03%. However, in between 1995–1999, it grows by

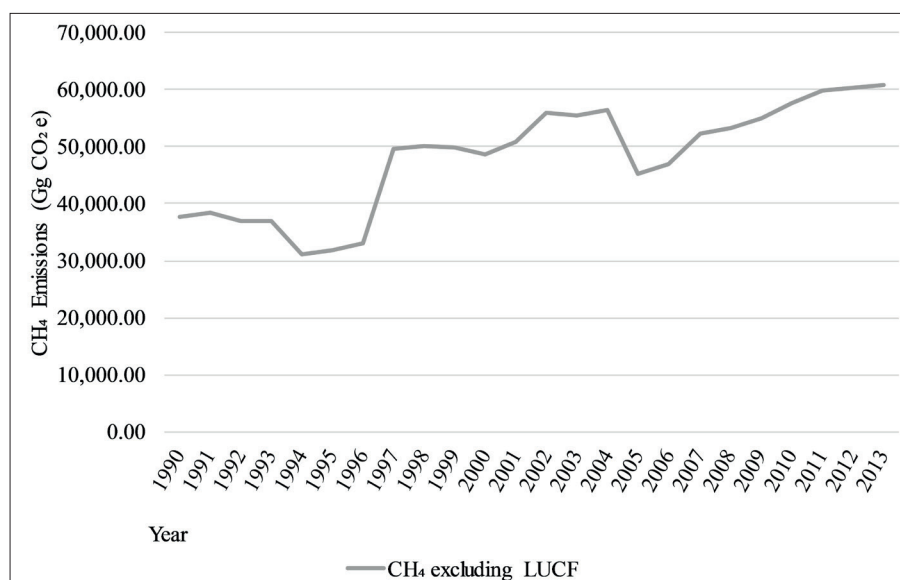


Fig. 4. Trends of CH_4 emission excluding LUCF (1990-2013)

64.52%. The trends of greenhouse gas emissions from this sector have shown a 12.96% of growth from 2000–2004. After 2004 the greenhouse gas emission from land use change and forestry had slight progress but downturns after 2012. Nevertheless, in 2013, it has still contributed a large share to Ethiopian greenhouse gas emissions. Generally, from 1990–2013, the average greenhouse gas emission from this sector was around 50739.73 Ggco_{2e} with a 19.76% average annual emission growth rate (Fig. 5, 6, 7, and 8).

Energy Sector

The energy sectors are one of the main anthropogenic factors that have a huge contribution to global increased greenhouse gas emissions. The energy sector discharges greenhouse gas emissions by burning or combustion of fossil fuels, combustion of biomass and electricity generation. This sector has been a colossal factor for carbon emission in the world, particularly in developed nations. Schreuder (2009) argued that co₂ emissions from fossil fuel burning and industrial processes have been accelerating at a global level with the growth rate of increase from 1.1% per year (from 1990–1999) to 3% per year from 2000–2004. The increasing pattern of fossil fuel emission has become exponential; for example, China and India have shown the highest carbon emissions with 67% and 88% increase respectively and Japan, the US, and Europe have respectively shown carbon emission increments by 23%, 19 %, and 6% (IEA 2012).

Developing countries have comparatively less carbon emissions than developed countries. It is because of this, the Kyoto Protocol leveled developing nations as a non-annex I country. However, their carbon emission is increasing from year to year. Biomass energy or the burning of wood-fuel has contributed to increased carbon emission in Sub-Saharan African countries. It was estimated that 658 million tons of wood-fuel were directly consumed by households and used to produce charcoal in 2012, which led to high carbon emission. However, on the other hand, electricity generation accounted for approximately 63 million tons of co_{2e} and that it shared 2% of the region's greenhouse gas emissions (Hogarth et al. 2015).

In Ethiopia, the total greenhouse gas emission from the energy sector has grown on average by 9.45% per year from 1990–2013. This sector is the third-largest sector that has contributed to greenhouse gas emissions in Ethiopia. The emissions from the energy sector were around 6274Ggco_{2e} in the 1990s and reached 17670.12Ggco_{2e}, which has increased by 217.99%. Even though Ethiopia did not produce energy from the combustion of fossil fuel it produces electricity from hydropower, which is clean from carbon emissions, but the other sectors (fuel combustion/ biomass energy) and transport sectors have the largest share of emissions in the energy sector as they have 3,918.2 Ggco_{2e} 12,881.3Ggco_{2e} in 2013. Other sectors (fuel combustion or biomass burning) cover 77.56% of the energy sector emissions whereas the transport sector has shared 14.67% of the energy sector emissions. The manufacturing industries and construction cover 5.6% of the energy sector emission (UNFCCC 2017). What makes this sector different from other sectors is that it has shown progressive increments from year to year. It had a 9.45% annual average growth rate from 1990–2013 (Fig. 5). This means the sector would be a vanguard greenhouse gas emission sector in the future.

Waste Sector

Greenhouse gas emissions from this sector include disposal of liquid and municipal solid waste through landfilling, composting, incineration, open burning, and treat-

ment of domestic and industrial liquid wastes. The gaseous emissions from this sector are predominantly CH₄ and N₂O. However, solid and liquid waste disposals are the dominant factors in the waste sector greenhouse gas emissions (MES-TI and EPA 2015).

In Ethiopia, the waste sector has a limited share of the national total greenhouse gas emissions. As clearly shown in Fig. 5, the waste sector has contributed to a total of 3081.21 Ggco_{2e} emissions per year on average ranging from 1990–2013. This figure seems insignificant but the sector has an average emission growth rate of 7.4% per annum. Different studies have also confirmed that this sector is one of the dreadful challenges of urban areas in Ethiopia that it would probably have sustainable greenhouse gas emissions. The growth rate of greenhouse gas emission in the waste sector increases by 390.38% in 2013 as compared with the 1990's waste sector emissions (Fig. 5, 6, 7, and 8). Wastewater handling, solid waste disposal on land, and waste incineration are the dominant subsectors that have contributed to greenhouse gas emissions in the waste sector with a share of 29.06%, 68.99% and 1.95 % respectively (UNFCCC 2017).

Industrial Processes and Product Use

This sector is very different from other sectors because it has adverse and spillover effects. It means that it could have effects not only at the source point but also far away from the source point. This means emissions at a point will have adverse effects at other points. In this sector, emissions are produced as a byproduct of the industrial process. Different kinds of industrial processes can lead to greenhouse gas emissions like mineral industrial sector (cement production, lime production, ceramics, soda ashes), chemical industries, metal industries (iron and steel production, aluminum production), and electronic industries (IEA 2012; IPCC 2006).

In Ethiopia, the industrial sector has still a trivial contribution to the nation's total greenhouse gas emissions as it has a total of 881.21Ggco_{2e} emissions on average from 1990–2013. Despite its triviality, the sector has an average emission growth rate of 20.05% per year, which is very high as compared with other sectors. From 1990–1994 the sector had an average greenhouse gas emission of 208.89 Ggco_{2e}. From 1995–1999, it had an average greenhouse gas emission of 323.03 Ggco_{2e}. From 2000–2004 the sector had an average greenhouse gas emission of 643.49 Ggco_{2e}. From 2005–2009, it had an average greenhouse gas emission of 1,732.36 Ggco_{2e} and finally, from 2010–2013, the industrial sector had an average greenhouse gas emission of 1,652.52 Ggco_{2e}. These periods have clearly shown that greenhouse gas emissions in the sector are upturning from year to year with increasing growth rates as shown in figure 5. Among the most subsectors that have contributed to greenhouse gas emission, metal production (48%) and cement production (51%) are the dominant subsectors. Other subsectors like lime, soda ash, and glass production have a trivial contribution to the industrial processes and product use emission (FDREMoEF 2015).

Bunkers Fuel Sector

Bunker fuels include fuels used for international aviation and maritime transport. This sector is nowadays increasingly influencing the global greenhouse gas emissions. Its trend has increased from time to time. Bunkers fuel had contributed to global greenhouse gas emission with 362.5 mtco_{2e} from maritime transport and 255.3 mtco_{2e} from aviation industries and the figure upturned constantly as it reached 488.8 mtco_{2e} from the maritime transport and 350 mtco_{2e} from aviation in 2000 and reached 565.8 mtco_{2e} for maritime and 413.8 mtco_{2e} for aviation fuel combustions. In

2005 and 2010 the greenhouse gas emission from maritime transport and aviation reached 643.7 mtco_{2e} and 455.3 mtco_{2e} respectively (IEA 2012).

The bunker fuel, like the waste and industrial sector, has trivial shares of the total greenhouse gas emissions in Ethiopia. All the emissions in this sector are attributable to the aviation industry. This sector has an average growth rate of 57.53% per year from 1990–2013 with an average emission of 458.65 Ggco_{2e}. From the year 1990–2000, the sector had an average greenhouse gas emission of 210.68 Ggco_{2e}. From the year 2000–2013, the bunker sector had an average greenhouse gas emission of 649.4 Ggco_{2e} (Fig. 5,6,7 and 8).

International Policy Instruments and Measures of Greenhouse Gas Emissions

The United Nations convened a conference in 1972 at Stockholm to deal with environmental problems, which was epitomized by a series of preceding environmental incidents like the trail smelter, Corfu channel, Torrey cannon or black tides. Although there were bilateral and unilateral efforts, before the Stockholm conferences, the international community had no global policy instruments to deal with the environmental problem (Kiss and Shelton 2007). The conference for the first time soaked up global efforts to address environmental problems hinting that environmental problems have global dimensions. The Stockholm conference brought up the Stockholm declaration and UNEP.

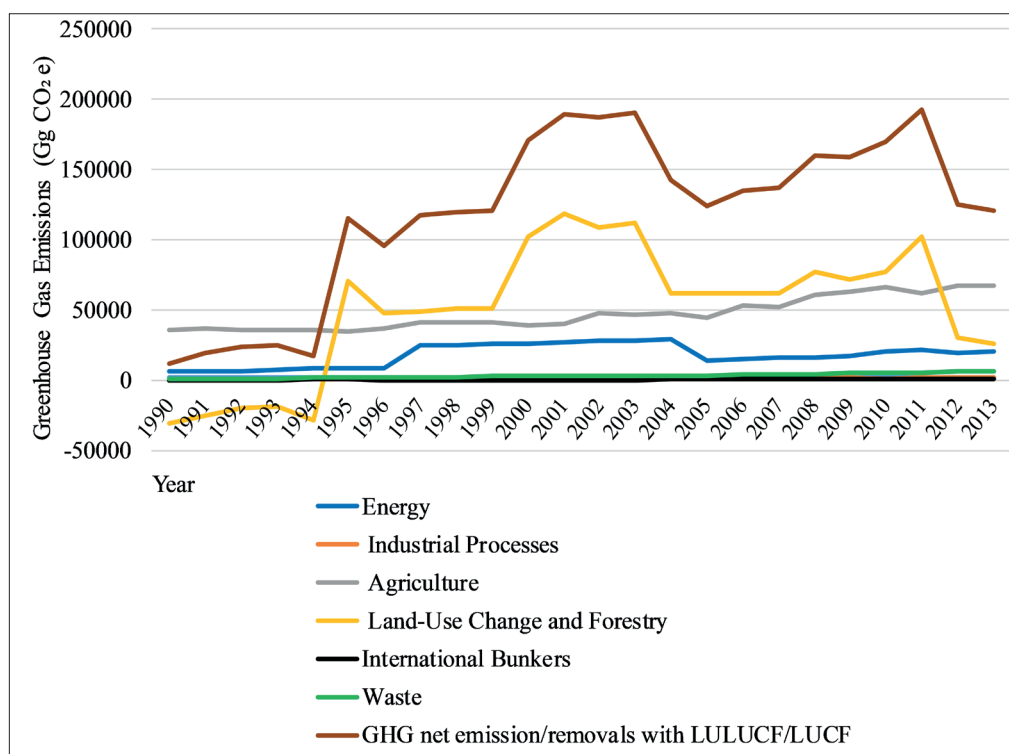


Fig. 5. Trends of greenhouse gas emission in terms of sectors (1990-2013)

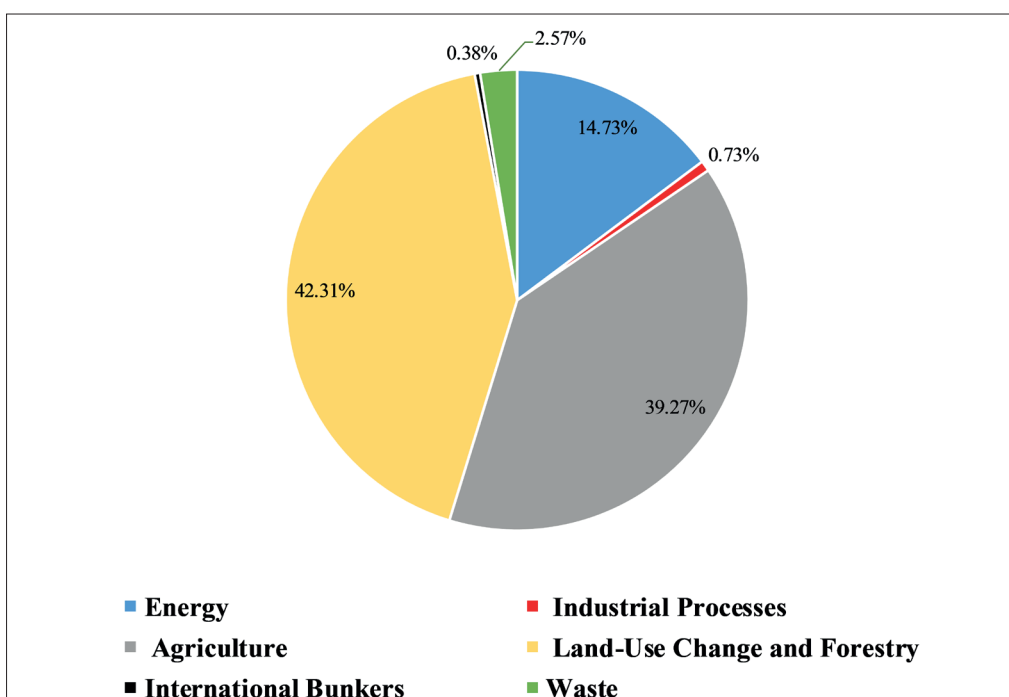


Fig. 6. Average greenhouse gas emission in terms of sectors (1990-2013)

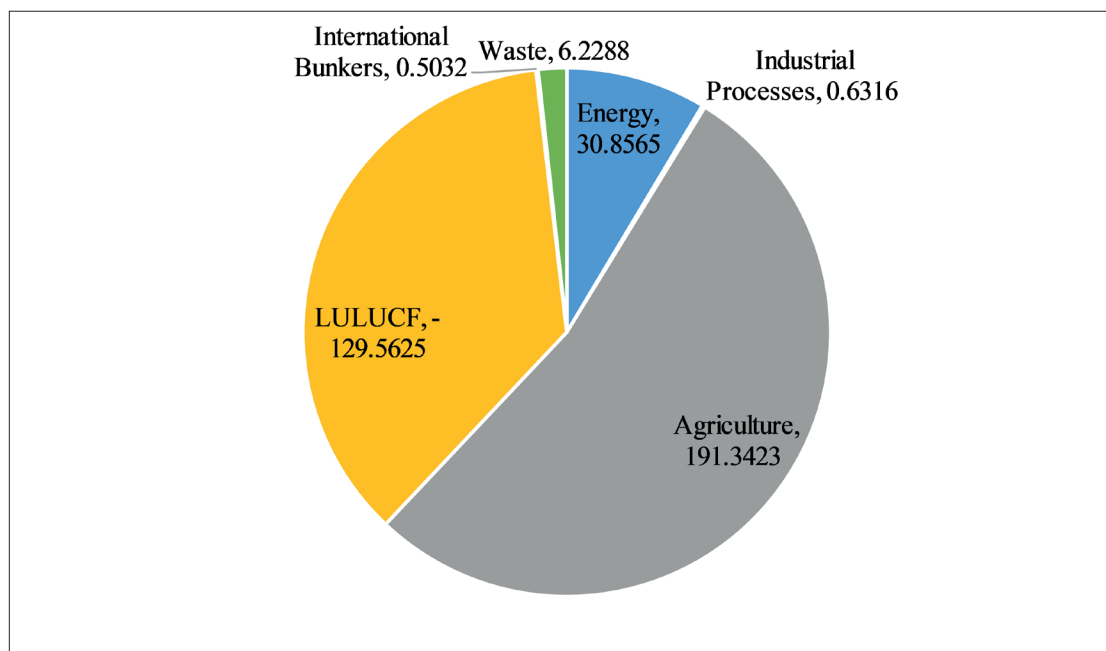


Fig. 7. Sectorial greenhouse gas emission in 1990 (percentage proportional to 1990 total greenhouse gas emission)

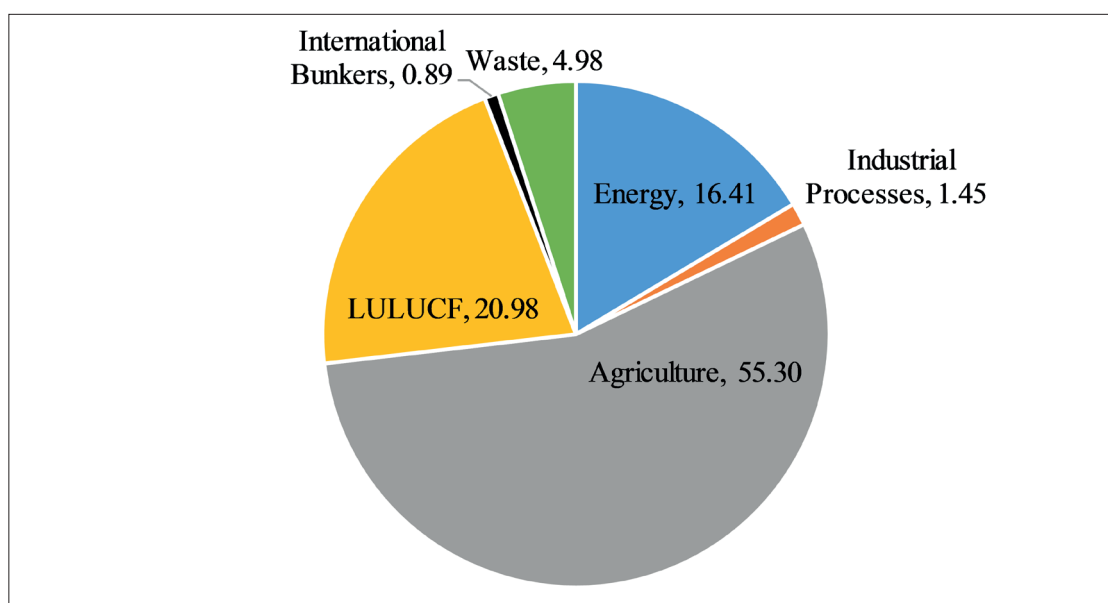


Fig. 8. Sectorial greenhouse gas emission in 2013 (percentage proportional to 2013 total greenhouse gas emission)

The Stockholm declaration recognized man as a primary agent in creating and molding his environment. So, anthropogenic factors are the primary causes of environmental problems. The declaration in article 6 of the principles intended to address toxic pollutants and pollution which are directly or indirectly related to greenhouse gas emissions reduction.

The discharge of toxic substances or of other substances and the release of heat, in such quantities or concentrations as to exceed the capacity of the environment to render them harmless, must be halted in order to ensure that serious or irreversible damage is not inflicted upon ecosystems. The just struggle of the peoples of ill countries against pollution should be supported (UN 1972).

UNEP is another international instrument, which is devised as one of the specialized agencies of the UN, in the Stockholm conference (Kraft 2007). This instrument was considered a forum for discussing environmental problems, influencing environmental policy and assessing the social and economic impacts of climatic change (Cohen and Waddell 2009). Consequently, UNEP in collaboration

with the world environment center (WEC) has identified 700 voluntary projects to cut greenhouse gas emissions. It was also successful as it has achieved 1.3 billion tons of co-reduction (Calhoun 2005).

The international community convened a conference in Austria in 1985. The conference instigated the development of global policies to address climate change and initiated the establishment of the intergovernmental organization that could assess the impact of climatic change. In 1988, in Toronto, Canada, the world conference on changing climate was held with the focus of developing policies and providing solutions to the challenges of climatic change. The conference called on the world to reduce greenhouse gas emissions by 20% from 1988–2005 and the creation of a global climate convention. The UNEP in collaboration with WMO created the intergovernmental panel on climate change (IPCC) in 1988. IPCC is initiated with the objectives of preparing comprehensive review and recommendations concerning climate change, the social and economic impact of climate change and possible responses to strategies (Sebastian 1999).

The other notable international policy instrument was the Rio Conference held in 1992. The conference adopted a treaty called the United Nations Framework Convention on Climatic Change. The UNFCCC is initiated to stabilize the greenhouse gas concentrations in the atmosphere. The convention created a forum for discussion on the major global initiatives on reducing greenhouse gas emissions (UNFCCC 2006). Five years later, the major but ill successful conference was held in Kyoto, Japan. The Kyoto Protocol has brought some quantitative measures on the reduction of greenhouse gas emissions. The protocol categorized the world countries into annex I countries (developed countries) and non-annex I countries (developing countries). It also recognized that developed nations were responsible for the majority of greenhouse gas emissions over the last centuries. As a result of this, the protocol tried to levy different responsibilities in developed and developing countries. Developed countries were subjected to emission reduction targets ranging from -8% to 10% of the 1990s emission. On the other hand, developing countries were advised to engage in the clean development process (Sebastian 1999).

The Kyoto protocol has introduced very flexible mechanisms for countries to follow to reach emission reduction targets. Different mechanisms of greenhouse gas emission reductions have been introduced as a result of the protocol. Joint Implementation, Emission Trading, and Clean Development are the basic mechanisms that are introduced in the Kyoto Protocol (Schreuder 2009).

Joint Implementation Mechanisms are «defined in Article 6 of the Kyoto Protocol, allows a country with an emission reduction or limitation commitment under the Kyoto Protocol (Annex I Party) to earn emission reduction units (ERUs) from an emission-reduction or emission removal project in another Annex I Party». Joint Implementation Mechanisms offer Parties a flexible and cost-efficient means of fulfilling a part of their Kyoto commitments (UNFCCC 2014). Joint Implementation mechanisms encourage carbon sink byways of planting the forest, cropland management, and re-vegetation. It can be implemented just among the developed nations (Schreuder 2009).

Emission Trading is another strategy used to reduce greenhouse gas emissions. It is a very flexible and market-based approach that is implemented among Annex I countries whereby countries can sell and buy emission units from countries which have positive carbon signs. Such a mechanism has tried to provide economic incentives to countries that have reduced greenhouse gas emissions.

Clean Development Mechanisms (CDM) is another strategy used to reduce GHG. It is defined in Article 12 of the Kyoto Protocol that «Annex I Parties can undertake emissions-reduction projects in developing countries (Non-Annex I), which lead to Certified Emission Reduction Credits. These credits can be used for compliance in the industrialized countries» (Schreuder 2009). This indicated that developed countries have the opportunity to engage in investments like greenhouse gas emission reduction projects in developing nations and can earn sellable certified emission reduction units.

Ethiopia as a developing country has to participate in CDM projects so as to reduce poverty by protecting the environment. After 2009, Ethiopia has registered in eight projects under CDM. Among these, three projects are CDM projects and the rest are POAs (a program of activities). The CDM projects are reforestation (Humbo Assisted natural regeneration project, located in southwest Ethiopia), Landfill gas (Repi Landfill Gas Projects in Addis

Ababa), and Methane Avoidance or wastewater (a tannery hub, construction of common effluent treatment plant for industrial waste in Modjo). Apart from this, Ethiopia has already registered five POAs (a program of activities) and four of them are related to the deployment of energy-efficient cook stoves for domestic use and one POA is related to Solar Programme (Ritika et al. 2017).

According to Mohammed (2011), the Humbo Assisted Natural Resource Project can be referred to as one of the success stories of CDM projects. Its achievement stems from the involvement of the local community to rehabilitate the degraded forest area, commitment of the stakeholders to entwine resources and technical capacity, and good institutional support from the Ethiopian Environmental Protection Authority. Hence, it rehabilitated the ecological system and enhanced the economic opportunities of the local community. The second CDM project, Repi CDM Project, is launched in Addis Ababa with the objective of capturing and flaring methane from solid wastes, which is found in Addis Ababa City Administration, Koshe. This project has given a great opportunity to Addis Ababa city administration as it unleashes better waste management practices by recycling it to produce electricity out it. The third CDM project is Methane Avoidance or wastewater (a tannery hub, construction of a common effluent treatment plant for industrial waste in Modjo town), this project appears to be an important opportunity to set up an environmentally friendly leather tanning cluster driven by a network of tanneries in the town and from or around Addis Ababa. The cluster gives priority to common effluent treatment plants to reduce the environmental impact of leather processing (Sandro and Ivan 2017). However, there are some cross-cutting restraint factors to CDM projects, which are relevant to the Ethiopian case. These factors are limitations in national CDM capacities, CDM system complexity, unfavorable national investment climate, smaller overall mitigation potential (represented by national GHG emission levels) and limited prior CDM experience (Ritika et al. 2017).

Generally, the Kyoto protocol was considered less successful because major greenhouse gas emission contributing countries like the US were failed to ratify the protocol (Obaidullah et al. 2016), and emerging economies, like China, India, and Brazil, which are contributing the highest greenhouse gas emissions were not induced with carbon caps as the protocol treated them in non-annex I countries. Nevertheless, EU countries had successful records in implementing the Kyoto protocol nations (Schreuder 2009). After the Kyoto protocol, series of negotiations and conferences were held in Marrakesh Accords (COP 7) in 2001, Copenhagen Accord (COP 15) in 2009, and the Paris Agreement (COP 21) in 2015.

The Paris Agreement can be considered as a concerted global response to climate change challenges. The goal is to keep the world temperature below a 2-degree Celsius increase as compared to the pre-industrial period. It has also aimed at strengthening the capacity of member states to deal with the impact of climate change. Hence, appropriate financial adaptations, technology transfer, mitigation or capacity-building frameworks have been used as instrumental tools to deal with climate change. This agreement has appreciated the differences in capacities among developing countries to deal with climate change. It is for this reason that the Paris Agreement creates a strong link between support and the degree of efficacy and commitments of the actions of developing countries. The Agreement acknowledges the need for support in order to enforce the agreement effectively and allows for a greater

commitment in the actions of developing countries; and enhances the effectiveness of adaptation planning (Pauw et al., 2019).

Nationally Determined Contributions (NDCs) have been crucial to achieving the Paris Agreement's adoption in 2015 and instrumental in its implementation over the coming decades. There are three key features of these climate action plans. First, NDCs are universal: the NDC has been submitted by nearly every party to the United Nations Framework Convention on Climate Change (UNFCCC). Second, NDCs provide considerable flexibility for countries to adjust their goals to national circumstances and priorities. Third, the Paris Agreement creates five-year review and update cycles designed to make NDCs more ambitious over time (Pauw et al., 2019).

However, like the preceding protocol, Kyoto Protocol, the US, the leading CO₂ emitter, Obaidullah et al (2016), has decided to withdraw from the Paris Agreement. This shows that there was no global consensus on actions directed toward the reductions of greenhouse gases. Lack of effective compliance mechanisms can be counted as a reason for the failures (Jonathan et al., 2018).

Policy Instruments and Measures of Greenhouse Gas Emissions in Ethiopia

Ethiopia as a developing nation has not subjected to carbon reduction quota or limitation. Rather it has to gear its efforts toward clean development mechanisms. The country, in doing so, has introduced environmental policies. There have been different laws, proclamations, directives, policies, and strategies that deal with environmental issues. The environmental policy that was introduced in 1997 by the council of ministers, intended to ensure sustainable development by protecting the environment. In 2010, environmental impact assessment has been issued in «Proclamation 299/2002 E.C.» This environmental policy, let alone how successful it is, has obliged every development project and program to execute impact assessments on the environment and ensure sustainable development. Parallel to this, the country has introduced environmental pollution control proclamation, «Proclamation 300/2002» in 2010. This proclamation forced development projects to take environmental impact estimates and evaluate the efficiencies and effectiveness of pollution control mechanisms as per the proclamation. In 2015, Proclamation 513/2007 of solid waste management was introduced by the country. The Proclamation was issued as a counter-response to the very deleterious solid wastes and intended to enhance values gained from it. These practices, in turn, have the capacity to decrease greenhouse gas emissions from wastes. The council of ministers has also introduced a very specific pollution control proclamation concerning industries in 2016. It was Proclamation 159/2008 of industrial pollution control. This Proclamation intends to make industrial developments compatible with environmental protection activities and it has issued pollution level limits. Besides, there are different directives like environmental impact assessment directives in 2011, and environmental protection plan directives in 2004 (FDREMoST 2016).

The major environmental policy that can be cited in the country is the 2011 Climate Resilient Green Economy (CRGE). This environmental policy has specifically address climate change and greenhouse gas emissions. The CRGE despite ambitious goals was envisioned to

achieve the middle-income status by 2025 while limiting greenhouse gas emissions around 250 Mt CO_{2e}. In doing so, the CRGE adopted sectorial approached initiatives and identified and prioritized around 60 initiatives to limit GHG emissions around 250 Mt CO_{2e} while achieving its development goals (FDRE 2012). The CRGE is based upon the following principles;

Improving crop and livestock production practices for higher food security and farmer income while reducing emissions, Protecting and re-establishing forests for their economic and ecosystem services, including as carbon stocks, expanding electricity generation from renewable sources of energy for domestic and regional markets, Leapfrogging to modern and energy-efficient technologies in transport, industrial sectors, and buildings (FDRE 2012).

Although attaining such goals needs a total expenditure of USD 150 billion in the next 20 years for GHG abatement costs, the government has selected four sectorial based initiatives: i) exploiting the vast hydropower potential, ii) large-scale promotion of advanced rural cooking stoves, iii) efficiency improvements to the livestock value chain and iv) reducing emissions from deforestation and forest degradation (REDD) (FDRE 2012, 2016).

Agriculture has been and is projected to be responsible for the largest share of Ethiopia's GHG emissions until 2030 (Wang and Mersmann 2019). The total greenhouse gas emission from agriculture which is attributable to livestock was around 65 Mt CO_{2e} in 2010 and with the implementation of Climate Resilient Green Economy (CRGE) it would be around 125 Mt CO_{2e} in 2030 and from crops sector, the total greenhouse gas emission was around 19 Mt CO_{2e} in 2010 that could be limited to 71 Mt CO_{2e} in 2030. The NDCs report of the country revealed that in 2013, 31% of the agriculture sector's emissions resulted from livestock, 39% from cropland and 24% from grassland. The remaining share of emissions includes direct and indirect nitrous oxide emissions from managed soils, biomass burning, urea application, and rice cultivation. In 2030, the share of livestock emissions is projected to rise to 45% while cropland emissions account for 32% of the sector's total emissions, and grasslands account for only 11%. The government has action plans like decreasing the number of livestock while increasing livestock productivity and shifting from higher GHG emitting livestock (enteric fermenting animals) to lower GHG emitting livestock (non-enteric fermenting animals) like poultry, increasing land productivity and intensifying irrigations to reduce GHG emissions from the agricultural sector. However, due to the increasing patterns of use of fertilizer, new land conversion to cropland every year, an increasing number of cattle every year, it could be very difficult to limit the greenhouse gas emissions to 71 Mt CO_{2e} in 2030 (FDRE 2012).

The other largest greenhouse gas emission sector is land use- land use change and forestry. In this sector, deforestation and forest degradation are the primary contributors to greenhouse gas emissions. The Climate Resilient Green Economy (CRGE) planned to reduce greenhouse gas emissions from this sector by providing efficient stoves, (biogas and electric stoves) to rural societies, afforestation/reforestation and forest management. In doing so, it intended to decrease emissions by 40 Mt CO_{2e} in 2030 from the sector. The Climate Resilient Green Economy (CRGE) has provided targets for each sector with preferable action plans. For example, in the

energy sector, the policy aimed at generating electric power from hydropower (renewable energy sources) around 28TWh by 2030 and decrease GHG emissions by 20 Mt CO_{2e} in 2030 as hydropower generation does not produce greenhouse gases and thus is mostly termed as a green source of energy (Owusu and Asumadu 2016).

In the industry sector, it has been found that the cement industry has about 70% (5 Mt CO_{2e}) abatement potentials. Other industrial sectors (leather, chemical, fertilizer, textile, paper, and pulp) account for 6 Mt CO_{2e} abatement potentials in 2030. And other energy-efficient technologies or equipment in the industrial sector have an estimated abatement potential of 6 Mt CO_{2e}. The use of biomass energy in the industrial sector is also estimated at around 4 Mt CO_{2e} abatements. In the transport sector, the construction of the electric rail network has an estimated 9 Mt CO_{2e} abatement potentials and the introduction of fuel-efficient vehicles will have also an estimated abatement potential of 3 Mt CO_{2e} in 2030 (FDRE 2012). Nevertheless, Ethiopia's NDC has estimated the transport sector to have an abatement potential of 10 MtCO_{2e}. Transport emissions have been increasing continuously as it was only sector 1.0 MtCO_{2e} in 1994, but in 2013 it was responsible for 5.5 Mt CO_{2e} emissions. According to the SNC, these emissions are projected to multiply five-fold until 2030, reaching 25.4 Mt CO_{2e}. Ethiopia's NDC puts the transport sector emissions at 40 Mt CO_{2e}, however, the CRGE and Ethiopia's Climate Resilient Transport Sector Strategy put it at 40.7 Mt CO_{2e} in 2030 (Wang and Mersmann 2019). Therefore, the CRGE has ambitious mitigation measures as it has focused on specific policy areas.

Moreover, Ethiopia tries to restrain greenhouse gas emissions by providing financial support for investments in low-carbon cooking and baking devices, providing financial support for small-scale irrigation, establishing financial provisions for farmers for improved inputs and equipment, and supporting setting up a continuing forest data inventory. Therefore, the country has a comprehensive set of climate change mitigation policies and strategies that already cover all relevant

sectors for emission mitigation, focusing in particular on agriculture, forestry, transport, power, and waste (Wang and Mersmann 2019).

CONCLUSION

Although developing countries have comparatively less share of global greenhouse gas emissions, their level of emission is growing from time to time. The agricultural sector and land-use management and forestry change have contributed a lot to their greenhouse gas emissions. Likewise, Ethiopia has a limited share of global and regional greenhouse gas emissions. However, its greenhouse gas emissions are showing upward trends from time to time with little swings in some periods. Although most greenhouse gas emitting sectors are showing increasing trends, the land use-land use change and forestry and agricultural sector have been contributing the huge shares for greenhouse gas emission in the country as both have 50739.73 GgCO_{2e} and 47093.63 GgCO_{2e} emissions per year on average from 1990–2013 respectively. The energy sectors has also contributed 17670.13 GgCO_{2e} per year on average from 1990–2013. However, other sectors, which have a trivial contribution to greenhouse gas emissions, have shown the highest annual growth rate. For example, the industrial sector has an annual average growth rate of 20.05% of greenhouse gas emissions. The energy and waste sector have also a 9.45% and 7.4% average annual growth rate of greenhouse gas emission respectively. This might show the potential of the sectors to dominate the other sectors in greenhouse gas emissions. Nevertheless, Ethiopia has introduced different policies in controlling the level of greenhouse gas emissions. Among them Climate Resilient Green Economy (CRGE), notably intended to limit the level of greenhouse gas emissions around 250mtco_{2e} (250000GgCO_{2e}) by implementing action plans concerning each sector. Therefore, if Ethiopia implemented all detail action plans of CRGE, it would have the capacity to limit greenhouse gas emissions. ■

REFERENCES

- Brown S., Graiz A., Ambagis S. and Pearson T. (2012). Baseline GHG Emissions from the Agricultural Sector and Mitigation Potential in Countries of East and West Africa. In CGIAR research program on climate change, agriculture and food security (CCAFS) (13). Copenhagen. CAIT. (2017). CAIT Country Greenhouse Gas Emissions: Sources and Methods. World Resource Institute.
- Calhoun Y. (2005). Environmental policy. Philadelphia: Chelsea House.
- Cohen S. and Waddell W. (2009). Climate change in the 21st century. Montreal: McGill Queens University Press.
- FDRE. (2012). Ethiopia's Green Economy strategy; Climate Resilient Green Economy. Addis Ababa: MoEFCC.
- FDRE. (2016). NATIONAL REDD+ STRATEGY. Strategy, DOI: 10.1596/24957.
- FDREMoEF. (2015). Ethiopia's Second National Communication to the United Nations Framework Convention on Climate Change (UNFCCC). Addis Ababa: FDREMoEF.
- FDREMoST. (2016). Environment and social management framework. Addis Ababa: MoST.
- Hogarth A., Haywood C. and Whitley S. (2015). Low-carbon development in Sub-Saharan Africa 20 cross-sector transitions. London.
- IEA. (2012). CO₂ Emissions from Fuel Combustion (III), DOI: 10.1787/co2_fuel-2012-en.
- IPCC. (2001). Climate Change 2001: The Scientific Basis. Contribution of Working Group I to the Third Assessment Report of the Intergovernmental Panel on Climate Change (Houghton J., Ding Y., Griggs D., Noguer M., Van der Linden P., Dai X., Maskell K. and Johnson C., Eds.). [online] Available at: www.ipcc.ch/report/ar3/wg1/ [Accessed 20 May 2020].
- IPCC. (2006). 2006 IPCC Guidelines for National Greenhouse Gas Inventories (Eggleston S., Buendia L., Miwa K., Ngara T. and Tanabe K., Eds.). Hayama, Japan: Institute for Global Environmental Strategies (IGES).
- Jonathan P., Jeffrey S., Tim S. and Sylvia I. (2018). The impact of the US retreat from the Paris Agreement: Kyoto revisited? Climate Policy, 18(7), 818-827, DOI: 10.1080/14693062.2017.1412934.
- Kiss A. and Shelton D. (2007). Guide to international environmental law. In Guide to International Environmental Law. Leiden: Nijhoff, DOI: 10.1163/ej.9781571053442.1-329.
- Kraft M. (2007). Environmental Policies and Politics. USA: Pearson Education.
- MESTI and EPA. (2015). National Greenhouse Gas Inventory Report; Ghana's Submission to UNFCCC. Republic of Ghana: MESTI and EPA.

- Mohammed B. (2011). Opportunities and challenges of carbon trade products in promoting sustainable development: the case humbo assisted natural regeneration project. Addis Ababa: Addis Ababa University. [Thesis].
- Obaidullah M., Samuel A. and Madina O. (2016). The relationship between carbon dioxide emissions, energy consumption and GDP: A recent evidence from Pakistan. *Cogent Engineering*, 3(1), DOI: 10.1080/23311916.2016.1210491.
- Olivier J. and Janssens M. (2012). Greenhouse-Gas Emissions. Netherlands: Netherlands Environmental Assessment Agency and EDGAR.
- Owusu P. and Asumadu S. (2016). A review of renewable energy sources, sustainability issues and climate change mitigation. *Cogent Engineering*, 3(1, 1167990), 14, DOI: 10.1080/23311916.2016.1167990.
- Pauw W., Castro P., Pickering J. and Bhasin S. (2019). Conditional nationally determined contributions in the Paris Agreement: foothold for equity or Achilles heel? *Climate Policy*, DOI: 10.1080/14693062.2019.1635874.
- Ritika T., Marie J. and Carsten W. (2017). Germany's carbon market cooperation with Ethiopia: Prospect for engaging with Article of the Paris Agreement. Berlin: DEHSt.
- Sandro S. and Ivan K. (2017). Case Study: Leather Industry Parks: Planning, Implementation, Benefits, Challenges and Experience. Vienna: The United Nations Industrial Development Organization.
- Sarkodie S. and Strezov V. (2019). Economic, social and governance adaptation readiness for mitigation of climate change vulnerability: Evidence from 192 countries. *Science of the Total Environment*, 656(150-164), 15, DOI: 10.1016/j.scitotenv.2018.11.349.
- Schreuder Y. (2009). The corporate greenhouse climate change policy in a globalizing world. London.: Zed Books.
- Sebastian O. (1999). The Kyoto Protocol – International Climate Policy for the 21st Century. In Alexander C. (Ed.), *Ecologic Institute: Science and Policy for a Sustainable World*. [online] Available at: www.ecologic.eu/422 [Accessed 20 May 2020].
- See M. (2001). Greenhouse gas emissions: Global business aspects. Berlin: Springer.
- UN. (1972). Declaration of the United Nations Conference on the Human Environment. Stockholm. United Nations Environment Programme.
- UNFCCC. (2006). United Nations Framework Convention on Climatic Change Handbook. Germany: Climate Change Secretariat.
- UNFCCC. (2014). Joint implementation mechanisms. [online] Available at: [www.unfccc.int/kyoto/\\$protocol/mechanism](http://www.unfccc.int/kyoto/$protocol/mechanism) [Accessed 25 September 2018].
- UNFCCC. (2017). Greenhouse Gas Inventory Data. [online] Available at: www.di.unfccc.int/detailed_data_by_party. [Accessed 15 January 2020].
- USAID. (2015). Greenhouse Gas Emissions in Ethiopia. Ethiopia: USAID
- Wang H. and Mersmann, F. (2019). Implementation of nationally determined contributions: Ethiopia country report. Dessau-Roßlau: Umweltbundesamt. (in German).
- World Bank. (2013). GDP per Capita Growth(% annual) Ethiopian Data. [online] Available at: www.data.worldbank.org/indicator/NY.GDP.PCAP.KD.ZG?contextual=aggregate&end=2013&locations=ET&start=1990 [Accessed 25 December 2019].

THE IMPACT OF THE SYRIAN CIVIL WAR ON LAND USE / LAND COVER IN AL-YARMOUK BASIN DURING 2010–2018

Yusra Al-Husban^{1*}, Ahmad Ayen²

¹ Department of Geography, The University of Jordan, Amman 11942 the Hashemite Kingdom of Jordan

² Queen Rania Center for Education and Information Technology, Amman 11814, Jordan

*Corresponding author: y.alhusban@ju.edu.jo

Received: December 05st, 2018 / Accepted: May 10th, 2020 / Published: July 1st, 2020

<https://DOI-10.24057/2071-9388-2018-73>

ABSTRACT. The study goal is to monitor and evaluate the significant changes in land use/land cover (LULC) in Al-Yarmouk basin (YB) within only 8 year. (YB) is shared between Syria, Jordan, Palestinian Authority, and Israel. (YB) has been affected not only by water scarcity, frequent drought conditions; But nowadays provide proof that the major factor responsible for the current of the significant changes in (LULC) in the study area is the Syrian civil war that began in mid-2011, and the Syrian refugee influx into Jordan has been massive, more than 660,935 Syrians were registered in three camps; Za'atari the largest refugee camp in the world, Azraq and the Emirate, according to the Official figures, with the highest density about 58 not 50 person look; Fig.5 in YB. Landsat Thematic Mapper Landsat 5 (2010) and 8-OLI (2018) covering a period of 8 years. An on-screen digitizing methodology has been employed. The images of the study area were categorized into four different classes: vegetation, built-up area, barren area, and water bodies. Normalized difference vegetation index (NDVI) was applied at a threshold value ≥ 0.1 to distinguish between the vegetated area and non-vegetated areas. IN this study, the NDVI and LULC based classification have indicated that significant change in (LULC) between a year 2010 and 2018. The Major change has been found in the vegetation area which decreased by (-12.02%), in addition, an increase of the built up area by (+1.69%). Al-Wehda dam area decreased by -0.08%. Linear regression trends showed a slight decrease in the mean rainfall during the study period (2010/2018). However, this finding is not statistically significant at the 95 % confidence level.

KEY WORDS: Land use/land cover change, remote sensing, GIS, Landsat, Syrian civil war

CITATION: Yusra Al-Husban, Ahmad Ayen (2020). The Impact OfThe Syrian Civil War On Land Use / Land Cover In Al-Yarmouk Basin During 2010–2018. *Geography, Environment, Sustainability*, Vol.13, No 2, p. 147-153

<https://DOI-10.24057/2071-9388-2018-73>

Conflict of interests: The author reported that there is no conflict of interest.

INTRODUCTION

Jordan has not only suffered from limited water resources and high population growth and it is classified as the most Arab countries that suffers from water scarcity in the region (Haddadin 2001); But Jordan was a heaven for migrations, especially from Palestine, Iraq, and finally from Syria as a result of the Syrian civil war. (YB) is the biggest and the most important in terms of river in Jordan and it suffering from drought (Al-Dardoor et al. 2013; Alsharifa et al. 2018; Gleick 2014). Since 2011, more than 660,935 of refugees have migrated southward to Jordan to escape the Syrian civil war that began in mid-2011 (UNHCR 2018¹; Francis 2015²). (YB) which is a branch of the – Jordan River watershed – shared by Syria, Jordan, and Israel; these countries are in a state of conflict over water sharing, especially between Jordan and, Israel (Comair et al. 2012; Shamir 1998; Tose et al. 2000; Haddadin 2009; Haddadin 2001; Rosenberg 2006; Al-Husban 2013). LULC analysis is important for agricultural planning, environmental studies, and drought monitoring (Anderson et al. 1976). LULC change detection is essential for understanding of landscape dynamic patterns within a specified period for sustainable management. Around the world, many researches focus on LULC changes using re-

mote sensing data. (Kwarteng, et al. 1997; Khawaldah 2016; Al-Bilbisi 2012; Rawat and Kumar 2015). This paper is based on two years of satellite data represents 2010, and 2018 to calculate LULC and NDVI changes, in (YB). We found that the LULC classified into four different classes namely; water bodies, barren area, vegetated area and built-up area. Normalized difference vegetation index NDVI have been used for analysis of change detection in many studies to distinguish between the vegetated area and non-vegetated areas (Singh, et al. 1989; Al-Husban 2019; Al-Husban and Zghoul 2017; Al-Husban and Almanasyeh 2017). On the other hand, rainfall is an important factor affecting, and indicator for drought conditions (Al-Husban 2013; Al-Husban and Makhamreh 2013), for that changes in the mean annual rainfall from the 12 meteorological stations located within the (YB) during the study period was analyzed using linear regression to test if there is a trend in the pattern of mean annual rainfall (increase/decrease or no trend).

STUDY AREA

Jordan is one of the countries most affected by the Syria crisis, with the second highest share of refugees compared to its population in the world, 89 refugees per 1,000 inhab-

¹ UNHCR (2018). *UNHCR Jordan, Printing date: 09 Apr 2018: Fact sheet.*

² Francis A. (2015). *JORDAN'S Refugee crisis, Carnegie Endowment for International Peace. [online]. Available at: www.carnegieendowment.org/2015/09/21/jordan-s-refugee-crisis-pub-61338 [Accessed 21 September 2015].*

itants Individuals. 527,803 of them live in Urban. The total number of Syrian refugees in Jordan by end of March 2018 is 660,935 (UNHCR 2018). YB represents the borders of Syria, Jordan and Israel joins to the Holly Jordan River (HJR). The northern portion of the Yarmouk River is the boundary between Jordan and Syria, and the southern portion is the boundary between Jordan and Israel. The total catchment area of the river measures 6,790 km², of which 1,406 km² about (20.7%) from the total area Locate within Jordan, and the rest within Syria, and Israel. YB located between 32°20'N to 32°46'N and 35°50'E to 36°20' Fig. 1. The topography of the study area is varied in terms of the elevation from 1146 m above mean Sea level (a.m.s.l) in the upper part, down to 222 m below mean Sea level (b.m.s.l) at its mouth; about 7% is classified as low land, while 64.8 % from the total area has elevation between 470 and 799 m. With respect to the slope, about 50.6% from the total area is flat and gently sloping, and only 2.5% is represents ridges. YB is hydrologically important; where the average of rainfall on its basin up to 400 mm / annually in the upper part of basin drop to 250 mm/annually at the lower part (ministry of water and irrigation 2017) and, as it is form the second major surface water resources, after the Jordan River, as the basin adjacent mountain areas and heights (Ajlun Mountains and Golan Heights (that stand at more than 1146 m) above sea level are the highest uplands to the east of the Jordan Rift Valley; and these areas receive the highest rainfall in the country (Alsharifa et al. 2018). The annual historical water discharge decreased from 467 MCM, to 14 MCM during the last few decades, As a result of the historical water conflict between Jordan, Syria, and Israel, since these all these countries are suffering from water resources scarcity, particularly Jordan In addition to the Population growth, immigration and refugees, (Alsharifa et al. 2018). Currently Syrian civil war, with the scarcity of water resources; more than 660,935 of refugees have migrated to Jordan,

and this is an emergency circumstance, forced the Jordanian government to complete the Disi Water Conveyance Project from the non-renewable Disi aquifer in 2013 over a distance of about 325 km from the Southern to the Northern of Jordan, to meet the needs of drinking and domestic use, (Ferragina and Greco 2008).

DATA AND METHODOLOGY

The LULC maps were extracted for detecting different changes in LULC during the tow selected years; 2010 and 2018. In order to achieve this goal, Satellite images of Landsat 5 and Landsat 8-OLI were acquired from USGS website www.glovis.usgs.gov (USGS 2019).

Digital image processing

The Landsat TM and OIL were prepared by using different pre-processing techniques to create LULC maps for the years of 2010 and 2018. The visible and NIR bands were combined to create layer stacking using ArcMap software, after that the Landsat were geometrically corrected using distinct ground features such as road crossing, then the Landsat images were mosaicked, subset and clipped to the borders of the (YB) (Farhan and Al-Bakr, 2012; AL-Taani et al. 2020).

Land Use/land cover

Based on reconnaissance surveys and additional information of the study area, the LULC was generated using different image processing and GIS functions for assessing its recent changes. The medium ground resolution with 30 meter of satellite images for the years of 2010 and 2018 were processed using ArcMap for mapping LULC by using an on-screen digitizing procedure of different Landsat images overlaid by the boundary of (YB) as a shape file. Four classes of LULC classification were identified as shown in Table 1.

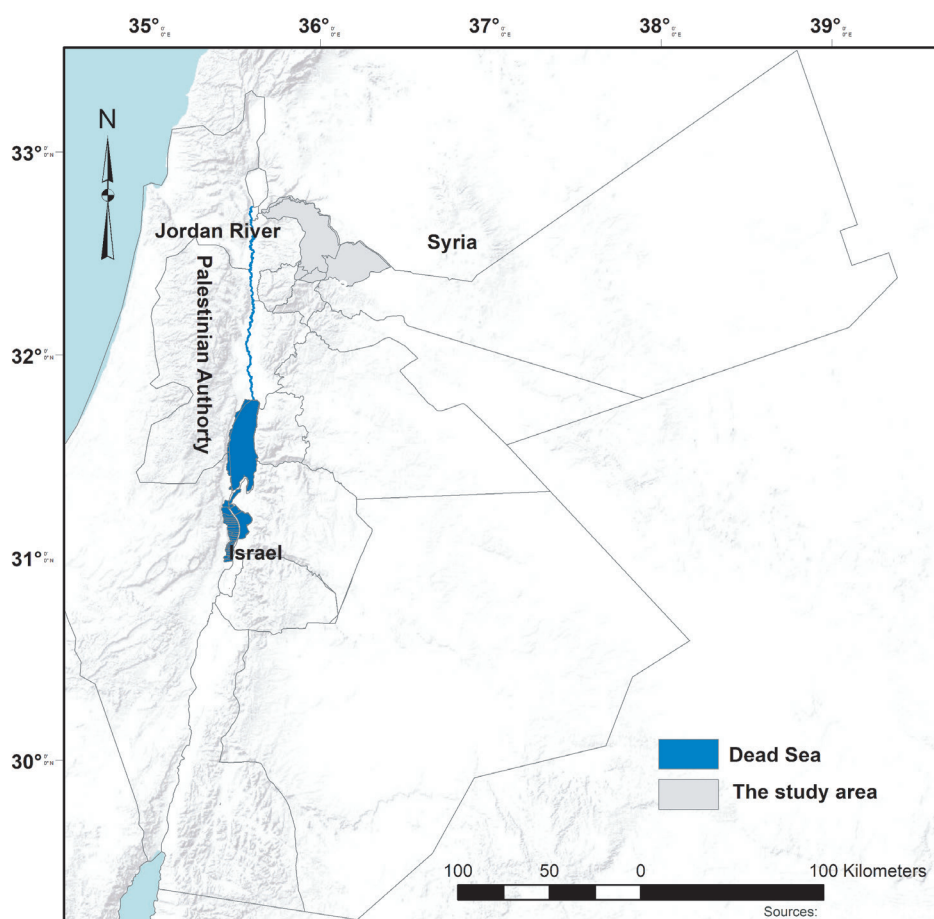


Fig. 1. The location of the Study area and the Riparian Countries

The visible and NIR bands were combined to create layer stacking using ArcMap software, after that the Landsat were geometrically corrected using distinct ground features such as road crossing, then the Landsat images were mosaicked, subset and clipped to the borders of the (YB). The digitizing technique was carried out to generate polygons by inclosing areas of different LULC types, such as built-up areas with specific boundaries, then, a new part of LULC was created and added as layers as input in ArcMap software. The new layer represents different types of LULC such as vegetated areas. Field surveys were executed during the study and supported with GPS to verify and correct results of recent LULC map (Farhan and Al-Bakri 2012).

NDVI: the red and near infrared bands were used to compute the NDVI for both dates (2010 and 2018). Using (Eq.1) (Rouse et al. 1974, USGS 2010³; Signals 2012):

$$NDVI = \frac{(NIR - Red)}{(NIR + Red)} \quad (1)$$

where, Near Infra Red (NIR) is the band 5 for the both images, and Red is band 4 for both images. The NDVI maps were reclassified at NDVI thresholds value ≥ 0.1 to separate the vegetation from the non-vegetation areas based on a threshold determined using raster calculator. The two NDVI layers were used to analyze the vegetation expansion changes and to calculate the changes of the vegetated areas.

NDVI changes between 2010 and 2018 was calculated applying (2018–2010). Both of the NDVI values exacted at value ≤ 0.1 value represent non-vegetated area, while NDVI values ≥ 0.1 represent vegetated area, Fig. 2.

IDW and Linear regression; the mean annual rainfall data from 12 meteorological stations distributed within the study area, was summarized into hydrological year. Hydrological

year used in this study starts from January to December (rainy months). The hydrological year rainfall of all stations were calculated for the years (2010–2017). Then Surface Interpolation Method was applied to convert the point data, which represents the twelve meteorological stations, into spatial surface (Al-Husban 2017). Inverse Distance Weighting (IDW) was applied in this study.

RESULTS

NDVI is an index based on spectral reflectance of the ground surface feature. Each feature has its own characteristic reflectance varying according to the wavelength (USGS 2000). NDVI value ranges between -1 to +1. A Higher value of NDVI infers the presence of healthy vegetation in the area while its lower value is the indicator of sparse vegetation. The NDVI value calculated from Landsat satellite image of the year 2010 ranges from 0.60 to -0.4. The upper part of the area having higher NDVI value belongs to the irrigated and forest areas, were found in the northern part of the (YB) and at the long of the main stream around the border between Jordan and Syria, where Al-Wehda dam constructed, in addition the high NDVI value in the western part of the basin. In comparison the NDVI 2010 values with the results of 2018 show a significant change across the whole region with NDVI value ranges from 0.50 to -0.1 (Fig. 2). Higher NDVI was found in scattered patches. The decrease in NDVI value indicates the change in the vegetated area mainly due to the decline of dense vegetated area and shifted from north to southern part far away from the border areas between Jordan and Syria.

Table 3. Information of satellite images used in this paper

Satellite Data	Bands	Acquisition Date	Spatial ground Resolution	Path and Row
Landsat (5) TM	All bands excluded band 6 (Shortwave Infrared)	2010 / August	30*30 m	Path 174 Row 38
Landsat (8) OLI	All bands excluded bands 10 and 11 (Thermal Infrared)	2018/August	30*30 m	Path 174 Row 38

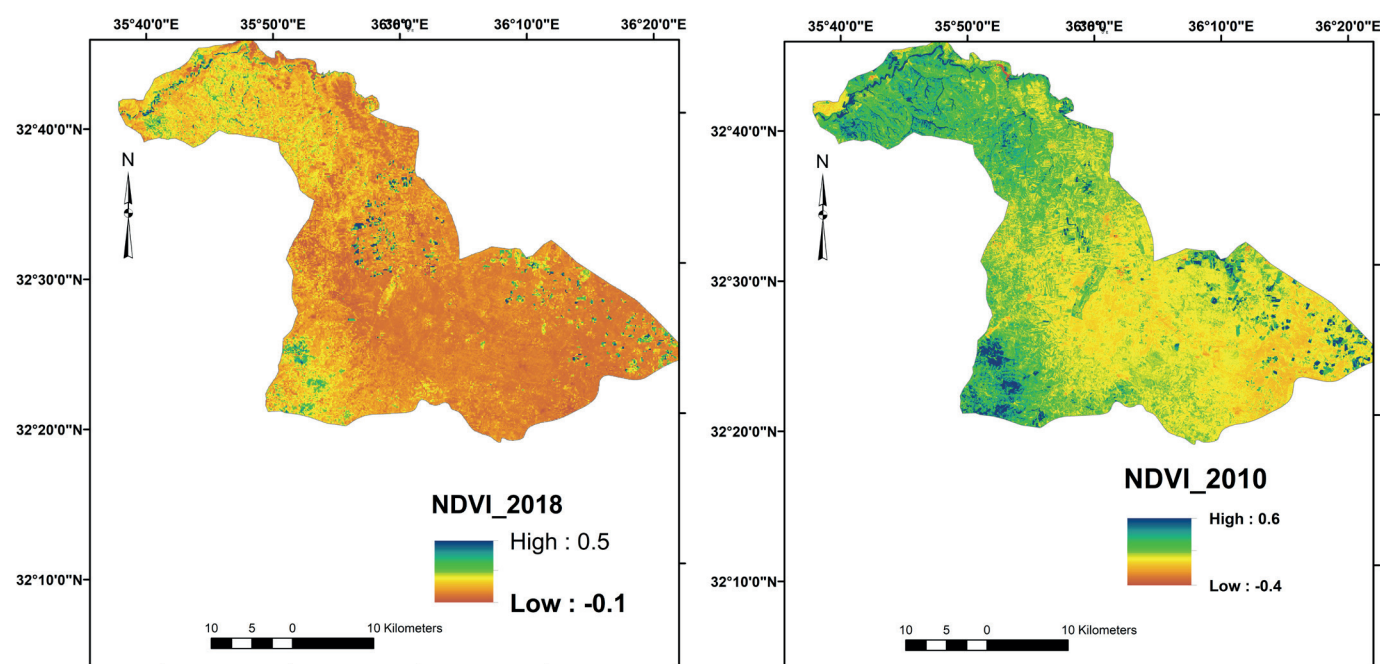


Fig. 2. NDVI variation in the study area in 2010 and 2018

³ USGS. (2010). What is NDVI? United States Geological Survey: Science for Changing World. [online]. Available at: www.ivm.cr.usgs.gov [Accessed 25 May 2020].

Image differencing method was applied for pixel-by-pixel comparison and was performed on the NDVI generated images of both dates. Image differencing was calculated using GIS tools (Raster calculator), to distinguishing the vegetation area from the non-vegetation area. Fig.3. The results indicated that the vegetation areas mainly the irrigated agriculture decreased by 12.02%, due to scarcity of water resources, as the amount of water allocated for irrigation decreased by 50% in order to meet the needs of water for the domestic uses. On the other hand, the bare area and the built-up area are increased by 8.42%, 1.69%, respectively, during the study period.

Both the two images were acquired in the same month (August) in order to minimize the impacts of seasonal differences of vegetation. To map changes that had occurred between the two dates, six spectral bands of both TM digital data were individually used as input to extract of the LULC, we applying digitizing on screen from the satellite images with the help of Google Earth. In this study, four land-cover classes could be identified. These LULC are Built-up area, vegetation area, Water bodies, and bare area. These four categories of land use/cover are definitions and summarized in table 2. The classified satellite image of the year 2010 and 2018 shows a significant change in LULC in the study area. The classified image of the year 2010, Fig. 4 shows that about 361.3 km² (25.7%) of the area is covered by vegetation, while the classified image of the year 2018 shows a significant reduction and the major change has been found in the vegetation cover area where the reduction about 13.86 km² (-12.02%) of vegetated area have been degraded between the year 2010 and 2018. The changes occur mainly due to the Syrian conflict. The results showed that the vegetation land have decreased from 361.3 km² to 192.4 km² during the

study period, built up area has increased from 136.7 km² in 2010 to 160.1 km² in 2018 which indicates that the number of population has increased during this period. In comparison, another increase was in barren area class was occurred during the study period, which increased by 74.82 km².

Linear regression In order to demonstrate the direct and rapid impact of the Syrian refugee crisis on the shrinkage of the LULC, and to exclude the effect of climate change on the dramatic decrease of vegetated area a linear regression and IDW were analyzed.

Linear regression was applied to examine and clarify the general trends in the annual mean rainfall, in the study area between (2010/2017). Simple linear regression, which studies the relationship between a response variable *y* (meteorological variable) and a predictor variable *x* (year), is essentially a trend test. Linear trend means that the rate of change over time is constant. The results of the analysis show that the gradient of trend is a slight negative, which indicates a decline in the mean rainfall in the study area. And the value of the regression coefficient (*b*) is 0.034 the negative values indicate an adcrease in the annual rainfall during the study period; but these findings are not statistically significant at the 95 % confidence level.

IDW Spatial interpolation method (IDW) for the time series (2010/2018) for all the twelve station was used to convert the point layer (meteorological stations) into spatial layer, as shown in Figure 6. In order to assess the change in the area of rainfall and to measure the area according to the mean of rainfall. The main results showed that no changes in the areas with the least mean of rainfall between the two dates. While the areas with highest mean rainfall decreased by 2%.

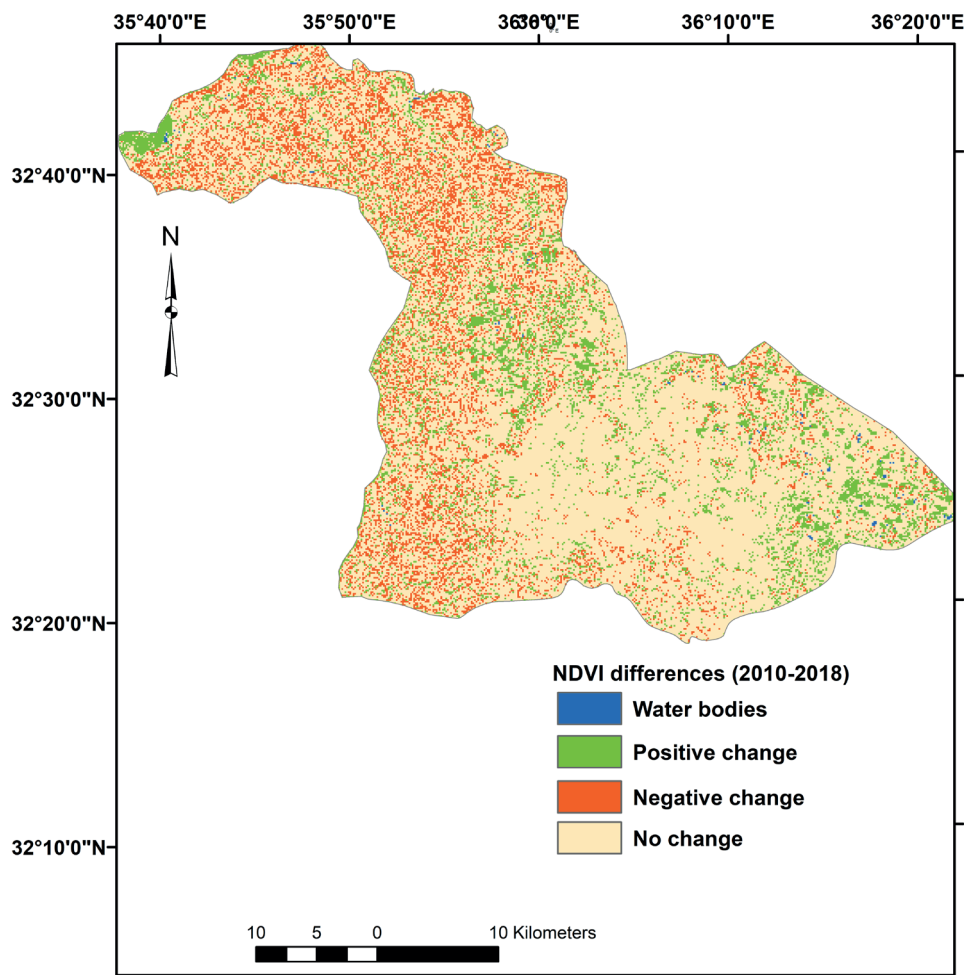


Fig. 3. Changes in NDVI during the period (2010–2018)

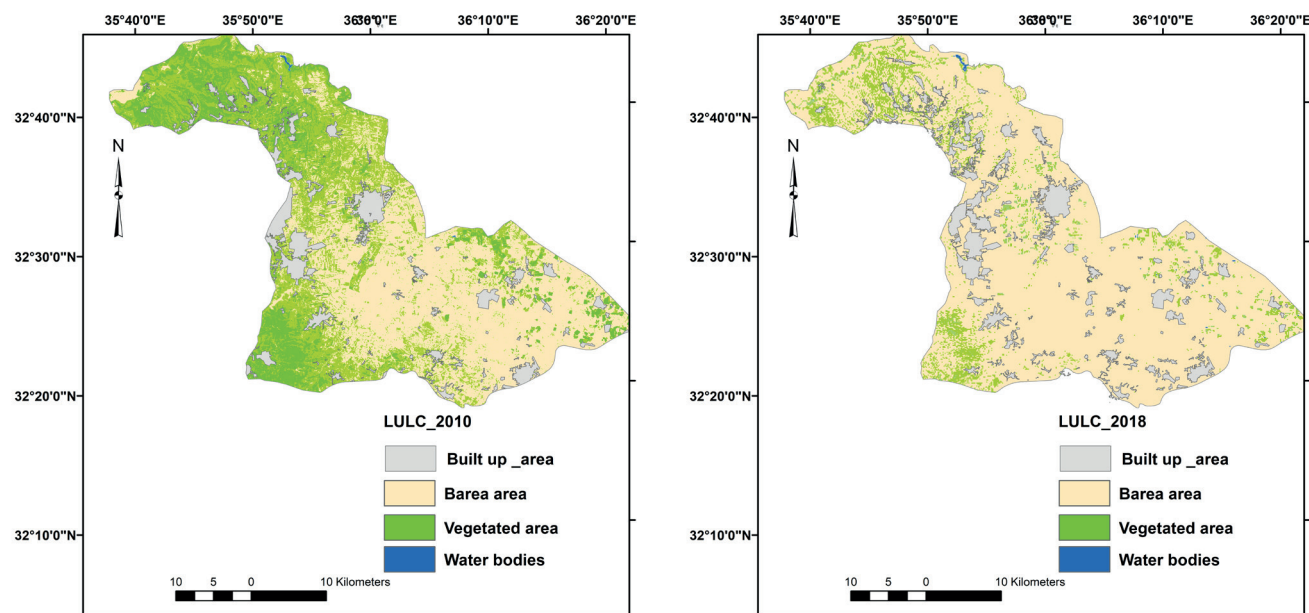
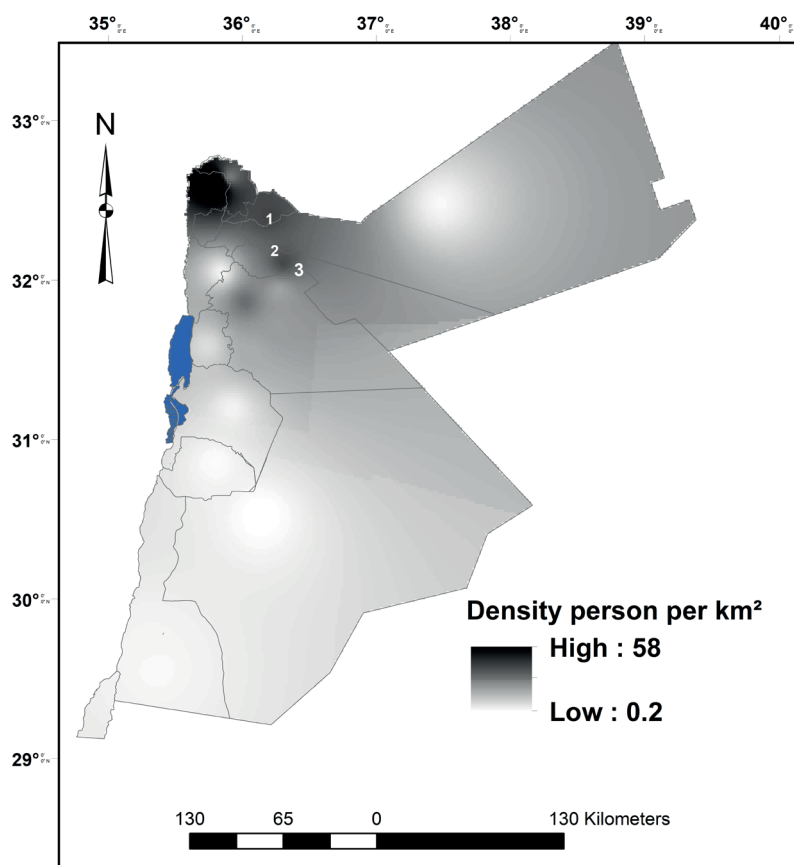


Fig. 4. LULC during the monitoring period (2010–2018)

Table 1. Grouping of the East Eurasia countries and regions according to their economic potential and growth rate (according to data for 2018)

LULC classes	Description	Area (km ²) 2010	Percentage (%) 2010	Area (km ²) 2018	Percentage (%) 2018	Changes (2010–2018) %
Water bodies	Al-Wehda dam	2.7	0.2	1.968	0.14	-0.08
Bare area	Barren or sparsely vegetated areas and bare soil.	905.3	64.4	1052	74.82	+8.42
vegetation	Irrigated lands and forested areas	361.3	25.7	192.4	13.68	-12.02
Built –up area	Includes all residential, commercial, and industrial development	136.7	9.7	160.1	11.39	1.69
Total		1,406	100.0	1,406	100.00	

Fig. 5. Syrian refugees by locality, Numbers (1-3) Za'atri, Azraq and the Emirate Camps respectively, and density person per km² (modified) from Data source: <https://data2.unhcr.org/en/documents/download/63034>

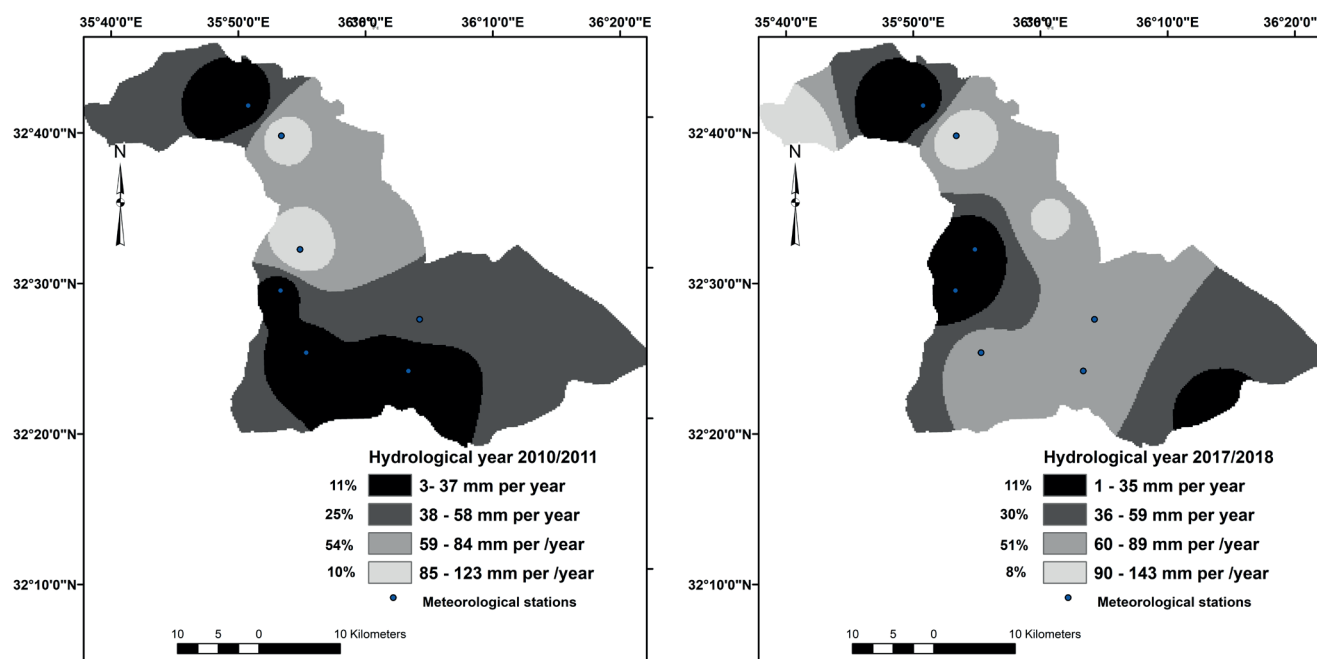


Fig. 6. IDW results and the locations of the meteorological stations

CONCLUSIONS

As the study goal is to highlight the direct and indirect effects of Syria crisis on freshwater resources through the impacts of refugee migration, land use change, and changes in water management practices in the Yarmouk–Jordan river watershed, which is the highest density of Syrian refugees, Fig. 5. NDVI index was used to monitor and evaluate the vegetation area, practically, the irrigated cropland in the study area during the dry summer months (June to September). Changes in the vegetation cover are shown in table 2 and Fig. 4. The analysis indicates a decrease in the vegetated by (-12.02%) within only 8 years in addition, an increase of the built up area by (+1.69%). Linear regression results showed that the mean annual rainfall characterized by fluctuations and contrast, and the changes have no statistically significant at the 95 % confidence level was found. Finally, (IDW)

spatial interpolation method showed decline of the areas with the highest mean rainfall by 1.4%. These results confirm the indirect impact of Syrian refugees on water for domestic purposes, which reduced the amount of water allocated for irrigated agriculture. The natural historical annual flow of the Yarmouk River is an estimated more of 400 MCM, The Current flow is around 14 MCM per year (Water Authority of Jordan 2017⁴). In addition, Ground water balance is (-14) MCM (Department of Statistics and World Food Program 2016⁵). Increases in water for domestic lead to a fall in per capita water from 140 m³ to 90 m³ by 2020, (Salman et al. 2018). The number of Syrian refugees in Jordan is about 1.4 million, representing 20% of the total population of Jordan. More than 3,500 million cubic meters are transported daily to Zaatari camp, and the per capita water supply in the northern cities has fallen below 68 liters per day in 2018. ■

REFERENCES

- Anderson J., Hardy E., Roach J. and Witmer R. (1976). A land use and land cover classification system for use with remote sensor data. Geological Survey Professional Paper No. 964, Washington DC. 28: Government Printing Office.
- Al-Bilbisi H. (2012). A two-decade land use and cover change detection and land degradation monitoring in Central Jordan using satellite images. *Jordan Journal of Social Sciences*. 5(1), 133.
- Comair G, McKinney D. and Siegel D. (2012). Hydrology of the Jordan River Basin: Watershed Delineation, Precipitation and Evapotranspiration, *Water Resource Management*, 26, 4281-4293.
- Al-Dardoor A., Al Taani A. and Hammouri N. (2013). Drought assessment using advanced GIS and remote sensing techniques: A case study of Yarmouk River Basin, unpublished Master thesis.
- Farhan I. and Al-Bakri, F. (2012). Use of GIS and Remote Sensing to Assess Soil Erosion in an Arid to Semiarid Basin in Jordan. In: *Proceedings of the International Conference on Sediment Transport: Modeling in Hydrological Watersheds and Rivers*, Istanbul, 145-152.
- Ferragina E. and Greco F. (2008). The Disi project: an internal/external analysis, *Water International*, 33, 451-463.
- Gleick P. (1993). Water and conflict: Fresh water resources and international security, *Int Secur* (18) 79-112.
- Gleick P. (2014). Water, Drought, Climate Change, and Conflict in Syria, *American Meteorological Society*. 331-340.
- Haddadin M. (2009). Cooperation and lack thereof on management of the Yarmouk River. *Water International*, 34, 420-431.
- Haddadin M. (2001). *Diplomacy on the Jordan: International Conflict and Negotiated Resolution*. Norwell, Mass: Kluwer Academic Publishers.
- Al-Husban Y. (2013). The Effect of Water Conflict on the Geomorphological of the Lower Yarmouk River during the Period (1960–2011), *European Journal of Scientific Research*, 327-337.
- Al-Husban Y. (2019). Urban expansion and shrinkage of vegetation cover in Al Balqa Governorate, the Hashemite Kingdom of Jordan, *Environmental Earth Sciences*, Springer, 78, 620.

⁴ Water Authority of Jordan, Department of Statistic. (2017). Unpublished data.

⁵ Department of Statistics and World Food Program. (2016). *The State of Food Security in Jordan (2013–2014) Analytical report*. Department of Statistics. Amman, Jordan. [online]. Available at: www.web.dos.gov.jo/wp-content/uploads/2016/10/food_2013-2014.pdf. [Accessed 25 May 2020].

- Al-Husban Y., (2013), Analysis of trends in temperature, selected stations in Arab Gulf during the period 1980–2011. *Journal of Social Sciences*, 42(1), 210-31.
- Al-Husban Y. and Zghoul M. (2017), Analysis of Drought Patterns in Azraq Depression (AD), During the Period (1984–2016). *International Journal of Applied Environmental Sciences*, 12(2), 341-358.
- Al-Husban Y. and Almanasyeh N. (2017). Accounting for the Level of Decline in the Dead Sea: Land Use and Land Cover Changes, 1984–2015. *The Arab World Geographer / Le Géographe du monde arabe*, 3(2-3), 317.
- Al-Husban Y. and Makhamreh Z. (2013). Trends in the Minimum Temperature and Number of Frost Events in the North-Eastern Badia of Jordan during the Period 1980–2010. *The Arab World Geographer / Le Géographe du monde arabe*, 16(4), 333-348.
- Al-Husban Y. (2017). Inverse Distance Weighting (IDW) for Estimating Spatial Variation of Monthly and Annually Rainfall in Azraq Basin during the monitor Period (1980–2016). *Al-Hussein Bin Talal University's journal of research*, 2(3).
- Rosenberg D. (2006). The Yarmouk River Agreements: Jordan-Syrian Transboundary Water Management, 1953–2004. *The Arab World Geographer*, 9, 23-39.
- Rouse J., Haas R., Schell J. and Deering D. (1974). Monitoring vegetation system in the Great Plains with ERTS. 3ed ERTS Symposium, Washington, D. C.: NASA SP-351. 1, 309-317.
- Salman M., Claudia C., Bucciarelli M. and Losacco M. (2018). An assessment of policies, institutions and regulations for water harvesting, solar energy, and groundwater in Jordan, A review and gap analysis, Rome: FAO.
- Shamir U. (1998). Water agreements between Israel and its neighbors. *Middle Eastern Natural Environments*, 103, 274–296.
- Al-Sharifa H., Chul H., Odeh T., Bhuiyan C. and Hussein H. (2018). Understanding the impact of droughts in the Yarmouk Basin, Jordan: monitoring droughts through meteorological and hydrological drought indices. *Arabian Journal of Geosciences*, 11, 103.
- Singh A. (1989). Digital change detection techniques using remotely-sensed data, *Int. J. Remote Sensing*, volume 10, p. 989-1003. *Sensing of Environment*, 37, 35-46, DOI: 10.1016/0034-4257 (91) 90048-B.
- Al-Taani A., Al-Husban Y., Farhan I. (2020). Land suitability evaluation for agricultural use using GIS and remote sensing techniques: The case study of Ma'an Governorate, Jordan. *The Egyptian Journal of Remote Sensing and Space Sciences*. DOI: 10.1016/j.ejrs.2020.01.001.
- Toset H., Gleditsch N., Hegre H. (2000). Shared rivers and interstate conflict. *Polit Geog*, 19, 971-996.

MAPPING TEMPERATURE AND PRECIPITATION EXTREMES UNDER CHANGING CLIMATE (ON THE EXAMPLE OF THE URAL REGION, RUSSIA)

Andrey N. Shikhov^{1*}, Rinat K. Abdullin¹, Andrey V. Tarasov¹

¹Perm State University, 15 Bukireva street, Perm, 614990, Russia

Corresponding author: shikhovan@gmail.com

Received: March 29th, 2019 / Accepted: May 10th, 2020 / Published: July 1st, 2020

<https://DOI-10.24057/2071-9388-2019-42>

ABSTRACT. The paper presents a series of maps of extreme climatic characteristics for the Ural region and their changes under climate warming observed in last decades. We calculate threshold, absolute and percentile-based indices with the use of daily temperature and precipitation dataset of 99 weather stations of Roshydromet. Extreme climatic characteristics were averaged by moving 30-year periods from 1951 to 2010 for temperature and from 1966 to 2015 for precipitation. The regression-based interpolation was used for mapping climatic extremes taking into consideration the influence of topography. Elevation and general curvature of the terrain are considered as independent variables. In addition, the changes of extreme characteristics between the 30-year periods were estimated. As a result, a series of maps of temperature and precipitation extremes for the Ural region has been created. The maps present not only spatial distribution of the climatic extremes, but also regional features of their changes under climate warming. In general, the revealed changes in extremes in the Ural region correspond to the trends observed on the most of the territory of Russia. There is a substantial decrease of the number of extremely cold days in winter, and the minimum winter temperature has a strong positive trend (up to 1-5°C/30 years). The maximum temperature in summer has a positive trend in most of the territory, but the increase rate does not exceed 2°C between 1951–1980 and 1981–2010. The precipitation extremes also increased up to 0.5-1.5 mm when comparing 1966–1995 and 1985–2015 periods.

KEY WORDS: climatic extremes, extreme temperature and precipitation indices, mapping, regression-based interpolation, Ural regio

CITATION: Andrey N. Shikhov, Rinat K. Abdullin, Andrey V. Tarasov (2020). Mapping temperature and precipitation extremes under changing climate (on the example of The Ural region, Russia). *Geography, Environment, Sustainability*, Vol.13, No 2, p. 154-165

<https://DOI-10.24057/2071-9388-2019-42>

ACKNOWLEDGEMENTS: This study was funded by the RFBR project No 18-35-00055 mol-a and RF President Grant MK-313.2020.5.

Conflict of interests: The authors reported no potential conflict of interest.

INTRODUCTION

Global warming leads to a change in both the mean and extreme values of climate variables. For decades, most analyses of long-term global climate change using observational data have focused on trends in mean values (Alexander et al. 2006). However, a change in extreme climatic characteristics may induce more substantial consequences, than in average. Last years, many studies examine the influence of global warming on the increase of climatic extremes and hazardous weather events (Frich et al. 2002; Groisman et al. 2005; Alexander et al. 2006; Bulygina et al. 2007; Zolina and Bulygina 2016; Mokhov and Semenov 2016). Changes in the frequency of occurrence of climatic extremes are under attention of the scientific community because the risks associated with them exceed the risks due to the changes in average values. In addition, the rate of increase of extremes can significantly exceed the same of the average values, which amplify the corresponding risks (Bardin and Platova 2013).

Expert Team on Climate Change Detection and Indices (ETCCDI) developed and recommended 27 indices of climate extremes, which can be derived from daily maximum and minimum temperature and daily precipitation. 16 of the 27 indices are temperature related and 11 are precipitation related (Alexander et al. 2006; Kiktev et al. 2009; Donat et al. 2013 a,b). The indices are used to estimate an intensity, frequency and duration of extreme temperature and precipitation events, and can be divided into five different categories.

Percentile-based indices of temperature and precipitation extremes. The temperature percentile-based indices show the coldest and warmest deciles for both maximum and minimum temperatures (TN10p, TN90p, TX10p and TX90p). The precipitation indices in this category represent the amount of precipitation falling above the 95th (R95p) and 99th (R99p) percentiles. Sometimes other percentiles are used, e.g. 95p or 99p for temperature extremes. The advantage of these indices is the possibility of their use for large areas with various climatic conditions. However,

the calculated threshold values of extremes are often not associated with hazardous weather and climate-related risks (Bardin and Platova 2013; Zolina and Bulygina 2016).

Absolute indices represent maximum or minimum values within a season or year. They include maximum daily maximum temperature (TXx), maximum daily minimum temperature (TNx), minimum daily maximum temperature (TXn), minimum daily minimum temperature (TNn), maximum 1-day precipitation amount (RX1day) and maximum 5-day precipitation amount (RX5day) (Alexander et al. 2006; Kiktev et al. 2009).

Threshold indices, which are defined as the number of days on which a temperature or precipitation value falls above or below a fixed threshold, such as number of frost days or number of days with very heavy precipitation (> 30 mm). The threshold values of the indices can coincide with the accepted criteria of hazardous or adverse weather events. However, threshold criteria are not suitable for large areas with various climatic conditions (Alexander et al. 2006; Kiktev et al. 2009).

Duration indices, which define periods of excessive warmth, cold, wetness or dryness or in the case of growing season length, periods of mildness. Growing season length, consecutive dry days and heat wave duration index are the most frequently used indices of this category.

Other indices, which do not fall into any of the above categories, characterized the diurnal temperature range, extreme temperature range, contribution from very wet days to annual precipitation etc. (Alexander et al. 2006; Kiktev et al. 2009).

Two global land gridded datasets of temperature and precipitation extremes have been developed for climate change monitoring purposes. The first was HadEX dataset which cover the period 1951–2003. It is not updated and most of the data is not publicly available (Donat et al. 2013a). A new dataset termed GHCNDEX is an operationally updated and based on daily observations of maximum and minimum temperatures as well as daily precipitation amounts from 29,000 weather stations (Donat et al. 2013b). The dataset is publicly available at <https://www.climdex.org>. It contains 26 of the indices recommended by the ETCCDI and updated until 2013 for the territory of Russia. However, the data has a substantial number of omissions.

The indices recommended by ETCCDI and their modifications are widely used to study observed changes in extreme climate events in Russia. Bulygina et al. (2007) used percentile-based indices to estimate the changes in annual and seasonal extreme characteristics of temperature and precipitation for 1951–2005, according to 857 weather stations of Roshydromet. A decrease in the number of extremely cold days, an increase in the number of extremely warm days and the number of extreme precipitation events have been found for most of the territory of Russia. Bardin and Platova (2013) compared long-term changes of temperature and precipitation extremes by seasons of a year, calculated from percentile-based indices, with changes of the mean values (for 1976–2009). They found substantial distinctions between the changes in means and extreme temperature (especially in winter season).

Last years, several studies have considered the changes of extreme precipitations in Russia. Zolina and Bulygina (2016) calculated the absolute and relative indices of precipitation extremes, and also the number of consecutive dry days (CDD) and consecutive wet days (CWD) indices for 1966–2012. They showed that the frequency and intensity of extreme precipitation increases in most regions of Russia. Also, the rise in duration both dry and wet periods was found for many regions, which indicated a significant

clustering of precipitation over time and an increase of probability of both floods and droughts events. Titkova et al. (2018) compared the frequency of extreme climatic events in winter season for 1970–2000 and 2001–2015. A significant decrease of very cold days, increase of very warm days and extreme precipitation events has been confirmed for most of Russia, especially for the European part of the country (ER). Zolotokrylin and Cherenkova (2017) analyzed the probable damaging effects of the observed increase of precipitation extremes on the environment and human activities for Russian regions with high population density.

So, the changes of temperature and precipitation extremes over entire Russia, observed during last decades, are relatively well-studied. At the same time, no such studies were performed at the regional scale level, which require an analysis of the geographical location of each weather station and consideration of the underlying surface influence on the spatial distribution of climate extremes. Some experience of climatic extremes mapping at the regional scale level is presented in the Atlas of hazardous hydro-meteorological events of the Perm region (Pyankov et al. 2017). However, the similar studies for other regions of Russia have not been conducted.

Worldwide, most of regional investigations of the climatic extremes examine the characteristics of extreme precipitation. A number of extreme rainfall characteristics are considered, such as probable maximum precipitation (PMP), intensity-duration frequency curve, probable maximum of precipitation for the period of 10 or 100 year, expected return interval of extreme precipitation events, e.g. 100 mm/day et al. (Beguería and Vicente-Serrano 2005). In some studies, not only daily precipitation extremes, but also extreme events lasting several days are considered (Beguería et al. 2009).

Mapping of other climatic extremes (e.g. temperature, wind speed extremes) at a regional scale level is considered in few publications. Blennow and Persson (1998) developed a GIS-based linear regression model for local-scale temperature interpolation and frosts probability. The model takes into account four independent variables – sky view factor, elevation, relative relief and presence of peat soil. Li and Zha (2018) proposed a method for mapping climate variables (including extreme temperature) based on random forest regression models.

The purpose of this study is to develop a series of maps of temperature and precipitation extremes and their changes under observed climate warming for the Urals region. Earlier, the maps of the mean annual and monthly values of temperature and precipitation and their changes for 1951–2015 have been created for the same territory (Abdullin and Shikhov 2019). Therefore, the second purpose of the study is to compare the trends in average and extreme characteristics.

DATA AND METHODS

Initial data

We used daily temperature and precipitation dataset (<http://aisori.meteo.ru/Climater>), compiled by All-Russian Research Institute of Hydro-Meteorological Information – World Data Center (RIHMI-WDC) as input data for mapping temperature and precipitation extremes. We selected the data from 99 weather station of Roshydromet, located within the studied region and near it (Fig. 1). Temperature dataset was analyzed for 1951–2015 and precipitation – for 1966–2015, because precipitation data is not homogeneous before 1966 (Bulygina et al. 2007). A digital elevation model (DEM) with 1 km resolution, obtained on the basis of the GMTED-2010 DEM (Danielson and Gesch 2011), was

used to find the relationships between extreme climatic characteristics and terrain properties (elevation, slope, aspect and curvature).

Extreme climatic characteristics are calculated for 30-year periods (1951–1990, 1971–2000, 1981–2010 for temperature extremes and 1966–1995, 1976–2005, 1986–2015 for precipitation extremes), since World Meteorological Organization (WMO) recommended the use of 30-year periods for climatological studies. The first 30-year interval (1951–1980) indicates the state of the climate before the start of contemporary rapid warming in the Northern Eurasia (Groisman and Soja 2009).

Four categories of indices, recommended by ETCCDI (Alexander et al. 2006) are calculated for temperature and precipitation extremes. Among threshold indices, number of days with minimum temperature $\leq -30^\circ$, maximum temperature $\geq 30^\circ\text{C}$ and heavy precipitation ≥ 30 mm (over above-mentioned 30-year periods) are calculated. The selected threshold values coincide with the criteria of adverse weather events, accepted in the most of studied regions. Annual minimum and maximum of temperature and annual maximum of daily precipitation, averaged over 30-year periods, are used as absolute indices. We also calculated percentile-based indices for temperature and precipitation extremes. Extreme temperature events are determined as the days with maximum temperature exceeding 99% percentile (99p), and with minimum temperature of less than 1% percentile (1p) of empirical distribution function for maximum and minimum

daily temperatures respectively. Extreme precipitation events are determined similarly, as daily precipitation exceeding 99% percentile of empirical distribution function, which was calculated from the entire studied period (1951–2015 for temperature, and 1966–2015 for precipitation).

Among the duration indices, we calculated only the average annual number of CDD for summer months. Its values may be related to the frequency and intensity of summer droughts and wildfire outbreaks, which occur every few years in different parts of the Ural region (Shikhov et al. 2019).

Programs and programming languages that were used in the study

The climatic data were processed with Python program language (Pandas library). The maps were constructed with ArcGIS 10.4.

Overview of the interpolation methods appropriate for climate mapping

Spatial distribution of both mean and extreme climatic characteristics is determined by both the geographical location (latitude, longitude) and characteristics of the underlying surface, especially in areas with rugged terrain. Various statistical methods have been developed to predict (interpolate) climatic variables in regions with sparse observation network and rugged terrain (Ninyerola et al. 2000; Weisse and Bois 2002; Vicente-Serrano et al. 2003). They can be subdivided into global and local methods.

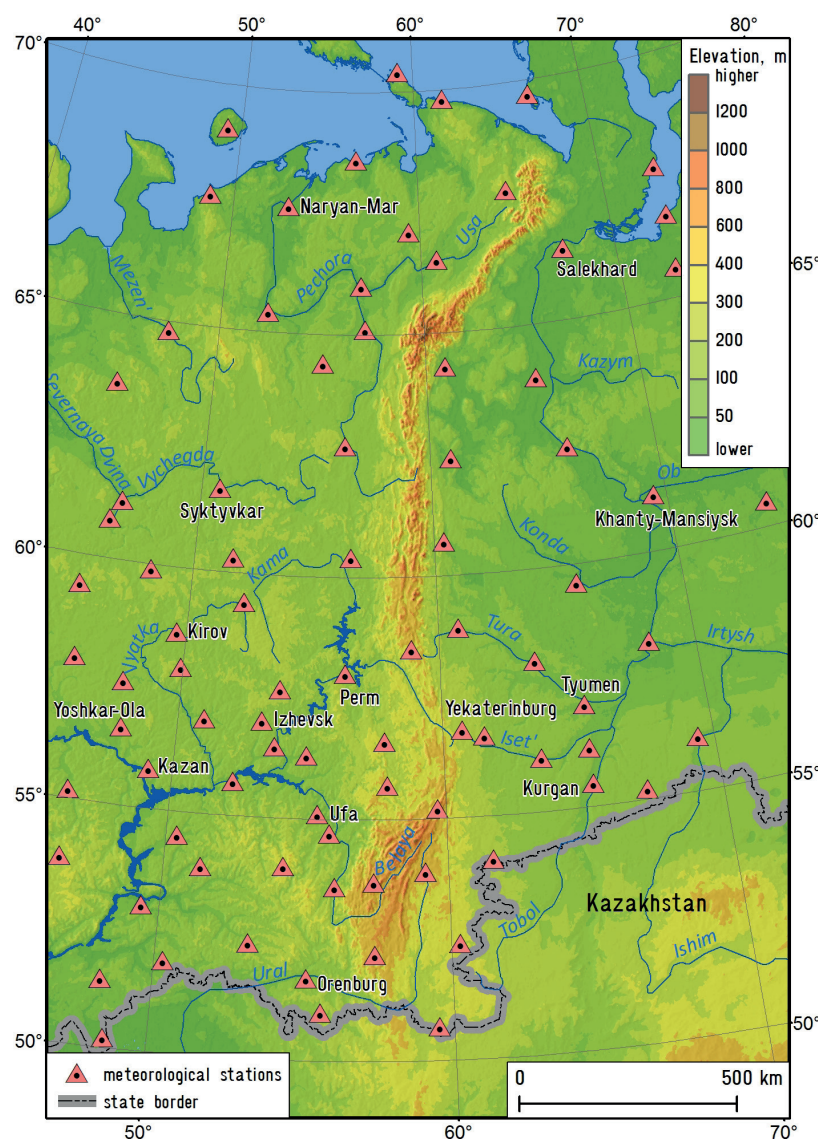


Fig. 1. Study area and location of the weather stations whose observations were used

A general practice of the use of global methods presume estimation of the relationships between climatic data and independent variables (predictors) such as latitude and longitude of the weather stations, topographic (e.g. elevation, aspect, slope, etc.) and/or geographic (e.g. distance to water bodies) variables. These relationships are used to produce climatic maps by means of empirical simple- or multiple-regression models. Such global regression-based estimate is inexact since the predicted values do not coincide with the measured values at weather stations (Goodale et al. 1998; Vicente-Serrano et al. 2003).

Among local methods, the most widely used for the climate mapping are various geostatistical techniques (Goovaerts 2000; Vicente-Serrano et al. 2003). Some of them based only on the climatic data recorded at the weather stations (e.g. simple kriging, ordinary kriging), while others use topographic/geographic information (e.g. cokriging or universal kriging).

Also, a group of 'mixed' methods combines global, local and geostatistical techniques (Ninyerola et al. 2000, Brown & Comrie 2002). These methods take into account both the physical relationships between climatic data and geographic/topographic variables, and the spatial correlation between weather stations data. Vicente-Serrano et al. (2003) showed that regression-based interpolation and geostatistical methods are most appropriate for temperature and precipitation mapping in the areas with rugged terrain.

Mapping of the climatic extremes with threshold indices

In this study, we used a 'mixed' interpolation technique which was firstly proposed to predict the spatial distribution of snow water equivalent (Shutov 1998). It combines spline interpolation with simple linear regression model. Earlier, we successfully used this technique for mapping of the frequency of hazardous weather events in the Perm region (Abdullin and Shikhov 2017). We could not use the multiple regression model based on several geographical and topographic variables, since the determination coefficients were not high enough (less than 0.85), except for the minimum daily temperature in winter.

The maps of threshold indices, as well as on absolute indices of climatic extremes were created based on the technique including five consecutive stages.

1. Fitting a linear regression between the calculated indices of climatic extremes (dependent variables) and terrain properties such as elevation, aspect, general curvature (independent variables), estimated for the location of each weather station;
2. Assessment of the regression significance at a threshold p-value of 0.05. The examples of a statistically significant regression are shown at Fig. 2;
3. Calculating of the values of indices under the assumption of a zero value of independent variables for each weather station according to the formula:

$$y_0 = y - ax_{st} \quad (1)$$

Where y_0 is the value of dependent variable under the assumption of a zero value of independent variable, y signifies the initial values of dependent variable, x_{st} is the value of independent variable in the location of each weather station and a is the coefficient in the linear regression equation (e.g. elevation-dependent gradient of temperature or precipitation);

4. Interpolation of the indices values from weather stations, calculated under the assumption of a zero value of the independent variable, using the method spline with tension. Spline interpolation method was selected due to its successful application in a number of climatic studies (Fick and Hijmans 2017; Chernokulsky et al. 2018);

5. Correction of interpolation results based on estimated regression between indices and independent variables with map algebra tool, according to the following formula:

$$y_0 = y + ax_f \quad (2)$$

where x_f signifies the values of independent variable (for example, elevation) in each grid cell. Then, the resulting grid was smoothed with mean filter.

So, large-scale variability of the indices, related to latitude and longitude of location, was taken into account with spline interpolation of the weather stations data, and mesoscale variability (related to underlying surface properties) was considered using regression models.

The resulting values in grid cells, corresponding to the location of the weather stations are equal to the observed values. The exception is only if the elevation was a single independent variable. In this case, initial values of elevation of the weather station, obtained from (<http://meteo.ru/>), may differ from the elevation values in the corresponding cells of the DEM. Consequently, the resulted value of the indices at the cell of weather station may differ from the observed value. In other cases, the initial values of independent variables were extracted from DEM.

Surface elevation is the main variable determining the spatial distribution of extremely high temperature (number of days with a maximum temperature $\geq 30^\circ\text{C}$) and heavy precipitations (≥ 30 mm/day). Large water bodies and urban heat islands have also some influence on the spatial distribution of a maximum temperature, but it is low-pronounced at a scale of 1:10 000 000. The linear regression between the number of days with temperatures $\geq 30^\circ\text{C}$ and elevation was estimated on the data from 36 weather stations located between 56 and 60° N. Thus, the influence of the large-scale (zonal) temperature gradient was reduced.

The number of days with heavy precipitation (≥ 30 mm/day), also correlate with surface elevation, but correlation coefficient is non-significant at 0.05 P-value. We used two-step approach with the introduction of additional variable, namely annual average maximum of daily precipitation. It has a statistically significant correlation with elevation at a 0.05 P-value (Fig. 3b), and also it has a strong correlation ($R^2 = 0.82$) with the number of heavy precipitation events (Fig. 2a). We supposed, that spatial distribution of the number of days with heavy precipitation is similar with average annual maximum of daily precipitation. So, we initially interpolate the annual average maximum of daily precipitation with elevation-dependent regression (Fig. 3b). Then, the corresponding values of the number of days with heavy precipitation were estimated for each pixel, using the linear regression (Fig. 2a).

The spatial distribution of the minimum daily temperature in winter is determined not by elevation, but by general curvature of the terrain (Fig. 2b). Indeed, the minimum temperature is much lower in landforms with negative curvature, than over elevated landforms, especially under anti-cyclonic weather conditions. Consequently, the frequency of extremely low temperatures should increase in the negative landforms. The relationship between the frequency of extremely low temperatures and general curvature was previously used for the Perm Region (Abdullin and Shikhov 2017). However, it is impossible to use it for the entire Ural region, since the frequency of the days with a minimum temperature $\leq -30^\circ$ strongly increases from south-west to north-east. Therefore, we applied a multiple linear regression which is based on three independent variables such as latitude, longitude and general curvature of the terrain, extracted from a smoothed DEM. The value of the multiple R^2 is 0.85.

Mapping of the climatic extremes with absolute indices and duration indices

To create the maps of the average annual maximum and minimum of temperature, as well as the average annual maximum of precipitation, we used the same relationships with the terrain properties, as for the corresponding absolute indices. The workflow of the creation of the maps includes the above-described five steps. The examples of the relationships between absolute indices of climatic extremes and terrain properties are shown at Fig. 3.

The number of CDD in summer has statistically significant inverse relationship with elevation of the weather station (at a 0.05 P-value). So, we interpolate CDD with elevation-dependent regression and obtained a reliable estimate of its spatial distribution.

Mapping of climatic extremes with percentile-based indices

Percentile-based indices of climatic extremes can be divided into two types, such as threshold values of temperature (1% and

99% percentiles) or precipitation (99% percentile) (type 1), and number of days with extreme temperatures or precipitations (type 2). Threshold values of extreme characteristics, calculated by percentile-based indices, have the same patterns of the spatial distribution, that corresponding absolute indices. So, we used interpolation with elevation-dependent regression to create the maps of 99p daily precipitation (calculated over the entire year and for cold season only), and for 99p maximum temperature in summer (Fig. 3a). The 1p minimum temperature in winter has statistically significant relationship with general curvature of terrain (Fig. 4b).

In turn, the spatial distribution of the number of days with extreme temperatures or precipitations (calculated by percentile-based threshold values) weakly correlated with underlying surface properties. Therefore, simple interpolation methods without considering any regressions are sufficient for mapping them.

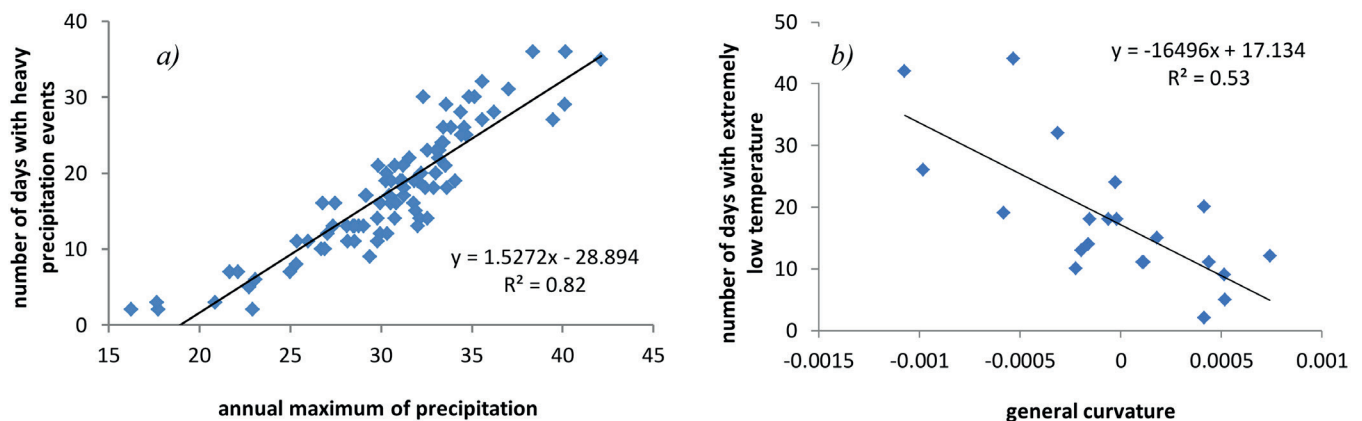


Fig. 2. Relationships between number of days with heavy precipitation and annual maximum of daily precipitation (a), and between number of days with minimum temperature $\leq -30^\circ\text{C}$ and general curvature (b)

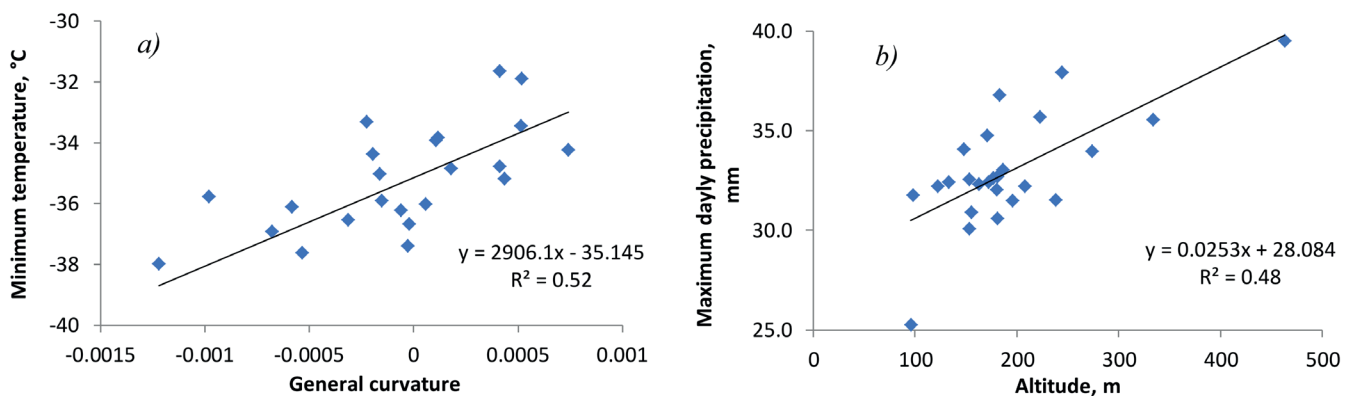


Fig. 3. Relationships of average annual minimum of temperature with general curvature (a), and average annual maximum of daily precipitation with elevation (b)

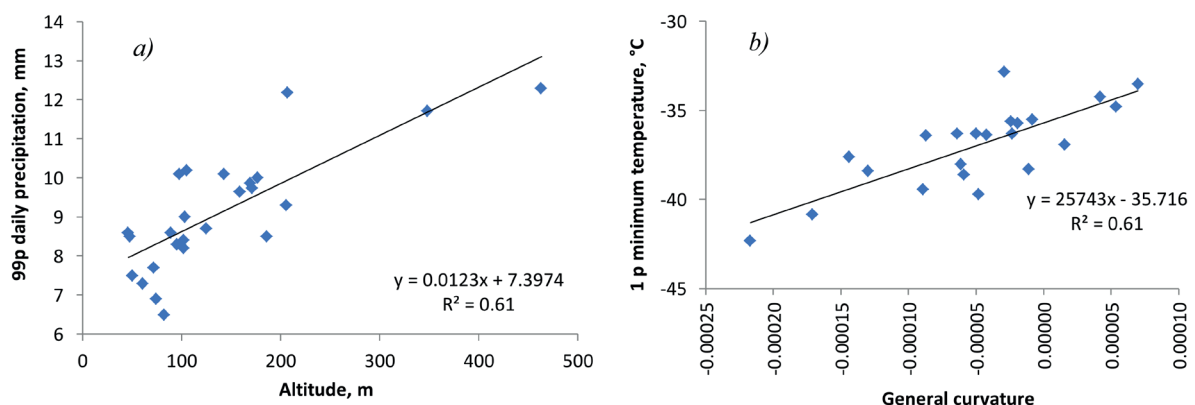


Fig. 4. Relationships of 99p daily precipitation in cold season with elevation (a), and 1p minimum temperature in winter with general curvature of the terrain (b)

RESULTS AND DISCUSSION

The created maps of the spatial distribution of temperature and precipitation extremes are shown at Fig. 5-11. We compared the climatic extremes indices for the first and last studied 30-year periods (1951–1980 and 1981–2010 for temperature extremes, 1966–1995 and 1986–2015 for precipitation extremes) and also calculated the difference between them to indicate the changes that have been occurred in the last decades. The difference maps (Fig. 5-11c) are more smoothed than initial maps of climatic extreme indices, since the above-described relationships of the indices with terrain properties (elevation, curvature) does not changes with time. Therefore, the difference maps indicate only large-scale variability of the indices, related to latitude and longitude of location, without substantial influence of the terrain.

Table 1 summarizes the average, minimum and maximum values of such differences over the Ural region.

In average for the Ural region, there was a substantial decrease of the frequency of extremely cold days in winter. In turn, the frequency of extremely warm days and extreme precipitation has increased. In accordance with this, the average annual maximum and minimum of temperature have also increased (especially the annual minimum of temperature) like the average annual maximum of precipitation.

The similar changes in temperature and precipitation extremes have been observed during last decades in the most of Northern Eurasia (Bulygina et al. 2007; Zolotokrylin and Cherenkova 2017; Titkova et al. 2018). However, the notable regional variations in climatic extremes changes are found within the Ural region, which may be related to both changes in the atmospheric circulation and geographical features of the location of weather stations. These regional variations are analyzed in more detail.

The average annual minimum of temperature ranges from $-44 \dots -47^{\circ}\text{C}$ east of the Polar Ural to $-31 \dots -34^{\circ}\text{C}$ west of the Southern Ural and also near the Yekaterinburg city (Fig. 5). It has increased by $1\text{--}5^{\circ}\text{C}$ between 1951–1980 and 1981–2010. The highest increase rate (up to $4\text{--}5^{\circ}\text{C}$ per 30 years) is observed in the south-east of the Ural (Sverdlovsk, Kurgan and Tyumen' regions), and the lowest rate is only 1°C per 30 years near the Polar Ural. The 1p minimum daily temperature in winter has also increased by $1\text{--}5^{\circ}\text{C}$ per 30 years (Fig. 6). The spatial distribution of the increase rate is similar to that of the average annual minimum of temperature. The number of extremely cold days in winter has been also significantly reduced (from 20–25 days/10 years in 1951–1980 to 4–8 days/10 year in 1981–2010) in the south-east of the Ural.

In general, the positive trend of minimum winter temperature corresponds to the observed decrease of temperature variance in high and middle latitudes of the Northern Hemisphere (Screen, 2014; Titkova et al. 2018). However, the regional variations are related to other factors. For instance, extremely cold winter seasons have been occurred in the south-east of the Urals in the 60s and 70s of 20th century (e.g. 1968–1969), when seasonal minimum of temperature ranged from -40° to -50°C . After 1984, such extreme cold days were not observed in this area, although long-term, but less severe frosts happened, in 2005–2006 and 2009–2010 winter seasons.

A relatively weak positive trend in the minimum winter temperature observed west of the Polar Ural may be related to the increase of the frequency of arctic air mass advection during cold season. The observed anticyclonic anomaly of 500hPa geopotential height and sea level pressure over the Barents and Kara Seas may contribute to this process (Titkova et al. 2018).

In addition to the changes of atmospheric circulation, the features of geographical location of the weather stations also affect the increase rate of the minimum winter temperature. For example, the weather stations located in the depressions or in the deep valleys such as Krasnoufimsk and Verkhneural'sk., reported an increase in the minimum winter temperature of only $1\text{--}2^{\circ}\text{C}/30$ years, whereas at neighboring stations the increase was much stronger (up to $3\text{--}3.5^{\circ}\text{C}/30$ years). Before the start of the contemporary climate warming extremely cold days observed more often on the entire territory (regardless of the topography features). Currently, severe frosts are mainly observed in depressions and in deep valleys of rivers. This pattern can be also related to the increase of temperatures of the air masses spreading from the Arctic to the Ural region (Kim et al. 2019).

The average annual maximum of temperature ranges from $+26^{\circ}\text{C}$ in the Polar Ural to $+35^{\circ}\text{C}$ west of the Southern Ural (Fig. 7). When comparing the periods 1951–1980 and 1981–2010, it has increased from $0.1\text{--}0.2^{\circ}\text{C}$ in the southeast of Ural to $0.6\text{--}0.7^{\circ}\text{C}$ in the north-west. The values of 99p maximum daily temperature in summer have increased by $0.5\text{--}1^{\circ}\text{C}$ in the most of the territory (Fig. 8). The highest increase rate (up to 2°C per 30 year) is observed to the west of the Ural ridge, in the Kirov region and Udmurt republic, which were most affected by the extreme heat wave of summer 2010. In the same time, the 99p maximum daily temperature decreased by $0.5\text{--}1^{\circ}\text{C}$ in the southeast of Ural (Kurgan and Tyumen' regions). This indicates the amplification of summer heat waves in the ER, with simultaneous reduction in Western Siberia. An increase of the maximum temperature in summer west of the Ural

Table 1. Average, maximum and minimum values of the difference of climatic extreme indices between two compared periods

Variable	Compared periods	Average difference	Minimum difference	Maximum difference
Average annual minimum of temperature, $^{\circ}\text{C}$	1951–1980 and 1981–2010	2.8	0.1	5.8
1p minimum daily temperature in winter, $^{\circ}\text{C}$	1951–1980 and 1981–2010	2.4	0.1	5.6
Average annual maximum of temperature, $^{\circ}\text{C}$	1951–1980 and 1981–2010	0.4	–0.1	1.0
1p maximum daily temperature in summer, $^{\circ}\text{C}$	1951–1980 and 1981–2010	0.6	–2.2	2.4
99p daily precipitation, mm	1966–1985 and 1986–2015	0.3	–3.1	2.1
Number of days with daily precipitation ≥ 30 mm	1966–1985 and 1986–2015	0.5	–4.1	4.3
Consecutive dry days in summer	1966–1985 and 1986–2015	0.4	–2.4	3.0

ridge is related to the rise in the frequency and intensity of blocking anticyclones in the Atlantic-European region (Cherenkova 2017). The decrease in extreme summer temperatures in the southeast Ural is also due to the same process, since arctic air masses spread to the Western Siberia along the eastern periphery of these blockings.

The number of extremely hot days in summer also amplified most strongly (by 7 days/10 years) in the Kirov region and Udmurt republic, and also west of the Polar Ural. On the contrary, it decreased by 1-3 days/10 years in the southeastern Ural (Kurgan and Tyumen' regions).

Average annual maximum of precipitation ranges from 15 mm on the Yamal peninsula to 35-40 mm along the Ural ridge and near Tyumen' city. The second local maximum near Tyumen' city is most likely due to the fact that southern cyclones which induced heavy precipitation are often moving through this area. Between 1965–1995 and 1985–2015, average annual maximum of precipitation has increased to 1-5 mm on the most part of the territory. The most substantial increase was observed in the Middle Ural and adjacent plains.

The threshold values of 99p daily precipitation ranges from 11 mm on the Yamal Peninsula to 20-22 mm along the Ural mountains. When comparing the 1965–1995 and 1985–2015 periods, it has increased by 0.5-1.5 mm in the most part of the Ural region (Fig. 9). Some weather stations in different parts of the Ural reported a decrease of 99p daily precipitation to 0.5-1 mm per 30 year, and up to 1.5 mm on the Yamal Peninsula. The observed increase of 99p daily precipitation is in concordance with positive trends in precipitation extremes changes which were previously found for the most part of Russia (Zolina and Bulygina 2016; Zolotokrylin and Cherenkova 2017).

The number of days with daily precipitation exceeding 30 mm ranges from 2 days/10 year on the Yamal Peninsula to 12 days/10 year on the Northern and Middle Ural ridge, with the observed maximum at the Biser weather station (58.51°N, 58.85°E). It has also increased to 1-3 days/10 year

when comparing 1965–1995 and 1985–2015 (Fig. 10). The negative trend is observed at some weather stations located in different parts of the region, mainly east of the Northern and Polar Ural, and also in the Orenburg region.

Comparing the changes of precipitation extremes between 1966–1985 and 1986–2015, it is important to consider that the highest precipitation amount and many extreme precipitation events in the Ural have been observed in 1989–1990 and 1992–1994 (Perevedentsev et al. 2013). These years already fall into the period 1966–1995. Therefore, the observed increase in precipitation extremes is relatively weak.

The distribution of the number of CDD in summer months ranges from 5-6 days in the northern part of the Ural ridge to 14-15 days in Orenburg region, where summer droughts are most frequent. The number of CDD had no significant changes between 1966–1995 and 1986–2015 on the most part of the Ural region. The most substantial increase (up to 2 days) occurred in the Kurgan region (Fig. 11). Strong droughts in southern part of the Ural region have been observed regularly, every 10-15 years (e.g. in summer of 1975, 1989, 1998 and 2010). However, a substantial increase in their frequency is not observed.

Comparison of the changes in average and extreme climatic characteristics

We compared the maps of the changes of temperature and precipitation extremes (1p and 99p threshold values) with the previously created maps of the changes in average annual and monthly temperature and precipitation for the same 30-year periods (Abdullin and Shikhov 2019). The Pearson correlation coefficients between the raster of changes (difference) in average and extreme values were calculated to estimate the similarity of their spatial distribution (Table 2).

It can be noted, that two of three correlation coefficients are statistically significant at a 0.05 P-value. . Indeed, both the average January temperature and 1p minimum winter

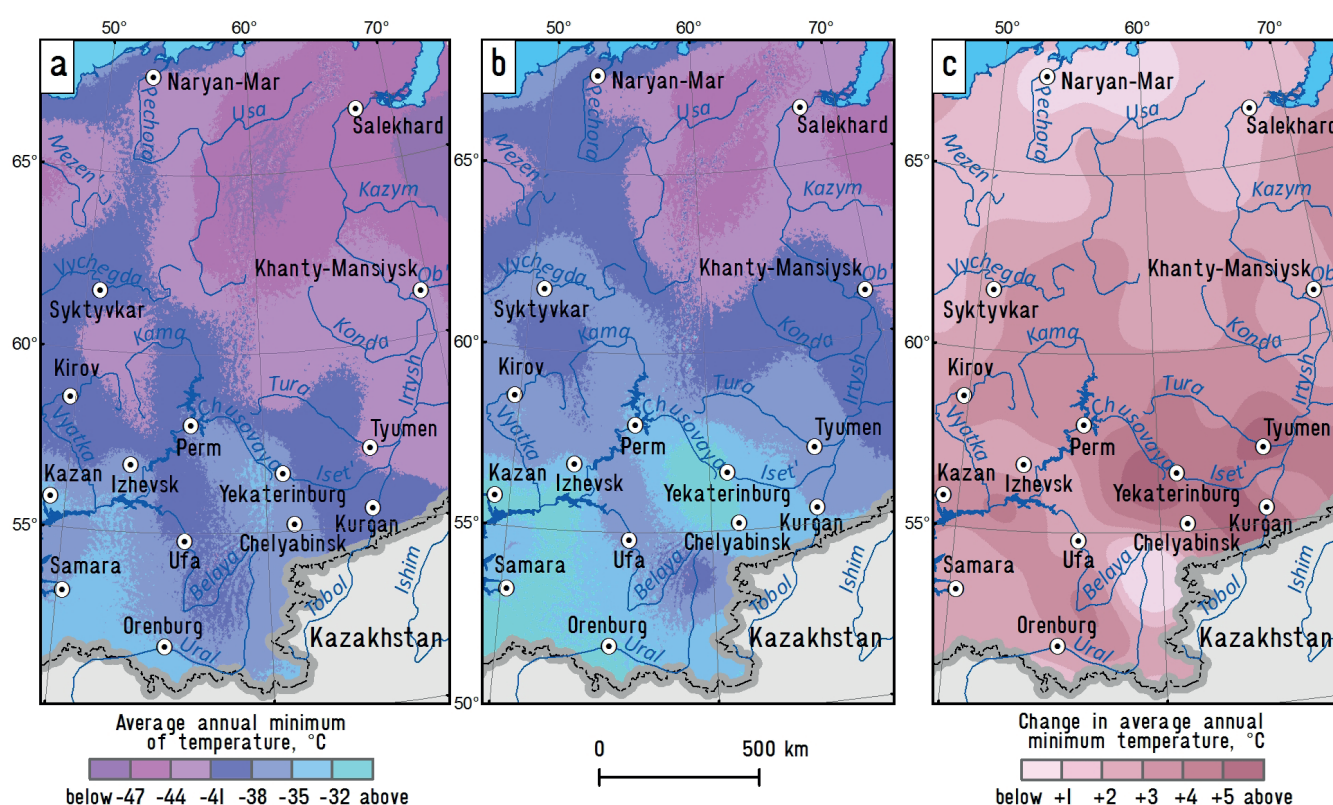


Fig. 5. Average annual minimum of temperature for 1951–1980 (a), 1981–2010 (b) and the difference between them (c)

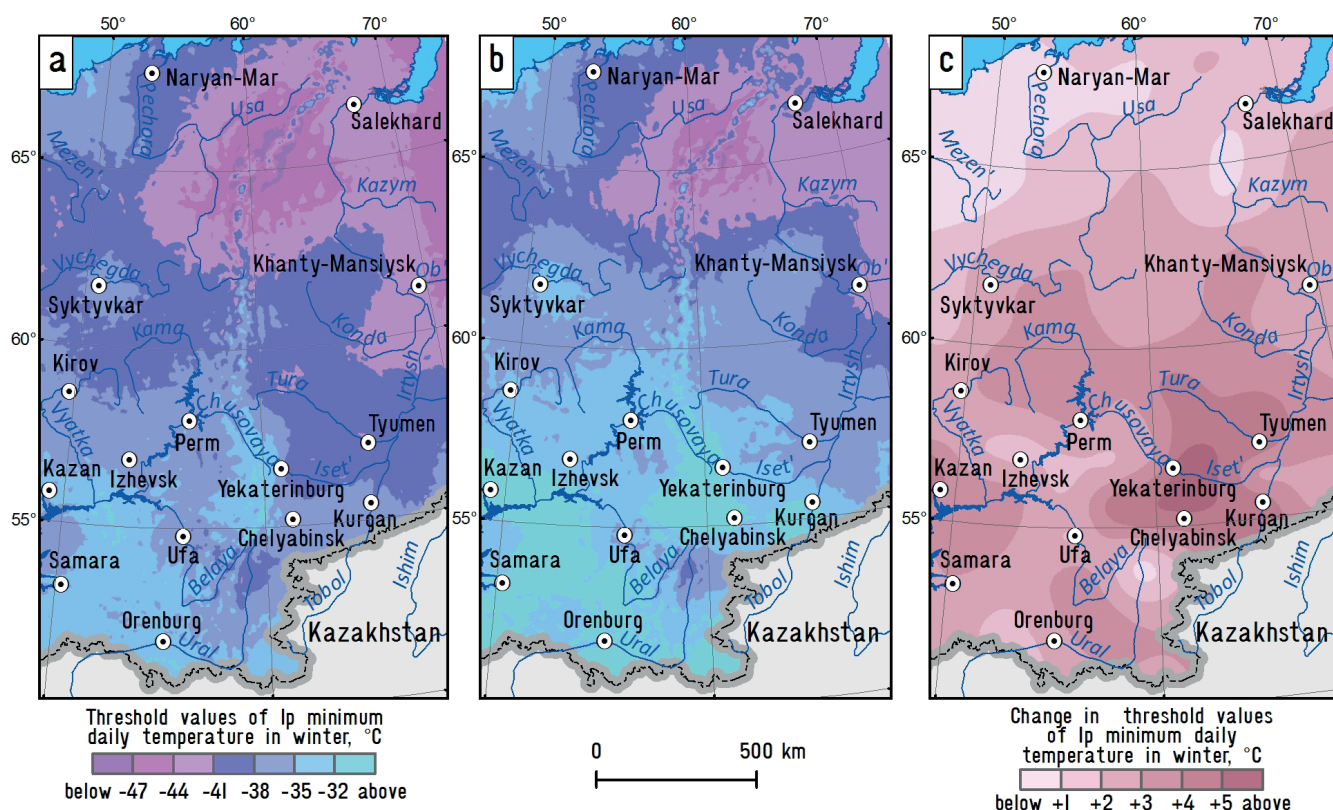


Fig. 6. Threshold values of 1p minimum daily temperature in winter for 1951–1980 (a), 1981–2010 (b) and the difference between them (c)

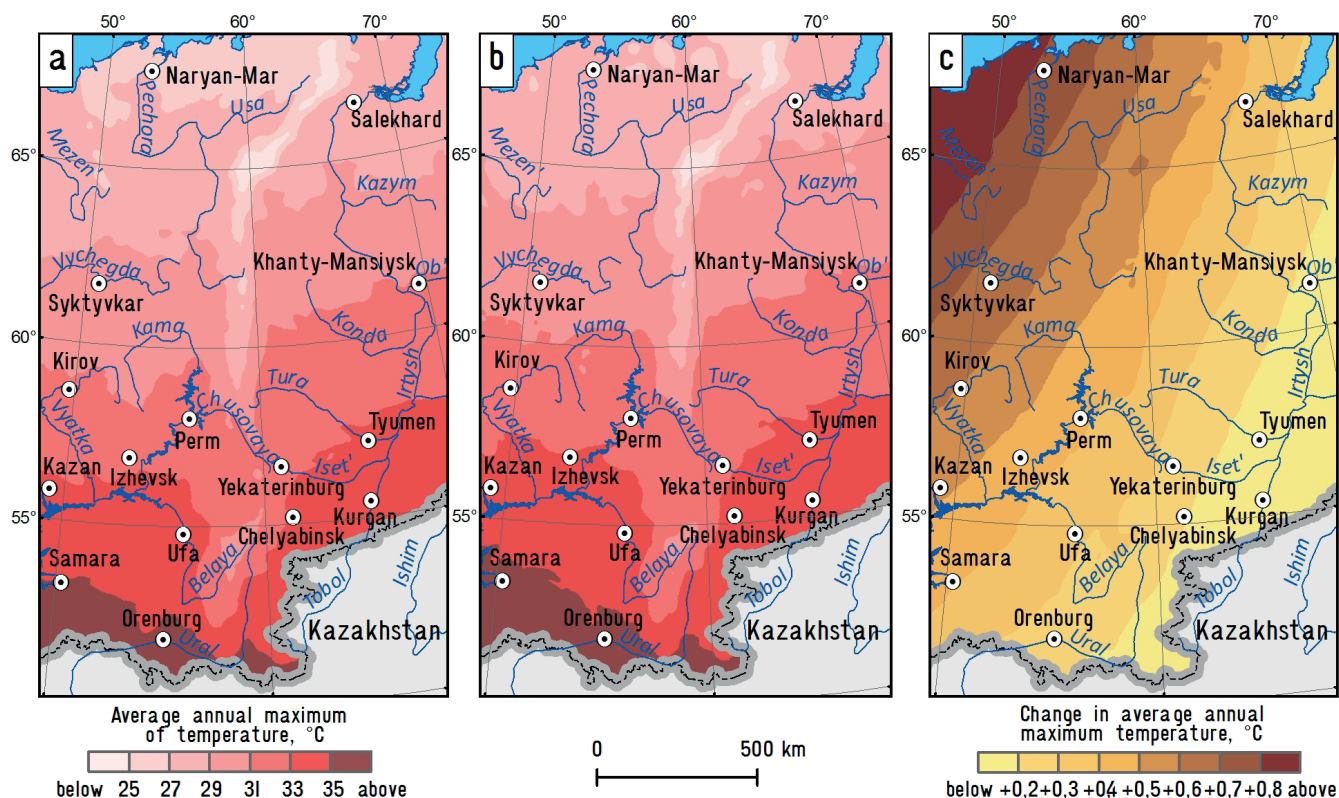


Fig. 7. Average annual maximum of temperature for 1951–1980 (a), 1981–2010 (b) and the difference between them (c)

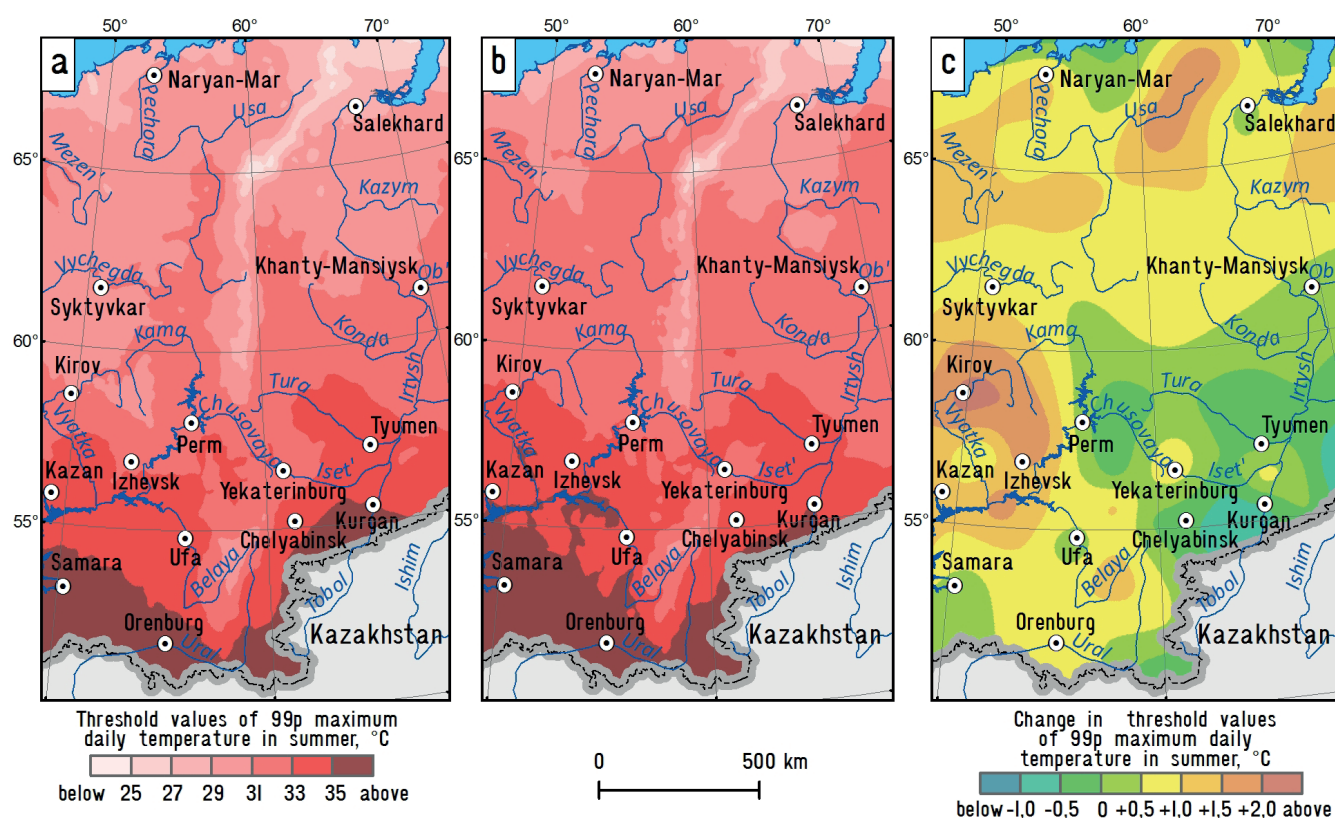


Fig. 8. Threshold values of 99p maximum daily temperature in summer for 1951–1980 (a), 1981–2010 (b) and the difference between them (c)

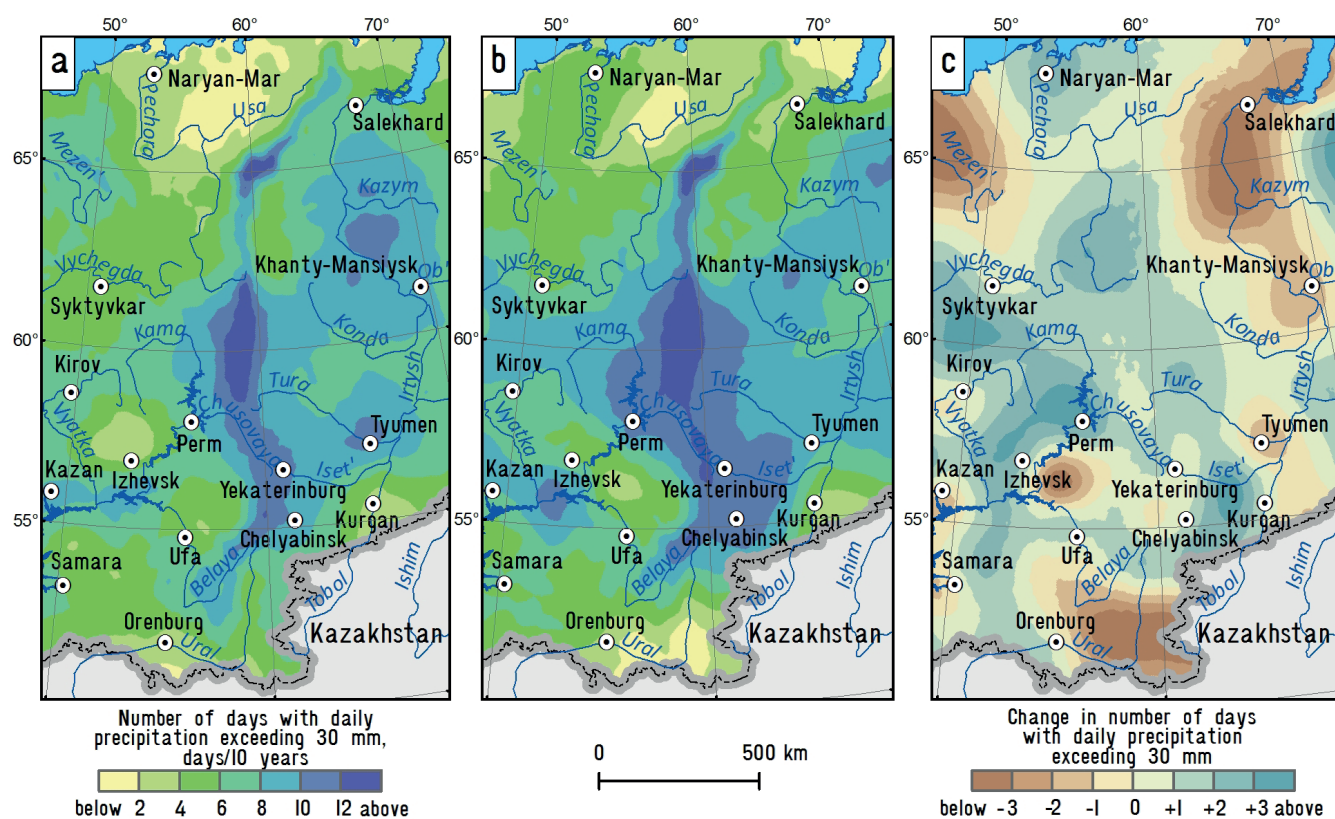


Fig. 9. Threshold values of 99p daily precipitation for 1966–1995 (a), 1986–2015 (b) and the difference between them (c)

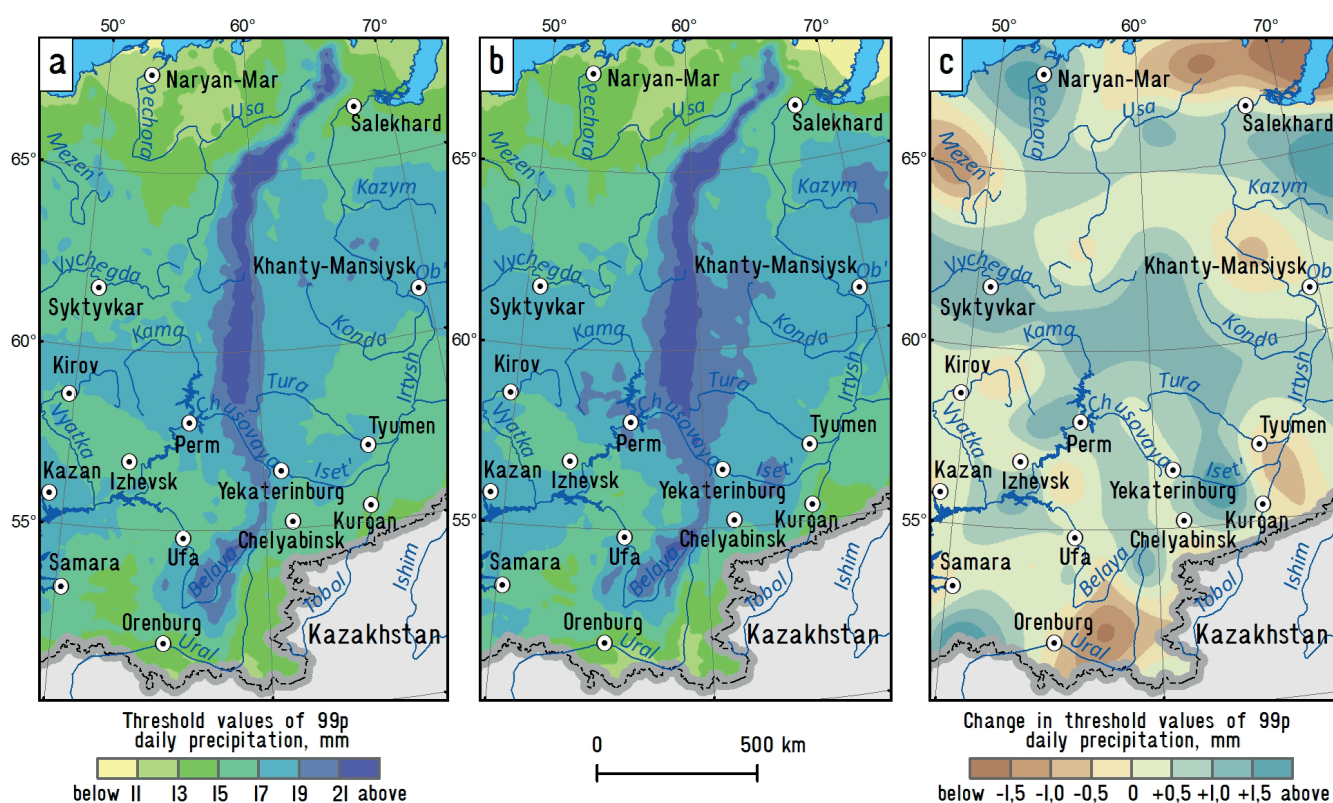


Fig. 10. Number of days with daily precipitation exceeding 30 mm averaged over 1966–1985 (a), 1986–2015 (b) and the difference between them (c)

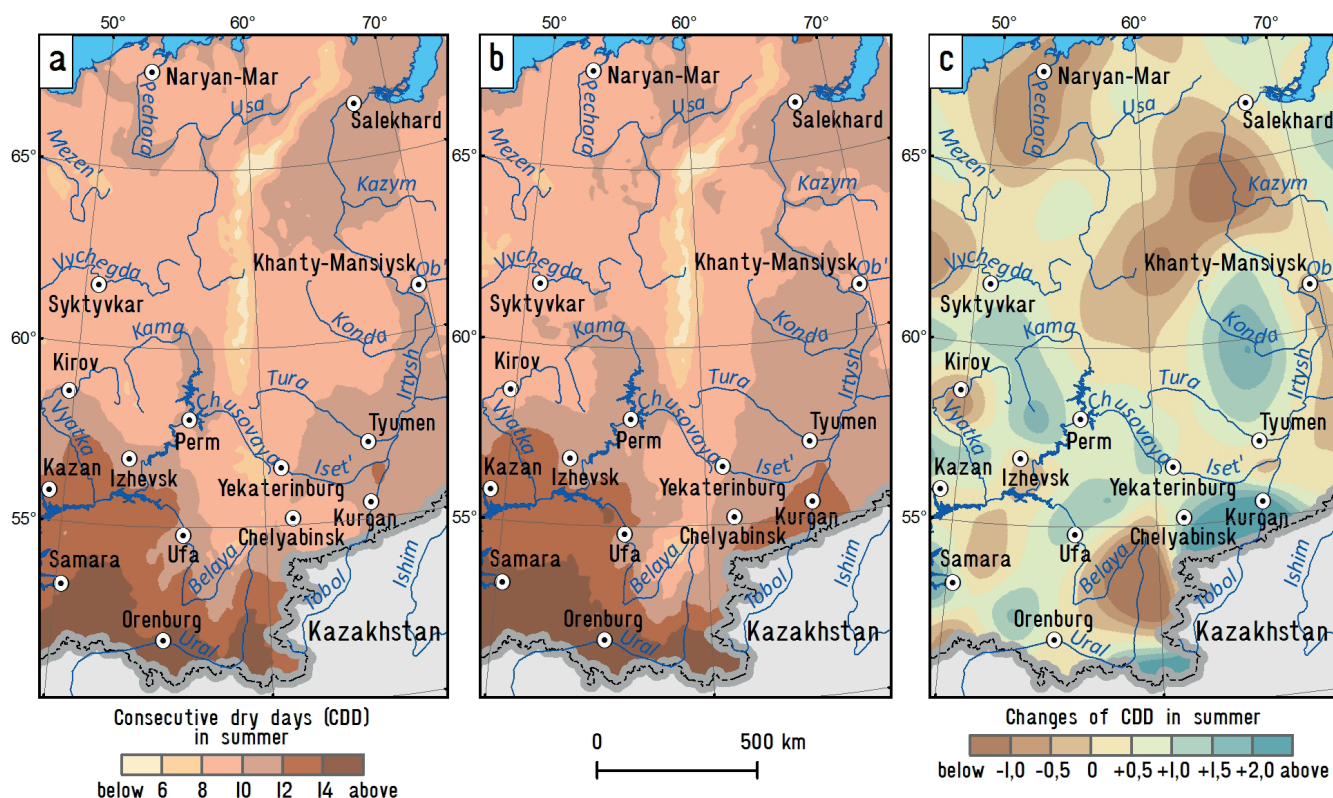


Fig. 11. Number of CDD in summer months averaged over 1966–1985 (a), 1986–2015 (b) and the difference between them (c)

Table 2. Pearson correlation coefficient between the changes in average and extreme temperature and precipitation (statistically significant coefficients at 0.05 P-value are highlighted)

Average parameter (difference)	Extreme parameter (difference)	Pearson correlation coefficient
Average January temperature (1951–1980 and 1981–2010)	1p minimum daily temperature in winter (1951–1980 and 1981–2010)	0.58
Average July temperature (1951–1980 and 1981–2010)	99p maximum daily temperature in summer (1951–1980 and 1981–2010)	0.11
Average annual precipitation (1966–1995 and 1986–2015)	99p daily precipitation (1966–1995 and 1986–2015)	0.69

temperature increased in the south of the Ural more than in the north, when comparing 1951–1980 and 1981–2010. As for the changes of average and extreme precipitation, their spatial distribution is similar since the most substantial increase was observed in mid-latitudes (between 55° and 60° N). Moreover, the area with a strongest increase of the average annual precipitation (up to 45 mm/30 years) overlaps with the same of 99p daily precipitation.

The changes in average July temperature and 99p maximum daily temperature are correlated very weakly, since the areas with strongest changes of such variables do not overlap. The maximum increase of average temperature in July between 1951–2010 and 1981–2010 was observed in the Northern Ural and Yamal Peninsula, while the 99p maximum daily temperature increased more substantially in Kirov region (which is probably due to the extreme heat wave of summer 2010).

CONCLUSION

The created maps not only show the spatial distribution of temperature and precipitation extremes in the Ural region, but also allow identify some regional features of its changes under observed climate warming. In general, the reported changes in extremes correspond to the trends observed on most of the territory of Russia in recent decades. There is a substantial decrease of the number of extremely cold days in winter. The 1p minimum temperature in winter also has a strong positive trend (up to 1–5°C/30 years). The 1p maximum temperature in summer has a positive trend in most of the territory, but the increase rate does not exceed

2°C between 1951–1980 and 1981–2010. The precipitation extremes also increased as for the entire year and in winter season. However, the maximum increase rate for 99p daily precipitation between 1966–1995 and 1985–2015 does not exceed 2.1 mm.

The observed changes of extreme temperatures and precipitation have substantial spatial variability, which is due both the changes of atmospheric circulation and the influence of topography. So, the 1p minimum winter temperature increased to 4–5°C in the southeast of the Ural and only to 1°C to the west of the Polar Ural. The 99p maximum temperature in summer most strongly increased in the Kirov region and Udmurt republic, which is due to the rise of the frequency of blocking anticyclones in summer. However, the same process lead to decrease of the maximum summer temperatures in the southeast of the Ural region. The 99p daily precipitation increased mainly in mid-latitude zone and reduced near the Arctic coast.

The maps of climatic extremes may be also useful to estimate the observed changes in the frequency and intensity of hazardous weather events. On the one hand, the number of extremely cold days is strongly reduced over entire Ural region, that is certainly favorable for people and economy. On the other hand, there is an increase in the frequency of summer heat waves as well as extreme precipitation events. This tendency is confirmed by the strong summer heat waves of 2010, 2012 and 2016, and also by several extreme precipitation events (exceeding 100 mm/day), which occurred in summer of 2013 and 2015 and caused substantial economic losses. ■

REFERENCES

- Abdullin R.K. and Shikhov A.N. (2017). GIS based modelling of spatial and temporal distribution of severe weather events. *Geodesy and Cartography = Geodezija i kartografija*, 78(2), 26–32 (in Russian with English summary), DOI: 10.22389/0016-7126-2017-920-2-26-32.
- Abdullin R.K. and Shikhov A.N. (2019). Mapping of current climate changes in the Ural. *Geodesy and Cartography = Geodezija i kartografija*, 80(1), 3–12 (in Russian with English summary), DOI: 10.22389/0016-7126-2019-943-1-3-12.
- Alexander L., Zhang X., Peterson T., Caesar J., Gleason B., Klein Tank A., Haylock M., Collins D., Trewin B., Rahimzadeh F., Tagipour A., Rupa Kumar K., Revadekar J., Griffiths G., Vincent L., Stephenson D., Burn J., Aguilar E., Brunet M., Taylor M., New M., Zhai P., Rusticucci M. and Vazquez-Aguirre J. (2006). Global observed changes in daily climate extremes of temperature and precipitation. *Journal of Geophysical Research*, 111, D05109, DOI: 10.1029/2005JD006290.
- Bardin M.Yu. and Platova T.V. (2013). Changes in thresholds of extreme temperatures and precipitation on territory of Russia with global warming. *Problemy ekologicheskogo monitoringa i modelirovaniya ekosistem*, 2013, 25, 71–93 (in Russian with English summary).
- Beguéría S. and Vicente-Serrano S.M. (2005). Mapping the hazard of extreme rainfall by peaks over threshold extreme value analysis and spatial regression techniques. *Journal of Applied Meteorology and Climatology*, 45(1), 108–124, DOI: 10.1175/JAM2324.1.
- Beguéría S., Vicente-Serrano S.M., López-Moreno J.I. and García-Ruiz J.M. (2009). Annual and seasonal mapping of peak intensity, magnitude and duration of extreme precipitation events across a climatic gradient, northeast Spain. *International Journal of Climatology*, 29(12), 1759–1779, DOI: 10.1002/joc.1808.
- Blennow K. and Persson P. (1998). Modelling local-scale frost variations using mobile temperature measurements with a GIS. *Agricultural and Forest Meteorology*, 89, 59–71, DOI: 10.1016/S0168-1923(97)00057-9.
- Brown D.P. and Comrie A.C. (2002). Spatial modeling of winter temperature and precipitation in Arizona and New Mexico, USA. *Climate Research*, 22, 115–128, DOI: 10.3354/cr022115.
- Bulygina O., Razuvaev V., Korshunova N. and Groisman P. (2007). Climate variations and changes in extreme climate events in Russia. *Environmental Research Letters*, 2(4), 045020, DOI: 10.1088/1748-9326/2/4/045020.

- Cherenkova E.A. (2017). Dangerous atmospheric drought in European Russia under recent summer warming. *Fundamental and Applied Climatology*, 2, 130-143 (in Russian with English summary), DOI: 10.21513/2410-8758-2017-2-130-143.
- Chernokulsky A.V., Kozlov F.A., Semenov V.A., Zolina O.G. and Bulygina O.N. (2018). Climatology of precipitation of different genesis in Northern Eurasia. *Russian Meteorology and Hydrology*, 43(7), 425-435, DOI: 10.3103/S1068373918070014.
- Danielson J.J. and Gesch D.B. (2011). Global multi-resolution terrain elevation data 2010 (GMTED2010): U.S. Geological Survey Open-File Report 2011-1073, 26 p.
- Donat M.G., Alexander L.V., Yang H., Durre I., Vose R., Dunn R.J.H., Willett K.M., Aguilar E., Brunet M., Caesar J., Hewitson B., Jack C., Klein Tank A.M.G., Kruger A.C., Marengo J., Peterson T.C., Renom M., Oria Rojas C., Rusticucci M., Salinger J., Elayah A.S., Sekele S.S., Srivastava A.K., Trewin B., Villarreal C., Vincent L.A., Zhai P., Zhang X. and Kitching S. (2013). Updated analyses of temperature and precipitation extreme indices since the beginning of the twentieth century: The HadEX2 dataset. *Journal of Geophysical Research Atmospheres*, 118(5), 2098-2118, DOI: 10.1002/jgrd.50150.
- Donat M.G., Alexander L.V., Yang H., Durre I., Vose R. and Caesar J. (2013). Global land-based datasets for monitoring climatic extremes. *Bulletin of American Meteorological Society*, 94(7), 997-1006, DOI: 10.1175/BAMS-D-12-00109.1.
- Fick S.E. and Hijmans R.J. (2017). WorldClim 2: new 1-km spatial resolution climate surfaces for global land areas. *International Journal of Climatology*, 37, 4302-4315, DOI: 10.1002/joc.5086.
- Frich P., Alexander L., Della-Marta P., Gleason B., Haylock M., Klein Tank A. and Peterson T. (2002). Observed coherent changes in climatic extremes during the second half of the 20th century. *Climate Research*, 19, 193-212, DOI: 10.3354/cr019193.
- Goodale C.L., Aber J.D. and Ollinger S.V. (1998). Mapping monthly precipitation, temperature and solar radiation from Ireland with polynomial regression and a digital elevation model. *Climate Research*, 10, 35-49, DOI: 10.3354/cr010035.
- Goovaerts P. (2000). Geostatistical approaches for incorporating elevation into the spatial interpolation of rainfall. *Journal of Hydrology*, 228, 113-129, DOI: 10.1016/S0022-1694(00)00144-X.
- Groisman P., Knight R., Easterling D., Karl T., Hegerl G. and Razuvaev V. (2005). Trends in intense precipitation in the climate record. *Journal of Climate*, 18, 1326-1350, DOI: 10.1175/JCLI3339.1.
- Groisman P.Y. and Soja A.J. (2009). Ongoing climatic change in Northern Eurasia: justification for expedient research. *Environmental Research Letters*, 4, 045002, DOI: 10.1088/1748-9326/4/4/045002.
- Kiktev D.B., Caesar J. and Alexander L. (2009). Temperature and precipitation extremes in the second half of the twentieth century from numerical modeling results and observational data. *Izvestiya RAN. Fizika atmosfery i okeana*, 45(3), 305-315 (in Russian with English summary), DOI: 10.1134/S0001433809030025.
- Kim K.-Y., Kim J.-Y., Kim J., Yeo S., Na H., Hamlington B.D. and Leben R.R. (2019). Vertical Feedback Mechanism of Winter Arctic Amplification and Sea Ice Loss. *Scientific Reports*, 9(1), Art. no. 1184, DOI: 10.1038/s41598-018-38109-x.
- Li L. and Zha Y. (2018). Mapping relative humidity, average and extreme temperature in hot summer over China. *Science of the Total Environment*, 615, 875-881, DOI: 10.1016/j.scitotenv.2017.10.022.
- Mokhov I.I., Semenov V.A. (2016). Weather and Climate Anomalies in Russian Regions Related to Global Climate Change. *Russian Meteorology and Hydrology*, 41(2), 84-92, DOI: 10.3103/S1068373916020023.
- Ninyerola M., Pons X. and Roure J.M. (2000). A methodological approach of climatological modelling of air temperature and precipitation through GIS techniques. *International Journal of Climatology*, 20, 1823-1841, DOI: 10.1002/1097-0088(20001130)20:14<1823.
- Perevedentsev Yu.P., Sokolov V.V. and Naumov E.P. (2013). Climate and environment of the Privolzhsky Federal District. Kazan, Kazan Federal University (in Russian).
- Pyankov S.V., Shikhov A.N. and Abdullin R.K. (2017). Modern methods and technologies in thematic atlas mapping (on the example of the AIS «Hazardous hydro-meteorological events of the Ural Prikamye region»). *Challenges in Geography = Voprosy Geografii*, 144, 208-226 (in Russian with English summary).
- Screen J.A. (2014). Arctic amplification decreases temperature variance in northern mid- to high-latitudes. *Nature Climate Change*, 4, 577-582, DOI: 10.1038/nclimate2268.
- Shikhov A.N., Perminova E.S. and Perminov S.I. (2019). Satellite-based analysis of the spatial patterns of fire and storm-related forest disturbances in the Ural region, Russia, *Natural Hazards*, 97(1), 283-308, DOI: 10.1007/s11069-019-03642-z.
- Shutov V.A. (1998). Investigations, analyses and modeling of different scaled spatial variability of snow storage. *Izvestiya, Seriya Geograficheskaya*, 1, 122-132 (in Russian with English summary).
- Titkova T.B., Cherenkova E.A. and Semenov V.A. (2018). Regional features of changes in winter extreme temperatures and precipitation in Russia in 1970–2015. *Led i Sneg*, 58(4), 486-497 (In Russian with English summary), DOI: 10.15356/2076-6734-2018-4-486-497.
- Vicente-Serrano S.M., Saz-Sánchez M.A. and Cuadrat J.M. (2003). Comparative analysis of interpolation methods in the middle Ebro Valley (Spain): Application to annual precipitation and temperature. *Climate Research*, 24(2), 161-180, DOI: 10.3354/cr024161.
- Weisse A.K. and Bois P. (2002). A comparison of methods for mapping statistical characteristics of heavy rainfall in the French Alps: the use of daily information. *Hydrological Sciences Journal*, 47(5), 739-752, DOI: 10.1080/02626660209492977.
- Zolina O. and Bulygina O. (2016). Current climatic variability of extreme precipitation in Russia. *Fundamental and Applied Climatology*, 1, 84-103 (in Russian with English summary), DOI: 10.21513/2410-8758-2016-1-84-103.
- Zolotokrylin A.N. and Cherenkova E.A. (2017). Seasonal changes in precipitation extremes in Russia for the last several decades and their impact on vital activities of the human population. *Geography, Environment, Sustainability*, 10(4), 69-82, DOI: 10.24057/2071-9388-2017-10-4-69-82.

MODELING AIR POLLUTION IN DONG NAI PROVINCE, VIETNAM

Nguyen T. Hung^{1*}, Irina I. Kosinova², Đang T. L. Anh¹

¹Vietnamese National University of Forestry, Xuan Mai Town, Chuong My District, 1000, Ha Noi, VietNam

²Voronezh State University, 1 Universitetskaya pl., 394018, Voronezh, Russia

*Corresponding author: Thanhhungln02@gmail.com

Received: April 8th, 2019 / Accepted: May 10th, 2020 / Published: July 1st, 2020

<https://DOI-10.24057/2071-9388-2019-44>

ABSTRACT. Data analysis shows that dust and CO have a very high concentration, causing air pollution. Meanwhile, SO₂ and NO₂ concentrations are lower than the permitted levels. The method inverse distance weighting (IDW) has been proved to be effective in modeling atmospheric pollution space in the study area. The results indicated that the air was contaminated. Pollution levels increase gradually in the following areas: Residential areas < Waste treatment areas < Industrial parks. The integrated pollution map shows that there have been signs of ecological insecurity in the dry season, so there should be measures to control the source of emissions into the environment.

KEY WORDS: AQI, Pollution air, Industrial, Residential, Waste treatment

CITATION: Nguyen T. Hung, Irina I. Kosinova, Đang T. L. Anh (2020). Modeling Air Pollution In Dong Nai Province, Vietnam. Geography, Environment, Sustainability, Vol.13, No 2, p. 166-174

<https://DOI-10.24057/2071-9388-2019-44>

Conflict of interests: The authors reported no potential conflict of interest.

INTRODUCTION

Air pollution is considered a global problem. Air pollution is caused by human activities such as burning of fuels (coal, oil, gas), forest burning, mining, metallurgy, etc. and natural activities like volcanic activity (Michelozzi et al. 1998; Ostachuk et al. 2008). The problem of air pollution is becoming increasingly serious. Forest area is decreasing, meanwhile, emissions (CO, CO₂, NO_x, ...) are increasing day by day, leading to greenhouse effects, which increase the temperature of the earth. The consequence is to upset the ecological circulation and climate change. In it, the most intuitive is the increase in diseases related to human respiratory tract (Raaschou-Nielsen et al. 2011; Pieters et al. 2015). According to statistics of the World Health Organization, up to 1.3 million people die from air pollution every year in major cities, and cause about 4.2 million premature deaths worldwide (WHO 2016; WHO 2018). China and India are the two countries that are considered to have high air pollution levels in the world (The new york time 2017). As a result, the number of deaths from lung cancer increases significantly (Shuo L. et al. 2018). Dong Nai is the southern province of Vietnam, one of the three satellite towns of Ho Chi Minh City. Many industrial parks with large scale are concentrated here. Accompanied by a huge number of employees and dense road system, often operating with high frequency. As a result, pollutants are released into the environment increasingly, leading to the risks of environmental pollution and human health.

MATERIALS AND METHODS

We used mobile observation stations to measure the parameters of the air environment at 80 monitoring points. Selected monitoring sites are areas with high pollution risk, including industrial zones (48 points), residential areas (23 points) and waste treatment areas (9 points). The monitoring parameters include

four basic pollution parameters (dust, SO₂, NO₂ and CO) and meteorological parameters (including temperature, humidity and wind speed). Samples were measured during 4 months of the dry season (December, January, March and April), and three months of the rainy season (August, September and October). Time to measure samples within 24 hours. Method AQI (air quality index) and method NPI (Nemerow integrated pollution index) used to assess the air quality. AQI and NPI are calculated according to formula 1 and 2 (Tran Hong Ha 2013; Yang et al. 2010).

$$AQI_i^{24h} = \frac{C_i^{24h}}{S_i^{24h}} \times 100 \quad (1)$$

$$NPI = \sqrt{\frac{PI_{iave}^2 + PI_{imax}^2}{2}} \quad (2)$$

C_i^{24h}: The average concentration of substance i.

S_i^{24h}: Permissible environmental standards of substance i

n: Number of pollutants.

PI = C_i/S_i, pollution index

IDW and kriging interpolation models have been used to model pollution space. Based on 5 test sample points, we conducted determination of correlation coefficient R² to estimate the accuracy of interpolation map results. Comparing the interpolation results of the two methods, we will choose the appropriate method to model air pollution in the study area. The formula for calculating R² is given by the following formula (Krause et al. 2005):

$$R^2 = \left(\frac{\sum_i^n (O_i - \bar{O})(P_i - \bar{P})}{\sqrt{\sum_i^n (O_i - \bar{O})^2} \sqrt{\sum_i^n (P_i - \bar{P})^2}} \right)^2 \quad (3)$$

O_i is the ith actual measured value.

\bar{O} is the actual measured average value.

P_i is the predicted value.

\bar{P} is the average predicted value.

n is the number of calculated values.

Table 1. Limits of basic parameters in air (Tran Hong Ha 2013; Yang et al. 2010)

Parameter	Standard ($\mu\text{g}/\text{m}^3$)	AQI value	Air quality	NIPi	Rank
Dust (TPS)	140	0-50	Good	$\text{NIPi} \leq 0.7$	Non-pollution
SO_2	50	51-100	Medium	$0.7 < \text{NIPi} \leq 1$	Warning line of pollution
NO_x	40	101-200	Bad	$1 < \text{NIPi} \leq 2$	Low level of pollution
CO	5000	201-300	Very bad	$2 < \text{NIPi} \leq 3$	Moderate level of pollution
		> 300	Dangerous	$\text{NIPi} > 3$	High level of pollution

RESULTS

Results of monitoring of seasonal parameters are shown in table 2. The study area has a tropical monsoon climate, with characteristics of very high temperature and humidity. This climatic feature greatly affects the dispersion of pollution in the atmosphere. Very high humidity (maximum humidity up to 85% in the rainy season, and 69% in the dry season), low wind speed (average 0.62 m/s in the rainy season and 0.58 m/s in the dry season) will limit the spread of pollutants in the air.

Data in tables 1 and 2 show that the maximum concentrations of SO_2 and NO_2 in the dry and rainy season are both lower than the permissible concentration limits. Their average concentration values are 2 to 3 times lower than the standard. This shows that the air has not been polluted by SO_2 and NO_2 . However, the concentration of dust and CO in the air is very high. dust and CO concentration is about 2-3 times higher than standard. A common feature of CO and dust is that the pollution level in the dry season is higher than in the rainy season (the average dust concentration in the dry season is nearly 2 times higher than in the rainy season. The CO content is 1.2 times higher than that in the rainy season). This proves that in the dry season, when the humidity decreases and there is no rain, the level of air pollution with dust and CO increases significantly. According to statistics of Dong Nai Department of Health, the number of people infected with respiratory diseases in the dry season in urban and industrial areas increased by more than 30% compared to the rainy season (Nguyen Trong Hai 2018).

The air quality index of the industrial zone is shown in Fig. 1 and Fig. 2. Most of the monitoring points in the industrial zone have very high dust concentrations in the dry season (2-3 times higher than the permissible concentration limits) and decrease gradually during the rainy season (Fig. 1). Locations that detect very high levels of dust pollution ($\text{AQI} > 300$) are Bien Hoa (BH-01, BH-02), Amata (AM-01), Nhon Trach (NT-01) and especially An Phuoc industrial zone (AP-01) with extremely high dust concentration ($\text{AQI} > 400$). This is a dangerous level, greatly affecting human health. In the rainy season, the concentration of dust drops sharply (about 50%

lower than in the dry season). A number of small industrial areas (TP-01, LK-01, BS-01, XL-01) have relatively low dust concentration. Industrial zones with high dust pollution are those producing construction materials, producing animal feed and processing rubber etc. Meanwhile, industrial zones producing clothing, shoes, assembling electronic components have lower dust pollution.

Fig. 2 shows the concentration of CO in the air in industrial areas. All monitoring point have high levels of CO ($\geq 5000 \mu\text{g}/\text{m}^3$). In particular, the concentration of CO in the dry months is much higher than the months in the rainy season. Most of the monitoring points have a CO concentration 1-2 times higher than the permissible concentration. Especially, in march, CO concentration is very high ($\text{AQI-CO} > 400$) in Long Thanh industrial zone (LT-02). This shows that the industrial park has a large amount of CO, which is very toxic and has a high risk of affecting human health. CO disperses into the air during incomplete combustion of wood, fuel (petroleum), coal. Especially coal is used a lot in industrial areas, it is the raw material to operate the incinerators.

The analysis results of air pollution data in residential areas are shown in Fig. 3 and 4. Based on Fig. 3, it can be affirmed that the dust concentration in residential areas is much lower than that in industrial areas. Except for Vinh Cuu residential area (VC-22 and VC-23). This area is under construction of roads, so the dust content in this area is very high ($\text{AQI} > 300$ in the dry season). The remaining residential areas have slight dust pollution, 1-2 times higher than the permissible concentration in the dry season, while in the rainy season, most of the sample sites have dust concentrations lower than the permissible concentration. The cause of dust spread in residential areas is mainly due to traffic activities.

Fig. 4 shows that the CO concentration in residential areas is also lower than in industrial areas. Most of the monitoring point have 1-2 times higher than the permitted level in the dry season and the CO concentration decreases gradually during the rainy season. However, in the Bien Hoa city area (BH-01, BH-03) there was an abnormally high CO concentration in march. The CO concentration was dangerously high ($\text{AQI} > 300$).

Table 2. Limits of basic parameters in air (Tran Hong Ha 2013; Yang et al. 2010)

Parameter	Rain season ($\mu\text{g}/\text{m}^3$)			Dry season ($\mu\text{g}/\text{m}^3$)		
	Mean	Min	Max	Mean	Min	Max
Dust	76.00	7.63	169.52	166.65	14.60	435.59
SO_2	21.19	10.64	30.40	21.62	11.38	27.23
NO_2	16.36	15.00	20.93	17.13	15.00	24.77
CO	5,873.25	5,000.00	8,474.75	6,552.43	5,000.00	12,574.94
Humidity %	65.23	57.63	85.38	60.45	52.03	69.38
Temperature $^{\circ}\text{C}$	31.82	29.60	33.15	32.40	30.20	33.78
Wind speed m/c	0.62	0.25	0.85	0.58	0.30	1.0

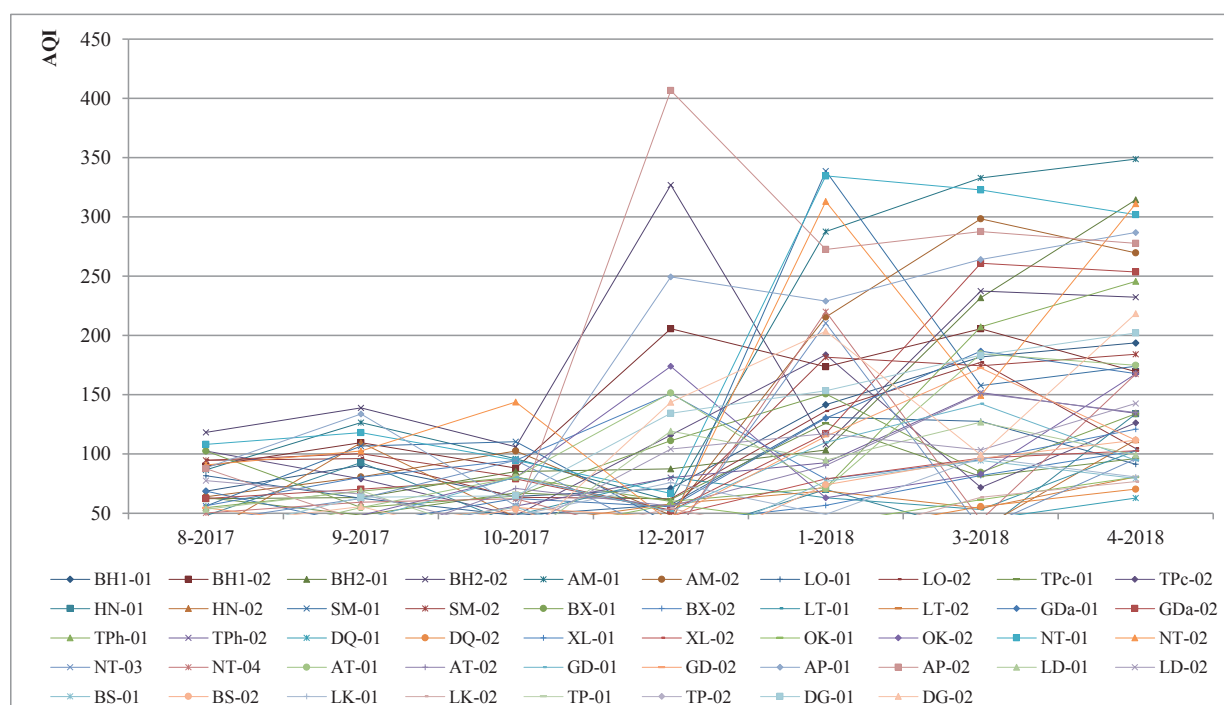


Fig. 1. AQI-dust Index in industrial areas

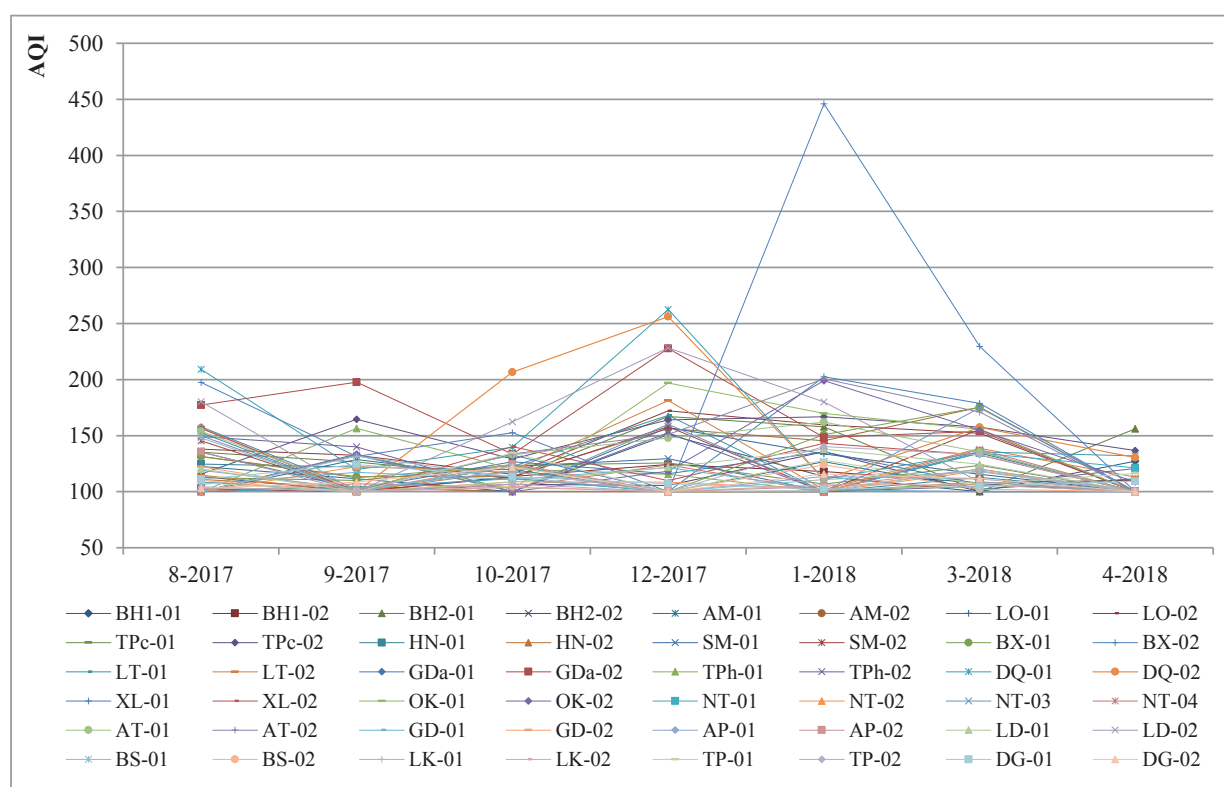


Fig. 2. AQI-CO index in industrial areas

In the waste treatment area, the dust concentration is quite high, most of the monitoring points in the dry season have AQI-dust value from 100-200. Dust concentration decreased significantly in the rainy season (Fig. 5). At that time, CO concentration was about 1-2 times higher than the permitted level (Fig. 6). Especially in Xuyen Moc waste treatment area (XM-06), there is a dangerous concentration of CO (AQI > 300). It can be seen that the level of pollution in the waste treatment area is lower than in the industrial zone but higher than the pollution level in the residential areas.

Based on the above analysis, it can be concluded that air pollution in the study area is mainly caused by dust and CO.

Pollution levels decrease in the following order: industrial park – waste treatment area – residential area.

According to Li et al. (2008), the choice of interpolation method depends on many factors (Sample density, sampling methods and data types affect the estimation of spatial interpolation). These factors will affect the ability to interpolate in different ways, resulting in differences in interpolation results. Therefore, it is difficult to select the appropriate spatial interpolation method for a given input data set. Several interpolation techniques were used to estimate pollution concentrations, including inverse distance weighting, splines, theissen triangulation, and kriging.

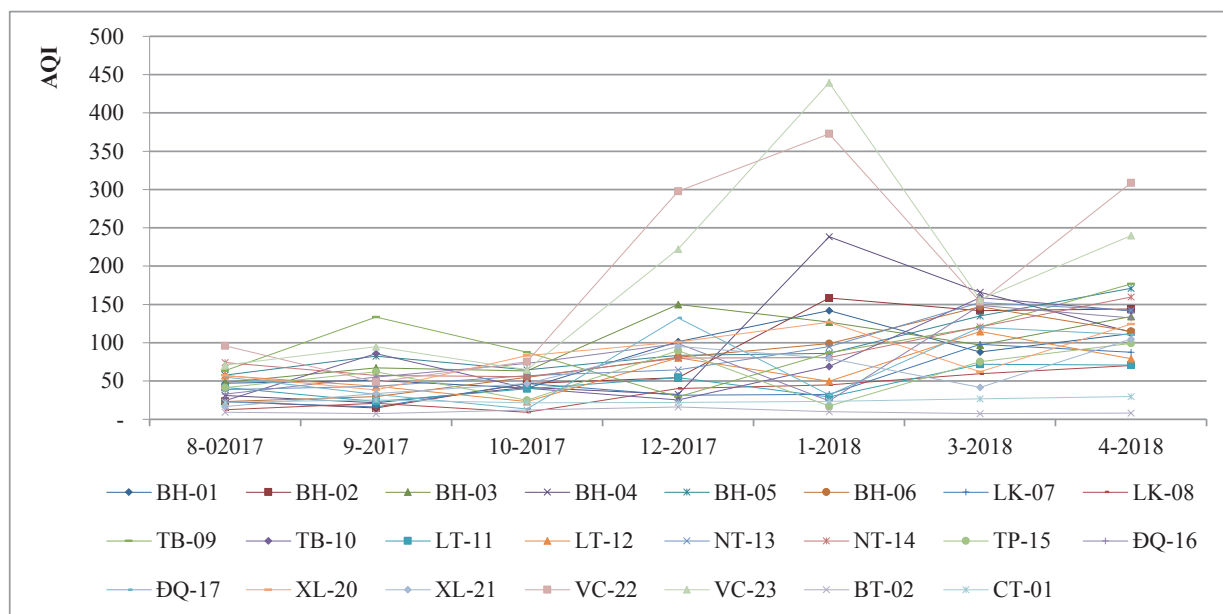


Fig. 3. AQI-dust index in urban residential areas

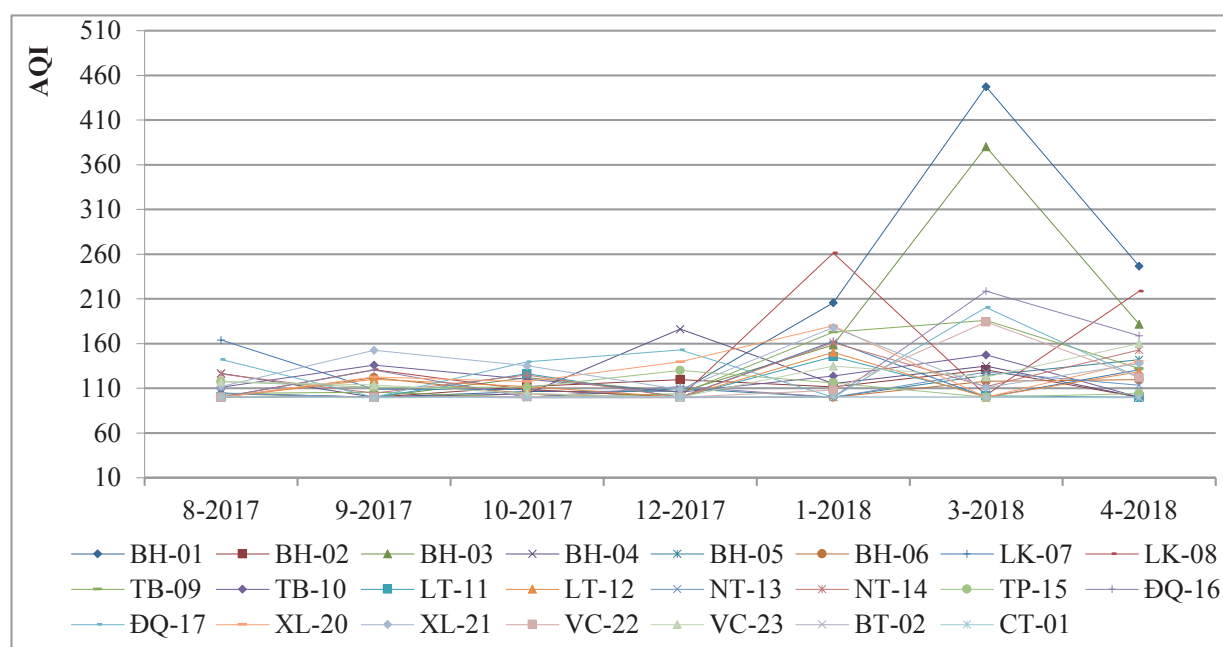


Fig. 4. AQI-CO index in urban residential area

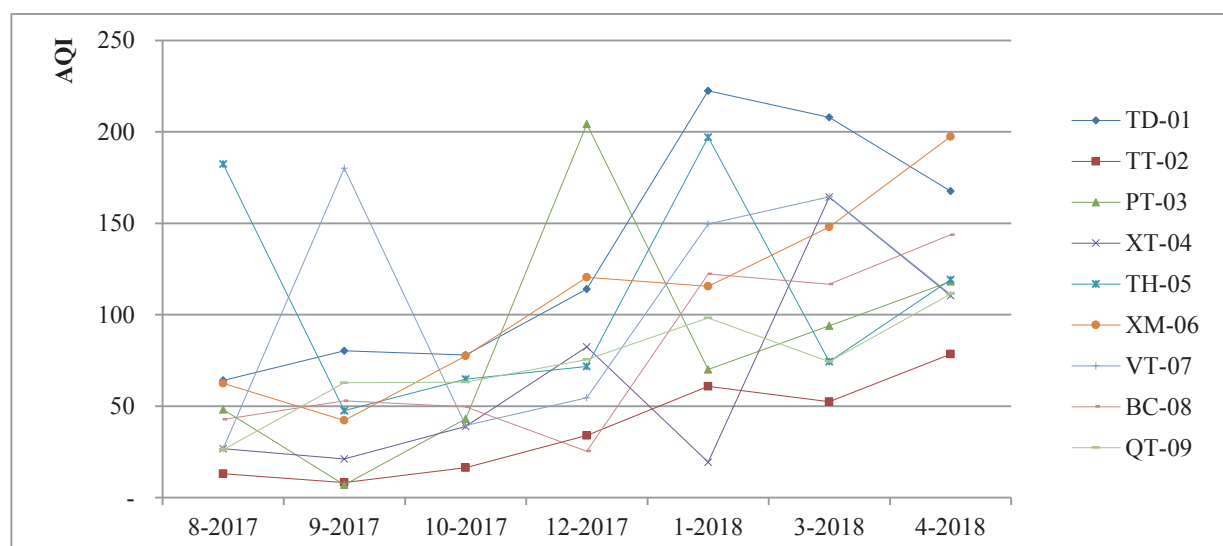


Fig. 5. AQI-dust index in solid waste disposal areas

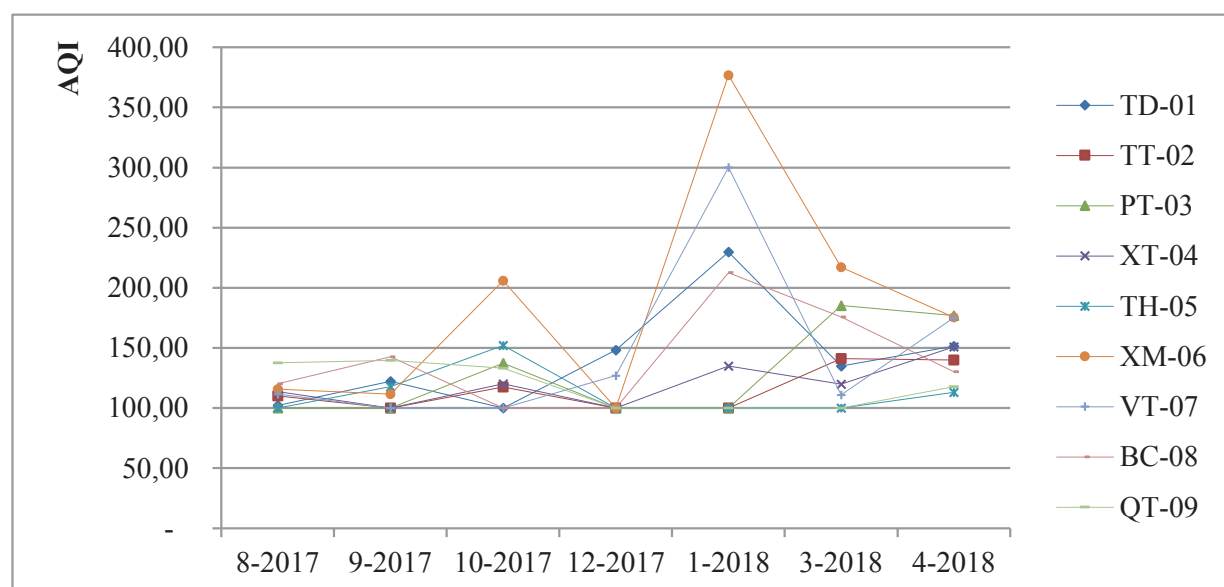


Fig. 6. AQI-CO index in solid waste disposal areas

IDW interpolation is also thought to be quite effective for modeling air pollution (Wong et al. 2004; Kumar et al. 2016). According Dilip Kumar (2011), IDW interpolation results in better results than kriging interpolation in assessing air pollution in Port Blair India (Dilip K. et al. 2011). Meanwhile, Jerrett suppose that kriging is the most commonly used method interpolation in air pollution studies (Jerrett et al. 2001). Therefore, to select the interpolation method for each specific case, it is common to use the method of comparing the interpolation value with the analytical value (Li et al. 2008; Oke et al. 2013). The results in table 3 show that the standard deviation difference of IDW is lower than that of Kriging. This shows that the IDW method gives an optimal result than the kriging method in interpolation of pollution values in the study area.

Interpolation results of air pollution distribution by IDW interpolation method were shown in Fig. 7 and Fig. 8. According to figure 7, in the northern and eastern Areas, air quality is good and medium ($AQI_{\text{dust}} < 100$). Meanwhile, in the southwest region, where most of the industrial and residential areas (about 80%) are concentrated, there is a very high level of dust pollution, air quality is at a bad level ($100 < AQI_{\text{dust}} \leq 200$). Vinh Cuu residential area (point 20) and waste treatment area (points 21, 24) have very bad air quality ($200 < AQI_{\text{dust}} \leq 300$). In particular, An Phuoc industrial park (point 68) is at dangerous air quality ($AQI_{\text{dust}} > 300$). However, in the rainy season, due to heavy and continuous rainfall (the

average annual rainfall is from 1900ml-2400ml, about 80% of the rainfall is distributed during the rainy season), leading to significantly improved air quality. Most of the area has good and moderate air quality. Only a small area has bad air quality in Nhon Trach Industrial Zone (point 61). Although the air quality is improved, the rain that carries the pollutants will pollute the soil and water. Figure 8 shows that the entire study area has relatively high levels of CO, air quality is at a bad level ($100 < AQI_{\text{CO}} \leq 200$). Concentration of CO does not decrease seasonally, in the dry season there is a waste treatment area (point 27) with very bad air quality ($200 < AQI_{\text{CO}} \leq 300$).

Based on the data of the test points, proceed to determine the R^2 coefficient, to evaluate the interpolation results. The R^2 value of the interpolation maps of Dust and CO pollution is shown in table 2.

Table 4 shows that the R^2 coefficient of dust is quite high (0.75) while the correlation coefficient R^2 of CO is very high (> 0.9). This can be explained by the fact that the CO concentration in the atmosphere of the study area is not too different (Figure 2). In contrast, dust content with significant differences between different areas, when interpolated, will have a lower correlation. However, with correlation $R^2 > 0.7$ can be seen, using IDW interpolation method is suitable to model air pollution in the study area.

Figure 9 shows the integrated pollution distribution of dust, SO_2 , NO_2 and CO. During the dry season, most of the study area has low pollution levels, only a small part of

Table 3. Compares the results between IDW and Kriging interpolation methods

Pollutant	Standard deviation of data	Standard deviation of IDW	Standard deviation of Kriging	Standard deviation difference	
				IDW	Kriging
Dust-rain	25.94	15.54	14.33	10.4	11.61
Dust-dry	62.09	35.16	28.89	26.93	33.2
SO_2 -rain	11.81	4.88	2.70	6.93	9.11
SO_2 -dry	11.37	4.80	2.76	6.57	8.61
NO_2 -rain	3.26	1.33	0.72	1.93	2.54
NO_2 -dry	4.96	2.18	1.92	2.78	3.04
CO-rain	14.52	7.49	3.83	7.03	10.69
CO-dry	28.94	13.12	6.49	15.82	22.45

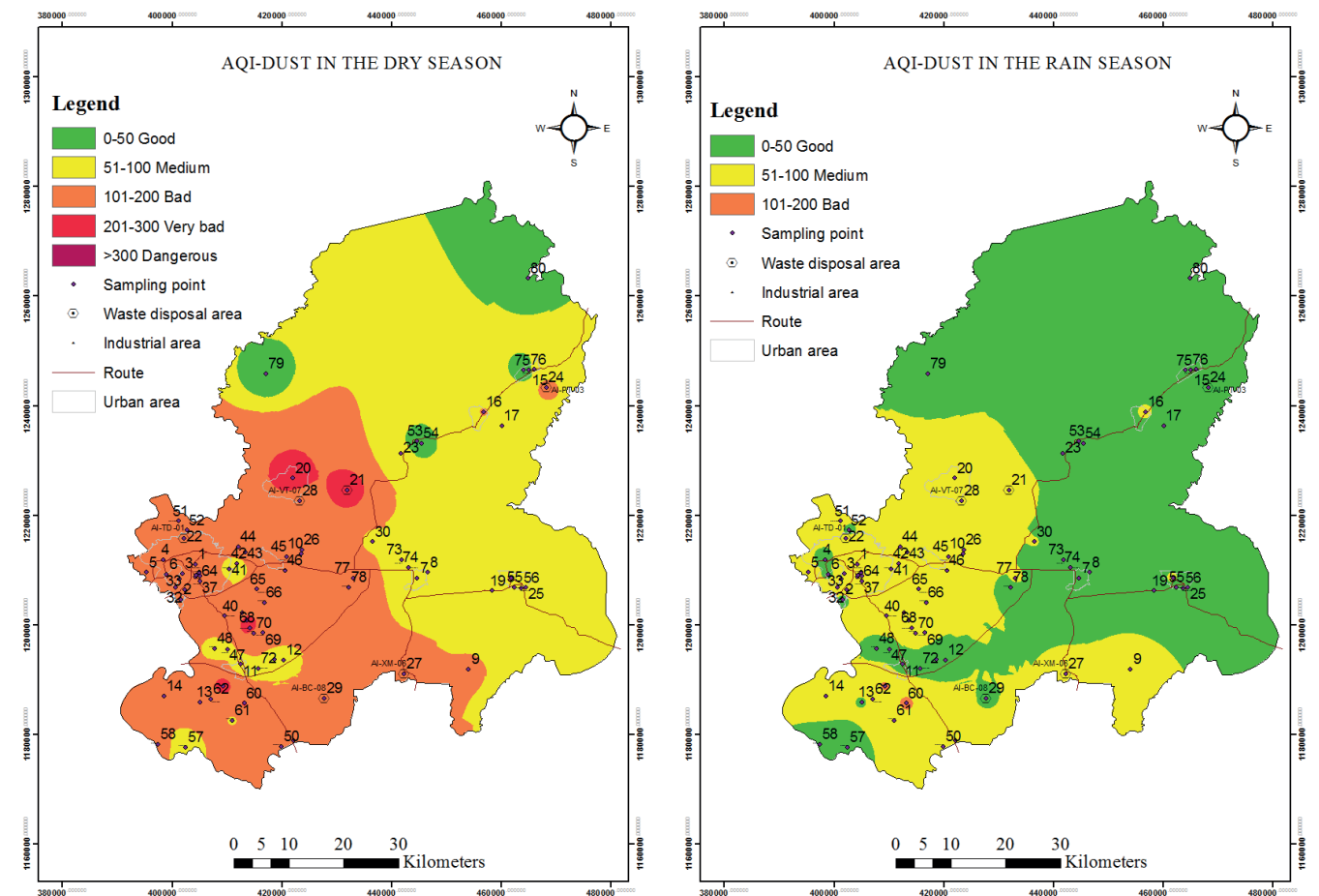


Fig. 7. Distribution of air pollution by dust

Table 4. Correlation analysis results

	Correlation Coefficients (Rainy Season)		Correlation Coefficients (Dry Season)	
	Dust	CO	Dust	CO
Coefficient R ²	0.75	0.97	0.73	0.91

the northern region has pollution pollution warning levels. The two locations were found to have moderate levels of combined pollution at the waste treatment area (point 21) and the Vinh Cuu residential area (point 20). In the rainy season, the complex pollution level decreases significantly. Most areas have pollution warning levels, a small area of low pollution levels. This proves the ability to self-clean the air in the rainy season is very high. However, this is also a sign that ecological non safety, when in the dry season, most areas, the air is slightly polluted, and some areas have moderate pollution levels, in the long run, it will affect human health. This is a result of the rapid increase in the number of industrial zones, the significant increase in the number of vehicles, especially the process of treating waste mainly by burning without effective measures to control the amount of gas discharged into the environment. Emissions not only include these basic substances, they can also include many other hazardous components such as heavy metals, benzene, etc Therefore, to ensure ecological safety as well as to protect human health, it is necessary to take measures to thoroughly treat the source of air pollution, especially in industrial areas (points 62, 68, 70) and waste disposal sites (points 21, 24 and 27).

DISCUSSION

We know that, to model spatial variations of air pollution concentration, dispersion models are often used. These models conceptualize pollution dispersion in terms of

deterministic processes, which are implemented through Gaussian plume equations (Gualtieri et al. 1998; Clench-Aas et al. 1999; Bellander et al. 2001; Pamela F.H. et al. 2011). However, to run these models requires a large data set, measuring many parameters at the same time, and data must be collected continuously over time (by hour or by day). This requires a complete monitoring system and the outcome depends on the size of the monitoring system. The common characteristic of developing areas is that environmental pollution has not been given enough attention and the system of equipment and technologies for environmental monitoring have not been fully established. Most air pollution data measurements are based on mobile stations and measurement of discontinuous air data. Mostly measure the concentration of substances in the air at a given time. Some authors argue that the interpolation model can be used effectively to model air pollution spaces without data on emissions and meteorology (Van L.M. 1993; Janssen et al. 2008; Candiani et al. 2013). In particular, IDW interpolation method is considered as an appropriate tool to analyze the change of air pollution space. The only input data is the pollutant concentration. This suggests that it is easy and economical to collect data, while meteorological and emissions data collection is more time-consuming and costly (Awkash Kumar et al. 2016). However, the disadvantage of the interpolation method is the need to use a dense network of monitoring points. Jerrett et al. (2005), estimated that a dense network of sampling sites ranging from 10 to

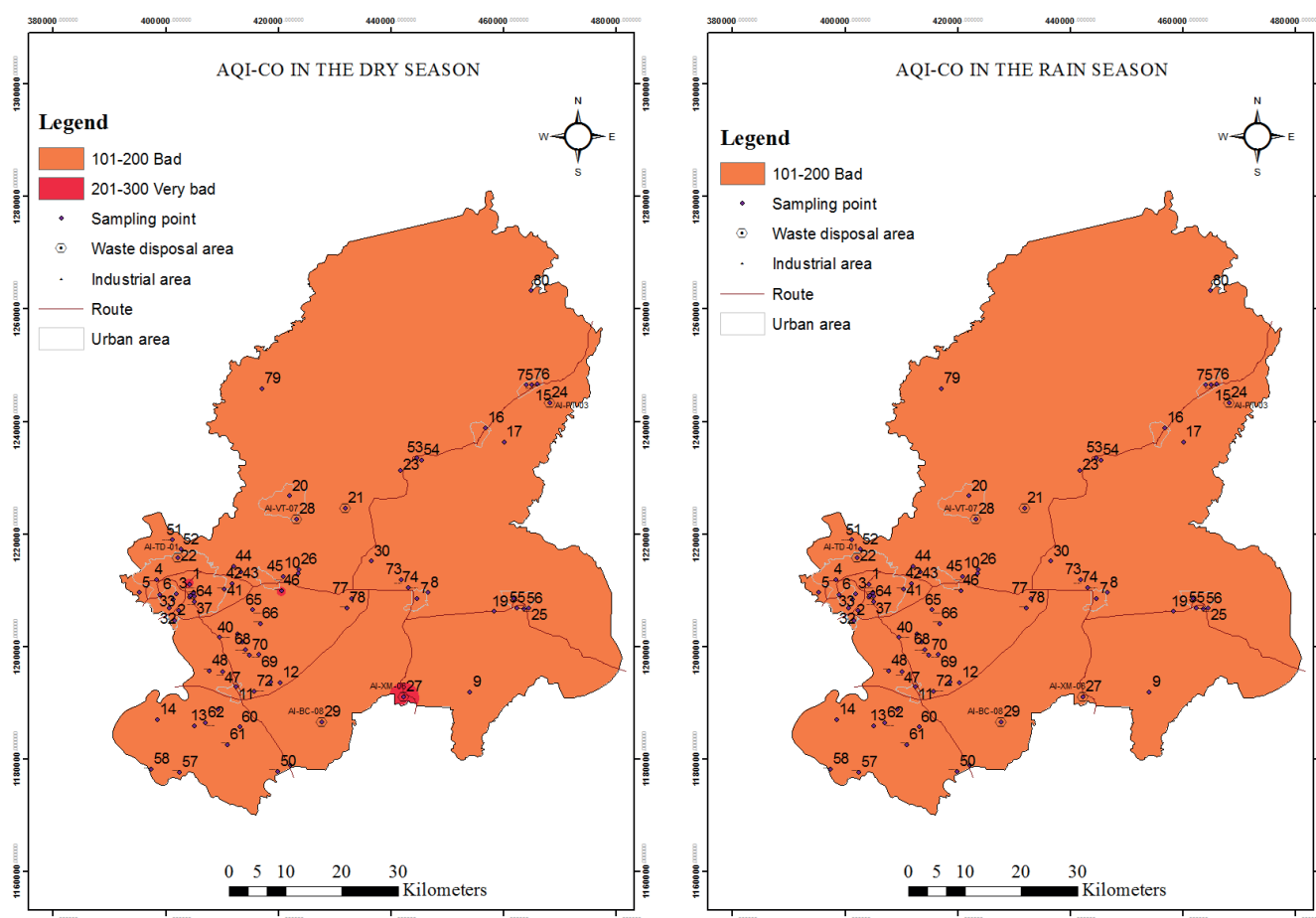


Fig. 8. Distribution of air pollution by CO

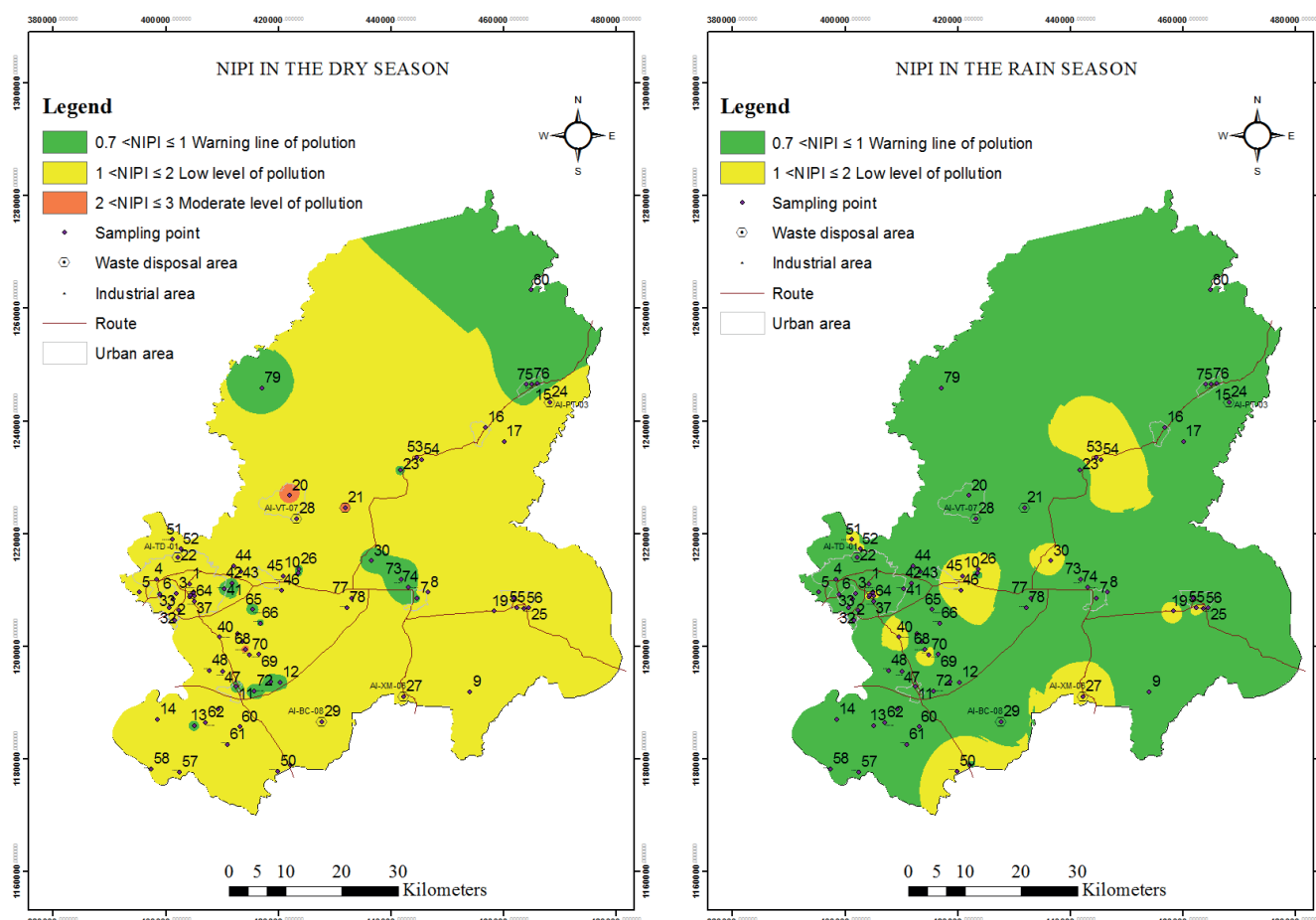


Fig. 9. Integrated air pollution map

100 stations is required for meaningful interpolation results depending on the size of the study area. Therefore, the use of interpolation method to model air pollution is considered as an appropriate option for study area.

For air environment, natural conditions such as wind speed, air humidity and topography are the major factors that influence the dispersion of pollution in the air. Characteristics of the natural conditions of the study area are relatively low wind speed (0.2 m/s – 1.0 m/s), flat terrain and an average humidity > 60%. With high humidity, pollutants, when released into the environment, will quickly absorb water and become heavier as a result they will be distributed closer to the ground. Combined with low wind speeds (almost static), flat terrain, pollutants tend to disperse around discharge sources. Pollution levels are highest at the source of discharge and the level of pollution decreases as the distance to the source of discharge is increased. The IDW inverse weighting method estimates the interpolation values based on the inverse distance from the interpolation point to the sample point. Therefore, the farther the distance, the lower the value of the interpolation point. This shows a similarity between the IDW interpolation model and the actual pollution dispersion in the study area.

In figures 7 and 8, areas with the highest pollution levels are shown polluted in concentric shapes, with a focus on monitoring points in industrial areas (points 62, 68, 70), residential area (points 20) and waste disposal sites (points 21, 24 and 27). These are areas with large discharge sources and continuous discharge into the environment. Meanwhile, in other areas such as in residential areas, and smokeless industrial areas such as garments, assembly of electronic

components, etc. pollution sources come mainly from traffic activities (scattered discharge sources), the pollution diffusion is more uniform. The correlation coefficient $R^2 > 0.7$ indicates that, the results of pollution modeling by the IDW interpolation method, although it is not possible to guarantee the high accuracy as when using complex air pollution dispersion models, but it is also somewhat reflect the extent and distribution of polluted areas.

CONCLUSION

The analysis results indicate that the study area has been polluted by CO and dust. Air quality varies from good to moderate, bad and dangerous in different areas. The most polluted air is in industrial zones, then in waste treatment areas and finally in residential areas. Air quality is subject to significant seasonal changes. In the dry season, pollution levels are almost double that in the rainy season.

Air pollution map created by IDW method has relatively high accuracy ($R^2 > 0.7$). Therefore, this method can be considered as effective in interpolation of air pollution values in the study area. The integrated pollution map shows a higher risk of ecological insecurity due to air pollution in the dry season. Therefore, measures are needed to reduce emissions, especially in the dry season.

The interpolation method is considered to be effective in modeling air pollution with developing areas, areas with limited monitoring and cost systems. With the input of a simple and low-cost data collection system, it can help visually depict polluted areas to warn of the dangerous increase of air pollution to human health. ■

REFERENCES

- Awkash K., Rashmi S., Anil K.D. and Rakesh K. (2016). Air Quality Assessment Using Interpolation Technique. *Environment Asia*, 9(2), 140-149.
- Bellander T., Berglind N., Gustavsson P., Jonson T., Nyberg, F. and Pershagen G. (2001). Using geographical information systems to assess individual historical exposure to air pollution from traffic and house heating in Stockholm. *Environmental Health Perspectives*, 109, 633-639.
- Candiani G., Carnevale C., Finzi G., Pisoni E. and Volta M. (2013). Comparison of reanalysis techniques: applying optimal interpolation and Ensemble Kalman Filtering to improve air quality monitoring at mesoscale. *Science of the Total Environment*, 458-460, 7-14.
- Clench-Aas J., Bartonova A., Grønskei K. E. and Walker S. (1999). Air pollution exposure monitoring and estimation. Part IV. Urban exposure in children. *Journal of Environmental Monitoring*, 1, 333-336.
- Dilip K.J., Sabesan M. and Kirubakaran R. (2011). Evaluation of Interpolation Technique for Air Quality Parameters in Port Blair, India. *Universal Journal of Environmental Research and Technology*, 1(3), 301-310.
- Gualtieri G. and Tartaglia M. (1998). Predicting urban traffic air pollution: A GIS framework. *Transportation Research Part D*, 3, 329-336.
- Janssen S., Dumont G., Fierens F. and Mensink C. (2008). Spatial interpolation of air pollution measurements using CORINE land cover data. *Atmospheric Environment*, 42(20), 4884-903.
- Jerrett M., Burnett R.T., Kanaroglou S., Eyles J., Brook J.R. and Giovis C. (2001). A GIS environmental justice analysis of particulate air pollution in Hamilton, Canada. *Environment and Planning, A*, 33, 955-973.
- Jerrett M., Arain A., Kanaroglou P., Beckerman B., Potoglou D. and Sahuvaroglu T. (2005). A review and evaluation of intraurban air pollution exposure models. *Journal of Exposure Analysis and Environmental Epidemiology*, 15, 185-204.
- Kumar A., Gupta I., Brandt J., Kumar R., Dikshit A.K. and Patil R.S. (2016). Air quality mapping using GIS and economic evaluation of health impact for Mumbai city, India. *Journal of the Air and Waste Management Association*, 66(5), 470-81.
- Krause P., Boyle D.P. and Base F. (2005). Comparison of different efficiency criteria for hydrological model assessment. *Advances in Geosciences*, (5), 89-97.
- Li J. and Heap A.D. (2008). A Review of Spatial Interpolation Methods for Environmental Scientists, *Geoscience Australia. Geoscience Australia Record 2008/23*, 137.
- Michelozzi P., Forastiere F., Fusco D., Perucci C.A., Ostro B., Ancona C. and Pallotti G. (1998). Air Pollution and Daily Mortality in Rome, Italy. *Occupational and Environmental Medicine*, 55 (9), 605-10, DOI:10.1136/oem.55.9.605. JSTOR 27730990. PMC 1757645. PMID 9861182.
- Nguyen Trong Hai. (2018). Report the situation of infection in 2018. Dong Nai Department of Health, 75-86. (in Vietnamese).
- Ostachuk A., Evelson P., Martin S., Dawidowski L., Yakisich J.S. and Tasat D.R. (2008). Age-related lung cell response to urban Buenos Aires air particle soluble fraction. *Environmental Research*, 107(2), 170-177, DOI: 10.1016/j.envres.2008.01.007. PMID 18313661.
- Oke A.O., Sangodoyin A.Y., Ogedengbe K. and Omodele T. (2013). Mapping of river water quality using Inverse Distance Weighted interpolation in Ogun/Osun river basin, Nigeria. *Landscape & Environment*, 7(2), 48-62.
- Pamela F.H. and Grace K.L. (2011). The Use of AERMOD Air Pollution Dispersion Models to Estimate Residential Ambient Concentrations of Elemental Mercury. *Water Air Soil Pollut*, 219, 377-388, DOI: 10.1007/s11270-010-0714-4.
- Pieters N., Koppen G., Van Poppel M., De Prins S., Cox B., Dons E., Nelen V., Int Panis L., Plusquin M., Schoeters G. and Nawrot T.S. (2015). Blood Pressure and Same-Day Exposure to Air Pollution at School: Associations with Nano-Sized to Coarse PM in Children. *Environmental Health Perspectives*, 123(7), 737-42, DOI: 10.1289/ehp.1408121. PMC 4492263. PMID 25756964.

- Raaschou-Nielsen O., Andersen Z.J., Hvidberg M., Jensen S.S., Ketzel M., Sorensen M. and Tjønneland A. (2011). Air pollution from traffic and cancer incidence: a Danish cohort study. *Environmental Health*, 10, 67, DOI: 10.1186/1476-069X-10-67. PMC 3157417. PMID 21771295.
- Shuo L., Lei Y., Yannan Y., Huichao L., Jing T., Sijia L., Ning W. and Jiafu J. (2018). Cancer incidence in Beijing, 2014. *Chinese journal of cancer research*, 30(1), 13-20, DOI: 10.21147/j.issn.1000-9604.2018.01.02.
- The new york time. (2017). India's Air Pollution Rivals China's as World's Deadliest, [online] Available at: www.nytimes.com/2017/02/14/world/asia/indias-air-pollution-rivals-china-as-worlds-deadliest.html. [Accessed 8 April 2019].
- Tran Hong Ha. (2013). National Technical Regulation on Ambient Air Quality. Ministry of Natural Resources and Environment, 1-3. (in Vietnamese).
- Van L.M. (1993). Testing interpolation and filtering techniques in connection with a semi-Lagrangian method. *Atmospheric Environment. Part A. General Topics*, 27(15), 2351-64.
- Wong D.W., Yuan L. and Perlin S.A. (2004). Comparison of spatial interpolation methods for the estimation of air quality data. *Journal of Exposure Analysis and Environmental Epidemiology* 14(5), 404-15, DOI: 10.1038/sj.jea.7500338.
- World Health Organization. (2018). Ambient (outdoor) air quality and health. [online] Available at: [www.who.int/en/news-room/fact-sheets/detail/ambient-\(outdoor\)-air-quality-and-health](http://www.who.int/en/news-room/fact-sheets/detail/ambient-(outdoor)-air-quality-and-health). [Accessed 8 April 2019].
- World Health Organization. (2016). Ambient air pollution: A global assessment of exposure and burden of disease. [online] Available at: www.who.int/phe/publications/air-pollution-global-assessment/en/ [Accessed 8 April 2019].
- Yang Z.P., Lu W.X., Long Y.Q. and Liu X.R. (2010). Prediction and precaution of heavy metal pollution trend in urban soils of Changchun City, *Urban Environ. Urban Ecol*, 23, 1-4.

THE STUDY OF LAND COVER CHANGE USING CHANGE VECTOR APPROACH INTEGRATED WITH UNSUPERVISED CLASSIFICATION METHOD: A CASE IN DUY TIEN (VIETNAM)

Si-Son Tong^{1*}, Thi-Lan Pham², Quoc Long Nguyen², Thi Thu Ha Le², Le Hung Trinh³, Xuan Cuong Cao², Adeel Ahmad⁴, Thi-Huyen-Ai Tong⁵

¹University of Science and Technology Ha Noi, Vietnam Academy of Science and Technology, 18 Hoang Quoc Viet 100000, Hanoi, VietNam

²Hanoi University of Mining and Geology, 18 Pho Vien, Bac Tu Liem, Hanoi, VietNam

³Le Quy Don Technical University, 236 Hoang Quoc Viet 100000, Hanoi, Vietnam

⁴University of the Punjab, Lahore, 54590, Pakistan

⁵Space Technology Institute, Vietnam Academy of Science and Technology, 18 Hoang Quoc Viet 100000, Hanoi, VietNam

Corresponding author: tong-si.son@usth.edu.vn

Received: June 13th, 2019 / Accepted: May 10th, 2020 / Published: July 1st, 2020

<https://DOI-10.24057/2071-9388-2019-62>

ABSTRACT. Investigating information on land cover changes is an indispensable task in studies related to the variation of the environment. Land cover changes can be monitored using multi-temporal satellite images at different scales. The commonly used method is the post-classification change detection which can figure out the replacement of a land cover by the others. However, the magnitude and dimension of the changes are not been always exploited. This study employs the mixture of categorical and radiometric change methods to investigate the relations between land cover classes and the change magnitude, the change direction of land covers. Applying the Change Vector Analysis (CVA) method and unsupervised classification for two Landsat images acquired at the same day of years in 2000 and in 2017 in Duy Tien district, the experimental results show that a low magnitude of change occurs in the largest area of direction I and direction IV regarding the increase of Normalized Difference Vegetation Index (NDVI), but the opposite trend of (Bare soil Index) BI in the rice field. Alternately, the high magnitude of change is seen in the build-up class which occupies the smallest area with 1700 ha. The characterized changes produced by the CVA method provide a picture of change dynamics of land cover over the period of 2000-2017 in the study area.

KEY WORDS: land cover change, change detection, change vector analysis, land cover dynamics

CITATION: Si-Son Tong, Thi-Lan Pham, Quoc Long Nguyen, Thi Thu Ha Le, Le Hung Trinh, Xuan Cuong Cao, Adeel Ahmad, Thi-Huyen-Ai Tong (2020). The Study Of Land Cover Change Using Change Vector Approach Integrated With Unsupervised Classification Method: A Case In Duy Tien (Vietnam). *Geography, Environment, Sustainability*, Vol.13, No 2, p. 175-184
<https://DOI-10.24057/2071-9388-2019-62>

Conflict of interests: The authors reported no potential conflict of interest.

INTRODUCTION

Land cover, the layer of physical material at the earth's surface, is composed of water, trees, grass, bare ground, etc. Land cover change is one of the most important domains in environmental change research. Investigating information on land cover changes is an indispensable task in studies related to the variation of the environment (Chen et al. 2003; Dewi et al. 2017; limanova et al. 2017). Change detection using satellite images has been proved to be an efficient approach with the advantages of rapidly collecting information, and multi-temporal, multi spatial resolution, which allows us to map land cover changes at different scales (Lambin and Strahler 1994; Chen et al. 2012). Various techniques for change detection using remote sensing data have been

developed and broadly applied. These techniques can be separated into two groups: post-classification comparison or two-date classification comparison; and temporal radiometric change analysis (Ding et al. 1998; Chen et al. 2012). The post-classification comparison is based on the classification results to determine the variations, which can produce a detailed change matrix of land cover classes. However, this group method does not allow detecting subtle changes in the classes, and the mechanism of changes is not discovered. Alternatively, a temporal radiometric change method analyses the variation curve or trajectory of spectral reflectances achieved by remote sensing sensors for successive times. Several methods using temporal radiometric changes have been developed such as rationing, band differencing, vegetation indices, principal component analysis, regression analysis, and

change-vector analysis (CVA) (Chen et al. 2003). Similarly, to other temporal radiometric change techniques, the CVA one hand can minimize the errors accumulating from the individual classification of two or more satellite images, and it measures not only the intensity of change but also the trend of the change for each pixel on multi-temporal satellite images (Dewi et al. 2017). In addition, the CVA method can process any number of spectral bands to generate a single band which represents the intensity of change between two or more satellite images (Molina et al. 2012). For these reasons, the CVA is a useful technique to investigate the information of land cover changes for various purposes as: detecting land-use/ land-cover change in rural-urban fringe areas (He et al. 2011); assessment of wetland dynamic (Landmann et al. 2013); monitoring changes in fuzzy shorelines (Dewi et al. 2017); detecting forest changes (Malila 1980). On the other hand, applying the CVA technique may face some challenges composed of: the reliable radiometry of images over a period of time, the difficulties of effectively detecting thresholds for separating the change or no-change of the magnitude pixels, and the problem of discriminating phenomenological types of the changes due to the use of a great number of bands for analysis (Cheng et al. 2003). These challenges limit the potential of such an effective technique as CVA for the land cover change monitoring.

This study aims to overcome these challenges and applies the CVA technique to investigate the land cover change of a rural area at a local scale. The CVA method produces the direction and the magnitude of changes but the categories of land cover. Implementing the CVA method in a case study area of Duy Tien district, Vietnam, we propose a mixture approach of the temporal radiometric change and the categorical information of land covers to assess the effectiveness of the method and to figure out the relations between land cover classes and their change components.

MATERIALS AND METHODS

Study area

The study area is in Duy Tien district of Ha Nam province, Vietnam, located in the center of the Red River delta with an area of 13,765 hectares composed of 19 communes and 2 towns (Fig. 1). Duy Tien was a purely agricultural district with the dominant land cover of the rice field. Recently, economic development required the exchange of a huge area of the agricultural land to industrial zones, dependent services, and residence expansion. Moreover, the very low valuation of rice cultivation led to the replacement of the rice fields with perennial trees or farms. The rapid change of land cover makes the need for monitoring not only the types of changes but also the direction of changes for environmental management of local government.

Date in use

To monitor the land cover changes of the study area, a Landsat 7 ETM+ satellite image acquired on 17/09/2000 and a Landsat 8 OLI image acquired on 17/09/2017 are used for analysis (Table 1). The specifications of the Landsat 7ETM+ and the Landsat 8OLI satellite image are illustrated in Table 2. The two images are the no-cloud cover, and they are processed at the Landsat Surface Reflectance High-Level Data products (level L1TP) by the United States Geological Survey (USGS). The effects of the atmosphere and the distortion of the images related to topography are minimized at this processed level (US Geological Survey 2016). All images have been systematically image-to-image registered with the Root Mean Square Error (RMSE) less than 12m, and they are adjusted to the 30 m spatial resolution (30 m x 30 m pixel size) in the Universal Transverse Mercator (UTM) projection zone 48N (Zanter 2017). The images are acquired at the late-season stage (the ripening phase) of rice which presents identical color and tone. These two images were acquired on the same day of years 2000 and 2017 at similar local time, similar solar zenith and solar azimuth angle; hence, this provides very good conditions to apply the CVA method. Although the images were acquired in different paths/rows, the study area is fully covered by both scenes.

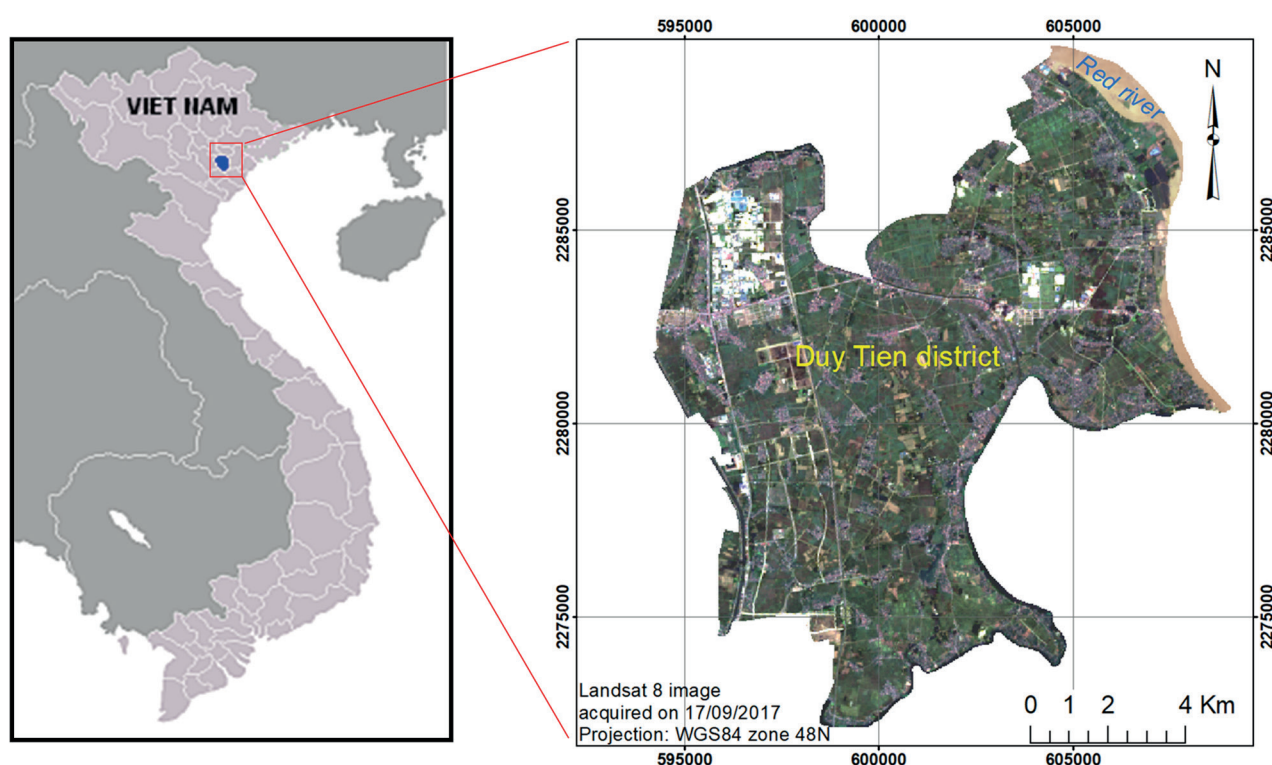


Fig. 1. Study area map of Duy Tien district

Table 1. Landsat images using in the study

Date	Sensor	Path/Row (ID)	Spatial resolution (m)	Acquisition time (UTM)
17 th Sep 2000	Landsat 7 ETM+	127/046	30	03h14'21"
17 th Sep 2017	Landsat 8 OLI	126/046	30	03h17'45"

Table 2. Specifications of bands of Landsat 7 ETM+ and Landsat 8 OLI

Landsat 7 ETM+ bands (μm)			Landsat 8 OLI and TIRS bands (μm)		
			Band 1	30 m Coastal/Aerosol	0.435-0.451
Band 1	30 m Blue	0.441-0.514	Band 2	30 m Blue	0.452-0.512
Band 2	30 m Green	0.519-0.601	Band 3	30 m Green	0.533-0.590
Band 3	30 m Red	0.631-0.692	Band 4	30 m Red	0.636-0.673
Band 4	30 m Nir	0.772-0.898	Band 5	30 m Nir	0.851-0.879
Band 5	30 m SWIR-1	1.547-1.749	Band 6	30 m SWIR-1	1.566-1.651
Band 6	60m TIR	10.31-12.36	Band 10	100 m TIR-1	10.60-11.19
			Band 11	100 m TIR-2	11.50-12.51
Band 7	30m SWIR-2	2.064-2.345	Band 7	30 m SWIR-2	2.107-2.294
Band 8	15 m Pan	0.515-0.896	Band 8	15 m Pan	0.503-0.676
			Band 9	30 m Cirrus	1.363-1.384

METHODOLOGY

CVA method

Ideally, the CVA method is described as a change vector with two components: a vector direction (the angle of the change) and a magnitude of the change between two or more images acquired in two dates (Malila 1980). The surface reflectance of an object measured on satellite images acquired in two dates corresponding to T1 and T2 are given by matrices $T1 = (p_{11}, p_{12}, p_{13}, \dots, p_{1n})$ and $T2 = (p_{21}, p_{22}, p_{23}, \dots, p_{2n})$. Where p_{in} are the surface reflectance and the number of the bands, respectively.

The change vector Δ is presented as:

$$\Delta^p = T2 - T1 = \begin{bmatrix} p_{21} - p_{11} \\ p_{22} - p_{12} \\ p_{23} - p_{13} \\ p_{2n} - p_{1n} \end{bmatrix}$$

The magnitude of changes ($|\Delta|$) between two dates are calculated from all the spectral reflectance change of the objects achieved on bands.

$$|\Delta^p| = \sqrt{(p_{21} - p_{11})^2 + (p_{22} - p_{12})^2 + (p_{23} - p_{13})^2 + (p_{2n} - p_{1n})^2}$$

The direction of change can be investigated by calculating the angle of the change vector. The angle of the change vector represents the types of land cover change over a period of time. The individual band of satellite images can be replaced by a band index or a band ratio to calculate the magnitude and the type of changes.

In this study, we use the Normalized Difference Vegetation Index (NDVI) and the Bare soil Index (BI) calculated from Landsat images to quantify the change of the land covers in Duy Tien. The NDVI displays the relationship between the quantity of chlorophyll in leaves and the spectral reflectance in the wavelength of red and near-infrared, thus the NDVI image is popularly used to research vegetation as estimating biomass, plant productivity, fractional vegetation cover (Rouse 1974; Richardson 1977). The BI is used to distinguish an

agricultural land and non-agricultural land (Jamalabad 2004). The NDVI and BI indexes are calculated by equations as:

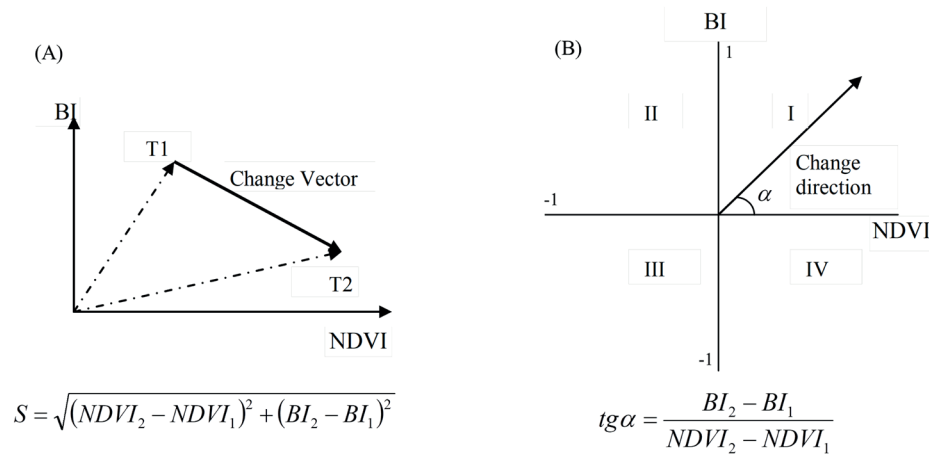
$$NDVI = \frac{(p_{Nir} - p_{Red})}{(p_{Nir} + p_{Red})}$$

$$BI = \frac{(p_{Swir} + p_{Red}) - (p_{Nir} + p_{Blue})}{(p_{Swir} + p_{Red}) + (p_{Nir} + p_{Blue})}$$

Where p_{Blue} , p_{Red} , p_{Nir} , p_{Swir} are the surface reflectance of the blue, red, near-infrared, and short wave infrared regions, respectively.

The CVA method is applied for the Landsat images captured in 2000 and 2017 to monitor the magnitude and the direction of changes using two components; the NDVI index and the BI index (Fig. 2). The direction of changes is clearly classified into four types of changes as type I, type II, type III and type IV corresponding to four possible corners of the change vector (Fig. 2B). The magnitude of change is then stratified into low change, medium change and high change using empirical thresholds detected by investigating the histograms of the image of the change magnitude combined with the knowledge of the study area (Fig. 3). As an example, the areas with rice no-change are checked with the values of the change magnitude image to define a threshold for the low change layer. The variations from rice fields into the other vegetation or infrastructures are used to define thresholds on the change magnitude image for the medium change or the high change layers, respectively (Fig. 3A, 3B).

The Landsat 8 OLI image captured on 17/9/2017 is performed classification to achieve a land cover map. To do the classification, we used the ISODATA method to cluster the images into 40 classes from running 20 iterations of all the bands of the Landsat 8 image. The unsupervised classification method is used in this study to maximize the possibility of distinguishing clusters based on spectral reflectance but it minimizes the impact of visual interpolation on results. A post-classification is implemented to combine the previous 40 classes into 8



S: The magnitude of change vector

α : The angle of change vector

$tg\alpha$: The direction of change vector

$NDVI_1$, $NDVI_2$, BI_1 , BI_2 : NDVI and BI index at date 1 and date 2 respectively

Fig. 2. Change Vector Analysis in two spectral dimensions and the equation for calculating (A) the magnitude of change and (B) the direction of change

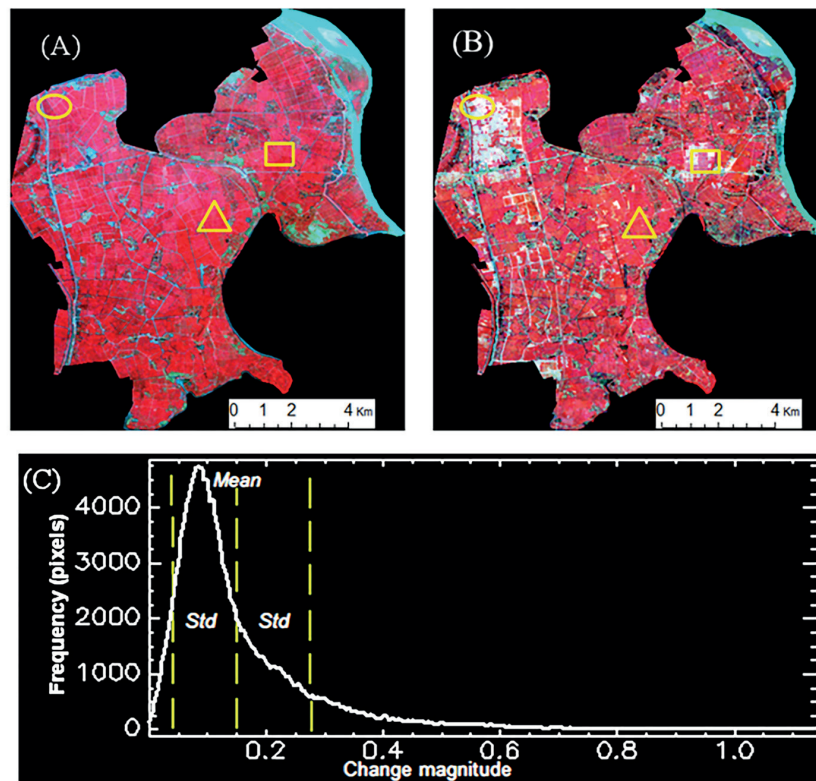


Fig. 3. (A) Pseudocolor composite of Landsat image acquired on 17/9/2000, and (B) on 17/9/2017 with the high change in the yellow ellipse, the medium change in the yellow rectangle, and the low change in the yellow triangle, (C) The histogram of the change magnitude image with the mean of 0.15 and the standard deviation (Std) of 0.12.

classification and field visiting

classes of the land cover map based on samples collected in the field (Table 3). The land cover map is overlaid with the change magnitude and the change direction maps to analyze the relationship between them. Field visiting was implemented on 14th September 2018 to observe the land covers in 47 locations in the study area. The information on field points is used to assess the accuracy of the land cover map.

RESULTS



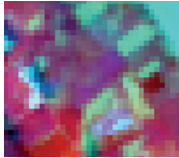

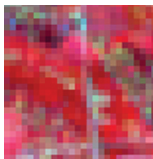

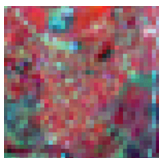



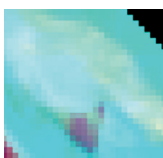

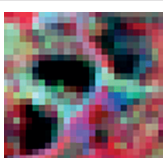

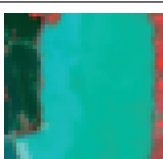

The change magnitude and the change direction

The two dimensional scatter plots in Fig. 4A and Fig. 4B represent the spatial relation of NDVI and BI in 2000

and 2017. NDVI and BI are two dimensions in the change vector coordinate. The trend of data points (red line) in Fig. 4 shows a negative correlation between NDVI and BI. To apply successfully the CVA method, it must be sure that the variation of the vegetation index is opposite to the variation of the bare soil index. Thus, the more negative correlation between them is, the higher ability of change determination is. The negative correlation between the two indexes approves the suitability of using NDVI and BI for detecting the change vectors which produce the reliable maps of the change magnitude and the change dimension for further analysis.

As seen in Fig. 5, the change direction is discriminated by four types (so-called Direction) of the changes over

Table 3. Keys for land cover classification

Land covers	Description	Landsat 8 image in 2017 (R G B = Nir, Red, Green)	Field image
Rice field	Rice at the ripening stage, homogeneous color and tone, high density of vegetation		
Annual vegetation	Vegetation as peanut, soya.. scatter distribution in the small, high, dry areas, presented as the mixture of colors		
Perennial trees	Fruit trees with small parcels planted surrounding houses		
Rural residence	Discrete shapes and colors with a mixture of vegetation and houses		
Build-up area	Road, constructions, industrial zone, playground grouped in specific shapes, white area.		
Bare land	Sand bars along the rivers presented as white regions		
Clear water	Fish ponds, canals showed as black surface on satellite images		
Turbid water	Water in Red river with the density of suspended sediment with bright surface		

2000–2017. Type I shows the increase in both of the NDVI and BI index, which covers only the area of rice field predominantly distributing in the study area. Type II represents the area with the increase of BI but the decrease of NDVI. This type of change is obviously seen in the changing area from the agricultural land to industrial zones or some roads as well. The degradation in both NDVI and BI values of Type III is found in the surrounding water surface such as the river of fishponds. The change in Type III may relate to the moisture variation of the land cover. The largest area of the change direction belongs to Type 4 defined by the increase of NDVI and the deduction of BI. Type 4 occupies all of the water surface and a vast area of vegetation. The distribution of Type 4 is complicated, thus, it needs to discuss more details when integrating with the

other data such as the land cover map and the magnitude change map.

Fig. 6 illustrates the magnitude of the land cover changes at three levels of low change, medium change, and high change corresponding to three threshold ranges as 0.0004-0.1428, 0.1428-0.2709, 0.2709-1.235 of the change magnitude. These thresholds are empirically defined by the correlation between the land cover changes and the mean, the standard variation of the histogram of the change magnitude image (showed in Fig. 3). Low magnitude change represents the variation of the spectral reflectance at an insignificant level that is not strong enough for indicating a replacement of a land cover class over the period 2000–2017. Hence, the low change level covers almost all of the study area. Medium change

level presents the transform between land covers which have similar physical specifications. The changes from rice to annual vegetation or to perennial trees are the examples of medium change level. This level of change distributes in small parcels scattered in the study area. However, the medium change of the river is an exception due to the variation of turbidity of water at the two dates. High change magnitude shows the replacement of a class by the other classes with different physical characteristics such as an exchange of rice by build-up area or bare soil by vegetation.

The map of land covers and accuracy assessment

Fig. 7 represents the distribution of 8 land cover classes in the study area on 17th September 2017. Although some vast industrial zones have been constructed in Duy Tien, the agricultural land occupies most of the area with 45% of rice, 9% of perennial trees and 6% of annual agriculture. Clear water is fishponds and canals, which are discriminated

from turbid water by the density of suspended sediment. The extremely high turbidity of up to 1 kg of sediment in 1 m³ water of the Red river, as reported by (Hoa 2001) leads to very high reflectance of visible wavelengths, thus the turbid water is clearly seen in the multispectral satellite image. Clear water and turbid water cover 11% and 3% area, respectively. Classes without vegetation as build-up area, rural residence, bare land occupy an amount of 26% area in which the bare land is some sandbars along Red river, cover only 1% of the study area.

Table 4 shows the user's accuracy and the producer's accuracy of each class of the land cover map built from Landsat 8 image acquired in September 2017. Totally, 47 field points have been used as the reference data for the accuracy assessment. The highest accuracy is found in the bare land and the turbid water with 100% of the right pixels because of the clear presentation of these features on the satellite image. The lowest accuracy is seen in the annual vegetation class with only 29% of the user's accuracy. This

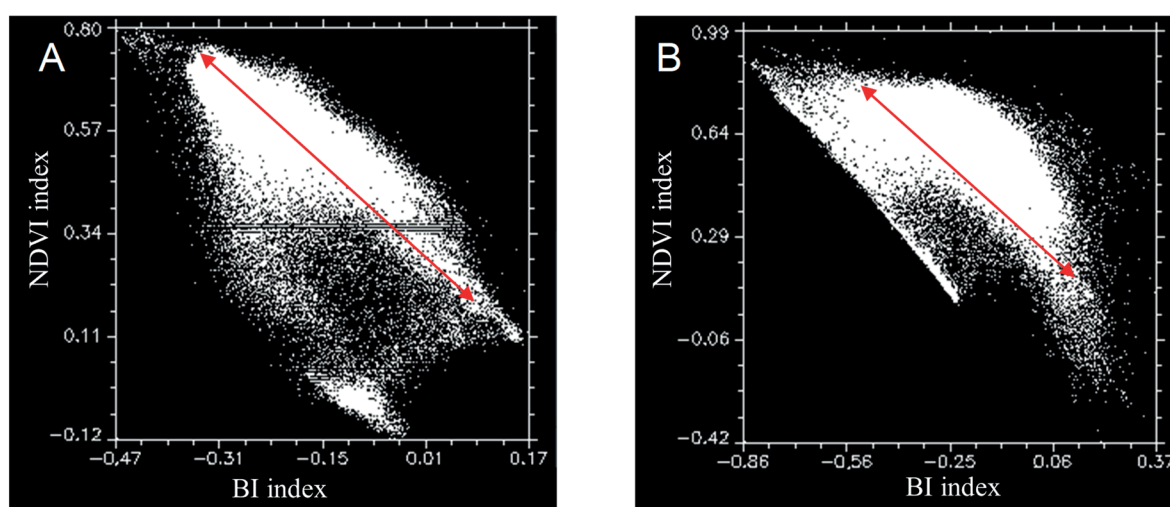


Fig. 4. (A) The scatter plot of NDVI and BI index (A) in 2000 and (B) in 2017

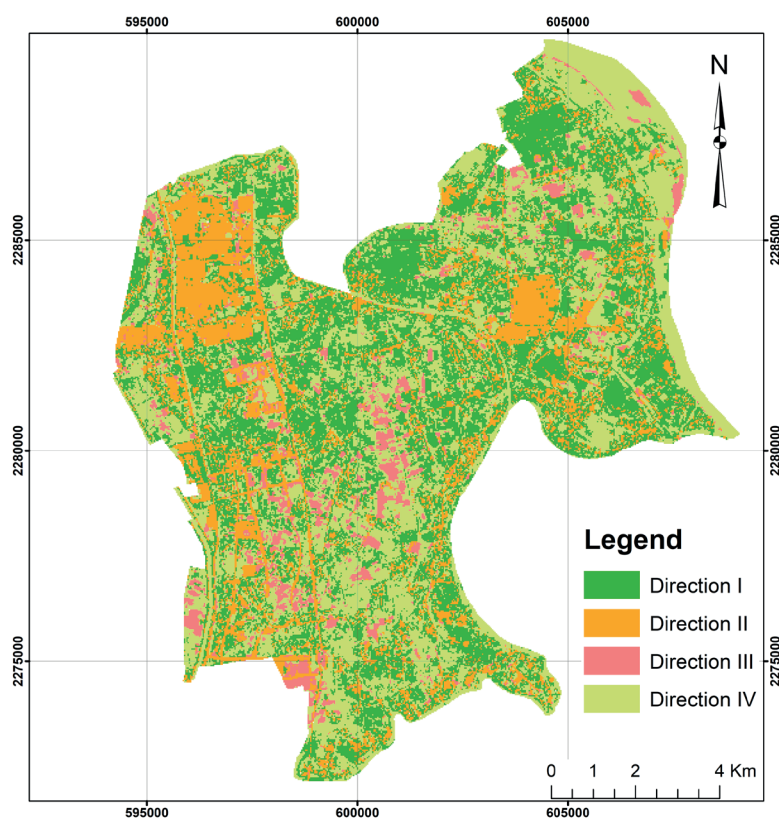


Fig. 5. The change direction map produced by applying the CVA method for the Landsat images acquired in 2000 and 2017

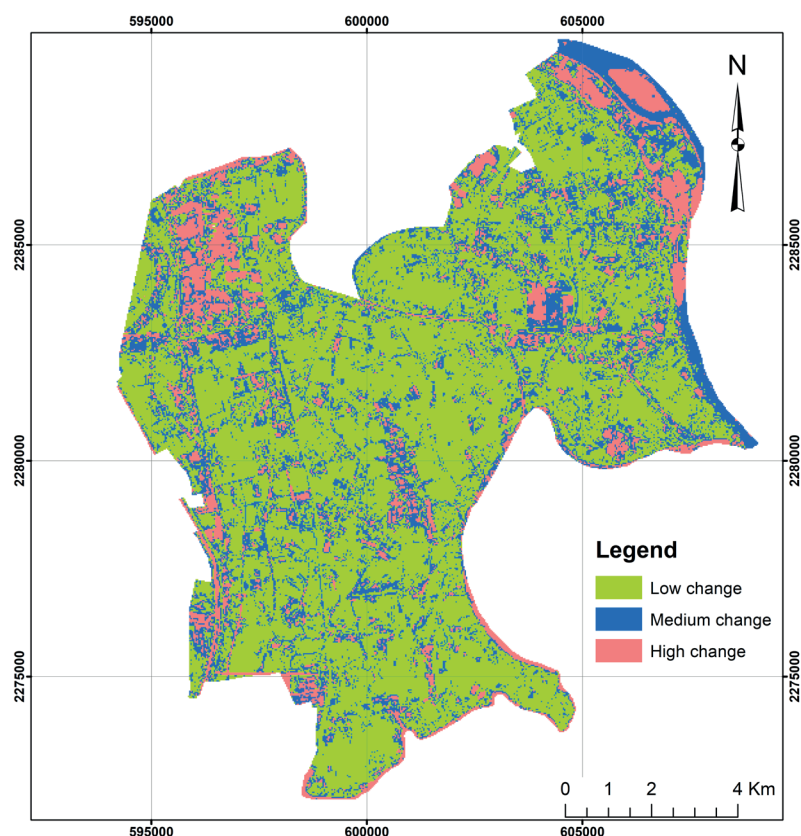


Fig. 6. The change magnitude map achieved by applying the CVA method for the Landsat images acquired in 2000 and 2017

number of accuracy is unexpected but it represents the difficulty to extract such a mixed class as annual vegetation in the agricultural rural area. Above all, the general accuracy of the map is 68%. The land cover map with this accuracy is acceptable in this experiment.

The assessment of temporal radiometric changes and the categorical information of land covers. As seen in Fig. 8A, the low magnitude of change occurs at the largest area

in the direction I (Type I) and direction IV corresponding to 4200 ha (32% of total area) and 2600 ha (20%). Direction I and direction IV are both increases of NDVI but the opposite trend of BI. Hence, these directions are related to vegetation such as rice with 23% in direction I, 16% in direction IV or perennial trees with 7% in direction IV (Fig. 8B). The medium magnitude of change covers the largest area of direction IV with 11% of the total area. However,

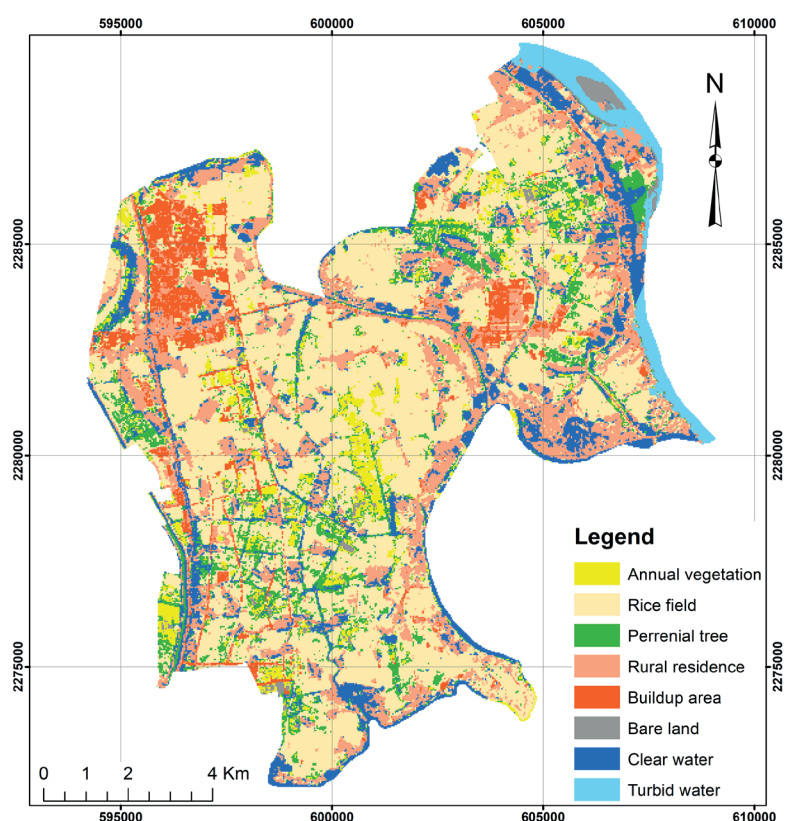


Fig. 7. Land cover map obtained from the image classification of the Landsat 8 image acquired on 17th September 2017

Table 4. Keys for land cover classification

Classified data	Reference points									
	Annual vegetation	Rice field	Perennial trees	Rural residence	Build-up area	Bare land	Clear water	Turbid water	Total points	User's accuracy
Annual vegetation	2	2	1	1	0	0	0	1	7	29%
Rice field	1	7	0	1	0	0	1	0	10	70%
Perennial trees	0	1	3	1	0	0	0	0	5	60%
Rural residence	0	0	1	6	1	0	1	0	9	67%
Build-up area	0	0	0	1	4	0	0	0	5	80%
Bare land	0	0	0	0	0	3	0	0	3	100%
Clear water	0	0	0	1	0	0	5	0	6	83%
Turbid water	0	0	0	0	0	0	0	2	2	100%
Total points	3	10	5	11	5	3	7	3	47	
Producer's accuracy	67%	70%	60%	55%	80%	100%	71%	67%		68%

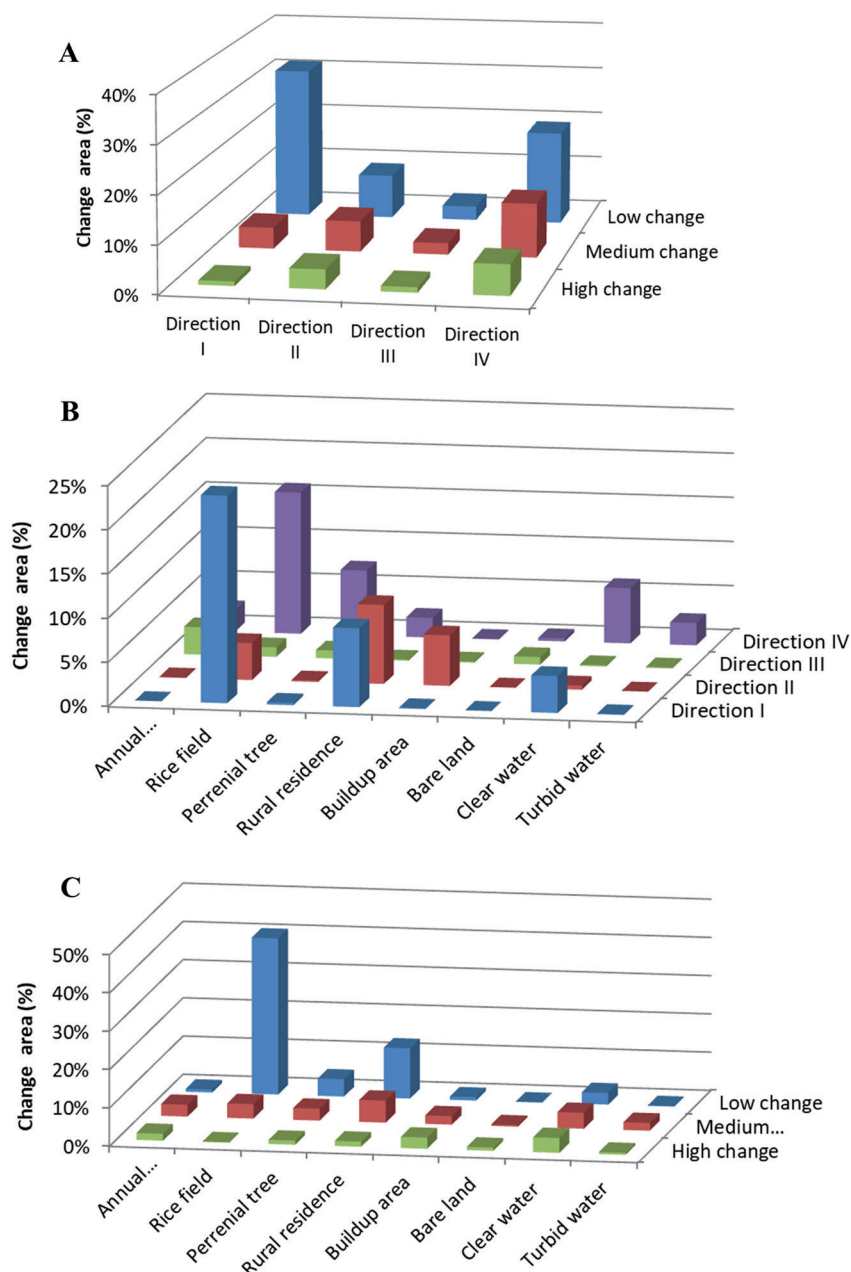


Fig. 8. Relations between (A) the change magnitude and the change direction, (B) the land cover and the change direction, and (C) the land cover and the change magnitude

this level of change does not emphasize a specific land cover class. The area of medium change is relatively equal for all the classes (Fig. 8C). Alternately, a high magnitude of change occupies the smallest area with 1700 ha (12% of total area), but it almost covers the build-up area with 3% and 4% of the clear water area. High change can obviously be observed in the satellite images due to the conversion of vegetation to the concrete surface which makes the absolute change of spectral reflectance. An amount of 519 ha (4%) of clear water felt in the high change area may be caused by the appearance of the vanishing of vegetation on the clear water surface. In addition, high change occurs mostly in direction IV area (6%) where the NDVI increases over the period 2000–2017. In sum, the results of the experiment show the correlation of the change magnitude, the change direction, and land cover classes. The characterized changes in land covers exploit the nature of change.

DISCUSSION

The CVA method is based on the radiometric change, which is an efficient approach by exploiting the hidden information of the changes through the change magnitude and the change direction. However, the challenges related to using spectral reflectance and the determination of thresholds of change may impact the accuracy of applying the CVA method. Thus, we discuss more of these issues.

As mentioned by (Chen et al. 2003), the radiometric changes of the images acquired at the two dates can be affected by disturbing factors caused by the temporal variation such as the different atmospheric conditions, solar angle, soil moisture, and vegetation phenology, etc. These quick variation conditions may contribute to the bias of the results more critical than the spectral reflectance change detected by the CVA method. To minimize the error coming from temporal variation, it is necessary to use the pair of satellite images acquired at as much similar as possible conditions. In this study, we use two images acquired on the same day of the year on 17th September in 2000 and 2017. The difference of several seconds of the acquisition times (Table 1) provides a radiometric signal at a similar solar zenith, horizontal angle. In addition, the study area suffers the sub-tropical climate with a cold season, thus, the time of cultivation is relatively stable over the years. The images acquired on the same day of year measures the spectral reflectance from the similar phenological stage of rice. Moreover, these two images are captured by the same family of satellite sensor (Landsat family), the same way of atmospheric correction, the same spectral resolution, and the same range of the accuracy of geometric correction. Thus, the satellite images used in this case are wonderful data to apply the CVA method to achieve the highest accuracy of results.

In the concept of CVA, this method is applicable to any number of spectral bands, even though any measurement scale of radiance is used (Malila 1980). However, the use of multispectral images can make the confusion and the difficulties to discriminate the categories of changes when analyzing the change directions. The more the number of image bands in use, the analysis of change direction is more complicated, especially in the study area with numerous types of land covers. Three methods to face this issue have been developed (Chen et al. 2003): trigonometric function of vector angle in two spectral dimensions (Malila 1980); principal component analysis in multi-temporal space (Lambin and Strahler 1994), and sector coding in more

than two spectral dimensions (Virag and Colwell 1987). The use of the sector coding method to separate the change direct into 4 categories in this study is the appropriate option for the study area. Each category represents a type of the change direction corresponding to two correlated components NDVI and BI index. The stratification scheme of the change direction can be used to figure out some causes of the changes which may not be detected by visual interpolation.

One of the most difficult tasks of the CVA application is the determination of appropriate thresholds to distinguish the change-magnitude pixels with change or no-change. However, there is no automatic or semi-automatic method to define the change thresholds because it is necessary to consider some ecological and spectral conditions corresponding to threshold selection and overall change sensitivity. As an example, a lower change threshold value may allow the inclusion of slightly changed wetlands into the change analyses, while a high threshold value may only include the locations of significantly changed areas (Baker et al. 2007). Hence, using the remote sensing analyst's expert knowledge of the study area is the best method to detect the change thresholds (Jano et al. 1998). In this study, we determine the change thresholds based on the mean and standard deviation of the histogram of the change magnitude image combining with the knowledge of land cover changes. The results proved that this approach is effective and it produces reliable maps of land cover changes in such a small known area as in Duy Tien. However, for a large scale area with the complication of land cover classes, the use of the CVA method with this method of threshold determination will face numerous challenges and it needs to be studied in future works.

CONCLUSIONS

The application of CVA using two components NDVI and BI index is an effective method to discover the dynamic of land cover/ land use changes. The CVA method does not only exploit the magnitude element but also the direction element of the changes which represent the nature of land cover changes using remote sensing data. On the other side, the results of the CVA application make it difficult to indicate the specific land covers that can obviously be obtained using a single classification of the satellite image. This study successfully applies both CVA and unsupervised methods to investigate the change information of land cover. The study shows that the CVA method using NDVI and BI index is suitable for Landsat images to monitor land cover change in such a purely agricultural area as Duy Tien district. The key step of the CVA method is the method to detect appropriate thresholds for stratifying pixels with change or no-change, for which the knowledge of the study area combined with the spectral reflectance of surface features is the most accurate approach. The change magnitude or change direction obtained from the CVA application can be disturbed by the temporal variation of the environment, the different sources of satellite images and the radiometric, geometric processing as well. Thus, the used satellite images must be carefully selected and processed to minimize the impacts of those disturbing factors. Overall, the CVA with the ability to measure the magnitude of land cover change is a promising method to monitor the growth of the plants from that we can estimate the production of crops. This application is necessary for an agricultural country like Viet Nam, and it may be employed for future studies. ■

REFERENCES

- Baker C., Lawrence R.L., Montagne C. and Patten D. (2007). Change detection of wetland ecosystems using Landsat image and change vector analysis. *Wetlands*, 27(3), 610-619, DOI: 10.1672/0277-5212(2007)27[610:CDOWEU]2.0.CO;2.
- Chen J., Gong P., He C., Pu R. and Shi P. (2003). Land-Use/Land-Cover Change Detection Using Improved Change-Vector Analysis. *Photogrammetric Engineering & Remote Sensing*, 69(4), 369-379, DOI: 10.14358/PERS.69.4.369.
- Chen G., Hay G.J., Carvalho L.M.T. and Wulder M.A. (2012). Object-Based Change Detection. *International Journal of Remote Sensing*, 33(14), 4434-4457, DOI: 10.1080/01431161.2011.648285.
- Dewi R., Bijker W. and Stein A. (2017). Change Vector Analysis to Monitor the Changes in Fuzzy Shorelines. *Remote Sensing*, 9(2), 147, DOI: 10.3390/rs9020147.
- He C., Wei A., Shi P., Zhang Q. and Zhao Y. (2011). Detecting land-use/land-cover change in rural-urban fringe areas using extended change-vector analysis. *International Journal of Applied Earth Observation and Geoinformation*, 13(4), 572-585, DOI: 10.1016/j.jag.2011.03.002.
- Hoa M.H. (2001). Morphological dynamics estuary of the delta in north Vietnam serves rational use of natural resources and environment in estuary area. Faculty of Geography, vol. Doctor, 147.
- Jamalabad M.S. and Akbar A.A. (2004). Forest canopy density monitoring, using satellite images. ISPRS Congress, Istanbul.
- Jano A.P., Jeffries R.L. and Rockwell R.F. (1998). The detection of vegetational change by multitemporal analysis of Landsat data: the effects of goose foraging. *Journal of Ecology*, 86(1), 93-99, DOI: 10.1046/j.1365-2745.1998.00232.x.
- Klimanova O., Naumov A., Greenfieldt Y., Prado R.B., Tretyachenko D. Regional trends of land use and land cover transformation in Brazil in 2001–2012. *Geography, Environment, Sustainability*. 2017; 10(4): 98-116, DOI: 10.24057/2071-9388-2017-10-4-98-116.
- Lambin E.F. and Strahler A.H. (1994). Change vector analysis in multi-temporal space: A tool to detect and categorize land-cover change processes using high temporal-resolution satellite data. *Remote Sensing of Environment*, 48(2), 231-244, DOI: 10.1016/0034-4257(94)90144-9.
- Landmann T., Schramm M., Huettich C., and Dech S. (2013). MODIS-based change vector analysis for assessing wetland dynamics in Southern Africa. *Remote Sensing Letters*, 4(2), 104-113, DOI: 10.1080/2150704X.2012.699201.
- Malila W.A. (1980). Change Vector Analysis: An Approach for Detecting Forest Changes with Landsat. In LARS Symposia, 385, Purdue University, Lafayette, IN, USA.
- Molina I., Martinez E., Arquero A., Pajaresand G. and Sanchez J. (2012). Evaluation of a Change Detection Methodology by Means of Binary Thresholding Algorithms and Informational Fusion Processes. *Sensors*, 12(3), 3528-3561, DOI: 10.3390/s120303528.
- Richardson A.J. and Wiegand C.L. (1977). Distinguishing vegetation from soil background information. *Photogrammetric engineering and remote sensing*, 43(12), 1541-1552.
- Rouse Jr J.W., Haas R.H., Deering D.W., Schell J.A. and Harlan J.C. (1974). Monitoring the Vernal Advancement and Retrogradation (Green Wave Effect) of Natural Vegetation. [Great Plains Corridor].
- US Geological Survey, version 6.4. (2016). Landsat 4-7 climate data record (CDR) surface reflectance. USGS Product Guide.
- Virag L.A. and Colwell J.E. (1987). An improved procedure for analysis of change in Thematic Mapper image-pairs. In International Symposium on Remote Sensing of Environment, 21st, Ann Arbor, MI, 1101-1110.
- Yan D., Elvidge C.D. and Lunetta R.S. (1998). Survey of Multispectral Methods for Land Cover Change Analysis. In *Remote Sensing Change Detection: Environmental Monitoring Methods and Applications*, Ann Arbor Press: Chelsea, MI, USA, 21-39.
- Zanter K. (2017). Landsat Collection 1 Level 1 Product Definition. United States Geological Survey version 1.0: LSDS-1656.



ges.rgo.ru/jour/

ISSN 2542-1565 (Online)